DEFORMATIONAL BEHAVIOUR, FAILURE MECHANISMS AND DESIGN CRITERIA FOR CONCRETES UNDER COMBINATIONS OF STRESS

By

J. B. Newman, B.Sc.(Eng.), A.C.G.I., D.I.C.

A Thesis submitted for the Degree of Doctor of Philosophy, in the Faculty of Engineering of the University of London

1973

Imperial College of
Science and Technology
London

ABSTRACT

Part I of the thesis examines the effectiveness of various methods of applying boundary conditions of stress or deformation to specimens of material with regard to the ability of such methods to induce uniform and definable stress states. A detailed study of previous investigations complemented by new analytical and experimental work indicates that certain techniques may cause considerable interaction between the specimen and loading device. Recommendations are made regarding the most suitable methods for testing heterogeneous materials such as concrete.

Part II investigates the response of concretes to boundary conditions of uniform stress and uniform strain. Equal biaxial compression is chosen as the basic stress state, since this can be attained using available and proven apparatus, with rigid-platen loading providing the uniform strain condition and uniform stress being applied hydraulically. The differences between the behaviour of the concretes under the two boundary conditions are shown to be heavily dependent on the degree of heterogeneity of the mix. The implications of this are discussed with particular reference to the use of test data for design purposes.

Part III examines the progressive breakdown of non-metallic brittle materials under short-term stress. Previous work indicates that distinct changes in the fracture process can be identified, the levels of change depending on the detection technique employed. A failure mechanism is postulated and proposals made regarding convenient methods of identifying the boundaries of each significant stage of material response. Definitions of failure based on these boundaries are suggested as upper and lower bound criteria suitable for structural design and the validity of these criteria is assessed by a series of tests in which concretes are subjected to regimes of repeated uniaxial compressive stress. Correlation is obtained between the deformational stability under such loading regimes and the upper and lower bound criteria evaluated for static stress conditions.

In Part IV, previous data on the ultimate strength of concretes under triaxial stress are analysed statistically to determine the influence of mix characteristics and environmental conditions on the failure envelopes. The conclusions drawn are used as the basis for a comprehensive experimental programme in which the deformational response of concretes to short-term triaxial 'compression' is studied using a specially developed hydraulic

triaxial cell. In the first part of the investigation a range of concretes with idealised gradings is tested to obtain general patterns of behaviour and it is shown that the proposed failure criteria can be evaluated satisfactorily for multiaxial as well as uniaxial stress states. The results are used in the formulation of the second series in which a range of practical concretes is tested.

In Part V the results from the triaxial tests are used to establish design criteria for concretes under combined states of stress. Information is presented in a form suitable for engineers and the method of using the design charts is demonstrated. Finally, suggestions are made regarding avenues of research which might profitably be followed in the light of the results obtained during the present project.

ACKNOWLEDGEMENTS

The Author acknowledges that a successful outcome to any experimental project is only possible through teamwork. Sincere thanks are, therefore, expressed to all individuals and organisations who made possible the work described in this thesis, and in particular to -

Professor A. L. L. Baker, who was responsible for the overall supervision of the project, for his continued encouragement.

Mr. K. Newman, who originally recognised the need for the research work, for his detailed supervision at the start of the project, continued advice and suggestions throughout the course of the programme and valuable comments during the preparation of this thesis.

Past and present members of the Concrete Materials Research Group, especially Mr. R. J. Glen, Mr. P. R. Mitchell and Mr. P. E. Corles, without whose technical expertise and conscientious and enthusiastic approach to the complex experimental techniques the project would have foundered at an early stage.

My wife, for patiently typing the endless and ever-changing manuscripts, presenting the final version in an eminently readable form and accepting at the same time the domestic deprivations demanded by research work.

The Construction Industries Research and Information Association for its generous financial support, and to its staff for their valuable help during the project.

TABLE OF CONTENTS

	Page No.
ABSTRACT	(i)
ACKNOWLEDGEMENTS	(iii)
TABLE OF CONTENTS	(iv)
SIGN CONVENTION AND UNITS	(xv)
GLOSSARY OF TERMS	(xvi)
1. AIMS OF PROJECT	1
1.1. Introduction	1
1.2. Previous Work of the Concrete Materials Research Group	2
1.2.1. Prior to 1963	2
1.2.2. Prior to 1965	3
1.2.3. After 1965	3
1.3. Current Project	4
PART I	
2. METHODS OF ACHIEVING AND EVALUATING DESIRED STATES OF STRESS OR STRAIN IN SPECIMENS	7
2.1. Introduction	7
2.2. Definition of the Problem	8
2.3. Factors involved in transmitting Load through Different Materials	9
2.3.1. Introduction	9
2.3.2. Uniform Boundary Strain	10
2.3.3. Uniform Boundary Stress	15
2.4. Review of Related Investigations	16
2.4.1. Introduction	16
2.4.2. Analytical Investigations	17
2.4.2.1. Results of Investigations	17
2.4.2.2. Conclusions	36
2.4.3. Experimental Investigations	36
2.4.3.1. Results of Investigations	36
2.4.3.2. Conclusions	54

2.5. Analytical Investigations of Stresses and Strains induced in Specimens for Different Boundary Conditions and Applied States of Stress or Strain 57

2.5.1. Introduction 57
2.5.2. Method of Analysis 58
2.5.3. Loading Configurations investigated 59
2.5.4. Results of Analyses 59
2.5.5. Discussion of Results 59

2.5.5.1. Assessment of Criticality of Stress State 59
2.5.5.2. Slabs and Prismatic Specimens under Uniaxial Compressive Load 70
2.5.5.3. Slab Specimens under Equal Biaxial Compression 72
2.5.5.4. Prismatic Specimen under Unequal Biaxial Compression 72

2.5.6. Conclusions 72

2.5.6.1. Introduction 72
2.5.6.2. Slab under Uniaxial Compression 72
2.5.6.3. Prism with H/W = 2.5 under Uniaxial Compression 73
2.5.6.4. Slab under Equal Biaxial Compression 73
2.5.6.5. Prism with H/W = 2.5 under Unequal Biaxial Compression 74

2.6. Experimental Investigation of Stresses and Strains induced in Slab Specimens under Uniaxial Compressive Load 74

2.6.1. Introduction 74
2.6.2. Details of Mortar Specimens 75

2.6.2.1. Selection of Mix 75
2.6.2.2. Details of Slab Specimens 76
2.6.2.3. Choice of Maximum Stress Levels and Determination of Elastic Constants for the Mortar 76
2.6.3. Test Series I - Assessment of the Load Transmission Characteristics for a Rigid Steel Platen Loading System 78

2.6.3.1. Introduction 78
2.6.3.2. Testing Arrangement 78
2.6.3.3. Test Procedure 79
2.6.3.4. Test Results 79
2.6.3.5. Discussion of Results 83
2.6.3.6. Conclusions 83

2.6.4. Test Series II and III - Evaluation of the Stress Distribution induced in Mortar Specimens under Uniaxial Loading applied through Rigid Platens with and without Intermediate Materials or 'Non-rigid' Platens 85

2.6.4.1. Introduction 85
2.6.4.2. Testing Arrangement 87

2.6.4.3. Details of Intermediate Materials and 'Non-rigid' Platens 90
2.6.4.4. Test Procedure 90
2.6.4.5. Test Results 90
2.6.4.6. Discussion of Results from Series II 101
2.6.4.7. Discussion of Results from Series III 107
2.6.4.8. Conclusions 108

2.7. Choice of Loading Procedures for Uniaxial, Biaxial and Triaxial Compressive Stress States 109

2.7.1. Choice of Boundary Conditions 109
2.7.2. Recommended Loading Procedures 110

2.7.2.1. Uniaxial Compression 111
2.7.2.2. Biaxial Compression 113
2.7.2.3. Triaxial Compression 114

PART II

3. AN EXAMINATION OF THE STATE OF EQUAL BIAXIAL COMPRESSION WHEN INDUCED UNDER UNIFORM BOUNDARY STRESS AND STRAIN 116

3.1. Introduction 116

3.2. Choice of Loading Techniques 117

3.3. Review of Previous Investigations into the Behaviour of Concrete under Biaxial Compression 119

3.3.1. Tests under Uniform Boundary Stress 119
3.3.2. Tests under Uniform Boundary Strain 119
3.3.3. Conclusions 119

3.4. Choice of Concrete Mixes, Curing Conditions and Specimens 125

3.4.1. Concrete Mixes 125
3.4.2. Curing Conditions 126
3.4.3. Specimens 127

3.5. Apparatus and Methods of Testing 127

3.5.1. Measuring and Recording System for Stresses and Strains 127
3.5.2. Cube Tests 128
3.5.3. Direct Tensile Tests 128
3.5.4. Uniaxial Cylinder and Prism Tests 128
3.5.5. Uniaxial and Biaxial Compression Tests under Near-uniform Boundary Strain 128

3.5.5.1. Introduction 128
3.5.5.2. Complex Stress Machine 129
3.5.5.3. Preparation of Specimen 131
3.5.5.4. Specimen Setting-up 132
3.5.5.5. Method of Testing 132

3.5.6. Biaxial Compression Tests under Near-uniform Boundary Stress 134

3.5.6.1. Introduction 134
3.5.6.2. Loading Technique to account for Secondary Restraint Stresses 135
3.5.6.3. Hydraulic Cell and Control System 136
3.5.6.4. Preparation of Specimens 136
3.5.6.5. Specimen Setting-up 139
3.5.6.6. Method of Testing 139

3.6. Uniaxial Compression Tests 141

3.6.1. Results 141
3.6.2. Discussion of Results 141

3.6.2.1. Stress-Strain Relationships 141
3.6.2.2. Incremental Strain Ratio 151
3.6.2.3. Onset of Stable Fracture Propagation (o.s.f.p.) 152
3.6.2.4. Volume Changes and Minimum Volume Level 155
3.6.2.5. Ultimate 158
3.6.2.6. Modes of Failure 158

3.7. Equal Biaxial Compression Tests 158

3.7.1. Results 158
3.7.2. Discussion of Results 163

3.7.2.1. Stress-Strain Relationships 163
3.7.2.2. Incremental Strain Ratio 168
3.7.2.3. Onset of Stable Fracture Propagation (o.s.f.p.) 171
3.7.2.4. Volume Changes and Minimum Volume Level 174
3.7.2.5. Ultimate 178
3.7.2.6. Failure Modes 179

3.8. Conclusions 182

3.8.1. Introduction 182
3.8.2. Cube Tests 182
3.8.3. Uniaxial Compression Tests 183

3.8.3.1. Stress-strain Relationships 183
3.8.3.2. Onset of Stable Fracture Propagation 183
3.8.3.3. Volume Changes 183
3.8.3.4. Onset of Unstable Fracture Propagation 184
3.8.3.5. Ultimate 184

3.8.4. Equal Biaxial Compression Tests 184

3.8.4.1. Stress-strain Relationships 184
3.8.4.2. Incremental Strain Ratio 185
3.8.4.3. Onset of Stable Fracture Propagation 185
3.8.4.4. Volume Changes 186
3.8.4.5. Onset of Unstable Fracture Propagation 186
3.8.4.6. Ultimate 187

3.9. Implications for Design 187

PART III

4. DEFINITIONS OF FAILURE 189

4.1. Introduction 189

4.2. The Fracture Process in Brittle Materials other than Concrete 190

4.2.1. Review of Previous Work 190
4.2.2. Conclusions 197

4.3. Review of Experimental Measurement of the Deformational and Cracking Processes for Concrete 197

4.3.1. Introduction 197
4.3.2. Behaviour and Conditions of Short-term Static Stress 199
4.3.3. Conclusions 212

4.4. Postulated Mechanisms of Failure for Concrete under Increasing Stress 212

4.5. Proposals for Detecting Various Stages of the Fracture Process 217

4.5.1. Introduction 217
4.5.2. Ultimate Level 218
4.5.3. Onset of Unstable Fracture Propagation (o.u.f.p.) 218
4.5.4. Onset of Stable Fracture Propagation (o.s.f.p.) 219

4.5.4.1. General Considerations 219
4.5.4.2. Detailed Procedure for assessing o.s.f.p. 225
4.5.4.3. Validity of Technique 227

5. INFLUENCE OF DIFFERENT REGIMES OF LOADING ON THE DEFINITIONS OF FAILURE 229

5.1. Introduction 229

5.2. Review of Investigations into the Behaviour of Concrete under Repeated Loading 230

5.2.1. Introduction 230
5.2.2. Uniaxial Tension 230
5.2.3. Uniaxial Compression 230
5.2.4. Flexure 234
5.2.5. Conclusions 235

5.3. Experimental Programme to Assess the Behaviour of Concretes under Repeated Uniaxial Compressive Loading 237

5.3.1. Introduction 237
5.3.2. Choice of Concrete Mixes, Curing Conditions and Specimens 238

5.3.2.1. Concrete Mixes 238
5.3.2.2. Curing Conditions 238
5.3.2.3. Specimens 238

5.3.3. Choice of Loading Regime 238
5.3.4. Apparatus 239

5.3.4.1. Loading Equipment 239
5.3.4.2. Strain Measurement 239
5.3.4.3. Measurement of Ultrasonic Pulse Velocity 240
5.3.5. Preparation of Specimens for Test 240
5.3.6. Method of Testing 240
5.3.7. Analysis of Strain Measurements 242
5.3.8. Results 243
5.3.9. Discussion of Results 253

5.3.9.1. Stages of Behaviour evaluated from Short-term Tests 253
5.3.9.2. Behaviour under Repetitive Loading 253

5.3.10. Conclusions 257

PART IV

6. STRENGTH OF CONCRETE UNDER TRIAXIAL COMPRESSION - AN ANALYSIS OF PREVIOUS WORK 259

6.1. Introduction 259

6.2. Representation of the Strength Envelope 260

6.3. Effect of Water Cement Ratio 264

6.4. Effect of Curing Regime prior to Test 268

6.5. Effect of Mix Type and Maximum Size of Aggregate 268

6.5.1. Mortars and Concretes 274
6.5.2. Lightweight Aggregate Concretes 274
6.5.3. Pastes 274

6.6. Effect of Volume Fraction of Aggregate 275

6.7. Conclusions 280

7. DEFORMATIONAL BEHAVIOUR OF CONCRETES UNDER UNIAXIAL TENSION AND TRIAXIAL 'COMPRESSION' STRESS STATES 282

7.1. Introduction 282

7.2. Choice of Concrete Mixes, Curing Conditions and Specimens 284

7.2.1. Concrete Mixes 284

7.2.2. Curing Conditions 287
7.2.3. Specimens 288

7.3. Apparatus and Methods of Testing 288

7.3.1. Measuring and Recording Systems for Stresses and Strains 288
7.3.2. Cube Tests 290

7.3.2.1. Apparatus 290
7.3.2.2. Method of Testing 291

7.3.3. Direct Tensile Tests 291

7.3.3.1. Apparatus 291
7.3.3.2. Method of Testing 293

7.3.4. Triaxial 'Compression' Tests 295

7.3.4.1. Introduction 295
7.3.4.2. Triaxial Cell and Control System 296
7.3.4.3. Loading Frame and Control System 299
7.3.4.4. Assembly Procedures 299
7.3.4.5. Method of Testing 301

7.4. Preparation of Specimens for Test 304

7.4.1. Introduction 304
7.4.2. Casting and Compaction 305
7.4.3. Curing 305
7.4.4. Surface Preparation 306
7.4.5. Strain Gauging 306
7.4.6. Assembly Procedure for Specimen/Platen/Sheath Unit 307

7.5. Triaxial Test Programme for Idealised Concretes 307

7.5.1. Concrete Mixes 307
7.5.2. Cube Tests 308

7.5.2.1. Results 308
7.5.2.2. Discussion of Results 308

7.5.3. Direct Tensile Tests 310

7.5.3.1. Results 310
7.5.3.2. Stress-strain Relationships 310
7.5.3.3. Onset of Stable Fracture Propagation (o.s.f.p.) 313
7.5.3.4. Volume Changes 317
7.5.3.5. Ultimate Stresses and Strains 317
7.5.3.6. Mode of Failure 322

7.5.4. Triaxial Compression Tests 324

7.5.4.1. Results 324
7.5.4.2. Stress-strain Relationships 324
7.5.4.3. Onset of Stable Fracture Propagation (o.s.f.p.) 338

7.5.4.4. Hypothesis for Behaviour at o.s.f.p. 358
7.5.4.5. Volume Changes 363
7.5.4.6. Onset of Unstable Fracture Propagation (o.u.f.p.) 375
7.5.4.7. Ultimate Stresses and Strains 382
7.5.4.8. Mode of Failure 388

7.5.5. Conclusions from Tests on Idealised Concretes 393

7.5.5.1. Cube Tests 394
7.5.5.2. Direct Tension Tests 394
7.5.5.3. Triaxial Compression Tests 394

7.6. Triaxial Test Programme for Real Concretes 398

7.6.1. Introduction 398
7.6.2. Concrete Mixes 399
7.6.3. Cube Tests 400

7.6.3.1. Results 400
7.6.3.2. Discussion of Results 400

7.6.4. Direct Tensile Tests 403

7.6.4.1. Results 403
7.6.4.2. Stress-strain Relationships 403
7.6.4.3. Onset of Stable Fracture Propagation 404
7.6.4.4. Volume Changes 409
7.6.4.5. Ultimate Stresses and Strains 409
7.6.4.6. Failure Modes 409

7.6.5. Triaxial Compression Tests 409

7.6.5.1. Results 409
7.6.5.2. Stress-strain Relationships 413
7.6.5.3. Onset of Stable Fracture Propagation (o.s.f.p.) 420
7.6.5.4. Volume Changes 436
7.6.5.5. Onset of Unstable Fracture Propagation (o.u.f.p.) 445
7.6.5.6. Ultimate Stresses and Strains 448
7.6.5.7. Modes of Failure 453

7.6.6. Conclusions from Test Series on Real Concretes 453

7.6.6.1. Cube Tests 457
7.6.6.2. Direct Tension Tests 457
7.6.6.3. Triaxial Compression Tests 459

PART V

8. DESIGN CRITERIA FOR CONCRETE UNDER COMBINED STATES OF STRESS 464

8.1. Introduction 464

8.2. Application of Results of Test Programme 465

8.2.1. Test Procedures and States of Stress 465
8.2.2. Test Specimens 466

8.2.3. Concrete Characteristics 467
8.2.4. Validity of Test Results 467

8.3. Definitions of Failure 470

8.4. Test Results 471

8.5. Stress Data as a Basis for Design 472

8.5.1. Introduction 472
8.5.2. Ultimate 472

8.5.2.1. Idealised Concretes 472
8.5.2.2. Real Concretes 473

8.5.3. Onset of Unstable Fracture Propagation (o.u.f.p.) 473
8.5.4. Onset of Stable Fracture Propagation (o.s.f.p.) 476

8.5.4.1. Idealised Concretes 476
8.5.4.2. Real Concretes 478

8.6. Design Charts for Stresses 479

8.6.1. Method of Representing Test Data 479
8.6.2. Ultimate 480
8.6.3. Onset of Unstable Fracture Propagation 481
8.6.4. Onset of Stable Fracture Propagation 481
8.6.5. Design Example 485

8.6.5.1. The Problem 485
8.6.5.2. Design Procedure 485
8.6.5.3. Concretes with other Aggregates 498

8.7. Strain Data as a Basis for Design 498

8.7.1. Onset of Stable Fracture Propagation (o.s.f.p.) 498

8.7.1.1. Idealised Concretes 498
8.7.1.2. Real Concretes 499

8.7.2. Onset of Unstable Fracture Propagation (o.u.f.p.) 499

8.7.2.1. Idealised Concretes 499
8.7.2.2. Real Concretes 500

8.8. Design Charts for Strains 500

8.8.1. Introduction 500
8.8.2. Onset of Stable Fracture Propagation 500

8.9. Influence of Thermal, Shrinkage and Creep Effects on the Design Criteria 501

8.10. Test Programme to Establish Design Criteria for a Particular Concrete 503

8.10.1. Specimens 503
8.10.2. Test Details 503

9. PRINCIPAL CONCLUSIONS AND RECOMMENDATIONS FOR FUTURE WORK 505

9.1. Introduction 505

9.2. Principal Conclusions 505

9.2.1. Conclusions from Part I 505
9.2.2. Conclusions from Part II 506
9.2.3. Conclusions from Part III 507
9.2.4. Conclusions from Part IV 508
9.2.5. Conclusions from Part V 510

9.3. Recommendations for Future Work 511

9.3.1. Introduction 511
9.3.2. The Stress State induced within Specimens under Load 511

9.3.2.1. Analytical Investigations (see 2.5.) 511
9.3.2.2. Experimental Investigations (see 2.6.) 511

9.3.3. Response of Concretes of Different Degrees of Heterogeneity to Boundary Conditions of Near-Uniform Stress and Near-Uniform Strain (see Chapter 3) 512
9.3.4. Detection of Fracturing Events (see 4.5.4.3.) 513
9.3.5. Influence of Loading Pattern on Various Stages of Material Behaviour (see Chapter 5) 513
9.3.6. Behaviour of Concrete under Multiaxial Stress States (see Chapter 7) 513

LIST OF REFERENCES 514

APPENDICES

A1. Loading and Measuring Devices Used in the Test Series 530

A2. Materials for Concrete Mixes 533

A2.1. Ordinary Portland Cement (Ex. Northfleet Works, Kent) 533
A2.2. Spherical Glass Aggregate (Ex. Redfearn Bros.) 533
A2.3. Thames Valley Flint Gravel (Ex. Thorney Mill Pit, Iver, Bucks) 534
A2.4. Crushed Limestone (Ex. Topley Pike, Derbyshire) 534
A2.5. Crushed Granite (Ex. Kirkmabreck, Creetown, Kirkcudbrightshire) 535

A3. Details of Concrete Mixes 536

A3.1. Mixes Ma, MBC, and 6IC 536
A3.2. Idealised Concrete Mixes 537
A3.3. Real Concrete Mixes 538

A4. Derived Results for Mortar Mix MA 539

A4.1. Onset of Stable Fracture Propagation (o.s.f.p.) and Ultimate Strength Levels for Mortar Mix Type MA under Uniaxial Compression and Tension 539

A4.2. Values for Elastic Constants for Mortar Mix Type MA tested under Uniaxial Compression after conditioning for 50 Cycles of Load 539

A5. Reduction of Stress and Strain Data 540

A5.1. Calibration of Equipment and Analysis of Data 540
A5.2. Calculations of True Strain on Electrical Resistance Strain Gauges from Output of Wheatstone Bridge Circuits 540
A5.3. Triaxial 'Compression' Test - Correction for Influence of Circumferential Strain on Axial Stress 543
A5.4. Equal Biaxial Compression Test in Hydraulic Cell-Calculation of Stresses 543

A6. Testing Machine and Specimen Assembly Procedures 547

A6.1. Complex Stress Machine 547

A6.1.1. Alignment of Frame and Platens 547
A6.1.2. Setting-up Procedure for Slab Specimens 547

A6.2. Equal Biaxial Compression Test in Hydraulic Cell 548

A6.2.1. Assembly of Platen/Specimen/Sheath Unit 548
A6.2.2. Procedure for Setting-up Specimen 551

A6.3. Triaxial Compression Test 552

A6.3.1. Assembly of Platen/Specimen/Sheath Unit 552
A6.3.2. Procedure for Setting-up Specimen for Biaxial and Triaxial Test 555

A7. Derived Results for Biaxial and Triaxial Test Series 556

A8. The Frictional Resistance of the Axial Load Piston of the Triaxial Cell 579

A9. The Effect of Pressure on Strain Gauges 582

SIGN CONVENTION AND UNITS

Sign Convention

Unless otherwise stated the sign convention used throughout this thesis is that of positive tensile stresses and strains.

Where a stress or strain has been normalised with respect to a parameter, the normalised value retains the original sign.

Units

As all apparatus used throughout this work is calibrated in the Imperial System it is therefore considered necessary to express all results in these units unless otherwise stated.

In order to convert to S.I. units the following factors should be used:

1 lbf.	=	4.4482 N.
1 in.	=	25.4 mm.
1 lbf./in.^{2}	=	0.006895 N./mm.^{2}

GLOSSARY OF TERMS

Discontinuity

A general term denoting the level of stress or strain at which the first significant fracture processes can be detected within a specimen of material under load using a given detection technique.

Incremental Strain Ratio (i.s.r.)

The ratio: $\frac{\text{increment of maximum tensile strain}}{\text{increment of maximum compressive strain}}$

measured for a specimen of material under a small increment of applied stress (see 4.5). For a uniaxial test the i.s.r. is synonymous with the tangent value of Poisson's ratio.

Onset of Stable Fracture Propagation (o.s.f.p.)

The level of stress or strain at the start of processes of fracture propagation within a specimen of material under load as detected by significant changes in i.s.r. (see 4.5.). This is a special case of discontinuity.

Onset of Unstable Fracture Propagation (o.u.f.p.)

The level of stress or strain at the start of processes of unstable fracture propagation within a specimen of material as defined by the start of an overall increase in volume following consolidation (see 4.5.).

Ultimate

For the tests described in this thesis, unless otherwise stated, ultimate is defined as the level of stress or strain corresponding to the maximum stress which can be applied to a specimen of material as calculated using the cross-sectional area of the specimen corrected for the current measured deformations (see 4.5.). For all other tests referred to, ultimate is based on the cross-sectional area of the specimen prior to loading.

Deviator Stress

Is defined as the axial stress superimposed on the confining pressure in a conventional hydraulic triaxial cell such that:-

Total axial stress = deviator stress + confining pressure

Volumetric Change

This is calculated using the following relationship for principal strains, unless otherwise stated:-

$$e_v = e_1 + e_2 + e_3 + e_1e_2 + e_2e_3 + e_3e_1 + e_1e_2e_3$$

'Effective' Water/cement Ratio

This ratio is based on the water added to the mix in excess of that capable of being absorbed into the aggregate. For the present series of each aggregate the water absorbtion capacity is taken to be the 24-hour value as determined in accordance with B.S. 812 [1] and each mix is made with pre-soaked aggregates in order to eliminate the uncertainty regarding their initial moisture contents.

Volume Fraction of Aggregate (V_a)

Defined as the ratio of the absolute volume of aggregate to the absolute volume of all materials added to the mix:-

$$V_a = \frac{M_a/G_a}{M_c/G_c + M_a/G_a + M_w/1.0}$$

where M_a = weight of aggregate
M_c = weight of cement
M_w = weight of water
G_c = specific gravity of cement
G_a = specific gravity of aggregate

Levels of Material Investigation

For the purposes of the present work the following classifications will be used:-

Microscopic Level

At this level the behaviour of an element of material ranging in size from molecular dimensions up to about 50 microns is studied. Within this size range the heterogeneous nature of a real material is evident and, for a composite material such as concrete, an investigation at this level will generally concentrate on one of the main constituent phases present such as the particles of unhydrated cement, gel structure or aggregate particles.

Macroscopic or Structural Level

At this level the events occurring when a representative element of material is subjected to a force or deformation are generally optically visible. The size of element ranges from about 50 microns up to several centimetres depending on the degree of heterogeneity of the material. Investigations at this level disclose the heterophase nature of real materials with each phase reacting in a different manner to the imposed forces or deformations. For a composite material, such as concrete, the interactions between the main constituent materials present will be evident.

Phenomenological or Overall Level

At this level the overall behaviour of a representative element of a material is studied, with the size of element chosen to be sufficiently large such that even composite materials can be considered homogeneous.

Stress (or Strain) Space

A general stress (or strain) state acting on a small element of material can be transformed into three principal stresses (or strains acting in orthogonal principal directions.

This principal stress (or strain) state can be represented by three coordinates using a system of orthogonal axes, each of the axes corresponding to values of one of the principal stresses (or strains). Stress (or strain) space refers to all possible locations defined by such a coordinate system.

The following terms are used in this thesis to describe particular portions of stress space:-

Hydrostatic Axis

The line defined by the locus of all points where the three principal stresses are equal.

Rendulic Planes

Defined as the locus of all points where at least two principal stresses are equal. There are three such planes in stress space.

Equivolumetric Stress Planes

Each plane is defined as the locus of all points where the average principal stress remains constant. There are an infinite number of such planes in stress space, each corresponding to a given value of average stress.

1. AIMS OF PROJECT

1.1. Introduction

During recent years considerable improvements have been made to the philosophy of design of concrete structures. These have now been embodied in a new Unified Code of Practice (CP 110)[2] which requires a structure to be analysed for compliance with various limit states of serviceability and ultimate strength.

Clause 2.4.1. of the Code requires that any analytical method used to assess compliance with these limit states should be based on as accurate a representation of the structure as is practicable.

In line with the improvements in design philosophy, advances have been made in the application of computer-based methods for the analysis of complex structures or parts of structures. Perhaps the most widely used of these techniques involves the use of finite elements. This method has been developed to such a high degree of sophistication that it is now possible to analyse three-dimensional problems with complex geometrical arrangements and boundary conditions.

If these computer-based techniques are to be used to analyse realistically the response of a concrete structure or element to the imposed loading conditions, information is required of the relevant material properties and the ways in which these change through the range of stress or strain states likely to be encountered by each element. Unfortunately data on the properties of concrete under various loading regimes, necessary for such an approach, are lacking. Moreover, the accuracy of data which are available is often in question due to uncertainties concerning the efficiency of the various testing systems employed in attempting to achieve given states of stress within specimens.

Because of this situation, CP 110 suggests that, for design purposes, the properties of concrete can be based on the results of short-term simple compression tests (Clause 2.4.2.1.). One shape of idealised stress-strain curve is specified, with a magnitude which varies with the cube crushing strength of the concrete under consideration. The

elastic modulus is also based on simple compression values which are assumed to vary mainly with crushing strength, while the Poisson's ratio is taken as 0.2 for all cases. Any inadequacies of such an approach are covered by adopting suitable partial factors of safety for loads and materials, and the Foreward to the Code states that, as improvements are made in design methods, these factors may be amended.

The Code envisages that design methods based on these assumptions will be generally adequate but states that, in certain cases, advantages may be gained by using a fundamental approach to assess the behaviour of a structure. In order to adopt such fundamental methods the urgent need for valid data regarding the behaviour of concrete under stress states other than simple compression has been recognised by the Concrete Materials Research Group (CMRG) started in 1961 by K. Newman and, to this end, a comprehensive programme of research has been initiated, of which the work reported in this thesis forms a part. In order to see how this particular project has been developed, and how it fits the general pattern of the overall research programme, it is useful to make a brief reference to the historical progress of the work of the Group.

1.2. Previous Work of the Concrete Materials Research Group

At an early stage the essential requirement was recognised for studying the behaviour of a hetereophase material such as concrete not only at the phenomenological or overall level, but also at the structural or microscopic level.

1.2.1. Prior to 1963

The work of the CMRG during this period was mainly of an exploratory nature carried out at the phenomenological level. The problem of the testing machine/specimen interaction effects was acknowledged, and attention was paid to determining the influence of specimen shape on the deformational and fracture characteristics of concretes [3] and also the influence of testing machine characteristics [4].
At the structural level Anson[5] attempted to explain the basis of the behaviour of concrete under uniaxial compression by developing a model representing relatively rigid aggregate particles embedded in a mortar matrix. The model simplified concrete into a two-phase material, and

assumed the mortar matrix to act as a system of rods joining particles of coarse aggregate. Although it may now be considered that such a model represents only an approximate analogy to the behaviour of such a material, it was invaluable in highlighting areas which required further investigation.

On the phenomenological level a direct test to measure the behaviour of concrete under uniaxial tension was developed by Ward [6], while Robinson [7] initiated work to study the behaviour of concrete under biaxial compression. Both these test programmes yielded valuable strength data and, during the latter programme, the process of progressive cracking was first investigated using various techniques including x-ray surveys.

1.2.2. 1963 to 1965

The work outlined above led directly to the initiation in 1963 of a co-ordinated research programme. At the outset of this programme, Vile [8] recognised the growing awareness by researchers of the considerable influence which the loading device may exert on specimens, particularly in the case of multiaxial boundary loadings. With this in mind he designed and developed apparatus to subject various concretes and mortars to biaxial stress states including compression-compression, compression-tension and compression-torsion. In the resulting test programme, which was aimed at providing phenomenological biaxial strength envelopes defined but much valuable information was obtained regarding the deformational behaviour and mechanisms of failure for various types of concrete. Perhaps the most significant outcome of the work was the identification of the start of significant fracture processes (termed 'discontinuity' level by Newman [9]) by measuring the changes of ultrasonic pulse velocity through specimens under load. Envelopes defining the discontinuity level for various combinations of biaxial stress were presented for use as safe limits for designers, and were soon adopted in the design of prestressed concrete pressure vessels [11 and 12].

1.2.3. After 1965

At the conclusion of the above research programme the then current state of the art regarding the behaviour of concrete under load, both at the

phenomenological and structural level, was more than adequately summed up during an International Conference organised jointly by the CMRG and the Cement and Concrete Association [13]. The considerable quantity of data presented at this Conference indicated areas which required further investigation and, as a result, in 1965 it was decided to focus the work of the CMRG to achieve the following three principal aims:-

(i) to measure the complete deformational characteristics of concrete at the phenomenological level when subjected to definable states of short-term uni- and multi-axial stress;

(ii) to investigate at the structural level the fundamental mechanisms which form the basis of observed phenomenological characteristics;

(iii) to present any data obtained in a form suitable for structural design applications, as well as for further analysis by research workers.

The basic need for a clearer understanding of the nature of the inter-particle behaviour of a composite material such as concrete under load, outlined in Item (iii), was met by a test programme which started concurrently with the phenomenological investigation described in this thesis. McCreath [14] studied the local behaviour of 2-phase idealised plate models of concrete under uniaxial compression, and was able to postulate a fracture mechanism. This mechanism, which was observed in 2-dimensional simplified concretes, was found to be invaluable in explaining many of the characteristics measured and observed phenomenologically in idealised and real concretes up to the start of significant cracking. Pigeon [15] under the Author's direction extended this work to further types of model and, using more sophisticated techniques of strain measurement, was able to examine the fracture process up to the point of complete disruption.

1.3. Current Project

The requirement for Items (i) and (ii) above has led directly to the work reported in this thesis, which is concerned mainly with measuring the deformational behaviour of concretes under definable triaxial 'compression'

stress states. In this project the possible effects of the testing machine on the validity of results have again been recognised but, above all, attention has been paid to the ways in which the data can be disseminated usefully to designers, etc. It was considered that the most suitable methods of presentation will evolve only after consultation with potential users of the data and so, during the course of the programme, a number of interim reports [16, 17, 18] and papers [19, 20] have been published in order to acquaint these users with the progress of the work. Two seminars, arranged in conjunction with CIRIA, have also been held at which the main results have been presented for comment. The first seminar, in 1969, was aimed at a relatively large audience consisting of specialists in many fields of concrete technology, concrete structural design and construction. In the second seminar, held in 1970, the principal data obtained up to that date were presented to a smaller group of experts consisting mainly of structural engineers, some of whom were members of committees responsible for drafting Codes of Practice.

Although the primary aim of these seminars was to ensure that the results of this programme would be presented in a manner suitable for design purposes, they were also used as an opportunity to ensure that any further work envisaged would be entirely relevant to practical structural problems. As a result of the various discussions the work of the investigation was concentrated into the following five main areas -

Part I

An investigation of testing machine/specimen interaction effects in order to make recommendations regarding a loading system likely to induce the most definable multiaxial stress states within an element of concrete.

Part II

Measuring the effect of the type of boundary loading condition (i.e. whether uniform stress or uniform strain) on the behaviour of concretes (under equal biaxial compression).

Part III

Identifying significant stages of material behaviour, and determining the influence of loading pattern on these stages.

Part IV

Obtaining the complete deformational behaviour and evaluating significant changes of material behaviour for both idealised and practical concretes under triaxial 'compression' states of stress.

Part V

Expressing the data obtained from Part IV in a manner suitable for practising structural designers, as well as research workers.

Throughout the work the opportunities to converse with groups of individuals concerned with the practical problems of structural design and construction on a relatively informal basis has proved extremely valuable in helping to maintain, as far as possible, the efficient progress of the research programme. They also emphasised the need to continue the work to include an investigation into the behaviour of concretes under triaxial 'extension' and compression-compression-tension stress states. This work is currently in progress under the Author's direction [21] and preliminary results have already been included in the design recommendations given in this thesis.

2. METHODS OF ACHIEVING AND EVALUATING DESIRED STATES OF STRESS OR STRAIN IN SPECIMENS

2.1. Introduction

Most problems in structural engineering require the analysis of the response of an assemblage of members to an imposed boundary condition which is mostly specified in terms of a force (or stress), and sometimes as a deformation (or strain). Unless there is some experimental evidence to indicate the likely response of the particular geometrical arrangement to the given forces or deformation, then recourse must be made to a more fundamental solution by using the characteristics of the individual materials comprising the structure.

For such a fundamental approach the stress-strain relationships of the materials must be determined, by subjecting representative elements to the whole range of boundary conditions which it is possible to encounter in the structure, unless the materials are such that it is possible to deduce properties in one stress or strain state from those in another.

Since boundary conditions are more commonly specified as applied loads, it is generally assumed that the properties of a material can be determined merely by applying a load in an arbitrary manner to the boundary of a representative element of the material, and measuring the resulting behaviour. Such an approach, however, neglects the possible influence of the structural characteristics of the material on the type of stress or strain field induced in an element by the particular method in which the boundary load is applied.

An example of this can be seen when considering the way in which boundary loads are applied in standard tests used to determine material properties. This is normally accomplished by loading a specimen through a rigid steel platen arrangement. Such a method will, however, induce a uniform state of stress only in an ideally elastic, homogeneous and isotropic material, and then only provided no secondary restraint stresses are present. For real materials such as concrete, this may be far from the case since, for such a multiphase type of material, the difference in mechanical properties between the various constituents will induce considerable stress, and hence strain, disturbances. Usually no attempt is made to reduce such restraint stresses.

Other possibilities exist, the most extreme being that of applying uniform boundary stress to an element. For a multiphase material, the wide variation in properties of the various phases present will cause a non-uniform strain, and hence stress, distribution to be induced. This distribution, however, is likely to be different from that induced by the uniform boundary strain condition.

Of these two principal methods of applying a load to a material in a test, the engineer must decide that which will provide the most relevant information for his purposes. This is discussed more fully in Chapter 3 when the difference in the response of two concretes is compared under the two types of boundary condition.

Having decided, therefore, on the type of boundary condition which it is intended to apply to the material, it is necessary to assess the efficiency of any loading technique in attaining the desired state of stress or strain within the element under load for the results to be of use to engineers. This problem is discussed in the following sections.

2.2. Definition of the Problem

In evaluating the stress state within an element of material under load, the magnitude and direction of principal stresses should be determined at a sufficiently large number of positions within the volume of material for a given set of conditions on the boundary of the volume. However, to the Author's knowledge no technique has yet been developed which is capable of directly determining stress. Thus, unless an approximate analytical method is used, the only possible approach to the problem is to determine the stress state from measurements of strain.

Such an approach, although widely used, suffers from one fundamental disadvantage, namely, that of requiring a complete and accurate knowledge of the constitutive relations for the material in order to determine the stress state at each point which has given rise to the corresponding measured strains. In other words, we require to know the complete stress-strain characteristics of the material before tackling the problem.

This presents a seemingly insurmountable dilemma for an analytical or experimental investigation if the objective is to check the validity of

tests which are intended to provide such complete stress-strain characteristics. Thus only by the use of simplifying approximations or assumptions can one arrive at some idea of the state of stress in a material.

The results of previous analytical and experimental investigations which have been carried out in an attempt to assess the stress state within specimens are outlined in the Section 2.4. Sections 2.5. and 2.6. describe the results of analytical and experimental investigations undertaken in order to provide additional data which could be used as an aid to formulating recommendations as to the effectiveness of certain loading techniques considered for the present project.

Before considering the various investigations, however, it is necessary to define the problems involved in transmitting loads from one material system to another, and this is the subject of the next section.

2.3. Factors involved in Transmitting Load through Different Materials

2.3.1. Introduction

In order to assess the fundamental load-carrying characteristics of a material it is usually required to subject the material to ideal boundary conditions of either uniform stress or uniform strain (see 2.1.).

In order to attain these conditions it is necessary to transmit the load via another material resting against, or attached to, the boundary of the specimen under test. The material adjacent to the specimen may form an intermediate layer between the specimen and the main loading device and, indeed, may form only part of a composite subsidiary loading unit.

It is the incompatability between the various materials forming the loading device and the material of the specimen, together with the conditions at the various interfaces, which can give rise to either positive (tensile) or negative (compressive) restraint stresses on the boundary of the specimen. Obviously these restraints are undesirable, and should be minimised, but they cannot be avoided completely with practical loading systems. Since they will, inevitably, be present it is necessary to assess their magnitude and sign before evaluating the results of tests to establish the fundamental properties of materials.

2.3.2. Uniform Boundary Strain

Many problems are associated with devices developed for applying a state of uniform strain to the boundary of a material since the load must necessarily be applied to a specimen through rigid platens. Under stress the lateral deformation of such a platen will tend to be either greater, or less than, that of the platen with the actual extent of the difference being influenced by the frictional characteristics of the platen/specimen interface.

Assuming elasticity, the lateral strain in the platen for zero frictional restraint will be:

$$e_{1_{plat}} = (\sigma_1 - \nu_{plat}(\sigma_2 + \sigma_3))/E_{plat} \quad .. \quad .. \quad .. \quad (1)$$

where E_{plat} = elastic modulus for platen material
ν_{plat} = Poisson's Ratio for platen material
$\sigma_1 = \sigma_2 + \sigma_3$ = principal stresses

but since $\sigma_1 = \sigma_2 = 0$ for uniaxial stress Equation 1 becomes:-

$$e_{1_{plat}} = -(\nu/E)_{plat}\sigma_3 \quad .. \quad .. \quad .. \quad (2)$$

Similarly the lateral strain in the specimen becomes:-

$$e_{1_{spec}} = -(\nu/E)_{spec}\sigma_3 \quad .. \quad .. \quad .. \quad (3)$$

If no material is interposed between the platen and specimen the loading device can be placed in one of the following categories:-

(1) the platen strains laterally less than the specimen

i.e. $(\nu/E)_{plat} < (\nu/E)_{spec}$

(2) the platen strains laterally more than the specimen

i.e. $(\nu/E)_{plat} > (\nu/E)_{spec}$

If full or partial frictional restraint is developed at the interface then the differential movement can cause restraint stresses to be transmitted across the boundary to influence the specimen. The likely form of distribution of lateral restraint at the platen/specimen interface is shown in Fig. 2.1. which indicates zero restraint on the axis increasing to a maximum towards the corners. This trend has been confirmed by the results of the analytical and experimental investigations described in Sections 2.4., 2.5. and 2.6.

Figures 2.1.(a) and (b) show the form of lateral deformation profiles under uniaxial compression for the above cases (1) and (2), both without friction and with full friction. For the sake of simplicity it has been assumed that plane sections remain plane under load.

If the restraint stresses increase above the level capable of being maintained by friction at the platen/specimen interface, then the form of restraint distribution suggests that slippage should start near the unloaded boundary and progress towards the axis. This process would undoubtedly cause considerable redistribution of stresses.

Now consider an intermediate layer of material interposed between the platen and specimen. The material can be classified in a similar manner to the previous cases namely:-

A. the material strains laterally to a degree equal to, or less than, the main loading platen

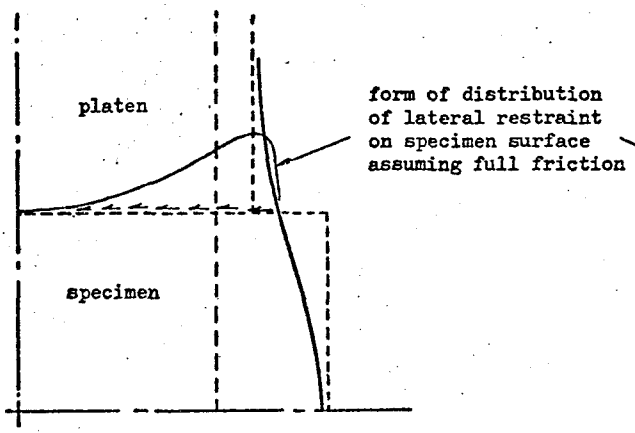
   i.e.

B. the material strains laterally to a level intermediate between the platen and specimen

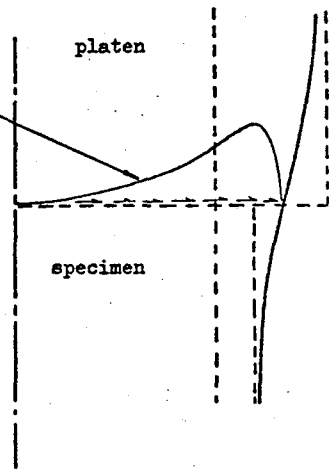
C. the material strains laterally to a degree equal to or greater than the specimen

   i.e.

Considering uniaxial compressive loads applied to the class of materials which form the subject of this thesis, loads are normally transmitted through platens which are laterally stiffer than either the intermediate



Case 1. (ν/E) platen $<$ (ν/E) specimen
no intermediate material
(a)



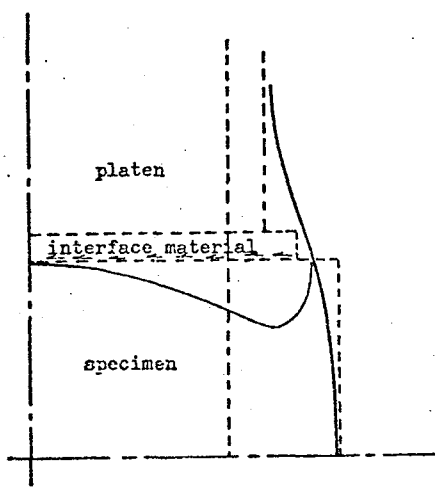
Case 2. (ν/E) platen $>$ (ν/E) specimen
no intermediate material
(b)

form of distribution of lateral restraint on specimen surface assuming full friction

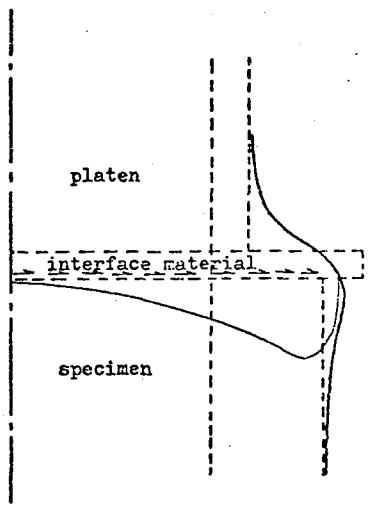
Legend

------ undeformed boundary and deformed boundary assuming no frictional restraint

~~~ deformed boundary assuming full frictional restraint



Case B. (ν/E) platen $<$ (ν/E) mat. $<$ (ν/E) specimen
(c)



Case C. (ν/E) mat. $>$ (ν/E) specimen
(d)

Figure 2.1. Lateral deformation profiles for a rigid platen/specimen system under uniform compressive load with and without an intermediate material.
~~~

material or the specimen. Case A.is thus unlikely to be met in practice, and materials falling within Cases B. and C. only will be considered.

Figures 2.1.(c) and (d) show the forms of lateral deformation profiles under uniaxial compression for the above Cases B. and C., without friction and with full friction, again assuming plane sections remain plane. As previously discussed the restraint stress across the loaded face for the case of full friction developed at the interface, is again assumed to be zero on the axis, reaching a maximum close to the unloaded boundary. As before, if the restraint stresses exceed those capable of being maintained by friction at any interface then slippage will occur, starting near the unloaded boundary and progressing towards the centre, resulting in a redistribution of stresses within the specimen.

Other factors, in addition to the differences in ν/E value between the various materials, and frictional characteristics at the various interfaces, will influence the stress distribution within the specimen. The most important of these which may influence the restraint stresses transmitted to specimens under loading through layered material systems are summarised in the following:-

1) Incompatability of ν/E value between the Various Materials

Typical values for materials considered in the investigations in the following sections, placed in order of increasing values of ν/E, are given in Table 2.1. Unless the restraint stresses are relieved by some form of slippage at the specimen boundary compressive restraint will be induced on the loaded boundary of a material if loaded through a material in a higher position in the table, i.e. through one with a lower numerical ν/E value. Conversely, if a material is loaded through a material below it in the Table, tensile restraint stresses will be developed.

2) Frictional Characteristics

Restraint stresses will be reduced significantly if the frictional resistance across the specimen/intermediate material interface can be lowered. A decrease in the frictional resistance across the intermediate material/platen interface will also reduce the restraint, but this effect is likely to be less pronounced. In most practical cases, the distribution of restraint stresses at the various interfaces is likely to cause partial

Material	Poisson's Ratio ν	Modulus of Elasticity E	ν/E
		10^6 lb./in.^{2}	10^{-10} in.^{2}/lb.
Mild steel	-0.33	30.0	-1.1
Zinc	-0.25	15.7	-1.6
Limestone	-0.21	14.0	-1.8
Copper	-0.343	17.5	-2.0
Glass	-0.228	10.6	-2.15
Brass	-0.35	14.59	-2.4
Granite	-0.25	10.0	-2.5
Concretes -			
Natural aggt.	-0.15 to -0.20	6 to 2	-2.5 to -10.0
(Mortar MA	-0.155	4.75	-3.26)
Lightweight aggt.	-0.15 to -0.20	3 to 1	-5.0 to -20.0
Aluminium	-0.345	10.2	-3.4
Lead	-0.43	2.5	-17.0
Bakelite	-0.32	1.0	-32.0
Perspex	-0.33 to -0.35	0.89 to 0.4	-36.9 to -87.5
p.t.f.e. (unfilled)	-0.42	0.58	-72.0
Epoxy resin (Araldite)	-0.38 to -0.35	0.5 to 0.35	-76.0 to -100.0
Celluloid (Xylonite)	-0.38 to -0.3	0.36 to 0.28	-105.6 to -107.1
Rubber	-0.5	0.0003	-166000

Table 2.1. Values of ν/E for Typical Materials

slippage which will considerably modify the stress distribution in specimens.

3) Thickness and Modulus of Rigidity of the Intermediate Material

The two factors are closely linked since they control the magnitude of shear stress which can be transmitted across the intermediate material. A larger thickness and/or lower modulus of rigidity will reduce the restraint stresses. One important assumption has been made so far to simplify the problem, namely that constant values of ν and E be ascribed to the various materials forming the specimen and loading unit. However, for the case of a concrete or mortar specimen under load ν and E change with stress level. This fact must be recognised when considering the restraint stresses imposed on the concrete, especially towards ultimate.

4) Surface Irregularities

Another assumption is that of the initial planeness of the various contacting surfaces. Obviously conditions will be severely modified if the surfaces are initially dimensionally incompatible or if they become distorted during loading.

2.3.3. Uniform Boundary Stress

The only practical way in which a state of uniform stress can be achieved on the boundary of a specimen of a heterogeneous material is by the use of some form of hydraulic loading. If a pure hydrostatic stress is required to be applied, then this can be relatively simply attained by immersing the specimen, surrounded with a suitable impermeable membrane if desired, in a fluid under pressure.

For a state of equal biaxial compression a similar technique can be used provided that the specimen can be isolated from the effects of the fluid pressure in one of the three principal directions.

For stress states other than the above, the problem becomes more complex since the hydraulic pressure must be applied in each direction independently. Thus in any given direction it will be necessary to contain the fluid such that the pressure is applied orthogonal to the face of the specimen, while at the same time eliminating (a) any effects of extrusion between

the surface of the specimen and the containment device and (b) effects of intrusion into the specimen surface.

Providing the above difficulties can be overcome then such a loading method should induce the desired boundary conditions close to uniform stress.

2.4. Review of Related Investigations

2.4.1. Introduction

The following sections outline the more important investigations, both analytical and experimental, which have been carried out to assess the stress state in specimens of materials under various boundary conditions of load.

The main stress states studied in the present experimental programme are uniaxial compression, biaxial compression and triaxial compression applied directly as principal stresses. Only those investigations relevant to such loading conditions are included.

The outline of the factors which may influence the transmission of load from the loading device to a specimen given in 2.3. are used to classify each investigation in terms of the type of problem solved. In most analyses the stress state within the specimen has been described in terms of stresses other than those in the three principal directions (i.e. as direct and shear stresses, octahedral stresses, etc.). Such methods of representation are considered by the Author to make interpretation of the results extremely difficult, and accordingly the results for each investigation have, where necessary, been recalculated to obtain the distributions principal stresses as proportions of the average applied boundary stress.

For some experimental investigations the data is available only in graphical rather than numerical form. In such cases the stress distributions have been evaluated from this data, which in many cases is limited in quantity, by a process of scaling.

2.4.2. Analytical Investigations

2.4.2.1. Results of Investigations

Details of the various investigations considered, together with the main results are given in Table 2.2. Figures 2.2 to 2.8 show typical detailed stress distributions for the most important of these investigations and these are also summarised in Table 2.3.

Although most of the information is given in the above Tables and Figures, it is useful to make additional comments on important points concerning some of the investigations and these are outlined in the following.

Filon [22, 23], Pickett [23, 26] and D'Appolonia and Newmark [27]

Due to the difference in assumed boundary conditions Filon's solution induces more severe restraint stresses near the loaded ends than those obtained by Pickett. Elsewhere in the specimen, and especially within the central 2/3rds of the cylinder, the results for both solutions compare very closely.

The solution due to D'Appolonia and Newmark shows the same trend as the above two solutions, but differs somewhat in magnitude particularly for the near-axial principal stress which is considerably less uniform throughout the specimen.

Goodier [24]

The boundary conditions used in this investigation, although not directly simulating those encountered in the present work, serve to indicate the effects of a poor loading distribution. The results show that for a concentrated load a lateral tensile stress is developed, which reaches a maximum at some distance from the loaded face and then decreases to uniformity. Even for a knife-edge load, the central $\frac{1}{3}$rd of a specimen with H/W = 2 remains under a uniform lateral stress which is confirmed by the work of Timoshenko and Goodier [25].

Greenberg and Truell [28], Edelman [29], Prentis [30] and Girivvallabhan and Mehta [39]

These investigations attempt to evaluate the likely effect on the measured E value if a specimen is loaded through rigid platens with all

Investigator	Specimen Shape	Boundary Conditions	Material Properties	Method of Analysis	Main Conclusions
Filon/Conway (22, 23)	Cylinder with H/D = 1	Uniform uniaxial compressive strain with periphery only restrained laterally (i.e. clamped ends)	Ideally elastic $\nu = 0.25$	Approximation using circular functions	(See Figure 2.2.) State of triaxial compression near the loaded ends which diminishes towards the centre of the specimen. Circumferential stress becomes tensile near centre of cylinder. Directions of principal stress coincide with axial and radial directions over central 2/3rds of cylinder. Maximum lateral deformation at mid-section with value 0.96 x unrestrained case.
Goodier (24)	Rectangular thin plate with various H/W ratios	Uniaxial compressive load applied through knife edges or thin strips	Ideally elastic	Strain energy	For H/W = 2 and knife edge load the maximum lateral tensile stress occurs at approximately 1/6 x H from loaded ends decreasing to uniformity at 1/3 H. Magnitude of lateral tensile stress decreases with increase in width of loaded strip but increases with reduction in H/W ratio of specimen.
Timoshenko and Goodier (25)	Rectangular plate with large H/W ratio	Concentrated uniaxial compressive load	Ideally elastic	Fourier series approximation	Axial stress becomes uniform at distance from loaded face equal to width of plate.

Table 2.2.(a) Summary of theoretical investigations to determine the stress state within specimens under various boundary conditions of load.

Investigator	Specimen Shape	Boundary Conditions	Material Properties	Method of Analysis	Main Conclusions
Pickett/ Conway (23, 26)	Cylinder with H/D = 1	Uniform uniaxial compressive strain with all points on loaded ends restrained laterally	Ideally elastic $E = 1$ $\nu = 0.5$	Fourier-Bessel series approximation	(See Figure 2.3.) State of triaxial compression near loaded ends which diminishes towards centre. Radial and circumferential stresses become tensile near periphery at between approximately 1/4 and 1/2 x H from loaded ends. Directions of principal stresses coincide with axial and radial directions over central 2/3rds of cylinder.
D'Appolonia and Newmark (27)	Cylinder with H/D = 1	Uniform uniaxial compressive strain with all points on loaded ends restrained laterally	Ideally elastic $E = 1$ $\nu = 0.5$	Approximated solid cylinder to lattice framework of pin-connected rods	(See Figure 2.4.) State of triaxial compression near loaded ends which diminishes towards centre. Circumferential stress becomes tensile near periphery between approximately 1/4 and 1/2 x H from loaded ends.
Greenberg and Truell (28)	Square prism of infinite length	Uniform uniaxial compressive strain with all points on loaded ends restrained laterally	Ideally elastic with $\nu = 0.33$	Strain energy (assuming plane strain)	E of restrained specimen 6.4% greater than for unrestrained case.
Edelman (29)	Cylinder with H/D = 1				E of restrained specimen 5.2% greater than for unrestrained case.
Prentis (30)	Cube				E of restrained specimen 5.8% greater than for unrestrained case.

Table 2.2. (b) Summary of theoretical investigations to determine the stress state within specimens under various boundary conditions of load.

Investigator	Specimen Shape	Boundary Conditions	Material Properties	Method of Analysis	Main Conclusions
Lisowski (31)	Cube	Uniform uniaxial compressive strain with (1) complete lateral restraint at loaded ends (2) partial slip allowed at loaded ends	Ideally elastic with $\nu = 0.25$	Finite difference for two-dimensional case	For complete end restraint the end zones are under a state of biaxial compression. Shear stresses on the ends increase from the axis to periphery which suggests that slip should occur near periphery. With such slip, simulated, large lateral tensile stresses develop near periphery which would probably lead to cracking.
Balla (32,33)	Cylinder with H/D = 2	Uniform uniaxial compressive strain on ends and uniform lateral stress over the curved surface to induce various rates of axial/ lateral stress. Radial and circumferenrial displacements at the periphery of each end constrained.	Ideally elastic with $\nu = 0.33$	Stress functions	Uniaxial Compressive Stress (Axial stress = 1, (See Figure 2.5.) Lateral stress = 0) State of triaxial compression near loaded ends extending to about 1/3 x H. Central 1/3rd of cylinder under almost uniaxial state of stress but with a small induced tensile component present in places. Equal Biaxial Compression (Axial stress = 0, (See Figure 2.6.) Lateral stress = 1) Considerable stress disturbances towards the 'unloaded' ends, with high tensile values near axis. Central 1/2 of specimen under near-uniform biaxial compressive stress. Hydrostatic Compression (Axial stress = 1, (See Figure 2.7.) Lateral stress = 1) Stress disturbances near ends but central 1/3rd of specimen under near-uniform hydrostatic compression. Triaxial Compression (Axial stress = 4, (see Figure 2.8.) Lateral stress = 1) Although high concentrations of triaxial compression exist near ends a large area of specimen is within ± 5% of applied stress

Table 2.2. (c) Summary of theoretical investigations to determine the stress state within specimens under various boundary conditions of load.

Investigator	Specimen Shape	Boundary Conditions	Material Properties	Method of Analysis	Main Conclusions
Hodgkins (34)	Long cylinder	Uniaxial Compressive Load applied to ends Various distributions of boundary stress assumed including uniform and parabolic	Ideally elastic $\nu = 0.33$	Stress potential functions	Local stress and strain disturbances insignificant below 0.75 x D from loaded face.
Hilsdorf (35)	Thin square plate	Uniaxial and various ratios of biaxial compression with (1) complete fixity between plate and specimen, and (2) with finite limiting values for coeff. of friction between plates and specimen ($\mu = 0.6$ for low loads $\mu = 0.1$ for high loads)	Steel platens: $E=2.1 \times 10^6$ Kg/cm.^{2} $\nu=1/3$ Concrete slab with: $E=0.2 \times 10^6$ Kg/cm.^{2} $\nu=1/6$ at low loads $E=0.1 \times 10^6$ Kg/cm.^{2} $\nu=1/2$ at high loads	Approximate analysis containing assumptions regarding stress and strain distributions, variation of material parameters, coeff. of friction and superposition of load transference and platen restraint effects	<u>For Uniaxial Compression</u> Lateral restraint stresses depend mainly on ratio (transverse deformation of platen/transverse deformation of concrete) for no sliding on loaded faces. These stresses increase with thickness of platen. For finite coeff. of friction, at low loads restraint stress = 0.13 x boundary stress (approx.) at high loads this ratio increases up to 0.3. <u>For Biaxial Compression</u> Under low values of equal biaxial compression only 40% of applied load is carried by concrete. Due to sliding, this proportion rises to about 90% at loads approaching failure. Proportion of load carried by specimen increases as the biaxial ratio decreases.
Niwa and Kobayashi (36)	Rectangular blocks with H/W ratios of 0.5, 1.0, 2.0, 4.0.	Uniform uniaxial compressive strain with complete lateral restraint	Ideally elastic	Self-equilibrating ortho-normal polynomial functions	Extent of central zone subject to uniform axial stress and negligible lateral stress varies with H/W ratio as follows:- <u>H/W ratio</u> <u>Approx. height of uniform central zone</u> 0.5 NIL 1.0 0.125 x H 2.0 1 x H 4.0 3 x H

Table 2.2 (d) Summary of theoretical investigations to determine the stress state within specimens under various boundary conditions of load.

Investigator	Specimen Shape	Boundary Conditions	Material Properties	Method of Analysis	Main Conclusions
Niwa, Kobayashi and Nakagawa (37)	Axisymmetric	Uniform uniaxial compressive strain with (1) complete lateral restraint at ends or (2) sliding at ends when coeff. of friction $\leqslant \frac{\text{shear stress}}{\text{axial stress}}$ for an element	Ideally elastic $\nu = 0.17$	Finite elements	(1) Triaxial compression stresses are induced near ends of specimens, with the axial stress reaching values up to 1.2 x applied stress for the completely restrained case. (2) Shear stress on loaded ends is zero on the axis and increases towards the periphery to reach a value of either 0.2 x applied stress for restrained case or μ x axial stress for the case of sliding. (3) The stress state within the specimen becomes more as uniform as μ decreases. For $\mu > 0.25$ the stress state is the same as for the fully restrained case.
Kosaka et Al (38)	Thin plate with various H/W ratios loaded through interface materials	Uniform boundary strain with complete lateral fixity at loaded ends	Specimen material Ideally elastic Interface material Ideally elastic with ν varying from 1 to $< 0.1 \times \nu$ of specimen	Finite elements (assuming plane strain)	For interface materials with $\nu < 0.1 \times \nu$ for specimen, large lateral tensile stresses are induced at ends of specimens. These tensile stresses reduce with decrease in H/W ratio.

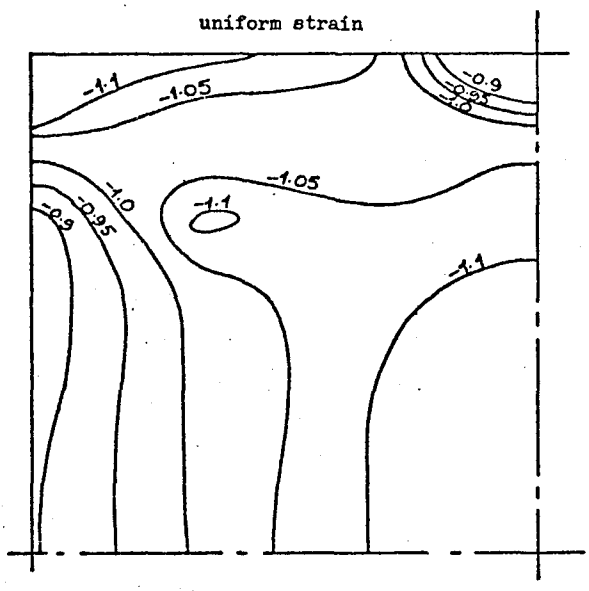
Table 2.2. (e) Summary of theoretical investigations to determine the stress state within specimens under various boundary conditions of load.

Investigator	Specimen Shape	Boundary Conditions	Material Properties	Method of Analysis	Main Conclusions
Girijavallabhan and Mehta (39)	Cylinders with various H/D ratios	Uniform boundary strain with complete lateral fixity at loaded ends	Ideally elastic with ν varying from 0.15 to 0.49	Finite elements	Restraint effects increase with decrease in H/D ratio and increase in ν For H/D = 2 ν — % increase in E over unrestrained case 0.15 — 0.3 0.20 — 0.9 0.25 — 1.7 0.30 — 2.4 0.35 — 3.6 0.40 — 4.4 0.45 — 6.8 0.49 — 8.1
Peng (40)	Cylinders with H/D = 2 loaded with various interface materials	Various boundary stress conditions applied, with configurations based on experimental results for granite specimens loaded under various platen arrangements including (1) complete lateral fixity (2) loading through rigid steel platens and (3) loading through Teflon inserts	Ideally elastic	Elastic analysis using Fourier/ Bessel functions and based on previous solutions (Filon, Pickett, D'Appolonia and Newmark, Balla)	Complete lateral fixity Triaxial compression near ends with max. stress concentration of 1.44 x average applied stress near the periphery of each end and minimum value of 0.89 x applied stress occurring at centre of end faces. Radial and circumferential stress changes from compressive to tensile towards centre section, with maximum tension of 0.06 x applied stress on axis. Loading through rigid platens Stress distributions similar to above but with maximum and minimum axial stress reduced to 1.20 and 0.95 x average applied stress respectively. Max. tensile radial stress is 0.02. Teflon inserts Soft inserts considerably modify the axial stress distribution with maximum axial stress concentration of 1.105 x average applied stress near centre of end face with minimum of 0.06 x applied near corners. Max. radial and circumferential tensile stress near centre of end face of 0.04 and 0.05 x applied stress respectively.

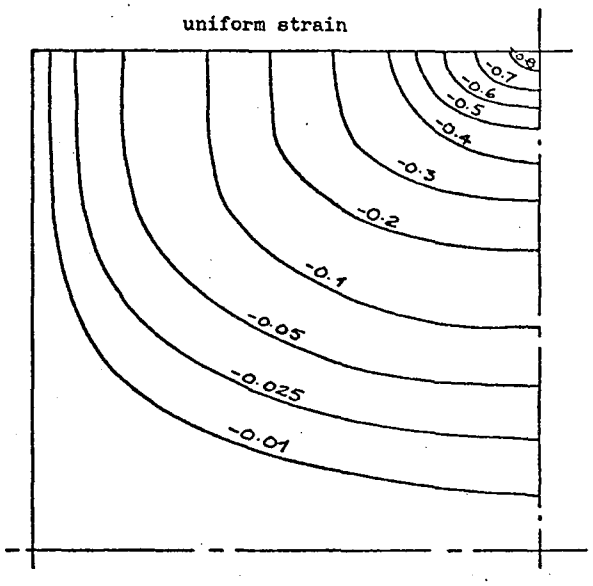
Table 2.2. (f) Summary of theoretical investigations to determine the stress state within specimens under various boundary conditions of load.

Investigator	Specimen Shape	Boundary Conditions	Material Properties	Method of Analysis	Main Conclusions
Brady [41]	Cylinder with H/D = 2 loaded by steel platen through various interfacial materials of various thicknesses	Uniform boundary strain	Ideally elastic E (10^6 lb/in^2) / ν Platens 30 / 0.3 Inserts 12 / 0.24 4 / 0.45 2 / 0.24 Specimen 2 / 0.24	Three dimensional finite elements	Soft inserts (ν/E insert > ν/E specimen) Tensile radial and circumferential stresses induced near ends of specimen which decreased with decreasing thickness of insert and become insignificant at a H/D ratio of insert of 0.01. Stress state almost uniaxial at distance equal to D from each end. Intermediate inserts (ν/E specimen > ν/E insert > ν/E platen) Triaxial compression throughout specimen but confined mainly to zones within D from end faces.

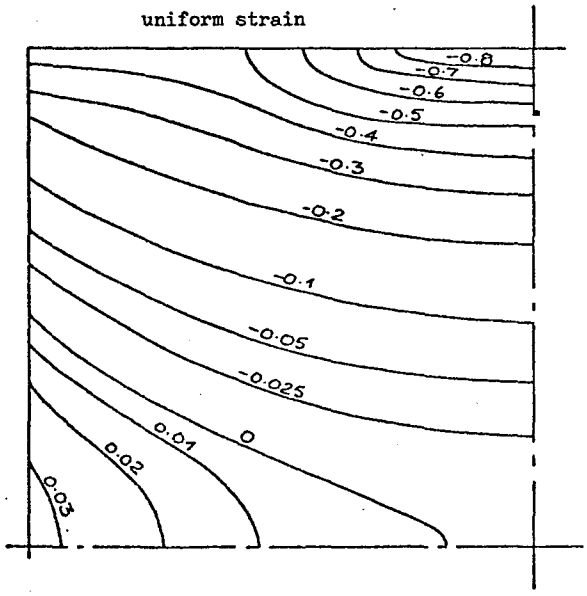
Table 2.2. (g) Summary of theoretical investigations to determine the stress state within specimens under various boundary conditions of load.



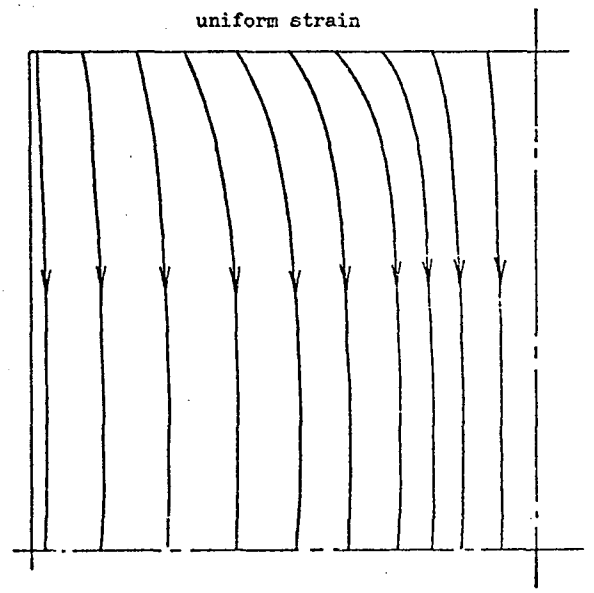
Near-axial stress



Near-radial stress



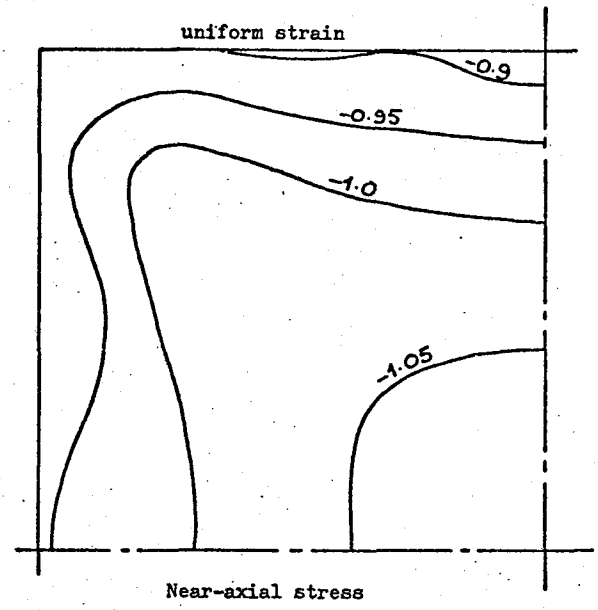
Near-circumferential stress

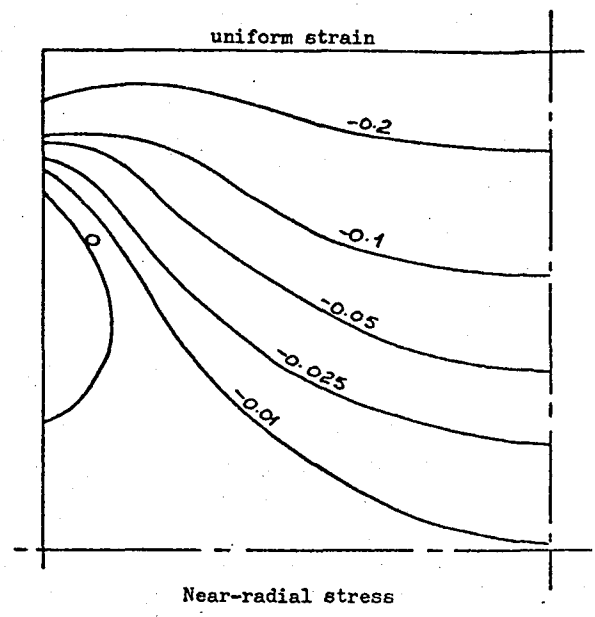


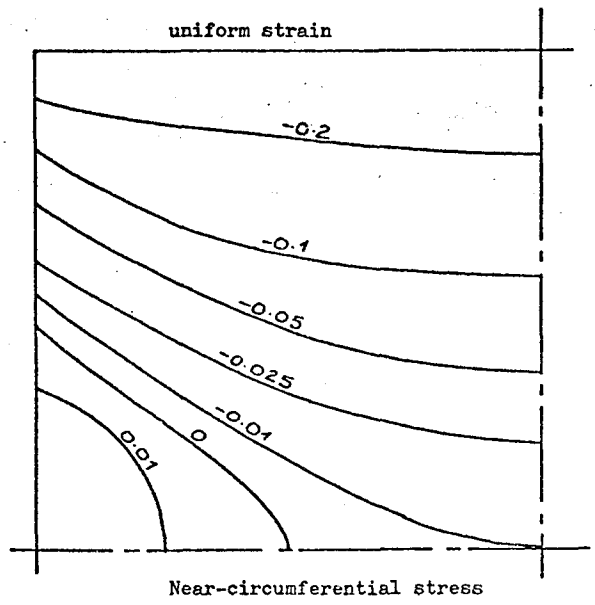
Isostatics of near-axial stress

Figure 2.2. Distributions of principal stresses and isostatics for a cylinder with H/D = 1 and restrained ends loaded under a uniform uniaxial compressive strain to induce an average applied boundary stress of - 1.0.

after FILON (22, 23)







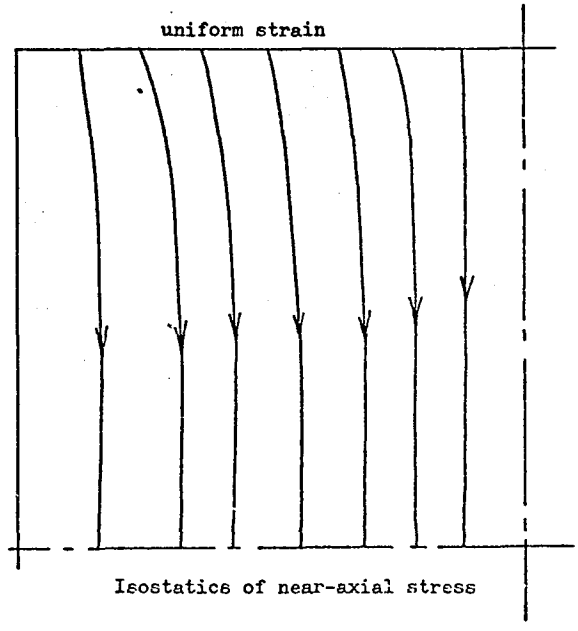
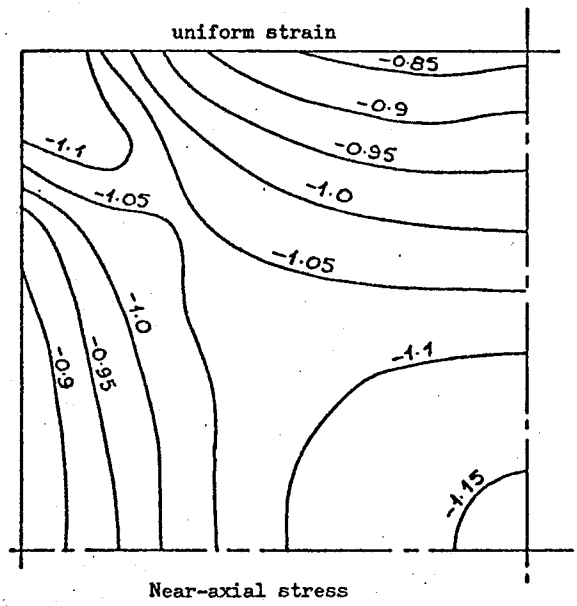
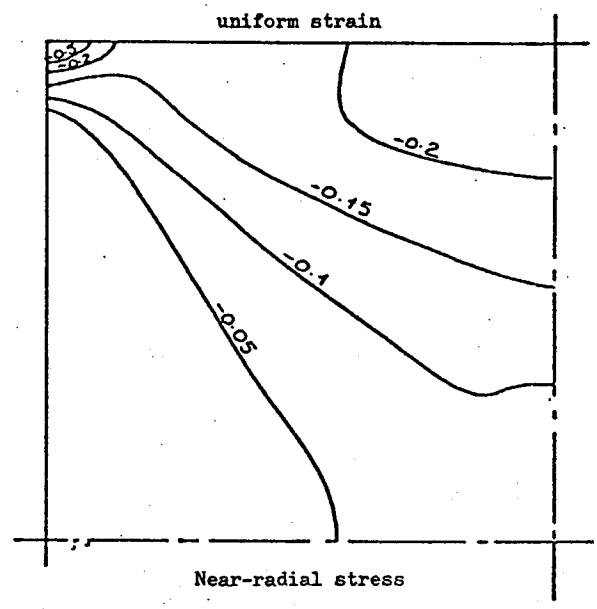
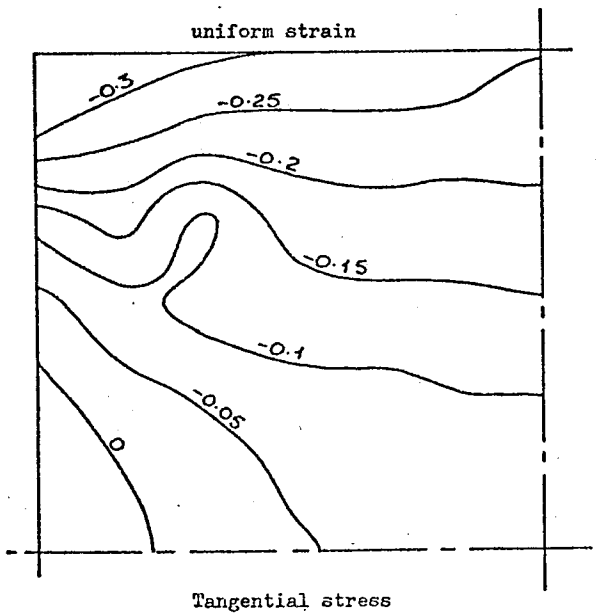


Figure 2.3. Distributions of principal stresses and isostatics for a cylinder with H/D = 1 and restrained ends loaded under a uniform uniaxial compressive strain to induce an average applied boundary stress of -1.0.

after PICKETT (23, 26)







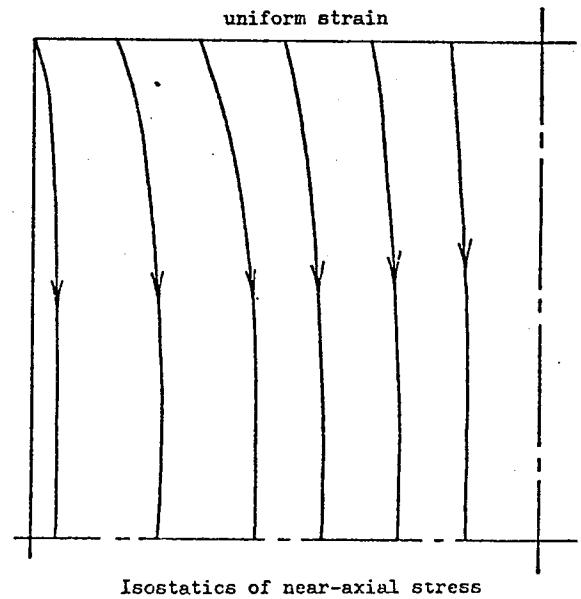
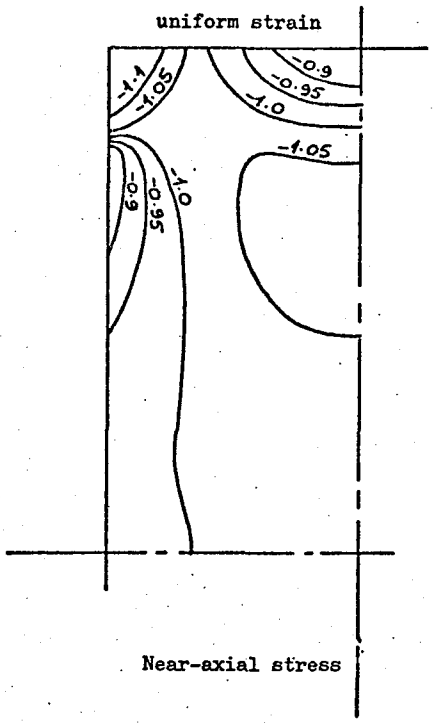
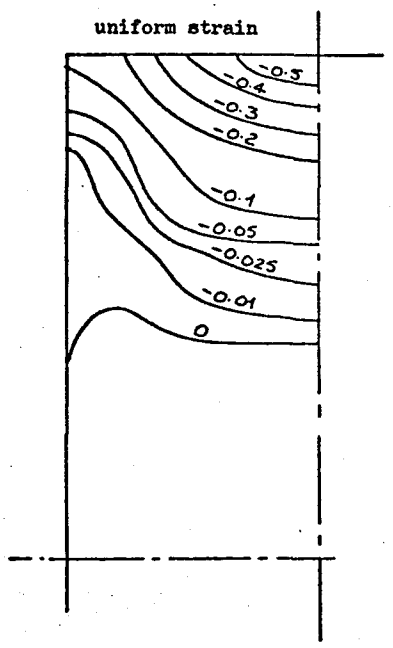


Figure 2.4. Distributions of principal stresses and osostatics for a cylinder with H/D = 1 and restrained ends loaded under a uniform uniaxial compressive strain to induce an average applied boundary stress of -1.0.

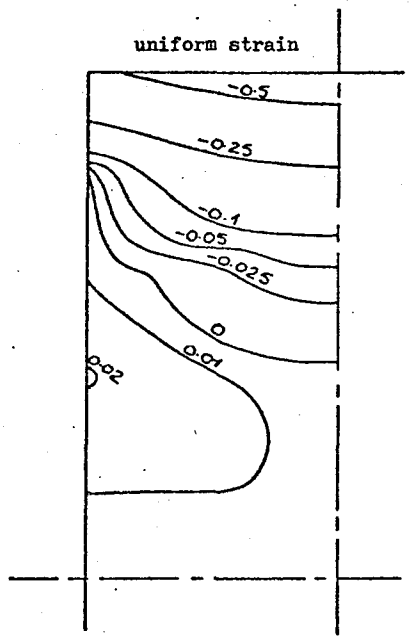
after D'APPOLONIA and NEWMARK (27)



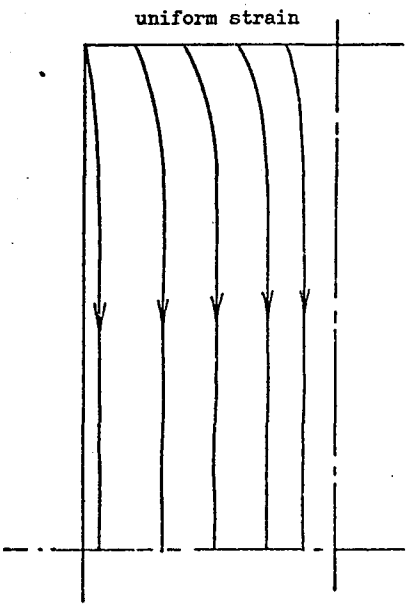
Near-axial stress



Near-radial stress



Near-circumferential stress



Isostatics of near-axial stress

Figure 2.5. Distributions of principal stresses and isostatics for a cylinder with H/D = 2 and restrained ends loaded under a uniform uniaxial compressive strain to induce an average applied boundary stress of -1.0. after BALLA (32,33)

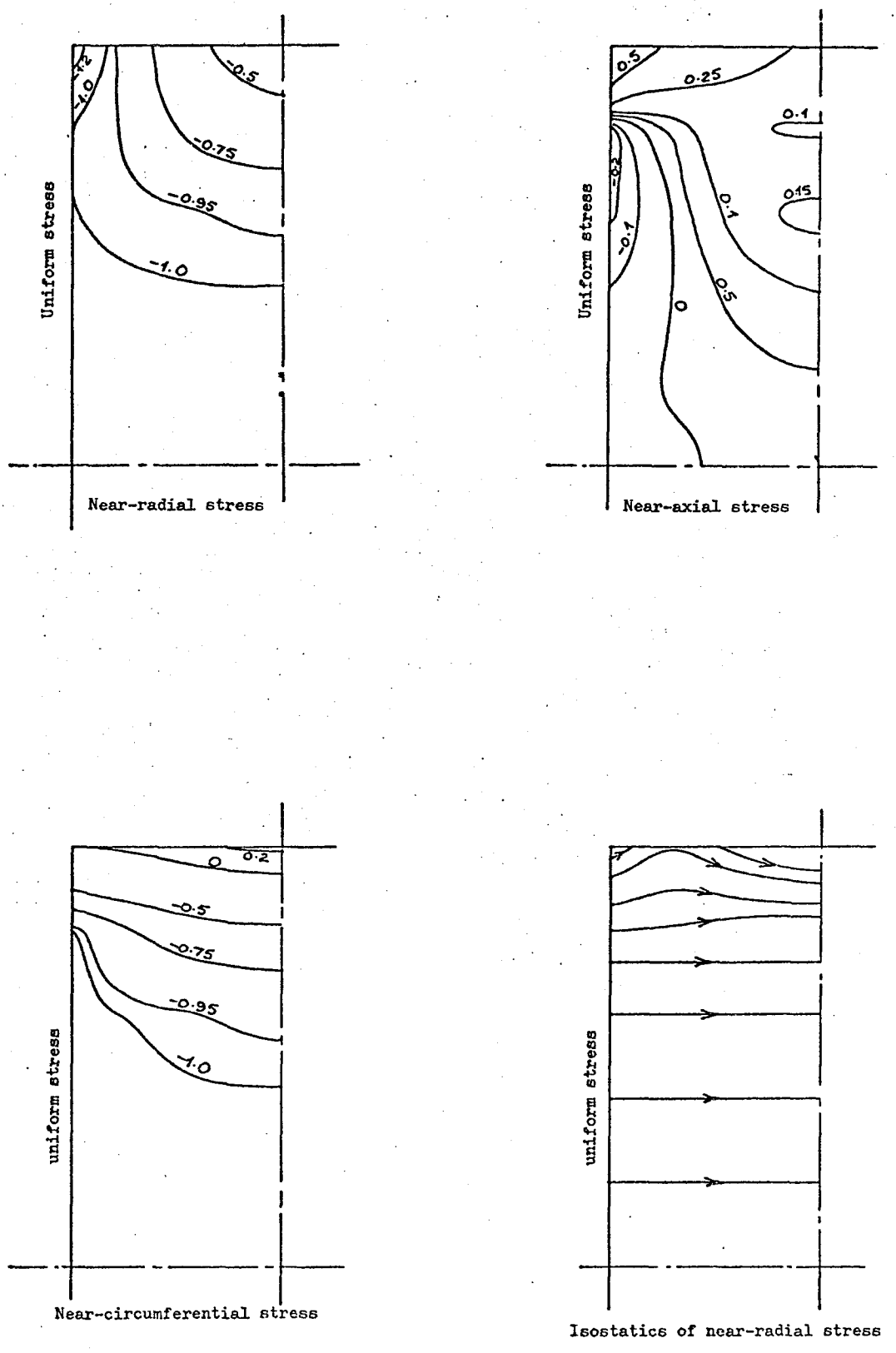
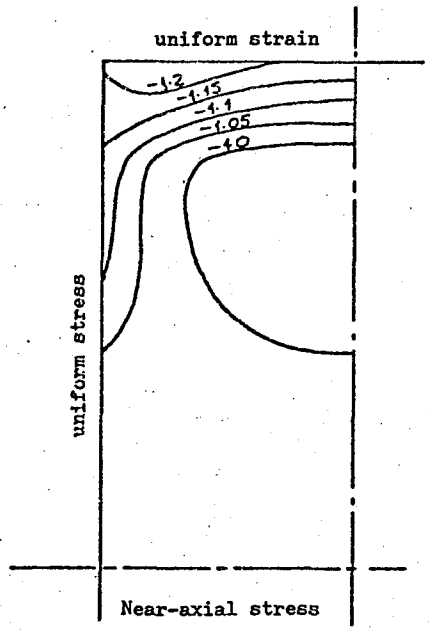
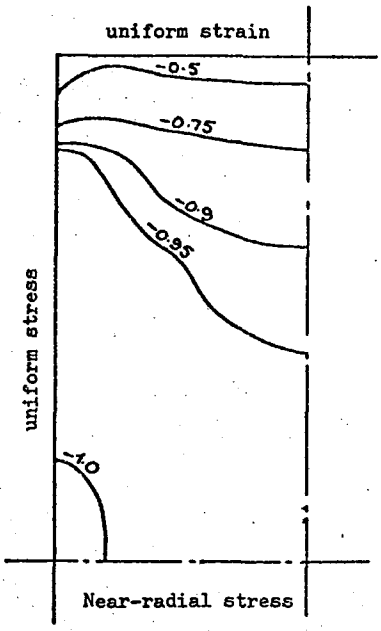


Figure 2.6. Distributions of principal stresses and isostatics for a cylinder with H/D = 2 and restrained ends loaded under a compressive stress of - 1.0 applied uniformly over the curved surface.

after BALLA (32, 33)





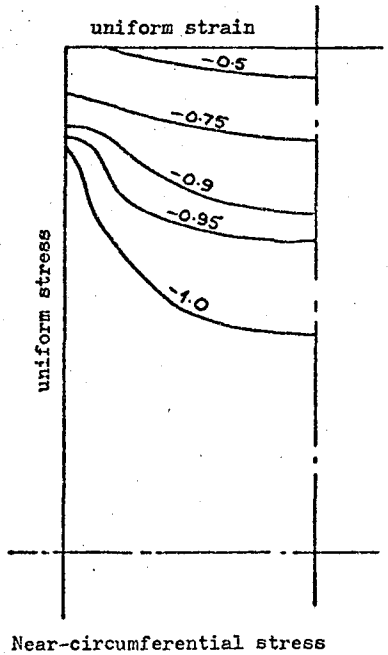
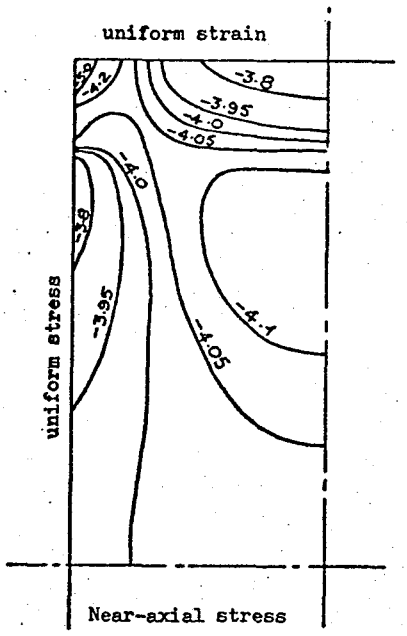
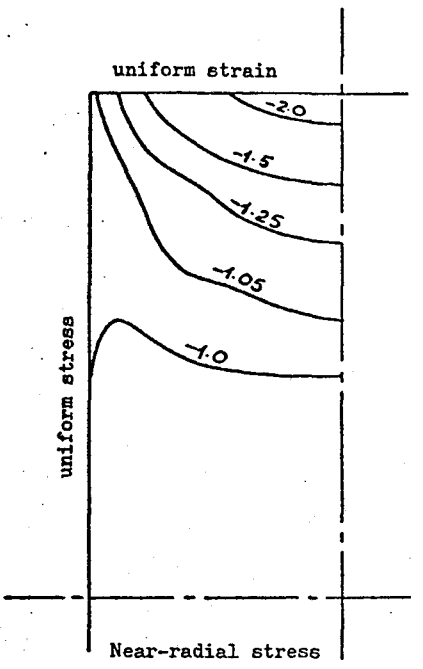
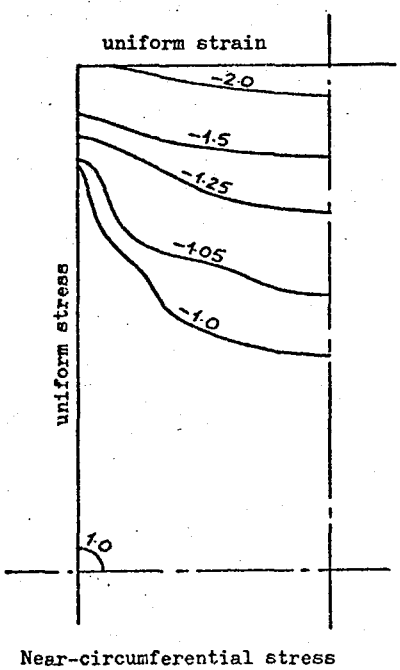


Figure 2.7. Distributions of principal stresses for a cylinder with H/D = 2 and restrained ends loaded under a uniform compressive strain to induce an average applied stress on ends of -1.0, and a compressive stress of -1.0 applied uniformly over the curved surface.

after BALLA (32, 33)







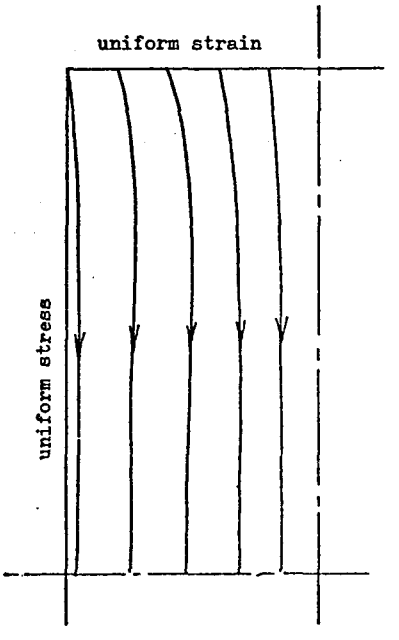


Figure 2.8. Distributions of principal stresses and isostatics for a cylinder with H/D = 2 and restrained ends loaded under a uniform compressive strain to induce an average stress on ends of -4.0, and a compressive stress of -1.0, applied uniformly over the curved surface.

after BALLA (32, 33)

Investigator	Approximate Direction of Principal Stress	Principal Stress/Average Applied Boundary Stress								
		Approximate Position as Coords. from Centre of Specimen of Width W and Height H								
		½W, ½H	¼W, ½H	0, ½H	½W, ¼H	¼W, ¼H	0, ¼H	½W, 0	¼W, 0	0, 0
Filon/Conway (22, 23)	Axial	-1.69*	-1.09	-0.69	-0.90	-1.05	-1.12	-0.90	-1.05	-1.13
	Radial	-0*	-0.20	-0.80	-0	-0.08	-0.12	0	0	0
	Circumferential	-0.44*	-0.60	-0.90	-0.01	-0.10	-0.12	+0.03	+0.01	0
Pickett/Conway (23, 26)	Axial	-1.40*	-0.90	-0.90	-0.89	-1.04	-1.04	-0.95	-1.04	-1.07
	Radial	-0.42*	-0.27	-0.29	+0.02	-0.05	-0.08	-0.01	0	-0.01
	Circumferential	-0.35*	-0.29	-0.29	-0.01	-0.06	-0.09	+0.01	0	-0.01
D'Appolonia and Newmark (27)	Axial	-2.02	-0.86	-0.85	-0.90	-1.07	-1.06	-0.85	-1.09	-1.18
	Radial	-0.32	-0.19	-0.25	0	-0.10	-0.15	0	-0.43	-0.09
	Circumferential	-0.53	-0.30	-0.25	-0.05	-0.13	-0.15	+0.03	-0.05	-0.08
Balla (32, 33)										
1)Uniax. compress. (Axial stress = 1 Lat. stress = 0)	Axial	-1.87	-0.95	-0.85	-0.95	-1.05	-1.05	-1.00	-1.00	-1.01
	Radial	-0.10	-0.40	-0.60	0	0	0	0	0	+0.01
	Circumferential	-0.47	-0.50	-0.60	+0.01	0	-0.01	0	+0.01	+0.01
2)Equal biaxial compression (Axial stress = 0 Lat. stress = 1)	Axial	-1.82	-0.35	-0.23	-0.15	-0.06	-0.12	0	-0.01	+0.02
	Radial	-1.29	-0.65	-0.40	-1.00	-1.00	-1.00	-1.00	-1.01	-1.02
	Circumferential	-0.59	+0.14	+0.23	-1.03	-1.00	-1.00	-1.00	-1.01	-1.02
3)Hydrostatic compression (Axial stress = 1 Lat. stress = 1)	Axial	-1.21	-1.23	-1.19	-1.07	-1.00	-0.98	-1.00	-1.01	-1.01
	Radial	-0.03	-0.40	-0.40	-1.00	-0.96	-0.93	-1.00	-1.00	-0.99
	Circumferential	-0.53	-0.43	-0.40	-1.02	-1.00	-0.98	-1.00	-1.01	-1.01
4)Triax. compress. (Axial stress = 4 Lat. stress = 1)	Axial	-5.70	-3.80	-3.62	-3.85	-4.05	-4.09	-4.00	-4.01	-4.02
	Radial	-0.82	-2.00	-2.23	-1.00	-1.02	-1.03	-1.00	-0.99	-0.99
	Circumferential	-1.94	-2.15	-2.23	-0.97	-1.01	-1.03	-1.00	-0.99	-0.99

Table 2.3. Stress state at various positions within specimens of material under an average applied boundary compression stress of -1.0 as obtained by different theoretical analyses.

points on the loaded ends completely restrained against lateral movement, as compared with the case of no restraint. Although the results of the analyses differ in detail the E value for a material with $\nu = 0.33$ is found, on average, to be approximately 5.2% higher than for the unrestrained case. This increase, which reduces as either the H/W value or ν for the specimen decreases, indicates the stiffening effect of the boundary restraint resulting from the induced triaxial compressive stress.

Niwa, Kobayashi and Nakagawa [37]

For complete end restraint, the boundary shear stresses increase from the axis towards the ends which is confirmed by the results of Lisowski [31]. The magnitude of the maximum stress developed is dependent on the frictional characteristics at the platen/specimen interface which determine the amount of sliding which can occur.

Balla [32, 33]

This investigation is important in that it includes cases of loading other than in uniaxial compression. The analysis has been checked by Green [42] and found to be essentially correct, except for some typographical errors which do not invalidate the results, which are presented in terms of octahedral stresses.

The chosen boundary conditions are intended to simulate conditions obtaining in a conventional hydraulic triaxial cell and consist of uniform axial strain over the loaded ends, with the displacement only of the peripheral points constrained, together with a uniform lateral stress over the curved surface. Various axial/lateral stress ratios for a cylinder with H/D = 2 are investigated and for the uniaxial case the results are similar to those obtained by other workers, with the same trends being exhibited for triaxial compression. In the case of equal biaxial compression, high tensile values of near axial principal stress are found to be induced near the 'unloaded' ends. This case is considered rather academic since, under practical conditions, the attainment of such a stress state would be achieved without any load, and hence any significant clamping effect, acting over the ends of the specimen. For the same reason, the stress disturbances found for the hydrostatic loading face may be unrealistically high since, using a conventional hydraulic cell arrangement, such a stress

state is applied by hydraulic pressure acting on all faces which will not tend to induce significant secondary restraints.

Hilsdorf [35]

This approximate analysis simulates the case of a thin concrete specimen loaded through rigid steel platens. The cases of both complete and partial lateral restraint are considered, and it is shown that at low loads relatively high values of restraint stress could be induced up to the point of sliding.

The analysis is extended to biaxial compression by superimposing the effects of load transference between the two sets of platens on the platen restraint stresses. It is shown that, at low loads, the concrete carries only approximately 40% of the applied load. This proportion rises to about 90% as the load is increased, due to sliding caused by a lowering of the coefficient of friction at the specimen/platen interface. It must be emphasised that the analytical method used is not rigorous and relies on many assumptions. Also, for the case of a specimen of finite thickness, restraint stresses will be developed at 90° to the plane of loading which will induce a zone of triaxial stress near the platens. Such a 'frame' of triaxially stressed material will, due to its rigidity, be likely to conduct more load than estimated, leaving the central portion of the specimen under near-biaxial stress at a value considerably lower than the applied stress.

Brady [41]

This investigation studies the effects of loading a specimen in uniaxial compression through rough steel platens, with materials of various values of ν/E and thickness interposed between the specimen and platens. It is shown that the restraint stresses become less compressive as the ν/E of the intermediate material increases and that, for a value greater than the specimen, large tensile stresses are induced at the ends. This confirms the results of other analyses [38 and 40]. As the thickness of a 'soft' intermediate material is decreased, the tensile stresses within the specimen become smaller.

The analysis is extended [43] to study the influence of testing method on the initiation of fracture (increase of voids) within cylinders of a

brittle material loaded in uniaxial and triaxial compression using steel end plates with and without soft inserts, the triaxial compression being obtained by a confining pressure applied to the cylindrical surface. The material studied is assumed to contain cracks, rather than pores, whose distribution was described by a statistical function. It is assumed that, under applied compressive stress, fracture initiates from closed cracks, when the shear stress on the cracked surface exceeds a critical value (evaluated using the McLintock-Walsh modification to the Griffith Criterion [44]). For applied tensile stress the fracture is assumed to initiate from open cracks when the tensile stress normal to the crack exceeds a critical value. The following main conclusions are drawn from the results:-

1) For compressive stress states fracture initiation probably starts around the end perimeters of the cylinder, the initiation stress depending on the geometry and properties of the specimen and loading plates. Within conical end-zones, large radial and tangential confining stresses are developed which inhibit the formation of microcracks.

2) The addition of a confining pressure produces a more uniform stress distribution.

3) When soft intermediate materials are used to transmit the load, tension cracks are initiated, and grow into the specimen, from positions on the end planes near the periphery. The fractured surface is concave inward and gradually aligns in the axial direction.

4) The true value of the stress required to cause fracture initiation (growth of voids) can be measured in a specimen of H/D ratio greater or equal to 2.0, providing deformation measurements are made in that portion of the specimen bounded by planes $\pm$ 0.25 x H on each side of the central plane.

2.4.2.2. Conclusions

The following main conclusions are for the case of uniaxial compression. For other states of stress the only investigation carried out is that by Balla [32, 33] for which the principal conclusions are given in Table 2.2.

Uniaxial Compressive Loading through Rigid Platens ($\nu/E_{plat} < \nu/E_{spec}$)

i) Compressive lateral restraint stresses are induced at the platen/specimen interface. These stresses are zero on the axis and increase towards the periphery to values limited either by the difference in mechanical properties of the platen and specimen material or by the frictional properties at the interface.

ii) This restraint causes lateral compression stresses to develop near the loaded boundaries. This induces a state of triaxial compression within specimens of finite thickness.

iii) The lateral compressive restraint stresses reduce with distance from the loaded face and may reach tensile values near the centre of the specimen. For complete fixity at the loaded boundaries, these restraints may reduce to insignificance and result in a near-uniform state of near-uniaxial stress at a distance from the loaded face equal to the width or thickness of the specimen, whichever is the greater.

Uniaxial Compressive Loading through Rigid Platens with Soft Intermediate Materials ($\nu/E_{mat} > \nu/E_{spec}$)

i) Large tensile restraint stresses are induced near the loaded ends of the specimen which increase with increasing value of ν/E for the intermediate material.

ii) Tensile restraint stresses decrease in magnitude with reduction in the thickness of the intermediate layer.

2.4.3. Experimental Investigations

2.4.3.1. Results of Investigations

All experimental methods for assessing the influence of the loading technique on the state of stress induced within a specimen of material are based essentially on estimating the stress from measurements of

deformation. Such an estimation can only be considered valid if (a) the constitutive relations for the material under test are known with certainty and (b) provided sufficient data is available regarding the distribution of strain throughout the entire material.

Since for materials such as rock or concrete the first of the above requirements cannot be satisfied, and the second is extremely difficult to achieve, some workers have chosen to adopt other materials for evaluating the effectiveness of loading techniques. In fact on the basis of the materials used, the investigations conducted to date can be divided into three main types as follows:-

Type 1 The shape of specimen is modelled in a material exhibiting photoelastic properties, to facilitate the measurement of internal strains.

Type 2 A material of known mechanical properties is used, such that the behaviour under any specified stress state can be calculated and compared with the behaviour observed under test conditions.

Type 3 A sample of material of largely unknown response to the range of induced stress states is used, and it is attempted to assess trends from measurements of surface strain or deformation.

Investigations using materials of Type 1 suffer from the main disadvantage that the behaviour of the model material, and the frictional characteristics at the loaded surfaces, may not resemble that of the material being modelled.

Type 2 materials can be chosen to approximate closely to brittle materials, such as rocks and concrete, within the 'elastic' range. Large differences are likely to be apparent both due to the disparity of frictional characteristics at the platen/specimen interface and of deformational behaviour at higher loads.

For investigations using materials within Type 3 it is impossible to deduce with any degree of certainty the actual state of stress within, or on,

specimens but some evaluation of the comparative effectiveness of loading techniques can be assessed.

Details of the various investigations considered are reviewed in Table 2.4., where the type of material (as outlined above) used in each case is also indicated. The main results of the investigations are also given in the Table and some more detailed typical results are shown graphically in Figures 2.9. to 2.12. Most of the information relevant to the present project is given in these Tables and Figures, but additional comments regarding important points concerning some investigations are made in the following:-

Coker (45, 46)

Comparison of Figures 2.9.(a) and (b) show the serious stress disturbances within the glass specimen when loaded through a soft intermediate material (rubber). Only small disturbances are apparant when using subsidiary platens of the same material as the specimen but the experiments showed that this arrangement is satisfactory only if such platens are sufficiently thick and of the same cross section as the specimen (see Figures 2.10.(c) and (d)).

Durelli (48)

From this investigation it was concluded that a slight change in the shape of the contact surface between the specimen and platen greatly increases the magnitude of the stress concentrations, but that these could be significantly reduced by interposing an optimum thickness of cardboard (0.25").

Conway (23)

In this investigation it is assumed that the strains induced and measured in the specimens are directly proportioned to the stresses. This assumption, however, neglects the 'Poisson effect' and, since no values are given for the particular resin under the stress freezing temperature used in the experiments, no stresses can be calculated. In spite of this drawback, useful information can be obtained by comparing the strain values measured under the various boundary conditions and Figure 2.10 shows the lateral strain profiles and principal strain trajectories obtained in the tests. Apparently, the use of p.t.f.e. sheets produces the most uniform distribution of strain but it should be pointed out that at the extremely low value of boundary stress used (102 lb/in^2) it is unlikely that extrusion of

Investigator	Specimen Shape and type of Material used*	Boundary conditions**	Magnitude of Load	Assessment of Stress State	Main Conclusions
Coker (45, 46)	1" x 1" x $\frac{1}{4}$" slab of glass with well-machined faces (Type 1)	Uniaxial compression through - 1) thick brass main platens 2) main platens and thin sheet of rubber 3) main platens and 0.4" subsidiary glass platens faces of all components well-machined	Approximately 1000 lb./in.^{2}	From strains measured photoelastically (probably combined with deformation measurements)	Case 1 (See Figure 2.9.(a) Axial stress near loaded faces increases from value of 0.7 at axis to 1.09 at corners. This trend reverses towards the centre of the specimen with the maximum value being 1.10 at centre and 0.98 at edges. Case 2 (See Figure 2.9.(b) Near loaded faces highest value of axial stress is 1.29 near axis reducing to 0.06 at corners. This trend persists to centre of specimen where variation is from 1.07 to 0.72. Case 3 (See Figure 2.9.(c) Axial stress at loaded boundary varies from 1.05 at axis to 0.97 at edges. At centre the variation is from 1.0 to 0.94. The distribution of lateral stress shows mainly compressive values near loaded faces which change to tensile towards centre of specimen (highest value is 0.06).
Frocht (47)	Rectangular blocks of photoelastic material with differing H/W ratios (Type 1)	Concentrated uniaxial compressive load	Undisclosed	From isochromatic fringes (shear strains)	Uniform state of stress in centre if $H/W \geqslant 2.5$.

*For definition of material type see text (2.4.3.1.)
**See Table 2.1. for values of (ν/E)

Table 2.4.(a) Summary of experimental investigations to determine the stress state within specimens of various materials under various loading conditions.

Investigator	Specimen Shape and type of Material used*	Boundary Conditions**	Magnitude of Load	Assessment of Stress State	Main Conclusions			
					Case	Highest strain Concentration	Position	Remarks
Durelli [48]	Rectangular block of bakelite with H/W = 2.65 (Type 1)	Uniaxial compressive load through - (A) lapped plane steel platens of width greater than and thickness equal to specimen (1) with no material interposed (2) with various thicknesses (0.027" and 0.033") of rubber interposed (3) with various thicknesses (0.036"-0.250") of cardboard interposed (4) with 2 x 0.15" thick lead sheets interposed. (B) slightly convex steel platens (1) with no material interposed (2) with 0.2" thick cardboard interposed (C) slightly concave steel platens	Undisclosed	From isochromatic fringes	A1	1.10	Near corners	
					A2	1.20 - 1.33	Between axis and corners	Increases with thickness of rubber.
					A3	1.4 - 1.05	Near corners	Decreases with thickness of cardboard up to 0.25".
					A4	1.14	On axis	
					B1	1.60	Near axis	
					B2	1.10	Near corners	
					C	3.80	Near corners	

Figure 2.4.(b) Summary of experimental investigations to determine the stress state within specimens of various materials under various loading conditions.

Investigator	Specimen Shape and type of Material used*	Boundary Conditions**	Magnitude of Load	Assessment of Stress State	Main Conclusions
Conway (23)	Cylinders of epoxy resin (Type 1)	Uniaxial compression through steel platens with - (1) p.t.f.e. sheets interposed (2) sheets of fine sandpaper interposed (3) ends of specimen clamped in steel sleeves	102 lb./in.^{2}	Using frozen stress technique combined with three-dimensional photoelasticity	(See Figure 2.10.) Increasing the restraint at the ends increases the strain disturbances, p.t.f.e. sheets induce the most uniform distribution.
Parrott (49)	150 x 150 x 19 mm. slab of aluminium (Type 2)	Uniaxial and biaxial compression through - (1) rigid steel platens (2) hydraulic platens based on pressurised rubber diaphragms	Up to 2200 lb./in.^{2}	From measurements of surface strain using E.R.S.G.s	(See Figure 2.11) For rigid steel platens the axial strain near the loaded ends tends to increase from the axis to the corner. The disturbances decrease towards the centre of the specimen. Loading through hydraulic platens produces uniform axial strains close to the theoretical value for all positions on the specimen and the effectiveness only slightly decreases with increasing load. Uniformity of strain remains for biaxial compression applied using different stress paths and is time independent.

Table 2.4.(c) Summary of experimental investigations to determine the stress state within specimens of various materials under various loading conditions.

Investigator	Specimen Shape and type of Material used*	Boundary Conditions**	Magnitude of Load	Assessment of Stress State	Main Conclusions
Seldenrath and Gramberg (50)	Cylinders of limestone and marble with H/D = 2 (Type 3)	Uniaxial compression through pads of 0.5 mm. thick rubber and 0.2 mm. copper located in recesses within steel platens with - (1) ends of specimen unrestrained (2) ends restrained by steel collars	Up to failure	From lateral deformation measured by extensometers	Clamping increases failure load by up to 75% for finer grained limestone but by less than 10% for coarser grained marble. Limestone specimens fractured by axial splitting while marble specimens exhibited distinct end 'cones'.
Hilsdorf (35)	20 x 20 x 5 cm. slabs of concrete (Type 3)	Uniaxial and biaxial compression using - (1) 5 cm. thick steel platens (2) 'Brush' platens	Up to failure	From measurements of overall deformation of specimen and surface strain measurements near loading face of rigid steel platen	<u>For uniaxial compression</u> Method of loading has no significant effect on strength. Measured E and ν values are higher for brush platens. <u>For biaxial compression</u> Near parabolic distribution of lateral restraint stress measured on platen near interface, with maximum value on axis. Ultimate strength lower for brush platens than for rigid platens. From a series of tests using combined brush platen and rigid platen loading it was decided that for steel platens under low loads specimens are subjected to about 50% of applied load (μ for interface = 0.5 approx.). At higher loads this proportion increases to about 80% (μ for interface = 0.2 app.).
Hughes and Bahramian (51)	4" cubes and 4" x 4" x $9\frac{5}{8}$" prisms of various concretes (Type 3)	Uniaxial compression through thick steel platens - (1) with no interposed material (2) with MGA pads interposed	Up to failure	From measurements of lateral surface strain	For steel platens only the cubes give higher strengths than prisms but the ratio prism/cube strength is not constant for all mixes. Loading through MGA pads considerably reduces the strength differences between the two types of specimen and induces more uniform, and larger, lateral strains in cubes. The strength for both prisms and cubes for all mixes is also reduced.

Table 2.4. (d) Summary of experimental investigations to determine the stress state within specimens of various materials under various loading conditions.

Investigator	Specimen Shape and type of Material used*	Boundary Conditions**	Magnitude of Load	Assessment of Stress State	Main Conclusions
Lachance (3)	Prisms and cylinders of paste, mortar and concrete with H/W from 1 to 4 (Type 3)	Uniaxial compression through various media of same c.s.a. as specimen - (A) Thick steel platens (1) without interposed material (2) various thicknesses of rubber interposed (3) various thicknesses of cardboard or plywood interposed (B) Thick platens of same material as specimen with contacting surfaces 'as cast' or ground plane	Up to failure of specimens	From overall lateral deformation measured by extensometers	(See Figure 2.12.) Case A (1) Under low loads loading through steel platens induces lateral deformation 'bulges' near loaded ends. These decrease from concrete to paste and disappear for H/W ratios above 2. Lateral deformation at centre increases with H/W ratio. Under higher loads No slipping at platen/specimen interface. Maximum lateral deformation at centre, with initial failure in central zone. Failure load decreases with increase is H/W up to 2.5 thereafter no further decrease. Case A (2) Significant 'bulges' at ends for all specimens and H/W ratios. Lateral deformation greater than for Case A and increases with thickness of rubber. 'Splitting' failure initiates near ends at lower loads than for Case A. Failure load increases with increase in H/W up to 2.5. Considerable slippage at surface of specimen during failure process. Case A (3) Cardboard and plywood considerably reduces lateral deformation disturbances. Case B Concrete platens reduce the lateral deformation disturbances provided that the platen and specimen surfaces are accurately ground.

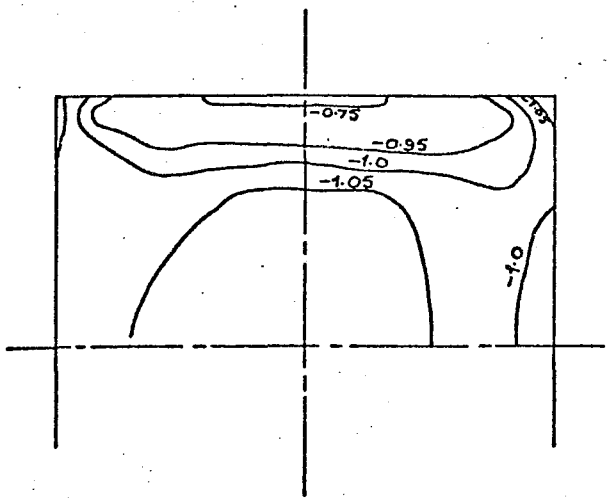
Table 2.4.(e) Summary of experimental investigations to determine the stress state within specimens of various materials under various loading conditions.

Investigator	Specimen Shape and type of Material used*	Boundary Conditions**	Magnitude of Load	Assessment of Stress State	Main Conclusions
Jordaan and Illston (52)	8" cubes of concrete (Type 3)	Uniaxial compression through - (1) platens consisting of four 2" thick unmachined steel plates (2) machined steel platens as above with MGA pads interposed	Up to 2000 lb./in.^{2}	From measurements of axial and lateral strains using 4" vibrating wire strain gauges cast into specimen	For unmachined platens, lateral tensile strains near ends are <u>larger</u> than those near centre. With MGA pads strains are more uniform, but larger, both near platen and within the central portion of the cube.
Beak (53)	(a) 150 x 150 x 300 mm. prism of normal concrete tested both in as-cast condition and after having 50 mm. ground from one end. (b) prism of lightweight aggregate concrete with 150 x 150 mm. cross-section and H/W ratio from 4.67 to 1 (Type 3)	Uniaxial compression through - (1) thick steel platens (2) 'brush' platens	Up to failure	From lateral deformation measured by Demec gauges	<u>For normal concrete</u> <u>In 'as cast' condition</u> Lateral deformation profile indicates considerable compressive restraint near steel platen with characteristic 'bulging'. For 'brush' platen, profile near ends indicates tensile restraint. <u>After removing end</u> Bulge under steel platen remains but the disturbance under the 'brush' platen is essentially eliminated. <u>For lightweight concrete</u> For H/W = 4.67, lateral deformation profiles for both methods of loading are similar to those for 'as-cast' specimens of normal concrete. Deformation in central ⅓rd zone is uniform and about 7% higher using brush platens. Prisms of both types of concrete tested using brush platens show no significant variation of measured strength with H/W ratio.

Table 2.4.(f) Summary of experimental investigations to determine the stress state within specimens of various materials under various loading conditions.

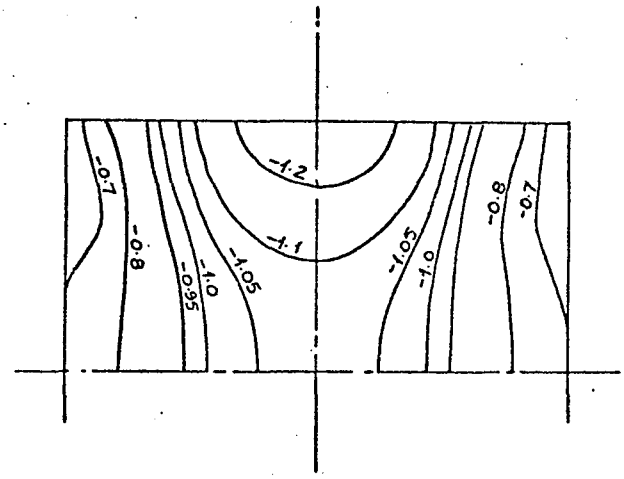
Investigator	Specimen Shape and type of Material used*	Boundary Conditions**	Magnitude of Load	Assessment of Stress State	Main Conclusions
Robinson and Vile (54)	4" x 4" x 12" prisms of mortar (Type 3)	Uniaxial compression through thick steel platens with various materials interposed	Up to 30% of ultimate	From lateral deformation as measured by extensometers	Characteristic 'bulged' lateral deformation profile near ends, with least disturbance given by 0.0012" thick layer of Febcure Super 90 curing compound. The effectiveness of this layer reduces as the specimens are dried but the ultimate strength is not influenced.
Vile (8)	10" x 10" x 4" slabs of mortar and concrete (Type 3)	Various ratios of bi-axial compression applied through thick steel platens with layer of Febcure Super 90	Up to 30% of ultimate	From measurements of surface strain using ERSG.s and photo-elastic coatings and deformation measurements throughout the thickness using extensometers	Central zone of specimens is under a uniform state of strain. The extent of this zone decreases to 6" x 6" with increasing load.
Peng (40)	1.25" diameter cylinders of granite with H/D = 2 and ends polished plane and parallel (Type 3)	Uniaxial compression through 6" dia. thick steel platens with - (1) no materials interposed (2) with 0.005" p.t.f.e. sheets (3) with 1.25" dia. x 0.075" thick hardened steel subsidiary platens (4) as (3) but with p.t.f.e. sheets between main and subsidiary platens (5) As (4) but with p.t.f.e. sheets between specimen and platen (6) with 1.25" dia. x 1.5" thick hardened subsidiary platens	Not disclosed but apparently well below ultimate	From measurements of axial and circumferential strains	Case 1 Strain profiles indicate large lateral compressive restraint near loaded ends. Case 2 Strain profiles indicate large lateral tensile restraints at ends with profiles similar to that of Case 1 within central zone of spec. Case 3 Doubly-curved strain profiles exhibited, with strains significantly larger than for Cases 1 and 2. Case 4 More uniform strains throughout specimen than for above cases. Case 5 More uniform strains than for above cases. Case 6 Almost ideally uniform circumferential and axial strains which remain up to failure of the specimen. For all cases the values of axial strain at the centre of the specimen are similar. For cases 1 and 2 the circumferential strain at the centre is significantly less than for the other cases which are all similar.

Table 2.4. (g) Summary of experimental investigations to determine the stress state within specimens of various materials under various loading conditions.



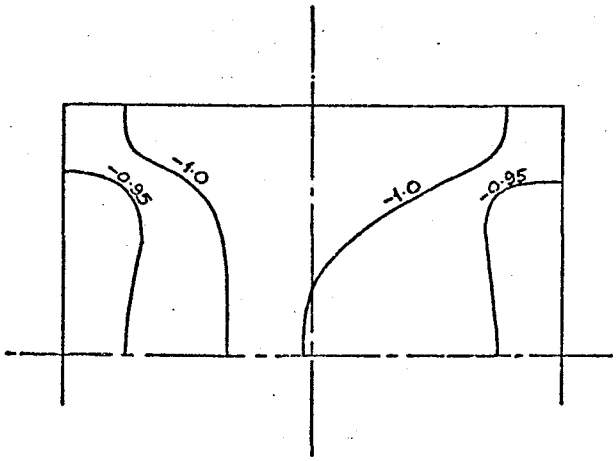
axial stress

(a) Loading through thick brass platens with no interfacial material

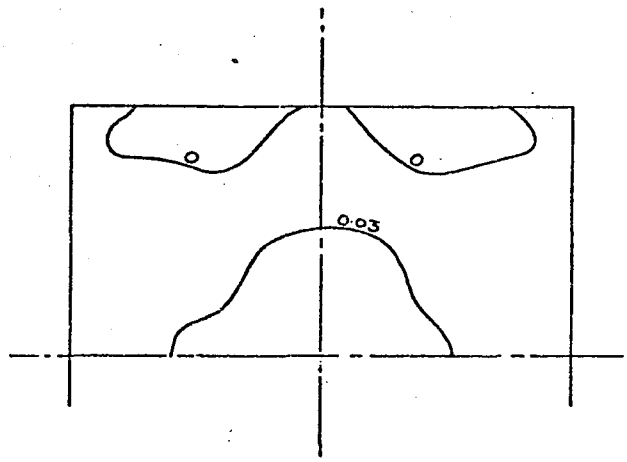


axial stress

(b) Loading through thick brass platens with thin rubber at interface



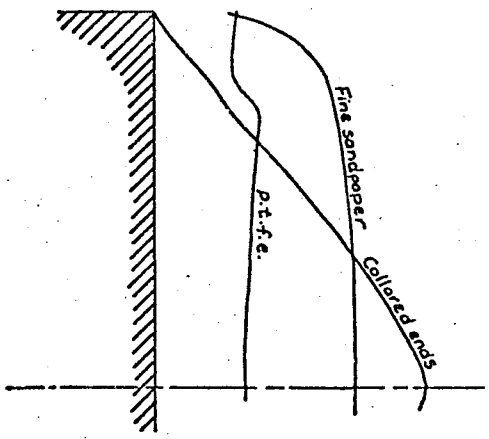
axial stress



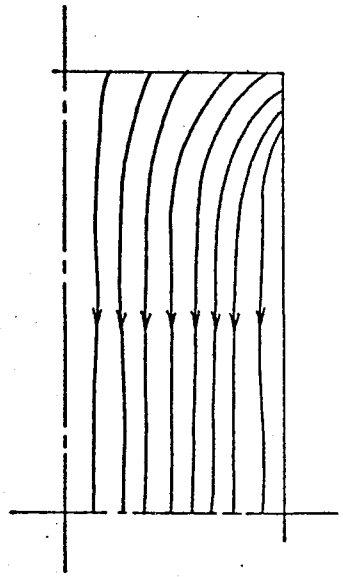
lateral stress

(c) Loading through thick brass platens with 0.4" thick glass subsidiary platens

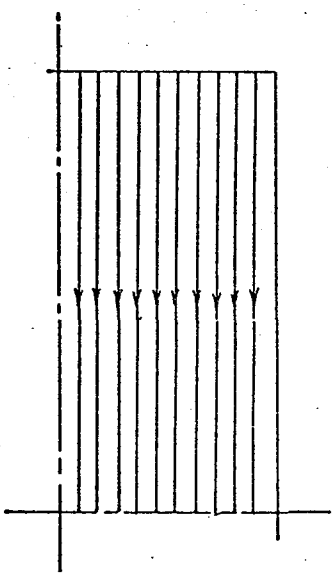
Figure 2.9. Distributions of stress for a 1" x 1" x $\frac{1}{4}$" slab of glass loaded under an average uniaxial compressive stress of -1 through various types of platen and interfacial material. after COKER (45, 46)



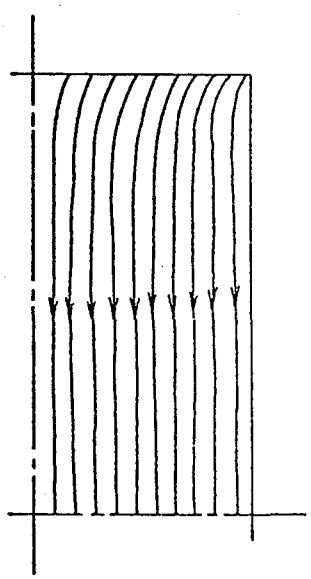
(a) Lateral deformation



(b) Isotenics of near-axial principal strain for collared ends



(c) Isotenics of near-axial principal strain for p.t.f.e. at interface



(d) Isotenics of near-axial principal strain for fine sandpaper at interface

Figure 2.10. Distributions of lateral deformation and isotenics for a cylinder of epoxy resin loaded under an average uniaxial compressive stress of -1 through steel platens and various types of interfacial material or end restraint.

after CONWAY (23)

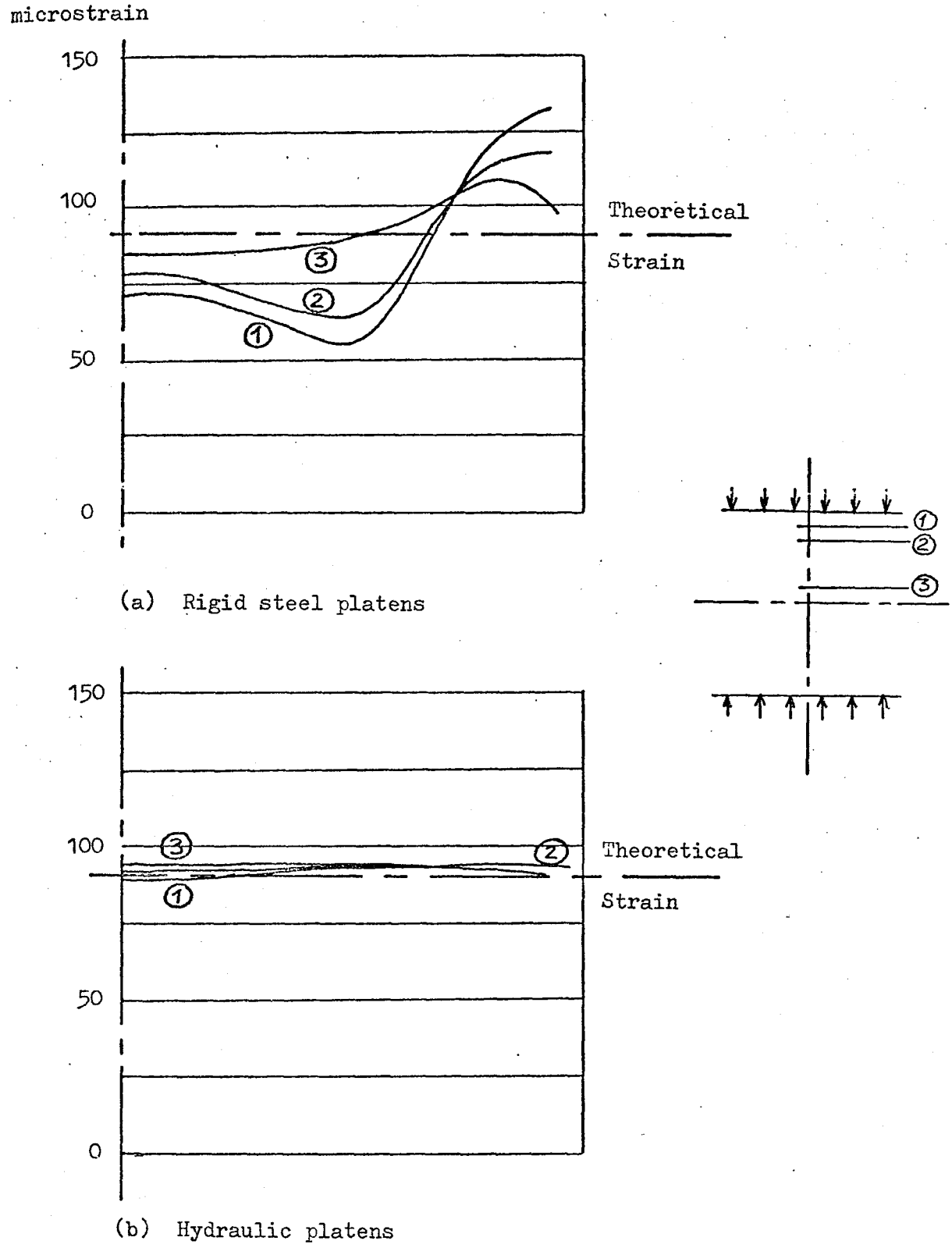
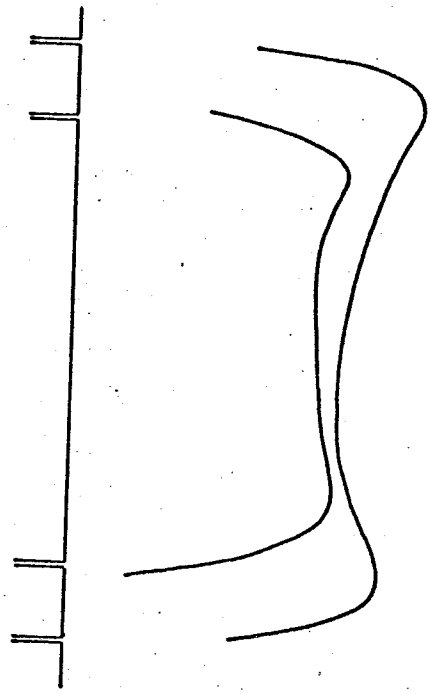
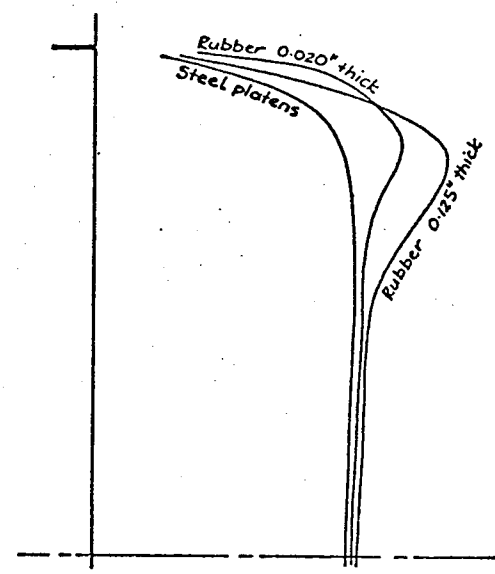


Figure 2.11. Distributions of axial strain for a 150 x 150 x 19 mm. aluminium slab loaded under an average uniaxial compressive stress of 2200 lb./in.^{2} through different types of platen.

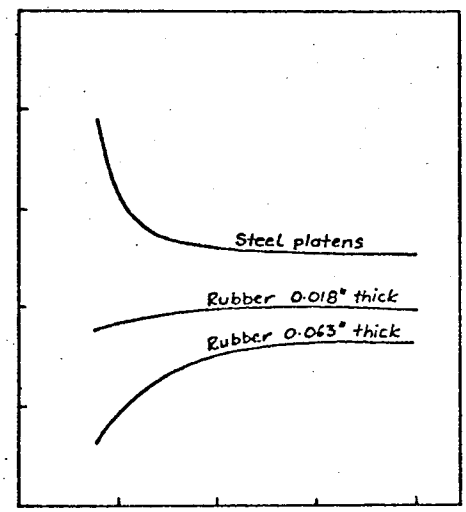
After PARROT (49)



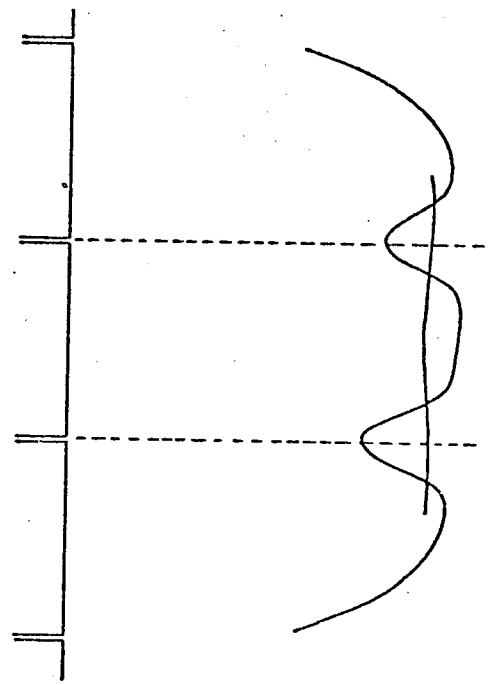
(a) Variation of lateral deformation profile with H/W ratio of concrete prisms



(b) Lateral deformation profiles for paste prisms with H/W = 3 loaded under uniaxial compression through steel platens with and without interface



(c) Variation of crushing strength with H/W ratio for concrete prisms loaded under uniaxial compression through steel platens with and without interface materials



(d) Lateral deformation profiles for a concrete cube loaded under uniaxial compression through a concrete cube platen

Figure 2.12. Lateral deformation profiles and variation of strength for various shapes of specimen loaded through various materials.

after LACHANCE [3]

this material will tend to induce significant tensile restraints.

Parrott [49]

In this investigation 'hydraulic' platens are compared with conventional rigid platens for applying uniaxial and biaxial loads.

Figure 2.11. shows typical results and clearly demonstrates the effectiveness of the hydraulic platens in reducing the strain disturbances in the direction of applied load.

The effects of extrusion of the rubber diaphragms were minimised by reducing the clearance between the clamping plates and the surfaces of the specimen both before, and during, testing. It should be emphasised, however, that all tests have been conducted at stresses below 2200 lb/in^2. Within this range the problems associated with extrusion may not have become significant.

Seldenrath and Gramberg [50]

The most important outcome of this work is a demonstration of the dependence of the behaviour under various loading conditions on the type of material tested.

The failure mode of the marble specimens suggests that, even with the specially developed loading pads, compressive restraint still exists at the specimen faces. This is confirmed by the form of the deformational profiles.

Lachance [3]

It was concluded that the presence of a framework of aggregate may be the cause of the 'bulging' of the lateral deformation profiles which are particularly evident for concrete specimens near the loaded ends (see Figure 2.12.(a)). This hypothesis was tested by loading a mortar specimen through several small steel platens, intended to simulate aggregate particles near the surface, and the resulting lateral deformation profile showe considerable 'bulging', similar to that obtained for concrete using a single main platen.

A soft intermediate material, such as rubber, also induces significant bulges in the lateral strain profiles (see Figure 2.12.(b)) and the same characteristics were observed for loading through steel platens of

smaller cross-section than the specimen. This tends to confirm that the extrusion of the rubber under load causes an axial stress concentration near the axis.

Figure 2.12.(c) shows the increase of failure stress with H/W ratio for rubber as the intermediate material, as compared with the decrease measured for tests using rigid platens only. In the case of the soft materials, vertical splitting failures were observed to initiate at the ends of specimens as compared with initiation from the central zone for rigid platens. Examination of the surfaces of the soft materials indicated that considerable slippage had occurred during the failure process.

Thick 'concrete' platens of the same material as the specimen under test considerably reduces the strain disturbances, provided all contact surfaces are accurately ground (see Figure 2.12.(d)). The few tests using intermediate materials, such as cardboard or plywood, apparently also indicate reduced strain disturbances (see Figure 2.13.(e)) but unaccountably, these improvements were not considered significant, the materials being classed as only slightly better than rubber.

Hilsdorf [35]

It was considered that the following two main requirements are essential for a study of the behaviour of materials under stress:-

1) The stress state in the specimen must be uniform, except for local disturbances caused by heterogeneity of the material.

2) It must be possible to determine the intensity of stress in the specimen, as a function of the applied loading, independently of the deformational properties of the material.

In an attempt to satisfy both these requirements a 'brush' platen arrangement was developed by splitting a steel platen longitudinally and transversely to form a large number of individual 'bristles', each with a high degree of lateral flexibility but with adequate buckling strength.

One possible drawback regarding the use of brush platens was recognised, namely that on non-uniform loading caused by the greater lateral bending of

the bristles near the outside edge of the platen compared with zero movement on the axis. It was calculated that such effects would be insignificant, but no assessment of the strain distribution within specimens was made to confirm this fact.

The deductions regarding the ineffectiveness of rigid steel platens are based on the assumption that test results for brush platen loading can be taken as the zero restraint datum.

Hughes and Bahramian [51]

The 'MGA pads', specially developed to reduce the frictional restraint between the rigid platen and specimens of concrete, consist of a sheet of 0.003" thick hardened aluminium adjacent to the specimen (with a ν/E value close to that of concrete) spread with a grease containing 3% MoS_2, with a Melinex polyester film placed above to provide a lateral expansion to counteract the lubricating inefficiency of the grease.

Loading through rigid platens with MGA pads considerably reduces the measured strength differences between prisms and cubes and induced more uniform, and larger, strains in cubes. However, an examination of the strength results shows that MGA pads reduce the strength of prisms, as well as cubes, for all mixes tested. This suggests that lateral tensile restraints are induced by the pads.

Jordaan and Illston [52]

The main requirements for the apparatus used in this investigation to apply multiaxial stresses to concrete specimens were:-

i) It should induce a reasonably uniform state of stress and strain in the loading directions.

ii) Any change in one of the loads should have little effect on the loads in the other directions.

The lateral strains at successive stages of loading in uniaxial compression indicate that, with the absence of MGA pads, the tensile strains near the platens are larger than those near the centre of the specimen. This observation conflicts with that found by most other workers where compressive restraints have been shown to exist near the loaded faces.

With MGA pads, the lateral tensile strains are more uniform, but generally greater in magnitude, throughout the specimen. This fact is noted by the Authors who state that MGA pads induce tensile strains over and above those caused by the 'Poisson effect'. This is undoubtedly due to extrusion of the pads even under the relatively low level of stress used in the tests (2000 lb/in^2 maximum).

Beak [53]

Brush platens, similar to those developed by Hilsdorf [35], were used as an alternative to the sliding layer and rigid-platen solution which was considered inferior due to the variation of induced shear stresses with thickness of the lubricating film.

For 'as cast' specimens of concrete the characteristic 'bulged' form of lateral deformation is evident for both rigid and brush platen loading.

It was not evident whether this profile was due to the effects of the platen or the particular configuration of material within the specimen caused by the casting process. The fact that the 'bulge' could be eliminated for brush platen loading, but not for rigid platens, by removing the end of the specimen was held to indicate that it was a material effect. With only this limited evidence, however, such an interpretation is open to question.

Robinson and Vile [54] and Vile [8]

After conducting a large number of trial tests under uniaxial compression using various interfacial materials with rigid platens, the least disturbance of lateral deformation was given by an intermediate layer of 'Febcure Super 90' curing compound. Apparantly this compound slightly penetrates the surface of the specimen, and hardens to form a viscoelastic layer which allows the steel platen to move freely relative to the specimen, even up to ultimate.

Although the strains and isochromatic patterns measured under biaxial loads applied using this compound indicate a central zone of the specimen to be under a uniform state of strain, the magnitude of the stress within this zone remains unknown.

2.4.3.2. Conclusions

The experimental investigations reviewed have consisted, basically, of measuring the deformational response of various shapes of specimen composed of three main types of material (see 2.4.2.) under compression, with the following boundary conditions:-

(a) Loading directly through rigid platens ($\nu/E_{platen} < \nu/E_{specimen}$)
(b) Rigid platen loading through soft intermediate materials ($\nu/E_{insert} > \nu/E_{specimen}$).
(c) Rigid platen loading through materials which 'bed-down' under load i.e. those with a low E value and low value of ν. (e.g. plywood, cardboard, etc.).
(d) Loading through platens of the same material as the specimen.
(e) Loading through non-rigid platens (i.e. 'brush' or 'hydraulic' platens).

From these tests the following main conclusions can be drawn regarding the effect of the above conditions:-

Loading directly through Rigid Platens

(1) Compressive lateral restraint stresses are induced at the platen/specimen interface. As predicted theoretically, these restraints increase from the axis towards the periphery and decrease towards the centre of the specimen.

(2) The restraint stresses, which increase with degree of roughness between the specimen and platen, tend to reduce the magnitude of the lateral deformation of the specimen.

(3) At low levels of load, the maximum lateral deformation occurs near the end zones of specimens giving characteristic 'bulged' lateral deformation profiles. At higher loads the position of maximum deformation changes to the central zone of the specimen.

(4) As the H/W ratio of a specimen is increased, the extent of the central zone under a near-uniform lateral deformation increases while the magnitude of the deformation within this zone decreases. At a H/W ratio of about 2.5, the central $\frac{1}{3}$rd of the specimen is under near-uniform strain which is in close agreement with theory.

(5) Failure initiates within the central zone of specimens and progresses towards the loaded ends where the restraint stresses inhibit fracture propagation.

(6) The failure load decreases with H/W ratio up to H/W = 2.5 (approx.) after which it remains essentially constant.

(7) The effect of the degree of boundary fixity on the behaviour of a specimen of a given shape depends both on the type and degree of heterogeneity of the material of which the specimen is composed, together with the characteristics at the interface (i.e. whether ground or unground, etc.).

(8) Considerable stress disturbances occur if the contact surface between the specimen and platen is not accurately plane.

Loading through 'Soft' Materials

(1) As predicted theoretically, tensile lateral restraint stresses are induced at the interface between the intermediate material and the specimen due to extrusion of the insert material. These restraints decrease towards the centre of the specimen.

(2) The restraint stresses increase with value of ν/E insert (as shown theoretically) and tend to increase the lateral deformation of the specimen, the maximum of which occurs near the loaded ends.

(3) The restraint stresses increase with thickness of the insert material which agrees with the results of theoretical analyses.

(4) The restraints apparently reduce with increasing H/W ratio, as evidenced by the increase in measured failure load. This increase occurs up to H/W = 2.5 (approx.), after which the failure load remains essentially constant at a value below that for rigid-platen loading. It may be, however, that this behaviour is due to slippage at high loads since evidence of this has been observed in the loading surfaces of soft materials after test, and is predicted theoretically.

(5) Failure initiates within the end zones of the specimen and progresses towards the centre.

Loading through Materials which 'bed-down' under Load

These materials considerably reduce the strain concentrations within specimens, particularly for cases where the loading surfaces of either the platen or the specimen are not accurately plane.

The particular merit of such materials is that although their E-value is very low they do not induce significant tensile or compressive restraint stresses in the specimen since their lateral movement under load is exceptionally small. In fact the E-value is generally so small that, under the range of loads normally applied, these materials soon compress to a limiting deformation.

Platens of the Same Material as the Specimen

These platens only reduce the stress concentrations if the contact surfaces are accurately plane and parallel. If this can be achieved then the complete platen/specimen assembly appears to act as a unit, with the characteristics of a monolithic specimen of the same total H/W ratio.

Non-rigid Platens

'Brush' Platens

Unfortunately a relatively small amount of data are available on which to base a quantitative judgment of the performance of this type of loading device. However, the following are the main conclusions which can be drawn from the reviewed investigations:-

(1) The lateral movement of the specimen may cause uneven flexing of the bristles, and thus tend to concentrate the load near the axis. Insufficient data is available to quantify this effect.

(2) The stress is applied as a series of concentrated loads. This may effect the behaviour of heterogeneous materials, and could account for the changes in deformational behaviour observed before and after removing the ends from specimens of concrete containing coarse aggregate.

(3) Higher lateral deformations are induced in specimens by brush platens than by rigid steel platens.

2.5. Analytical Investigation of Stresses and Strains induced in Specimens for Different Boundary Conditions and Applied States of Stress and Strain

2.5.1. Introduction

Many previous analytical methods of assessing the effects of boundary conditions on the stress or strain distribution within loaded specimens (reviewed in Section 2.4.1.) rely on the use of simplifying approximations to achieve solutions. The accuracy of such solutions, therefore, is dependent on the validity of these approximations. Modern computational techniques such as Dynamic Relaxation, Finite Difference and Finite Element methods have greatly reduced the degree of approximation required to solve problems concerned with complex geometrical arrangements and loading conditions. Of these, Finite Element Methods provide the most widely used techniques, and in recent years much time and effort has been devoted to the development of associated computer programmes.

In their basic form these programmes can provide solutions for the stress and strain distribution within structures consisting of elastic, but not necessarily isotropic, materials provided the arrangement remains a continuum during the loading process and assuming conditions of plane stress or plane strain. Such programmes have recently become generally available as research tools, but are of limited use since most real civil engineering problems concern three-dimensional stress states, and materials which are inelastic and which become discontinuous during loading. Specialised computer programmes have been developed for the solution of these more complex problems but the author has found difficulty in locating a programme which would be immediately useable without requiring extensive, and time consuming, modifications or using excessive computational time or storage.

It has been decided, therefore, for the purposes of obtaining an indication of the stress and strain state within loaded specimens, to modify a relatively well-developed programme suitable for the elastic solution of plane problems so that it does not require excessive computer time or storage.

The cases investigated using this programme have been chosen to simulate, as closely as possible, the following:-

(a) Slab specimens loaded under the various boundary conditions of uniaxial compression in the supplemental programme described in 2.6.

(b) Slab specimens loaded under equal biaxial compression using a loading arrangement similar to that used for the tests described in Chapter 3.

(c) Specimens with a height/width ratio of 2.5 under uniaxial and axisymmetric triaxial compression, as used for the triaxial investigation described in Chapter 7.

2.5.2. Method of Analysis

The Finite Element programme used for the analyses is based on the FESS series developed at Swansea University [55]. The main modification to the programme is the addition of a contour plotting programme developed for use with the Calcomp automatic plotter [56] and subsequent restructuring in the form of overlays, to maintain the same core storage. Other modifications include the insertion of subroutines for automatic node and element generation, and a simplification of the method of data input so that material properties can be assigned easily to each element.

Triangular elements have been considered satisfactory for all the analyses, although other programmes of the FESS series are available in which the more versatile isoparametric elements can be used. No attempt is made to represent discontinuous boundaries between materials of different types as it is intended to investigate the effects of loading with full fixity between the loading device and the specimen.

All loading configurations investigated have been analysed to provide solutions to both the plane stress and plane strain cases. However, as there appears to be no significant differences between the results for the two cases, only those for the plane stress case are shown.

Since all the problems analysed concern arrangements symmetrical about the vertical and horizontal axes, computational time and storage is reduced by considering only that portion of the arrangement in one quadrant and appropriately constraining the boundaries formed by the axes.

2.5.3. Loading Configurations Investigated

All cases are analysed linearly elastically assuming, for each system considered, complete fixity at the boundaries between the various components. It is acknowledged that the use of such assumptions will not accurately simulate practical cases involving the loading of brittle materials up to failure, but the solutions obtained should serve to illustrate comparative trends in behaviour.

For each type of loading and specimen arrangement, the material properties are chosen to represent the mean values for the mortar mix (Type MA) used for the experimental programme described in Section 2.6. These mean values, based on the results of short term uniaxial compression tests, are as follows:-

$$E \text{ mortar} = 4.74 \times 10^6 \text{ lb/in}^2$$
$$\nu \text{ mortar} = 0.155$$

For the steel components of the loading devices, the following values are taken as representative:-

$$E \text{ steel} = 30.0 \times 10^6 \text{ lb/in}^2$$
$$\nu \text{ steel} = 0.30$$

Full details of the various cases considered are given in Table 2.5., and Figures 2.13. and 2.14. show the dimensions of the arrangements and the mesh configurations used.

To enable direct comparisons to be made in all cases the boundary conditions are chosen such that the same mean compressive stress (1000 lb/in^2) is induced in the axial direction.

2.5.4. Results of Analyses

The distributions of maximum and minimum principal stress over the specimen for Cases 1 to 8 are shown in Figures 2.15. to 2.18.

2.5.5. Discussion of Results

2.5.5.1. Assessment of Criticality of Stress State

With a specimen of material it is evident from the stress distributions obtained experimentally that, under realistic loading conditions, there are

Case	Specimen Shape	Boundary Conditions	Mean Stress induced within Specimen		Mesh Layout	Remarks
			Axial	Lateral		
Slab and Prismatic Specimens under Uniaxial Compression						
1	10" x 10" x 4" slab	Uniform load through 10" x 4" faces	1000 lb./in.^{2}	NIL	See Figure 2.13.	Uniform stress.
2	10" x 10" x 4" slab	Uniform deformation of 0.001045" on 10" x 4" faces	1000 lb./in.^{2}	NIL	See Figure 2.13.	Uniform strain (to be compared with Case 1).
3	10" x 10" x 4"	Uniform load through 10" x 4" x 4" steel platens	1000 lb./in.^{2}	NIL	See Figure 2.13.	Uniform stress through rigid platens.
4	10" x 10" slab	Uniform load through $9\frac{1}{2}$" x 4" x 4" steel platens	1000 lb./in.^{2}	NIL	See Figure 2.13.	This case is intended to simulate the use of rigid platens of smaller c.s.a. than the specimen (compare with Case 3).
5	10" x 10" x 4" slab	Loaded through 10" x 4" x 4" steel platens using male portion of steel spherical seating unit with concentrated load applied*	1000 lb./in.^{2}	NIL	See Figure 2.14.	Platen/spherical seat unit of same dimensions as used for the tests described in Chapter 3 with a load concentration typical of that experienced in practice*. (Compare with Case 3).

* The extent of the load concentration was assessed using carbon-paper impressions for load applied through the female seating unit.

Table 2.5.(a) Details of analytical investigations to determine the stress state within specimens under various boundary conditions of load.

Case	Specimen Shape	Boundary Conditions	Mean Stress induced within Specimen		Mesh Layout	Remarks
			Axial	Lateral		
Slab and Prismatic Specimens under Uniaxial Compression (contd.)						
6	10" x 10" x 4" prism	Load applied with uniform deformation of 0.0011192" on 4" x 4" x 4" steel platens	1000 lb./in.^{2}	NIL	See Figure 2.14.	Simulates the case of a specimen with H/W = 2.5 as used for tests in Chapter 7.
Slab Specimen under equal Biaxial Compression						
7	10" x 10" x 4"	Uniform load through $9\frac{1}{2}$" x 4" x 4" steel platens	1000 lb./in.^{2}	1000 lb./in.^{2}	See Figure 2.14.	This case simulates the geometrical layout of the specimen/platen unit of the Complex Stress Machine used for the tests in Chapter 3 but with full restraint effects in operation.
Prismatic Specimen under Biaxial Compression						
8	10" x 10" x 4"	Axial load applied with deformation of 0.0010799" on 4" x 4" x 4" steel platens together with lateral uniform load	1000 lb./in.^{2}	250 lb./in.^{2}	See Figure 2.14.	This case simulates a typical test conducted in the hydraulic cell (see Chapter 6 where specimen is loaded with combination of near uniform axial strain and uniform confining pressure.

Table 2.5. (b) Details of analytical investigations to determine the stress state within specimens under various boundary conditions of load.

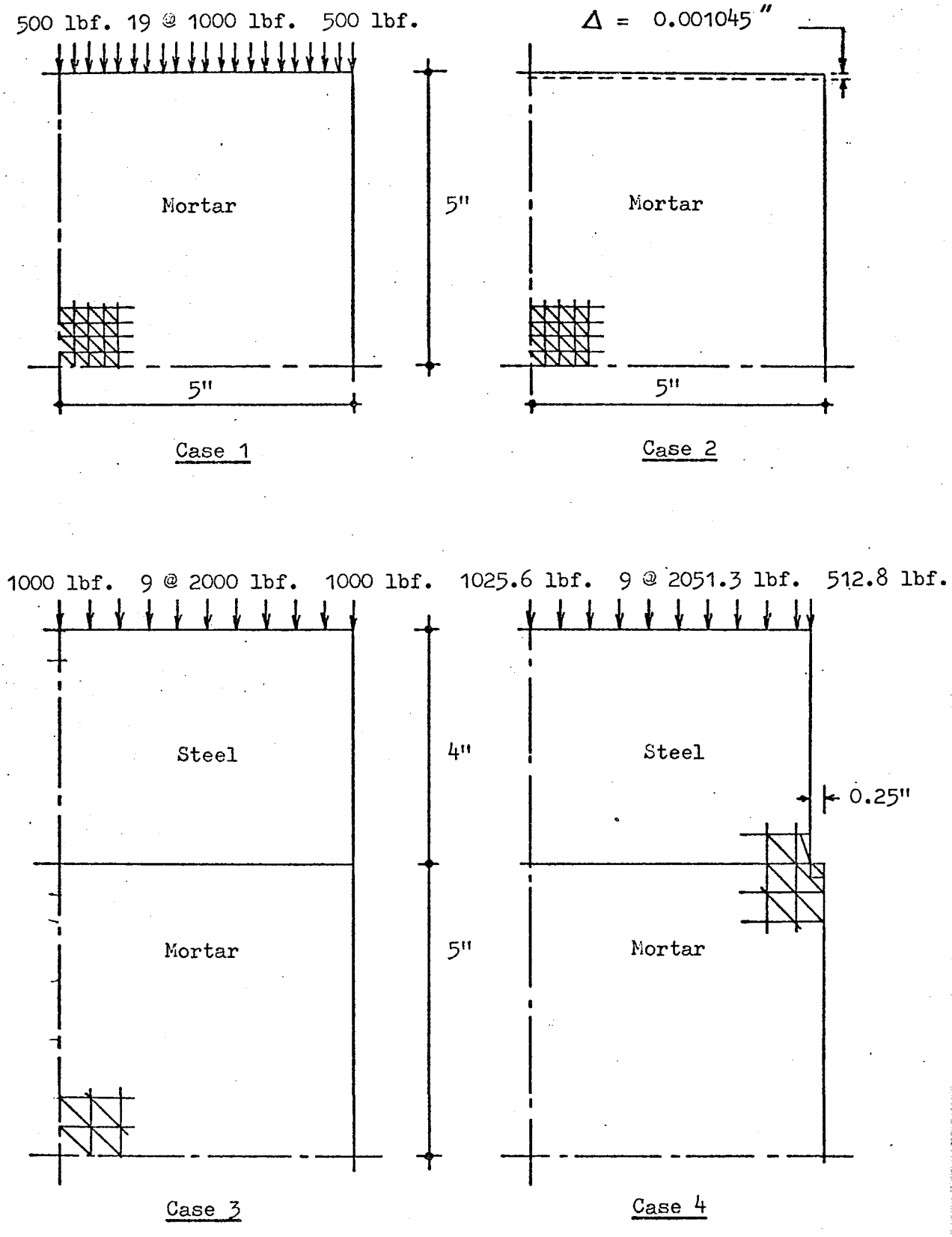


Figure 2.13. Diagrams showing dimensions, loading configurations and mesh layouts for Cases 1 to 4.

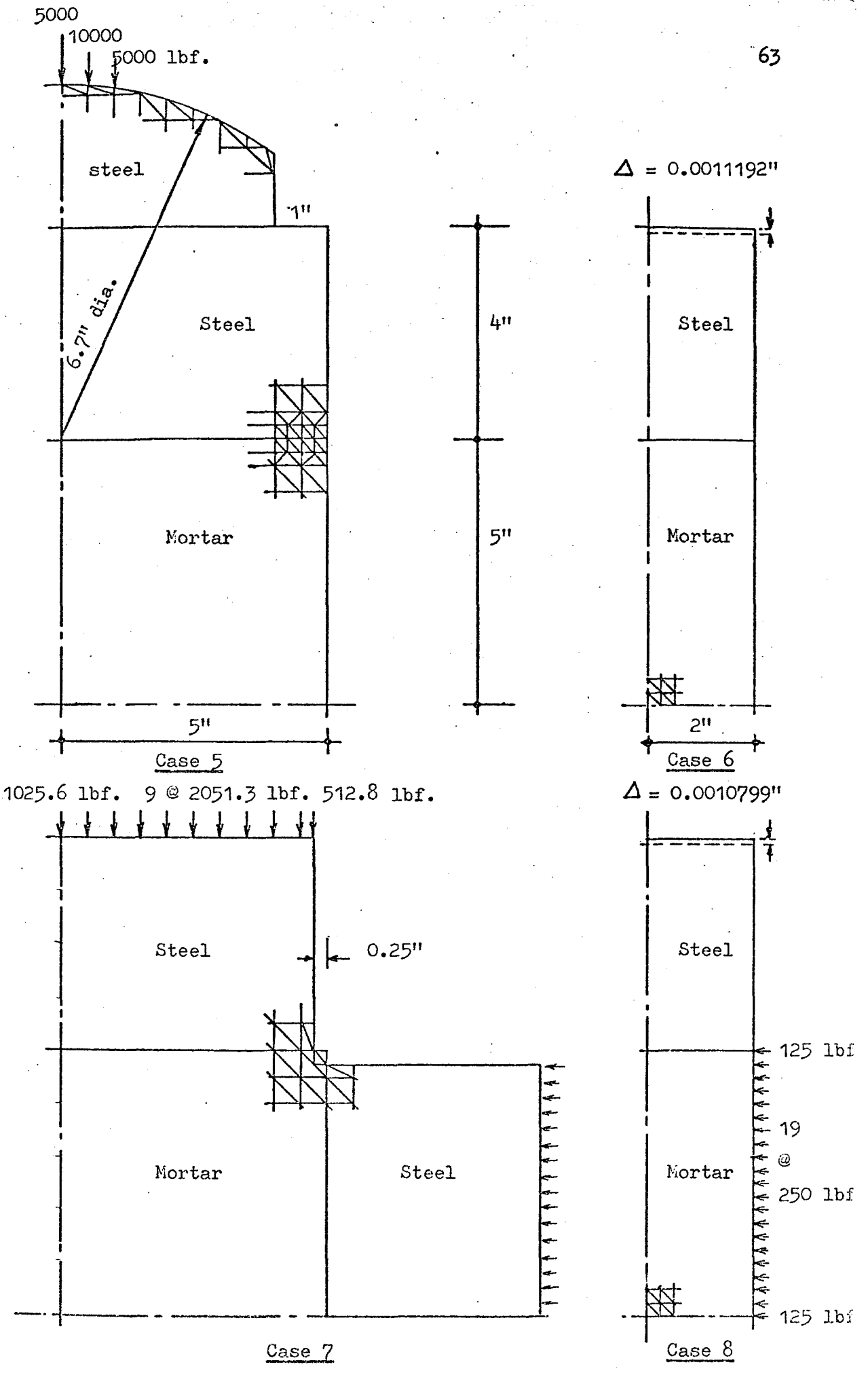
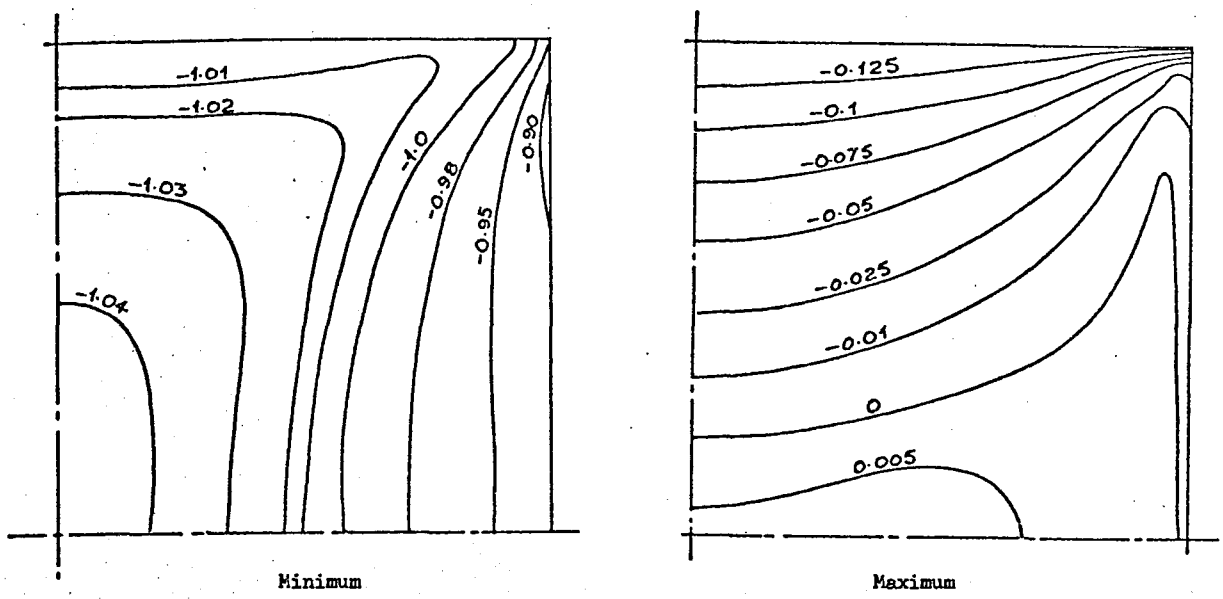
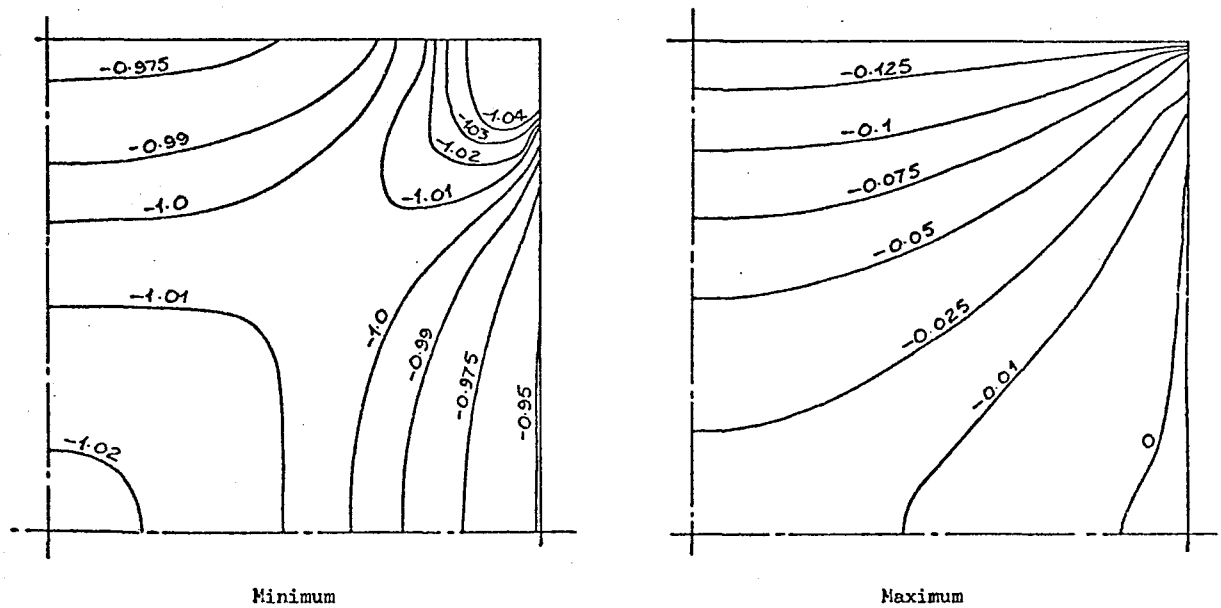


Figure 2.14. Diagrams showing dimensions, loading configurations and mesh layouts for Cases 5 to 8.

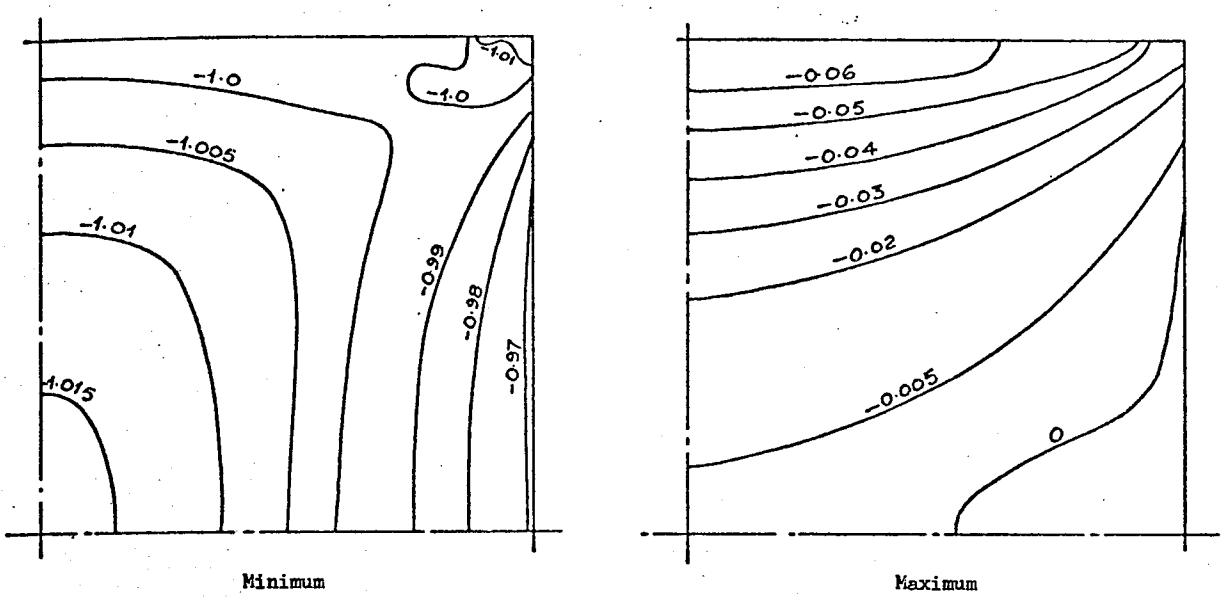


Case 1 Uniform Boundary Stress

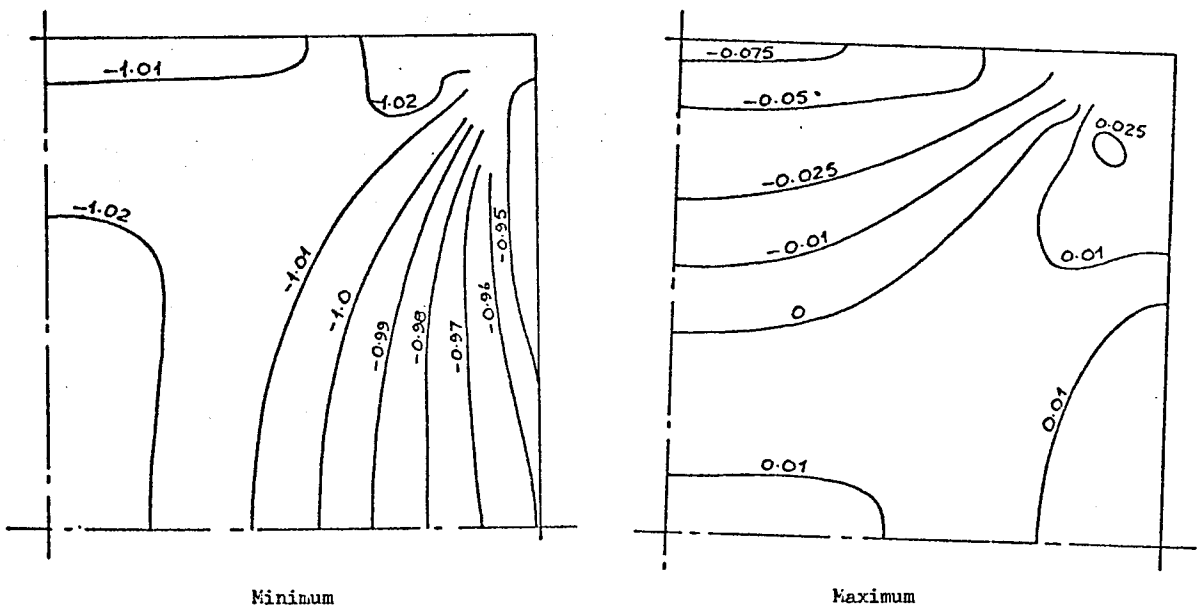


Case 2 Uniform Boundary Deformation

Figure 2.15. Distributions of principal stresses for slabs loaded under an average uniaxial compression of -1.0 applied directly to the boundary.

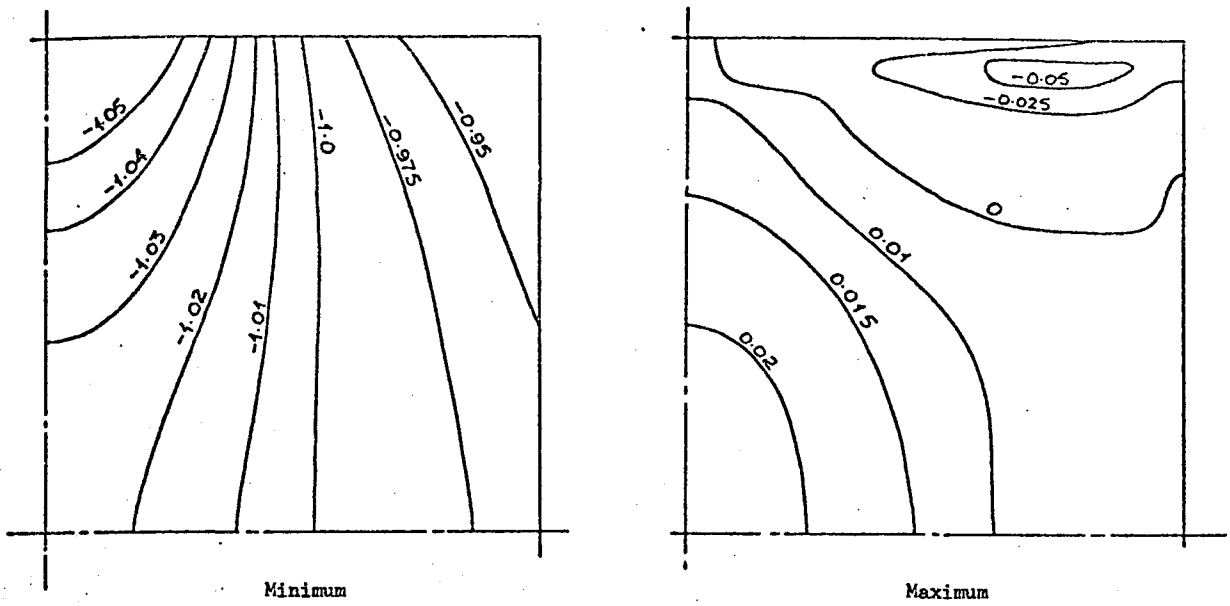


Case 3 Uniform boundary stress through platen of same cross-section as specimen

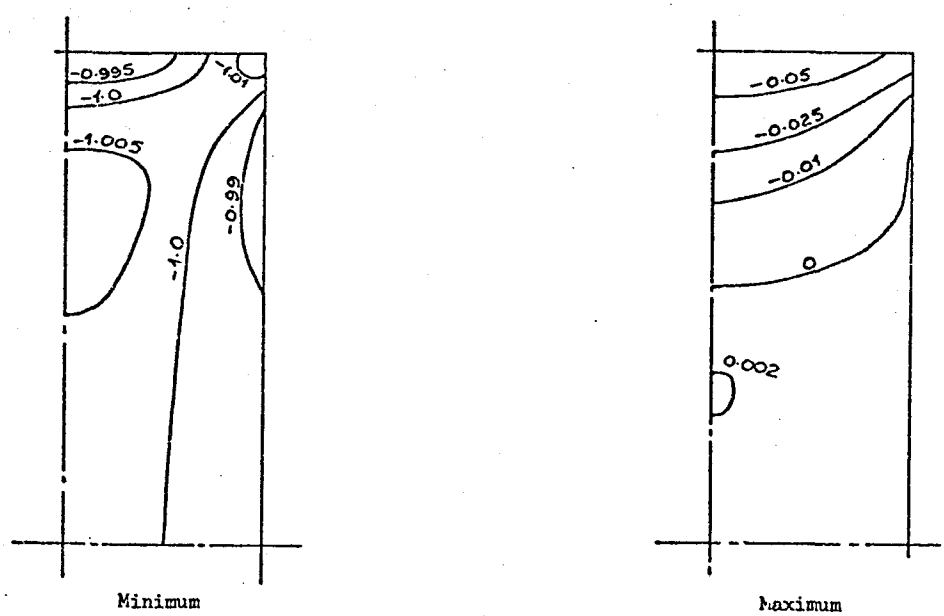


Case 4 Uniform boundary stress through platens of smaller cross-section than specimen

Figure 2.16. Distributions of principal stresses for slabs loaded under an average uniaxial compression of -1.0 applied through steel platens.

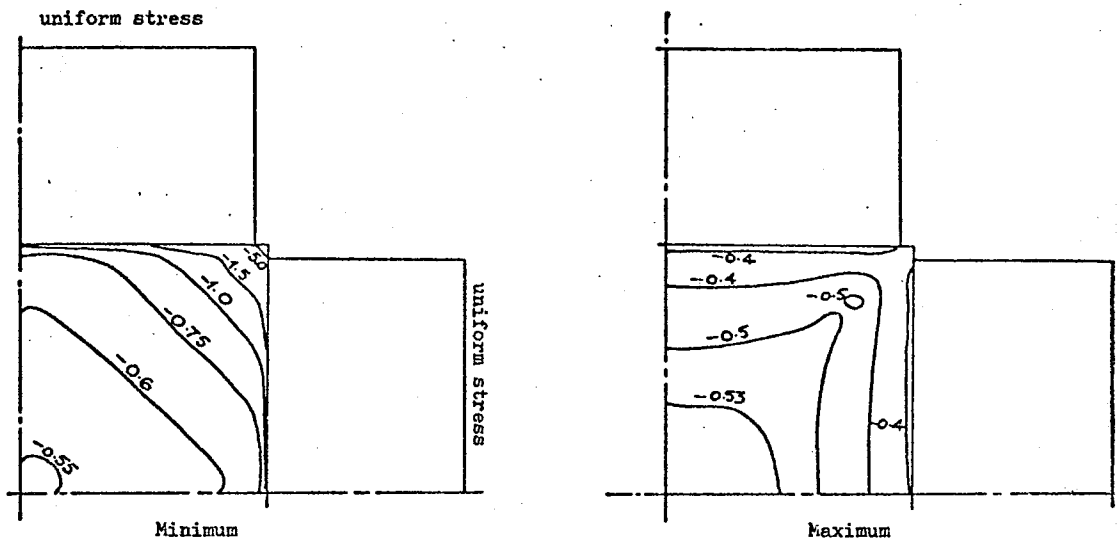


Case 5 Slab loaded through platen/spherical seating unit

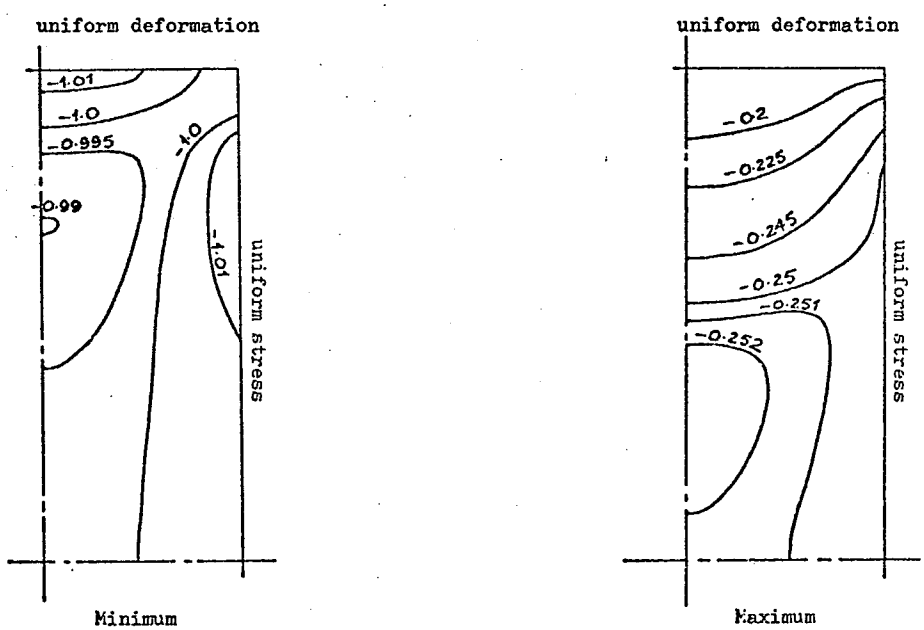


Case 6 Prism loaded through steel platens under uniform boundary deformation

Figure 2.17. Distributions of principal stresses for specimens loaded under an average uniaxial compression stress of -1.0.



(a) Case 7 Slab loaded under equal biaxial compression of -1.0, -1.0 through steel platens



(b) Case 8 Prism loaded under an average biaxial compressive stress of - 1.0 axially and -0.25 laterally

Figure 2.18. Distribution of principal stresses for specimens loaded under biaxial compression.

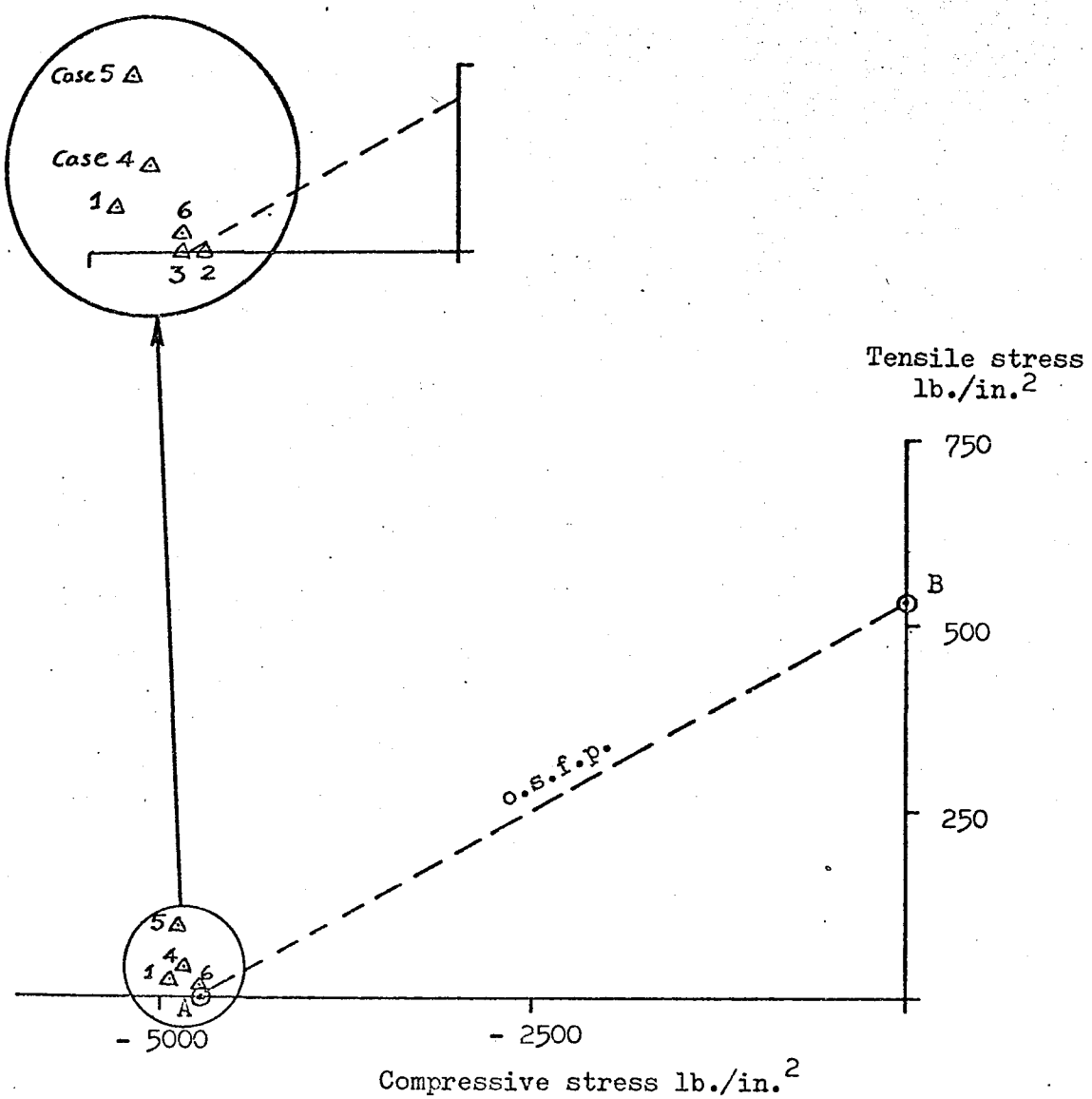


Figure 2.19. Envelope of stress at o.s.f.p. for mortar MA in the biaxial compression-tension zone showing the stress states at the most critical point for Cases 1 to 6 of the finite element analyses.

considerable local disturbances of stress and strain. At some points, therefore, the type and magnitude of the stress state may be such as to cause the initiation of fracturing. In order to assess whether a given combination of stress at a particular location within a specimen is likely to initiate fracturing, it is necessary to compare that state with an envelope defining the states of stress which are known to be critical in this respect. Such an envelope, marking the transition from subcritical to critical behaviour, can be obtained by subjecting the material to known states of stress and determining the set of conditions which cause the material to reach a given limiting condition.

A suitable method, used satisfactorily by the Concrete Materials Research Group for the assessment of criticality of strain conditions in a mortar matrix surrounding aggregate particles (14, 15, 57 and 58) involves representing the stress at each point within a specimen by co-ordinates in stress space, and comparing their position with an envelope defining the start of significant fracture processes. If the stress state at point under consideration lies inside the envelope then it is likely to be 'safe', while if outside then it is likely to be in an 'unsafe' or 'critical' condition.

In the present experimental analysis a mean stress of a given, but arbitrary, value has been induced within the material and the resulting distribution of stress has been assessed. A comparative measure of the criticality of different cases is given by measuring the distances from the stress co-ordinates corresponding to each point on the specimen to the envelope. The larger the distance, the greater will be the tendency for the material to fracture under the particular stress state.

As the method of analysis used constrains the stresses developed at any point to lie on the biaxial plane, a realistic method of estimating criticality is by comparing a particular stress state with a suitable envelope obtained under conditions of biaxial compression and compression-tension. One such envelope which, it is considered, represents a significant stage in the fracture process is that defining the onset of stable fracture propagation (o.s.f.p.) (see Section 4.5.). This envelope, therefore, is used as the criterion for judging the criticality of stress state.

Based on the results of the tests to determine the stresses at o.s.f.p. for the mortar mix used in Section 2.6., which the present analysis is intended to simulate, and the trends for a mortar under biaxial compression observed in Chapter 3, the envelope shown in Figure 2.19. has been constructed. Points A and B represent the measured stress states at o.s.f.p. for the mortar (Mix MA) under uniaxial compression and tension, respectively and the remainder of the envelope has been constructed as a linear relationship. Such an approximation does not depart significantly from the shape of the envelope as measured experimentally [8] and is sufficiently accurate for the present purpose. Details of the method of comparison for the various anlyses are described in the following sections.

2.5.5.2. Slab and Prismatic Specimens Under Uniaxial Compressive Load

Table 2.6. shows the stress conditions at the most critical point in the specimens for an applied average compressive stress of 1,000 lb/in^2. Each point has been judged as the most critical, for the particular case considered, by plotting all points for that case and comparing with the o.s.f.p. envelope. Since the arbitrary choice of applied stress (1000 lb/in^2) results in all stress coordinates lying inside the envelope, those lying closest to the envelope represent the most critical point. For ease of comparing the various cases, the resulting values have been scaled up by the ratio of the o.s.f.p. stress under uniaxial compression (4231 lb/in^2) to the average applied compressive stress used in the finite element analyses (1000 lb/in^2). These stress states (for cases 1 to 6) are indicated on Figure 2.19.

It is evident from Figure 2.19. that Case 5, where a concentrated load is applied through the spherical seating unit, induces the most critical stress state of the uniaxial cases considered, since the most critical point for this case lies farthest from the o.s.f.p. envelope. It also appears that Case 4, where the load is applied through platens of a smaller cross-section than the specimen, is more critical than Case 3 where the platen cross-section is the same as the specimen. Case 1, where the boundary stress is applied uniformly to a free surface of a specimen, is more critical than for the case where a uniform boundary deformation is induced (Case 2).

Case	Principal Stresses at Most Critical Point - lb./in.^{2}	
	Maximum	Minimum
1	+5	-1040
2	0	-990
3	0	-1003
4	+10	-1020
5	+20	-1030
6	+2	-1003

Table 2.6. Principal stresses at the most critical point in specimens subjected to a uniaxial compressive load to induce an average compressive stress of 1000 lb./in.^{2} as obtained from Finite Element analysis.

The critical stress state for the prismatic specimen (Case 6) is similar to those for Cases 2 and 3 and lies close to the trueuniaxial stress state.

The critical stress state for the prismatic specimen (Case 6) is similar to those for Cases 2 and 3 and lies close to the true uniaxial stress state.

2.5.5.3. Slab Specimens under Equal Biaxial Compression

Figure 2.18.(a) shows the considerable disturbance of stress when a slab is loaded under equal biaxial stress through steel platens attached rigidly to the surfaces of the specimen. The material within the central section of the specimen is under a state of near-uniform biaxial compression, but with a magnitude of approaching only approximately 50% of the applied stress. This confirms the results of previous theoretical (see Section 2.4.1.1.) and experimental analyses (see Section 2.4.2.1.).

2.5.5.4. Prismatic Specimen under Unequal Biaxial Compression

Figure 2.18.(b) shows for a specimen with H/W = 2.5, the considerable agreement between the stresses induced within at least the central 50% of the specimen and the applied stresses, even assuming complete fixity at the platen/specimen interface.

2.5.6. Conclusions

2.5.6.1. Introduction

The analyses, which for all cases are based on assumptions of plane strain and linear elasticity have, for all but the case of equal biaxial compression, resulted in stress distributions which are not particularly critical, as assessed by the criterion described in 2.5.5.1. This indicates that these assumptions may not realistically simulate practical loading conditions. However, the following conclusions, although not considered to provide a quantitative estimate of the stress concentrations likely to be encountered, are useful in that they indicate trends in behaviour.

2.5.6.2. Slab under Uniaxial Compression

(i) Laterally restraining the loaded boundaries of a specimen induces biaxial compression stress states near the loaded ends of specimens. The lateral component of compression reduces in magnitude towards the central zone of the specimen, and may change to tension in some cases.

(ii) For all cases the most critical stress state always occurs within the zone under combined compression and tension and it is, therefore, from this zone that failure will probably initiate.

(iii) For complete fixity of the loaded boundary, and a constant value of induced mean axial stress, a uniformly applied load (Case 1) induces larger and more critical stress concentrations than a uniformly applied deformation (Case 2).

(iv) For a uniformly distributed load applied through a thick steel platen, a more disturbed and more critical stress state is induced within the specimen if the cross-sectional dimensions of the loading face of the platen are not equal to those of the specimen.

(v) Load applied through a steel platen/spherical seating unit (Case 5) induces by far the most disturbed and critical stress state of all cases considered.

2.5.6.3. Prism with H/W = 2.5 under Uniaxial Compression (Case 6)

(i) Laterally restraining the loaded boundaries of a prism induces biaxial compression stress states near the ends. This compression decreases to zero at a distance of approximately H/4 from the ends, after which the stress state is compression-tension.

(ii) The most critical stress state lies within the zone under combined compression and tension, and failure will probably initiate from a position near the centre.

(iii) The stress state is slightly more critical than for a similarly loaded slab (Case 3) but both lie close to the true uniaxial case.

2.5.6.4. Slab under Equal Biaxial Compression (Case 7)

Considerable stress disturbances are induced when a specimen is loaded through steel platens rigidly attached to the specimen boundary, such that the central zone is under only approximately 50% of the applied stress.

This suggests that a test in which a specimen is loaded through steel platens, with some degree of restraint against movement at the platen/specimen boundary, will tend to overestimate the true biaxial strength of the material.

2.5.6.5. Prism with H/W = 2.5 under Unequal Biaxial Compression (Case 8)

(i) For combined loading, using steel platens and confining pressure, the induced stresses within the central 50% of the specimen are in close agreement with the applied boundary stresses.

(ii) Towards the rigid platens, the axial compressive stress tends to increase while the lateral compressive stress decreases. This suggests that failure should be initiated within the central zone.

The above would tend to support the choice of testing arrangement adopted for the triaxial compression test series described in Chapter 7.

2.6. Experimental Investigation of Stresses and Strains induced in Slab Specimens under Uniaxial Compression Load

2.6.1. Introduction

The analytical investigation described and discussed in 2.5. provides useful qualitative information on the type of stress disturbances likely to be encountered using various loading conditions. Even for the case of rigidly fixed boundaries, however, the resulting stress states do not appear to be as critical as would be expected from the differences in measured deformation and strength outlined in 2.4.

It is considered essential, therefore, to attempt to assess, from strain measurements, the complete stress pattern in a specimen of concrete or mortar under practical conditions of load. The uniaxial compression loading configuration has been adopted since it is only for this case that the material characteristics relating stress to strain (E and) can be evaluated without any serious doubts as to their validity.

The loading arrangement used to apply the load to the specimens is the rigid steel platen and spherical seating unit developed by Vile [8] for the uniaxial and biaxial compression facilities of the Complex Stress Machine (see Section 3.5.5.2. and Appendix 1). This was designed in order to apply uniform boundary strain to concrete and mortar specimens.

The investigation is divided into three parts as follows:-

Series 1

Measurements of the surface strains on the loading platen block to assess the effectiveness of the loading arrangements in applying uniform strain to the boundary of a slab specimen, and a similar assessment of the performance of the loading arrangement after being modified to minimise some of the measured loading disturbances.

Series 2

A measurement of the surface strains on an 'as cast' mortar slab specimen to evaluate the magnitude and direction of principal stress and strain in the specimen, using the loading arrangement developed in Series 1 with, and without, various materials interposed at the specimen/platen interface.

Series 3

(i) As Series 2 but using a mortar specimen with all surfaces ground plane and parallel with and without intermediate materials inserted at the platen/specimen interface.

(ii) As Series 3 (i) substituting 'Mortar platens' for the rigid steel platens, but without an intermediate material.

(iii) As Series 3 (ii) substituting 'Brush platens' for the rigid steel platens, but without an intermediate material.

2.6.2. Details of Mortar Specimens

2.6.2.1. Selection of Mix

The choice of maximum size of aggregate in the mix is partly governed by the size of electrical resistance strain gauge (E.R.S.G.) rosettes used for measurements of surface strain, and partly by the requirement for a specimen to be approximately representative of the heterogeneity of most specimens used in practice. As a compromise it has been decided to use the largest size of aggregate consistent with the use of 10 mm. long strain gauges, which were chosen so that a large enough number of individual strain values can be obtained over the specimen. The ratio of length of E.R.S.G./maximum size of aggregate is therefore slightly above 2, which would generally be considered to measure strain to within 7% of the average field value [8, 59, 60 and 61]. This is judged acceptable considering the relatively large number of rosettes used.

As the remainder of the mix parameters are not considered critical for this investigation it has been decided to use a mortar mix type MA designed for a previous investigation [8]. Details of the constituent materials and their proportions for this mix are given in Appendices 2 and 3 respectively.

2.6.2.2. Details of Slab Specimens

In addition to the three 4" x 10" x 10" slabs cast for the strain measurement test, three 4" x 4" x 12" prisms and three 4" x 4" x 20" tensile specimens were cast for determining the stress-strain relationships and ultimate strength under uniaxial load.

A further four 4" x 4" x 12" prisms were cast for use as mortar platens for the tests described in 2.5.4.

All specimens were prepared using rigid steel moulds constructed in accordance with tolerances based on those specified in B.S. 1881 [62].

The curing procedure adopted for all specimens is intended to mature the specimens under ambient laboratory conditions for a sufficient length of time to remove all significant effects of age from the test results. This is achieved by removing the specimens from the moulds 24 hours after casting, and placing them under water at 20°C. for 21 days. After this period the specimens are removed from the water and stored under initially wet hessian for 21 days, the hessian being allowed to dry out gradually under laboratory conditions. The specimens are then exposed directly to laboratory air for a minimum of eight weeks prior to being tested.

2.6.2.3. Choice of Maximum Stress Levels and Determination of Elastic Constants for the Mortar

Three prisms and three tensile specimens were cast from the same batch of mortar as the 10" x 10" x 4" slabs used in the investigations of stress distribution described in the following sections. These specimens were cured in the same manner as the slabs, namely 21 days under water, 21 days under damp hessian in the laboratory and a further 2 months exposed directly to laboratory air.

Three prisms were loaded to failure under uniaxial compression at a loading rate of 2000 lb/in^2 per minute and the corresponding maximum (lateral) and minimum (axial) principal strains measured continuously by 60 mm. electrical resistance strain gauges. The stress and strain relationships were analysed to determine the o.s.f.p. level (using the method described in 4.5.) and ultimate strength for each specimen. The principal results are given in Appendix 4.

The tensile specimens were loaded uniaxially at a loading rate of 100 lb/in^2 per minute and the variation of axial and lateral strains used to determine the o.s.f.p. level, which in all cases coincided with ultimate (see Appendix 4).

For the tests to assess the load transmission characteristics of the platen/seating loading arrangement (Series 1), where strains of relatively small value were measured on the steel platen block, it is necessary to apply as high a load as possible without exceeding the o.s.f.p. level for the mortar. A stress level of 4000 lb/in^2 was chosen to be below the lower 95% confidence limit for the mean o.s.f.p. level (4196 lb/in^2).

For the tests involving measurements of strain on the surface of mortar specimens (Series 2 and 3), where the strains were considerably larger, a lower stress level of 3000 lb/in^2 was chosen. This is considered essential to ensure that the mortar does not disrupt even at those points of the specimen at which stress concentrations were induced.

The elastic constants for the mortar at this stress level were evaluated from the three remaining mortar prisms by loading each prism to 3000 lb/in^2 and measuring the resulting maximum and minimum principal strains with 60 mm. electrical resistance strain gauges. Since the slab specimens were conditioned by cycling a number of times to the maximum stress before taking strain measurements, the prisms were also cycled at least fifty times before test. After the cycling process, the axial and lateral strains were measured at the 3000 lb/in^2 stress level, the test being repeated until the difference between successive reading for each gauge was less than $\pm$ 1 microstrain, which was the normal scatter of the measuring system.

The secant values for the elastic constants E and ν for each specimen are given in Appendix 4, the mean values being assumed to apply for the mortar slabs used in the platen restraint tests.

2.6.3. Test Series 1 - Assessment of the Load Transmission Characteristics for a Rigid Steel Platen Loading System

2.6.3.1. Introduction

The steel platen/spherical seating system designed for the Complex Stress machine is intended to be loaded by a 6" diameter hydraulic ram and to transmit the load so as to apply uniform strain to the 4" x 10" face of a 4" x 10" x 10" slab specimen, with no rotation of the spherical seating after initial contact (8).

To satisfy the above requirements the platen/seating arrangement has been designed as a composite unit, in mild steel, using the concept of a beam on an elastic foundation, the centre of rotation of the spherical seating being fixed at the centre of the loading face of the platen.

Although the dimensions and design of the platen unit appear sufficient to satisfy the requirement of applying uniform boundary strain, it was thought necessary to attempt to confirm this fact in a preliminary test series before embarking on the main series concerned with measuring the strain distribution in a loaded mortar specimen.

Results of the tests on the platen block, however, indicate considerable strain disturbances within the block, and a modification was made to the loading arrangement in order to improve the situation. The effectiveness of the modification was checked by repeating the tests.

2.6.3.2. Testing Arrangement

The loading arrangement used for the investigation was designed primarily for use in the Complex Stress machine. However, use of this machine involves a lengthy process for setting up specimens for test, and so the procedure has been simplified by transferring the specimen and loading unit to an Amsler 300 tonf. uniaxial compression testing machine. This machine combines excellent load measuring characteristics with the facility for accurately maintaining load. The 6" diameter loading ram fitted to the Complex Stress machine is simulated in the testing arrangement by using a

6" diameter steel disc bearing on the top face of the female seating unit. Details of the arrangement are shown in Figure 2.20. which also shows the layout of the strain gauge rosettes on the surface of the main rigid steel platen block. The outputs from the gauges were measured and recorded by a Solartron Automatic Data Logger.

2.6.3.3. Test Procedure

The mortar specimen and loading arrangement were conditioned prior to test by cycling the system at least 25 times from zero up to a maximum load which induced an average stress of 4,000 lb/in^2 in the specimen. This stress was kept well below the o.s.f.p. level for the mortar in order to prevent internal disruption of the material, and to enable the same specimen to be used for a relatively large number of individual tests.

For the main tests, the load maintaining the facility of the testing machine was used to hold the load at a convenient value (which induced an average compressive stress of 3874 lb/in^2 in the mortar specimen) while the 60 individual strain gauges were scanned by the Solartron Automatic Data Logger at a recording rate of 2 channels per second.

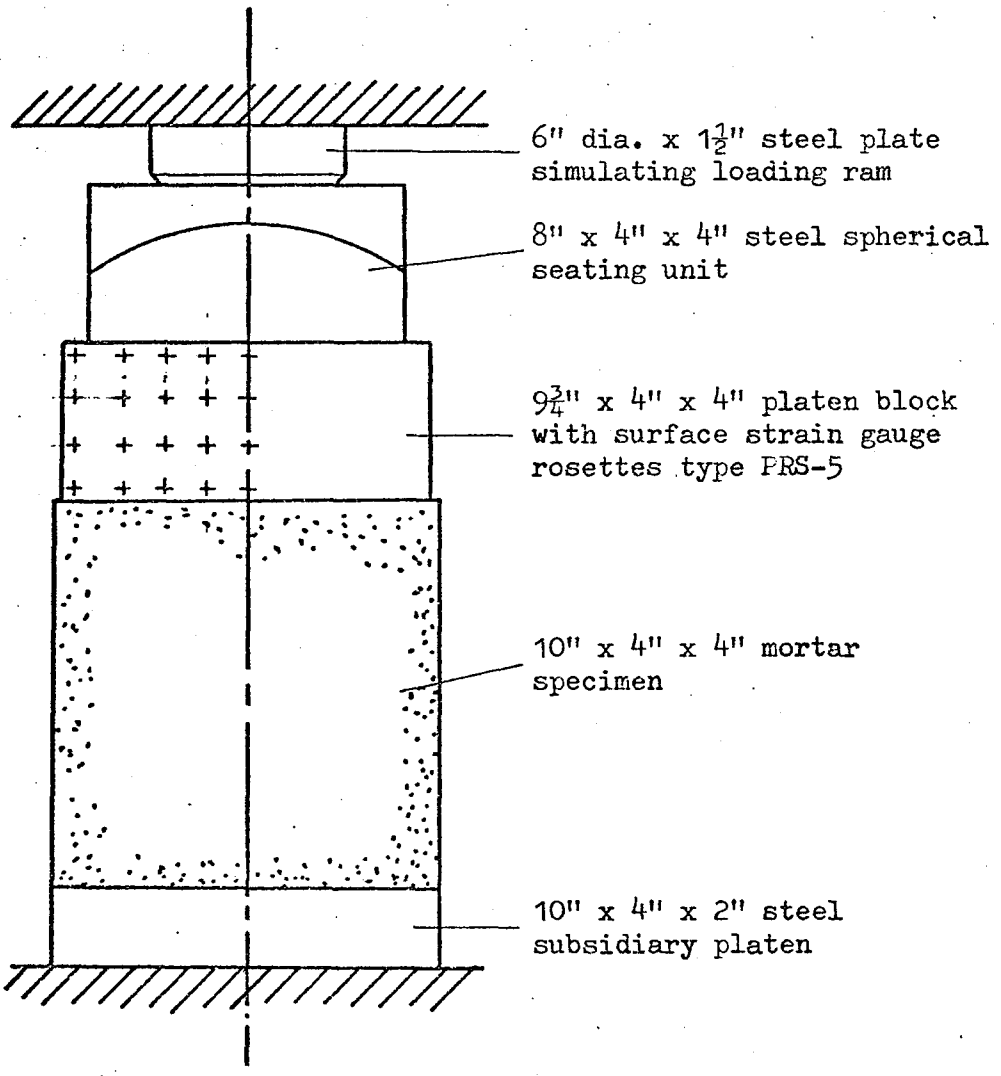
Each test was repeated until the strain difference between the unloaded and loaded condition for each strain gauge remained within $\pm$ 1 microstrain, which was the normally expected scatter of the measuring system.

2.6.3.4. Test Results

The principal strains and their directions are calculated from the three corrected strains measured by each rosette using standard relationships. In deriving the magnitudes of the associated principal stresses a condition of plane stress is assumed, together with values of E and ν of 30×10^6 lb/in^2 and 0.3 respectively for the steel.

The variation of minimum principal strain across the line of rosettes nearest to the specimen face, as a proportion of the mean minimum principal strain across the platen for the same rosette positions, is shown in Figure 2.21.

The isobars and isostatics of minor principal stress derived from the values of principal stress at each rosette position is shown in Figure 2.22.



All steel contact surfaces ground to ± 0.0001"

Figure 2.20. Schematic diagram showing testing arrangement for determining strain distribution over the surface of a rigid steel platen under uniaxial compression

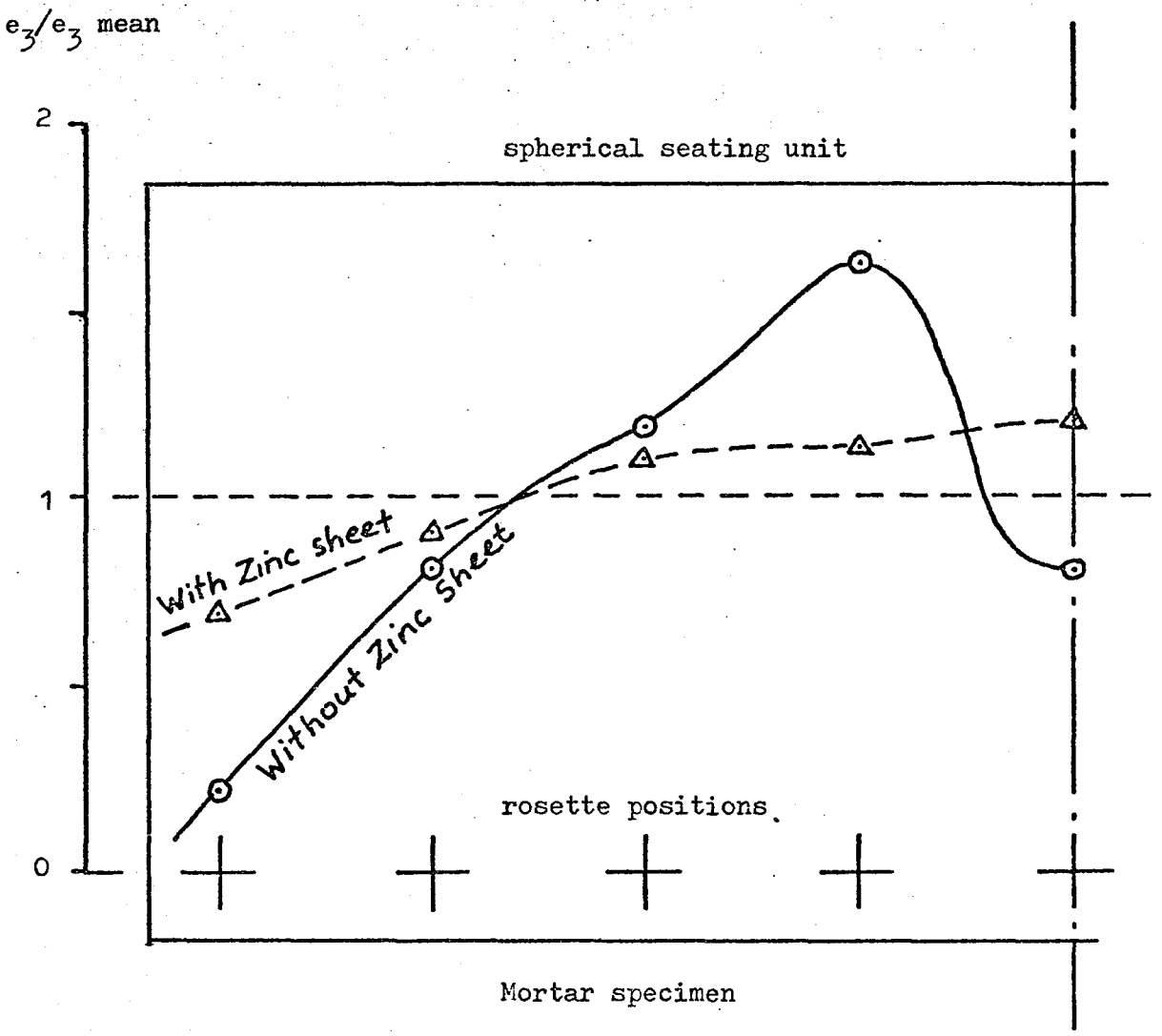
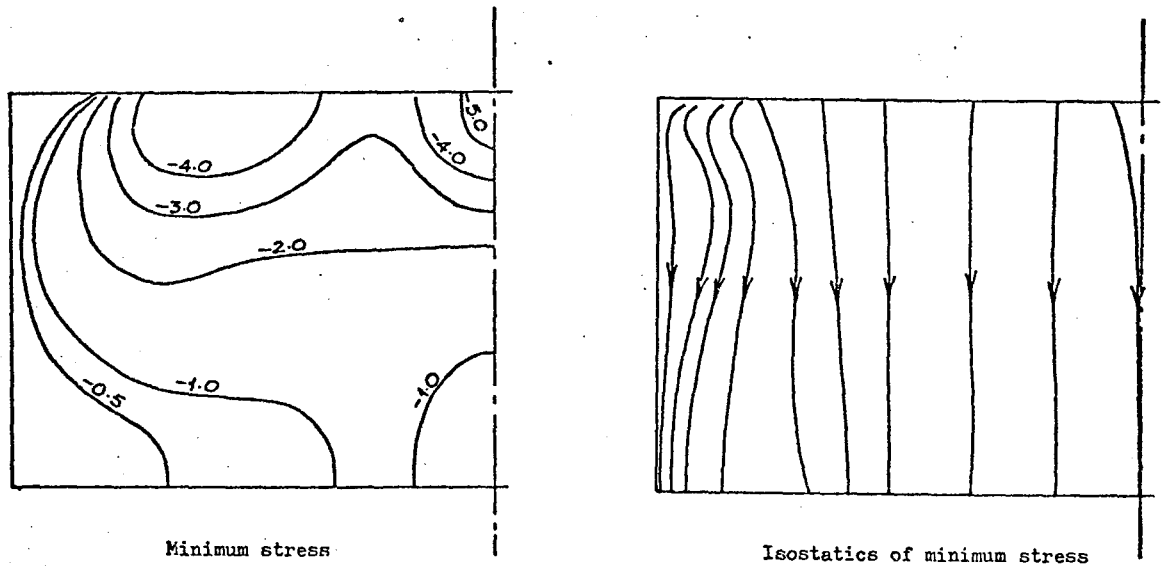
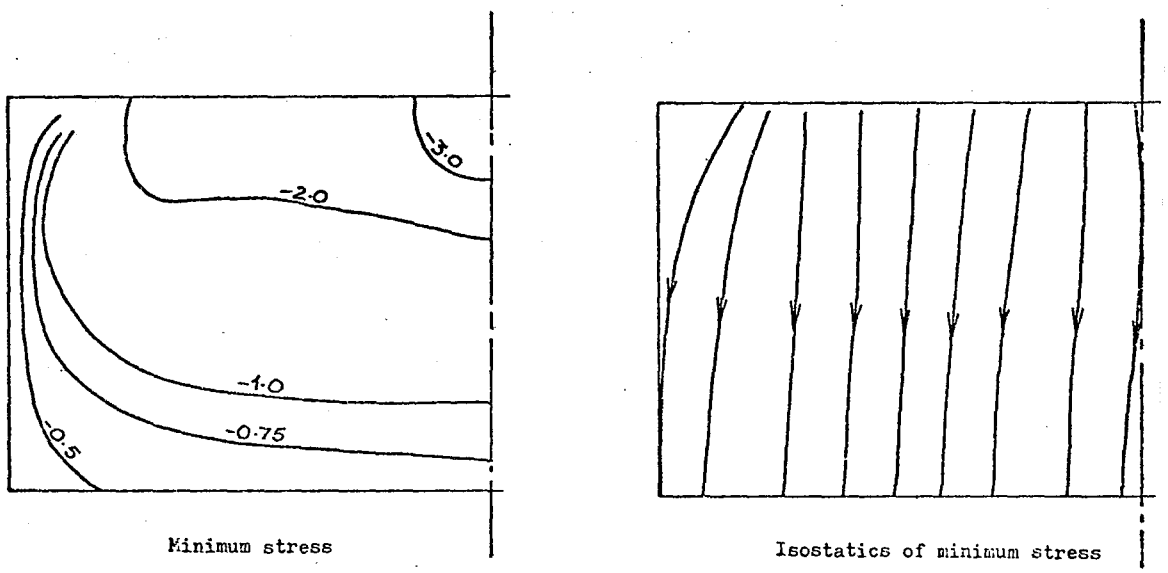


Figure 2.21. Distribution of minimum principal strain near the loading face of the platen block under an average applied uniaxial compressive stress of 3874 lb./in.^{2} with and without zinc sheet between the platen and seating unit.



(a) Without zinc sheet at platen/seating interface



(b) With zinc sheet at platen/sealing interface

Figure 2.22. Normalised isobars and isostatics of minimum principal stress for a rigid steel platen block loading a mortar slab and loaded by a ram and spherical seating assembly, with and without a zinc sheet at the interface, under an average applied uniaxial compressive stress 3874 lb./in.^{2}.

2.6.3.5. Discussion of Results

Figure 2.21 indicates that the loading arrangement does not apply uniform strain to the surface of a mortar slab specimen, as assessed by measurements of minimum principal surface strain near the platen loading surface. The corresponding calculated minor principal stress in the block increases from zero at the edge of the block to a maximum near the centre, and the disturbances in the isostatics of minor principal stress, shown in Figure 2.22.(a) indicate that this may be due to the characteristics of the contact surface between the platen and the male seating unit, as these disturbances are particularly evident near the edge of the seating unit.

The disturbances of strain throughout the whole platen block are also evident from Figure 2.22.(a) which show, in particular, high stress concentrations beneath the centre of the seating unit of up to five times the average applied stress on the loading face of the platen block. This is further evidence that the interface between the seating unit and the platen may be the main cause of the non-uniformity of loading.

2.6.3.6. Conolusions

It must be emphasised that the following conclusions are based on measurements of surface strain and corresponding surface stresses calculated assuming elasticity.

Examination of Figure 2.22.(a) shows that the average minimum principal stress across sections of the platen block perpendicular to the loading direction decreases to values below the average applied stress, as the loading face of the block is approached. Thus the surface strains and stresses are probably not representative of those within the body of the block as illustrated in Figure 2.23. However, since the internal stress and strain distribution cannot be determined, the surface measurements only are available to assess the efficiency of the loading system and, on this basis, the system does not apply uniform strain.

This inefficiency is probably due to the properties of the spherical seating unit/platen block interface since it is adjacent to this interface that high stress concentrations and disturbances are found.

The zone near the edge of the seating unit is under a particularly disturbed state of strain and stress as illustrated by the isostatics given in Figure 2.22.(a).

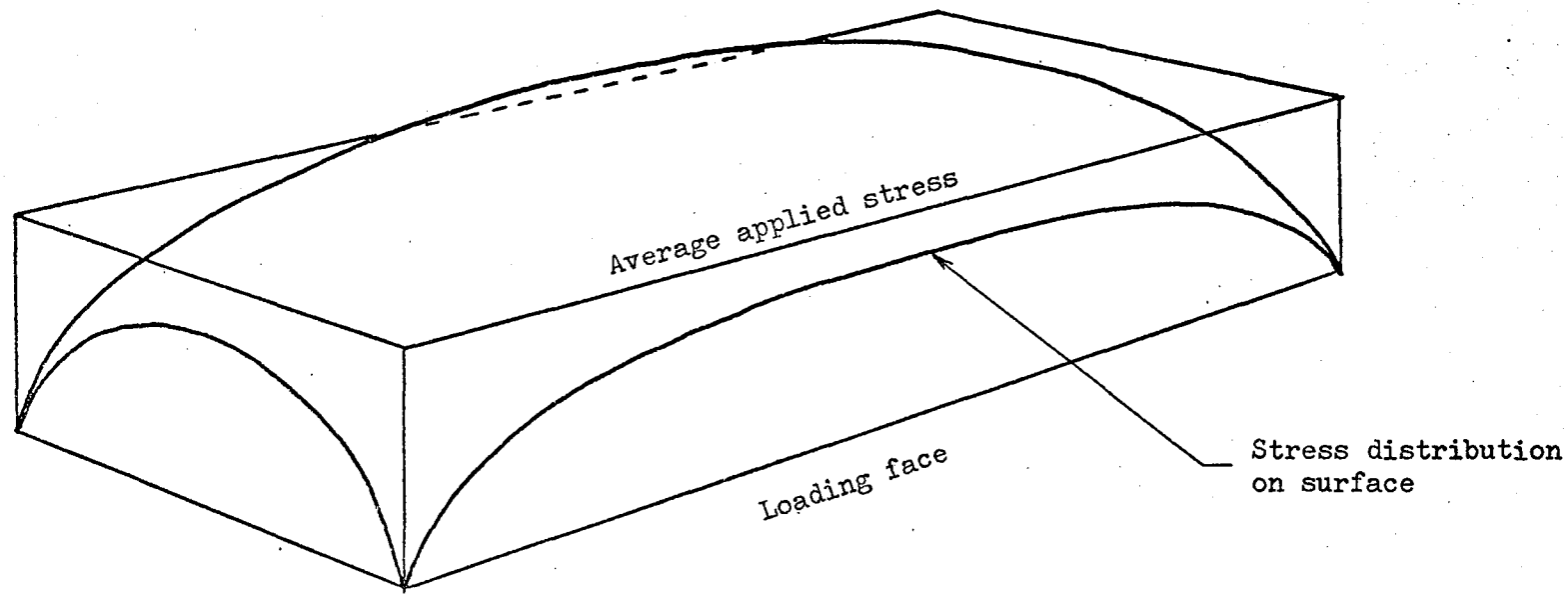


Figure 2.23. Schematic diagram showing possible distribution of minimum principal stress near the loading face of a platen block when applying a uniaxial load to a specimen.

In the light of the above, the most effective way of improving the load application characteristics of the loading arrangement would seem to be by modifying the seating unit/platen block interface so as to allow some 'bedding down' under load.

The method adopted to achieve this is to insert a relatively soft material at the interface. A 0.0035" thick zinc sheet has been found to be the most suitable of the various materials investigated, and the improved effectiveness of the modified arrangement is demonstrated by reference to Figure 2.21. which shows more uniform strain near the loaded face of the platen block.

Further confirmation of the improved load transmission characteristics is given by Figure 2.22.(b) which, when compared with Figure 2.22.(a) for the loading system without the zinc, show considerably less disturbed isostatics and a more uniform minimum principal stress distribution respectively.

It should be pointed out that other methods of improving the loading arrangement were investigated, including inserting various thicknesses of mild steel stiffening plates between both the ram and spherical seating units and/or between the seating unit and the platen block. Inclusion of the plates, however, produced no significant improvement in measured surface strains and so the loading arrangement with the zinc sheet was adopted for the tests to determine the stress distribution in a mortar specimen, which are described in the following section.

2.6.4. Test Series 2 and 3 : Evaluation of the Stress Distribution induced in Mortar Specimens under Uniaxial Loading applied through Rigid Platens with and without interfacial materials or 'Non-rigid' Platens

2.6.4.1. Introduction

As previously mentioned, frictional restraint effects at the platen/specimen interface can lead to large stress disturbances within specimens of material tested using rigid-platen loading devices. Many attempts have been made to overcome the problem by inserting various materials between the specimen and the platens. However, reference to the published work on the subject (see 2.4.2.) discloses a serious lack of knowledge regarding the actual stress induced in the specimens by the various systems adopted. This uncertainty regarding the stress conditions within test specimens has led

to much criticism of the validity of the results of tests performed under rigid-platen loading.

Assessment of the stress conditions within specimens is considered essential by the Author, not only to prove or disprove the validity of available test results, but also to provide a basis for the choice of a reliable loading method to study the behaviour of concrete under multiaxial stress states in order to provide valid design information.

Ideally, for the above purposes the stress state in specimens should be assessed under multiaxial, as well as uniaxial, loading conditions. However, the only method of determining stress state relies on measuring the strain state and converting this to stress via a knowledge of the relationship between stress and strain.

As the relationships between stress and strain can only be evaluated reliably under uniaxial loading conditions, using specimens of a suitable shape to minimise the end restraint effects, this is the only stress state which can be studied.

The investigation described in the following sections is, therefore, concerned with uniaxial compressive loading only, using various materials interposed between the rigid platens and the specimen and also by using 'non-rigid' platens. It should be noted, however, that, in many cases, measurements of strain showed multiaxial stress states to exist at least on the specimen surface, which obviously could not be evaluated with complete accuracy using material constants obtained from uniaxial tests.

The various intermediate materials and platen types used are chosen as a result of studying previous work on the subject described in 2.4.2. and can be broadly classified into three main groups as follows:-

(a) intermediate materials which, when used with rigid platens attempt to reduce interfacial friction between the specimen and the platen;

(b) intermediate materials which 'bed down' under load to 'even-out' the stress concentrations due to uneven contact between the specimen and rigid platen without, it is hoped, inducing lateral tensile or compressive restraint;

(c) non-rigid platens which, on applying stress to the surface of specimens, are intended to deform laterally to the same extent as the specimen at all stages of loading and thus exert no restraint.

In addition a fourth class of materials have been used where it is attempted to match the lateral deformational characteristics of the specimen such that

$$(\nu/E)_{insert} \simeq (\nu/E)_{specimen}$$

The test commenced with Series 2 using an 'as cast' mortar slab specimen which had undergone no surface treatment prior to test. During the course of the tests it was noted that slight irregularities on the face of the specimen seriously affected the stress distribution (as noted in 2.4.2.). Similar effects were noted due to dimensional irregularities caused partially by mould tolerances but mainly by differential shrinkage of the specimen after casting. Accordingly, a further test series (Series 3), similar in scope to the first but using selected interfacial materials and platen types was conducted, using a slab specimen which was ground all over to a tolerance of approximately 0.001" just prior to test.

2.6.4.2. Testing Arrangement

For the tests conducted using interfacial materials, the 4" x 10" x 10" slab specimen is loaded in each case through the modified loading unit from the complex stress machine. This modification, effected by inserting a 0.035 thick zinc sheet between the platen and the spherical seating unit, is shown in Section 2.6.3. to significantly improve the stress and strain state in the platen near the platen/specimen interface and over the remainder of the platen surface.

The testing arrangement, essentially the same as that used in Series 1 and loaded using the same Amsler Testing Machine (see Appendix 1), is shown in Figure 2.24., together with the layout of the rosettes of 10 mm. long strain gauges on the mortar slab. A general view of the system is shown in Figure 2.25.

For the testsconducted using 'non-rigid' platens, the testing arrangement remains essentially the same, but with the steel block replaced by the particular platen.

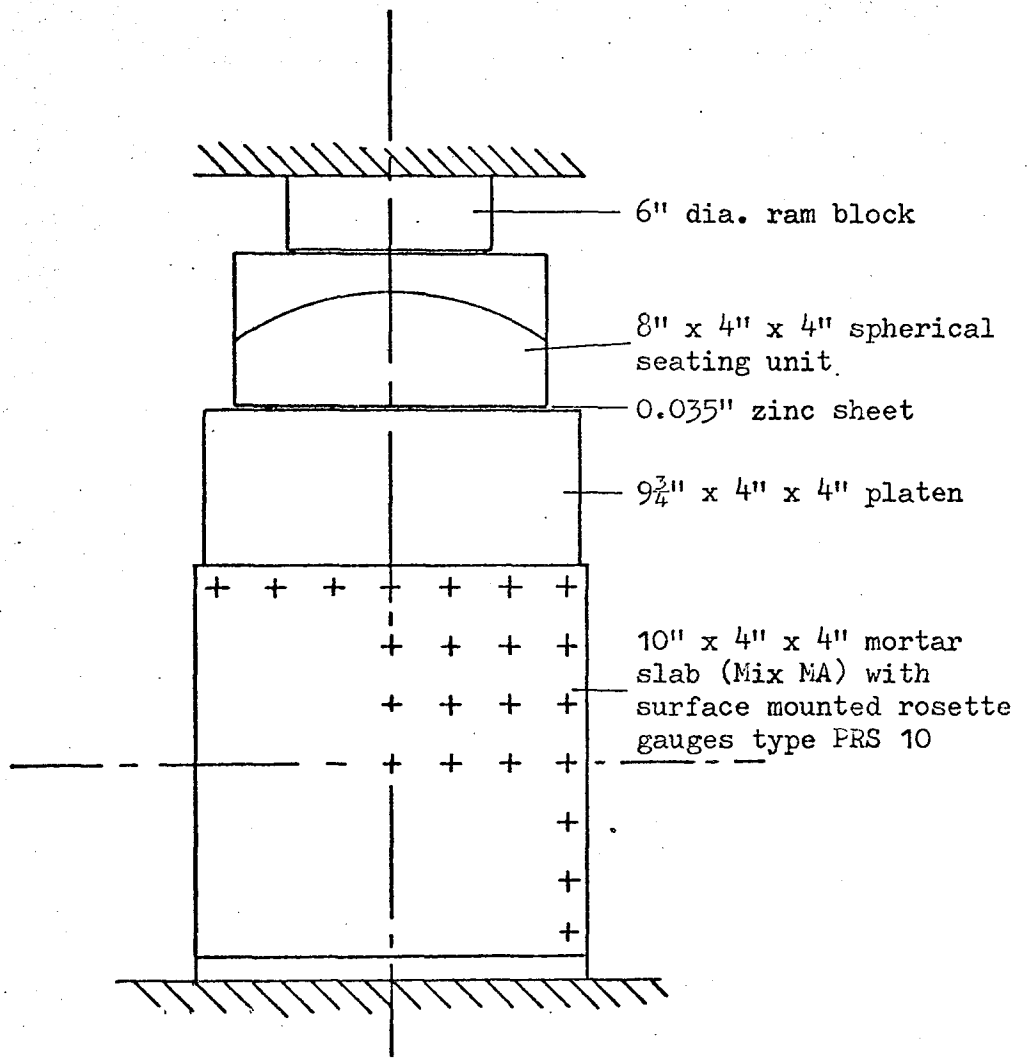


Figure 2.24. Schematic diagram showing arrangement of platen/spherical seating unit on strain gauged mortar specimen for determining surface stress distribution under uniaxial compression.

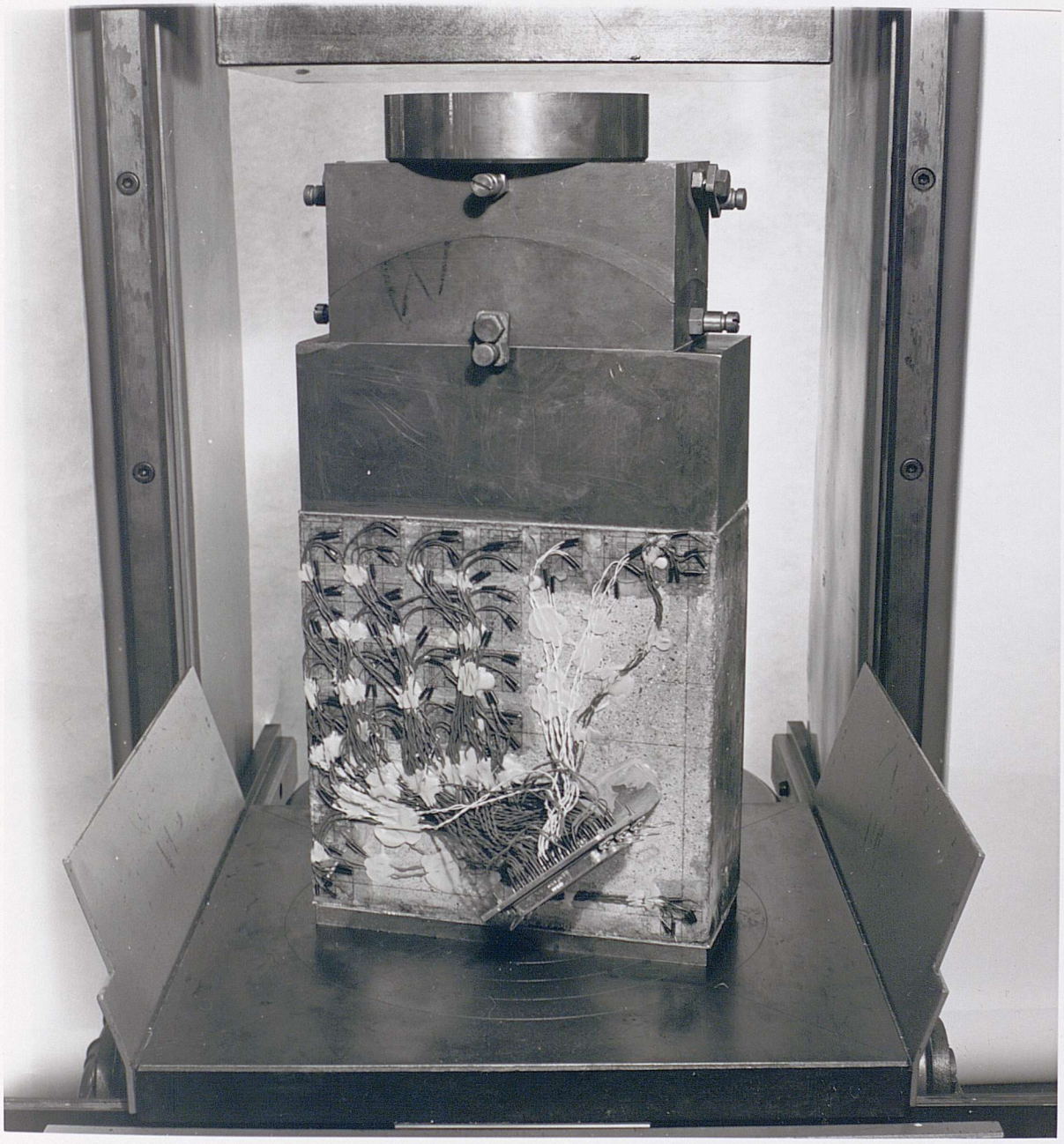


Figure 2.25 General view of strain-gauged mortar slab and rigid platen loading arrangement in testing machine.

Details of the various materials interposed between the specimen and platen block and the types of 'non-rigid' platens investigated are given in the following section:-

2.6.4.3. Details of Intermediate Materials and 'Non-rigid' Platens

As already discussed, the intermediate materials and platen types have been chosen with reference to the relevant published work summarised in 2.4.2. The materials are classified into four main groups as shown in Table 2.7.

2.6.4.4. Test Procedure

The mortar specimen and loading arrangement were conditioned prior to each test by load cycling at least ten times from zero up to the maximum load which induces an average compressive strength of 3200 lb./in.^{2} in the mortar.

The intermediate material, if any, was then inserted between the platen and specimen and a load of 52.8 tonf. applied using the load maintaining facility of the Amsler Testing Machine. This load is calculated to apply an average stress of 3000 lb./in.^{2} to the mortar slab.

The resulting induced strains over the surface of the slab were measured using a Solartron Data Logger recording at a rate of 2 channels per second.

The above procedure was repeated with the specimen and loading arrangement rotated through 180° in the testing machine to check the effects of possible incorrect alignment. Insignificant differences were found in the strain distributions for the two tests and the distributions shown are based on the mean values.

2.6.4.5. Test Results

Figures 2.28. to 2.31. show, for the tests of Series 2, the distributions of maximum and minimum principal stress over the surface of the slab specimen under the various loading configurations. The magnitudes of the principal stresses have been calculated from the strains indicated by the rosette gauges by assuming plane stress relationships and values of E and ν for the mortar (as measured in 2.7.3.1.) of 4,750 x 10^6 lb./in.^{2} and 0.155 respectively. The corresponding results for Series 3 are given in Figures 2.32. to 2.34. All distributions shown in Figures 2.28. to 2.34. are represented in normalised form with respect to the average stress of 3000 lb./in.^{2} applied to the mortar slab.

Test Series	Material or Platen Type	Total Thickness (in.)	ν/E Value	Remarks
Intermediate Materials with similar Lateral Deformational Properties to Specimen				
2	Zinc	0.035	-1.6×10^{-10}	
2	Aluminium	0.009	-3.4×10^{-10}	3 sheets
Intermediate Materials which primarily 'bed-down' under Load				
2 and 3	Jointite gasket material	1/16	-	Used with 0.003" thick aluminium sheet adjacent to specimen to minimise extrusion effects.
Intermediate Materials which primarily reduce Interfacial Friction				
2 and 3	Febcure 'Super 90'	0.0012	-	2 coats brushed on surface at 24 hour intervals. Final coat applied 24 hr. prior to test.
2	Stauffer's Grease	-	-	Pad consisting of thin layers of grease between 4 layers of polythene.
2 and 3	M.G.A. Pads	-	-	Pad consisting of 0003" thick hardened aluminium adjacent to specimen with grease (with 3% M_oS_2) film. Melinex polyester film above grease.
'Non-rigid' Platens				
3	Mortar Platens	4	-3.26×10^{-10}	Ground surfaces with same cross-section as specimen.
3	Brush Platens	4	-	See Figures 2.26 and 2.27 for details

Table 2.7. Details of intermediate materials and platen types used in Series 2 and 3.

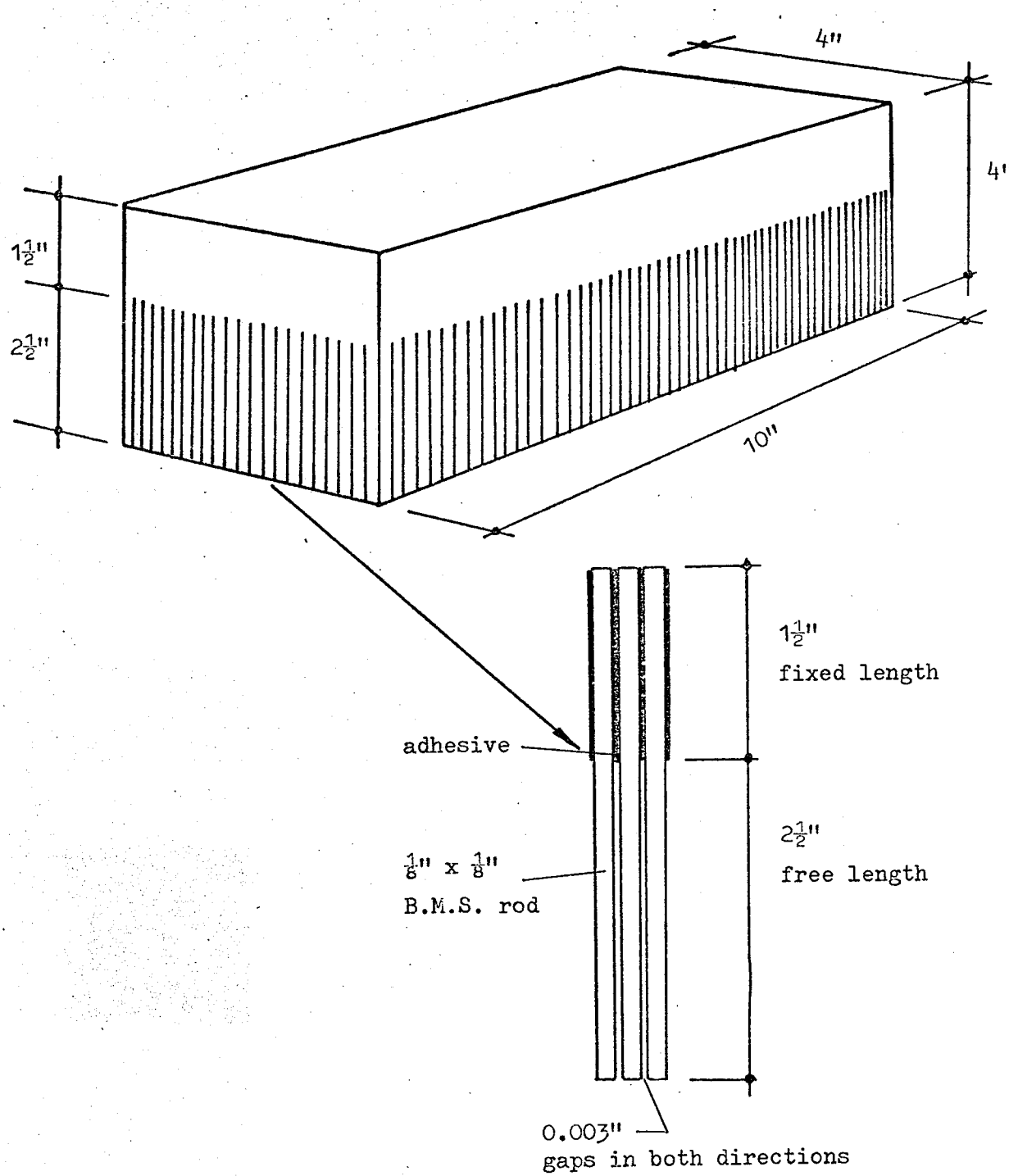


Figure 2.26. Schematic diagram showing details of brush platens.

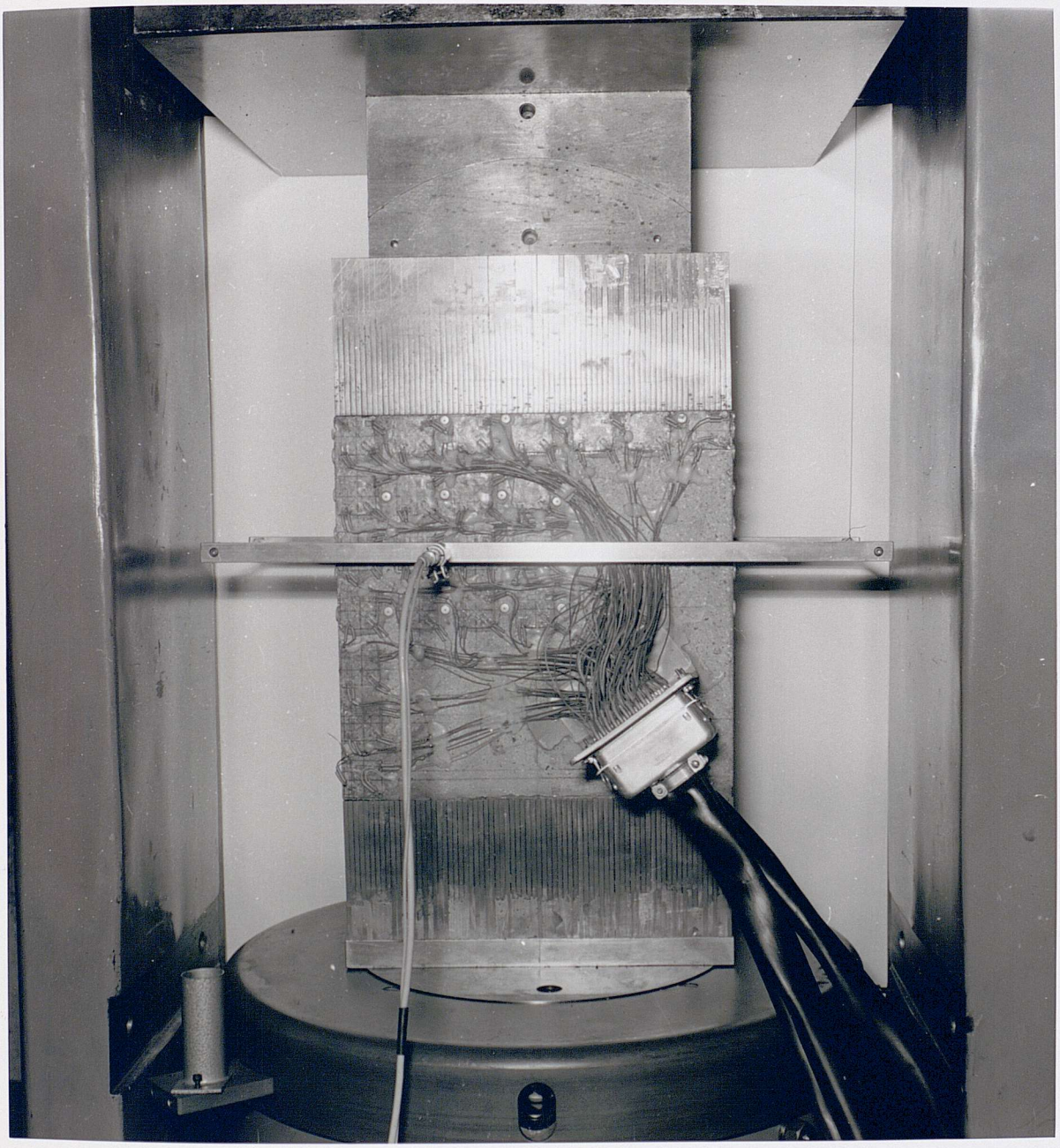
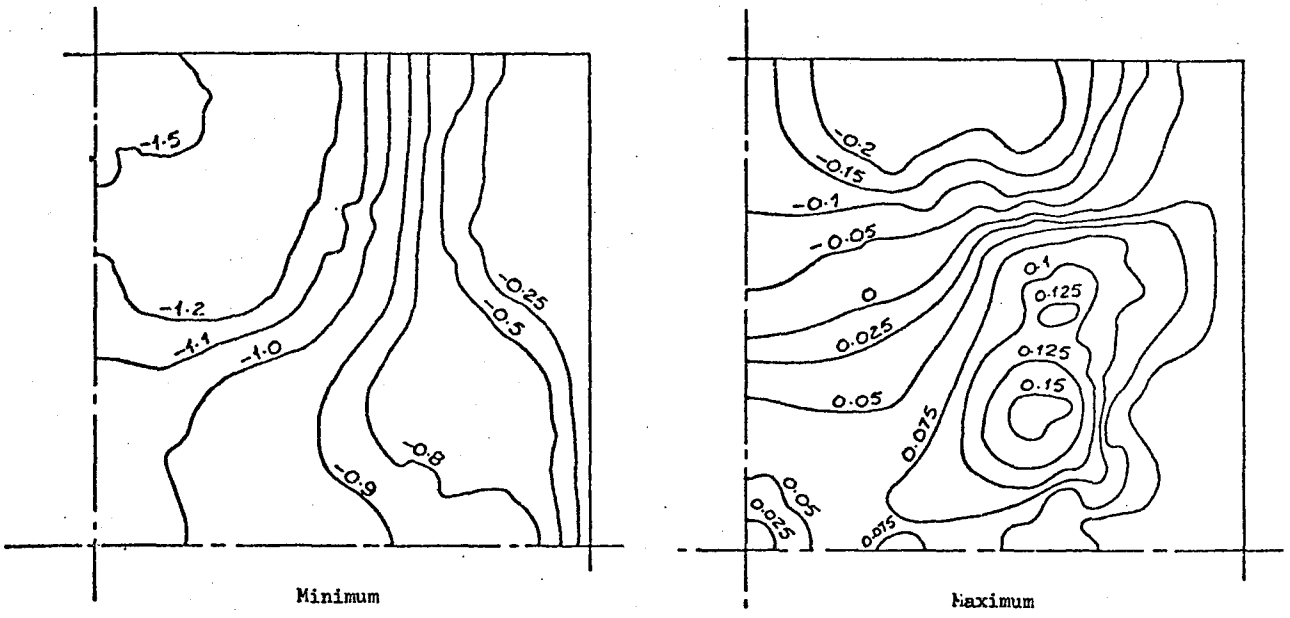
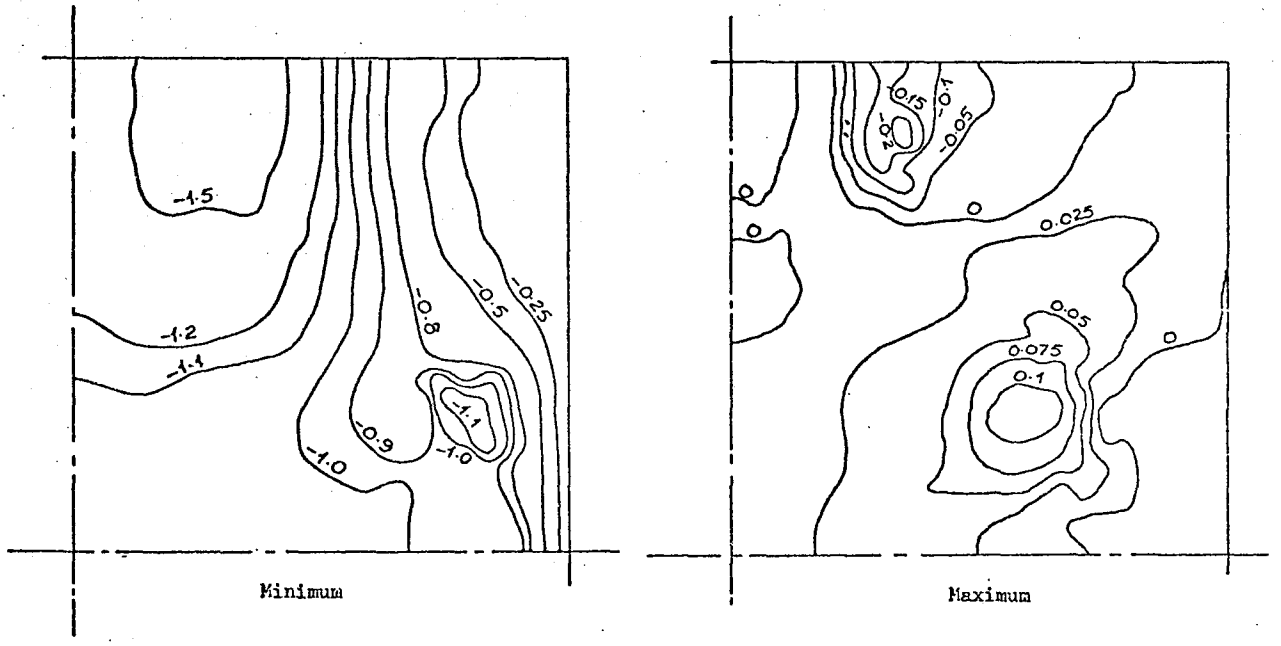


Figure 2.27. General view of strain gauged mortar slab and brush platen loading arrangement in testing machine.

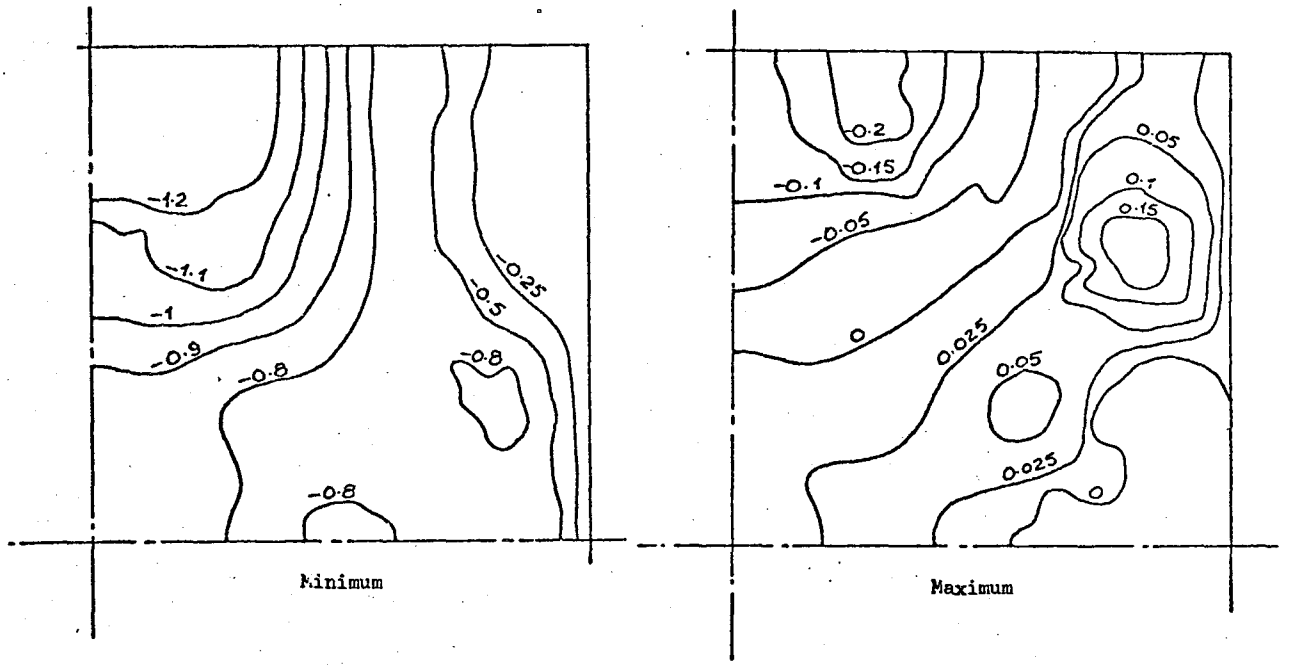


(a) No intermediate material

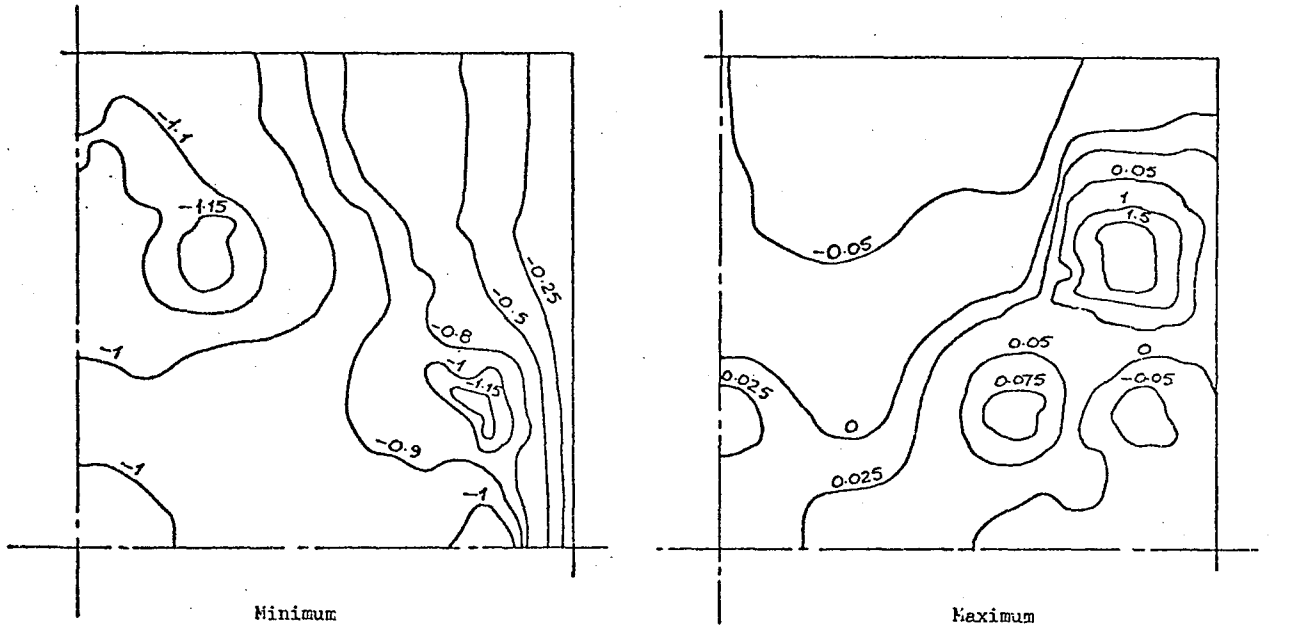


(b) 0.035" Zinc Sheet

Figure 2.28. Distributions of principal stresses over the surface of the as-cast mortar slab under an average compressive stress of -1.0 applied through a steel platen with and without an intermediate material (Series 2).

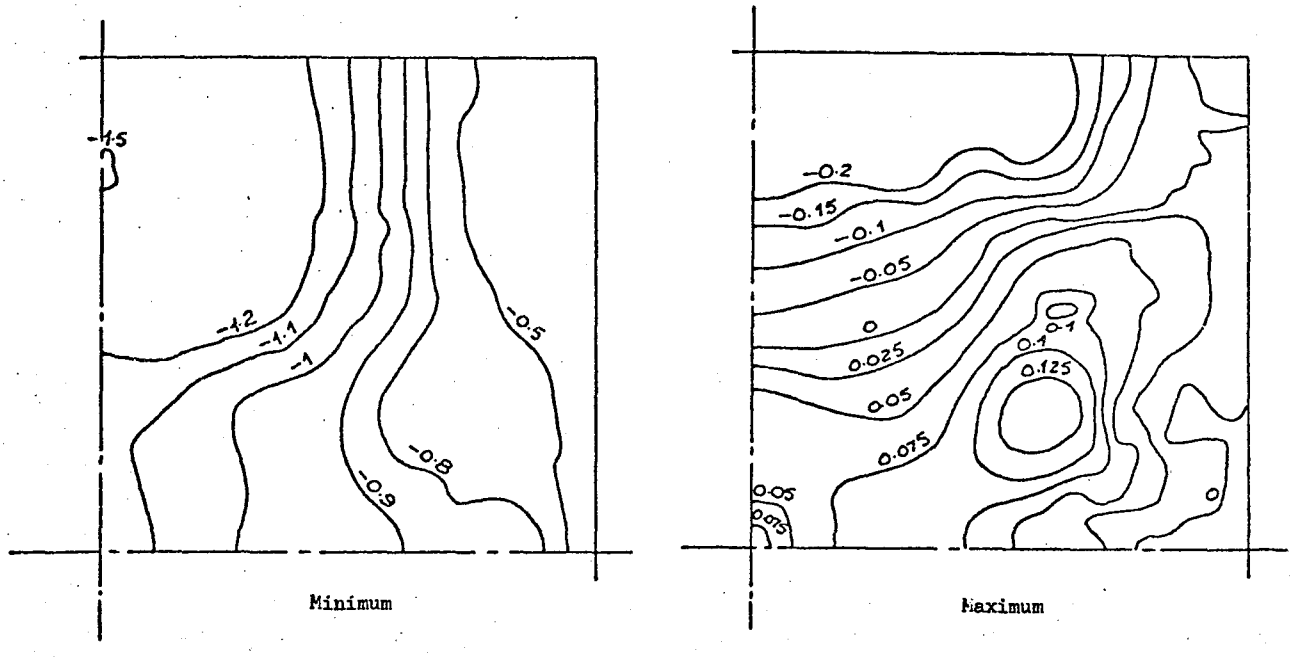


(a) 0.009" Aluminium Sheet

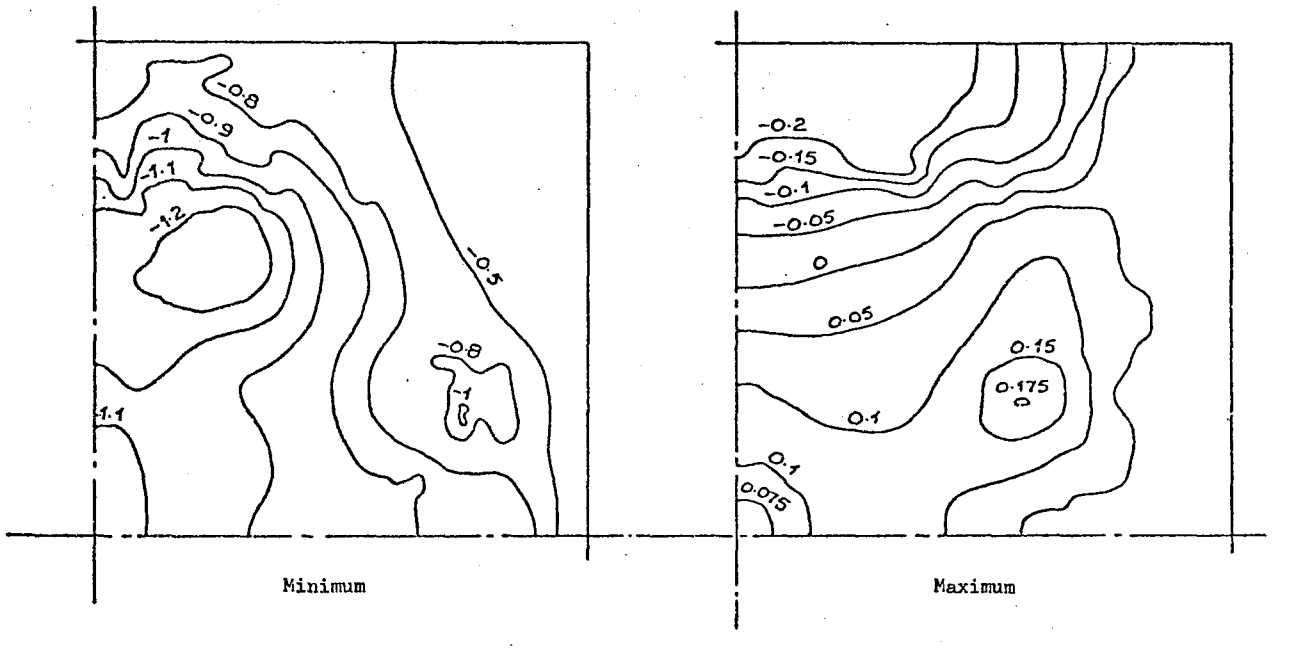


(b) 1/16" Jointite

Figure 2.29 Distributions of principal stresses over the surface of the as-cast mortar slab under an average compressive stress of -1.0 applied through a steel platen with various intermediate materials (Series 2).

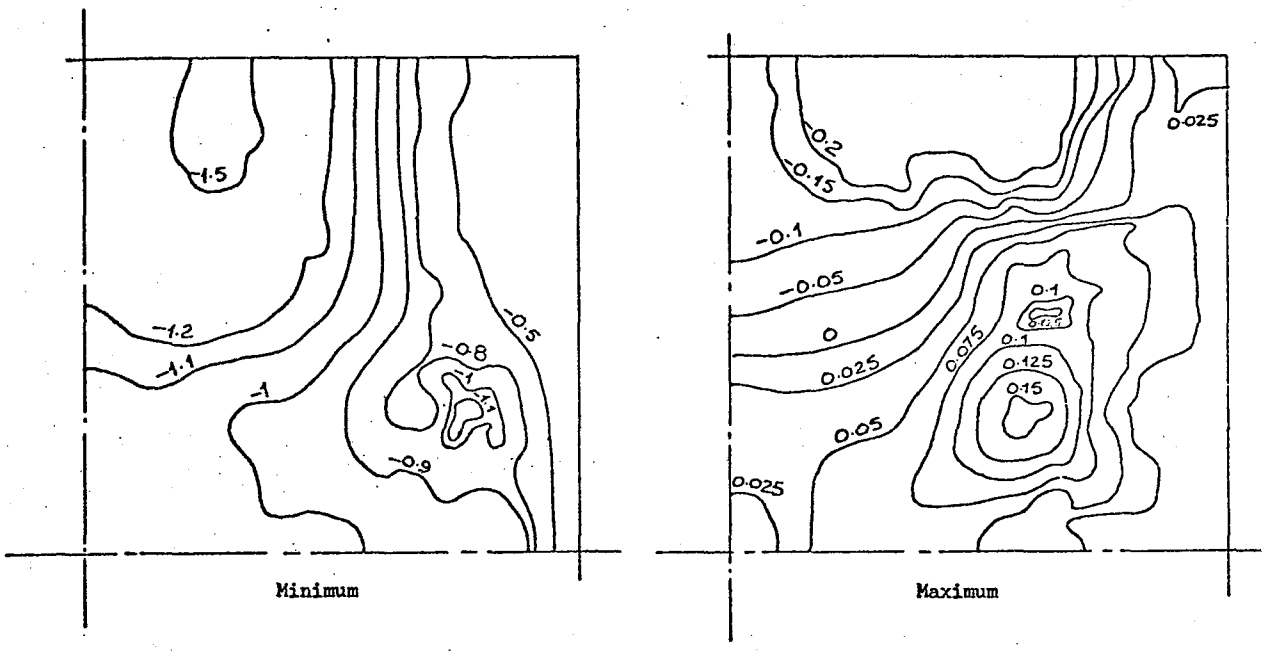


(a) 0.0012" Febcure



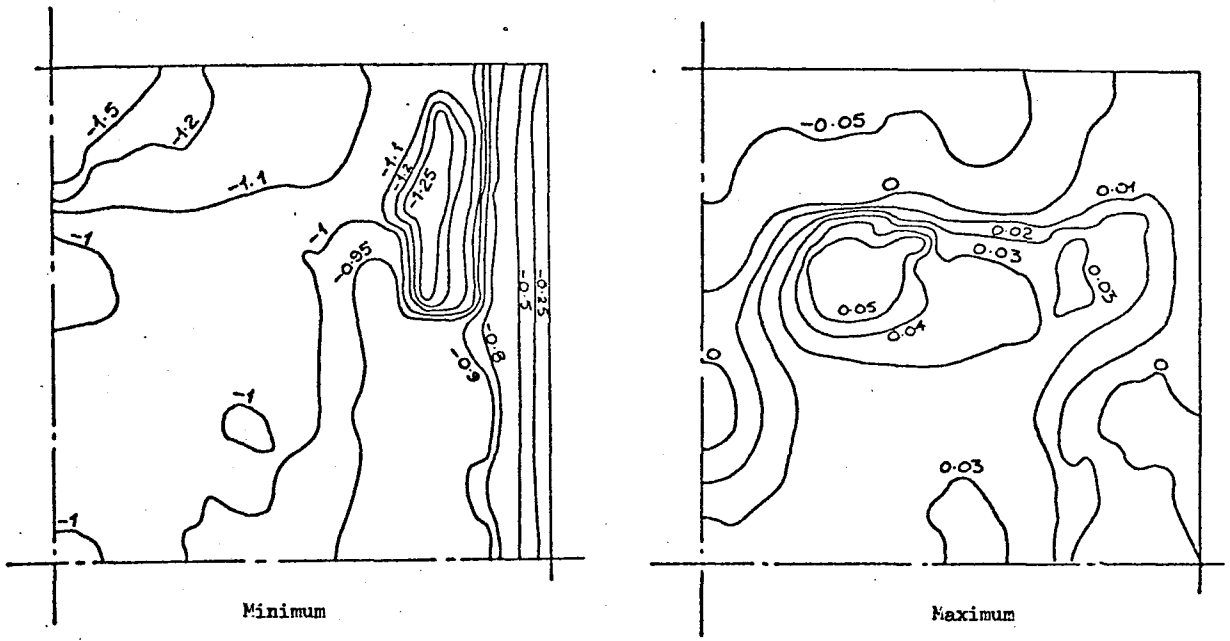
(b) Stauffer's Grease

Figure 2.30. Distributions of principal stresses over the surface of the as-cast mortar slab under an average compressive stress of -1.0 applied through a steel platen with various intermediate materials (Series 2).

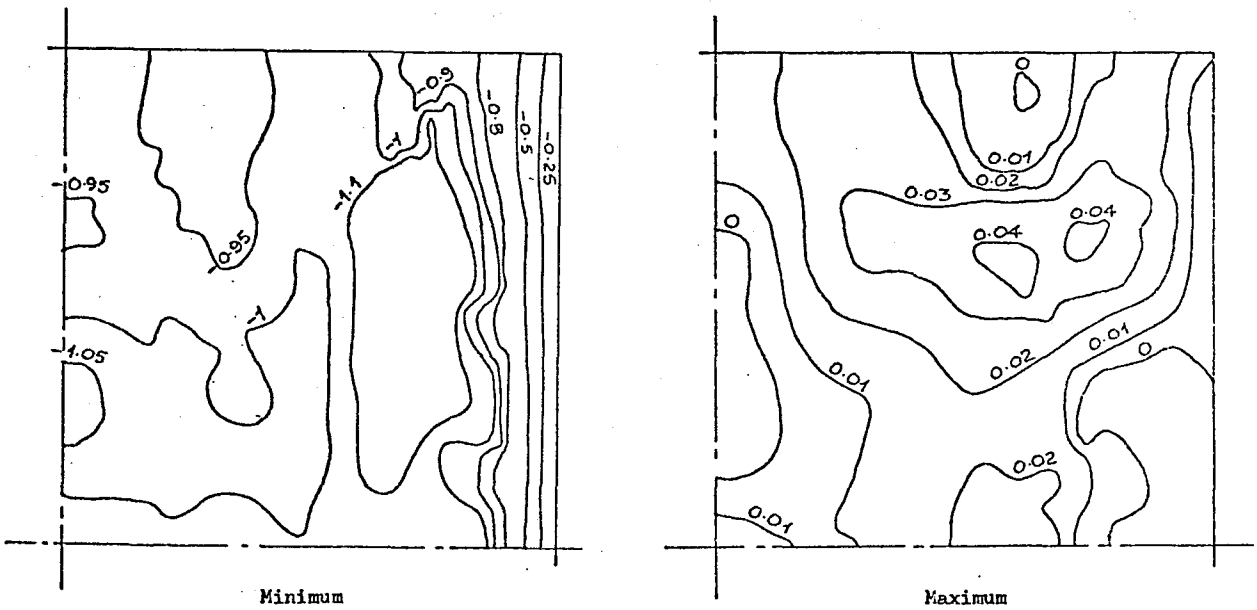


MGA Pads

Figure 2.31. Distributions of principal stresses over the surface of the as-cast mortar slab under an average compressive stress of -1.0 applied through a steel platen with MGA pads at the interface (Series 2).

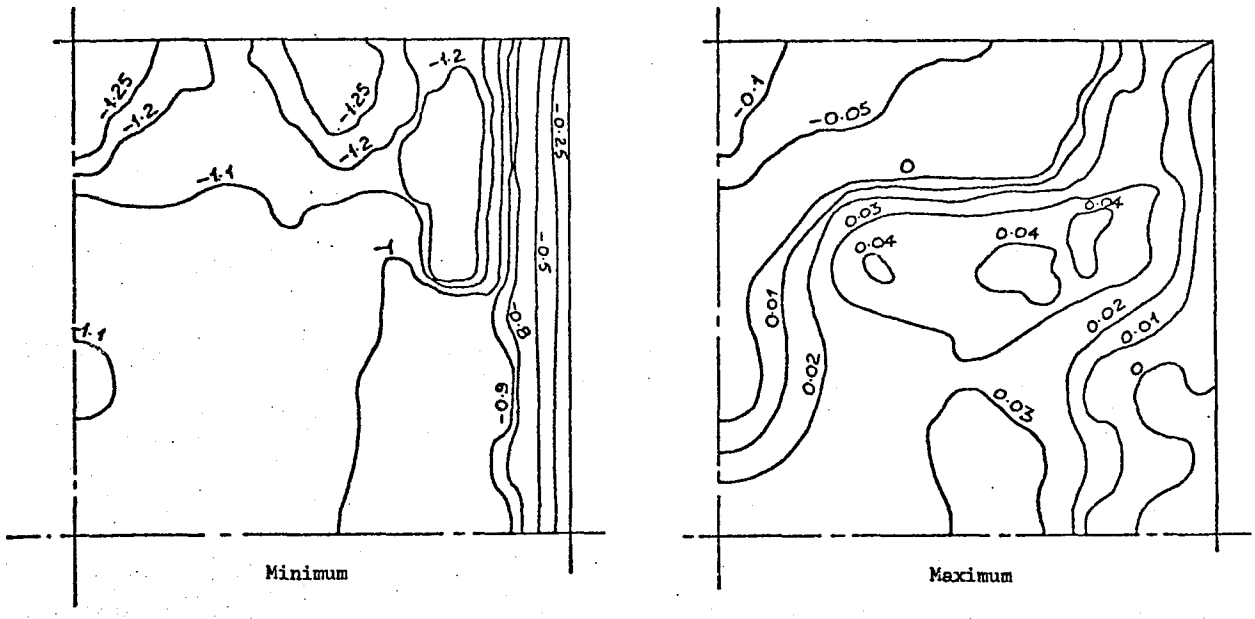


(a) No intermediate material

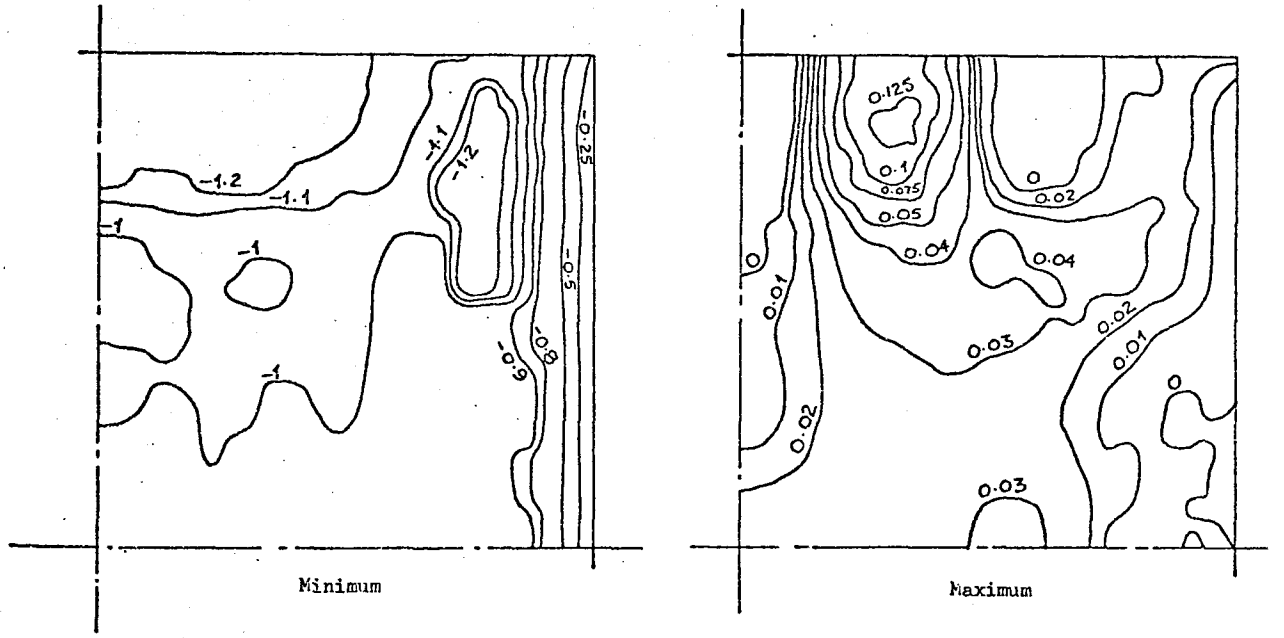


(b) 1/16" Jointite

Figure 2.32. Distributions of principal stresses over the surface of the ground mortar slab under an average compressive stress of -1.0 applied through a steel platen with and without an intermediate material (Series 3).

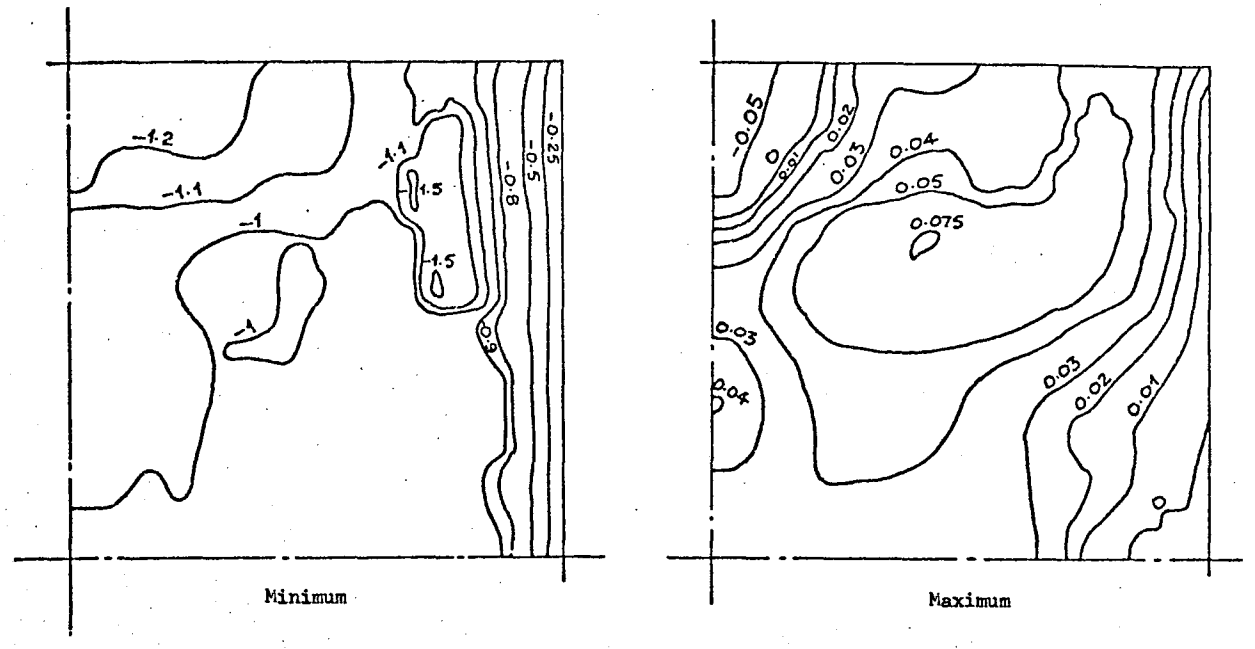


(a) 0.0012" Febcure

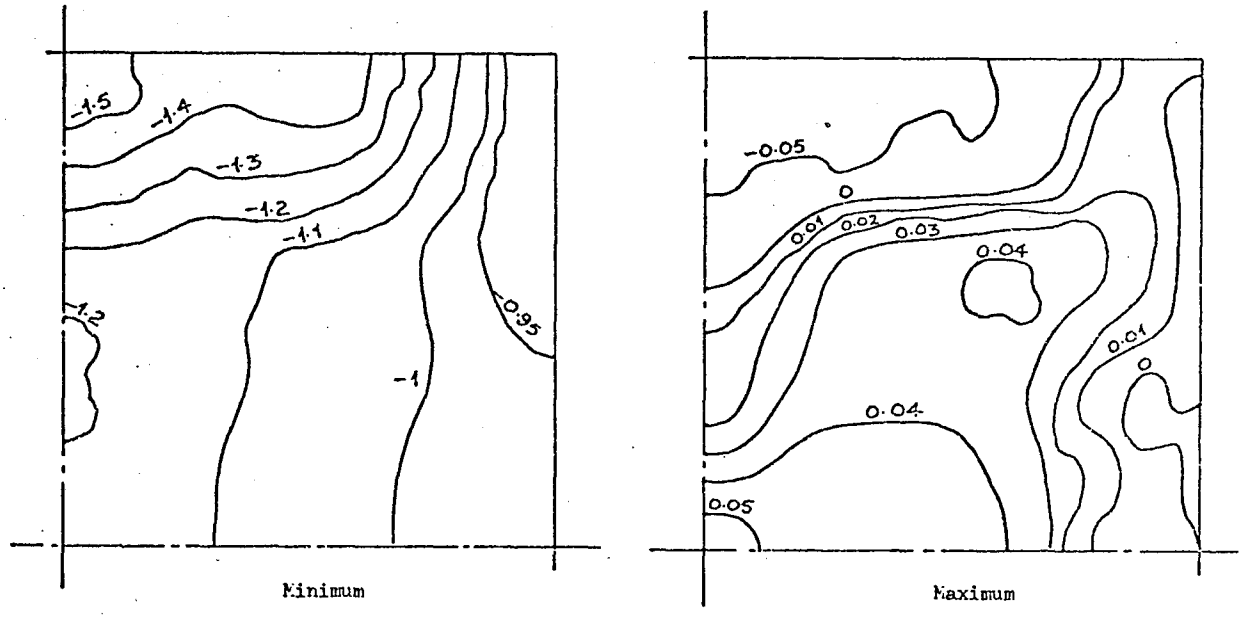


(b) MGA Pads

Figure 2.33. Distributions of principal stresses over the surface of the ground mortar slab under an average compressive stress of -1.0 applied through a steel platen with various intermediate materials (Series 3).



(a) Mortar Platens



(b) Brush Platens

Figure 2.34. Distributions of principal stresses over the surface of the ground mortar slab under an average compressive stress of -1.0 applied through a steel platen with various intermediate materials (Series 3).

The degree of criticality of the various loading configurations is assessed following the procedure described in 2.5.5.1., and the stress state at the most critical point is shown in Table 2.8. and Figure 2.35. for Series 2 and in Table 2.9. and Figure 2.36. for Series 3.

2.6.4.6. Discussion of Results from Series 2

(i) Stress Distributions for Plain Mortar with no Intermediate Material

The distributions shown in Figure 2.28.(a) indicate extremely high disturbances of stress as compared with those evaluated for the theoretical model of a slab similarly loaded through a spherical seating unit, but assuming complete fixity at the specimen/platen interface, as described in 2.5. (Case 5). Both the experimental and theoretical analyses, however, show the same trends, namely, the minimum principal stress reducing from values above the average applied stress near the centre of the specimen to values below the average near the free faces. The magnitudes of the differences are considerably larger for the experimental case.

For the maximum principal stress, both theory and experiment indicate induced compressive restraints near the platen/specimen interface. The magnitude of this restraint reduces to zero at a distance from the interface, after which the remaining zone of the specimen is under tension. In the experimental case, the boundary between the compression and tension zone extends approximately from the corners of the slab to intersect the vertical axis at $\frac{1}{3}$rd of the depth of the slab. On the other hand, for the theoretical model the zone extends for the centre of the interface to approximately $\frac{1}{4}$ of the depth down the free face. The disparity between theory and experiment is also evident by considering the magnitudes of the maximum principal stresses, which for the experimental case are much larger.

(ii) Stress Distributions for Intermediate Materials which attempt to match the Lateral Deformation of the Specimen and Materials which bed-down' under load

Apart from some local differences the distributions for minimum principal stress (see Figure 2.28.(b) and 2.29.) show the same trends as for the plain mortar case.

The corresponding distributions of maximum principal stress are also generally similar to those for the plain mortar, although the position of

Intermediate Material	Principal Stress at Most Critical Point as a Proportion of the Applied Boundary Stress	
	Maximum (Tension)	Minimum (Compression)
No intermediate material	0.150	- 0.800
Feb	0.125	-0.900
Stauffer's Grease	0.175	-0.800
MGA Pads	0.150	-0.800
Zinc	0.100	-0.900
Aluminium	0.150	-0.250
Jointite	0.150	-0.500

Table 2.8. Principal stresses measured at the most critical point on the surface of the Series 2 mortar specimen loaded to an average compressive stress of 3,000 lb./in.^{2} through various intermediate materials.

Legend

⊙ for average applied stress of 3000 lb./in.^{2}
△ extrapolated for average applied stress of 4731 lb./in.^{2}
N = no intermediate material
Z = zinc sheet
A = aluminium sheet
J = Jointite
F = Febcure
G = Stauffer's grease
M = MGA pads

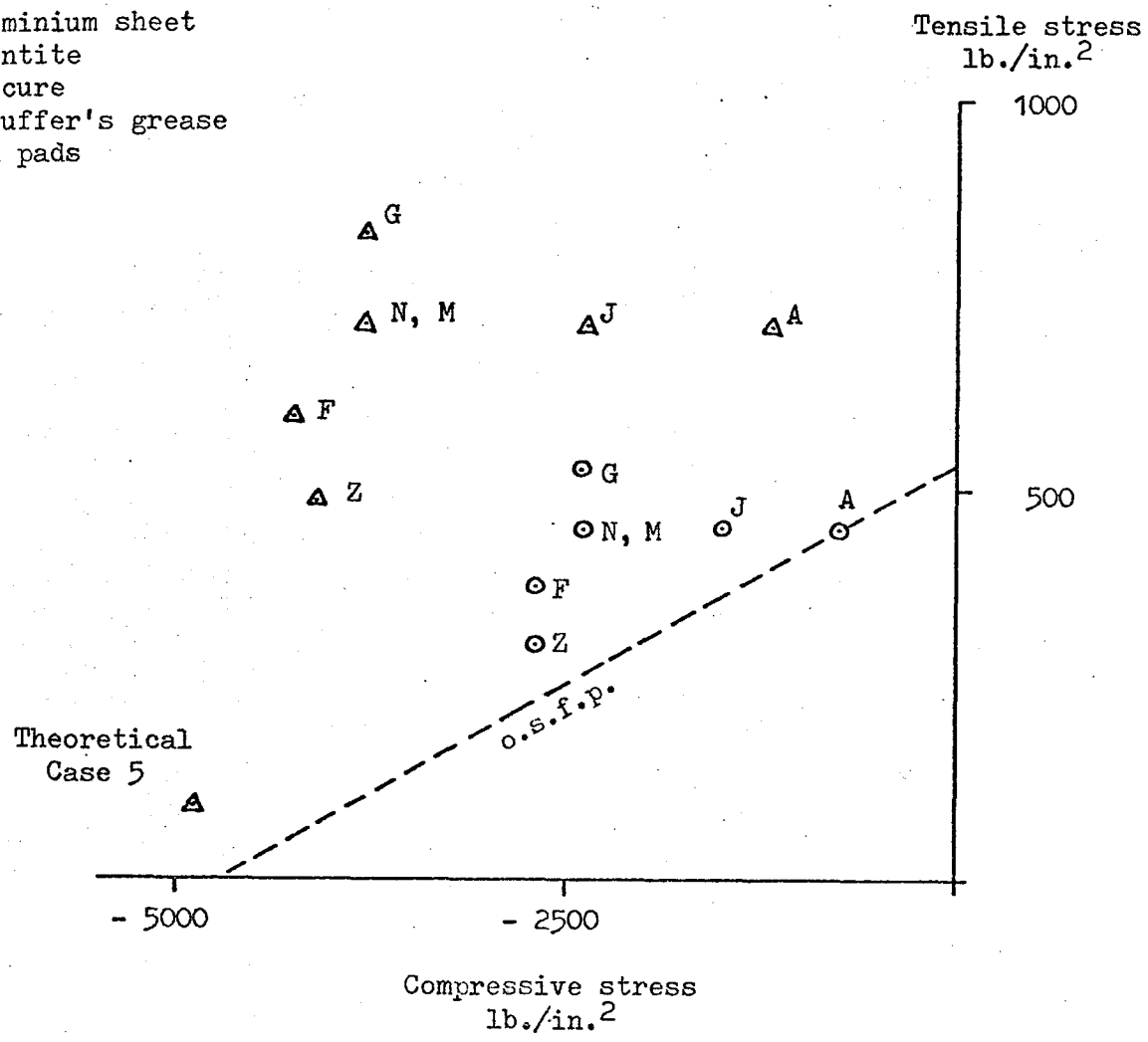


Figure 2.35. Envelope of stress at o.s.f.p. for mortar MA in the biaxial compression-tension zone showing the stress states at the most critical point for tests of Series 2.

Intermediate Material or Platen Type	Principal Stress at Most Critical Point as a Proportion of the Applied Boundary Stress	
	Maximum (Tension)	Minimum (Compression)
No intermediate material	.05	-1.00
Jointite	.04	-1.10
Feb	.04	-1.00
MGA pads	.125	-1.20
Mortar Platens	.075	-1.00
Brush Platens	.05	-1.08

Table 2.9. Principal stresses measured at the most critical point on the surface of the Series 3 mortar specimen loaded to an average stress of 3,000 lb./in.^{2} through various intermediate materials and types of platen.

Legend

⊙ for average applied stress of 3000 lb./in.^{2}
△ extrapolated for average applied stress of 4731 lb./in.^{2}
N = no intermediate material
J = Jointite
F = Febcure
M = MGA pads
MP = mortar platens
B = brush platens

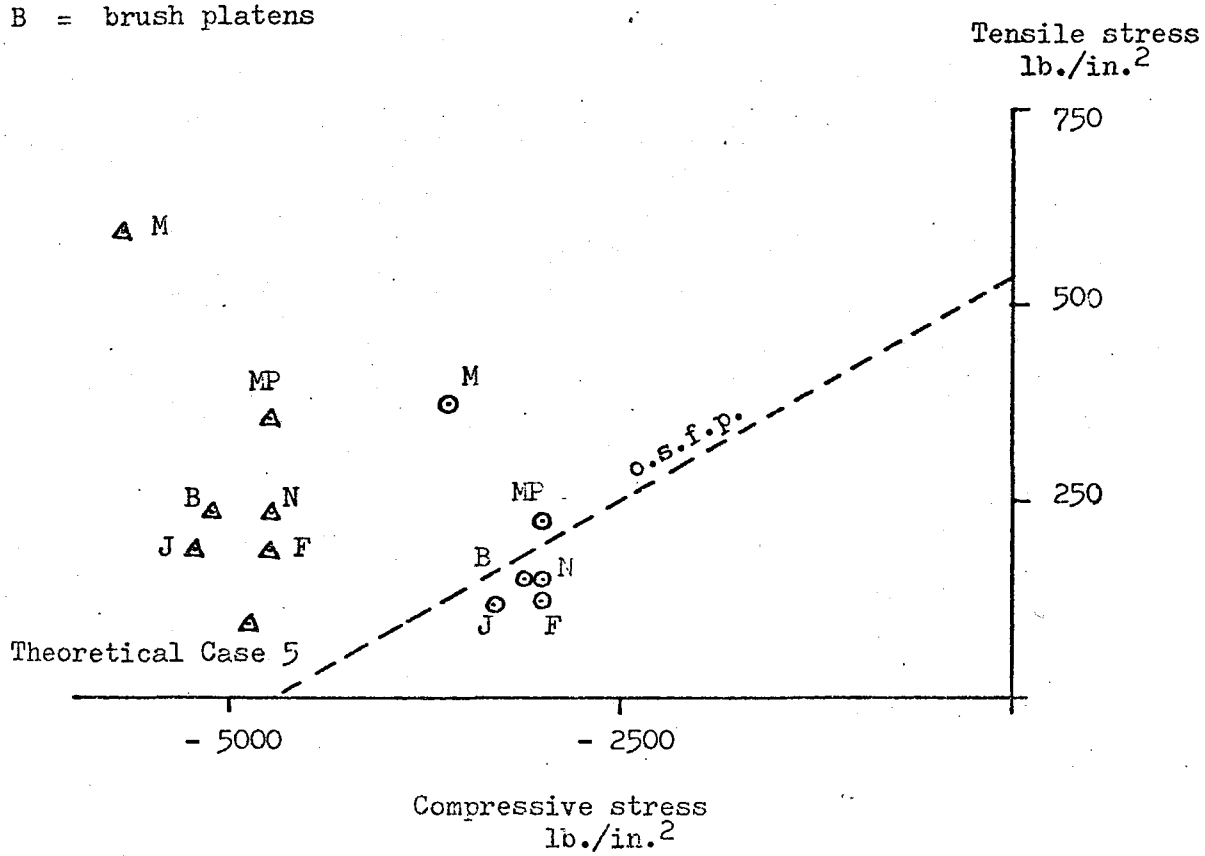


Figure 2.36. Envelope of stress at o.s.f.p. for mortar MA in the biaxial compression-tension zone showing the stress states at the most critical point for tests of Series 2.

the most tensile stress zone changes between cases which considerably effects the criticality of stress state.

(iii) Stress Distributions for Intermediate Materials which primarily reduce Interfacial Friction

Unlike the preceding group of materials the minimum principal stress distributions (see Figures 2.30. and 2.31.) show considerable local disturbances which are not evident for the plain mortar. The corresponding maximum principal stress distributions, however, appear to compare well with the plain mortar case.

(iv) Criticality of Stress State

For all cases the stress state at the most critical point is a combination of compression and tension. The various critical stress states shown in Figure 2.35. indicate that even at an average applied compressive stress level of 3000 lb/in^2, which is well below that at the o.s.f.p. level (4731 p.s.i.), the stress state lies outside the o.s.f.p. envelope except for the aluminium interface which lies on the envelope.

For this stress level a friction-reducing intermediate material appears likely to cause a reduction in the level of boundary stress necessary to cause material breakdown, with the most critical case being Stauffer's grease, due undoubtedly to its extrusion under load. The 'matched deformation' and 'bedding-down' materials, on the other hand, appear to induce less critical states, with the plain mortar lying between the two groups.

If the stresses are linearly extrapolated for an assumed case of an applied boundary stress of 4731 lb/in^2, which is the o.s.f.p. stress for the mortar under uniaxial compression, the increase in criticality compared with that found experimentally at the same applied stress (see 2.5.3.1. Case 5, which is also shown in Figure 2.35.) is evident.

This disparity of results may be due to the following reasons:-

(a) The strains measured on the surface of the specimen are not truly representative.

(b) The values for E and ν for the mortar obtained from a uniaxial compression test may not be valid in a combined stress field.

(c) The loaded surfaces of the specimen may be out of plane, or contain local irregularities which are sufficient to cause high stress concentrations.

(d) The assumptions made in the theoretical analysis are not realistic.

2.6.4.7. Discussion of Results from Series 3

(i) Stress Distribution for Plain Mortar with no Intermediate Material

By comparing Figures 2.28.(a) and 2.32.(a) it is apparant that there is a similarity between the distribution of minimum principal stress for the 'ground' and 'as cast' specimens. The Figures show, however, that the magnitude of the maximum principal stresses caused by the restraints at the specimen/platen interface are significantly lowered for the ground specimen. This indicates the importance of ensuring an accurately plane loading face, a conclusion confirmed by other investigators [231].

(ii) Stress Distribution for Loading through Rigid Platens with Intermediate Materials

For all intermediate materials used in this series, with the exception of the MGA pads used with the ground specimen, the stress distributions, when compared with those measured in Series 2 for the 'as cast' specimen, indicate a significant lowering of the restraint stresses. For the MGA pads, however, the tensile restraint stresses induced are only slightly lower in magnitude, and this case is the most critical in that it will tend to lower the applied stress level at which significant material disruption will start.

(iii) Stress Distribution for Loading through Non-rigid Platens

The use of mortar or brush platens appears not to significantly affect the distribution of either minimum or maximum principal stress as compared with the plain mortar case.

(iv) Criticality of Stress State

As for Series 2, the stress state at the most critical point for all loading configurations is a combination of compression and tension (see also 2.5.5.). Figure 2.36. shows that, for a stress of 3000 lb/in^2 the MGA pads give a critical stress state well outside the o.s.f.p. envelope. This indicates a possible effect of extrusion inducing high

lateral tensile stresses. The stresses induced by the mortar platens lie just outside the envelope, but all other cases lie close together in a zone within.

Comparison between Figure 2.35. and Figure 2.36. for the stress states extrapolated to an average boundary stress of 4731 lb/in^2 (the o.s.f.p. level under uniaxial compression) shows the distinct tendency for the stresses at the critical points to approach the true uniaxial point. This process of extrapolation, however, emphasises the criticality of the MGA pads.

2.6.4.8. Conclusions

Before drawing conclusions from these test series, it must be emphasised that the stress distributions are based on measurements of strain over the surface of previously conditioned mortar specimens under a relatively low level of load. The stress distributions have been derived from the strain values by using plane stress assumptions and values of E and ν obtained from a uniaxial compression test. Thus, the data may not accurately reflect the true stress conditions within a specimen even at low values of applied stress and they will undoubtedly be unrealistic at levels sufficient to cause significant material breakdown. However, the test data allows comparisons to be made between the various loading configurations, since the same specimen and strain measuring equipment has been used for all cases.

With the above restrictions in mind, the following main conclusions can be drawn from the series:-

1. For both 'as-cast' and ground mortar specimens loaded through rigid steel platens with no intermediate materials, the surface stress distribution conforms qualitatively with, but is more disturbed than, that obtained from a theoretical elastic model of the loading configuration which assumes complete fixity at the platen/specimen interface.

2. For most intermediate materials investigated, the 'as-cast' mortar specimen induces both larger secondary restraint stresses, and a more disturbed primary compressive field, than the ground specimen. The importance of ensuring accurately plane loading surfaces is

emphasised by the increase in criticality of the stress state at the most critical point within the 'as-cast' specimens for the various interfaces, compared with the tendency of the stresses at the most critical point in the ground specimens to approach the true uniaxial case.

3. Intermediate materials which attempt to match the lateral deformation of the specimen behave in a similar fashion to those which primarily 'bed-down' under load. Both classes, however, induce slightly less critical stress states than plain rigid platens, and considerably less critical states than grease-based friction-reducing pads, due probably to the effects of extrusion of the latter type.

4. From the results of the series it is not possible to clearly distinguish between the effects of 'matched deformation' or 'bedding-down' materials and the friction-reducing layer of Febcure, in that all classes induce stress states with a similar degree of criticality.

This tends to confirm the opinion that Febcure, in common with the other two classes, does not experience significant extrusion at the level of applied load.

5. The use of 'mortar' platens tends to induce a more critical stress state within specimens than 'brush' platens, but neither appear to show significant advantages over the use of plain rigid steel platens at the level of load considered.

2.7. Recommended Loading Procedures for Uniaxial, Biaxial and Triaxial Compressive Stress States

2.7.1. Choice of Boundary Conditions

Two fundamental possibilities exist for the application of load to specimens of a given material:-

(a) a condition of uniform boundary stress, or

(b) a condition of uniform boundary strain.

Provided no secondary restraint stresses or strains are induced in attaining the above conditions it would be expected that, in general, a material will

respond in a different manner to each state of loading. The difference in response to a given volume of material may be dependent on the heterogeneity of the material, in that a homogeneous material is likely to respond in a similar manner to both types of boundary condition, whereas a heterogeneous system will undoubtedly exhibit large differences.

These differences will be caused by the manner in which the load is transmitted through the structure of the material. For a material such as concrete, consisting of relatively stiff inclusions embedded in a softer matrix, a uniform boundary strain will tend to concentrate the stress at the inclusions, whereas a uniform boundary stress will tend to induce higher strains in the matrix.

The differences in response of such a material will, however, probably reduce for material which is remote from the loaded boundaries. For a fine-grained material, where the degree of heterogeneity is low, the distance from the loaded boundaries required to ensure nearly identical behaviour under the different systems of load will be less than that required for a coarse-grained composite. In general, therefore, the response of a material to a given boundary condition of load will depend on the degree of heterogeneity of the material in relation to the size of the representative volume element under test. If the size of specimen is relatively small compared with the grain size, which may be inevitable in practice, some differences in behaviour are to be expected and a choice must be made regarding which type of loading condition more nearly represents the loading situation for which the data is to be used. In Chapter 3 this subject is discussed in detail when a comparison is made between the behaviour of concretes of different degrees of heterogeneity when subjected to the two types of loading condition.

However, one further point must be considered before a choice of fundamental boundary condition is made, namely, the ability of any given loading device to attain the desired condition without imposing secondary restraint effects, and this is discussed in the following sections.

2.7.2. Recommended Loading Procedures

In this section, suggestions are made as to the effectiveness of various systems of loading in inducing either of the fundamental boundary conditions for various states of stress, based on the evidence discussed previously in the Chapter.

2.7.2.1. Uniaxial Compression

The uniform stress boundary condition requires the development of a hydraulic loading technique, with the attendant problems of preventing extrusion of the hydraulic medium. Such extrusion will tend to impose tensile secondary restraint stresses which will have the effect of promoting any mechanism of failure. To date, no evidence has been found of a hydraulic device capable of loading sufficiently large specimens of a material such as concrete to a magnitude of uniaxial stress sufficient to cause complete disruption, Such devices have been used successfully for investigating the material behaviour of specimens relatively low stress ranges [49] and are in the development stage for applying stresses up to 12000 lb/in^2 to small specimens of rock [232].

It would appear that fewer problems are associated with the design and use of rigid loading devices intended to produce a state of uniform boundary strain. However, analytical (see 2.4.1. and 2.5.) and experimental (see 2.4.2. and 2.6.) investigations of the stress state induced within specimens loaded in this manner, indicate that such a system may impose compressive restraints which in turn induce considerable strain, and hence stress, disturbances within specimens.

In order to eliminate such restraint effects the loading device can be modified by either (a) inserting a friction-reducing material between the platen and specimen, (b) inserting a material which primarily 'beds-down' under load, (c) inserting a material which attempts to deform laterally to the same extent as the specimen or (d) adopting a non-rigid loading device. Previous experimental evidence (see 2.4.2.) and evidence obtained during the present test series (see 2.6.) suggests that intermediate materials which attempt to match the lateral deformation of the specimen and materials which primarily 'bed-down' induce considerable less critical stress states than those based on a grease layer which primarily reduce friction, but the results of the present tests suggest that the former classes of material do not substantially improve the stress or strain state within specimens compared with that obtained using rigid-platens only. The use of 'non-rigid' platens such as 'mortar' or 'brush' platens also does not appear to solve the problem (see 2.6.4.).

From the available analytical and experimental evidence it would appear that, for the case of uniaxial compression, the most effective method of

attaining the required stress and strain state is by choosing a specimen shape such that any boundary restraint stresses are confined to zones near the loaded surfaces thus leaving a substantial volume of the specimen without significant restraints. In adopting such a method, the state at the boundary becomes less of an influence on the resulting behaviour of material within this central volume. In fact if, for a given material with a given degree of heterogeneity, the volume is sufficiently remote from the boundary, the loading condition may not significantly affect the performance of the material which may respond to uniform boundary strain and uniform boundary stress in the same manner (see 2.7.1.).

Thus, for investigating the deformational and failure characteristics of a material under uniaxial compression choosing a suitable specimen shape appears to be the most effective in inducing the desired stress or strain state. However, the experimental and analytical investigations discussed previously emphasise that the following must be considered before carrying out any such test:-

1. The material should be loaded such that no significant restraint stresses are induced at the boundaries. It is particularly important to ensure that tensile stresses are not present since these will tend to initiate failure from the end zones of the specimen, where the stress state is undefined, at a much lower level of applied stress (see 2.4.2.). Thus, materials based on grease layers which may extrude under load should be avoided (see 2.6.), but some form of interfacial layer of a material which primarily 'beds-down' under load will be satisfactory (see 2.4.2. and 2.6.).

2. The specimen should have a height/width ratio of at least 2:5, if no attempt is made to reduce compressive restraint stresses at the platen/specimen interface.

3. It should be ensured that the loaded surfaces of the specimen and the surfaces of the loading device are plane and parallel. It is recommended that this be achieved by a process of grinding using an accurately aligned toolroom grinding machine with diamond abrasive wheel and suitable clamping devices.

4. The loading platen should be sufficiently stiff to prevent distortion which nay lead to uneven loading. This is of particular importance if a spherical seating device is used to minimise the risk of eccentric loading, since such a device may tend to concentrate the load at the centre of the platen (see 2.5.) due to the distortion and/or mismatch between the male and female components.

   It is also of importance to ensure that the seating unit locks under load such that a state of uniform strain is applied throughout the loading history despite the degree of anisotropy of the material [63].

5. The loading platens should be at least as large as the specimen cross section, and preferably of the same nominal cross-sectional dimensions as the specimen to be tested, as platens of a smaller than the specimen induce stress disturbances (see 2.4.2. and 2.5.).

6. Any deformation measurements should be made with the central third of the specimen, where the stress state is uniform and relatively definable (see 2.4.1., 2.4.2., 2.5. and 2.6.).

2.7.2.2. Biaxial Compression

Again, the choice must be made between the adoption of a system of loading to apply either near-uniform boundary stress or near-uniform boundary strain. As previously emphasised, a heterogeneous material will undoubtedly respond to the two systems of load in a different way, especially for small volume elements of a material with a relatively large grain size.

The analytical evidence (see 2.4.1. and 2.5.) indicates that any restraints on the boundaries will cause a more severe disturbance of stress and strain within specimens where two loading directions are involved. Such restraints, if compressive, cause the load to be concentrated near the loaded boundaries, leaving the central portion under a state of stress much lower in magnitude than that desired.

For biaxial compression, the total applied load in any one direction need not be transmitted to the specimen, as is the case for a uniaxial state of stress, since it is possible for some loads to be conducted through the

loading device used to apply the load in the other direction due to frictional restraint at the specimen/platen interfaces. This will be the case for most practical testing arrangements where rigid platens are used for the application of uniform boundary strain. It is, therefore, essential to eliminate as far as possible these frictional restraints by using an intermediate material. Unfortunately no material has been found particularly satisfactory in this respect during the present experimental investigation although materials which 'bed-down' or reduce friction without extrusion may be the most suitable (see 2.6.).

For uniform boundary stress it is considered that some form of hydraulic loading through two orthogonal sets of platens [49, 232] will provide the best solution, provided that the extrusion problems can be satisfactorily overcome up to the loads required to produce failure. As the effectiveness of such a device has not been demonstrated at high loads, a hydraulic cell arrangement would appear to be the most convenient loading technique. Unfortunately this method will apply only axisymmetric states of stress to specimens. Nevertheless, it is essential to study the response of a material to biaxial stress applied using uniform boundary stress in order to assess the degree of criticality as compared with the uniform strain condition (see Chapter 3). This is necessary since, unlike the case of uniaxial stress, the specimen shape cannot be chosen to ensure that a representative volume of material is sufficiently remote from the loaded boundaries and, therefore, for practical sizes of specimens, the material response is likely to be different for the two cases.

2.7.2.3. Triaxial Compression

Just as the biaxial case with no secondary restraints is considerably more difficult to achieve than unrestrained uniaxial compression, so the attainment of a definable triaxial stress state with no secondary stresses will be even more elusive. For uniform boundary stress, hydraulic loading in three orthogonal directions is desirable but extremely difficult. to develop due to the associated problems of extrusion. For uniform strain applied through rigid loading devices it is absolutely essential to eliminate friction between the platens and specimen and, for the reasons discussed previously, such a solution is not practical at present.

A suitable compromise, which appears from theoretical analysis (see 2.4.1. and 2.5.) to induce a secondary restraint-free stress and strain state, is

that of loading a specimen through a combination of uniform boundary strain and uniform boundary stress. Such a method has been used satisfactorily for many years as the conventional triaxial test for soils and latterly for concretes and rocks. The technique involves the immersion of a specimen in a hydraulic fluid, using an impermeable boundary membrane to prevent intrusion, and applying a superimposed load through rigid-platens. The effects of the boundary restraints, inevitably present for the rigid device are minimised by choosing a suitable specimen shape, as discussed for the case of uniaxial compression, and all the relevant recommendations already outlined in 2.7.2.1. must be followed.

3. AN EXAMINATION OF THE STATE OF EQUAL BIAXIAL COMPRESSION WHEN INDUCED UNDER UNIFORM BOUNDARY STRESS AND STRAIN

3.1. Introduction

As discussed in Chapter 2, the reaction of a material to a given state of stress can be studied by subjecting a representative element to one of two fundamental boundary conditions: namely, uniform strain or uniform stress.

For any combination of stresses these two extremes must induce differing responses in the material depending on (a) its degree of anisotropy and (b) its degree of heterogeneity, with respect to the shape and size of the volume element under test (see 2.7.).

A relatively homogeneous and isotropic material, which in the present context implies a material with small-sized inclusions (with respect to the size of the specimen) evenly distributed in a matrix, should exhibit relatively small differences in deformational behaviour and strength under the two boundary conditions always provided that the material remains coherent throughout the loading process. For a more heterogeneous and anistropic material, i.e. one containing relatively large sized inclusions unevenly distributed in the matrix, significant differences may be apparant.

These differences in the response of a material will be exhibited even assuming that such ideal boundary conditions can be attained. In practice, however, the secondary restraint effects induced by the loading technique used could also be significant and, as shown in Chapter 2, may tend to induce a disturbed stress or strain state within specimens. The degree of disturbance will depend on the type of loading device used to apply the particular boundary condition required.

A state of near-uniform strain can be attained by loading through rigid-platens, provided that they are sufficiently stiff and that the frictional restraint at the specimen/platen interface is sufficiently low. The condition of near uniform boundary stress is conveniently obtained by some form of hydraulic loading, where the problem of stiffness does not arise and the effect of frictional resistance is insignificant. In this case, however, care must be taken to eliminate the effects of extrusion of the hydraulic fluid (or its container) in order to prevent tensile stresses being induced.

In general, therefore, unless the specimen shape and size can be suitably chosen different information will be obtained by loading concrete under the two fundamental boundary conditions. Information obtained from such tests should only be used for design applications in which the actual loading condition is of a similar nature to that imposed under the test conditions. If there is any doubt regarding the condition in the structure under consideration then the most conservative data, for whatever type of boundary condition this is associated, must be employed.

It is, therefore, of importance to the users of design information to assess quantitatively the differences in behaviour of concretes when loaded under boundary conditions closely allied to those of uniform strain and uniform stress. To the author's knowledge no attempts at comparison have been made directly, and the present chapter is concerned with an initial investigation into the behaviour of a coarse aggregate concrete and a fine mortar (which forms the matrix of the concrete) as representing differing degrees of heterogeneity, under the two conditions.

3.2. Choice of Loading Techniques

The only practical method of achieving a boundary condition of near-uniform boundary strain is by loading a specimen through rigid-platens, while the uniform stress condition is conveniently obtained by some form of hydraulic device.

For rigid-platen systems it is imperative to eliminate, or at least minimise, the frictional restraint at the platen/specimen interface and in Chapter 2 the problems associated with this have been discussed in detail.

For hydraulic loading, the main problem is that of possible extrusion of the membrane which contains the fluid, and which is in direct contact with the specimen (see Chapter 2). This extrusion, although significant where individual 'hydraulic platens' are used to apply asymmetrical states of stress, can be prevented if both the membrane and specimen are immersed in the fluid. Unfortunately such a technique allows only symmetrical compressive stress states to be applied, such as hydrostatic triaxial or equal biaxial (if the stress in one direction is eliminated). In spite of these limitations it is considered that this is the only reliable method of achieving a restraint-free uniform boundary stress condition.

As a knowledge of the behaviour of concrete under hydrostatic stress will serve no useful purpose as regards providing design data for engineers (although it is shown in Chapter 7 that it provides an insight into the failure mechanism for concrete) the state of equal biaxial compressive stress has been chosen for this investigation. Such a stress state is not only of practical significance, but has been the subject of a previous investigation [8]. Results from the present test series will, therefore, allow the data derived from that investigation to be used more realistically.

In order to achieve the uniform boundary strain condition under equal biaxial compression it is essential to minimise the boundary restraint due to the difference in the lateral deformations of the rigid loading platen and the generally less stiff specimen. From the available evidence (see Chapter 2) it would appear that the most uniform stress state within a material under such a loading configuration is given by using an intermediate layer which primarily 'beds-down' under load or one which attempts to reduce friction without the tendency to extrude.

Vile [8] satisfactorily obtained a considerable amount of design data regarding the behaviour of concretes under biaxial compression by using a friction-reducing material (Febcure Super 90 curing compound) which apparantly does not extrude under load (a fact which is supported by the experimental evidence given in 2.6.) and which also prevents moisture loss from specimens. This technique has, therefore, been adopted for this investigation.

For the rigid-platen loading condition, companion slab specimens have been tested in uniaxial compression using the same loading device. Unfortunately it is not possible to use this philosophy for the case of hydraulic loading, and so uniaxial tests for this series have been performed using rigid-platen loading on specimens with a sufficiently large height/width ratio to minimise the end restraint effects. It is conceded that such a testing arrangement will not give results which truly reflect the behaviour under uniaxial hydraulic loading, but will be a close approximation.

In the following section previous investigations which have studied the behaviour of concretes under biaxial compression are reviewed, in an attempt to assess the difference between the results obtained using the two types of boundary condition.

3.3. Review of Previous Investigations into the Behaviour of Concrete under Biaxial Compression

3.3.1. Tests under Uniform Boundary Stress

Although such a boundary condition has been attempted using hollow cylinders under hydraulic pressure [65] it is generally considered that such a test induces considerable stress and strain gradients which would have a significant effect on the results. In the main, therefore, investigators have adopted solid cylinders tested in a hydraulic cell arrangement, with the component of pressure in the axial direction eliminated and with the specimen sealed against ingress of fluid.

Under such a test, Richart et Al [66] found that specimens of mortar and concrete exhibited equal biaxial strengths of approximately 1.3 x uniaxial, this proportion being greater for higher quality mixes. It is likely that the test imposed relatively high restraint stresses in the axial direction due to the friction between various components of the loading device.

Using a similar arrangement Chinn and Zimmerman [67] found various grades of concrete to give an equal biaxial compressive strength of approximately 1.25 x uniaxial. In this case the effect of axial restraint was estimated, and the concrete quality did not appear to influence the results to a significant extent.

3.3.2. Tests under Uniform Boundary Strain

It is on such condition that much attention has been devoted since it enables the entire stress field to be investigated. Two main loading methods have been adopted namely (a) rigid-platen devices with, or without, an intermediate layer interposed between them and the specimen or (b) non-rigid loading platens.

Figures 3.1. to 3.4. show typical strength results obtained in the most important of such investigations, and these are also summarised in Table 3.1. which gives brief details of the type of test conducted and the material under consideration.

3.3.3. Conclusions

The following main conclusions can be drawn from the investigations:-

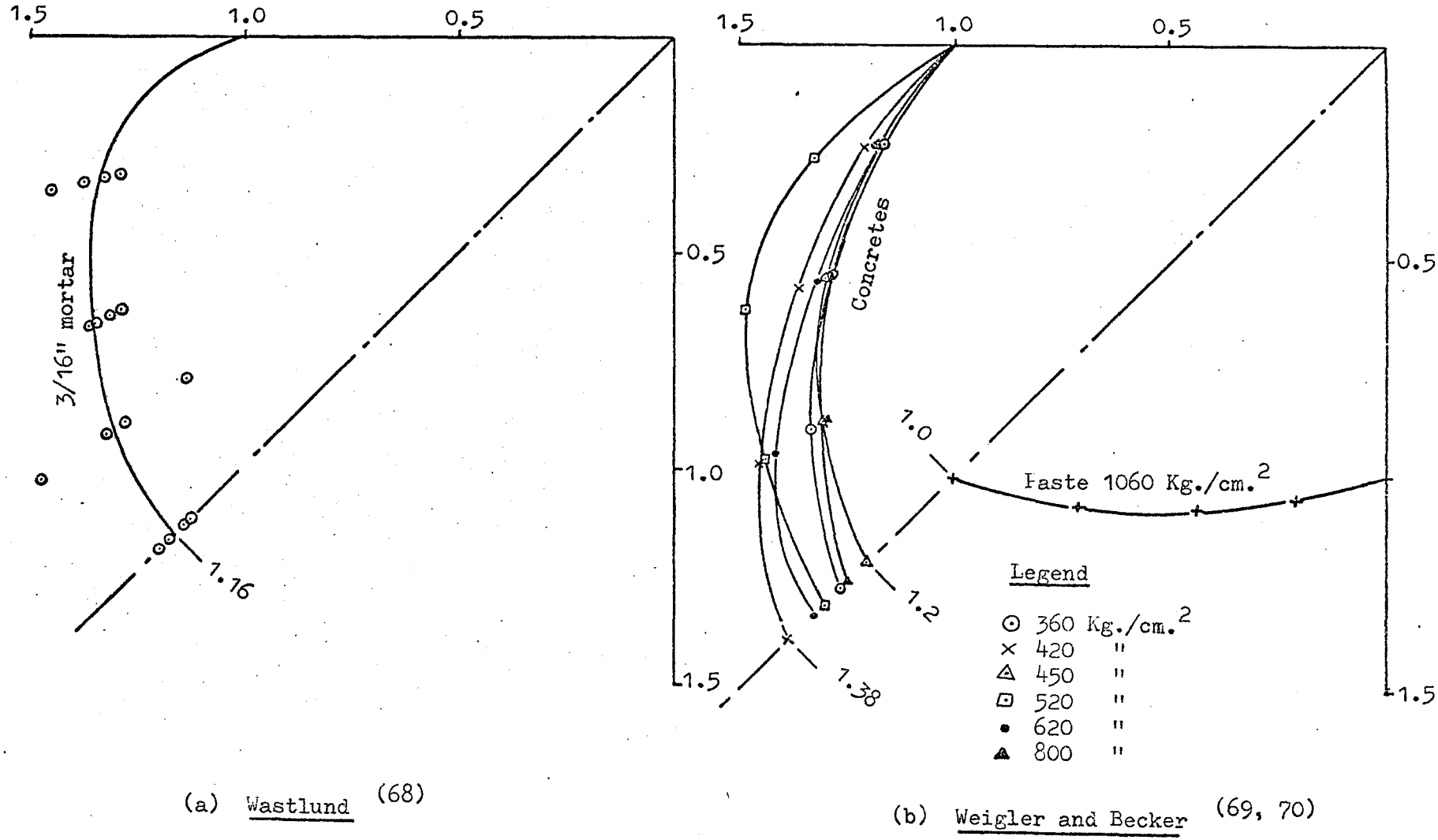
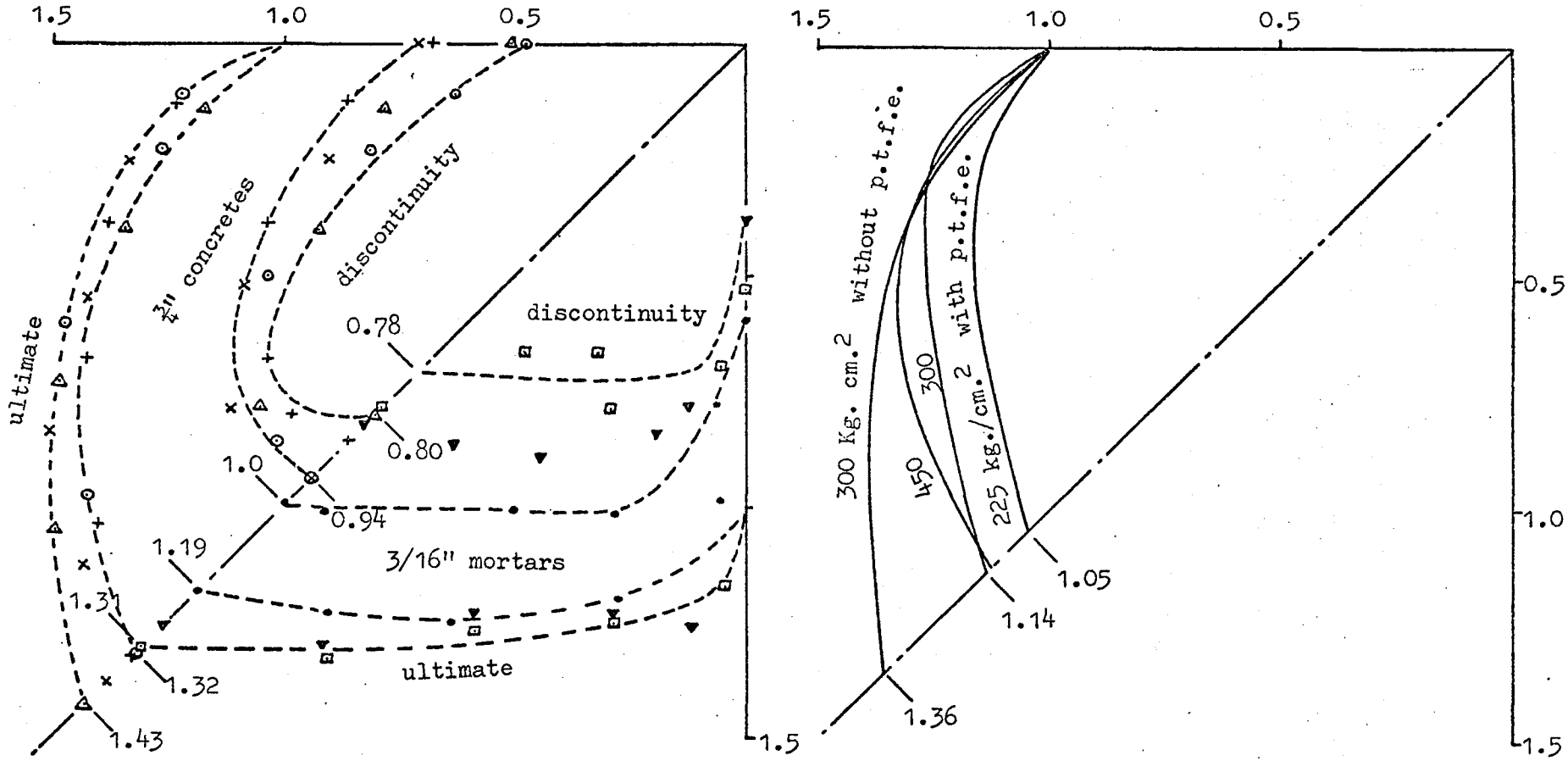


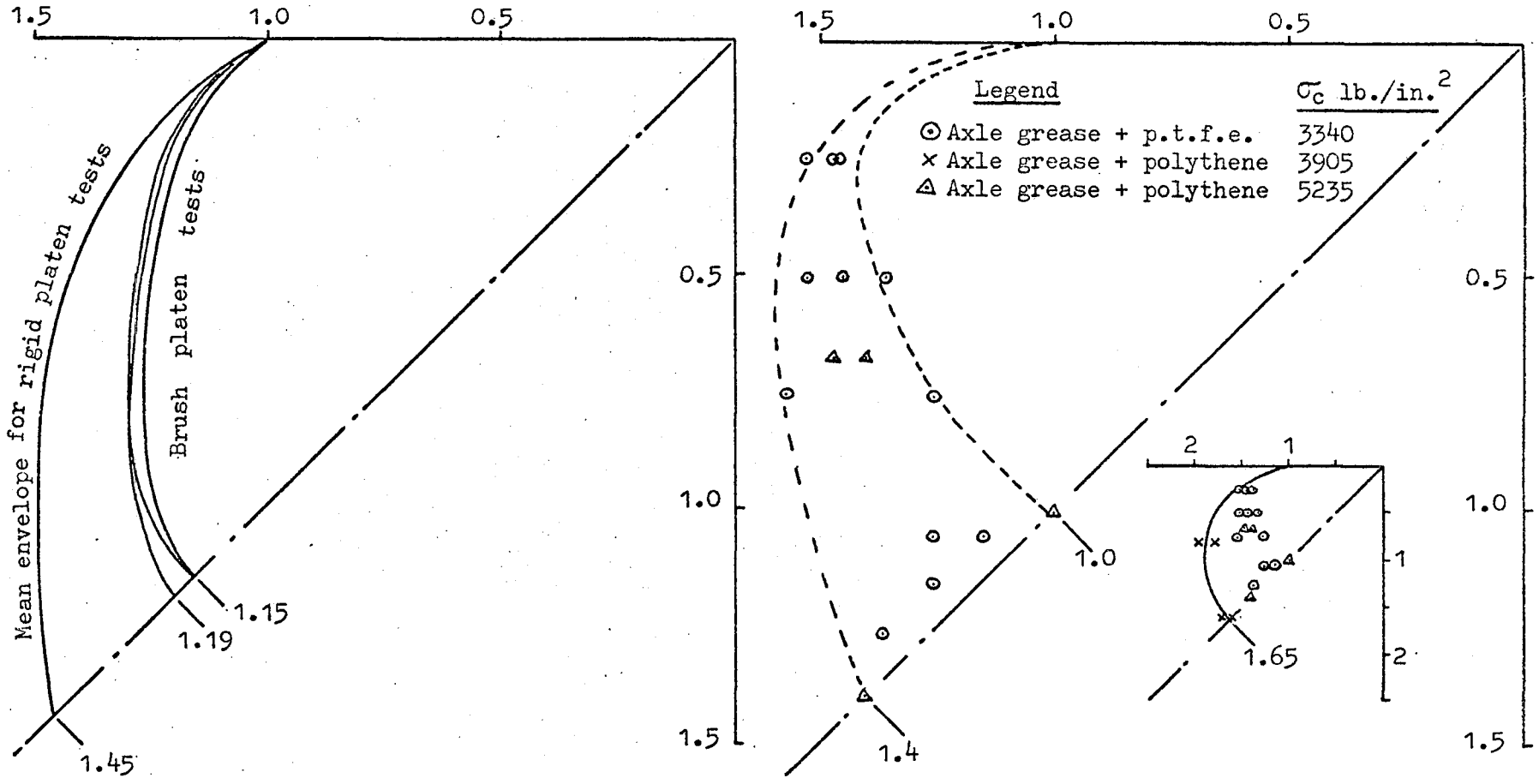
Figure 3.1. Ultimate strength envelopes normalised with respect to the uniaxial compressive strength for concretes tested under biaxial compression



(a) Vile (8)

(b) Opitz (71)

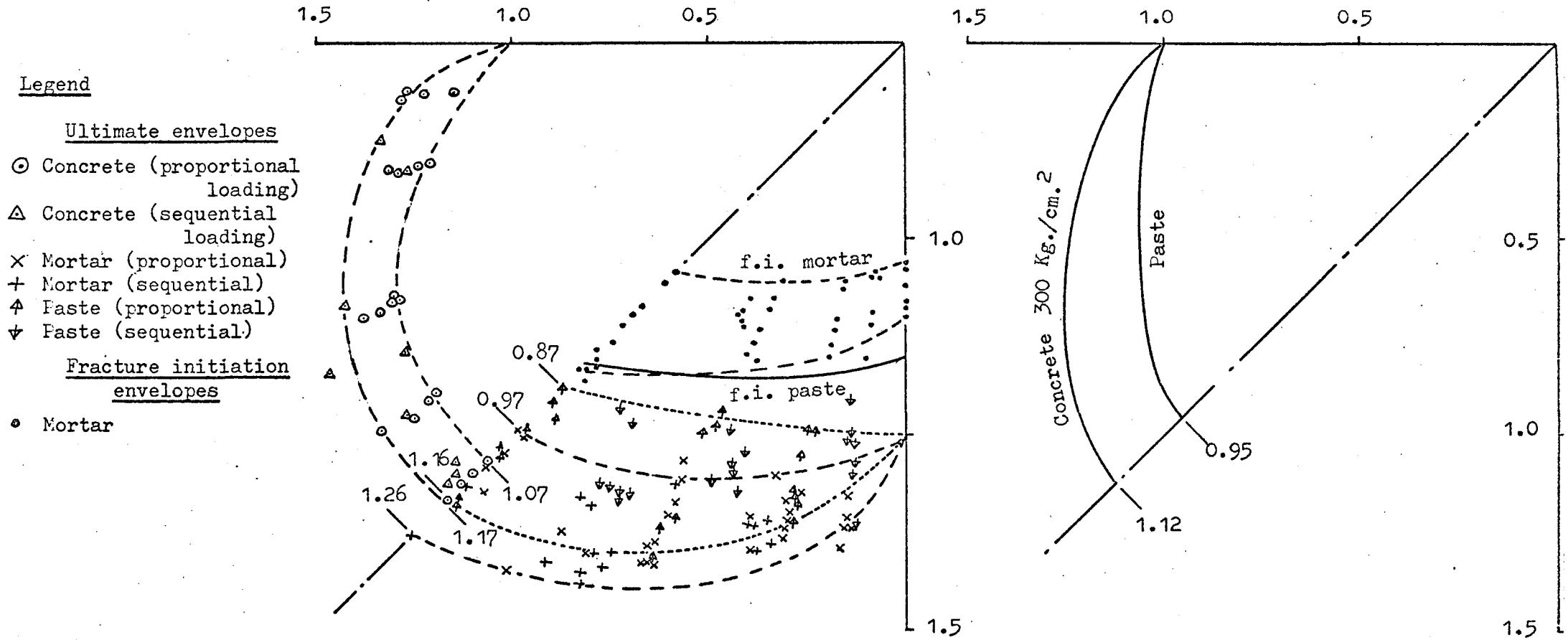
Figure 3.2. Ultimate strength and discontinuity envelopes normalised with respect to the uniaxial compressive strength for concretes tested under biaxial compression



(a) Kupfer (72)

(b) Mills and Zimmerman (73)

Figure 3.3 Ultimate strength envelopes normalised with respect to the uniaxial compressive strength for concretes tested under biaxial compression



(a) Kobayashi and Kononagi (74)

(b) Stegbauer and Linse (75)

Figure 3.4. Ultimate strength and fracture initiation envelopes normalised with respect to the uniaxial compressive strength for concretes tested under biaxial compression.

INVESTIGATOR	MATERIAL TYPE	MAXIMUM SIZE OF AGGREGATE	SPECIMEN DIMENSIONS	METHOD OF LOADING	RATIO $\sigma_{biax.}/\sigma_{uniax.}$		REMARKS
					MAXIMUM	UNDER EQUAL BIAXIAL COMPRESSION	
Wastlund (68)	Mortar	3/16 in.	15x15x15 cm. (5.91x5.91x5.91 in.)	Rigid platens with rubber sheets	1.35	1.16	See Figure 3.1.(a). Uniaxial tests performed in different apparatus.
Weigler and Becker (69,70)	Cement Paste Concretes 360-800 kg/cm.^{2} (5100-11400 lb./in.^{2})	- 7 mm. (.28 in.)	10x10x2.5 c.m. (3.94x3.94x0.98 in.)	Rigid platens	1.08 1.29 - 1.49	1.00 1.20 - 1.38	See Figure 3.1.(b). Uniaxial tests performed in different apparatus.
Vile (8)	Mortars	3/16 in.	10x10x4 in.	Rigid platens with 'Febcure' at interface	1.24 - 1.31 1.45 - 1.51	1.19 - 1.31 1.32 - 1.43	See Figure 3.2.(a). Discontinuity envelopes determined. Also tested 3/8 in. and lightweight aggregate concretes.
Opitz (71)	Concretes 225-450 kg/cm.^{2} (3200-6400 lb./in.^{2}) Concrete 300 kg/cm.^{2} (4300 lb./in.^{2})	Not reported	20x20x5 cm. (7.87x7.87x1.97 in.)	Rigid platens with p.t.f.e./brass intermediate layer without intermediate layer	1.17 - 1.34 1.36	1.05 - 1.14 1.36	See Figure 3.2.(b).
Kupfer et Al (72)	Concretes 190-590 kg/cm.^{2}	15 mm. (0.6 in.)	20x20x5 cm. (7.87x7.87x1.97 in.)	Rigid platens Brush platens	1.49 1.26 - 1.30	1.45 1.15 - 1.19	See Figure 3.3(a). Tests carried out under constant rate of strain.
Mills and Zimmerman (73)	Concretes	3/8 in.	$2\frac{1}{4}$x$2\frac{1}{4}$x$2\frac{1}{4}$ in.	Rigid platens with intermediate layer of axle grease between p.t.f.e. or polythene sheets	1.50 - 1.97	1.0 - 1.65	See Figure 3.3.(b).
Kobayashi and Koyanagi (74)	Cement Paste Mortar Concrete	- 4 mm. 15 mm.	10.5x10.5x10.5 cm. (4.13x4.13x4.13 in.)	p.t.f.e. sheet with silicone grease. Rubber sheet	1.32 1.37 1.43	0.87-1.16 0.97-1.26 1.07-1.17	See Figure 3.4.(a). Tested under sequential and proportional loading. Measured fracture initiation envelopes. Also tested lightweight concretes.
Stegbauer and Linse (75)	Cement Paste Concrete 300 kg/cm.^{2} (4300 lb/in.^{2})	- Not reported	20x20x5 cm. (7.87x7.87x1.97 in.)	Brush platens	1.07 1.26	.95 1.12	See Figure 3.4.(b). Tested other grades of concrete and lightweight concrete.

Table 3.1. Summary of strength results for biaxial tests of cement pastes, mortars and concretes containing natural aggregates.

1. Due to the lack of data obtained from biaxial tests employing hydraulic loading to achieve uniform boundary stress no valid comparisons can be made with uniform strain conditions.

2. For rigid-platen or non-rigid platen loading the maximum ratio between biaxial strength and uniaxial strength is not attained under equal biaxial compression. In fact, in most cases, the maximum value is given under a stress ratio of approximately 2 : 1.

3. Cement pastes under either rigid or non-rigid platen loading exhibit maximum biaxial strength ratios of between 1.07 and 1.12, with equal biaxial ratios between 0.95 and 1.02.

4. Mortars and concretes give considerably higher maximum biaxial and equal biaxial strength ratios than pastes for all types of rigid and non-rigid platen loading, the ratio increasing slightly with maximum size of aggregate.

5. Non-rigid platens, and rigid platens with a friction reducing intermediate layer, give biaxial strength ratios lower than those obtained using rigid platens without lubricant.

3.4. Choice of Concrete Mixes, Curing Conditions and Specimens

3.4.1. Concrete Mixes

As stated in 3.3. the mixes have been chosen to represent different degrees of heterogeneity, since it is considered that the effect of the boundary loading condition on the induced stress or strain distribution will be most affected by this factor.

Vile [8] had carried out an extensive programme of investigation into the behaviour of various types of concrete under biaxial compression, using a rigid-platen loading device. Of the mixes studied by Vile, concrete designated 6IC, containing gravel aggregate of $\frac{3}{4}$" maximum size, appeared to be the most satisfactory for the present work since it best illustrated the differences in deformational behaviour and ultimate strength between uniaxial and biaxial loading. The mortar phase of Mix 6IC, designated Mix MBC by Vile, is also tested in order to represent a concrete with a lower degree of heterogeneity.

Full details of the constituent materials and their proportions for the two mixes are given in Appendices 2 and 3 from which it can be seen that the 'effective' water/cement ratio does not remain constant for the two mixes. Vile, in fact, intended that a constant 'effective' w/c ratio of 0.55 be attained, but assumed an incorrect water absorbtion for the aggregates of only 50% of the correct value.

In Chapter 7, the deformational and strength characteristics of mixes are compared on the basis of constant 'effective' w/c ratio and the problems of such an approach are discussed. Basically, the difficulty lies in defining the amount of water available to contribute to the hydration process and the quantity which remains absorbed in the aggregate. In order to provide additional data it has been decided to adopt Vile's original mix proportions, leading to correct 'effective' w/c ratios of 0.52 and 0.46 for the mortar and concrete mixes respectively, in order to investigate the change in behaviour if only 50% of the water in the aggregate is assumed to be available for cement hydration. Such a departure from accepted practice is considered justifiable, since the aim of the present series is to compare the behaviour of concretes and mortars representing large differences in heterogeneity under different boundary loading conditions rather than to investigate in detail the effect of mix parameters.

3.4.2. Curing Conditions

During his test programme Vile [8] found the best friction-reducing intermediate material to be 'Febcure' applied to saturated surfaces of specimens. As the present tests are intended mainly to furnish comparisons, rather than provide general design data, it has been decided to depart from the philosophy outlined in 7.2.2. and to test saturated rather than dried specimens.

The curing conditions, therefore, have been kept as close as possible to those used by Vile, and entail curing under B.S. conditions for 25 days at which time the specimens are painted with two coats of 'Febcure Super 90' and stored in laboratory air until tested at 28 days $\pm$ 1 day. This variation in the age at test is unavoidable due to the time-consuming nature of the tests and is taken into account by testing a sample of each type of specimen at 27, 28 and 29 days respectively. The effects of the age differential are found to be insignificant.

3.4.3. Specimens

As discussed in 7.2.3., the maximum aggregate size of $\frac{3}{4}$" ensures that minimum cross-sectional dimensions of specimens given below: provide representative volume elements.

Test Specimen	Minimum Cross Section
Direct Tensile	4" x 3"
Cube	4" x 4"
Prism for Uniaxial Compression	4" x 4"
Cylinders for Uniaxial and Biaxial Compression	4" diameter
Slabs for Uniaxial and Biaxial Compression	4" x 10"

For both the slabs and cylinders tested under biaxial compression, the unstressed direction coincides with the vertical direction as cast, and thus the tests can be considered comparable with respect to the effects of anisotropy.

In order to assess the effects of anisotropy and specimen shape on the behaviour of concrete, companion cubes, prisms and slabs are loaded uniaxially in compression.

3.5. Apparatus and Methods of Testing

3.5.1. Measuring and Recording System for Stresses and Strains

It is required to accurately, and continuously, measure strains in zones of specimens where the stress or strain state is the most uniform and definable. To this end 60 mm. electrical resistance strain gauges are used, which measure average strains on the surface of cylindrical and prismatic specimens.

For the slabs, 60 mm. strain gauges were attached to the surface for measuring the strain in the stressed directions while the strain in the

unstressed direction, a knowledge of which is extremely important for a study of the fracture mechanism, was measured by strain gauges fixed within a small diameter hole cast in the specimens. This method has been chosen, after extensive trials with several types of specially designed transducers, in order to obviate the necessity for using external transducers with the attendant difficulties of their attachment to the specimen. Full details of the layout of the holes and gauges are given in 3.5.5.3.

The loads applied by the various systems were measured by pressure transducers whose outputs, together with the associated strains on the specimens, were recorded using a Modulog automatic digital data logger recording at a rate of 10 channels per second to a sensitivity of $\pm$ 1 microstrain.

3.5.2. Cube Tests

Full details of the method of performing the cube tests are given in 7.3.2. For the purposes of comparison with other specimens of this series the 'Febcure' coating was not removed from the loaded surfaces prior to test.

3.5.3. Direct Tensile Tests

Details of the tests are given in 7.3.3. Prior to test the 'Febcure' coating was removed from the surfaces of the specimens in contact with the gripping device to prevent slippage.

3.5.4. Uniaxial Cylinder and Prism Tests

These tests were carried out in a 300 Tonf. Amsler testing machine, using the same subsidiary platen and spherical seating unit as for the cube tests. As in the case of the cubes, the 'Febcure' coating was not removed from the loaded surfaces prior to test.

The stressing rate adopted was the standard 2000 lb/in^2/min. [62] and the deformational behaviour was measured using surface-mounted 60 mm. strain gauges.

3.5.5. Uniaxial and Biaxial Compression Tests under near-uniform Boundary Strain

3.5.5.1. Introduction

The Complex Stress Machine used by Vile proved highly successful in carrying out a comprehensive programme of tests in which specimens of concrete were

loaded under various biaxial stress ratios [8]. The basic design details of this apparatus have already been adequately described [75].

A preliminary series of tests carried out during the current test programme disclosed, however, certain difficulties of operation and deficiencies in the design which it was thought necessary to correct prior to performing the main test series. Details of these faults, and the modifications made to the machine in an attempt to improve them, are described in the following sections.

3.5.5.2. Complex Stress Machine

As stated above the machine, as manufactured according to Vile's specifications, required modification to improve its performance. The faults found, together with the remedial measures taken to minimise them, are described in the following, and the general layout of the modified apparatus is shown in Figure 3.5. and summarised in Appendix 1.

(i) Stiffness Characteristics

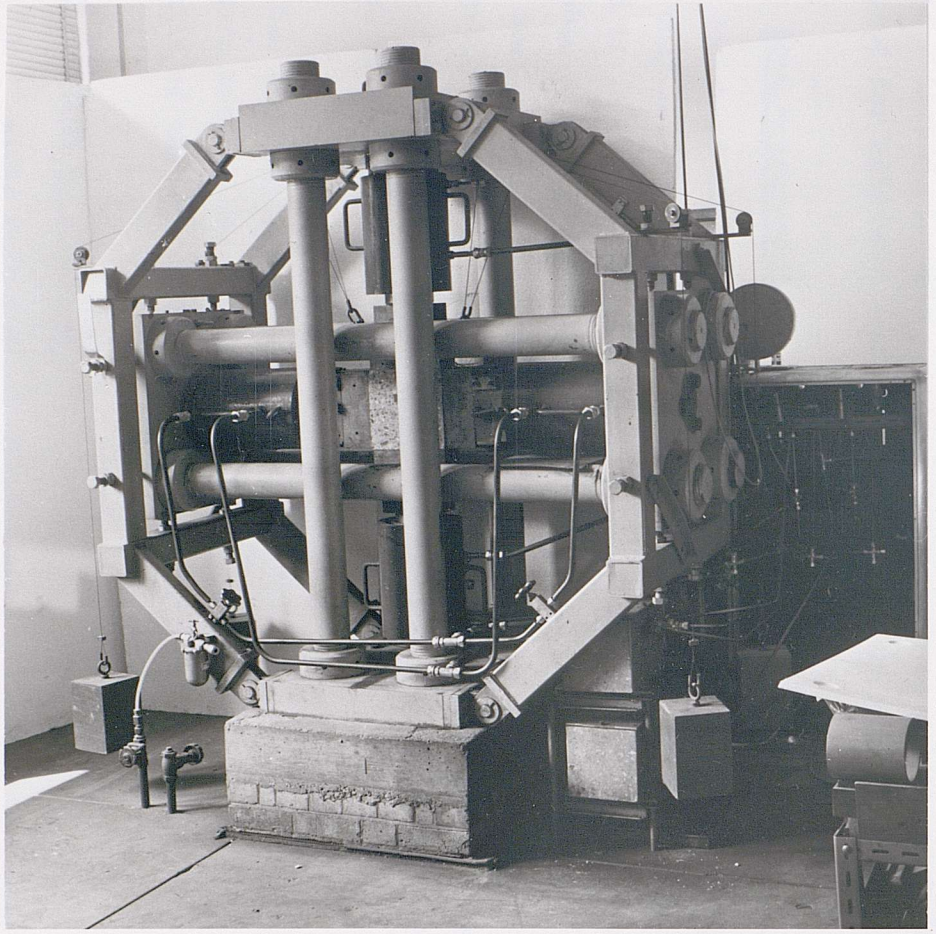
The mode of failure of specimens indicated that the machine was excessively 'soft' in the directions of loading, in spite of being designed to exceed the stiffness requirements suggested by Sigvaldason [4].

The problem was considered to be due mainly to the excessive length of oil column behind the hydraulic rams prior to applying load, and partly to the use of large-bore oil pipework.

Accordingly, the oil column was reduced by inserting mild-steel spacer discs behind the rams, and the oil pipework was replaced by small bore tubing. In addition the layout was rationalised to reduce the oil path length from the pumps to the rams.

(ii) Load Control and Measuring System

In the original machine, the rate and level of the load transmitted in each direction was controlled by the continual adjustment of needle valves. Such valves are extremely non-linear in operating characteristics, being highly sensitive at high pressures. Accurate load control was thus difficult to achieve and, as a



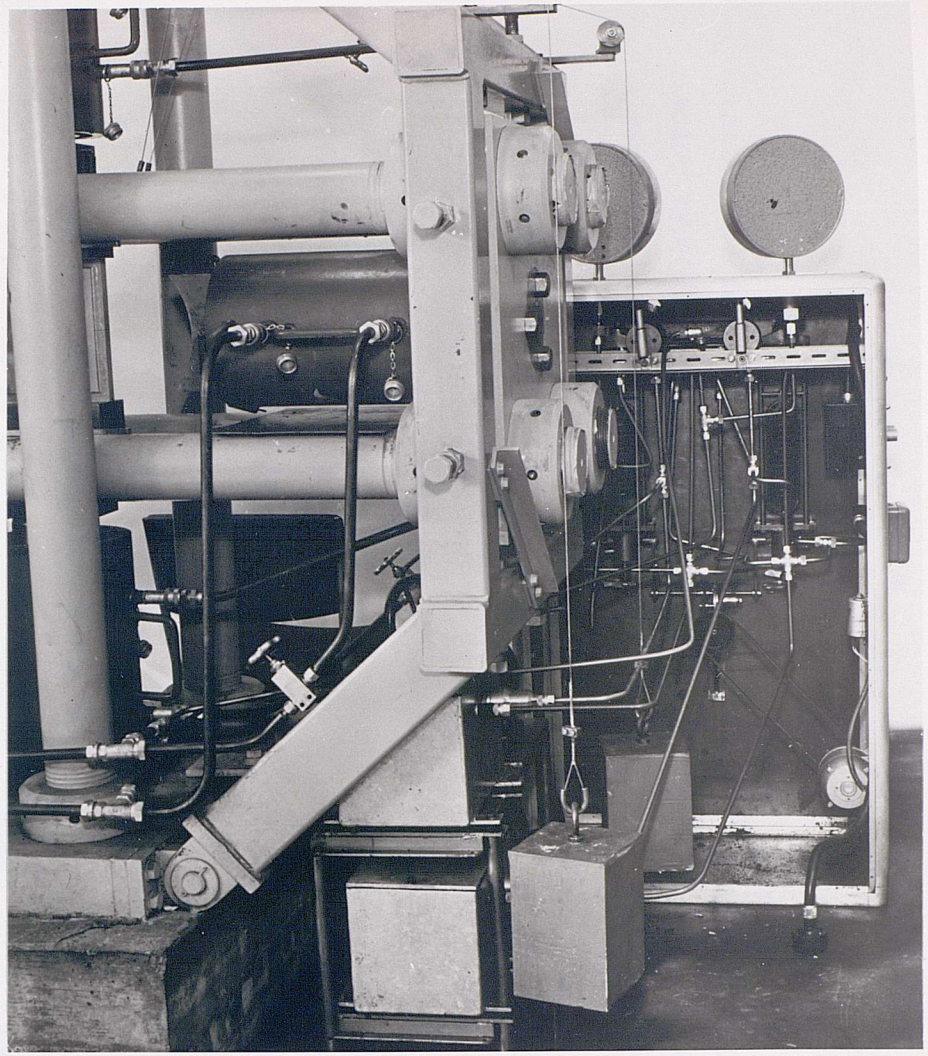


Figure 3.5. General views of Complex Stress Testing Machine and control system.

result, the control console was completely redesigned around Amsler type load maintainer valves, which are linear in operation. A rear view of the new console is shown in Figure 3.5.

(iii) Platen Units

The dimensions and surface finish of the platen blocks were found to be outside acceptable limits, thus causing considerable stress disturbances. Accordingly, the platens were remachined to the tolerances specified in B.S. 1881 [62] and examined periodically to check if distortion had occurred. It was found that the plain unhardened mild steel blocks frequently required remachining during the test series.

(iv) Alignment of Machine Frames and Specimen

Accurate alignment of the two main machine frames, and the setting-up of specimens for test, proved exceedingly difficult due to the number of degrees of freedom for movement of the system, and lack of a stable reference guide.

After numerous attempts a satisfactory procedure has eventually been adopted for alignment and this is outlined in Appendix 6.

(v) Load Measurement

The design of the original machine incorporated pressure gauges as the only means of load measurement. For continual recording of load it is considered essential to use some form of transducer capable of being connected to a data logger. It was decided that the most convenient form of measurement would be by incorporating sensitive pressure transducers in the oil circuit close to the rams, and protected from shock loading by interposing a length of tubing which acted as a 'snubber'.

The two transducers were calibrated against a load cell interposed in turn between the vertical and horizontal pairs of platens. Details of the equipment are given in Appendix 1.

3.5.5.3. Preparation of Specimen

The 10" x 10" x 4" slabs were cast in steel moulds conforming to the tolerance

requirements of B.S. 1881. Using a plastic covered steel former, a 0.25" diameter steel hole normal to, and in the centre of, the 10" x 10" faces, was cast through the 4" thickness of each slab in order to provide a location for the transverse strain gauges.

On removing the specimens from the moulds the steel former was withdrawn leaving the plastic tubing inserted in the holes. After demoulding the specimens were cured as described in 3.4.2.

At 14 days after casting the specimens were removed from water and their faces ground precisely plane and parallel, to within approximately 0.001", using a water lubricated and cooled diamond cup wheel. This procedure was adopted following the conclusions drawn in Chapter 2.

After the grinding process, which entailed the use of a specially developed jig device fitted to the grinding machine, the specimens were immediately returned to water for completion of the curing regime.

At 25 days the specimens were coated with two coats of 'Febcure Super 90', the second coat being applied as soon as the first had dried.

When the second coat was dry the areas over which the strain gauges were to be attached were scraped clean of 'Febcure' and laitence, and allowed to dry to ensure efficient bonding of the strain gauge adhesive. After this procedure, and after removing the plastic tubing from the transverse hold, the 60 mm. strain gauges were attached in the positions shown in Figure 3.6.

3.5.5.4. Specimen Setting-up

The process eventually adopted, after extensive trials to determine the best method of minimising non-axial loading, is described in Appendix 6. This technique has proved relatively simple to perform and reduces the time necessary to prepare the apparatus for test.

3.5.5.5. Method of Testing

The two types of test conducted using the Complex Stress Machine are uniaxial and equal biaxial compression. For the uniaxial compression case the vertical load frame only is used. For biaxial compression the hydraulic systems applying load through the two frames are linked, such that they operate

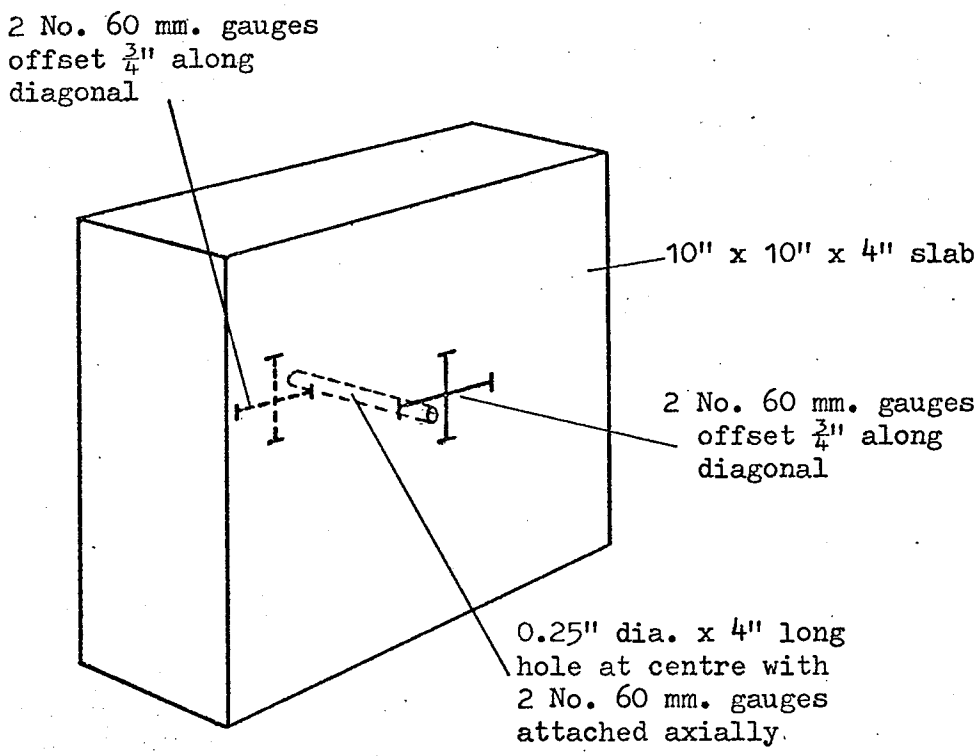


Figure 3.6. Positions of electrical resistance strain gauges on slab specimen.

from a single pump and control valve. This ensures an accurately proportional loading path, identical to that used for the tests conducted under near-uniform stress using the hydraulic cell.

As for the other types of specimen tested the coatings of 'Febcure' were not removed from the loaded surfaces prior to test.

The stressing rates for the uniaxial and equal biaxial tests are 2000 lb/in^2 per minute and 1000 lb/in^2 per minute respectively, as used by Vile [8].

Since the deformation of the slabs is of a low order, calculation of the stresses acting on the slabs is based on the cross-sections of the specimens in the two stresses directions as measured immediately prior to test.

3.5.6. Biaxial Compression Tests under near Uniform Boundary Stress

3.5.6.1. Introduction

The hydraulic cell used for the triaxial 'compression' tests, and described in Chapter 7, is designed such that additional facilities for carrying out triaxial 'extension' tests can be incorporated.

Essentially, the basic problem is to eliminate the component of stress in the axial direction, while applying confining pressure and hence equal biaxial compressive stress to the cylindrical surface of the specimen. This is achieved by inserting a sealing unit between the piston unit and the specimen, to replace the spherical seating unit used for 'compression' tests.

Using such an arrangement, the stress acting in the axial direction will, in actuality, depend on (a) the frictional resistance of the piston, which opposes the induced axial extension of the specimen, and (b) the disparity in cross-sectional area between the specimen and piston. If the cross-section of the specimen is lower than that of the piston, then separation of the specimen/sealing unit interface will tend to occur with possible implosion of the impermeable membrane at this position. For cases where the specimen dimension is larger than the piston, a resultant compression will be induced in the axial direction.

The reliability of the test is, therefore, highly dependent on the accuracy of measurement of the cross-sectional dimensions of the specimens and the correct evaluation of the frictional restraint of the piston unit. Such a dependency is undesirable, since the aim of the test is to load specimens of concrete with the assurance that no significant secondary restraint stresses are induced. To overcome this difficulty due allowance must be made for the likely errors of measurement and calibration and a technique intended to accomplish this is described in the following section.

3.5.6.2. Loading Technique to account for Secondary Restraint Stresses

The specimens are cylinders of the 'waisted' type, requiring a compressive load to be applied in the axial direction in order to nullify the effects of the reduced diameter for each value of confining pressure applied. This procedure gives the advantage of ensuring that the end zones of the specimens are under triaxial compression and hence unlikely to initiate failure.

The 'waisted' cylinders are subjected to the three following types of test, full details of the method of calculation of the compensating axial loads for the various types of test being given in Appendix 5.

(i) 'Null' tests

Where the axial compensation load exactly cancels out the stress in the specimen, as calculated using mean values for cross-sectional dimensions of the piston and 'waisted' portion of each specimen, frictional restraint, and calibration constants.

(ii) 'Tensile' tests

For these cases the axial compensation load is based on the above mean values plus or minus an appropriate tolerance, in order to give the worst case of under-estimated load. Thus, it will be highly probable that a slight tensile stress will exist in the axial direction.

(iii) 'Compression' tests

As for (ii), except that the signs of the various tolerances are chosen to give the worst case of over-estimated load, such that a resultant compressive stress is likely to be induced in the axial direction.

Three specimens of each mix have been subjected to each of the above tests and the spread of results should, therefore, enclose the true value for an axially unrestrained specimen.

3.5.6.3. Hydraulic Cell and Control System

Details of the hydraulic cell and confining pressure control system are given in 7.3.4.2. For 'extension' tests, of which equal biaxial compression is a special case, the spherical seating unit, through which the axial deviator load is applied in the case of 'compression' tests, is replaced by a specially designed platen unit shown in Figure 3.7. and Figure 7.3. This unit, when sealed to the piston, and the interface between it and the specimen is enclosed by the impermeable sheath, ensures that no component of confining pressure acts, except on the annular area represented by the difference between the cross-sections at areas of piston and specimen.

To guard against the possibility of oil penetrating the double seals of the platen unit, the interface between it and the piston is vented to atmosphere. In fact, no leakage was experienced during the entire test series.

For the biaxial series the axial compensation load is applied by hydraulic pressure acting on the upper surface of the piston balancing annulus. The system to control this pressure is shown in Figure 3.8. and is used in conjunction with the confining pressure control system (see Figure 7.3.) by closing valves A and B and removing the lengths of pipework adjacent to the cell.

3.5.6.4. Preparation of Specimens

The 4" diameter x 10" long cylindrical specimens were cast in the same steel moulds as used for the triaxial 'compression' series and cured in the manner described in 7.4.3.

At 14 days after casting the specimens were removed from water and their end faces ground plane and parallel using a diamond cup-wheel.

The specimens were then accurately 'waisted' to a nominal 3.9" diameter over the central 6" portion, using a lathe fitted with a tool-post grinder and diamond-impregnated grinding wheel. The transition between the 'waisted'

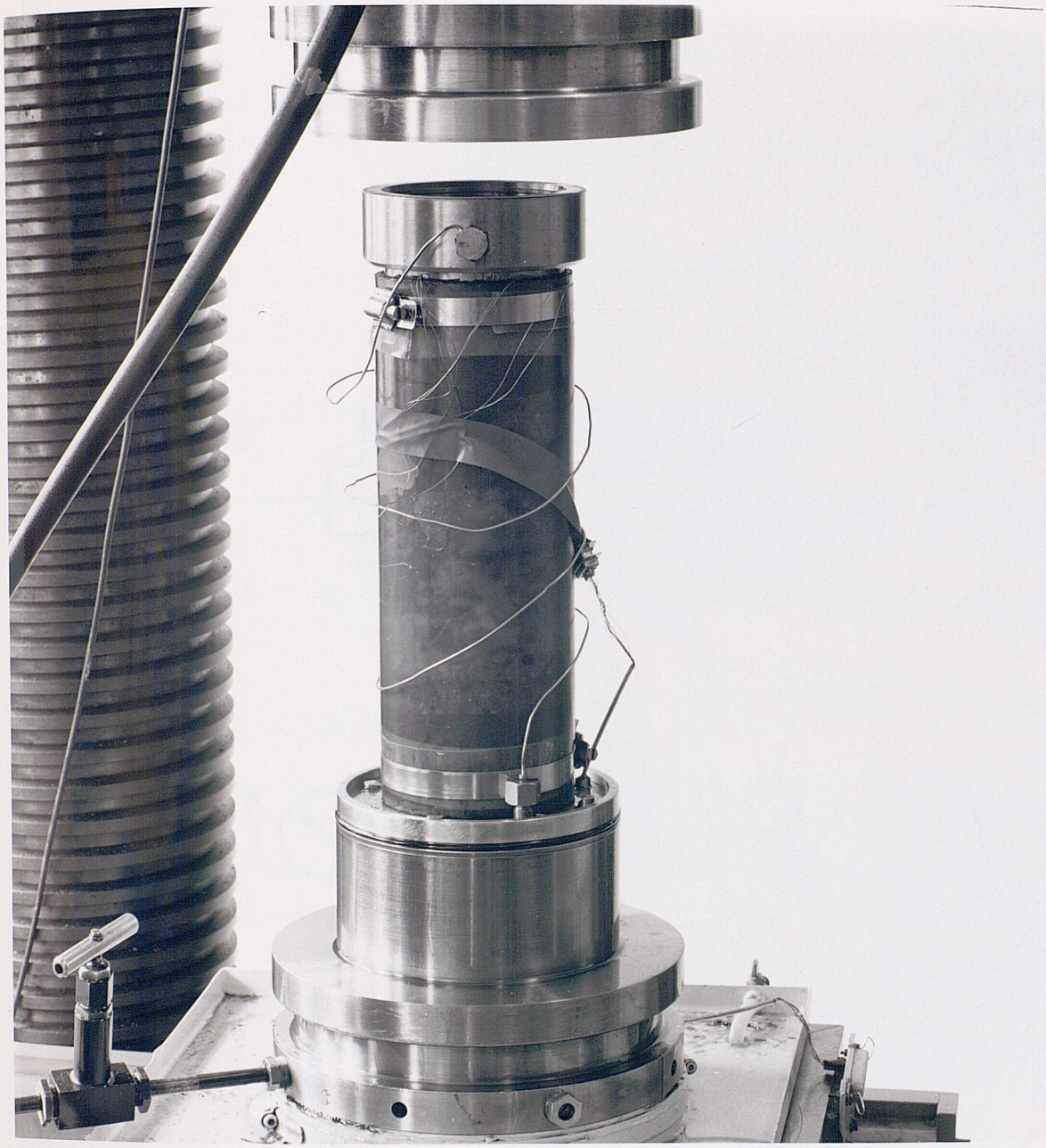


Figure 3.7. View showing arrangement of specimen/platen/sheath unit prepared for an equal biaxial compression test in the hydraulic cell

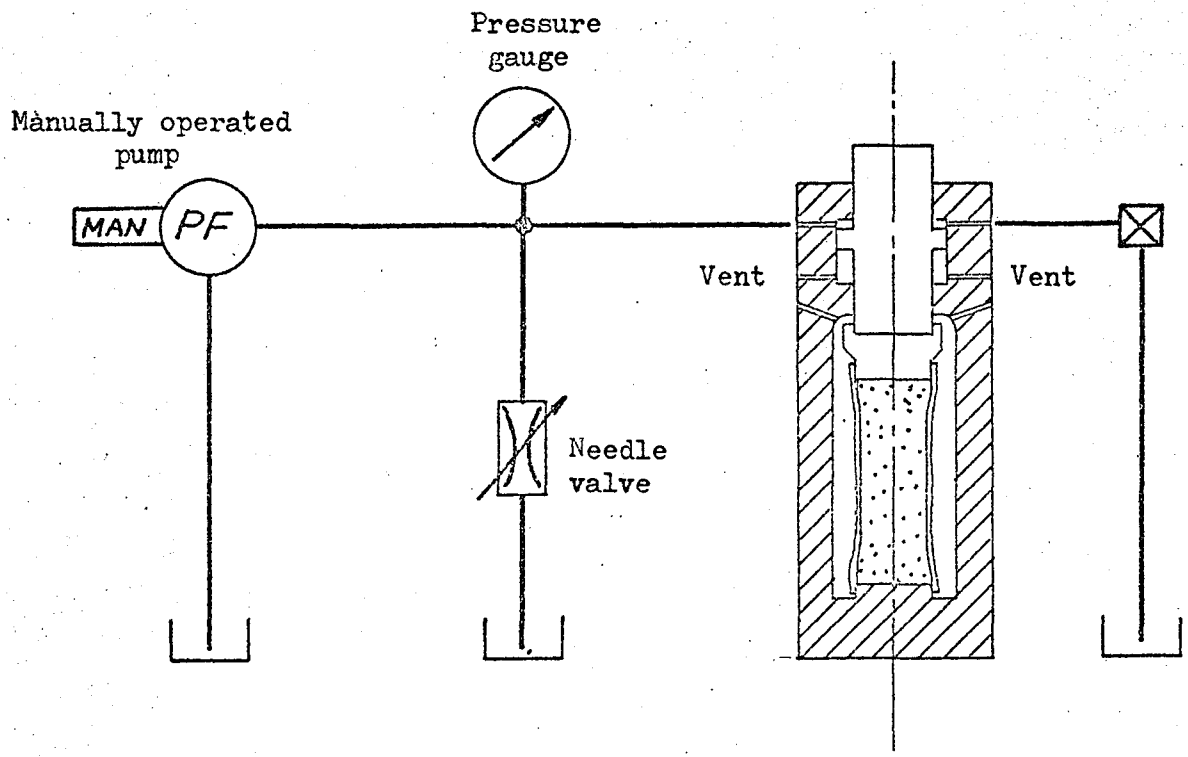


Figure 3.8. Pressure control system for applying axial compensation load in equal biaxial compression tests.

and 'unwaisted' sections was made smooth in order to ensure the minimum of stress concentrations. The effectiveness of this is demonstrated by the fact that none of the eventual failure planes of the specimens pass through the transition zones.

At 25 days the specimens were coated with 'Febcure Super 90', as for the remainder of the test series, and 60 mm. strain gauges attached to the surface in positions as detailed in 7.4.5. and following the same procedure.

3.5.6.5. Specimen Setting Up

Full details of the assembly process, in which the upper platen unit and lower platen is fitted to the ends of the cylinders and the impermeable sheath clamped in position, is given in Appendix 6.

The preparation of the test apparatus essentially follows the procedure outlined in 7.3.4.4., except that the piston is sealed into the upper platen unit using a screw jack interposed between the top of the piston and the loading frame.

3.5.6.5. Method of Testing

In order to preserve uniformity of testing technique, the coatings of 'Febcure' are not removed from the surfaces of the specimens prior to test. The loading path used for the tests, and shown in Figure 3.9. is achieved by increasing the confining pressure at a rate of 1000 lb/in^2 per minute and applying, at the same time, the calculated axial compensating load at a proportional rate using a handpump for sensitivity of control. A handpump is also used to apply the axial load, again from considerations of sensitivity of control.

Values of confining pressure, axial and circumferential strains were measured and recorded continuously throughout the test, at a rate of 10 channels per second. Each test was terminated when the specimen failed due to cleavage across a plane normal to the axis of the cylinder.

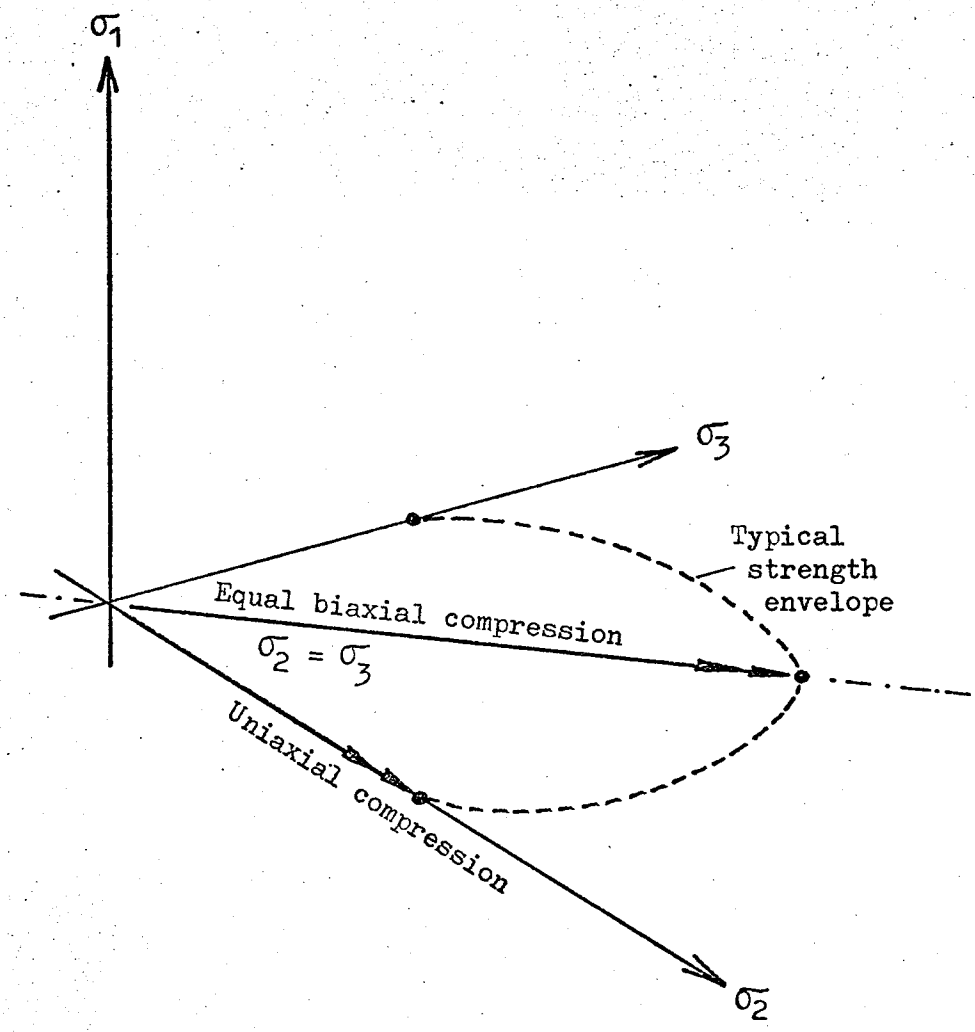


Figure 3.9. Loading path used for equal biaxial compression tests.

3.6. Uniaxial Compression Tests

3.6.1. Results

The complete stress-strain relationships are stored in the form of computer printouts with the Concrete Materials Research Group. The principal derived results for the cylinder, prism and slab tests are given in Appendix 7. For definitions of the various significant levels of material behaviour (onset of stable fravture propagation, onset of unstable fracture propagation and ultimate) see 4.5.

For ease of comparison, the values of stress and strain at the various levels of change of material behaviour (o.s.f.p., o.u.f.p. and ultimate) for the mortar and concrete are represented diagramatically in Figures 3.10 to 3.13, in terms of the 95% confidence limits for the means.

The results are summarised qualitatively in Table 3.2. where the behaviour of the various types of specimen of a given mix is compared, as well as the behaviour of given specimens of different mixes.

3.6.2. Discussion of Results

3.6.2.1. Stress-Strain Relationships

The stress-strain relationships for the cylinder, prism and slabs tests for the mortar mix MBC and concrete mix 6IC are shown in Figures 3.14. and 3.15. respectively while Figure 3.16. shows the mean relationships for the two mixes.

The relatively small variations within the batches of three specimens of a given type, apart from some divergence which is to be expected near ultimate, indicate a uniform mix, consistent loading method and a representative strain measuring technique.

The higher strains given by the slabs of both mixes, as compared with the corresponding cylinders and prisms, indicate that the restraint effects produced by a rigid-platen loading technique, using a friction reducing intermediate material ('Febcure'), induce considerably higher deformations within the central portion of slabs especially as ultimate is approached. It is possible to ascribe this phenomenon to three main causes as follows:

PROPERTY	MORTAR	CONCRETE
Stress Strain Relationships		
Variability -		
Between specimens of a given type	Extremely small variations up to ultimate for all types of specimen.	Extremely small variations initially, with some divergence approaching ultimate.
Shape and Magnitude of Relationships -		
Differences between specimens	Cylinders and prisms almost identical, slabs exhibit higher strains at all stress levels.	Cylinders and prisms almost identical up to approx. 75% ultimate. Slabs almost identical up to approx. 50% ultimate, after which higher strains exhibited.
Differences between materials	Strains lower in the concrete than the mortar at all stress levels.	
Incremental Strain Ratio-Stress Relationship		
Variability -		
Between specimens of a given type	Much wider variations for cylinders and prisms than for slabs.	Slightly wider variation for slabs than cylinders or prisms.
Shape and Magnitude of Relationships -		
Differences between specimens	Cylinders and prisms similar and showing a decrease of i.s.r. then near constant portion followed by sharp increase. Slabs show no initial decrease and much shorter constant portion.	Cylinders and prisms similar but show no initial decrease. Slabs also show no initial decrease and constant portion is much shorter.
Differences between materials	Stress levels at end of constant portion higher for mortar slabs than for concrete but are the same for cylinders and prisms. i.s.r. values for near constant portion of relationship lower for concrete than mortar.	
Onset of Stable Fracture Propagation		
Differences between specimens	Relatively large differences with stress and strain levels highest for cylinders and lowest for slabs.	As for mortar.
	Stress level as a proportion of ultimate highest for cylinders and lowest for slabs.	As for mortar.
Differences between materials	Stress levels similar for prisms and cylinders of both materials but significantly higher for mortar slabs than for concrete.	
	Strain levels considerably higher for mortar than concrete.	
	Stress levels as proportion of ultimate are significantly greater for concrete cylinders and prisms than mortar, but similar for the slabs of both mixes.	

Table 3.2. (a) Summary of results obtained from uniaxial compression tests.

PROPERTY	MORTAR	CONCRETE
Volume Change-Stress Relationship		
Variability -		
Between specimens of a given type	Relatively large variations for cylinders and prisms, extremely small variation for slabs up to approx. 75% ultimate.	Small variation for cylinders and prisms until near ultimate. Relatively large variation for slabs.
Shape and Magnitude of Relationships -		
Differences between specimens	Almost identical shape for all specimens (particularly cylinders and prisms) up to start of volume increase.	As for mortar.
Differences between materials	Larger rates of volume decrease for mortar than concrete.	
Onset of Unstable Fracture Propagation		
Differences between specimens	Stress and strain levels highest for cylinders and lowest for slabs.	As for mortar.
	Stress level as a proportion of ultimate highest for cylinders and lowest for slabs.	As for mortar.
Differences between materials	Stress levels and strain levels considerably smaller for concrete than mortar. Stress levels as a proportion of ultimate significantly higher for mortars than concretes.	
Ultimate		
Differences between specimens	Stress levels highest for cylinders and lowest for slabs, but differences small.	As for mortar.
	Tensile and compressive strain levels highest for slabs and lowest for cylinders.	Tensile and compressive strains highest for slabs and lowest for prisms.
	Volumetric strains highest for cylinders and lowest for slabs.	Volumetric strains highest for slabs but lowest for cylinders.
Differences between materials	Stresses and strains lower for concrete than for mortar.	

Table 3.2. (b) Summary of results obtained from uniaxial compression tests.

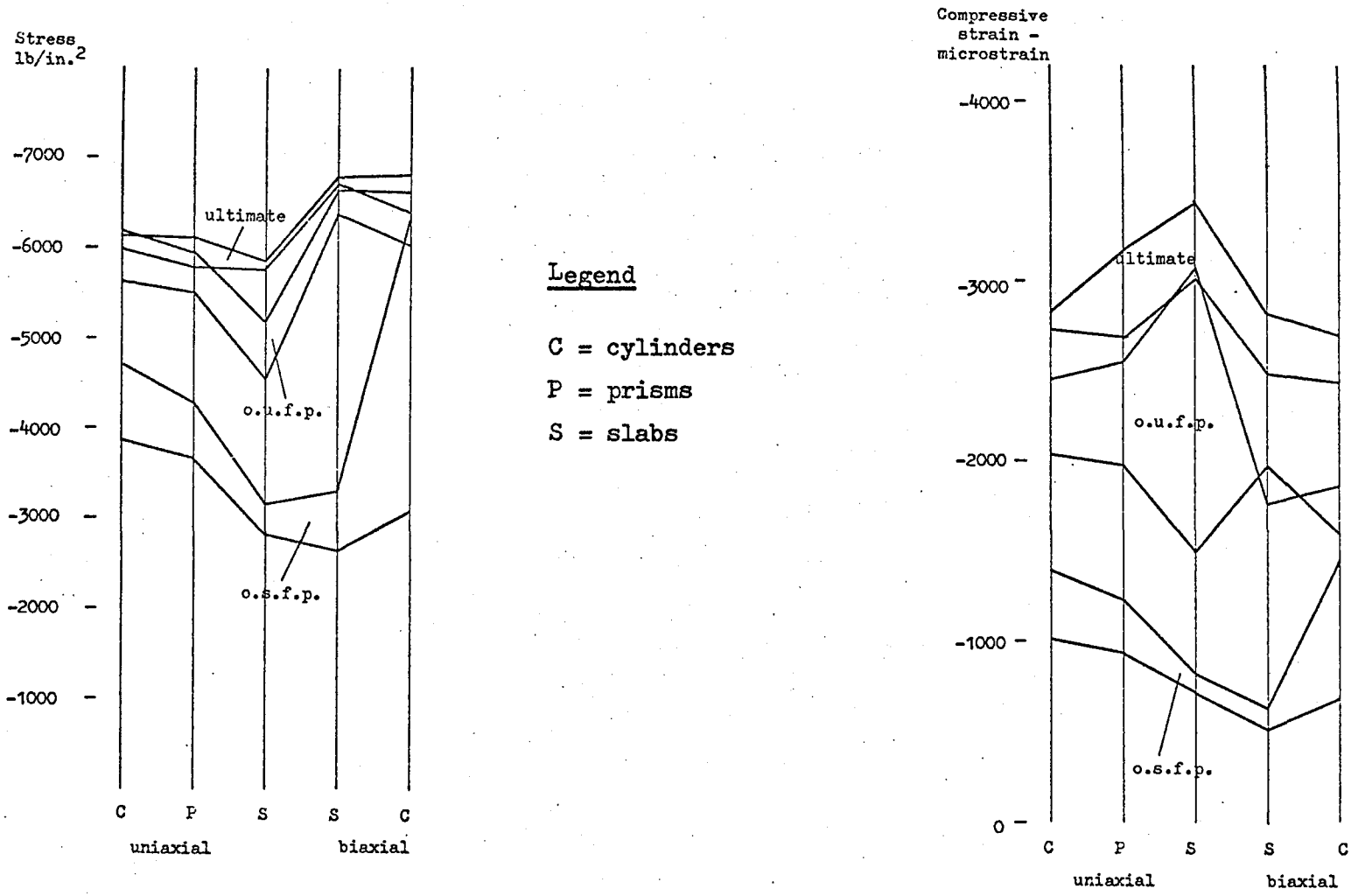


Figure 3.10. Variation of stress and compressive strain at o.s.f.p., o.u.f.p. and ultimate for various types of specimen of Mix MBC under uniaxial and equal biaxial compression in terms of 95% confidence limits for the means.

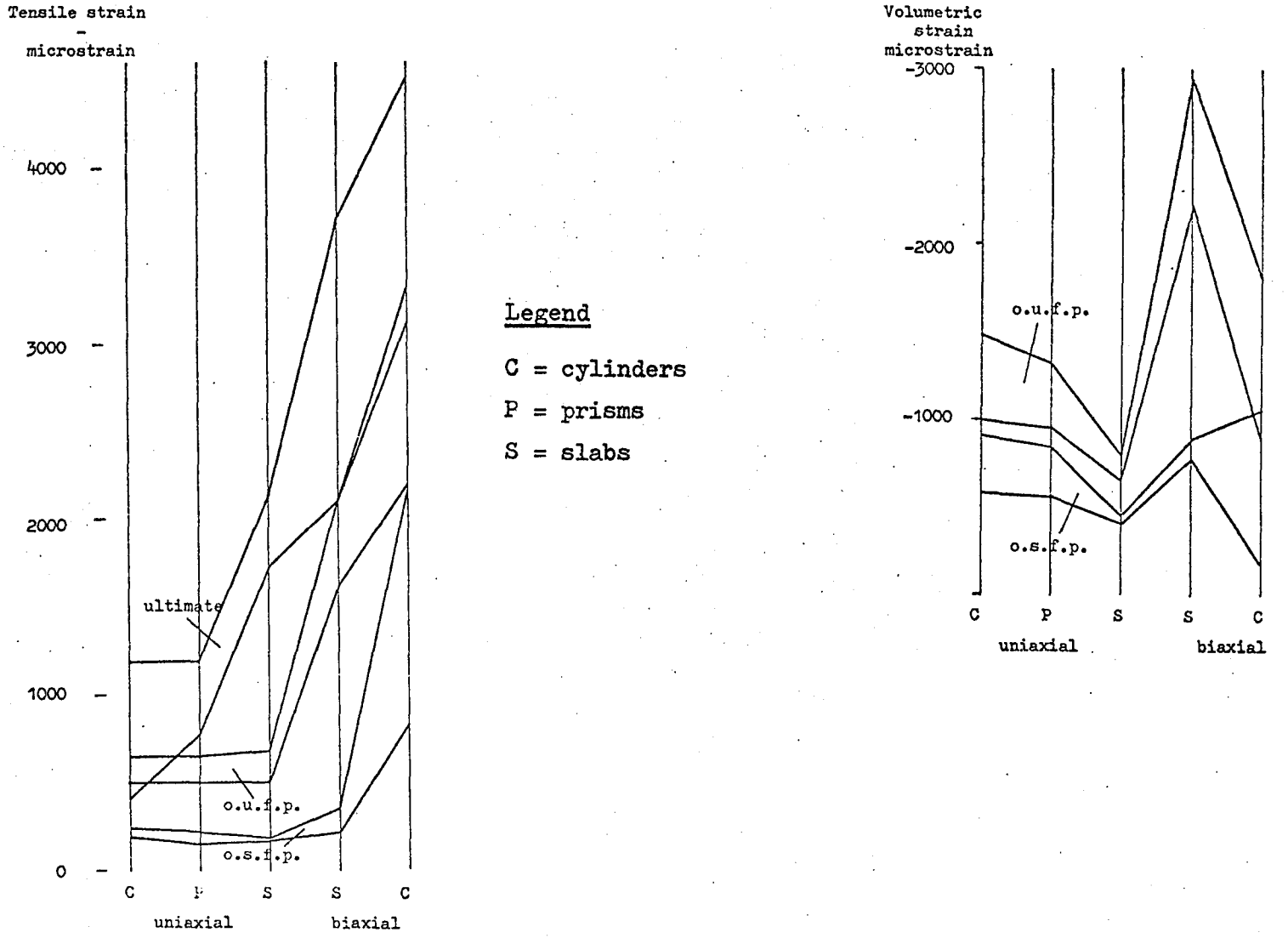


Figure 3.11. Variation of tensile and volumetric strain at o.s.f.p., o.u.f.p. and ultimate for various types of specimen of Mix MBC under uniaxial and equal biaxial compression in terms of 95% confidence limits for the means.

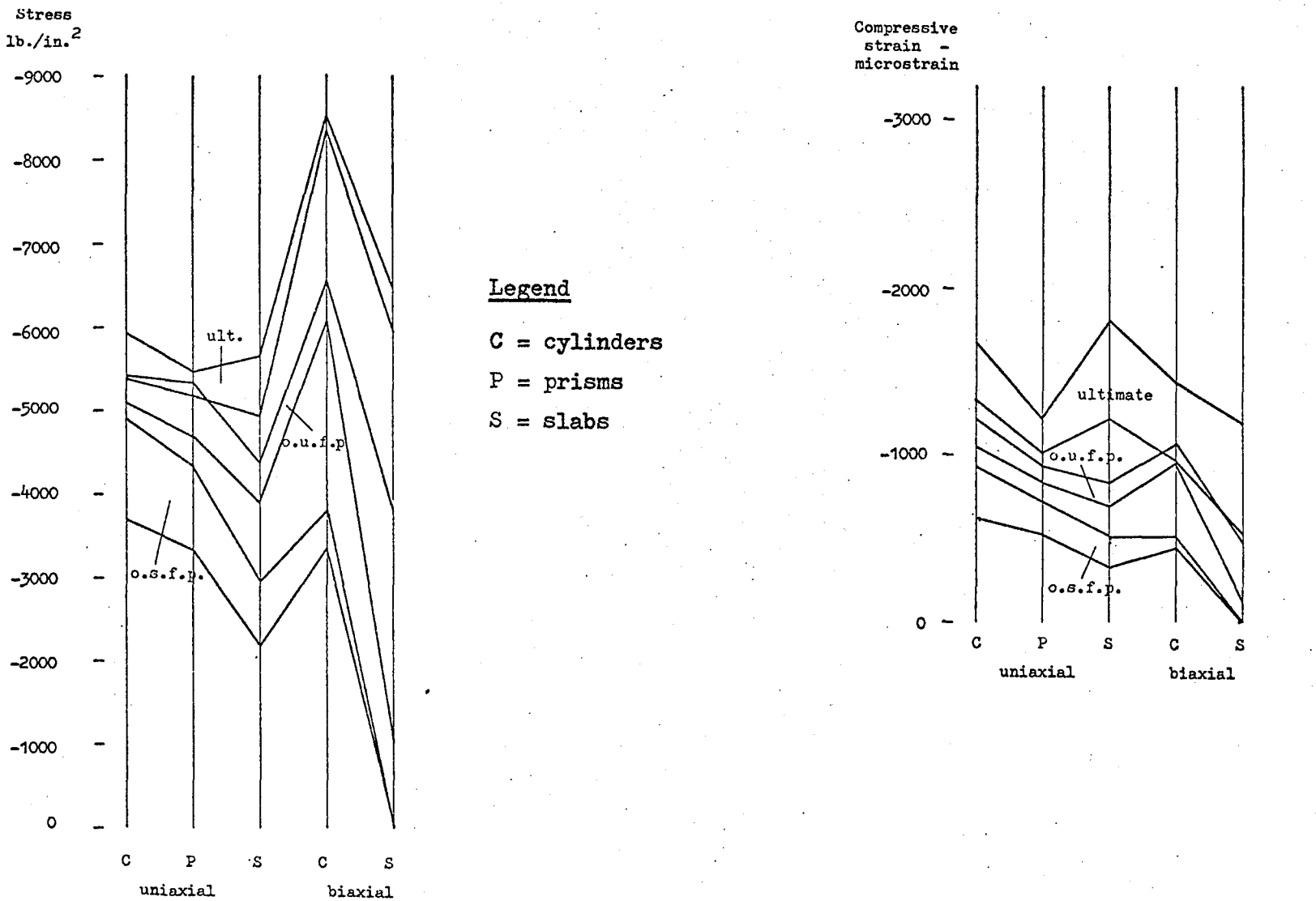


Figure 3.12. Variation of stress and compressive strain at o.s.f.p., o.u.f.p. and ultimate for various types of specimen of Mix 6IC under uniaxial and equal biaxial compression in terms of 95% confidence limits for the means.

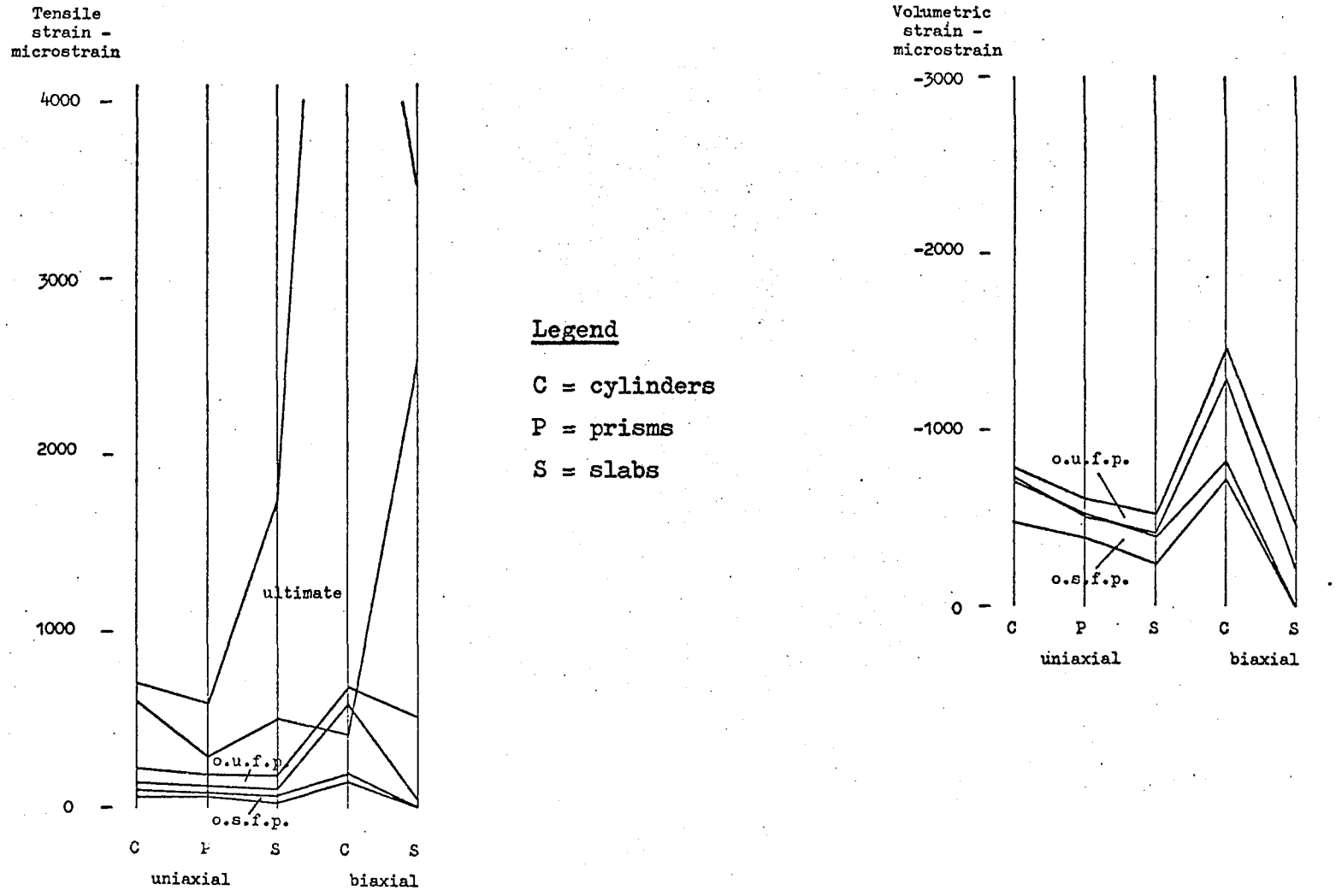
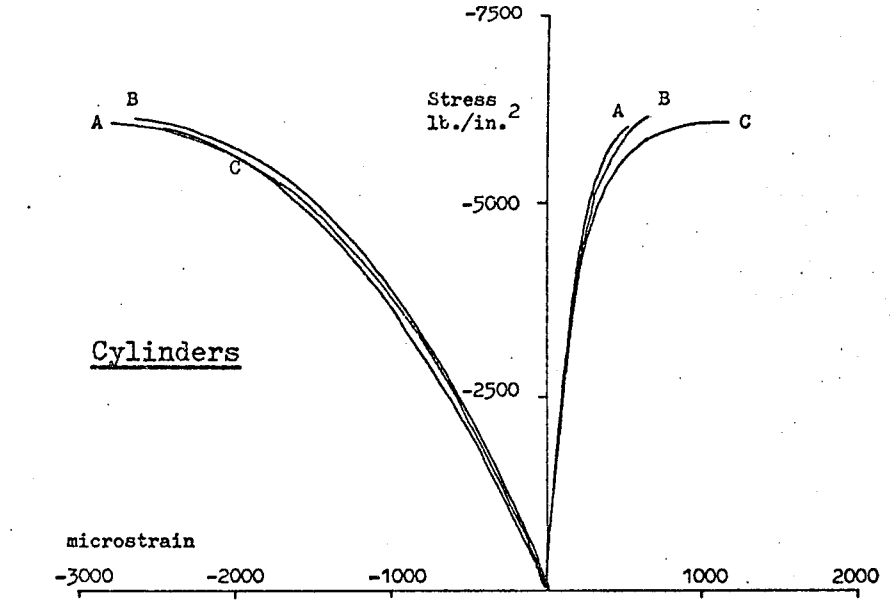
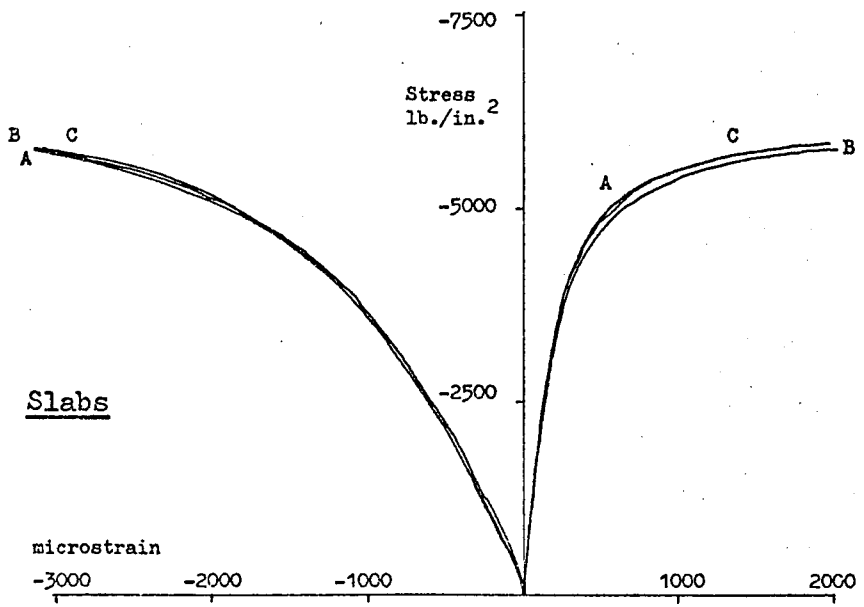


Figure 3.13. Variation of tensile and volumetric strain at o.s.f.p., o.u.f.p. and ultimate for various types of specimen of Mix 6IC under uniaxial and equal biaxial compression in terms of 95% confidence limits for the means.





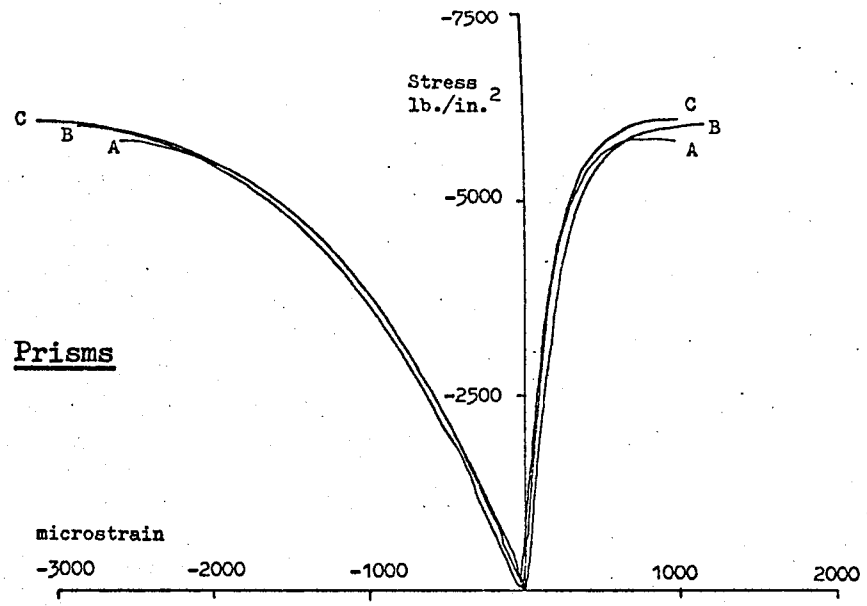
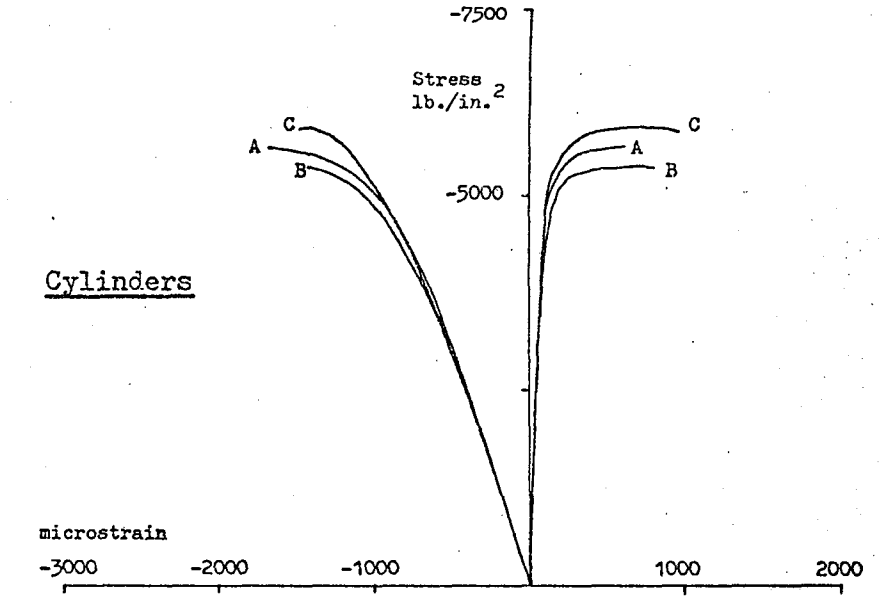
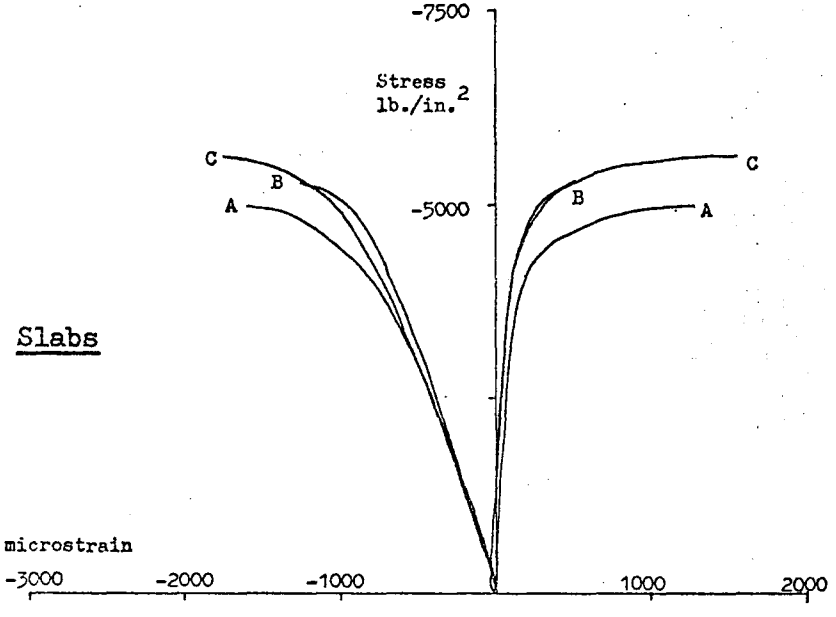


Figure 3.14. Variation of axial and lateral strains with axial stress for specimens of Mix MBC under uniaxial compression.





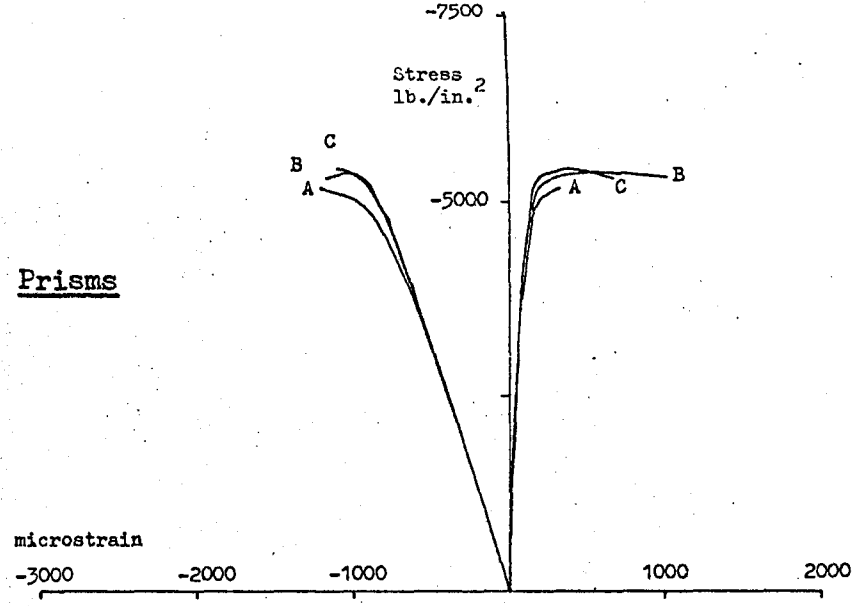
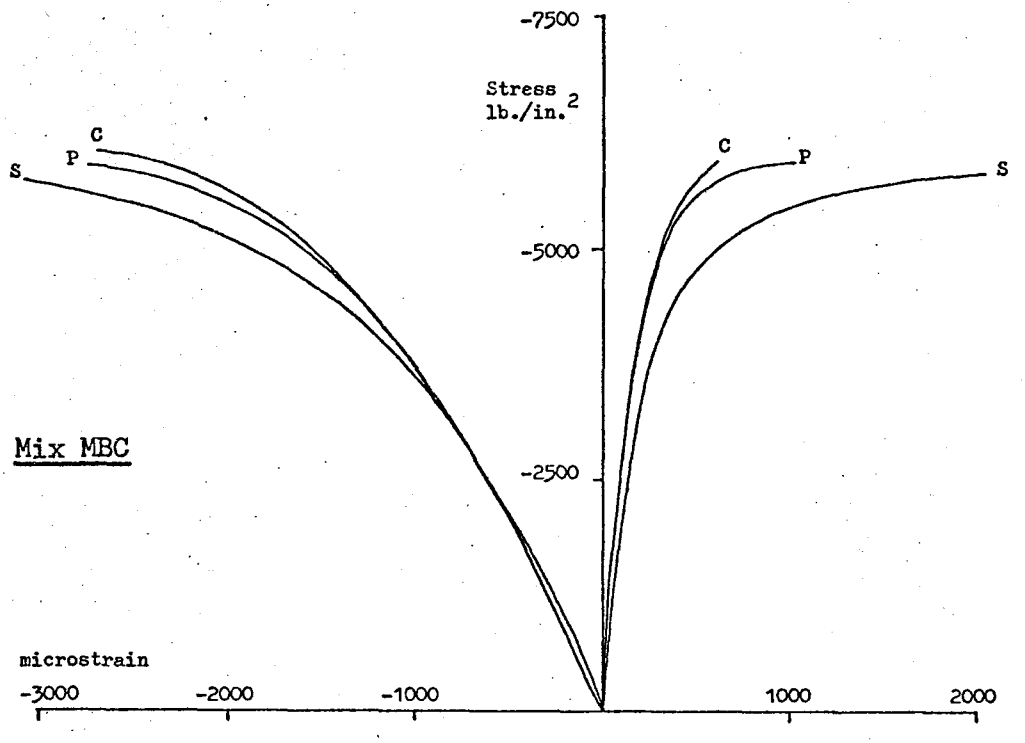


Figure 3.15. Variation of axial and lateral strains with axial stress for specimens of Mix 6IC under uniaxial compression.



Legend

C = cylinders
P = prisms
S = slabs

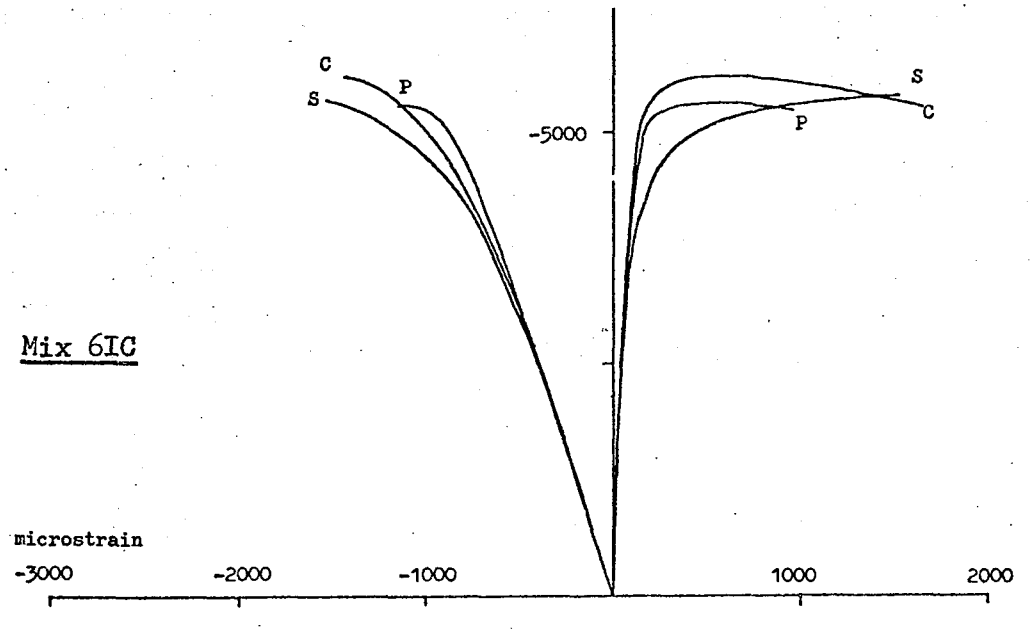


Figure 3.16. Variation of mean relationships between axial and lateral strains and axial stress with type of specimen for Mixes MBC and 6IC under uniaxial compression.

(i) The behaviour may be dependent on the relative sizes of the different types of specimens [77], or on the volume of material surrounding the portion within which strain measurements are made. Such an explanation is supported by the fact that the curves for the prisms lie slightly below those for the cylinders. If this were due to the effect of casting direction the reverse would be expected [78].

(ii) The loading platens of the Complex Stress Machine may apply restraints such that a higher degree of triaxial compression is induced within the slabs than within the prisms or cylinders, thus promoting a different deformational behaviour. This is not confirmed by any associated increase in ultimate strength for the slabs as compared with the prisms or cylinders (see 3.6.2.5.).

(iii) The platen may tend to deform and/or the friction-reducing interface may tend to flow under load, such that the stress is concentrated through the central portion of the slabs. In Chapter 2 compressive stress concentrations of between 1.0 and 1.2 x the average boundary stress are found, in fact, in the central zone of ground slabs loaded uniaxially through the rigid platens and 'Febcure' as the intermediate material. The corresponding tensile stress induced is between 0.02 and 0.03 x the average applied boundary stress. These effects would tend to induce higher tensile and compressive strains in the material, but may not affect the ultimate strength due to strain redistribution.

Of the possibilities (iii) appears to offer the most likely explanation.

The lower strains induced in the concrete, as compared with the mortar, at a given stress level are probably due to the stiffening effect of the increased volume fraction of aggregate. This is discussed fully in Chapter 7.

3.6.2.2. Incremental Strain Ratio

The technique described in 4.5. is used to assess the onset of stable fracture propagation (o.s.f.p.). Briefly, this method involves the

determination of the point of departure from linearity of the relationship between tensile and compressive strains from the variation with stress of the incremental strain ratio (i.s.r.). In the case of a uniaxial state of stress the i.s.r. values are equivalent to the tangent values of Poisson's Ratio at various levels of stress. The i.s.r. values at various stress levels, derived from the relationships between tensile and compressive strain are shown in Figure 3.17.for the mortar and in Figure 3.18. for the concrete mix.

The variation of i.s.r. with increasing stress level follows the pattern characteristic of a uniaxial test, namely, fairly wide variations at the start of loading followed by a region of almost constant i.s.r. which is terminated by a rapid increase which indicates fracture propagation in the 'axial splitting' mode. The lower values of i.s.r. within the near-constant portion as exhibited by the concrete are probably due to the effect of the increased content of aggregate [79].

3.6.2.3. Onset of Stable Fracture Propagation (o.s.f.p.)

The levels of stress and strain at o.s.f.p., assessed using the technique described in 4.5., for the various specimens of mortar and concrete are shown diagramatically in Figures 3.10. to 3.13. which indicate that considerable differences exist between the various types of specimen for a given mix.

It is not only the magnitude of stress or strain which varies between the specimen types, but also the proportion of ultimate stress at which o.s.f.p. occurs. For the mortar, the mean values of stress at o.s.f.p. for the cylinders, prisms and slabs, as proportions of the corresponding mean ultimate stresses are 70.8%, 66.6% and 50.8%, respectively, while for the concrete the values are 76.)%, 71.8% and 48.5%.

Comparison between Figures 3.10. to 3.11. with Figures 3.12. to 3.13. clearly demonstrates the lowering of the values of strain at o.s.f.p. for all types of uniaxial specimen as the aggregate content of a mix is increased, due to the stiffening effects discussed previously. However, corresponding changes in stress at o.s.f.p. are not indicated. In fact, the levels of stress are similar for cylinders and prisms of both mixes, although significantly higher for mortar slabs than for concrete. In Chapter 7 it is found that the stress at o.s.f.p. definitely reduces as the volume fraction of

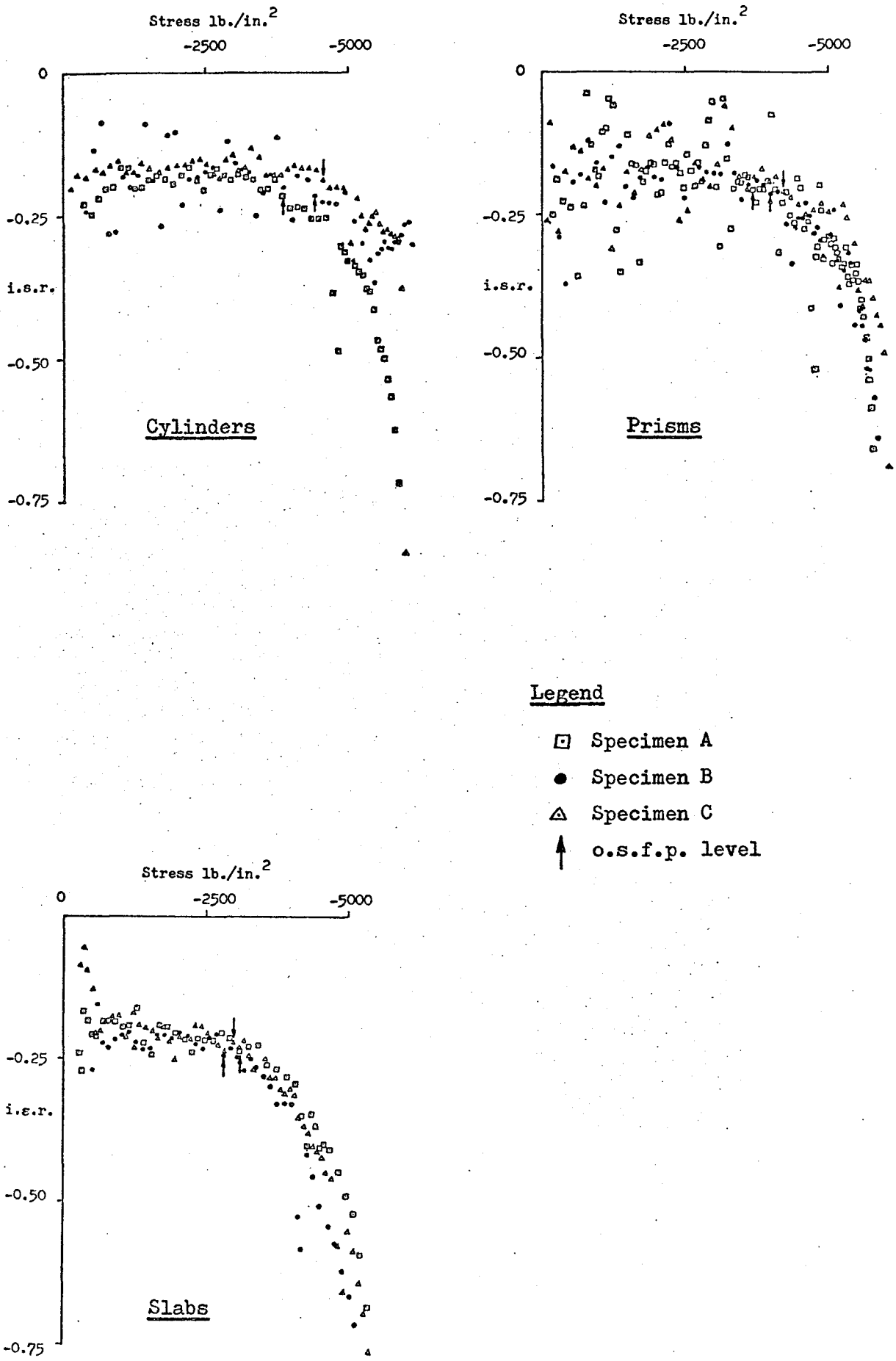
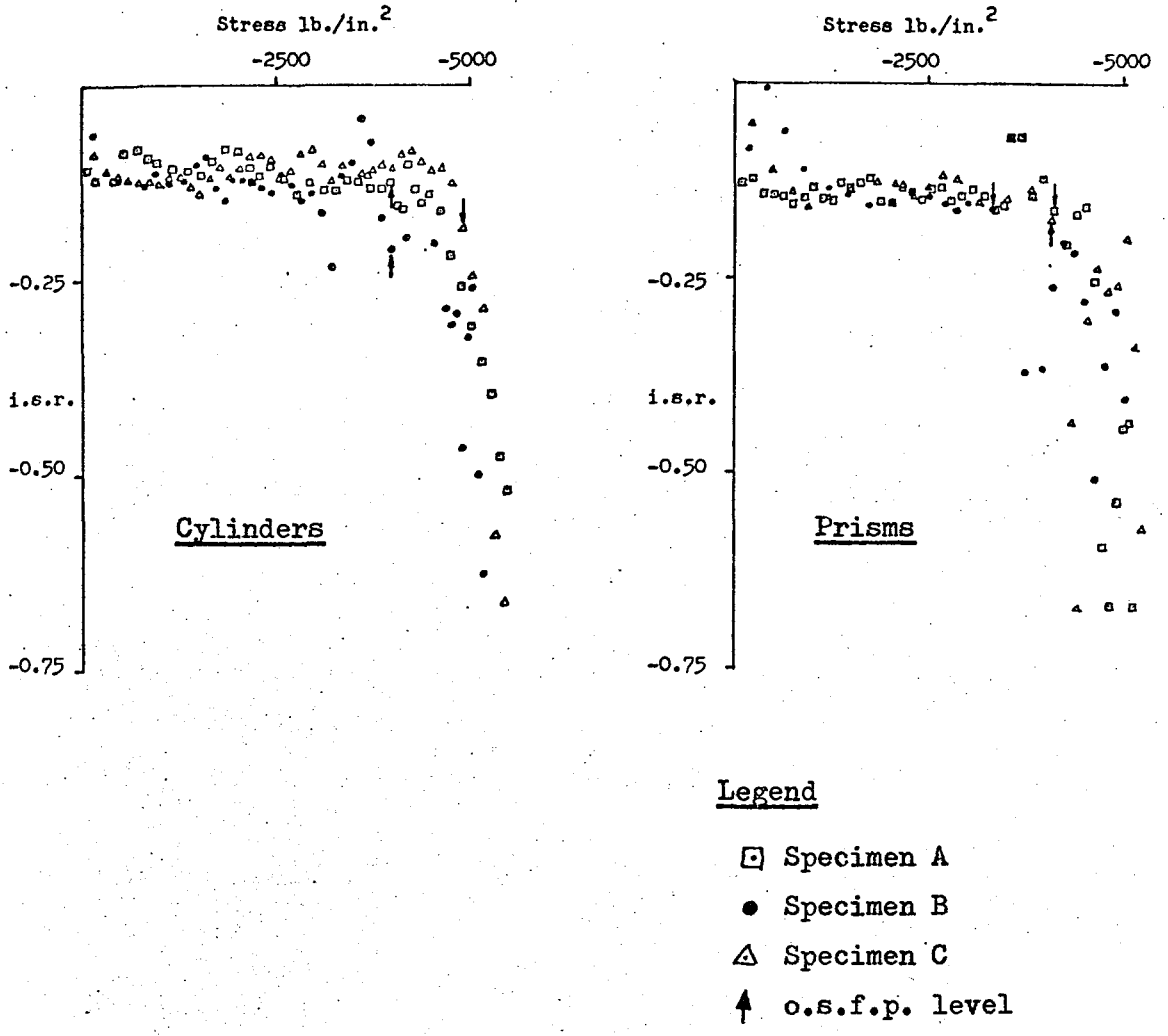


Figure 3.17. Variation of incremental strain ratio with axial stress for specimens of Mix MBC under uniaxial compression.



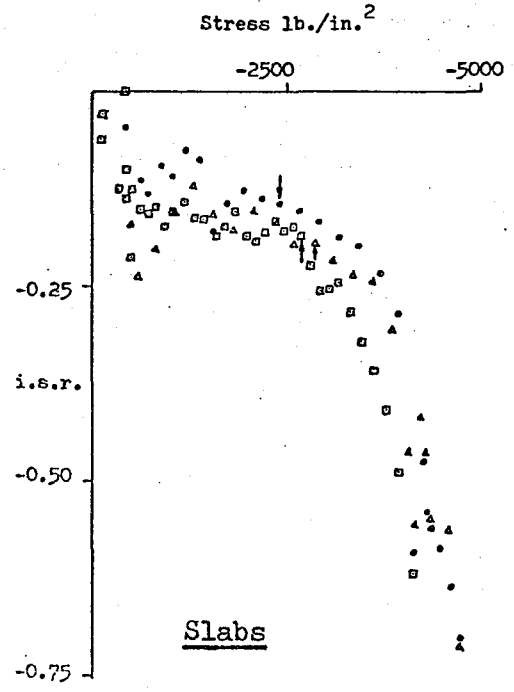


Figure 3.18. Variation of incremental strain ratio with axial stress for specimens of Mix 6IC under uniaxial compression.

aggregate increases, and no explanation can be found for the present behaviour of the cylinders and prisms in this respect.

Another feature of the results that is somewhat surprising is the slightly higher values for o.s.f.p. stress, as a proportion of ultimate given by the cylinders and prisms of concrete as compared with the mortar. A decrease would be expected with increasing heterogeneity of the mix, as discussed in Chapter 7. Such a decrease is, in fact, exhibited by the stress at the onset of unstable fracture propagation (minimum volume) as a proportion of ultimate, and is discussed in the following section. Reference to Chapter 7 shows that, for concretes under uniaxial compression, considerable fluctuations in the ratio of the stress at o.s.f.p. to the stress at ultimate are given as the volume fraction of aggregate increases, and thus the apparent anomaly may be due to a similar fluctuation.

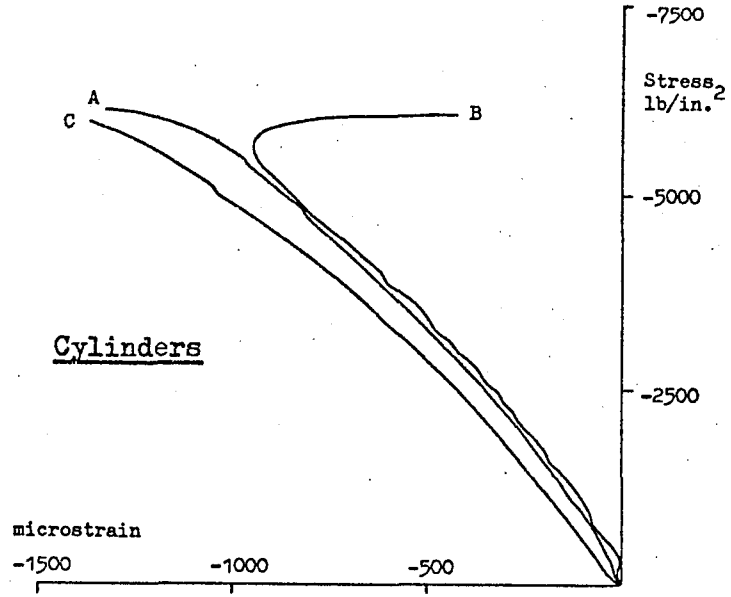
3.6.2.4. Volume Changes and Onset of Unstable Fracture Propagation (o.u.f.p.) Level

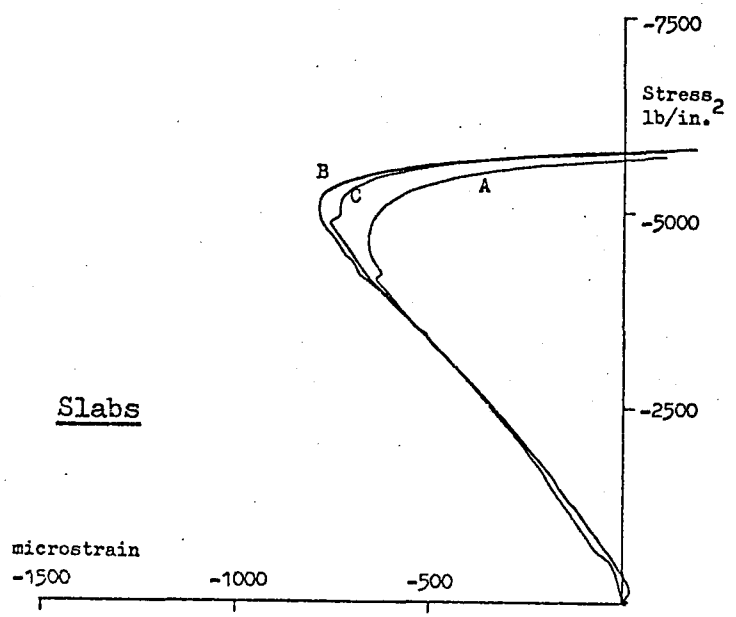
Figures 3.19. and 3.20. show the variation of volumetric strain with stress for the cylinders, prisms and slabs of the mortar and concrete respectively.

For both mixes the initial rate of volume decrease with stress is almost identical for all types of test. As ultimate is approached, however, differences become apparent, especially for the concrete, with the volume starting to increase at a lower stress level for the slabs as compared with the prisms and cylinders. This is shown in Figures 3.10. to 3.13. which indicate the comparatively low values of stress and strain at o.u.f.p. (minimum volume) for the slabs. The mean values of stress at o.u.f.p., as proportions of the mean ultimate stresses for the cylinders, prisms and slabs, are 98.0%, 96.4% and 82.7% respectively for the mortar, with the corresponding values for the concrete being 93.2%, 84.1% and 77.7%.

Thus, from the standpoint of volume changes as well as the stress-strain relationships the behaviour of slab specimens is somewhat dissimilar to that exhibited by cylinders and prisms.

Comparison between the volume change relationships and the strain at o.u.f.p. for the two mixes shows clearly the larger volume decreases induced in the mortar, compared with the concrete, at given stress levels. This behaviour is probably related to the proportion of relatively stiff aggregate





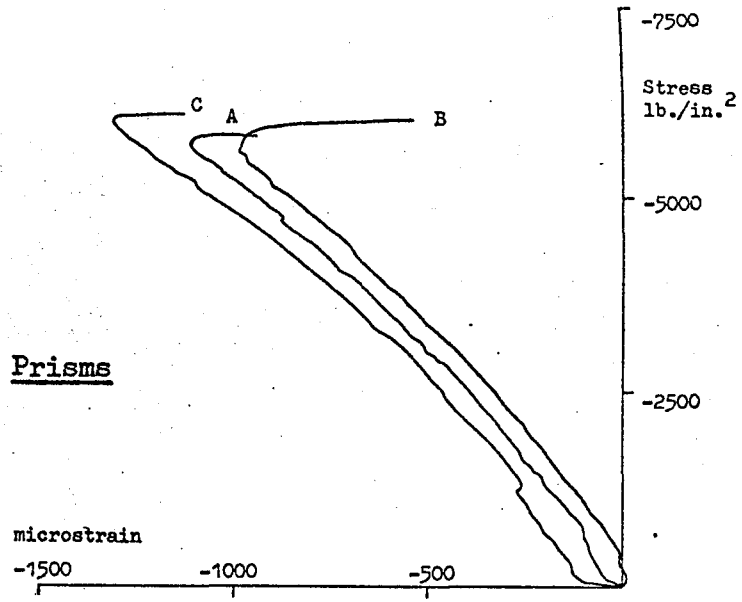
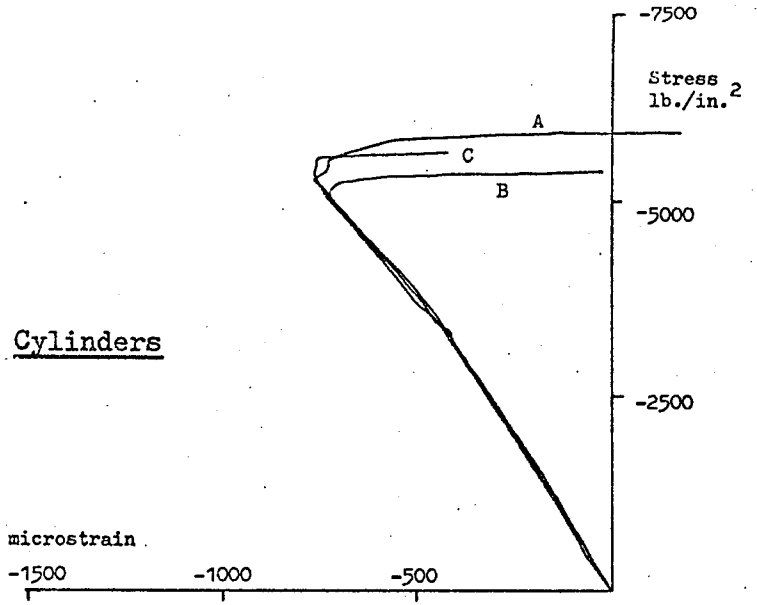
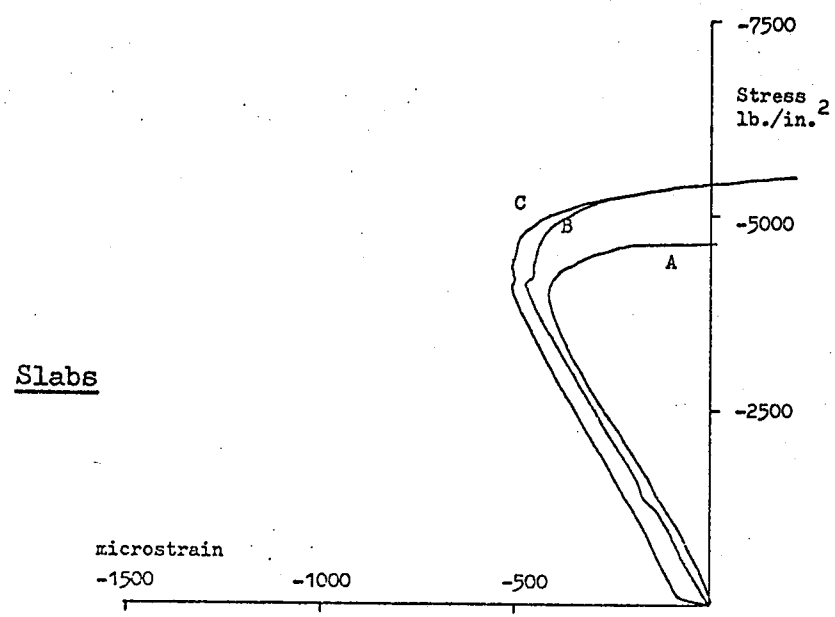


Figure 3.19. Variation of volumetric strain with axial stress for specimens of Mix MBC under uniaxial compression.





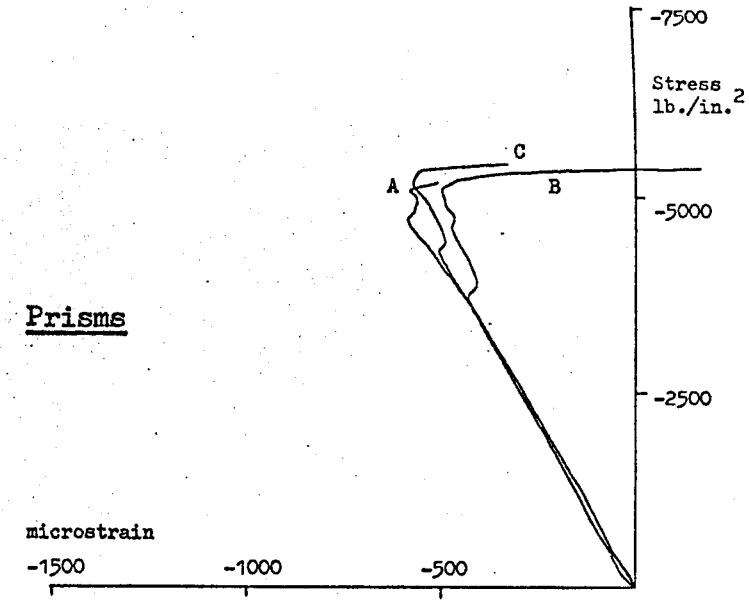


Figure 3.20. Variation of volumetric strain with axial stress for specimens of Mix 6IC under uniaxial compression.

in the softer matrix as discussed in Chapter 7, and is reflected in the values of stresses and strains at the o.u.f.p. level which are considerably lower in the concrete than the mortar.

3.6.2.5. Ultimate

Unlike the stresses at o.s.f.p. and o.u.f.p. the differences in strength between the different types of specimen of each mix are relatively insignificant. This is probably due to the considerable redistribution of strain occurring near ultimate which will tend to 'iron-out' any disparities.

The significantly lower stresses and strains at ultimate for the concrete compared with the mortar is a further demonstration of the effect of increasing heterogeneity in causing strain concentrations and thereby promoting the fracture process. This is discussed fully in Chapter 7.

3.6.2.6. Modes of Failure

For all specimens, fracturing occurred in the 'axial splitting' mode and appeared to initiate within the central zone. (See Figures 3.24. and 3.25.).

3.7. Equal Biaxial Compression Tests

3.7.1. Results

The complete stress-strain relationships are stored in computer card and printout form with the Concrete Materials Research Group. The principal derived results for the slab and cylinder tests are given in Appendix 9. For a definition of the various levels of material behaviour see 4.5.

For ease of comparison the values of stress and strain at the various significant levels of change of material behaviour (o.s.f.p., o.u.f.p. and ultimate) for the mortar and concrete are represented in Figures 3.8. and 3.9. respectively, in terms of the 95% confidence limits for the means.

The results are summarised qualitatively in Table 3.3., where the behaviour of the various types of specimen of a given mix is compared, together with the behaviour of specimens of different mixes. Comparisons are also made in the Table between the behaviour under uniaxial and biaxial stress.

PROPERTY	MORTAR	CONCRETE
Stress Strain Relationships		
Variability -		
Between specimens of a given type	Extremely small variations for slabs but extremely large variations for cylinders.	Extremely small variations for slabs except approaching ultimate. Extremely large variations for cylinders.
Comparison with uniaxial case	Slabs slightly less variable than when tested under uniaxial compression.	As for mortar.
Shape and Magnitude of Relationships -		
Difference between specimens	Considerably higher tensile strains at given stress level for cylinders. The compressive strain is slightly lower for cylinders, but this decrease is not significant.	As for mortar, but tensile strains are significantly lower for cylinders.
Difference between materials	Tensile strains at given stress level are slightly higher for cylinders of mortar during initial stages of load, and considerably higher for slabs of mortar. Compressive strains significantly higher for both cylinders and slabs of mortar throughout entire load range.	
Comparison with uniaxial case	Higher tensile and lower compressive strain at given stress level than for uniaxial case.	As for mortar.
Incremental Strain Ratio-Stress Relationship		
Variability -		
Between specimens of a given type	Low variability for slabs, but extremely high variability for cylinders.	As for mortar.
Comparison with uniaxial case	Higher variations for slabs than when tested under uniaxial compression.	As for mortar.

Table 3.3. (a) Summary of results obtained from equal biaxial compression tests.

PROPERTY	MORTAR	CONCRETE
Incremental Strain Ratio-Stress Relationship (contd.)		
Shape and Magnitude of Relationships		
Difference between specimens	Slabs show slight increase in i.s.r. for initial application of load, while cylinders show slight reduction. This is followed by near constant portion after which i.s.r. increases rapidly.	Slabs as for the case of mortar. For cylinders i.s.r. increases from start of loading.
	Extremely high values of i.s.r. for cylinders as compared with slabs.	As for mortar.
Differences between materials	i.s.r. values significantly higher for mortar slabs than concrete slabs. No conclusions possible for the cylinders due to the variability of results.	
Comparison with uniaxial case	Slabs show higher values of i.s.r. than when tested under uniaxial compression.	As for mortar.
Onset of Stable Fracture Propagation		
Differences between specimens	Lower values of stress (both in absolute terms and as proportions of ultimate) and strain for slabs than for cylinders.	Higher values of stress and strain for slabs since for cylinders o.s.f.p. occurs at start of loading.
Differences between materials	Concrete slabs exhibit higher stress and lower strains than concrete, while the mortar cylinders exhibit higher stress and strains than for the concrete (where o.s.f.p. occurs at start of loading).	
Comparison with uniaxial case	Stress at o.s.f.p. similar for uniaxial and biaxial slabs but compressive strain lower and tensile strain higher for uniaxial.	Stress at o.s.f.p. higher for slabs under biaxial compression than under uniaxial but similar to uniaxial cylinders and prisms.
	For biaxial cylinders the stress and compressive strain at o.s.f.p. is similar to uniaxial cases but variability precludes clear comparison, The tensile strain, however, is considerably higher than for uniaxial.	Compressive strain is similar to uniaxial slabs and lower than uniaxial prisms and cylinders. Tensile strain is significantly higher than uniaxial cases.

Table 3.3. (b) Summary of results obtained from equal biaxial compression tests.

PROPERTY	MORTAR	CONCRETE
Volume Change-Stress Relationship		
Variability between specimens of a given type	Relatively large variations for cylinders and prisms, extremely small variation for slabs up to approximately 75% ultimate.	Small variation for cylinders and prisms until near ultimate. Relatively large variation for slabs.
Shape and magnitude of relationship		
Differences between specimens	Almost identical shape for all specimens (particularly cylinders and prisms) up to start of volume increase.	As for mortar.
Differences between materials	Larger rates of volume decrease for mortar than concrete.	
Onset of Unstable Fracture Propagation		
Differences between specimens	Stress and strain levels highest for cylinders and lowest for slabs. Stress level as a proportion of ultimate highest for cylinders and lowest for slabs	As for mortar.
Differences between materials	Stress levels and strain levels considerably smaller for concrete than mortar. Stress levels as a proportion of ultimate significantly higher for mortars than concretes.	
Ultimate		
Differences between specimens	Stress levels highest for cylinders and lowest for slabs, but differences small. Tensile and compressive strain levels highest for slabs and lowest for cylinders. Volumetric strains highest for cylinders and lowest for slabs.	As for mortar. Tensile and compressive strains highest for slabs and lowest for prisms. Volumetric strains highest for slabs and lowest for cylinders.
Differences between materials	Stresses and strains lower for concrete than for mortar.	

Table 3.3. (c) Summary of results obtained from equal biaxial compression tests.

PROPERTY	MORTAR	CONCRETE
Ultimate (contd.)		
Differences between specimens	Stress and compressive strain values similar for both types of specimen. Tensile strain significantly higher for cylinders.	Stress and compressive strain significantly higher for slabs. No definite conclusions can be drawn regarding tensile strains due to excessive variability.
Differences between materials	Stress considerably higher for concrete slabs than mortar slabs but significantly lower for concrete cylinders than mortar cylinders. Compressive strains considerably higher for mortar specimens. Variability of tensile strains allows no definite conclusions to be drawn.	
	Stress slightly higher for biaxial cases than uniaxial cases. Compressive strain slightly lower and tensile st strain considerably higher for biaxial cases.	For biaxial slabs stress considerably higher than uniaxial cases but only slightly higher for biaxial cylinders. Compressive strains slightly, but not significantly, lower for biaxial cases with tensile strains higher (although their variability precludes any definite conclusions being drawn)

Table 3.3. (d) Summary of results obtained from equal biaxial compression tests.

The principal results are discussed more fully in the following sections. For the biaxial cylinder tests the terms 'null', 'compressive' and 'tensile' refer to the types of test described in 3.5.6.2.

3.7.2. Discussion of Results

3.7.2.1. Stress-Strain Relationships

Figures 3.21. to 3.24. show the stress-strain relationships and the mean curves (with 95% confidence limits for the means indicated) for the biaxial slab and biaxial cylinder tests on the mortar and concrete respectively. The figures clearly demonstrate the considerable variation in deformational behaviour exhibited between the cylindrical specimens tested in the hydraulic cell, as opposed to the uniformity exhibited by the slabs which is comparable with that for the uniaxial tests. This variation cannot be ascribed to the type of test performed on a particular cylinder (i.e. whether 'null', 'compressive' or 'tensile') since the variations show no trend in this respect.

It is likely, therefore, that the 'scatter' is due either to (a) the lack of secondary restraint effects in the cylinders as compared with the slabs and/or to (b) the different types of boundary conditions imposed in the two types of test.

For the cylinder tests stress redistribution is prevented, or reduced, by a hydraulic boundary loading condition, and the behaviour is extremely 'brittle' resulting in a single cleavage plane perpendicular to the unstressed direction. The fracture process is thus highly dependent on the most critically orientated crack, or groups of cracks, within the specimen and this criticality will vary from specimen to specimen.

In the case of the slabs, the near-uniform boundary strain condition allows the development of restraint stresses in the unloaded direction. The material will, therefore, be capable of redistributing stress under such loading. The resulting behaviour will, therefore, be less brittle as evidenced by the multiplicity of eventual failure planes (described in 3.7.2.6.) and will not be so highly dependent on the most critical cracks.

Comparing the two types of biaxial test, the hydraulically loaded specimens of both mortar and concrete show distinct increases in steepness of the stress/compressive strain relationship as compared with those loaded through rigid platens, while the corresponding stress/tensile strain relationships are less steep. This rotation of the two stress-strain curves towards the tensile axis for the near uniform boundary stress condition is similar to that given by increasing the biaxial stress ratio (see below) and it has

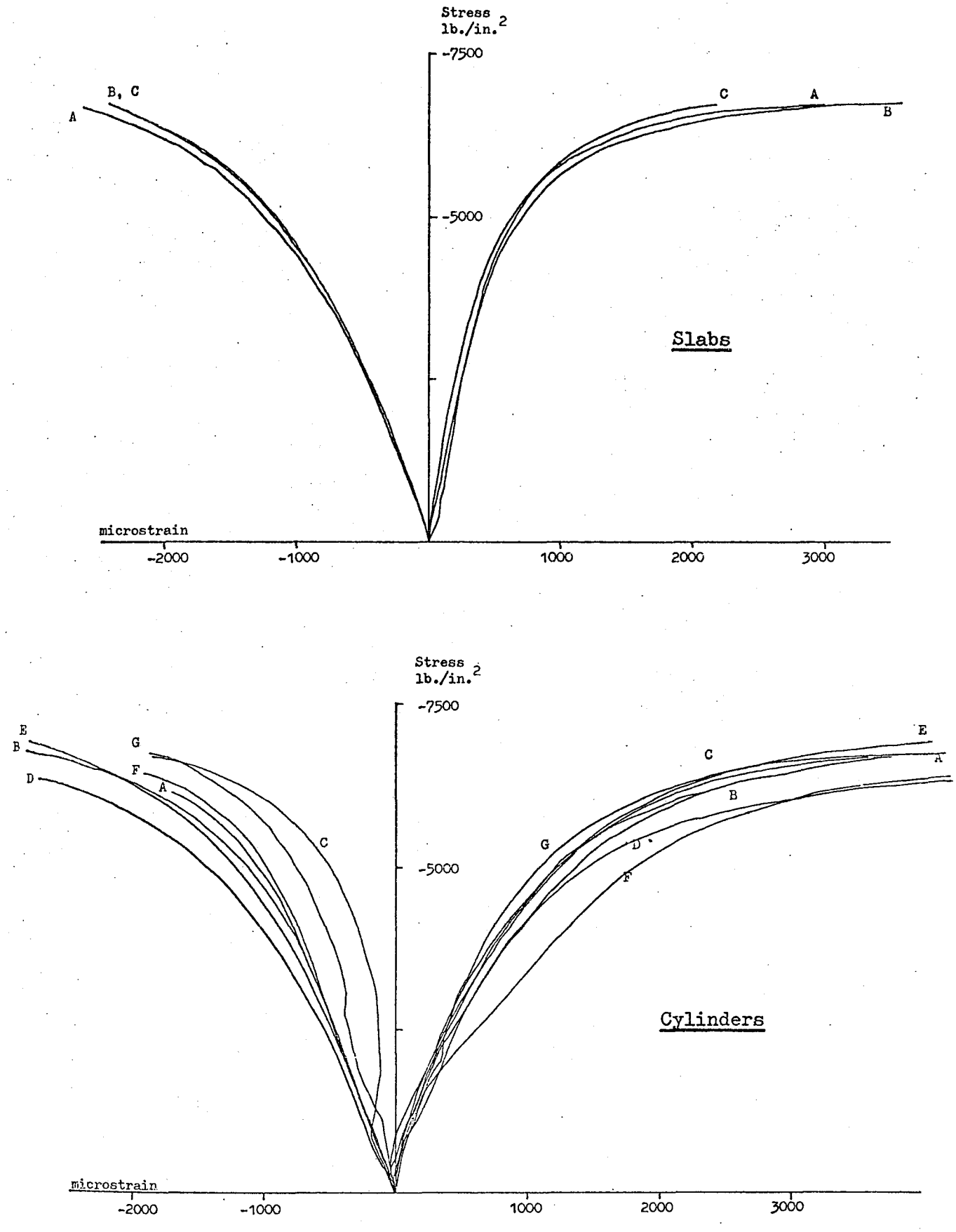


Figure 3.21. Variation of compressive and tensile strains with stress for specimens of Mix MBC under equal biaxial compression.

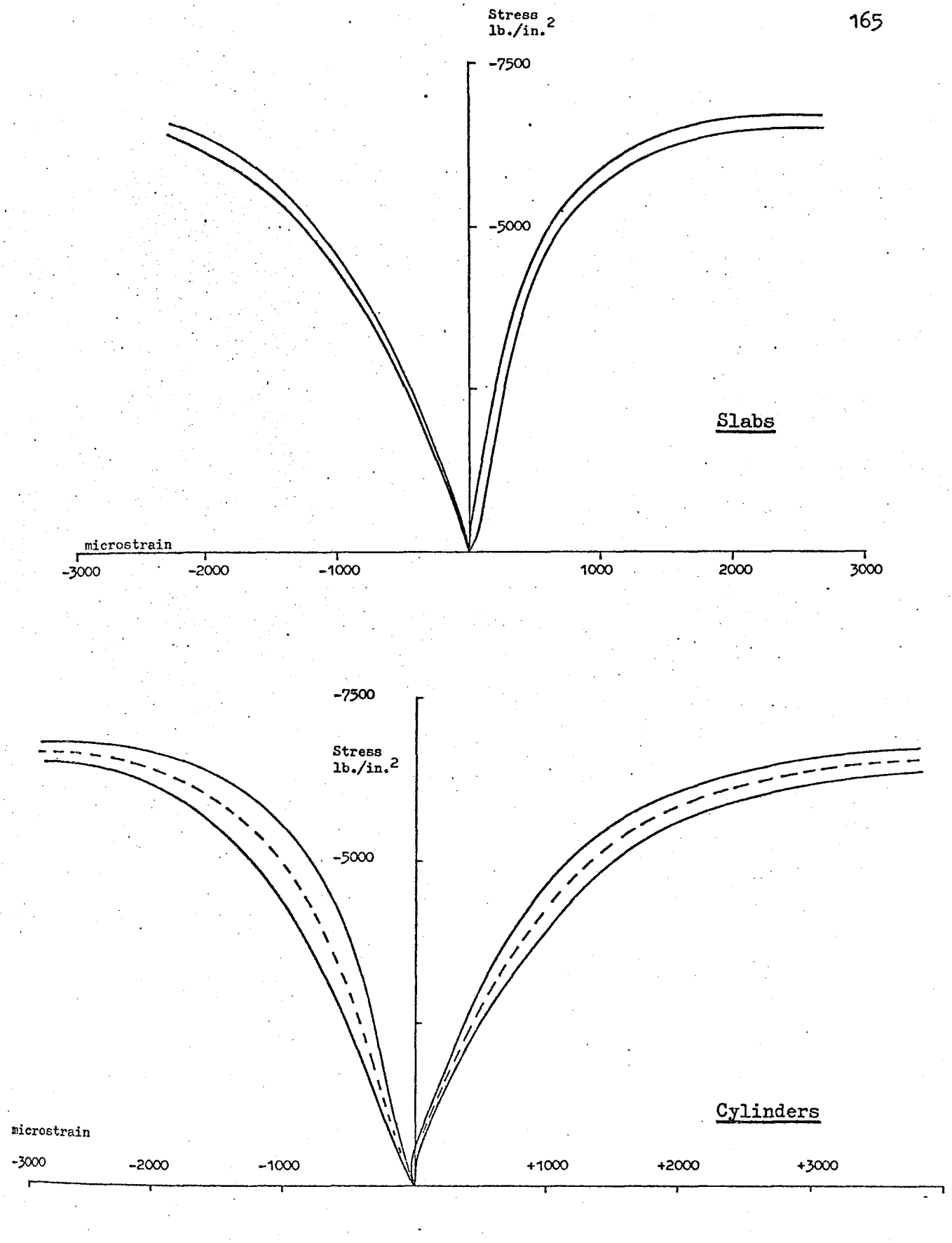
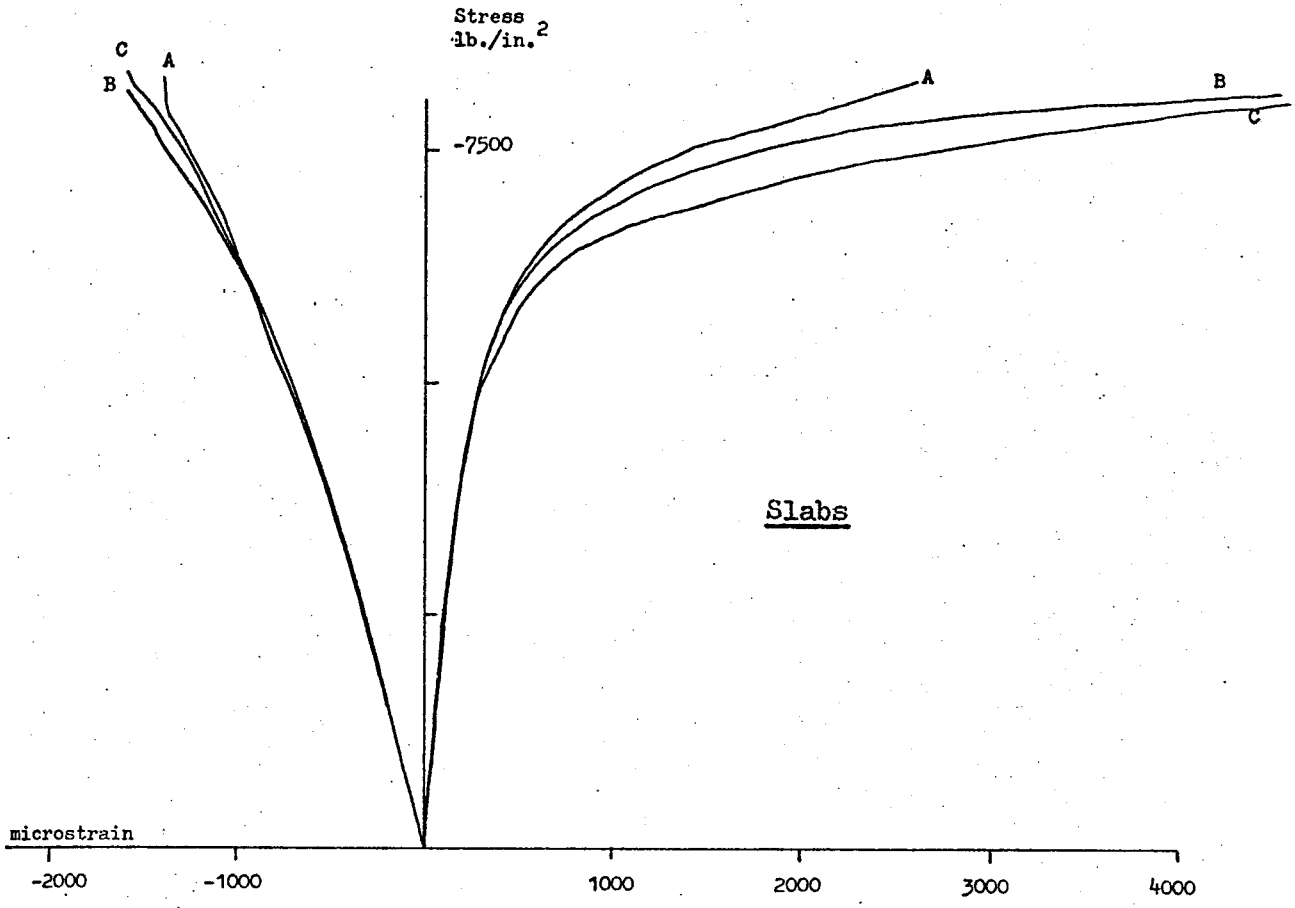


Figure 3.22. Variation of compressive and tensile strains with stress for specimens of Mix MBC under equal biaxial compression in terms of 95% confidence limits for the mean.



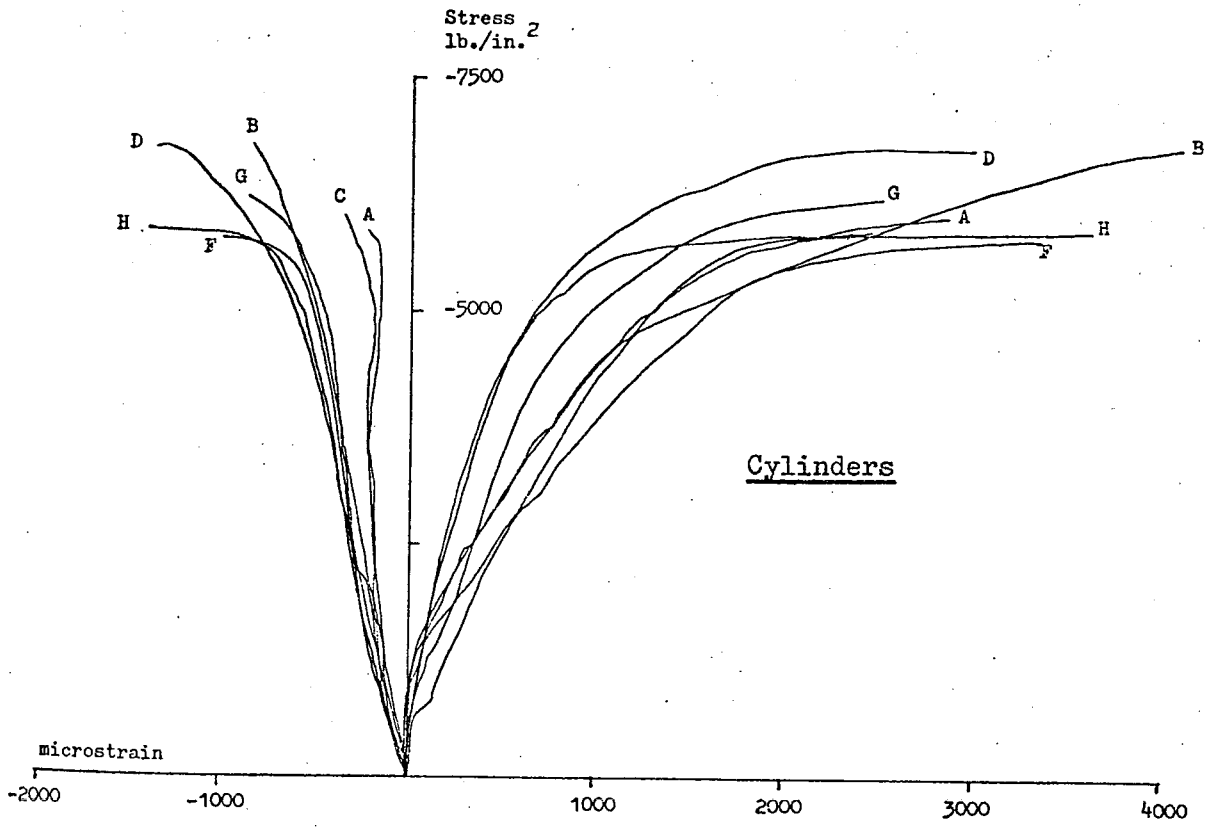
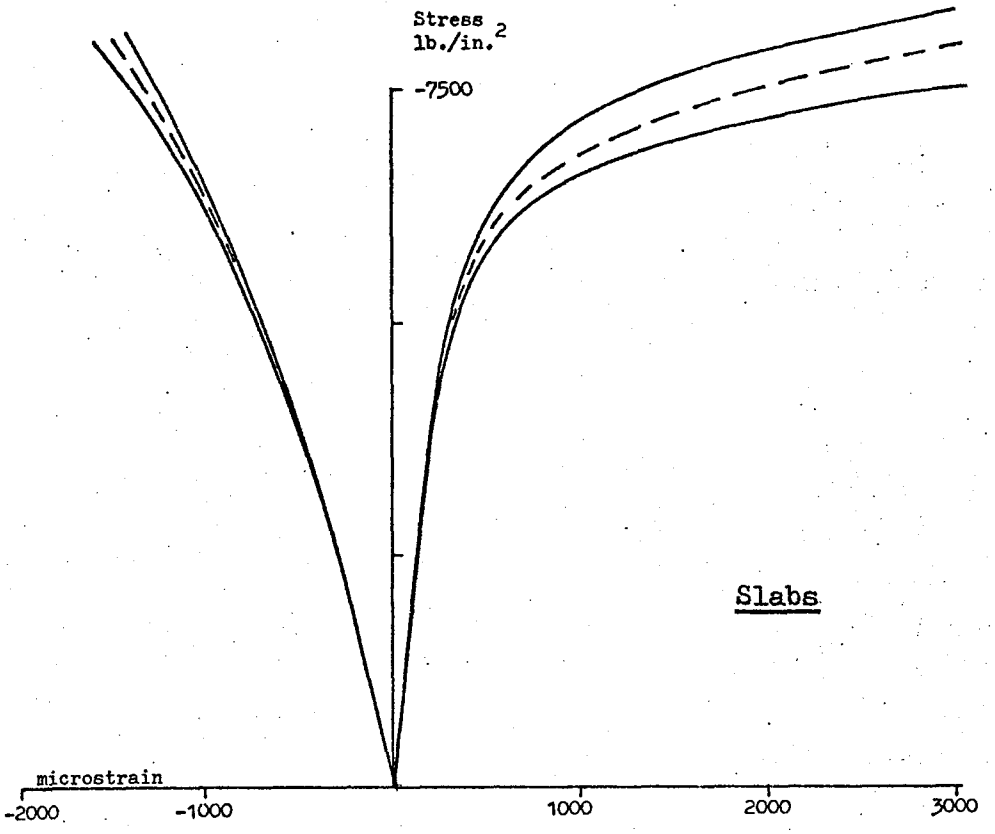


Figure 3.23. Variation of compressive and tensile strains with stress for specimens of Mix 6IC under equal biaxial compression.



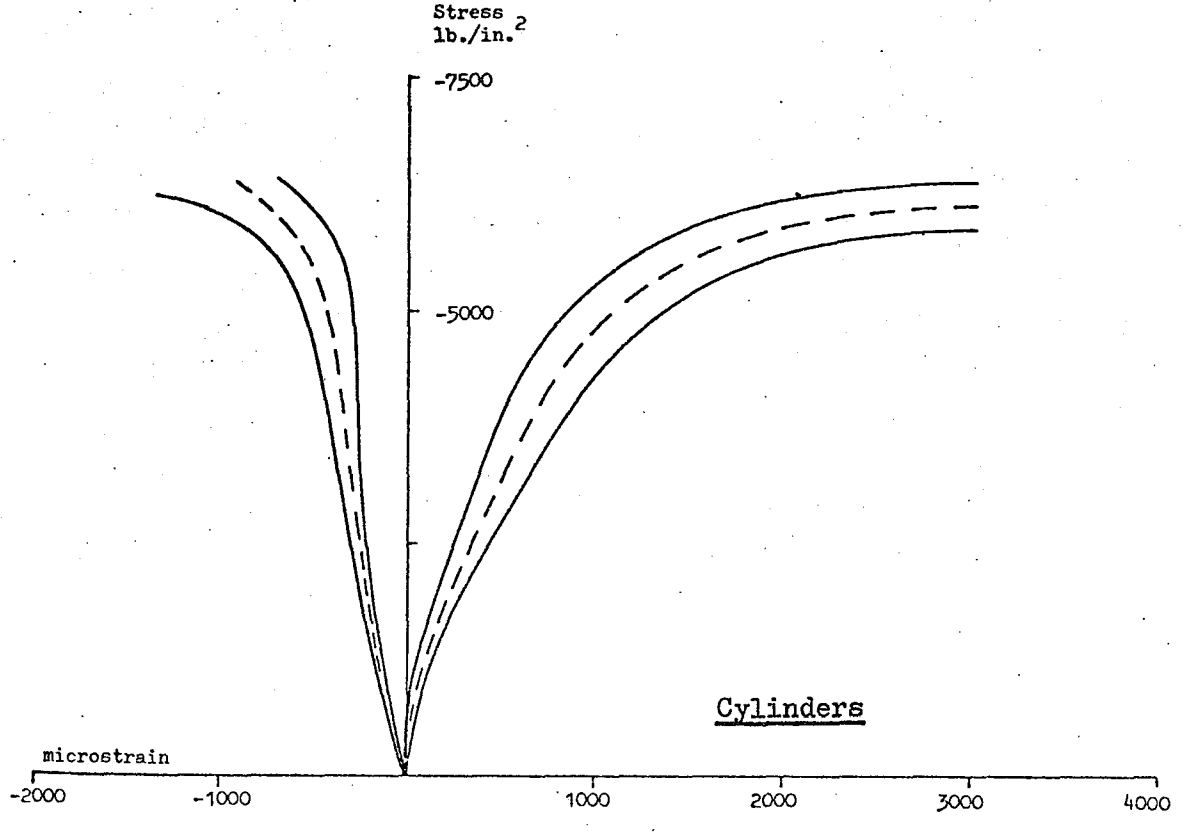


Figure 3.24. Variation of compressive and tensile strains with stress for specimens of Mix 6IC under equal biaxial compression in terms of 95% confidence limits for the means.

been suggested that such behaviour may be symptomatic of a lack of restraint against potential microcracking [230].

The larger tensile strains exhibited by the cylindrical specimens would be expected, since the restraint to movement in the unstresses direction is likely to be lower than in the slab tests. However, it would be expected that such increases in tensile strain would lead to corresponding increases in the ability to deform compressively in the stressed direction. The fact that the compressive strains are lower for the slabs suggests that the region within which strains are measured is not subject to stresses as high as those imposed on the boundary of the specimens. Such a situation would undoubtedly arise if the completely free movement of the specimen surfaces is prevented, thus promoting some degree of 'load shedding' into the platens. This effect is demonstrated in 2.5.5.3. where, for a rigidly loaded slab under conditions of complete restraint, the centrol portion is found to be under only 50% of the applied biaxial boundary stress.

Thus, from the stress-strain relationships, it would appear that the tests under near-uniform boundary strain are not completely free from restraint effects while, as anticipated, those under near-uniform boundary stress behave in a manner suggesting considerably less boundary restraint.

Comparing the relationships for the two mixes demonstrates the increased stiffness of the concrete, in that both sets of biaxial stress/compressive strain curves are considerably steeper than those corresponding to the mortar. This is also the case for the stress/tensile strain relationships for the slabs but the difference between the cylinder tests for the two mixes is less significant.

For both mixes the stress/compressive strain curves are steeper for the biaxial cases than the uniaxial, while the stress/tensile strain curves are less steep due to the effect of the principal stress in the orthogonal direction. Such behaviour has been observed for concrete specimens tested by Nelissen [80], Kupfer et Al [72], Stegbauer [75] and Liu et Al [230] using 'brush' platens and Vile [8] using rigid platens, where the steepness of slope changes with increasing biaxial stress ratio.

3.7.2.2. Incremental Strain Ratio

Figures 3.25. and 3.26. show, for the mortar and concrete respectively, the variation of incremental strain ratio with applied biaxial stress for

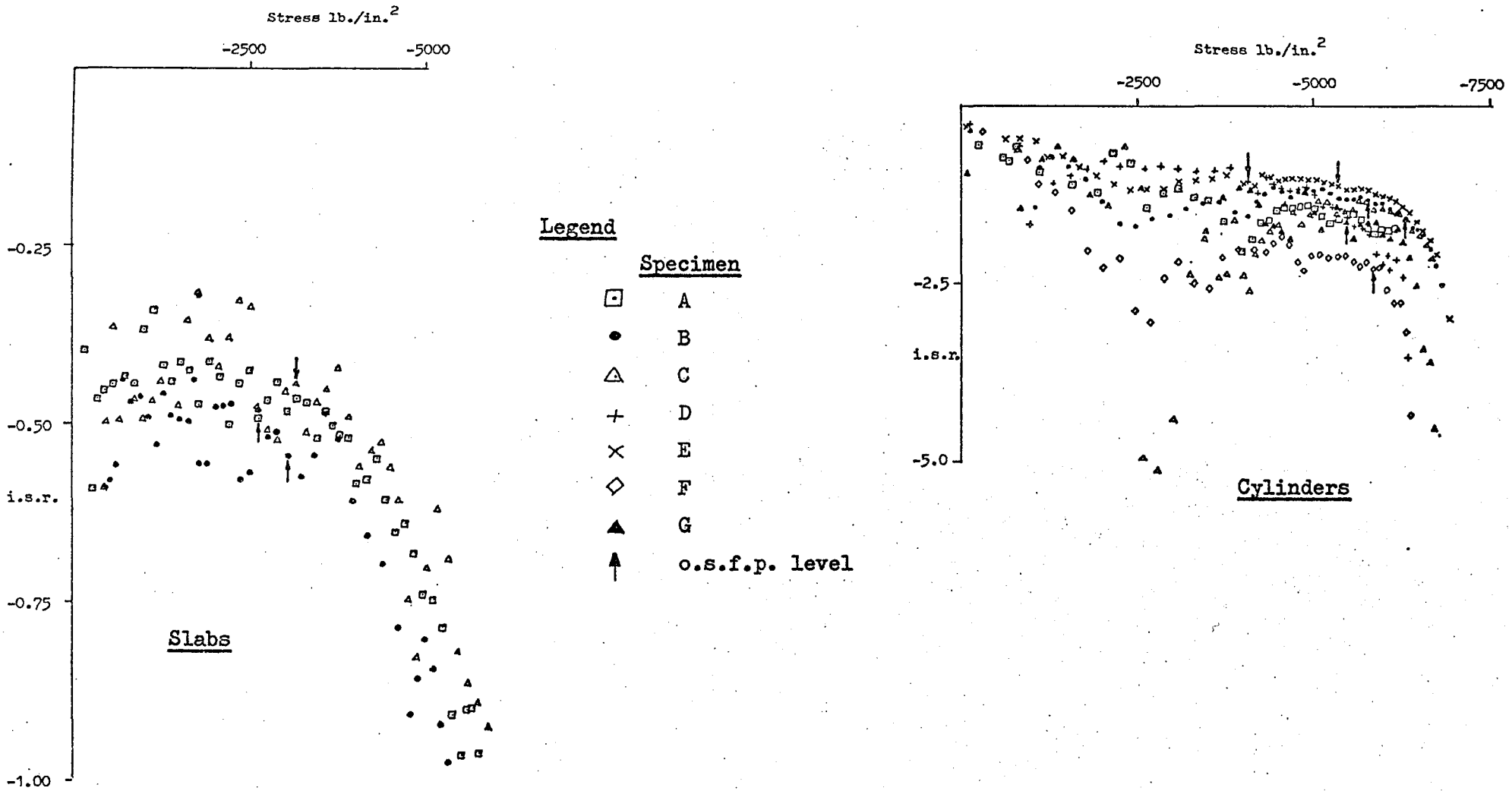


Figure 3.25. Variation of incremental strain ratio with stress for specimens of Mix MBC under equal biaxial compression.

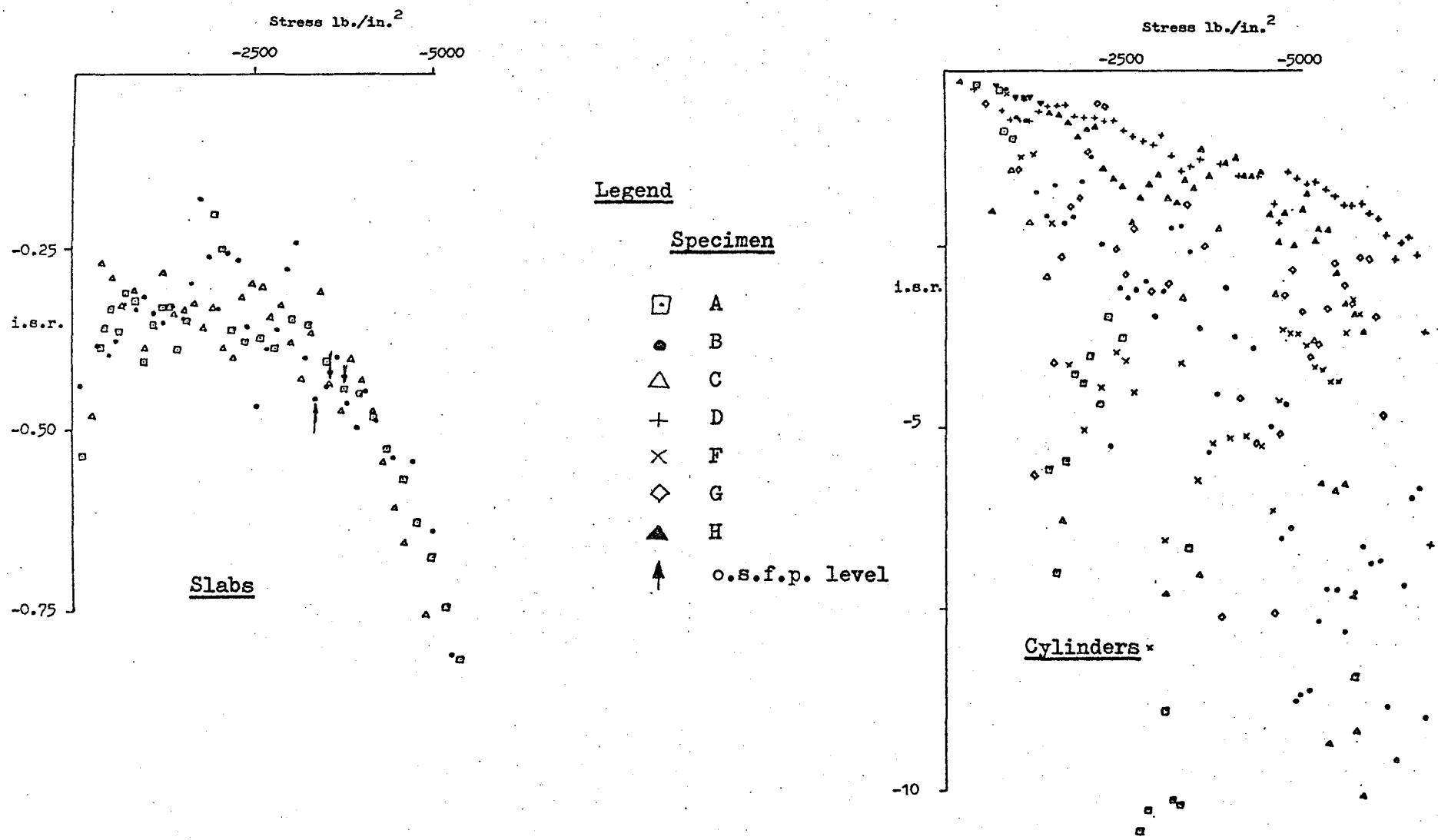


Figure 3.26. Variation of incremental strain ratio with stress for specimens of Mix 6IC under equal biaxial compression.

the two types of specimen. The relationships for the slabs of both mixes, although more variable, are of a form similar to that for the uniaxial tests, and show a decrease in i.s.r. for initial application of load, followed by a nearly constant portion which is terminated by a rapid increase to failure.

The relationships for the cylinder tests differ in that they are much more variable, and for the mortar the i.s.r. values reduce slightly during the early stages of load to become nearly constant before increasing to failure. In some cases the initial decrease is followed by a slight increase up to the constant portion, while for the concrete the i.s.r. increases from the start of loading.

Another distinct difference between the cylinder and slab tests is in the magnitude of the i.s.r. values. These are an order of magnitude greater in the cylinders, as compared with the slabs, demonstrating the larger deformational component in the unstressed direction for a given deformation in the plane of the biaxial stress.

In comparison with the cases of uniaxial compression both mixes show higher values of i.s.r. under biaxial compression due to the effect of the load in the orthogonal direction.

3.7.2.3. Onset of Stable Fracture Propagation (o.s.f.p.)

The values of stress and strain at o.s.f.p. for the biaxial specimens of both mixes, are indicated in Figures 3.10 to 3.13., together with the corresponding values for the various uniaxial tests. The stresses at o.s.f.p. for both biaxial and uniaxial tests are also represented on the biaxial plane in Figures 3.27 and 3.28.

It is clear from the figures that for the mortar, lower values of stress and strain at o.s.f.p. are given for the slabs as compared with the cylinders, whereas the reverse is the case for the concrete mix. No explanation can be found for this behaviour.

The concrete slabs show higher values of stress and lower strains at o.s.f.p. than for the mortar, with the corresponding proportions of ultimate being only slightly lower for the concrete (42.5% compared with 45.6% for the mortar). This trend is in broad agreement with the results

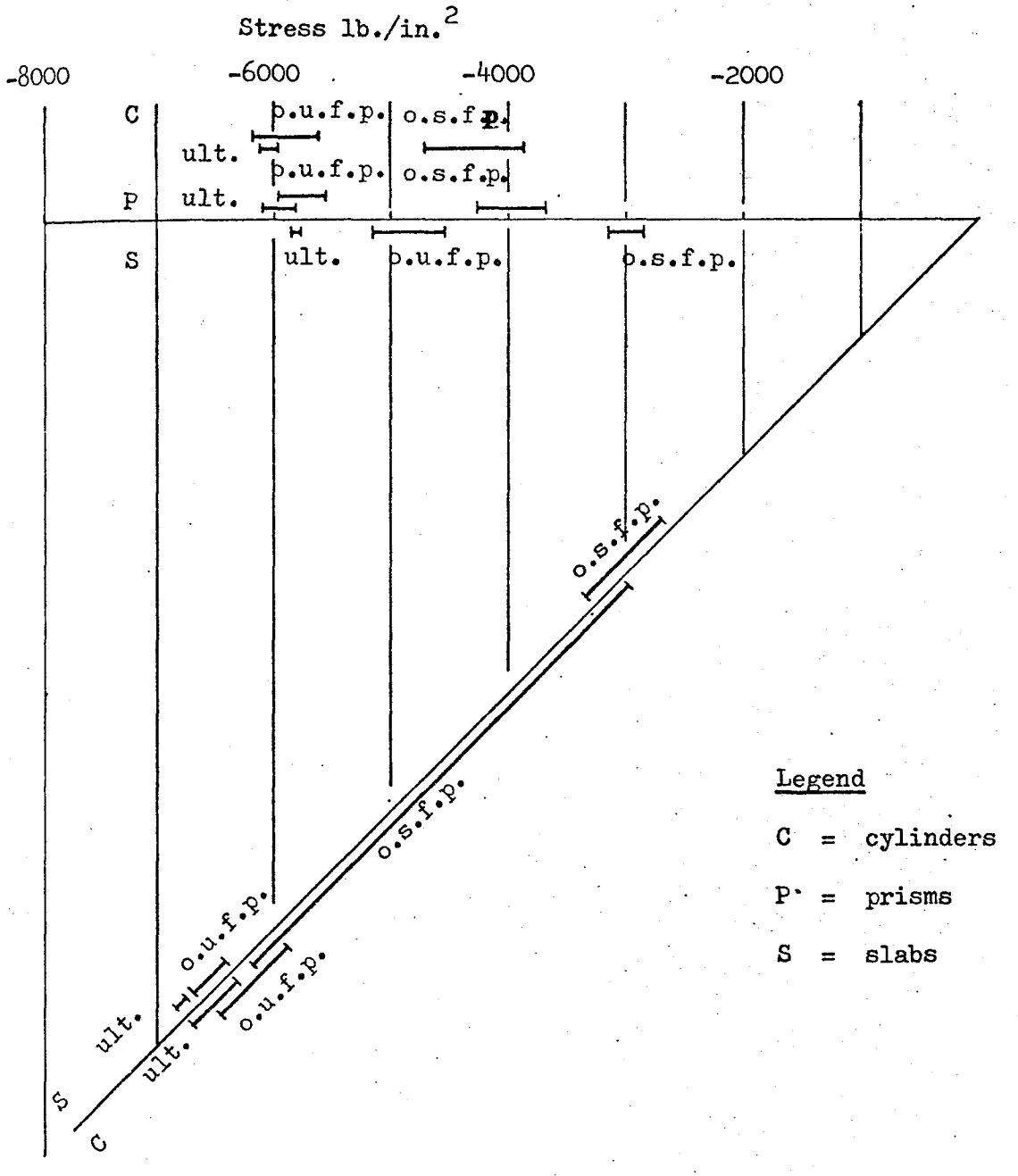


Figure 3.27. Stress levels at o.s.f.p., o.u.f.p. and ultimate for specimens of Mix MBC under uniaxial and equal biaxial compression in terms of 95% confidence limits for the means represented on the biaxial stress plane.

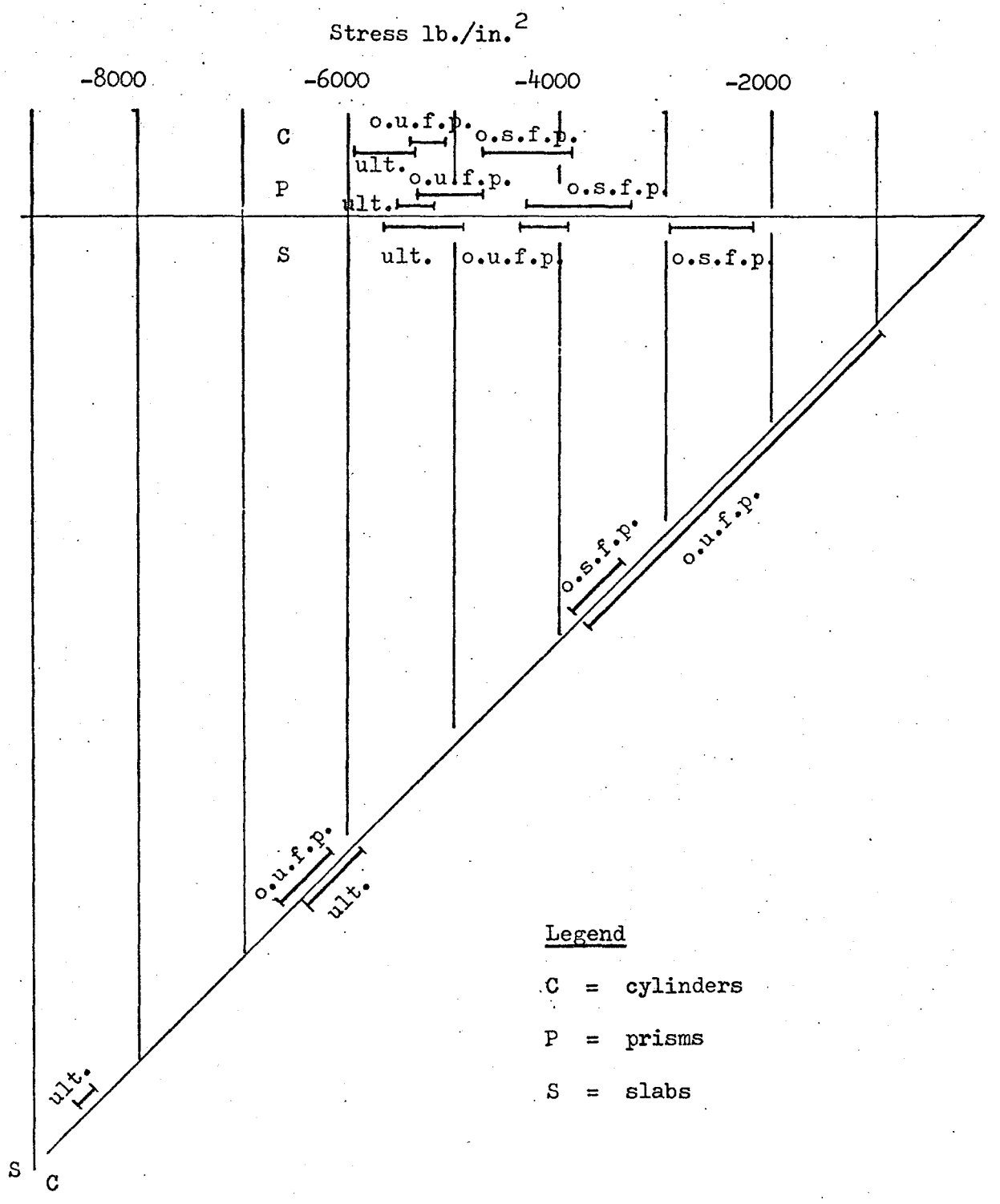


Figure 3.28. Stress levels at o.s.f.p., o.u.f.p. and ultimate for specimens of Mix 6IC under uniaxial and equal biaxial compression in terms of 95% confidence limits for the means represented on the biaxial stress plane.

obtained by Vile [8] for the discontinuity level, using a similar loading technique (discontinuity being defined as the level at which the ultrasonic pulse velocity started to decrease significantly), and is due to the increased aggregate content (a) increasing the strength under biaxial compression as induced by rigid-platen loading due to particle interference effects, (b) increasing the stiffness of the composite material, and (c) promoting the fracture process as a result of increased heterogeneity.

The significant feature of the results, however, is that the above is not the case for hydraulically loaded specimens. The cylinders of concrete appear to experience fracture propagation from the start of loading whereas for the mortar cylinders the o.s.f.p. stress level is a high proportion (73.7%) of ultimate.

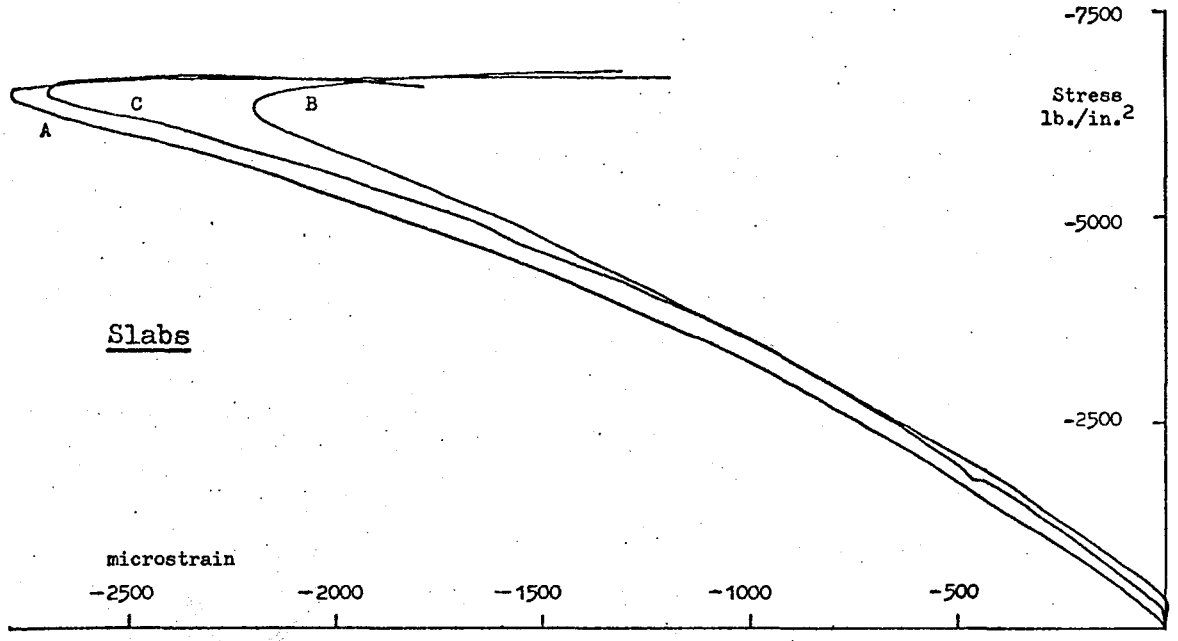
The above suggests that under rigid-platen loading, with the associated secondary restraints, the fracturing processes in the relatively heterogeneous concrete are inhibited, while under the uniform boundary stress condition (with reduced restraints) fractures are free to propagate.

The fact that the o.s.f.p. level for the mortar cylinders is a higher proportion (73.7% of ultimate compared with 45.6% for the slabs) indicates that the hydraulic loading does not, in itself, promote early disruption but that the behaviour of the concrete cylinders is primarily a function of the heterogeneity of the material.

The stress at o.s.f.p. is similar for both the uniaxially and biaxially loaded mortar slabs while the compressive and tensile strains for the biaxial case are lower and higher, respectively. For the concrete slabs, however, the stress at o.s.f.p. is higher than for the uniaxial case and, in this respect, reflects the differences in ultimate stress.

3.7.2.4. Volume Changes and Onset of Unstable Fracture Propagation (o.u.f.p.)

Figures 3.29. and 3.30. show the relationships between volume change and applied stress for the slabs and cylinders of mortar and concrete respectively. The relationships for the slabs generally exhibit the characteristics associated with a compression test, namely, a volume decrease, the rate of which increases with stress up to a certain stress



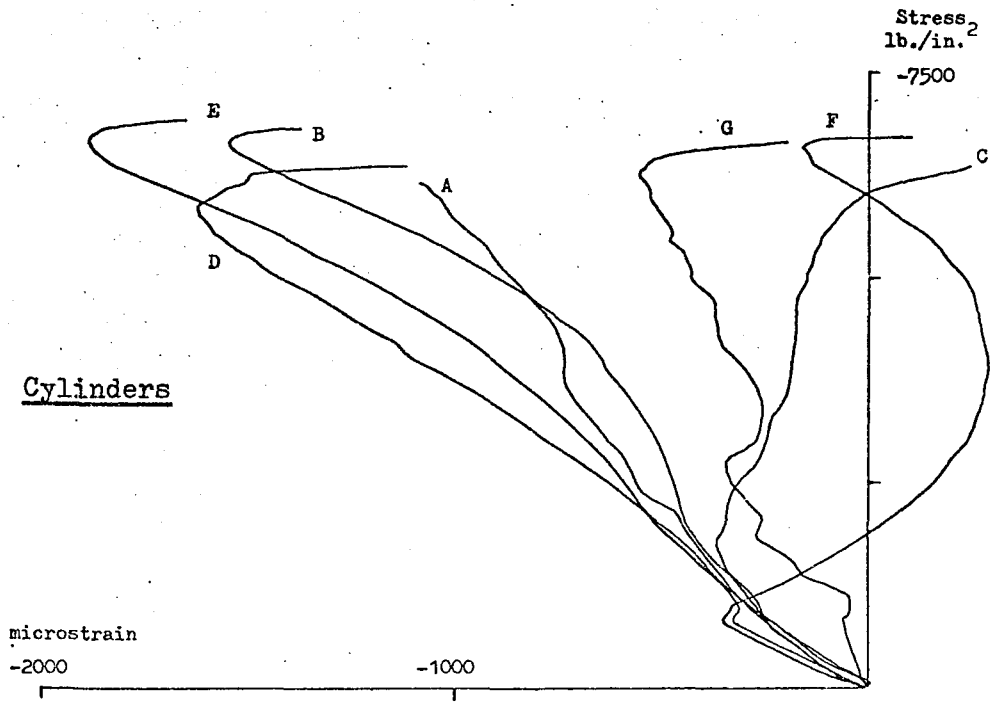
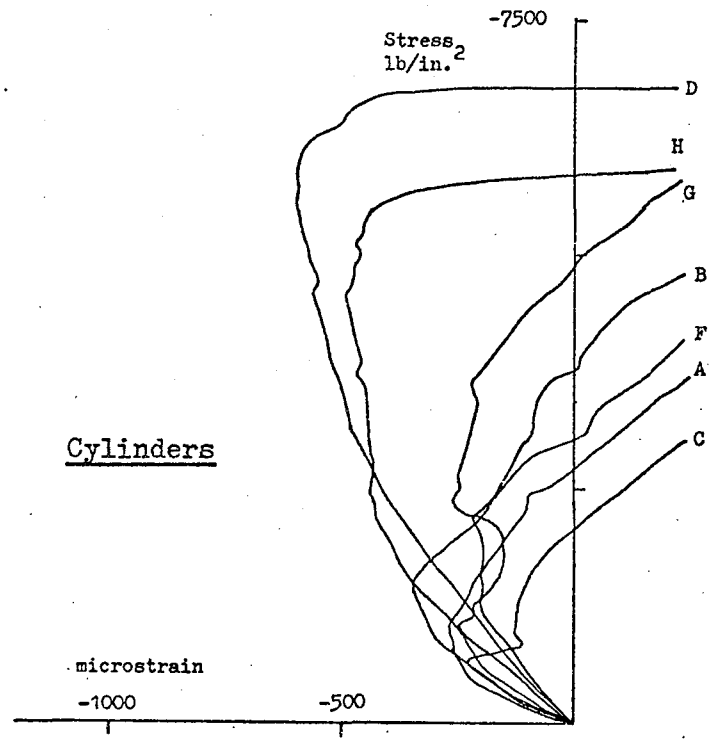


Figure 3.29. Variation of volumetric strain with stress for specimens of Mix MBC under equal biaxial compression.



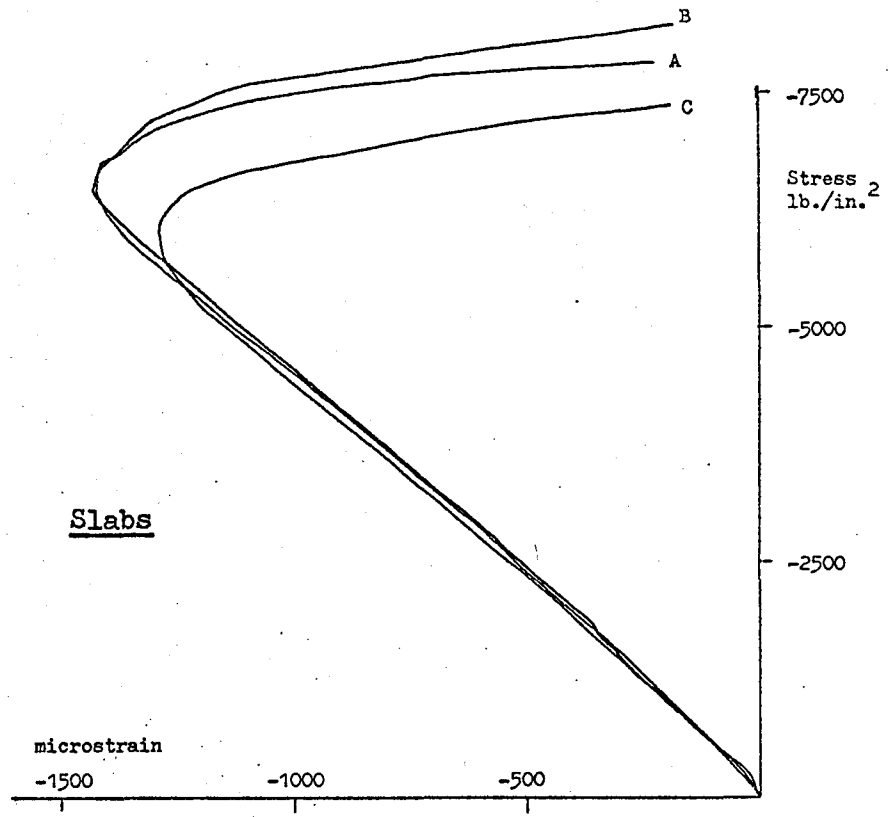


Figure 3.30 Variation of volumetric strain with stress for specimens of Mix 6 IC under equal biaxial compression.

level, after which the trend reverses such that the volume starts to increase to failure. This trend is not distinct for the cylinders since, in these cases, the relationships are extremely variable as would be expected from the variations in stress-strain relationships discussed previously.

The obviously feature of the sets of curves is the extremely large volume decreases given by the slabs of both mixes, and some of the cylindrical specimens of mortar, as compared with those for the corresdponding uniaxial tests. This is similar to behaviour noted for tests using 'brush' platen loading by Nelissen [80], Kupfer et Al [72] and Stegbauer et Al [75], where greater volume decreases were observed as the biaxial stress ratio increased. However, for the biaxial cylinders of concrete the o.u.f.p. (minimum volume) level occurs at a very low stress as expected from the low o.s.f.p. level, and thus the volume decreases are extremely small.

For both types of biaxial specimen the decrease in volume exhibited by the concrete is smaller than that for the mortar. This follows from the increased content of relatively stiff aggregate in the concrete. This increase in aggregate content also produces more nearly linear volume decreases for the slabs.

The 95% confidence limits for the mean values of stress and strains at o.u.f.p. for the two types of biaxial specimen, together with the corresponding levels for the uniaxial tests, are shown in Figures 3.10. to 3.13. for the mortar and concrete respectively. These indicate the close proximity of this level to the ultimate strength for the mortar, with the stresses for the biaxial slabs and cylinders, as proportions of the mean ultimate strengths, being 96.5% and 95.8% respectively. The mean stresses at o.u.f.p. for the slabs and cylinders of concrete, as proportions of the corresponding mean ultimate strengths, are 75.1% and 39.1% respectively, proportions considerably below these for the mortar indicating the effect of the aggregate content.

The stress and compressive strain values at o.u.f.p. for the mortar cylinders and slabs are similar, whereas the tensile strain is significantly higher for the cylinders. For the concrete, on the other hand, the cylinders reach o.u.f.p. at a lower level of stress and strain compared with the slabs which is similar to the case at o.s.f.p. These observations suggest that

the hydraulically loaded condition allows the fracture processes to proceed uninhibited by restraints, and that this effect is more clearly evident as the aggregate content is increased.

The effect of increasing the aggregate content is also reflected in the differences in stress and strain levels between the corresponding specimens of the two mixes. The stress values at o.u.f.p. for the mortar slabs vary between 107.4 and 112.1% of the mean of the uniaxial tests, depending on the particular uniaxial specimen tested, while the biaxial cylinders correspondingly vary between 104.2 and 109.0%

For the concrete, the stresses at o.u.f.p. for the slabs vary between 112.2 and 119.3% of the ultimate uniaxial strength, proportions only slightly higher than those for the mortar. The cylinders, on the other hand, reach the o.u.f.p. level at between only 43.0% and 45.8% of the uniaxial strength.

The corresponding strains at o.u.f.p. level are also higher for the biaxial cases than the uniaxial except for the case of the concrete cylinders where the early breakdown induces a lower compressive but a higher tensile strain.

3.7.2.5. Ultimate Stresses and Strains

Figures 3.10. to 3.13. respectively, show the ultimate stresses and strains for the two types of mortar and concrete specimen tested in equal biaxial compression. As would be expected, for the ultimate condition the strains show considerable variation between specimens of the same group. The Figures also indicate trends of a similar nature to those observed for the strains at o.u.f.p. In view of the above the strains at ultimate will not be discussed and it is suggested that the strains at o.u.f.p. be used for any design purposes (see Chapter 8).

The 95% confidence limits for the mean stresses at ultimate for the mortar indicate almost identical ultimate stresses for the biaxial slabs and cylinders, suggesting that for such a relatively homogeneous material the test method does not effect this property.

Only slight differences between the two types of specimen are found, when considering the mean ultimate strength in biaxial compression as a proportion

of the mean ultimate strength for the various types of uniaxial specimen tested. For the slabs, the proportion varies between 111.3% and 116.2% while the values corresponding to the cylinders are slightly lower at 109.0% to 113.8%.

The above results for the mortar are to be contrasted with those obtained for the concrete. The 95% confidence limits for the mean ultimate stresses under biaxial and uniaxial compression clearly show the considerably higher strength obtained for the biaxial slabs as compared with the cylinders. This is reflected in the values of mean strength in biaxial compression, as a proportion of mean ultimate uniaxial strength, which in the slabs varies between 149.3% and 158.8% depending on the type of uniaxial specimen tested, while the corresponding proportions for the biaxial cylinders are 110.0% to 117.0%

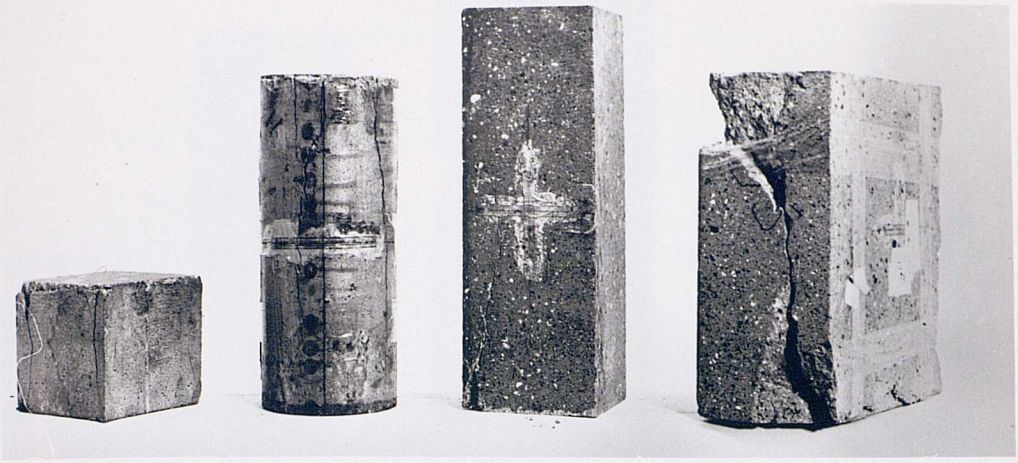
Thus the biaxial tests on cylinders performed in the hydraulic cell give ultimate strengths as proportions of the uniaxial strength which vary only slightly with the volume fraction of aggregate. For the biaxially tested slabs this is not the case, and increasing the aggregate content increases the strength by a large amount. For the mortar slabs the biaxial strength is not significantly different from the biaxial cylinder results for both mixes.

3.7.2.6. Failure Modes

Figures 3.31. and 3.32. show the modes of failure for typical specimens of mortar (Mix MBC) and concrete (Mix 6IC) respectively.

The cylinder, prism and slab specimens of mortar loaded under uniaxial compression exhibit the characteristic axial splitting fracture pattern leaving cones of inert material near the loaded ends due to platen restraint. The concrete specimens similarly loaded, show a larger number of fractured surfaces than the mortar due to the increased heterogeneity of the mix.

For the mortar slab tested under equal biaxial compression the appearance is similar to the corresponding uniaxial case except that the specimen is more subdivided by clearly defined planes of failure. Cones are again evident adjacent to the loaded faces. The biaxially loaded concrete slab, as in the corresponding uniaxial case, exhibits multiple fracture planes





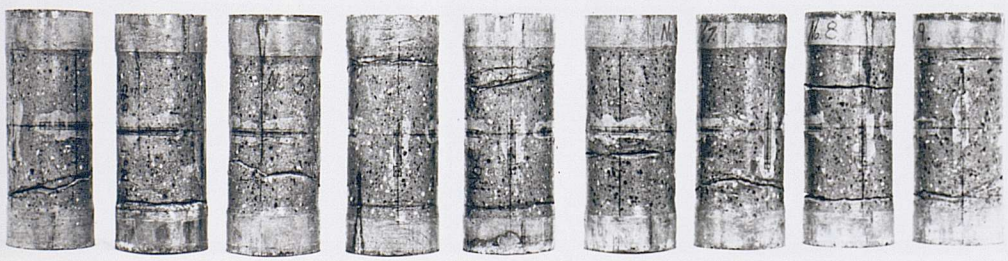


Figure 3.31. Views showing specimens of Mortar Mix MBC after failure in uniaxial and equal biaxial compression tests: (Top to bottom)
Cube, cylinder, prism and slab under uniaxial compression,
Slab under equal biaxial compression,
Cylinders under equal biaxial compression.



Figure 3.32. Views showing specimens of Concrete Mix 6IC after failure in uniaxial and equal biaxial compression tests: (Top to bottom)
Cube, cylinder, prism and slab under uniaxial compression,
Slab under equal biaxial compression,
Cylinders under equal biaxial compression.

such that the material outside the end cones is completely disintegrated.

The biaxially loaded cylinders of mortar contrast with the slabs in that only one, or in some cases two, simple fracture planes are evident, and these are aligned parallel to the direction of applied stress. The concrete cylinders, however, always exhibit single failure planes which are composed of multiple fractures caused by the heterogeneity of the mix.

An interesting feature of the cylindrical specimens is that those of the mortar tend to fail nearer to the unwaisted ends than the concrete. However, this trend is not reflected in the ultimate strengths of the specimens.

3.8. Conclusions

3.8.1. Introduction

The series of tests has been carried out in order to investigate the influence of the loading method on the behaviour of concretes of different degrees of heterogeneity (see 3.1.). The loading methods have been chosen to approximate as closely as possible to boundary conditions of uniform stress and uniform strain, using equal biaxial compression as the basic stress state (see 3.2.). Companion tests have been carried out under uniaxial compression in order to assess the effect of heterogeneity on the behaviour of various types of specimen.

The tests have been performed on (a) a concrete mix containing river gravel aggregate of $\frac{3}{4}$" maximum size, with an 'effective' water/cement ratio based on the assumption that the aggregate will retain water equivalent to approximately 50% of its water absorption capacity and (b) a mortar mix containing the same sand/cement ratio as the concrete with the 'effective' w/c ratio also based on the above assumptions. Specimens from the two mixes were cured in water for 25 days (under B.S. conditions) and then sealed with 'Febcure' curing compound tested under short-term uniaxial or equal biaxial compression at 28 days $\pm$ 1 day. The principal conclusions drawn from the tests are as follows:-

3.8.2. Cube Tests

The cube strength for the mortar is significantly lower than for the concrete (see Appendix 3). As the reverse trend is obtained for the ultimate strength of the various types of uniaxial specimen tested, this indicates the effect

of the end-restraint of the steel loading platen in inducing a state of triaxial compression throughout specimens with a low height/width ratio.

3.8.3. Uniaxial Compression Tests

3.8.3.1. Stress-Strain Relationships

1) For both the mortar and concrete mixes the stress-strain relationships for cylinders are almost identical to those for prisms. For slabs, however, higher compressive and tensile strains are measured at all corresponding stress levels, probably due to the friction-reducing interface tending to flow under load resulting in the load being concentrated near the centre of the relatively wide specimens.

2) The axial and lateral stiffness is greater for the concrete, as compared with the mortar, due to the higher concentration of relatively stiff aggregate.

3.8.3.2. Onset of Stable Fracture Propagation

1) For both the mortar and concrete mixes the stress at o.s.f.p., the stress at o.s.f.p. as a proportion of ultimate and the corresponding compressive and tensile strains are slightly lower for the prisms than for the cylinders, while those for the slabs are considerably lower.

2) The magnitude of the stress at o.s.f.p. for both concrete and mortar is similar for each corresponding type of specimen, but the corresponding compression and tensile strains at o.s.f.p. for the concrete are considerably smaller in magnitude than those for the mortar. This disparity of strain level demonstrates the effect of the content of relatively stiff aggregate but, as a consequence, it would be expected that the stress level would be lower for the concrete due to its increased heterogeneity. That this trend is not observed indicates the compensating effect of the larger 'effective' w/c ratio of the mortar.

3.8.3.3. Volume Changes

1) For the mortar mix, the relationship between the volume decrease and initial increase in stress is almost identical for all types of specimen. Approaching ultimate, however, the volume starts to increase at a significantly lower stress level for the slabs.

2) For all types of specimen smaller volume changes are given by the concrete than by the mortar due to the effect of the high content of relatively incompressible aggregate.

3.8.3.4. Onset of Unstable Fracture Propagation

1) For all types of specimen, the stresses and strains at o.u.f.p. are considerably lower for the concrete than for the mortar, as expected from the content of relatively stiff aggregate.

2) The stress at o.u.f.p. as a proportion of ultimate is lower for the concrete than the mortar which indicates that the effects of heterogeneity override those due to the disparity of 'effective' w/c ratio.

3.8.3.5. Ultimate

1) The ultimate strength of the mortar slabs is significantly lower than that for the cylinders and prisms, but for the concrete the strengths for all types of specimen are similar.

2) The ultimate strengths of the concrete specimens are significantly lower than that of the corresponding types for the mortar due to the effect of heterogeneity overriding the increase expected from the larger 'effective' w/c ratio of the mortar.

3.8.4. Equal Biaxial Compression Tests

3.8.4.1. Stress-Strain Relationships

1) For both the concrete and the mortar mix, the stress-strain relationships are considerably more variable for the near-uniform boundary stress tests than those conducted using near-uniform strain, due probably to the inability of the former test to redistribute stress or strain from a critical zone or zones.

2) For both the hydraulic and rigid-boundary conditions of loading, the stress-compressive strain curves for both mixes are steeper than those obtained under uniaxial compression, while the stress-strain tensile relationships are less steep. Such a 'rotation' towards the tensile strain axis is characteristic of biaxial loading.

3) The steepness of the compressive stress-strain relationships for both mixes is increased under hydraulic loading, while the steepness of the corresponding stress/tensile relationships is decreased. This increased 'rotation' of the relationships towards the tensile strain axis for the near-uniform boundary stress condition suggests increased 'biaxiality' of loading (see (2) above) and hence indicates the presence of lower secondary restraint effects.

4) The stress-strain relationships for the concrete are considerably steeper than for the mortar due to the effect of the content of relatively stiff aggregate.

3.8.4.2. Incremental Strain Ratio

1) The relationships between the i.s.r. and stress for slabs of both mixes under near-uniform boundary stress show characteristics similar to those observed under uniaxial compression namely, an increase (i.e. becoming more positive) indicating crack closure for the initial application of load and then a near constant portion followed by a continual decrease (i.e. becoming more negative) due to progressive fracture propagation.

2) For the hydraulically loaded specimens of mortar, the above behaviour is modified in that the i.s.r. values decrease slightly with initial load before becoming nearly constant, and subsequently continually decreasing, due to crack propagation. The concrete specimens exhibit i.s.r. values which increase continually throughout the test.

3) The i.s.r. values are approximately an order of magnitude greater for the hydraulically loaded cylinders than for the rigid-platen loaded slabs. This is a clear indication of the reduced restraints induced in the cylinders.

3.8.4.3. Onset of Stable Fracture Propagation

1) The level of stress at o.s.f.p. for the mortar slabs loaded under biaxial compression through rigid platens is almost identical to that for the uniaxially loaded slabs. Following from the differences in the stress-strain relationships the compressive strain for the biaxially loaded mortar slabs is thus less than, and the tensile strain greater than, that for the uniaxially loaded slabs.

2) The variability of results for the o.s.f.p. stress levels for the mortar cylinders under biaxial compression is considerably greater than for the slabs but it is, nevertheless, evident that the level is higher for the cylinders. The corresponding compressive and tensile strains are also considerably higher for the cylinders.

3) Fracture propagation for the concrete cylinders tested biaxially under near-uniform boundary stress occurs from the start of loading.

3.8.4.4. Volume Changes

1) The relationships between stress and volume change for the biaxial slabs of both mortar and concrete exhibit the same characteristics as for the uniaxial tests. For the biaxially loaded cylinders, however, the variation is considerable and the above trends, although evident, are less distinct.

2) The volume changes measured for the biaxial slabs, and some of the biaxial cylinders, of both mortar and concrete are considerably greater than those under uniaxial compression.

3) Due to the increased content of relatively stiff aggregate, the volume changes measured for the concrete cylinders and slabs under biaxial loading are less than those for the mortar.

3.8.4.5. Onset of Unstable Fracture Propagation

1) The stress at o.u.f.p. for the mortar slabs and cylinders under biaxial compression is close to the ultimate stress level. It is significantly higher than the ultimate level for the uniaxially tested slabs but only slightly higher than that for the prisms. The compressive strain at o.s.f.p. is essentially the same for both types of specimen but the tensile strain is significantly higher, and hence the volumetric strain is significantly lower, for the cylinders.

2) For the hydraulically loaded cylinders of concrete the stress at o.u.f.p. is considerably lower than for the slabs. In fact, the stress levels at o.u.f.p. and ultimate for the cylinders correspond approximately to the o.s.f.p. and o.u.f.p. levels, respectively, for the slabs. This results in the compressive, tensile and volumetric strains at o.u.f.p. for the cylinders being considerably lower than for the slabs.

3) The o.u.f.p. stress level for the mortar cylinders and slabs and the concrete slabs is essentially the same but that for the concrete cylinders is considerably lower.

3.8.4.6. Ultimate

1) For the mortar, the ultimate stress level for the hydraulically loaded biaxial cylinders is between 9% and 14% higher than that for the uniaxial specimens. The level for the slabs is essentially the same, being between 1% and 16% higher than that for the uniaxial specimens. For the concrete the ultimate strength for the cylinders is between 10% and 17% higher than for the uniaxial specimens but the strength for the slabs is between 49% and 58% higher.

This clearly demonstrates (a) the lack of secondary restraints for a fine-grained material under both near-uniform boundary stress and boundary strain and a coarse grained material under near-uniform stress and (b) the large restraints induced in a coarse-grained material when loaded under near-uniform boundary strain.

3.9. Implications for Design

It is obvious from the foregoing that there are considerable differences between the patterns of behaviour for concrete under near-uniform boundary stress and near-uniform boundary strain, and that the extent of the differences is dependent on the degree of heterogeneity of the mix tested. These facts must be recognised, therefore, when test data is used for design purposes, and full consideration must be given to comparing the test conditions with those obtaining in the structure.

In many instances it may not be possible to assess accurately the type of boundary condition acting on an element of material within a structure. In such cases, for safety the condition inducing the most critical state in the material should be chosen, and this would appear from the results of the present test series to be the application of uniform boundary stress. Under such a condition, practical mixes of concrete, which are relatively heterogeneous due to their coarse aggregate content and hence will tend to initiate and propagate fracture at an early stage of loading, will reach a critical stage of fracture earlier than under rigid-boundary loading since the failure processes will not be inhibited by secondary compressive restraints.

In the present investigation the stresses have been applied using proportional loading paths. The response of a concrete element may be modified for sequential loading, although opinions differ as to the actual effect. Some investigators [233, 234] suggest that sequential is the more critical of the two cases, while others [74] have observed no significant differences. More data is, thus, required in order to clarify the situation for design purposes.

4. DEFINITIONS OF FAILURE

4.1. Introduction

It has been evident for some considerable time that under increasing load concrete, in common with many multiphase materials essentially brittle in nature, undergoes processes of internal disruption prior to complete breakdown and subsequent loss of load-carrying capacity. These processes, however, are not discernable by examination of the overall stress-strain characteristics of the material under a given system of load, as no 'yield' point is evident, (i.e. there is no rapid increase in deformation without a corresponding increase in stress) and the curve is continuous to failure.

This latter fact has led engineers to focus attention on the one point on the stress-strain curve which is relatively easily reproduced, the point at which the specimen under test ceases to carry load. Generally the stress required to achieve this state is known as the 'strength' and it has been found to vary considerably with a number of factors, quite apart from the actual composition of the concrete mix and age and condition of the specimen under test. The most important among these factors are rate and duration of loading, type of stress state and previous loading history, all of which have received relatively little attention.

The strength of a given mix used for design purposes is usually taken to be that attained under short-term simple static stress (using a specimen of given age and condition) [2]. A working stress considered to be safe for the conditions of loading is obtained by reducing the strength by a predetermined factor. This factor is generally chosen by experience and intuition owing to lack of suitable data, and may not be based on a sound knowledge of material behaviour. In fact it is possible that the procedure is founded on the erroneous concept that at relatively low stresses concrete behaves elastically since the stress-strain curve appears nearly linear.

Recently, however, the use of concrete has been extended to include more complex structures under more severe stress and environmental conditions, necessitating the development of rationalised design criteria. The philosophy of design has also been modified in that it is now required to consider the possibility of the structure reaching certain 'limit states' [2]. It is therefore essential to study the breakdown of the material under various systems of load and to determine at what stage it ceases to exhibit properties essential for the purpose intended.

Section 4.2. reviews the experimental evidence and theories concerning the progressive breakdown of brittle materials other than concrete under various types of loading, while 4.3. examines the behaviour of concrete under short-term static load. This latter section is lengthy but it must be noted that, to the Author's knowledge, it represents most of the relevant work upon which could be based rational design criteria and significant improvements to the material.

The two types of research into the behaviour of a material will be noted. These consist of a) investigation at the structural level to establish the internal characteristics and fundamental behaviour of the material itself and, (b) phenomenological investigations concerned with the overall behaviour of the type of specimen used. It is results of the former type of research which are needed before a real understanding of the capabilities of concrete as a material can be attained. Unfortunately, however, it is the results of such research that are lacking.

Work carried out using both the above approaches will be examined, but the main aim is to study the fundamental behaviour of concrete under load and to compare the results with those obtained for materials similar in nature, and finally to consider the possible application of our knowledge to the development of design criteria.

4.2. The Fracture Process in Brittle Materials other than Concrete

4.2.1. Review of Previous Work

As far back as 1923 Adams and Williamson [81] inferred the presence of open cracks, rather than pores, in rock after measuring a lowering of the compressibility of rock with increasing hydrostatic pressure up to several kilobars, after which it remained approximately constant. Walsh [82] supported this explanation in suggesting that such cracks might have a large length/width ratio of the order of 10^3 since they close even under a slight pressure, whereas approximately spherical pores would require much higher pressures. Birch [83], in fact, showed that confining pressures above 25000 lb./in.^{2} were required to eliminate the effects of cracks and porosity on the stress-strain relationship for rocks.

The propagation of these pre-existing cracks, or the initiation of new ones, affects the deformational characteristics of the material, in particular the changes in volume under stress. Direct measurements of the volume

changes occurring when marble and soapstone specimens were loaded under simple compression made by Bridgman [84] showed an almost linear decrease in volume up to a critical stress, after which the materials dilated to failure. This dilatation has also been found by Matsushima [85], for igneous rocks such as granite, and by Handin et Al [86] for relatively porous rocks under triaxial compression.

Handin et Al found, by measuring changes in pore volume, that the density increased with deviator stress up to a critical level after which dilation processes predominated and eventually led to fracture. This dilation was detected in tests even under confining pressures of several kilobars. Matsushima [87] also detected significant decreases in ultrasonic pulse velocity for rocks under monotonic loading in the direction perpendicular to the maximum compressive stress at about approximately 50% of ultimate. Just prior to final failure the velocity decreased sharply in this direction but not in the direction parallel to the compressive load which suggests alignment of cracks in the direction of maximum compression.

The fundamental mechanism of fracture which could explain the above phenomena was studied by Brace and Bombolakis [88] by introducing thin straight cracks into a brittle material. Under systems of plane compressive stress it was observed that these cracks, which were aligned at various angles to the direction of maximum compression did not propagate catastrophically to failure.

Instead, branching cracks were found to extend from positions near the original crack tips and to increase in length gradually with increasing load until reaching a limited length. The branching cracks always tended to align themselves in the direction of maximum compressive stress.

Further evidence contributing to an understanding of the progressive failure process was provided by the tests of Cook and Hodgson [89]. They loaded cylinders of sandstone and quartzite under uniaxial and triaxial compression at an axial stress rate of 20 bars/second and measured the resulting deformation with transducers connected to an oscilloscope. For monotonically increasing stress, the modulus of elasticity increased during early stages of load which suggested crack closure. At higher stress levels, the modulus tended to decrease, and this was considered to be due to a sliding process. This sliding was inhibited for tests conducted at higher

confining pressures. For small cycles of load superimposed on the main loading cycle, the modulus for each successive cycle increased with increases in the maximum stress level of the cycle. This was also thought to be consistent with a sliding process. It was noted that the energy loss, as represented by the amount of hysteresis, decreased with each cycle which was considered to be due to surface energy supplied to new surfaces.

One of the most extensive fundamental investigations into the process of brittle fracture was carried out by Hoek [90]. He developed a modified form of the original Griffith Theory, [237 and 238] based on the McClintock and Walsh modification [44], to allow for crack closure. It was shown that such a theory agreed with the results obtained for most rocks under triaxial compressive states of stress if, in some cases, the interlocking of crack surfaces was assumed.

The actual mechanism of fracturing was studied using glass plate models in which inclined open cracks were machined. The plates were loaded in states of uniform uniaxial or biaxial compressive stress while the resulting strain distribution around the crack was assessed photoelastically. Fracture initiation occurred from positions near the crack tips, as noted by Brace and Bombolakis [88]. After aligning themselves in a direction parallel to the maximum compressive stress these cracks remained stable with increasing load up to a stress of over three times the initiation stress level. It was concluded from the results of the plate model tests that an open crack would only account for the failure of a specimen under uniaxial compression, or under states of stress in which one principal stress is tensile, and that failures from a single open crack would tend to produce a fracture surface parallel to the maximum compressive stress.

Similar experiments carried out on glass plates into which initially closed cracks were induced, showed considerable differences in behaviour. In such cases short cracks, aligned in the direction of maximum compressive stress, formed along the main crack at a certain stress level. These multiplied with load prior to the formation of branching cracks. The critical orientation of the initial crack was found to be $27\frac{1}{2}^{\circ}$ to the direction of maximum compression. It was postulated that experimental results could be explained by assuming fracture initiation from a series of short 'open' cracks separated by sections of contacting surface with a consequently high frictional resistance. Fracture propagation, in the form of

branching cracks near the original crack tips, occurs when the frictional resistance of the contacting crack surfaces is exceeded.

Detailed experiments carried out on quartzite specimens under uniaxial compression gave results which agreed with those predicted by the above hypothesis. Fracture initiation was observed at microcracks within grain boundaries orientated at between 20 and 30 degrees to the direction of compressive stress, compared with the $27\frac{1}{2}^{o}$ predicted.

Initiation occurred at between 70% and 80% of the ultimate strength, as predicted by the original Griffith theory. At approximately 85% of ultimate, sliding of crack surfaces occurred according to the modified Griffith theory. This sliding was inhibited by grain interlocking, and fracture propagation eventually occurred when the interlocking grains failed, causing the joining of arrays of cracks. The final fracture surface did not necessarily coincide with the critical crack orientation predicted by the modified theory. It was pointed out that the final phase in the fracturing process would depend on the grain structure of the rock with severe interlocking occurring for lightly packed, well-cemented, types which would raise the stress level required for propagation considerably above that for initiation.

Murrell [91] found the deformational behaviour of limestone under triaxial compression to depend on the value of confining pressure. For pressures between 0 and 16000 lb./in.^{2} the stress-strain relationships were curvilinear with no sharp changes in slope. In all cases ultimate failure was distinct and followed by a drop in load to a value supported by surface friction. Above 16000 lb./in.^{2} the stress-strain curve exhibited a definite 'knee' after which considerable deformation occurred. This pressure was described as the 'brittle-ductile transition' and was considered to represent the stage at which the shear stress on the fracture plane was insufficient to cause sliding. After failure the specimens remained coherent across the fracture plane and above about 25000 lb./in.^{2} no drop in load was experienced.

Brace et Al [92] used measurements of the electrical resistivity of water-saturated rocks to investigate the cracking processes occurring under load. It was deduced that most cracks were closed above confining pressures of about 2 Kb. A later extension of this work [93] showed that for

increases in compressive deviator stress, under a given confining pressure, the resistivity increased due to initial closure of pre-existing cracks. At stresses just below 50% of ultimate the resistivity started to decrease, probably as a result of the formation of new, or the extension of existing, cracks.

Brace, Paulding and Scholz [94] used electrical resistance strain gauges to measure the volume changes occurring when specimens of granite were tested under uniaxial and triaxial compression. As the deviator stress was initially increased the volume decreased sharply due to the closure of pre-existing cracks and flaws. Further increases of stress induced a linear volume decrease close to the linear compressibility of the material. This behaviour was considered to be associated with 'elastic' behaviour since no permanent strain remained after load cycling within the stress range. Above a certain stress level of between 33% and 67% of ultimate deviator stress, the volume started to increase due to crack growth even under high confining pressures. This level of stress, marking the end of the linear portion, remained constant as a proportional of ultimate and independent of the confining pressure for a given rate of loading, but decreased with a decrease in the loading rate.

Two mechanisms of cracking were proposed, the most likely, after consideration of measurements of linear compressibility, being cracks branching in the direction of maximum compression from near the tips of inclined pre-existing cracks. It was thought that failure did not occur simply as a result of the propagation of a critical crack but that, in rocks, such critical cracks may stabilise.

The above conclusions were confirmed by measurements of the changes in electrical resistivity of rocks under triaxial stress [93]. Under hydrostatic stress, increases in the electrical resistivity indicated crack closure for pressures up to 2 Kb. Under a given confining pressure the resistivity increased slightly as the deviator stress was increased in compression, again suggesting the initial closure of pre-existing cracks. At stresses just below 50% of ultimate, the resistivity started to decrease and fell rapidly just prior to ultimate for all rocks tested except marble, which was of a ductile nature. From these results, and the results of other workers, the process of brittle fracturing of rock in compression was considered to give rise to four zones in the stress-strain relationship as follows [95]:

Zone I — Initial crack closure producing a 'toe' in the stress-strain curve.

Zone II — Elastic distortion of the mineral grains.

Zone III — Elastic distortion of grains with loosening of grain boundaries due to frictional sliding. The formation of open axial cracks causing dilatent behaviour.

Zone IV — The formation of faults from the crack systems, leading to mechanical instability.

The above mechanism of failure was also supported by the work of Bieniawski [96] from the results of testing specimens of igneous and metamorphic rock in static uniaxial, biaxial and triaxial compressive stress. Examination of the specimens prior to test established the presence of randomly orientated and distributed cracks. On initial application of load, an increase in the E value was measured. This was attributed to the closure of cracks inclined at an angle to the direction of maximum compressive stress. The range of stress over which closure occurred was small, indicating that most pre-existing cracks were of the closed variety.

With a further increase of stress, the volumetric strain - maximum compressive stress relationship indicated a stage of linear consolidation which was terminated by a tendency of the volume to increase. This increase was considered to be due to fracture initiation in the form of branching cracks, originating from near the tips of the initial cracks, similar to the type postulated by Hoek [90] and Brace et Al [92], and subsequent stable fracture propagation. The level of deviator stress at which fracture initiated, for the rock tested, varied from 27.5% to 23.5% under uniaxial compression reducing under high triaxial stress states.

The direction of stable propagation was investigated by carrying out compressibility tests on rock samples previously subjected to stresses above and below the fracture initiation stress. Comparison of the compressibilities in the axial and lateral direction indicated the predominant direction of propagation to be parallel to the direction of

maximum compressive stress.

Tests carried out on glass plates, containing artificially induced open or closed cracks at random orientations, indicated a progressive process of stable propagation. The most critical crack initiated branching cracks and this was followed by initiation of the next crack in order of weakness, the process continuing until the crack arrays coalesced.

For rocks, the region of stable fracture propagation was assumed to extend up to the minimum volume level, after which a zone of unstable propagation lead to ultimate failure. Microscopic examination of slices of specimens subjected to stresses within this unstable zone, showed extensive grain shattering. This critical stress level was found to be approximately 80% of ultimate and coincided with a sudden change in the pattern of propagating cracks. If the stress was maintained above this level the material always subsequently failed, while below the level ultimate breakdown would not occur. It was concluded that the minimum volume level could be taken to represent the transition between stable and unstable propagation.

The process of fracturing was studied in detail by Scholz [97] using sensitive accoustic detection apparatus to record a number of microfracturing events, and their position, in rock samples under compressive loads. His results again support the previous hypothesis of fracture mechanism. At low stresses the frequency of the fracturing events was low and fairly constant until about 50% of ultimate deviator stress, when the number of events started to increase. Just prior to ultimate there was a drastic increase in the amount of microfracturing with the events spaced in, or near, the eventual plane of failure.

The microseismic activity within a rock under triaxial compression was also studied by Barron [98] using an ultrasonic translator detector. By effectively integrating the microseismic output from the specimen under load, a stress level was identified after which the noise increased rapidly to failure. It was found that this level coincided closely with the start of dilatation, as defined by the departure from linearity of the stress-volumetric strain relationship, and this was considered to mark the onset of fracture initiation.

4.2.2. Conclusions

The main conclusions drawn from the work reviewed in the previous section are summarised in Table 4.1. which shows the probable processes of failure occurring as a brittle material is subjected to increasing deviator component of compressive stress. It is clear that the behaviour can be divided into four identifiable zones as follows:-

Zone I — Closure of pre-existing cracks.

Zone II — Local fracture initiation from pre-existing cracks in a stable manner.

Zone III — Propagation of cracks in a stable manner to form arrays of cracks.

Zone IV — Coalescing of crack arrays and sliding of crack surfaces in an unstable manner, terminated by complete disruption.

Assessment of the above zones depends on the method of detection used and it would appear that a study of the structure of a material may disclose changes prior to those changes being evident phenomenologically.

4.3. Review of Experimental Measurement of the Deformational and Cracking Processes for Concrete

4.3.1. Introduction

For the brittle materials discussed in the previous section, the failure process has been found to consist of distinct stages identified by definite changes in material behaviour.

The following review of investigations into the response of concrete under load has been carried out in order to determine whether similar characteristics are evident for a more heterogeneous system.

Most of the work on concrete has been concerned with a study of the behaviour under short-term static loading. Although such investigations provide valuable information regarding the probable failure mechanism for concrete, it should be emphasised that this information is of limited use as the basis for design criteria applicable to more complex loading regimes. This is discussed more fully in Chapter 5.

OBSERVED MATERIAL BEHAVIOUR UNDER INCREASING DEVIATOR STRESS	DEDUCED CHANGES IN INTERNAL STRUCTURE	APPROXIMATE STRESS LEVEL
Compressibility decreases to a constant value and electrical resistivity increases after relatively small increase of hydrostatic pressure [81, 82, 92, 93].	Pre-existing 'open' cracks with large length/width ratio	Prior to Load.
Decrease in volume [84, 89, 94], increase in density [86, 92, 93] and elastic modulus [89, 96].	Crack closure	
From Structural Investigations Crack initiation in single branching mode from existing open cracks, or multiple mode from closed cracks, with branches aligned in direction of maximum compressive stress [88, 90, 96]. Cracks reach a limited length.	START OF FRACTURE INITIATION	Approximately 30% ultimate.
From Phenomenological Investigations Decrease in USPV [87], dilatation [84, 85, 86, 87] and decrease in elastic modulus [89] and electrical resistivity [93] and increase in microseismic events [97, 98].		23 to 67% of ultimate depending on material, stress state and method of detection.
From Structural Investigation Sliding of crack surfaces causing joining of crack arrays [90, 96]	START OF FRACTURE PROPAGATION	Approximately 80 - 85% ultimate
From Phenomenological Investigations Rapid fall in electrical resistivity [93] and shattering of grain boundaries [96] rapid increase of microseismic events [97]. Increase in overall volume [94, 96].		From 80% ultimate to just prior to ultimate.

Table 4.1. Fracture processes occurring when a brittle material is subjected to increasing deviator component of compressive stress.

4.3.2. Behaviour under Conditions of Short-Term Static Stress

As early as 1928, Richart Brandtzaeg and Brown [66, 99] inferred from measurements of strain on cylinders of plain concrete under simple short term compression that the behaviour was nearly elastic just after initial loading, becoming more inelastic as the load was increased.

Conversion of principal strains to volume changes showed that, as the stress was increased, the overall volume decreased to a minimum before reversing and increasing to failure. The stress corresponding to this point of minimum volume was termed 'critical stress' and was taken to mark the onset of discontinuous behaviour of the concrete, culminating in failure by a splitting mode. Further work [100] on reinforced concrete beams and eccentrically loaded columns indicated 'critical loads' of between 70% and 90% of ultimate, as defined by the same criterion.

That cracking occurred at early stages in the loading history was first observed by Thomas [101] who detected it on the surfaces of specimens using a microscope, Carlson [102] quoted strains of 80 microstrain at the start of cracking (for one specimen only). Using more sophisticated means (extensometers and a microscope) Evans [103] detected very small cracks on the exterior faces of briquettes of concrete in tension and beams in flexure at various load stages.

Berg [104] observed cracks 4-5 microns wide and several millimetres long to occur on the tension face of flexure specimens at a stress of approximately 70% of ultimate, with the start of cracking corresponding to a strain of 100 microstrain.

Using the same definition as first postulated by Richart et Al [66, 99] Hognestad [105], measuring strains on the compression face of reinforced concrete columns loaded eccentrically, showed the 'critical load' to vary between 80% and 90% of ultimate, being greater for higher forces in the reinforcement compared with total internal compressive force. In a later investigation Hognestad et Al [106] concluded that the critical stress for beams loaded in flexure was between 71% and 96% of ultimate stress.

The methods discussed so far have depended on measurements made on the boundaries of specimens to infer the internal behaviour of concrete under load. An important technique introduced by Jones [107] enabled an

independent assessment to be made. This technique involved the measurement of the velocity of ultrasonic pulses transmitted through concrete under load. From specimens tested in simple compression, flexure, and direct and indirect tension it was concluded that the cracks detected by the method were always of a tensile nature. The stress at which the cracking started, as indicated by a rapid decrease in pulse velocity, varied with the type of specimen, method of loading and ultimate strength of the concrete. For short-term simple compression tests using bobbins cracking started at 65% of ultimate stress, while for direct tension it was detected as early as 59%. Theoretical calculations of the strain level at cracking showed that, in compression and tension, it occurred at a tensile strain of 150 and 70 microstrain respectively.

Blakey and Beresford [108, 109], by measuring surface strains with electrical resistance strain gauges attached to the tensile face of beams in flexure (3rd point loading), found that the strain between the central loading points remained essentially constant up to a given load stage which varied between 60 and 70% ultimate. The corresponding strains varied between 70 and 100 microstrain. After this stage the load-strain curve deviated from linearity and sudden increases in strain were detected by some gauges, while others indicated relaxations. This effect was associated with the formation of microcracks which were related, although did not immediately lead, to final collapse. This conclusion is important as it indicates that microcracks may remain stable in a stress field until the magnitude of the local stress is sufficient to cause propagation.

A similar investigation carried out by Todd [110] again showed the load-strain curve to be almost linear up to a strain of approximately 100 microstrain, corresponding to a calculated stress of between 63% and 75% of the maximum. It was suggested that the strain level marked the onset of cracking.

The ultrasonic pulse method to detect the onset of cracking was again used by Jones and Kaplan [111] to study the cracking process in concrete cubes under simple compression. Results of the investigation indicate that, for richer mixes with a low water/cement ratio, the onset of cracking occurs at a slightly higher stress level as a proportion of ultimate, than for leaner mixes with a higher water/cement ratio and that this level increased very slightly with age of the specimen. The main conclusion, however, was that

the start of initial cracking depended on those properties of aggregates which influence the bond between the aggregate and matrix.
Concrete containing smooth round gravel started to crack at a lower stress level than that containing angular aggregates of coarser surface texture, the variation being between 50% and 70% of ultimate. From this investigation it would appear that the amount and type of aggregate in a concrete mix plays an important role in the initiation of cracks. It is thus of interest to include at this point the work of Dantu (112, 113) which provides qualitative, if not quantitative, evidence of aggregate inclusions causing strain concentrations. By studying the strain distribution in and around large aggregate inclusions in a very fine mortar matrix he showed that the strain level in the mortar could be itensified up to about five times the average strain, at the compressive stress level used.

Rusch (114), again using the concept of critical stress marked by the reversal in direction of volume changes, considered that for short-term simple compression this corresponded to a stress of approximately 75% of ultimate. The use of another independent method for detecting internal breakdown was also reported, and consisted of measuring the accoustic emissions from concrete under load. These emissions, which were assumed to be caused by the formation of cracks, were found to start at a stress of about 50% of ultimate, and to increase rapidly at about 75%. This may be evidence of distinct stages in the disruption process after the initial cracking point, and the increase in noise at 75% of ultimate may indicate extremely unstable behaviour following relatively stable processes.

An interesting series of experiments was performed by Glucklich (115) who tested concrete and mortar in simple compression using a normal testing machine with, and without, a spring in series with the specimens. The strength given by the concretes tested in the 'soft' machine was only 30% of that given in the unadapted machine. The failure mode exhibited by the specimens tested in the soft machine was a single axial crack, whereas many internal cracks were observed in the specimens tested normally. For mortar, on the other hand, no strength difference was given by the two loading methods and the failure was always accompanied by a single axial crack.
It was concluded that the spring provided a source of kinetic energy which overcame the arrest of crack growth caused by the stiff aggregate particles in the concrete. Thus the crack which grows initially will always lead to failure in the soft machine, and the tests indicate that this cracking

starts at about 30% of ultimate for normal concrete.

Hansen [116] using the ultrasonic pulse technique showed, for cubes tested in simple compression, that the stress at the end of the linear portion of the stress-strain curve and the stress at which microcracks were first detected were almost coincident. The microcracking level, as a proportion of the failure stress, was found to increase markedly for ages up to about 7 days and then to remain fairly constant. Cubes stored in water cracked at 65-70% of ultimate, whereas those stored in air cracked earlier at 45-50%. This was suggested to be due to the weaker aggregate-matrix bond developed under unfavourable curing conditions, and confirms earlier work[111].

The first direct method studying the formation of internal cracks in concrete was reported by Hsu et Al [117]. They removed thin slices perpendicular to the direction of loading from cylinders previously strained to various levels, and examined these microscopically after staining. The main conclusions drawn from the investigations were that microcracks exist at the coarse aggregate/mortar interface even before loading and that these were the weakest link in the system. Above approximately 30% of maximum stress, these bond cracks increase in length, number and width with increasing strain, this level corresponding to the end of the near-linear portion of the stress-strain curve. However, if it is to be expected that cracks formed under stress would align predominantly parallel to the direction of loading i.e. perpendicular to the direction of slicing and the technique would thus be insensitive to such cracking. At about 70-90% of maximum stress, cracks through the mortar increase rapidly and bridge between bond cracks. Above this level continuous crack patterns form, the paths taken tending to a minimum length through the mortar. Curvature of the stress-strain relation was assumed to be due to the continual reduction in the number of possible load paths caused by the cracking process, which eventually led to complete loss of load carrying capacity. A further part of this programme [118] used x-days in place of direct microscopic observation to study the internal structure of concrete before, and after, loading in simple compression. This again showed that cracks existing prior to loading were predominantly of the bond type and the importance of those due to drying shrinkage was stressed. After straining to a level corresponding to a point on the descending portion of the stress-strain curve, bond cracking was found to have increased markedly accompanied by interconnecting cracks through the matrix.

It was again noted that the matrix cracks tended to extend in such a manner as to minimise their length and that this caused preferential formation between closely-spaced aggregate particles.

Kaplan [119] defined initiation of microcracking as the start of significant deviation from linearity of the stress-strain curve as assessed by a mathematical procedure. Surface strains were measured on mortar and concrete specimens of various mixes tested under simple compression, flexure, direct and indirect tension. This investigation is of importance as it represents one of the first attempts to discover logically the individual influence of various mix parameters on the behaviour of concrete. The results and conclusions will thus be given more fully as follows.

For flexure the strains and stresses (calculated assuming elastic behaviour) both at, or near, failure and at initiation of microcracking decreased with increase in the volume fraction of (a) fine aggregate in mortar of a given water-cement ratio or (b) coarse aggregate in a concrete with a given mortar ratio. The cracking and near ultimate strains for concrete decreased from 160 to 85 microstrain and 210 to 150 microstrain respectively (with almost identical values for the mortars). For concretes the stresses at cracking as a proportion of ultimate remained fairly constant or decreased slightly as the volume fraction of coarse aggregate was increased and both stresses depended on the type of aggregate and water/cement ratio. For a water/cement ratio of 0.5 the average ratios for limestone and gravel aggregate were 76% and 71% respectively, while those corresponding to a water/cement ratio of 0.6 were both 73%.

For the direct tension and splitting tests the stresses and strains at cracking also decreased with increase in volume fraction of aggregate. The strains were independent of aggregate type and water/cement ratio, whereas the stresses were affected in a manner similar to the flexural case. For gravel aggregate concretes the cracking stress as a proportion of ultimate was about 60% which for the limestone aggregate the ratio was about 68%.

In simple compression the compressive strains at cracking and near ultimate for mortars and concretes decreased as the volume fraction aggregate increased. Strains were again independent of the type of aggregate or water cement ratio. Stresses were dependent on these latter mix

characteristics, being greater for limestone aggregate and water/cement ratio concretes of 0.5 than for gravel and water/cement ratio of 0.6.

The ratio of cracking stress to ultimate varied only between 46% and 51% for all tests.

It is suggested that cracking initiation may be more dependent on a critical strain than stress, and that the distributions of internal stress and strain are affected primarily by the proportion and properties of the coarse aggregate for a given matrix.

A method of detecting a critical cracking stage used by Oladapo [120] involved the assessment of the load stage which caused significant non-uniform changes in the strain distribution. It was conceded that the criterion chosen defined a stage of advanced cracking and that cracking preceding this stage appeared to be a gradual process.

By measuring the strain distribution on the tensile face of flexure specimens it was shown that both the critical and ultimate load increased with increasing strength of the mix (i.e. aggregate/cement ratio decreasing simultaneously with the water/cement ratio). The corresponding critical strain increased from 50 to 100 microstrain. The critical load stage as a proportion of ultimate increased with increasing strength of mixes from 70% to 85%.

The critical stress (calculated assuming elasticity) compared directly with the indirect tensile strength given by cylinder splitting tests, but no comparison of strains was made. Linear dependence of maximum load in flexure on critical strain and load was also observed and it was postulated that the relation between the rates of loading and crack propagation may give rise to increases in strength under dynamic conditions.

Yokomichi et Al [121] studied internal cracking level by recording and measuring the elastic waves produced when cracks form. The number of cracking signals was compared with the deformational and visual behaviour of polished surfaces of specimens of various concrete mixes under uniaxial cyclic compression. It was found that curvature of the stress-strain relation increases as the number of cracking signals increases and the results indicate that a rapid increase in signals corresponded

with a large increase in the residual strain of the load cycle. Visual examination of the surface at early stages of loading showed bond cracks, predominantly around large particles of aggregate, which were parallel to the direction of loading (which was perpendicular to the layers as cast) for mixes with low water/cement ratios, and on the underside of aggregate particles for high water/cement ratios. As the load was increased, cracks through the mortar matrix bridged between pairs of bond cracks until, at very high stresses, isolated mortar cracks formed.

Various methods of establishing the existence of microcracks in concrete and the load at which they become unstable and propagate (termed 'discontinuity' by Newman [9], were used by Robinson [7]. An x-ray technique confirmed the results of Hsu et Al [117] and Slate and Olsefski [118] in showing that small cracks exist in concrete prior to loading. In specimens of mortar with preplaced coarse aggregate particles and also specimens of normal concrete, cracks were observed to extend and mainly bond cracks to develop under uniaxial compression, the presence of coarse aggregate particles and large air voids influencing this process to a great extent. Accoustic emissions recorded during testing indicated isolated cracking occurring at very low stresses which did not significantly affect the mechanical behaviour. Integration of the emissions showed that at a certain stress the energy dissipation level increased significantly indicating cracking. This stress level decreased with increasing volume fraction from 70% ultimate for plain mortar to 60% for mortar with 6 pieces of aggregate.

The ultrasonic pulse technique indicated stress levels at which the pulse velocity decreased significantly. For mortars with, and without, preplaced aggregate, two such levels were observed, both decreasing with increase in volume fraction of aggregate and examination of the data also shows corresponding decreases in lateral cleavage strain. The first stress level varied between about 45% and 30% of ultimate (with corresponding lateral strains between 330 and 180 microstrain) and was considerably less pronounced than the second level which varied between about 70% and 45% of ultimate. Since the levels gradually merged with increasing aggregate content the second level was thought to represent cracking due to stress concentrations caused by the coarse aggregate, which gradually overshadowed cracking in the mortar phase. For normal concretes only one stress level was detected which varied between approximately 40% and 50% of ultimate

(with corresponding lateral strains between 80 and 60 microstrain). That the cracking detected by the pulse velocity technique was sufficient to influence the lateral strain was reflected in the increases of Poisson's Ratio which occurred at, or very close to, the critical stress levels. Considerable creep was experienced at each load stage after the second stress level. X-ray analysis of the cracking process under load showed that the stress range over which small cracks interconnected and developed parallel to the loading direction, until inches long in all cases, included the second critical stress level as determined by ultrasonic pulse technique.

Vile [8] again defined discontinuity in concrete as the stress at which the ultrasonic pulse velocity through loaded specimens decreased rapidly, as it was found difficult to determine from stress-strain curves. Saturated mortars, normal and lightweight aggregate concretes, with identical sand/cement ratios, were tested under uniaxial compression and tension, biaxial compression and compression-tension, using mixes in which only one parameter was intentionally varied so that its individual effect could be studied. It should be noted that prior to test all specimens were subjected to cycles of stress to a level of approximately 30% and 20% of ultimate for uniaxial and biaxial tests respectively.

Discontinuity stress as a proportion of ultimate varied between: (a) 65% and 77% for mortars in uniaxial tension (b) 58% and 74% for mortars in uniaxial compression (c) 60% and 77% for normal concretes in tension, and (d) 44% and 70% for normal concretes in compression. Cleavage strains corresponding to the above conditions varied between: (a) 75 and 100 microstrain (b) 180 and 200 microstrain (c) 40 and 60 microstrain, and (d) 35 and 200 microstrain respectively.

For a given mix an increase in the water/cement ratio decreased the stress both at discontinuity and ultimate. For compression no definite trend was noted regarding the discontinuity stress as a proportion of ultimate but in tension it occurred earlier with increasing water/cement ratio. No trends were noted for cleavage strain values at discontinuity.

For uniaxial stress increasing the proportion of coarse aggregate in a given mix showed no definite trends regarding the value of ultimate and discontinuity stress or discontinuity as a proportion of ultimate. The

cleavage strain, however, decreased markedly but was relatively independent of type, shape and size of aggregate.

For biaxial states of stress the discontinuity and failure envelopes were similar in shape. The cleavage strain at discontinuity increased with increasing mean normal stress, greater increases being observed for mortars than concretes. Discontinuity stress as a proportion of ultimate, after increasing markedly for the first increase in intermediate principal stress, then remained almost constant for mortars and lightweight concretes and generally increased slightly for normal concretes.

Below the discontinuity level for both uniaxial stress and biaxial compression the mortars and lightweight concretes maintained constant values of 'elastic modulus' and 'Poisson's Ratio'. Similar behaviour was observed for normal concretes except in biaxial compression when considerable increases in E and slight increases in Poisson's Ratio were noted. After discontinuity the changes were rapid. Also below discontinuity the creep rate was very slow becoming increasingly more rapid above the level.

Ruetz [122] investigated the cracking process in concrete under uniaxial compression by detecting the accoustic emissions with sensitive transducers. Under constant, and fairly short-term, rates of stressing the lateral strain and noise intensity both increased markedly at about 90% of ultimate. Under short-term constant strain rates the increases in these quantities occurred much earlier and at lower levels of lateral strain for mixes containing larger sizes of aggregate.

For uniaxial tension Illston [123] found that for stresses above 50% of short-term ultimate large plastic strains were induced by sustained loading. Below the level the creep remained proportional to the applied stress.

Isenberg [124] using x-rays to study the formation of cracks in slices cut from hollow cylindrical concrete specimens previously loaded in combined compression and torsion concluded that adjacent surfaces of aggregate particles are preferred locations for bond and mortar cracking. For crushing modes, cracks in the mortar mostly tended to spread interpartically, with some ending in the mortar. For cleavage modes it was observed that cracks could exist within the mortar without forming a major cleavage crack. This was explained by assuming 'blunting' of the crack tips on the spaces

containing the coarse aggregate particles, which implies an increase in tensile strength with increase in volume fraction of aggregate for a given mortar matrix.

Desayi and Sen [125] determined critical points in the loading history from stress-strain relations obtained under simple compression by examining the logarithmic variations of stress and strain. For short-term tests the resulting curves were found to consist of three linear portions, the first ending, for the mixes tested, at a stress of between 15% and 25% of ultimate, the second (termed the 'true ultimate strength') at a stress of from 70% to 90% of ultimate.

An extension of the above work was reported by Desayi and Viswanatha [126] in which concrete cylinders of various mixes were tested in simple compression, longitudinal and lateral strains being measured by extensometers. Two methods of determining the 'true ultimate strength' were compared and were defined by: (a) the stress at which the volumetric strain changed direction, and (b) the upper critical stress determined from log stress-long strain plots. The specimens were apparently tested in the air-dried condition and for mixes of decreasing compressive strength the true ultimate strength defined by (a) remained a constant 84% of ultimate, while that defined by (b) decreased from 82% to 77½%.

Plate models of concrete were used by Shah and Winter [127] to study the strain distributions around aggregate particles in a mortar matrix. The model consisted of a single inclined thin plate of aggregate and, loaded under uniaxial compression, the resulting strain distribution measured by electrical resistance strain gauges. It was found that strains increased monotonically up to an applied load of about 40% of ultimate, at which point cracks formed along the aggregate/mortar interface and were indicated both visually and by the strain readings. As the load was increased tensile cracks were formed near the aggregate tips aligned in the direction of applied load, allowing sliding at the aggregate/mortar interface. The strain distribution produced by further load increases indicated that stresses were re-distributed such that an increasing proportion of the load was carried by the surrounding mortar matrix, until this finally failed in a crushing mode at a stress below that determined for the pure mortar.

Beres [128] defined a 'lower critical stress' as that producing minimum voids in normal dense aggregate concrete. This stress was assumed to mark the onset of structural 'loosening' and was measured by observing the start of either volume increases or a decrease in 'Poisson's Ratio', both being calculated on an incremental strain basis. This 'lower critical stress' is not to be confused with the 'critical stress' of Richart et Al [66] designated 'upper critical stress' by Beres, the latter being determined by the stress for minimum volume calculated from total strains. Prisms of various concrete mixes were tested in uniaxial compression and strains measured using electrical resistance strain gauges. It was found that the lower critical stress which corresponded to the point of inflexion of the volumetric strain-compressive stress curve, varied between 50% and 82% of ultimate for the mixes tested. It decreased with age (or strength) of a given mix, the decrease being greater for mixes of higher water/cement and aggregate/cement ratios. The proportion increases, however, for mixes of lower water/cement and aggregate cement ratios.

The onset of microcracking was detected by Hughes and Bahramian [129] using the ultrasonic pulse technique on specimens of normal aggregate concrete under simple compression. Results of the tests indicate that prisms of concrete made with a given volume fraction of coarse rounded aggregate, decreasing the volume fraction of total aggregate increased the ultimate stress, volume fraction of cement and cement/water ratio being raised simultaneously to achieve approximately constant workability. However, the cracking stress decreased from 56% to 45% of ultimate for the same variations.

Under similar conditions but using a smaller volume fraction of angular aggregate the ultimate stress increased while, in this case, the cracking stress increased from 63% to 72% of ultimate.

The internal behaviour of concrete under load was studied by McCreath [14] using idealised two-dimensional plate models (each simulating a thin slice through a concrete mix) loaded under uniaxial compression. Each model consisted of four cylindrical aggregate particles, arranged to represent a section through a face-centred cubic packing corresponding to a particular volume fraction of aggregate, surrounded by a very fine mortar matrix. The strain distribution around the inclusions under load was measured by a

combined photoelastic and strain gauge technique and, from a knowledge of the strains necessary to cause fracture initiation in mortar determined from the strain response of specimens of plain mortar subjected to various states of stress, the critical point in the model was predicted from which fracture should initiate. For each model representing a different volume fraction of coarse aggregate the critical point was located in the mortar at the centre of symmetry of the aggregate packing, and this was confirmed from tests to failure in which the initial crack at this location propagated around the aggregate particles. It was found that the average strain in the composite material at crack initiation gradually decreased as the volume fraction of the coarse aggregate was increased, the trend comparing favourably with results from tests on idealised three-dimensional models of concrete in which the crack initiation point was defined as start of increase of the ratio lateral composite strain/axial composite strain. However, this value of strain for the plate models was considerably lower than for the three-dimensional concretes.

The author [57] defined a lower bound discontinuity as the point of significant departure from linearity of the volume change/minor principal strain relationship, which was assumed to indicate measurable void formation within the material.

From surface strains measured on air-dried specimens of mortar and concrete under short-term uniaxial compression it was found that discontinuity, as defined above, could be detected easily, there being large superimposed volume increases above this level. The ultrasonic pulse velocity technique when used on the same specimens indicated a considerably higher critical stress level for all mixes tested.

As an independent check that the volume change approach was sufficiently sensitive to detect the first significant formation of voids under loading specimens, previously loaded in uniaxial compression, were subjected to hydrostatic pressure and the resulting deformational response measured. A close correlation was obtained between the discontinuity level and the stress at which the deformation under hydrostatic pressure indicated the closing of cracks aligned parallel to the direction of previously applied stress.

Discontinuity determinations were also successfully carried out using surface strain measurements taken on specimens under combined axial

compressive stress and confining pressure. Preliminary work, using mortar specimens, showed the discontinuity level, as a proportion of maximum axial stress, reached a maximum at a certain value of confining pressure and then decreased gradually.

Hughes and Ash [130] detected discontinuity, using the ultrasonic pulse velocity technique, for bobbin-type specimens of concrete loaded under short-term uniaxial tension at constant rates of strain. Cracking was found to occur at stress levels between 40% and 100% of ultimate, the proportion decreasing with increasing size and roughness of aggregate. For cement paste, cracking and ultimate were coincident.

Pigeon [15] studied the process of both fracture initiation and propagation under uniaxial compression within idealised two dimensional models of concrete consisting of various arrays of cylindrical aggregate particles in a fine mortar matrix. The technique used was an improved version of that developed by McCreath [14] and, in general, the results confirmed those obtained by McCreath with the following additional conclusions:-

i) The strains required to cause fracture initiation for a given concentration of aggregate remained independent of the type of particle array.

ii) For volume fractions of coarse aggregate above approximately 25%, there are only relatively small changes in the strains required to cause fracture initiation.

iii) Unlike McCreath's tests no definite cracks were observed, the mode of failure being zones of disruption in the matrix, which gradually extended towards the aggregate boundaries as the load increased.

iv) After significant disruption of the mortar matrix crack propagation always followed a path around the aggregate boundaries as well as through the matrix.

In addition to the above tests the behaviour of cylinders of gap-graded cements containing various types of aggregate was studied. The results indicated that angular particles caused fracture to initiate at lower values of strain than rounded.

The cracking process in concrete under uniaxial tension was studied by Stroeven [131] who used an optical technique to measure the development of strains to a sensitivity of 0.1 microstrain. A decrease in Poisson's Ratio was detected at stress levels between 60% and 80% of ultimate.

4.3.3. Conclusions

The main conclusions drawn from the work reviewed in the previous section are summarised in Table 4.2. which, as in the case of other brittle materials (see Table 4.1.), is presented in the form of a process of failure occurring under increasing stress. In addition, the various factors which may influence the structural changes occurring under load are outlined.

It appears that the behaviour is similar to that observed in 3.2. for rocks, etc. and two main identifiable changes in response of the material, prior to complete disruption under load, are evident, namely:-

(i) Onset of Localised Cracking
After which the material exhibits distinct inelastic properties but still behaves in a relatively stable manner.

(ii) Onset of Continuous Cracking
After which the material starts to disrupt in a relatively unstable manner in that cracks continue to propagate even when the load is maintained constant. This causes dilatation and serious loss of load carrying capacity.

As in the case of rock materials the assessment of the level at which the material undergoes significant internal changes depends on the method of detection used. In general, the structural investigations again disclose changes at an earlier stage than they become apparent phenomenologically.

4.4. Postulated Mechanisms of Failure for Concrete under Increasing Stress

It is evident that, in a heterogeneous material such as concrete, defects exist even prior to the application of load. These defects are due to a number of causes, the main ones being:-

(i) Discontinuities in the cement paste matrix due to its complex morphology. Such flaws range in size from a number of angstrom units at the gel lattice level, to several microns, or above, for isolated or continuous capillary pores.

OBSERVED MATERIAL BEHAVIOUR UNDER INCREASING STRESS	DEDUCED CHANGES IN INTERNAL STRUCTURE	APPROXIMATE STRESS LEVEL	INFLUENCING CHARACTERISTICS
Presence of cracks detected microscopically [117] and from x-rays [7, 118].	Pre-existing cracks	Prior to load	Shrinkage, thermal effects, etc.
From Structural Investigations Bond cracking [117, 121, 127] and matrix cracking increases depending on spacing of particles of aggregate [14, 15, 124] with cracking aligned in direction of maximum compressive stress as load increases [127].	START OF LOCALISED STABLE CRACKING	30 - 40% ultimate	Spacing of particles for a given mix, etc.
From Phenomenological Investigations Decrease in USPV [107, 111, 7, 116, 8, 129] marked changes in strain response [110, 108, 109, 119, 120, 8] start of significant accoustic emissions [122, 7, 121, 114] increase in creep strains [8, 123] measurable void formation [57].		45 - 90% ultimate	Method of detection, type of aggregate, type of specimen, state of stress, rate of loading, curing conditions and level decreases with - (a) increase in w/c ratio (b) increase in volume fraction of aggregate (c) decrease in age (d) decreasing roughness and angularity of aggregate.
From Structural Investigations Formation of continuous crack patterns through matrix and around aggregate particles [117, 118, 121, 14, 15]	START OF CONTINUOUS CRACKING	70 - 90% ultimate	Spacing of aggregate particles for a given mix, etc.
From Phenomenological Investigations Further increase in USPV [7, 8] increase in volume [66, 99, 114, 126, 128] marked increase in accoustic emission [114] and change in stress-strain relationship [125]. Considerable creep effects [7] visible surface cracking [101, 103, 104].	Unstable behaviour caused by reduction in number of load paths due to cracking (leading to complete disruption).	70 - 90% ultimate	As for localised stable cracking (detected phenomenologically).

Table 4.2. Failure processes occurring when concrete is subjected to load.

(ii) Voids caused by shrinkage or thermal movements due to the incompatability between the properties of the various phases present in the composite material.

(iii) Discontinuities at the boundary between aggregate particles and the paste or mortar matrix, caused by segregation.

(iv) Voids present in the composite material as a result of incomplete compaction.

Apart from the discontinuities at the aggregate boundaries, which are aligned in certain directions relative to the casting direction [130a, 130b], the above pre-existing flaws are randomly distributed and orientated within the material. They also exhibit a range of shapes and sizes.

The stress or strain state applied to the boundary of an element of a composite material generates a strain field within the material, which is dependent on the distribution of the component phases, and the size, shape and distribution of flaws. It has been shown that the local strain in a matrix can be increased by up to an order of magnitude, compared with the average field strain, as a result of the presence of relatively hard inclusions [112, 113, 57, 133, 134, 15, 132]. Such strain concentrations are further intensified to far higher orders of magnitude due to the presence of flaws, particularly those with high aspect-ratios [135]. These flaws, therefore, are considered to be the nucleation sites for any load-induced cracking.

As the boundary strain on an element of concrete is increased, the local strain concentrations will also proportionally increase until the conditions around a critical flaw (critical by shape and/or by orientation) cause the crack to extend in such a way as to reduce the local strain concentrations. In a predominantly tensile stress state the crack will tend to extend a direction at 90° to the direction of maximum tensile stress [135]. This extension will occur in an unstable fashion, unless the crack front moves into a zone of increased stiffness or a plane of weakness [136] or a region with a lower level of strain. If the applied stress is predominantly compression the crack will tend to propagate in a direction parallel to the maximum compressive stress. In this case the extension starts, not from the actual tips of the pre-existing flaw as in tension, but from positions near the crack tips [90, 96]. This branching is such as to reduce the strain concentrations and, once the crack has extended and strain redistribution has occurred, the individual crack configuration remains stable during further increases of applied stress or strain.

As the applied stress is further increased other cracks, either in local strain fields of lower order or with less critical geometry and/or orientation, progressively initiate branches. The resulting crack configurations also remain static with increasing average applied stress, and this process continues as the applied stress increases, until more pre-existing flaws have initiated branched cracks.

On increasing the load to a higher level a stage is reached when the branched flaws start to propagate and, as for the initiation process, the distribution defining the number of cracks affected at the various stress levels will be superimposed on that defining the occurrence of branching from pre-existing flaws. It is likely that the processes of branch initiation and propagation overlap one another, with no definite stress level marking the transition. Diagrammatically, the distributions are shown in Figure 4.1. in which they are assumed to be Gaussian. During this cracking propagation stage each crack of the system extends in a relatively stable manner in that, if the applied load is maintained at a given level, the process ceases. The start of the process is defined by the Author as the onset of stable fracture propagation (o.s.f.p.) and will be used as the basis for a lower bound failure criterion.

Further increases of load will cause the crack system to propagate to such an extent that it becomes unstable. This instability is associated with a release of strain energy sufficient to cause self-propagation. During this stage the propagation will continue even if the load is not increased and the start of the stage is defined by the Author as the onset of unstable fracture propagation (o.u.f.p.) and will form the basis for an upper bound failure criterion.

A stage will be reached eventually when the material is so sub-divided that strain redistribution is impossible. The concrete can no longer, therefore, support further increases of applied stress and must either catastrophically disrupt or the load must be decreased. The mode of disruption, and the pattern of failure, will be dependent on the method of control of boundary load or strain, boundary conditions and shape of specimen.

For predominantly tensile states of stress, the stress range between onset of fracture propagation and final collapse will be extremely short, as compared with that associated with behaviour under compressive stresses.

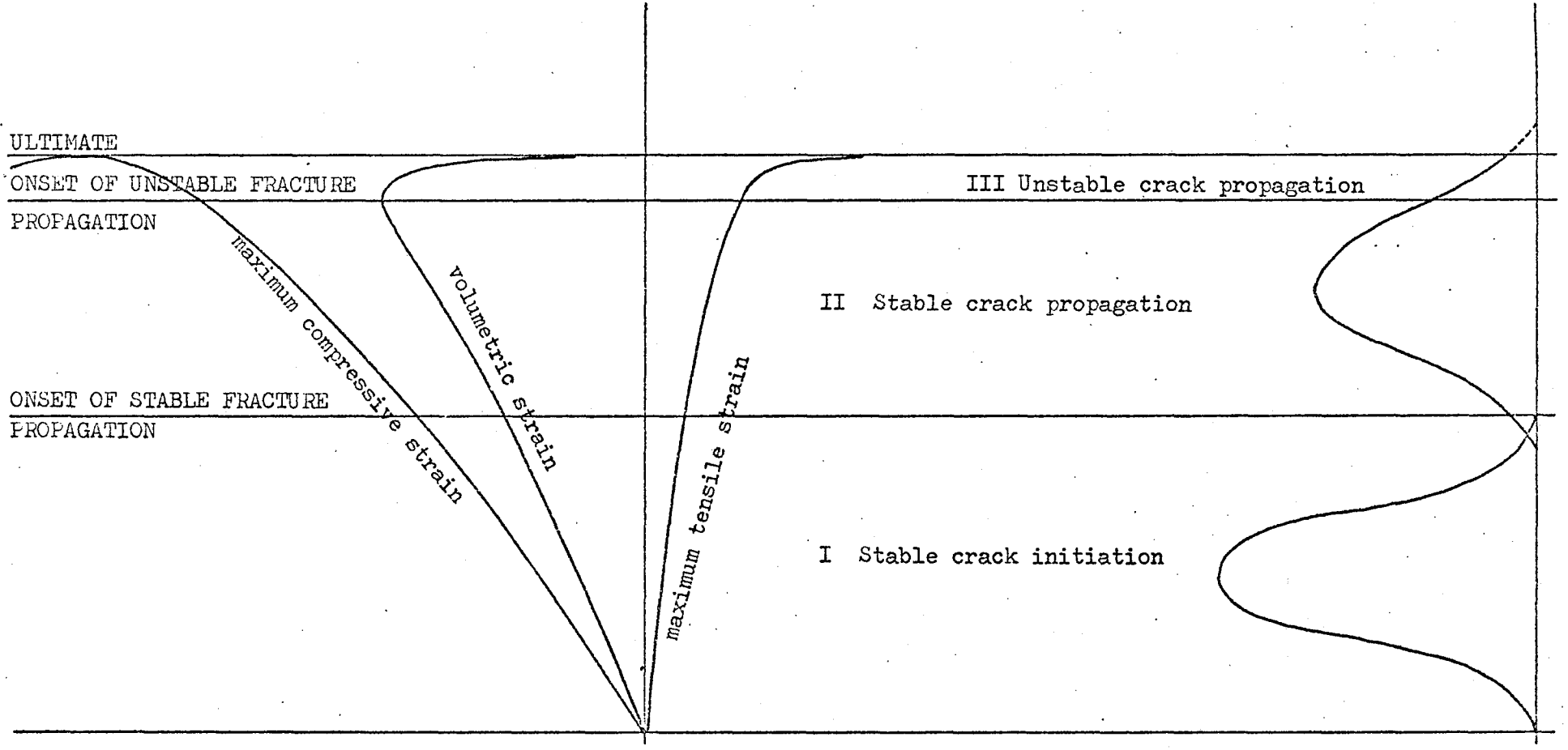


Figure 4.1. The stages of cracking in concrete in terms of (a) stress-strain relationships and (b) distribution of crack initiation and propagation.

In formulating any criterion, or criteria, for the failure of concrete it would appear desirable to identify the various levels marking significant changes in material behaviour. The detection of these levels is discussed in the following section.

4.5. Proposals for detecting Various Stages of the Fracture Process

4.5.1. Introduction

In the previous sections it has been suggested that the behaviour of concrete prior to reaching the ultimate condition can, in common with other brittle materials, be divided into three principal stages separated by two distinct levels of change in material behaviour, namely:-

(i) Onset of stable fracture propagation
(ii) Onset of unstable fracture propagation

These two levels of change, together with the ultimate level, appear, therefore, to be capable of providing useful reference points for failure criteria, particularly if such criteria are to be used as the bases of the design of structures for compliance with various limit states [2] (see Chapters 5 and 8).

A review of the investigations has disclosed, however, serious discrepancies in the levels of stress at which the significant changes are detected, due to the differences in methods of assessment. This is clearly demonstrated in Table 4.2. where the start of stable cracking has been found, from phenomenological observations, to occur throughout a range of stress between 45% and 90% of ultimate, whereas structural changes have been detected between 30% and 40% of ultimate.

An accurate and unequivocal definition of each zone of behaviour is, therefore, of paramount importance before an examination of the significance of these levels in structural design can be made, prior to adopting them as design criteria. To this end, methods for assessing the various stages of behaviour have been developed by the Author in order to detect the transition between each stage of behaviour with accuracy, simplicity and without significant operator or apparatus dependency. The methods are based on measurements of overall (phenomenological) behaviour, since it is considered that at present these provide the only practical means of detection, and are described in the following sections.

4.5.2. Ultimate Level

In most cases the ultimate level can easily be detected for 'brittle' type failures by measuring the maximum load which the material can withstand. It may, however, be difficult to accurately measure the corresponding material strains. For more ductile or plastic behaviour the problem is one of defining ultimate failure. For such material behaviour, the deformation induced under applied loads approaching ultimate may increase at such a rate that the load does not decrease but may, in fact, increase. An example of this is in a triaxial 'compression' test performed under a high confining pressure. As the axial load on the boundary of the specimen is increased, the cross-sectional area of the middle zone of the specimen over which the strain measurements are taken, may increase at a rate such that the nominal stress, calculated on the basis of the original cross-sectional area of the specimen, continues to increase.

In order to overcome the problem the ultimate level is defined in the present test series as the maximum stress level sustained by the specimen, calculated on the basis of the actual cross-sectional area of the zone of the specimen over which the strains are measured. This definition ignores the cracks or voids which may be induced in the specimen by the load, and assumes the material to be continuous throughout the cross-section. The assumption is as valid as the normally accepted definition of failure of brittle materials, which also does not account for discontinuities.

4.5.3. Onset of Unstable Fracture Propagation (o.u.f.p.)

This process is associated with crack propagation which may occur even when the load is maintained constant. Rusch [114, 137] has shown, for uniaxial compression, distinct differences in behaviour above and below a critical stress level. Below the critical stress, a load maintained at a given level produces a deformation which increases to a final value. This limiting value of strain increases with stress level but no catastrophic failure occurs. Above the critical stress, however, the deformations continue to increase to eventual complete disruption.

There is also evidence to suggest that this stress level may mark the limit between quasi-stable and unstable behaviour under repeated loading (see Chapter 5).

The critical stress level has been shown to coincide closely with the level after which the overall volume of the material increases. This level of minimum volume, termed 'true ultimate strength' by some investigators [125], and 'critical stress' by others [99, 114], is easily detected and is unique since it is marked by a complete reversal of the volume change/stress relationship. It can be measured using conventional deformation measuring techniques, and is not likely to vary significantly with the sensitivity of the measuring equipment.

A typical volume change/stress relationship is shown in Figure 4.1. This indicates a continuing process of consolidation, which gradually reverses as the minimum level is approached. Perhaps a more fundamental definition of this critical stress would be the level after which equivalent volume tends to increase, in other words, the stress at the point of inflexion of the curve. Such a definition would, however, require the tangents to the curve to be evaluated and this would lead inevitably to variations in assessment depending on the chosen intervals between data points and the method of calculation etc.

In the present work, therefore, the minimum volume level has been used to define the transition from stable to unstable behaviour. This level is assessed from volumetric strain values obtained from principal strain measurements using the relationship:-

$$e_v = e_1 + e_2 + e_3 + e_1e_2 + e_2e_3 + e_3e_1 + e_1e_2e_3$$

For small strains the second and third order terms are normally excluded as being insignificant. For strains above approximately 10000 microstrain these terms become relatively large and must be taken into account.

4.5.4. Onset of Stable Crack Propagation (o.s.f.p.)

4.5.4.1. General Considerations

This level is associated with the transition from completely stable behaviour, and quasi-elastic properties, to relatively stable but inelastic behaviour, and marks the start of significant deformation under sustained and cyclic loading. The assessment of the start of stable crack propagation, however, is heavily dependent on the sensitivity of the measuring technique, whereas the o.u.f.p. and ultimate levels described above can be detected relatively easily with conventional stress and strain measuring apparatus.

The onset of significant cracking has been assessed using visual and x-ray examination, strain measurements, ultrasonic pulse transmission characteristics, and accoustic emission techniques (see Table 4.2.) which, for a given type of test, detected the onset of significant cracking at stress levels from 30% to 90% of ultimate depending on the technique used. Such a wide variation of results is of little use to designers and, therefore, it is essential to devise a simple and sensitive procedure for determining the start of significant material breakdown. As previously stated, processes of branching crack initiation and stable crack propagation probably overlap, and both involve the proliferation of cracking within the material. It is likely, therefore, that it will be extremely difficult to separate the two modes on the basis of accoustic emission, ultrasonic pulse transmission characteristics, visual or x-ray examination. The distinction between the modes may, however, be demontrated by studying the processes of void formation. It seems highly probable that the branching mode, being a phenomenon local to each individual pre-existing flaw and serving only to induce stabilisation, will not induce significant voids in the material, However, when these branching cracks propagate, their effect on the volume of the material should become apparent.

If the relationship between the volume change of concrete and increasing stress is studied, then a typical curve as illustrated in Figure 4.1. is obtained. As stated in 4.5.3. the curve indicates consolidation which gradually reverses as the minimum volume level is approached. Thus there must be superimposed on the consolidation a dilatation process which tends to reverse the overall change in volume, and to detect the onset of void formation it is necessary to separate the two processes. This will be impossible to achieve using the volume change-stress relationship and so another technique must be devised.

In 4.4. a cracking process is postulated, the main mode being crack extension due to branch initiation, followed by propagation both tending to occur in a direction parallel to the direction of maximum principal compressive stress or perpendicular to the direction of maximum principal tensile stress. If such extension produces voids, then the resulting change in strain in the direction of extension should be much less than in the orthogonal directions.

A series of trial tests under monotonically increasing compression confirmed the occurrence of this phenomenon both for uniaxial and triaxial states of

stress. Figure 4.2. shows the typical relationship between axial and lateral strain found for a triaxial compression test, which indicates near linear behaviour up to a critical level. After this level the lateral strain increases faster than the axial.

Unfortunately, the end of the linear portion is ill-defined on this form of representation, and a clearer indication of the end of linear behaviour is obtained by considering the ratio $\frac{\text{increase in lateral strain}}{\text{increase in axial strain}}$ for small increments of stress. For a uniaxial state of stress this ratio, defined as the incremental strain ratio (i.s.r.), is synonymous with the tangent value of 'Poisson's Ratio'.

As a further check on the validity of the assumption that crack extension induces significant voids, a further series of tests were carried out in which specimens previously loaded in uniaxial compression were subjected to a hydrostatic stress [18]. Figure 4.3. summarises the results of the tests and shows that for specimens with different degrees of heterogeneity previously loaded above the o.s.f.p. level, the principal strain ratio under subsequently applied hydrostatic compression increases rapidly. This, therefore, strongly suggests the closing of cracks aligned mainly parallel to the direction of previously applied compressive stress.

The variation of incremental strain ratio (calculated using the centre-difference method) with stress level for a typical test is shown in Figure 4.4. This clearly shows the expected increase after the critical stress is exceeded. The random variation of values prior to the critical stress is due to the unavoidable scatter of the strain measuring and recording system, coupled with local cracking phenomena over the strain-gauged portion of the specimen. This latter phenomenon is particularly evident for pure tensile modes of failure. The variation about the mean value of the ratio due to the measuring system variation of $\pm$ 1 microstrain is indicated on the diagram. If the increments of stress are decreased in an attempt to assess the critical level more precisely, this strain variation will increase the scatter of the incremental strain ratio.
In order to facilitate the determination of critical stress the following procedure has been evolved and used for uniaxial, biaxial and triaxial compression tests.

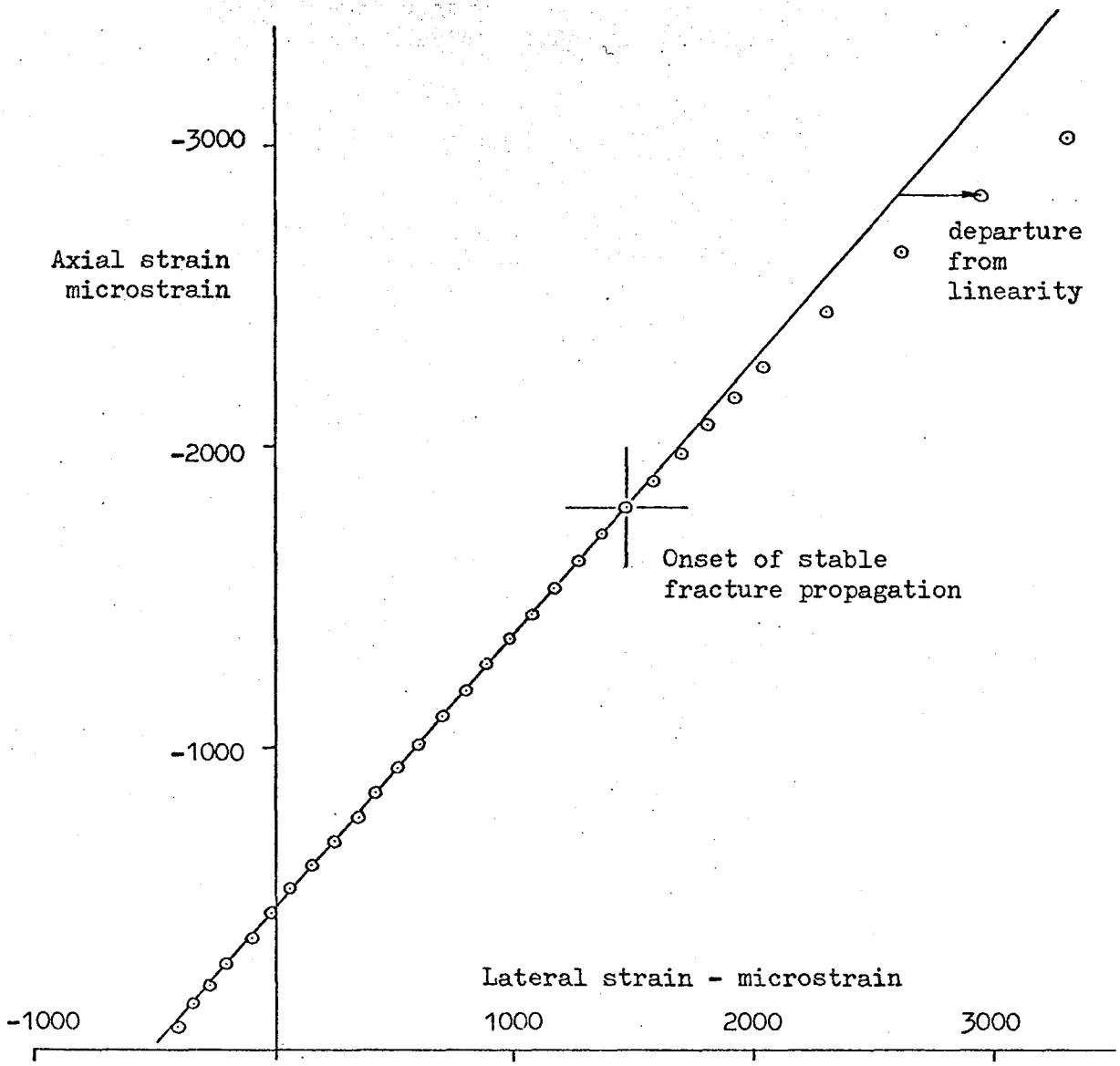


Figure 4.2. Relationship between axial and lateral strain during deviator loading for limestone concrete under a confining pressure of 989 lb./in.^{2}.

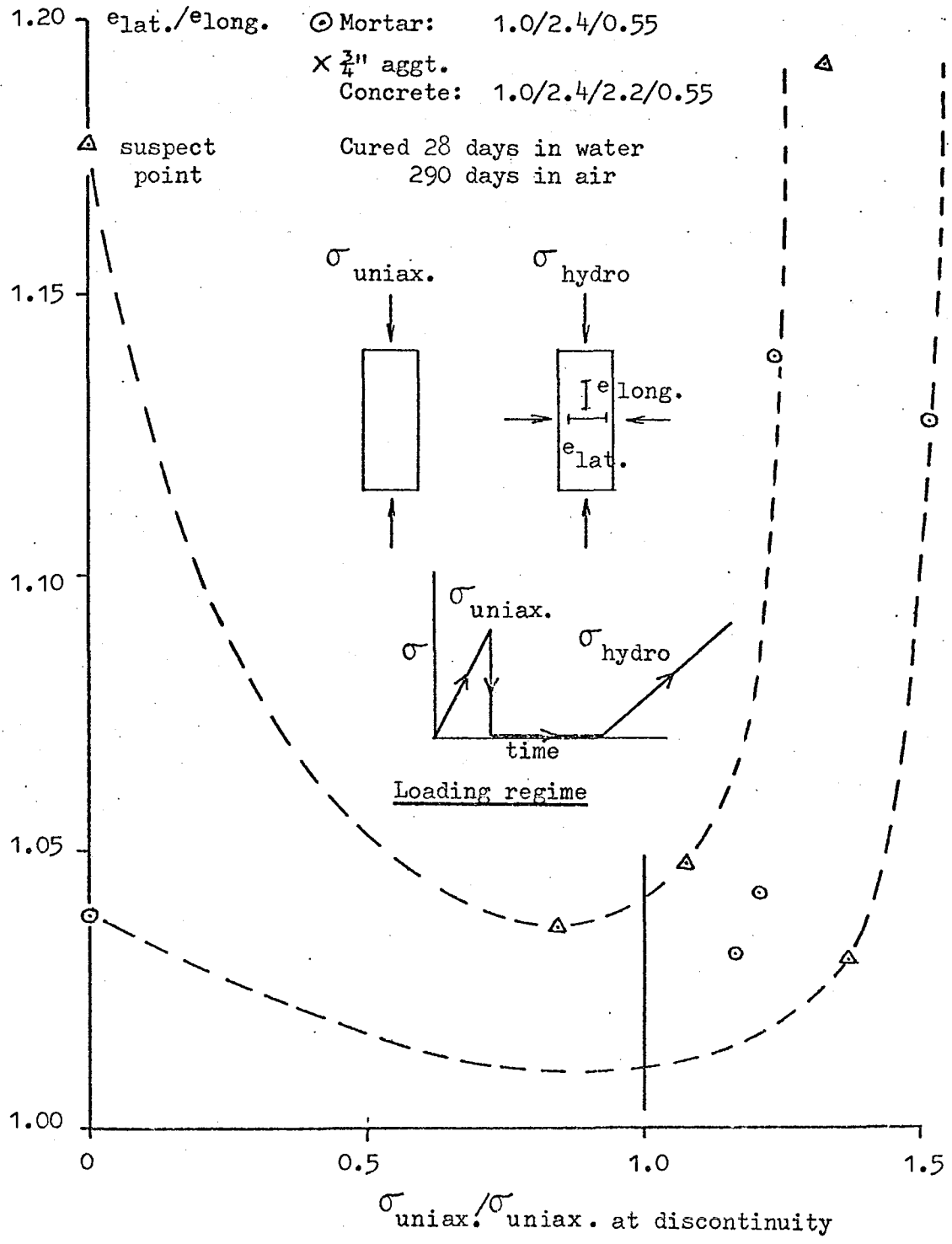


Figure 4.3. Variation of principal strain ratio under hydrostatic stress with previously applied uniaxial stress level.

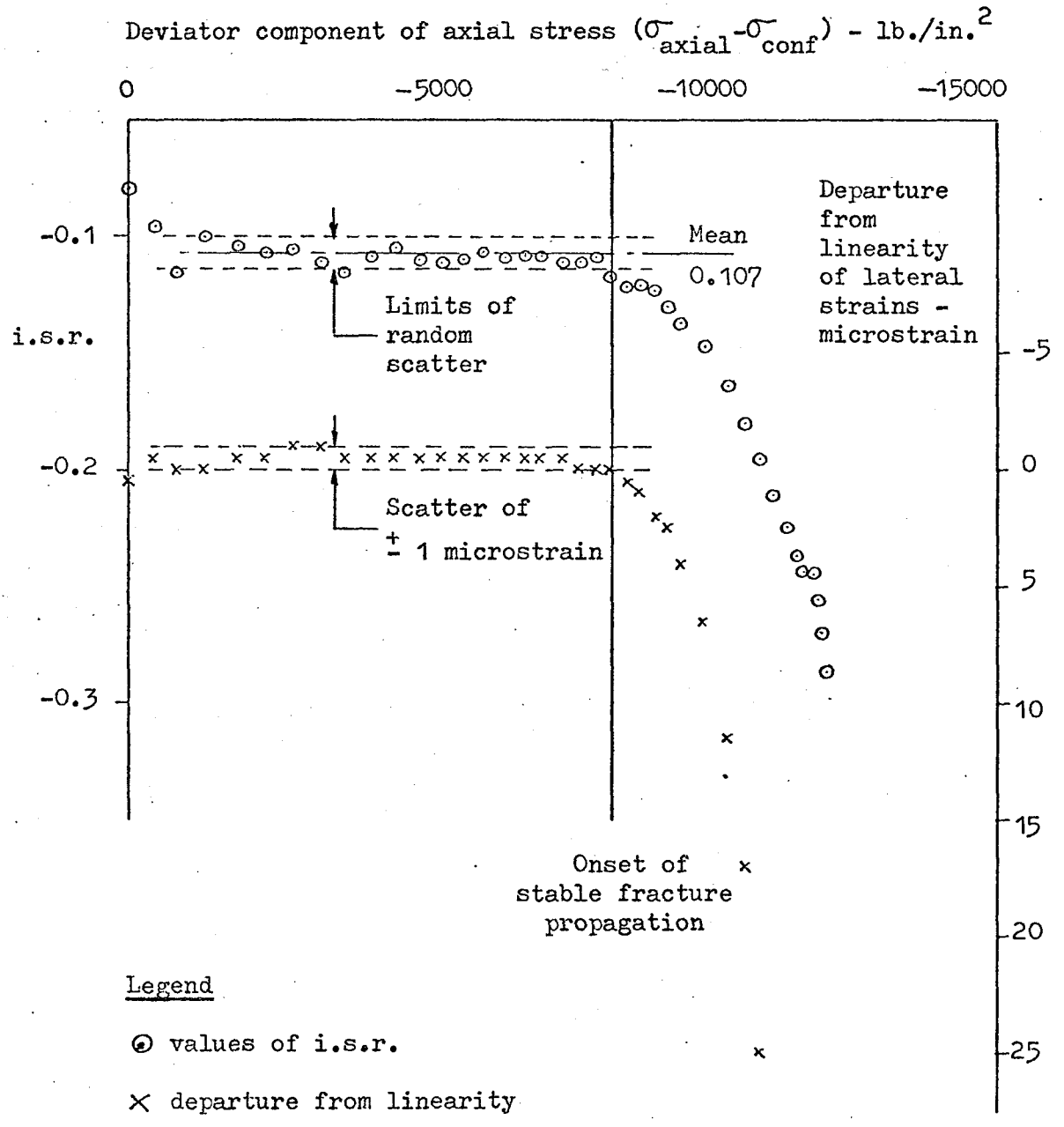


Figure 4.4. Variation of incremental strain ratio and departure from linearity of the lateral strain during deviator loading for limestone concrete under a confining pressure of 989 lb./in.^{2}

4.5.4.2. Detailed Procedure for assessing o.s.f.p. Level

1. Calculate for each increment of axial stress (of approximately 250 lb/in^2) the ratio:-

$$\frac{\text{increase of maximum tensile strain}}{\text{increase of maximum compressive strain}}$$

This ratio is defined as the incremental strain ratio (i.s.r.) and is ascribed to the mean stress level of the increment.

2. Plot the variation of i.s.r. with stress level (see Figure 4.4.). This variation generally shows initial non-linear behaviour due to crack closure, followed by a near-constant portion which is terminated by a rapid increase.

3. For the near constant portion calculate the expected limits of variation of i.s.r. about a mean value due to the random scatter R of the strain measuring device (taken as 1 microstrain for the present series) as follows:-

$$\text{Variation of i.s.r.} = \pm \frac{1}{2}\left[\frac{e_1 + R}{e_3 - R} + \frac{e_1 - R}{e_3 + R}\right]$$

4. Position a mask indicating the upper limit, mean and lower limits, as calculated in 7, horizontally over the near-constant portion of the i.s.r. vs stress relationship to obtain the largest containment of points (see Figure 4.4.).

5. Calculate the approximate mean i.s.r. from the points lying within the upper and lower limits on the mask and represent as a horizontal line on the i.s.r. vs stress plot.

6. Refit the mask such that the mean on the mask coincides with the mean on the plot.

7. Compute the true mean of the i.s.r. using all points lying within the upper and lower limits on the mask by a least squares estimation or similar method. The last point lying within the mask represents the approximate o.s.f.p. level.

8. The mean i.s.r. as calculated in 11 is used to represent the mean slope of the near linear portion of the maximum tensile strain vs maximum compressive strain relationship (see Figure 4.2.).

9. The amount by which each value of maximum tensile strain departs from the near linear portion of the relationship is calculated assuming, for the sake of convenience, that this linear portion is defined by the mean slope (as calculated in 7) and the approximate o.s.f.p. level (as assessed in 7).

10. Plot the variation of the departure from linearity of the maximum tensile strains with stress level (see Figure 4.4.) from which the end of the near linear portion is clearly defined as the last point inside the scatterband defined by the points within the near-constant portion.

    This level is ONSET OF STABLE FRACTURE PROPAGATION.

It should be noted that if the approximate o.s.f.p. level as assessed in 7 is in error then the determination of the true o.s.f.p. level will not be affected.

As stated earlier, the 'scatter' of the incremental strain ratio prior to the onset of stable fracture propagation is due to random errors in the strain measuring and recording system superimposed on the strain variations caused by local cracking over the length of the strain gauges. For specimens loaded compressively, this local cracking appears not to produce large strain variations. For uniaxial tensile loading, on the other hand, the variations caused by local cracking are significant and, coupled with those due to the insensitivity of the strain measuring system compared with the extremely low value of compressive strain induced, give rise to extremely large variations in incremental strain ratio. In such cases, it has been found difficult to use the procedure described above for determining the critical stress, and another equivalent technique is used which dispenses with the need to calculate the incremental strain ratio.

In this latter method, the relationship between axial and lateral strain is plotted directly and the linear portion exhibiting random variation enclosed within two parallel lines representing the 'scatter' band. The

onset of stable fracture propagation is defined as the last load stage before the points all lie outside the scatter band. A typical plot for a uniaxial tensile test is shown in Figure 4.5.

4.5.4.3. Validity of Technique

The validity of the techniques described above for the identification of o.s.f.p. is supported by a trial series of tests carried out by the Author which indicate the onset of stable fracture propagation for an idealised concrete mix containing Vca = 26% (see Appendix 3, mix Ref. I_{26}) under uniaxial compression to coincide closely with a definite increase in the number and intensity of micro-fracturing events detected. The detection technique, developed from that used by Barron [98] involved placing the probe of a Hewlett-Packard Ultrasonic Translator (Type 4905A) against the surface of concrete cylinders tested under monotonically increasing load, and feeding the signal directly to a sensitive ultraviolet recorder. Whereas the X-Y recorder used by Barron tended to integrate the output due to its relatively high inertia, the U-V apparatus was able to detect discrete pulses of accoustic energy. At the start of loading a relatively large number of events was recorded, possibly due to 'bedding-down' processes but after this initial period the events became less significant and were widely spaced. At a critical load stage, which corresponded to a stress level of 52% of ultimate, the events started to increase in number and intensity until final disruption occurred. The o.s.f.p. level for this mix was found to be 45% of ultimate which indicates the slightly reduced sensitivity of the accoustic technique. Although a number of reasons prevented the completion of the test series it is considered that, with more development, the apparatus could be used to detect fracturing events with a higher degree of precision.

Having defined methods of detecting the changes in material behaviour for concrete under uniaxial loading, which may prove suitable as bases for design criteria, it is necessary to examine the influence of other types of loading on these definitions. This is the subject of the following Chapter and Chapter 7.

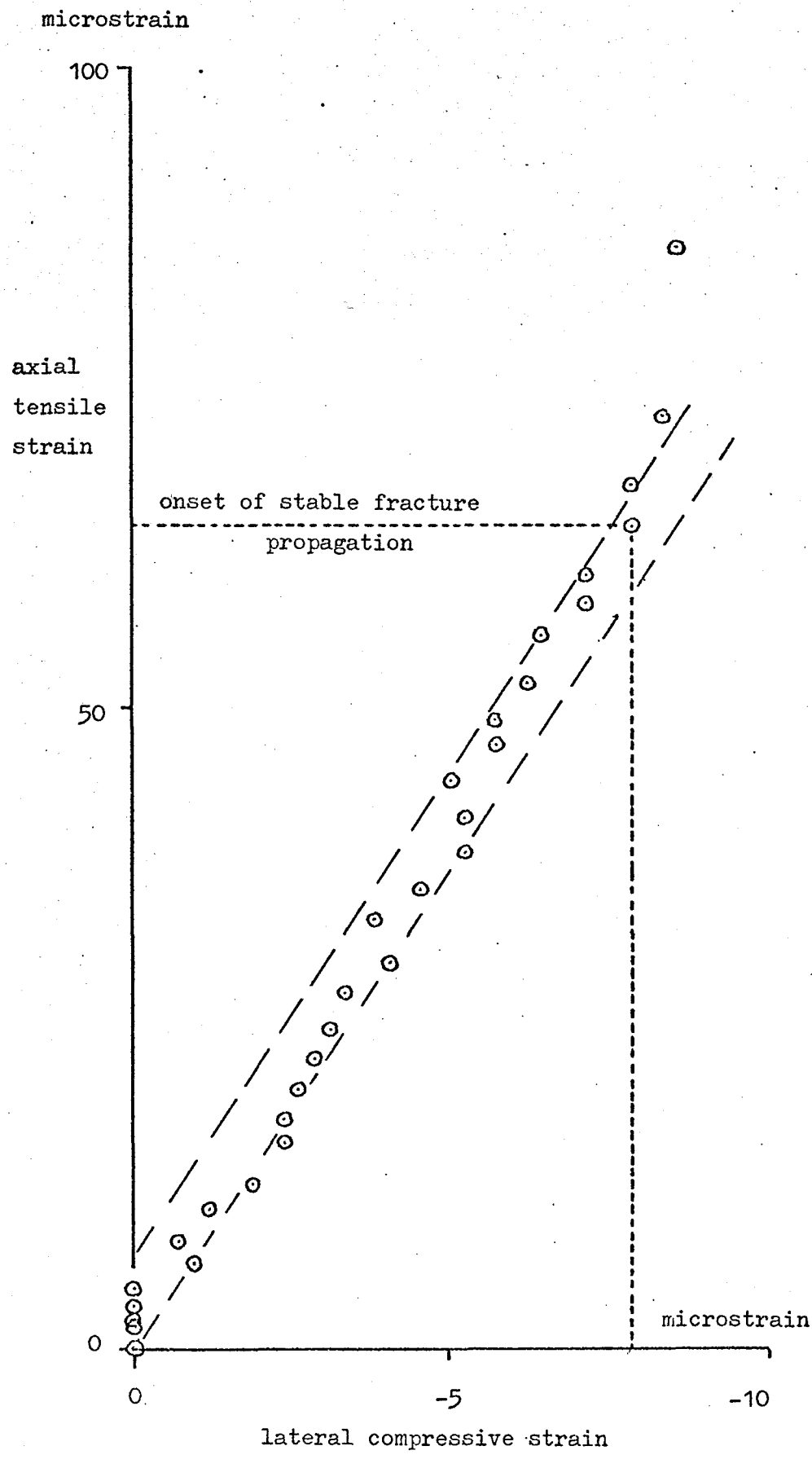


Figure 4.5. Typical relationship between axial and lateral strain for a concrete under short-term uniaxial tension.

5. INFLUENCE OF DIFFERENT REGIMES OF LOADING ON THE DEFINITIONS OF FAILURE

5.1. Introduction

The probable process of internal disruption which occurs in concrete subjected to load has been discussed in Chapter 4. For short-term loading, evidence has been given for the existence of a number of stages of material behaviour, each stage being terminated by relatively easily identifiable changes in deformational response (see 4.5.). Based on this evidence suitable techniques have been postulated for identifying these stages which can be summarised as follows:-

Stage I — Quasi-elastic behaviour.
Terminated by the o.s.f.p. level, which is defined as the level after which the i.s.r. increases.

Stage II — Inelastic but stable behaviour.
Terminated by the o.u.f.p. level, which is defined as the start of overall dilatation.

Stage III — Unstable behaviour.
Terminated by the ultimate level, which is defined as the level after which deformation continues to increase under a constant or decreasing stress level.

If these levels of change in behaviour are to provide the bases for useful failure criteria, it is necessary to attempt to identify any relationship between them and the performance of concrete under more practical loading regimes. In fact only a limited number of such attempts have been made.

Vile [8], for example, has shown that the 'discontinuity' level which, when detected by changes in ultrasonic pulse velocity tends to occur at a slightly higher stress level than the end of Stage I, corresponds closely with the occurrence of significant deformation under sustained uniaxial compressive load. The work of Jordaan et Al [52] has implied that within Stage I the principal of superposition can be invoked with regard to the estimation of creep deformation.

Rusch [114, 137] and Shah and Chandra [138] have shown that, for uniaxial compression, a load sustained within Stage III will eventually cause

complete disruption, whereas within Stages I and II sustained loads induce deformations which tend to a finite limit.

The relation between the short-term and the properties under sustained loads, has, therefore, been established and it would appear that the adoption of the o.s.f.p. and o.u.f.p. levels as lower and upper bound failure criteria, respectively, is justified for these types of loading. Such a relationship must also be established for other, more severe, regimes.

One such regime, which is of practical importance in structural design, is that of repetitive loading. It is likely that such loading will, due to its nature, tend to accentuate any processes of disruption within the material. In the following sections the behaviour under this type of loading is considered in an attempt to identify any relationships between it and the levels of change evident in short-term static tests which would prove useful in formulating design criteria.

5.2. Review of Investigations into the Behaviour of Concrete under Repeated Loading

5.2.1. Introduction

Most of the studies within this category are concerned with phenomenological behaviour, with only a small proportion attempting to deduce the mechanism of fatigue failure from fundamental tests. Apparantly, behaviour under three types of loading only has been investigated, namely uniaxial tension, uniaxial compression and flexural tension, and this is reviewed in the following sections.

5.2.2. Uniaxial Tension

Only one investigation into the behaviour of concrete under simple tension has been found. The work was carried out by De Joly in 1898 and is cited by Mills and Dawson [139]. Tensile stress states were induced in briquettes of mortar or cement paste which were subjected to cyclic stresses at frequencies between 26 and 92 c.p.m. A fatigue limit of about 50% of static ultimate was indicated and the number of cycles to failure was found to be proportional to the reciprocal of the cycling frequency.

5.2.3. Uniaxial Compression

Van Ornum [140] subjected cubes of neat cement paste and concrete to cycles

of simple compression at an age of 28 days. Similar behaviour was found for both materials with no fatigue limit indicated and a fatigue strength of about 55% of static ultimate at 7000 cycles.

Tests carried out on prisms of concrete at ages of 28 days and 1 year were the first to show the changing relationship between stress and strain under increasing numbers of cycles of load. It was found that the relationship, initially concave downwards became increasingly more linear with the slope gradually reducing to about 70% of the original value, indicating progressive breakdown. Towards failure the relationship became more concave upward, tending towards an S-shape. Again no fatigue limit was found and the fatigue strength was about 55% of static ultimate at 10000 cycles.

An important method of representing the results of fatigue tests on concrete was introduced by Graf and Brenner [141] which indicated graphically the effect of stress range on the number of repetitions of load necessary to cause failure. The main conclusions arrived at from tests under uniaxial compression were that (a) raising the minimum compressive stress of the load cycles caused the maximum stress necessary to cause failure after a given number of cycles to increase in direct proportion, (b) the rate of loading had an insignificant effect on the fatigue strength, but lower rates gave slightly lower strengths and larger deformations, and (c) the fatigue strength as a percentage of static ultimate, decreased slightly with decreases in static ultimate strength. The fatigue strength at 2×10^6 repetitions was 64% of the static ultimate.

During the tests, surface cracking was visible after only a few cycles of applied load, again indicating progressive breakdown.

Antrim and McLaughlin [142] compared the behaviour of normal and air-entrained concrete under cycles of uniaxial loading, at a frequency of 3000 cycles per minute, up to maximum stress levels of between 66% and 84% of static ultimate. No significant difference in fatigue response was found for the two types of concrete and there was no evidence of a fatigue limit. The fatigue strength at 10×10^6 cycles was 57% of static ultimate.

Similar tests reported in 1961 [143] covered lightweight aggregate concretes. Two mixes (3800 and 6000 lb/in.^{2} strength) were tested at 500 and 1000

cycles per minute but again no difference was found in the fatigue response. As in the previous investigation no fatigue limit was found and the fatigue strength at 10 x 10^6 cycles was again approximately 55% of static ultimate.

The gradual change in stress-strain characteristics during repetitive loading tests was also noted by L'Hermite [144]. Non-linear behaviour measured for the first load cycles became more linear which is in broad agreement with the observations of Van Ornum [140] and Bennett and Raju [145]. The suggested cause of the phenomenon was the 'ironing out' of internal stress concentrations.

It was noted during the tests that cracking sounds were heard only if the previous maximum stress was exceeded during a loading cycle. The results of Yokomichi et Al [146] also substantiate this fact. They found that hardly any new crack signals were detected until the previous maximum load had been exceeded.

Beres [147] measured the volume changes occurring when prisms of concrete with a height/width ratio of 4.0, were subjected to repeated stress. The stress range was varied between tests, but the same near-zero lower limit was used for all specimens. Although few details of the test were reported, the principal conclusions are highly significant. It was found that for a relatively low upper stress limit the volume of the specimen of the specimen continued to decrease with continued cycling. For a high upper limit, the volume increased continually, and led to eventual failure in some cases. For intermediate upper stress limits, the volume increased with increasing cycles but tended to stabilise and for such tests the specimens did not fail. Beres stated that his tests suggested that the 'lower critical stress' (see 4.2.) almost corresponds to the 'fatigue limit', but no definition of 'fatigue limit' was given.

Confirmation of the fatigue strength results of Graf and Brenner [141] and Antrim and McLaughlin [142] was provided by Bennett and Raju [145] who reported the results of repeated load tests on prismatic specimens of concrete. The prisms were loaded at 190 cycles per minute, a relatively low rate of loading compared with that used by other investigators, using stress ranges from 3.5% to between 53% and 85% of the static ultimate strength. The results indicated a fatigue strength of 62.1% and 57.6% at 2 x 10^6 and 10 x 10^6 repetitions respectively.

Similar behaviour was noted for specimens of cement paste and mortar.

Tests were also conducted in which the variation of stress-strain characteristics with number of load repetitions were measured. For these measurements to be made the fatigue tests were interrupted at intervals and a cycle of static loading inserted. A possible shortcoming of this method may be the effect of short rest periods on the fatigue response [148]. The results supported those of Van Ornum [140] in that the ascending portion of the stress-strain curve gradually reversed curvature (convex to concave) with increasing cycles of load, while the descending portion remained concave. The concavity of the ascending portion was taken to be associated with the closure of the horizontal component of cracks, and this theory was substantiated by a decrease of ultrasonic pulse velocity in the direction of load. Measurements of secant E value for the descending stress-strain curves showed a continual reduction with the number of repetitions as a proportion of the static value, the reduction apparently being independent of the stress range.

A study of the crack formation on the surfaces of fatigued specimens showed bond cracks to form the major proportion of all cracks (70%). This proportion was significantly higher than that found in static tests (55%), but both types of loading induced almost identical orientations of cracks which were aligned predominantly in a direction parallel to the applied load. A larger number of cracks was found in fatigue specimens loaded to 75% ultimate than in those loaded statically up to 95% ultimate. This more extensive crack system was confirmed by the larger decreases in transverse ultrasonic pulse velocity during repetitive loading failure, which were nearly three times greater than those observed in static tests to failure.

An approach similar to the above was made by Shah and Chandra [138] who repetitively loaded 2" x 2" x 6" sealed prisms of cement paste and concrete, using ranges of uniaxial compression from a minimum stress of 10% up to a maximum of 60%, 70%, 80% or 90% of the short-term ultimate strength. The chosen rate of loading of 4 cycles per minute was low enough to enable continuous measurement of strain and ultrasonic pulse velocity to be made without interruption of the loading sequence. The concrete specimens loaded to 80% or 90% of ultimate failed after 82 and 17 cycles respectively. In each case failure was preceded by continuous dilatation, a decrease in ultrasonic pulse velocity and an increase in pulse attenuation. It was

noted that initially the velocity was lower, and the attenuation higher, at the minimum stress limit than at the maximum level but towards failure the reverse was the case. The pastes loaded to 80% and 90% ultimate also failed, but after about twice the number of cycles sustained by the concrete. For the remaining stress ranges, the specimens did not fail and the concrete or paste experienced continued dilatation, albeit only slight in the case of the paste.

The above results agreed closely with the postulation of a 'shakedown limit' made by Shah and Winter [149], who concluded that concrete loaded below this limit (80% to 95% of ultimate) could withstand the load without more damage, while above the limit the damage would become increasingly severe.

It was concluded, from the above results, and from microscopic examination, that cyclic stressing resulted in progressive microcrack propagation.

5.2.4. Flexure

Much of the work into the fatigue behaviour of concrete has been carried out under flexural loading i.e. under induced stress and strain gradients.

Clemmer [150], using plain concrete beams clamped at one end and loaded as cantilevers by a point load at the free end at 40 cycles per minute, showed that the fatigue strength was slightly higher for mixes with higher cement contents. For this regime of unreversed cyclic loading a fatigue limit of approximately 53% of static ultimate was found. Unfortunately data from this series of tests is questionable owing to the indefinable stress state obtained by the method of loading.

Crepps et Al [151, 152, 153] investigated the behaviour of mortar and concrete under completely reversed cycles of flexural loading, at a slow rate of 10 cycles per minute, with programmed rest periods. A limitation of the test was that the material properties undoubtedly changed during each test. A fatigue limit of approximately 55% of the static ultimate strength was evident, and this limit could be raised by prior cycling to a stress below the original limit. Aggregate-matrix bond cracking was noted during the tests, and this cracking increased with the number of load cycles. Strain measurements also indicated progressive failure and, prior to complete disruption the strain increased. The fatigue limit concept was checked by noting whether the strains continued to increase or tended

to a maximum value as the cycles increased.

Kesler [154] found the rate of loading to have a negligible effect on the fatigue strength of concrete for loading rates between 40 and 44 cycles per minute, with no evidence of a fatigue limit up to 10×10^6 cycles.

An attempt at understanding the mechanism of fatigue failure in concrete subjected to flexural loading was made by Murdoch and Kesler [155]. A model of concrete was used in which single limestone inclusions of various shapes were embedded near the tensile faces of beams of mortar. It was reasoned that, as the limestone and mortar exhibited almost identical elastic properties, bond would determine the behaviour under load. The inclusions, in fact, reduced the static strength by between 13% and 47% depending on the shape of the particle, with the fatigue strength being the same as a proportion of static ultimate. It was hypothesised that fatigue failure initiated at the matrix-inclusion interface and this was supported by the fact that the failure planes almost always included part of this interface.

The results of the above investigations, together with those of Graf and Brenner [141] were represented in diagrammatic form by Neal and Kesler [156] who concluded that the fatigue strength, as a proportion of the static ultimate was independent of mix parameters. This conclusion is supported by the results of Bennett and Raju [145].

5.2.5. Conclusions

Unfortunately, the relatively small amount of information regarding the deformational response of concrete to repeated loading does not allow the corresponding structural changes to be assessed in detail. There is also a lack of sufficient data which would enable the influence of parameters such as mix characteristics, etc. to be determined.

In spite of these disadvantages, the following important conclusions can be drawn from the investigations reviewed:-

(i) A 'fatigue limit' of approximately 55% of static ultimate appears to exist for tensile or flexural states of stress [139, 150, 151, 152, 153] below which level the strains tend to increase to a finite value, and above which they continue to increase, with

the number of cycles [151, 152, 153]. Probst [157] has concluded that this fatigue limit is coincident with the 'elastic' limit.

(ii) No definite fatigue limit appears to exist for concrete under repeated cycles of compression loading [140, 142, 143]. At low stresses, however, the material behaves in an ultra-stable manner, as evidenced by continued consolidation with increasing number of cycles [138, 147].

(iii) At intermediate values of stress, progressive breakdown occurs under repeated compressive loading, but the volume increases tend to stabilise [138]. This suggests the occurrence of stable fracture processes and under these conditions the material does not completely disrupt.

(iv) At high values of stress the volume continues to increase until complete disruption occurs [13, 147, 138].

Thus it would seem that the behaviour repeated loading can be divided into three stages as follows:-

At Low Stresses

Ultra-stable Behaviour

Within this stage the material does not suffer any loss of load-carrying capacity.

At Intermediate Stresses

Quasi-stable Behaviour

During this stage significant voids are formed, due to progressive fracturing, and the material deforms to a finite limit as the number of load repetitions increases.

At High Stresses

Unstable Behaviour

Progressive fracturing causes continual void formation during this stage, leading to complete disruption after relatively few cycles of load.

The available evidence suggests, therefore, that the stress levels marking the boundaries of the various stages of behaviour under short-term monotonic loading may be useful for predicting the likely response of the material under other, more complex, loading regimes including that of repeated loading.

Owing to the insufficient amount of data available, it is considered essential at this stage to conduct a pilot, but detailed, investigation to confirm this fact with respect to the performance of concrete subject to repeated loading conditions, and this is described in the following sections.

5.3. Experimental Programme to Assess the Behaviour of Concretes under Repeated Uniaxial Compressive Loading

5.3.1. Introduction

This investigation is of limited scope only, and consists of firstly, measuring in detail the deformational behaviour for specimens of two concretes of differing degrees of heterogeneity under short-term uniaxial compression, in order to determine the levels of stress at onset of stable fracture propagation, onset of unstable fracture propagation and ultimate.

Secondly, having established these levels, a correlation is obtained between them and the deformational stability of the two mixes under various levels of short-term repeated uniaxial compression. In the present series the stability is assessed from detailed measurements of volumetric strain.

It should be pointed out that only the principal results of the work are described and discussed, and the considerable amount of data necessary for their evaluation is omitted (although is available for reference). The work, although restricted at present to uniaxial compression, is being extended under the Author's direction to cover multiaxial stress states [21].

The two concretes tested are of the 'idealised' type as tested in the triaxial series described in Chapter 7. In order to examine the correlation between the various stages of material behaviour and the deformational response of the specimens under repetitive loading, the mixes have been chosen such that the levels of o.s.f.p. o.u.f.p. and ultimate are significantly different in each case.

5.3.2. Choice of Concrete Mixes, Curing Conditions and Specimens

5.3.2.1. Concrete Mixes

As stated in 5.3.1., the concrete mixes are chosen to ensure a significant difference between the levels of stress and strain marking the boundaries between the various stages of behaviour. The mixes used are members of the series of concretes with idealised gradings incorporating spherical glass aggregate in a fine mortar matrix as tested in the triaxial programme (Chapter7). Two mixes of the range are studied, containing volume fractions of coarse aggregate of 26% and 46%. Full details of the constituent materials and their proportions in the mixes are given in Appendices 2 and 3 respectively.

5.3.2.2. Curing Conditions

The curing regime is identical to that used for the triaxial series as described in Chapter 7.

5.3.2.3. Specimens

For the maximum aggregate size of $\frac{3}{4}$", a 4" minimum dimension of specimen is considered satisfactory (see Chapter 7). Following the recommendations made in Chapter 2, a 4" diameter x 10" long cylinder has been adopted in order to achieve a state of uniaxial compression within the central zone of the specimen.

5.3.3. Choice of Loading Regime

One of the most severe loading regimes which an element of a structure may be required to withstand is that of a fluctuating load superimposed on a mean value of dead and live load. Under the action of the stresses induced by such a system, the fracture mechanism is likely to cause significant disruption which may lead to failure at relatively low levels of maximum stress compared with the static strength of the material.

For the present preliminary test series it is considered that the maximum quantity of information can be obtained from tests in which a fluctuating uniaxial compressive load is applied to specimens. A loading rate of 2000 lb./in.^{2} per minute has been adopted for the entire test programme. This is a relatively low rate, compared with that usually adopted for fatigue testing, and is used for the following reasons:-

a) It enables the deformational behaviour to be measured accurately and continuously throughout the test.

b) It corresponds to the standard rate at which the uniaxial control tests are conducted.

c) Structures subjected to large ranges of loading will probably be subject to relatively low rates of stress change compared with the rapid changes which may be experienced for small stress reversals.

The loading regime for each test consists of the following:-

1. Stress increasing monotonically at a rate of 2000 lb./in.^{2} per minute from a minimum level, determined by the lowest level of load capable of being controlled by the servo-mechanism of the testing machine, to the required maximum value.

2. Stress decreasing monotonically at a rate of 2000 lb./in.^{2} per minute from the maximum level to the minimum level.

3. The above cyclic regime repeated until the specimen becomes deformationally stable or completely disrupts.

5.3.4. Apparatus

5.3.4.1. Loading Equipment

The Amsler Compression Testing Machine used for the tests is described in Chapter 7. Automatic control of the ascending and descending loading rate is effected by using an Amsler Hydropacer servo-control mechanism, the load being reversed manually at the upper and lower limits to ensure accuracy.

Owing to the suspect behaviour of the spherical seating unit of the Amsler testing machine the load is applied through a subsidiary spherical seating unit and hardened steel platens, as described in Chapter 7.

5.3.4.2. Strain Measurement

The strains are measured on the surface of the specimen within the central zone which is considered to be under a significantly uniform state of stress

and strain. The complete deformational behaviour within this zone is measured by attaching 60 mm. electrical resistance strain gauges in the axial and circumferential direction as described in Chapter 7.

The strains are continuously recorded at a rate of 1 channel per second using a Peekel automatic data logger, capable of measuring to a sensitivity of 1 microstrain.

5.3.4.3. Measurement of Ultrasonic Pulse Velocity

Further evidence of the progressive breakdown of the concrete is obtained by measuring the ultrasonic pulse velocity across the specimen. In order to achieve the highest degree of sensitivity, a Cawkell Ultrasonic Materials Tester Type UCT 2 capable of resolving to a pulse time of 0.01 microsecond, is used. The energy transmitted by the apparatus has been increased by replacing the original transducers with a pair specially designed and constructed by the Civil Engineering Department of University College, London. These improved transducers are accoustically connected to the curved surface of the cylinders through brass sole-plates specially designed and constructed at Imperial College, and kept in contact with the specimen through elastic bands and a grease layer. Figure 5.1. shows the arrangement of the transducers on a specimen.

5.3.5. Preparation of Specimens for Test

The procedure adopted is identical to that used for the triaxial series and described in Chapter 7.

5.3.6. Method of Testing

The lower 4" diameter subsidiary platen is accurately located at the centre of the lower machine platen using a dowel. This enables the specimen and upper spherical seating unit to be correctly aligned in the testing machine such that the risk of uneven loading is minimised. Before each test the uniformity of loading is checked at a low level of stress, by comparing the strains measured at opposite ends of the diameter of each specimen. If significant differences are detected the specimen is realigned until they disappear.

The Hydropacer Unit is balanced at the lowest controllable load level. This level induces a nominal stress of 150 lb./in.^{2} in the specimens which remained constant for all tests. After selecting the setting of the timing

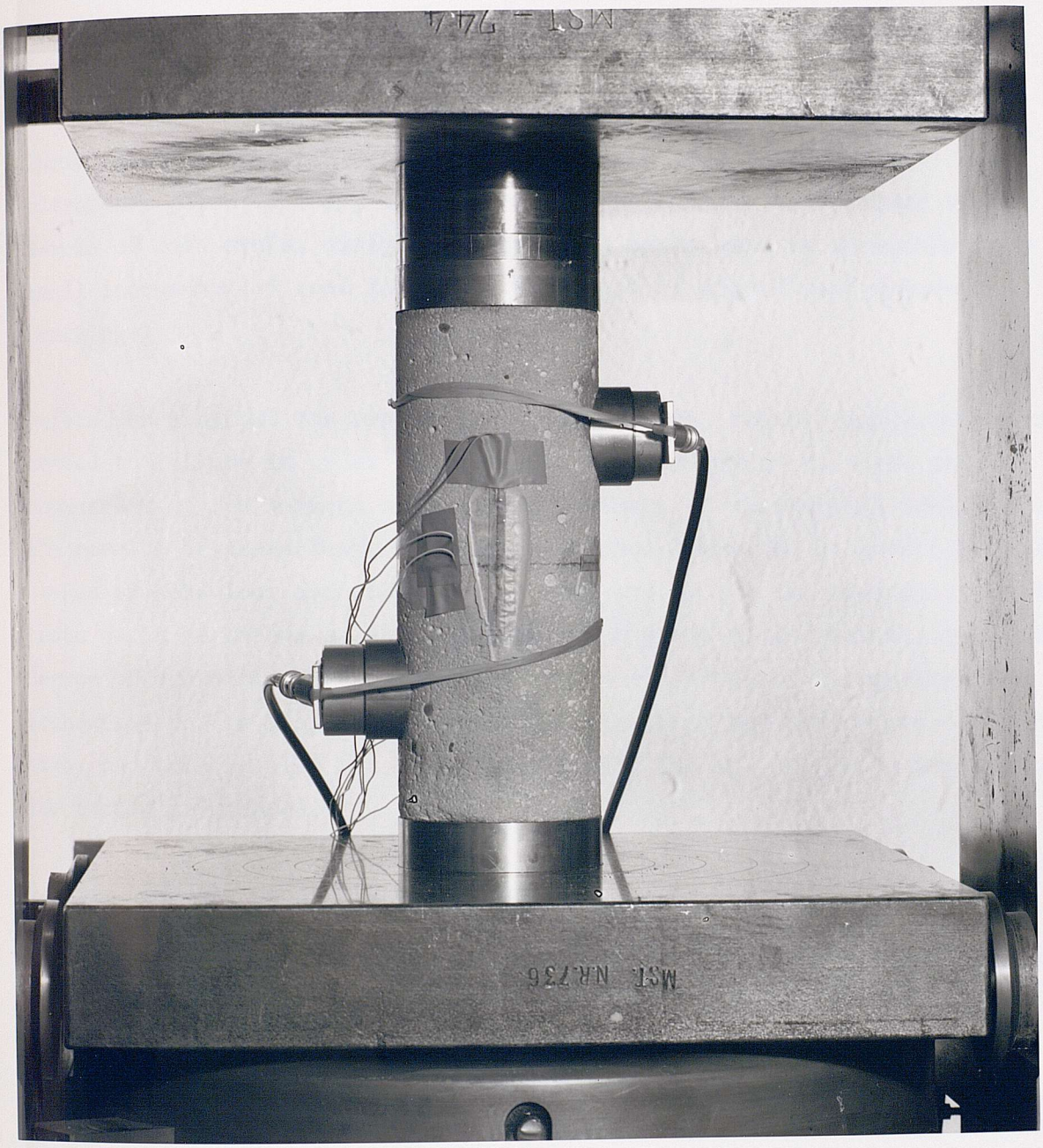


Figure 5.1. General view of cyclic test specimen showing arrangement of ultrasonic pulse transducers.

mechanism for the rate of stress of 2000 lb./in.^{2} per minute, the automatic control is switched on to increase the stress to the desired maximum level. At the maximum level the switch is reversed to reduce the stress at the controlled rate to the minimum level after which the switch is again reversed to start the next cycle.

During each loading cycle the strains are recorded continuously. The ultrasonic pulse velocity is measured at the maximum and minimum stress levels of each cycle, except for the first cycle when it is measured at small increments of load to detect the start of significant internal cracking.

Before carrying out the repetitive loading tests, control specimens were tested to failure in order to determine their ultimate strength and the boundaries of the various stages of behaviour. A statistical analysis of the results of these tests enabled confidence limits to be ascribed to the stages of behaviour such that the maximum stress for the repetitive loading tests could be chosen so as to lie within a given stage with a reasonable degree of certainty. Each test provided more information regarding the boundaries to the stages if the maximum stress of the cycles was sufficiently high, and this enabled the confidence limits for the stages to be revised as the series progressed.

5.3.7. Analysis of Strain Measurements

For the first cycle of loading the onset of fracture propagation level is determined using the procedure described in 4.5., while the onset of unstable fracture propagation (defined as the minimum volume level) is evaluated from the volumetric strains. Significant cracking, as detected by the ultrasonic technique, is marked by an increase in pulse velocity following a period of constant value.

The main aims of the test series are (a) to identify progressive cracking within concrete specimens as the number of cycles of loading is increased, and (b) to correlate the cracking characteristics with the range of stress imposed.

As discussed in Chapter 3 any significant cracking will tend to produce voids in the material which will lead to an increase in volume. Accordingly the measured axial and circumferential strains are converted to volumetric

strains using the small strain relationship:-

$$e_v = e_{axial} + 2e_{lateral}$$

The resulting development of volumetric strains with each successive load cycle enables the test to be categorised into one of three groups:-

1. Consolidation to stability
2. Dilatation to stability
3. Dilatation to complete disruption

The relation between the above characteristic types of deformation and the stage of material behaviour to which the specimen was cycled is discussed in the following.

5.3.8. Results

In Tables 5.1. and 5.2. the levels of stress marking the boundaries to the various stages of material behaviour for the mixes containing 26% and 46% of coarse aggregate respectively, are indicated.

As discussed in 4.7., the development of cracking within specimens undergoing repetitive loading is assessed from a detailed study of the resulting volume changes as obtained from the measured principal strains.

In many of the tests, a large number of loading cycles were applied before a trend in behaviour was clearly established. It has been necessary, therefore, to store the data from the tests in a form suitable for analysis and subsequent graphical representation by computer. All data is available for retrieval but, since the complete deformational behaviour of concretes similar to those used in the present test series is described in detail in Chapter 7, only the derived volumetric strains will be considered.

For each mix the volume changes occurring during progressive load cycling are generally too small to be distinguished when plotted directly. Accordingly, for clarity, these changes have been represented as offsets from a base line using the method of calculation as shown in Figure 5.2.

Figures 5.3. to 5.8. show the relationships between these offset volumetric strains and stress level, as the load is cycled for specimens of each mix.

Specimen ref.	Stress at o.s.f.p.	Stress at start of USPV decrease	Stress at minimum volume	Ultimate stress	Maximum stress of cycles	Remarks
	---------- lb./in.^{2} ----------					
1	4744	5169	7669	8891	8891	Control test to failure.
2	3323	7130	7762	8865	8865	Control test to failure.
3	-	-	-	-	6260	Consolidated to stability after 40 cycles.
4	4245	5882	-	-	7647	Dilated to failure after 38 cycles.
5	3798	6239	-	-	6710	Filated to stability after 68 cycles.
6	3253	6595	-	-	7246	Consolidated to stability after 23 cycles.
7	3393	7309	-	-	7611	Consolidated to stability after 29 cycles.
8	-	6952	-	-	7630	Consolidated to stability after 50 cycles.
9	3402	6952	7673	-	7816	Dilated to failure after 93 cycles.
10	-	-	-	-	3630	Consolidated to stability after 10 cycles.
11	3265	6595	-	-	8030	Dilated to failure after 71 cycles.
12	-	-	-	-	3021	Consolidated to stability after 5 cycles.
Mean	3678	6536	7701	8878		
95% C.L.		±444	±60	±25		

Table 5.1. Summary of Results for Repetitive Loading Tests for Idealised Concretes with a V_{ca} of 26%.

Specimen ref.	Stress at o.s.f.p.	Stress at start of USPV decrease	Stress at minimum volume	Ultimate stress	Maximum stress of cycles	Remarks
	lb./in.^{2}					
1	3403	5882	6782	7447	7447	Control test fo failure.
2	3478	6239	6844	8093	8093	Control test to failure.
3	3659	6239	6815	8021	8021	Control test to failure.
4	2405	-	7233	-	7241	Dilated to failure after 70 cycles.
5	2914	-	6198	-	6531	Dilated to failure after 79 cycles.
6	3874	-	-	-	5965	Dilated to stability after 70 cycles.
7	3724	-	-	-	5423	Dilated to stability after 11 cycles.
8	3582	-	-	-	4508	Dilated to stability after 30 cycles.
9	3778	-	-	-	3987	Dilated to stability after 40 cycles.
10	-	-	-	-	2981	Consolidated to stability after 29 cycles.
11	-	-	7083	-	7473	Dilated to failure after 10 cycles.
12	-	-	-	-	2502	Consolidated to stability after 4 cycles.
Mean	3424	6120	6826	7854		
95% C.L.		±233	±310	±401		

Table 5.2. Summary of Results for Repetitive Loading Tests for Idealised Concretes with V_{ca} of 46%.

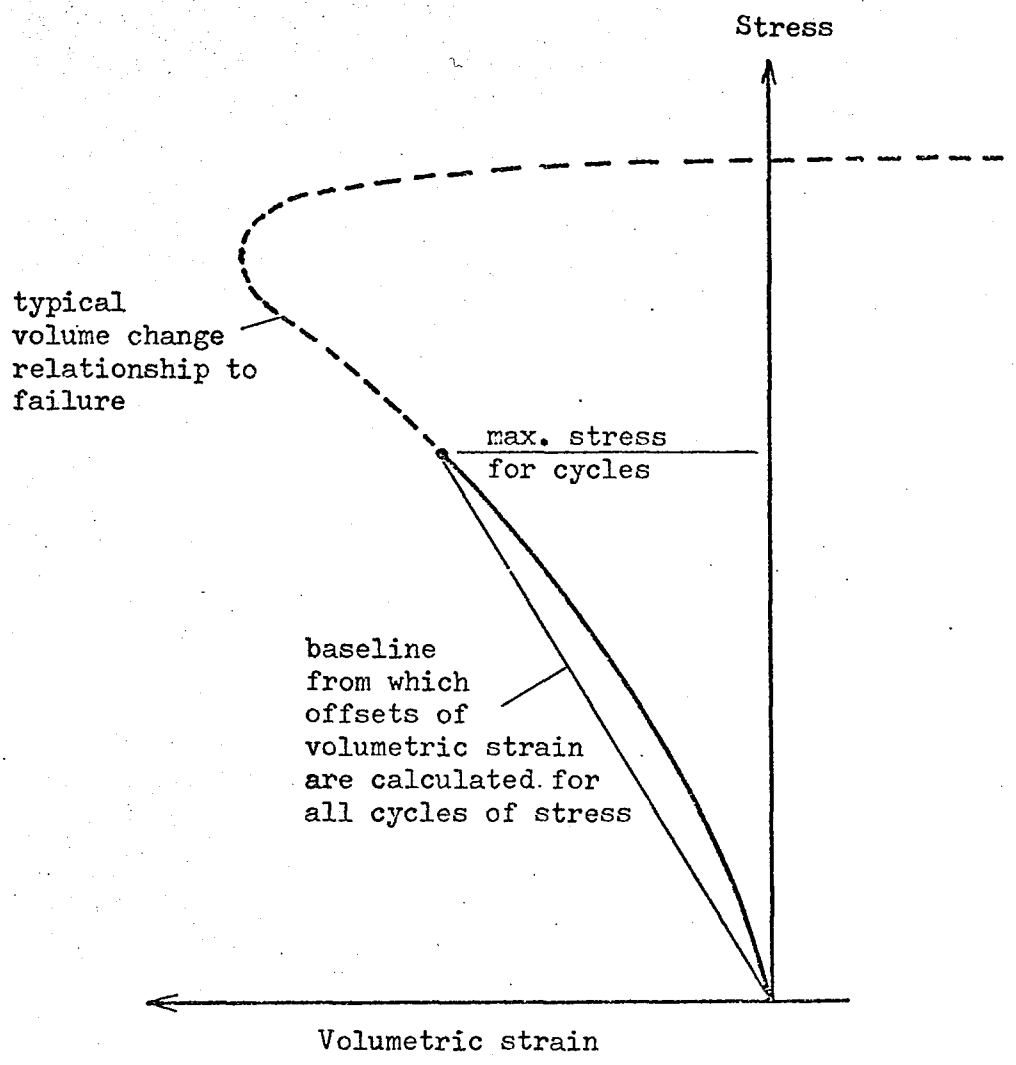


Figure 5.2. Method of calculating volumetric strains as offsets from baseline derived from first cycle of loading.

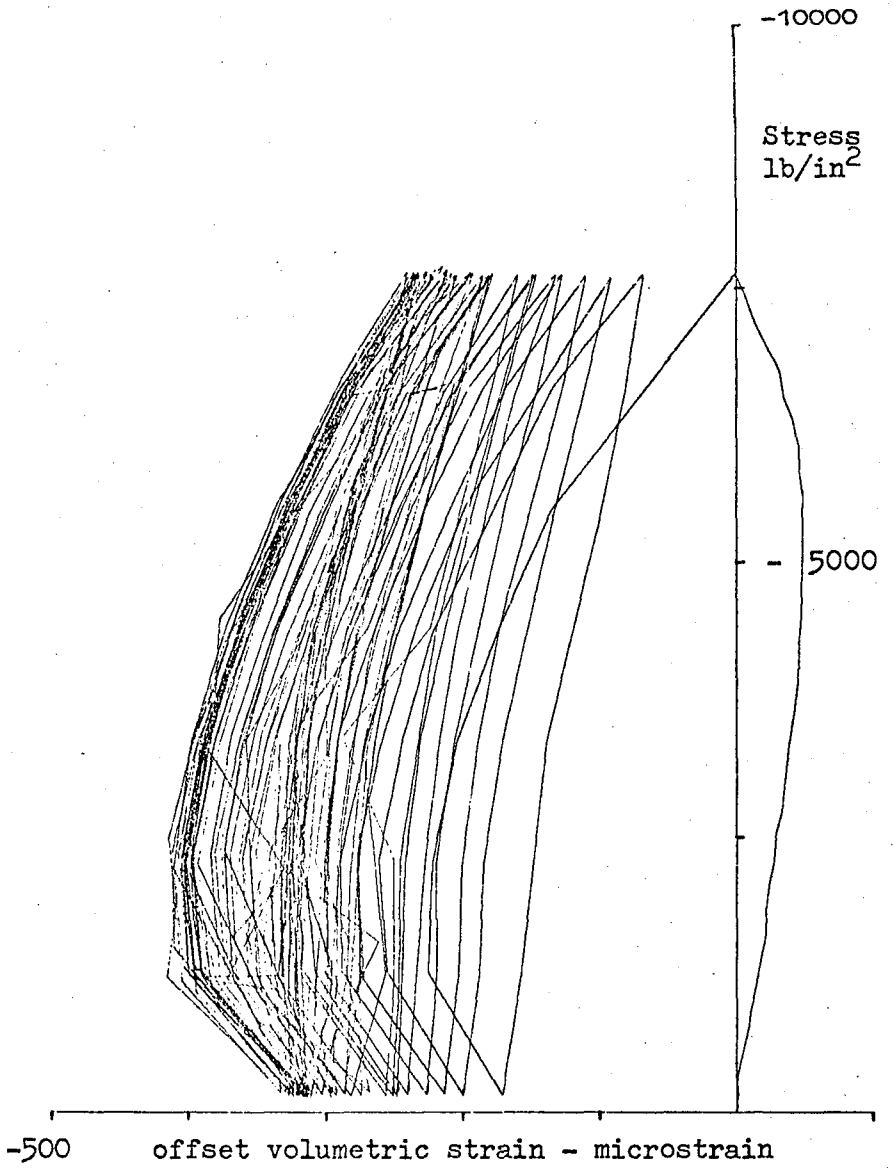


Figure 5.3. Variation of offset volumetric strain with cycles of stress for Specimen No. 7 of idealised concrete with Vca = 26%.

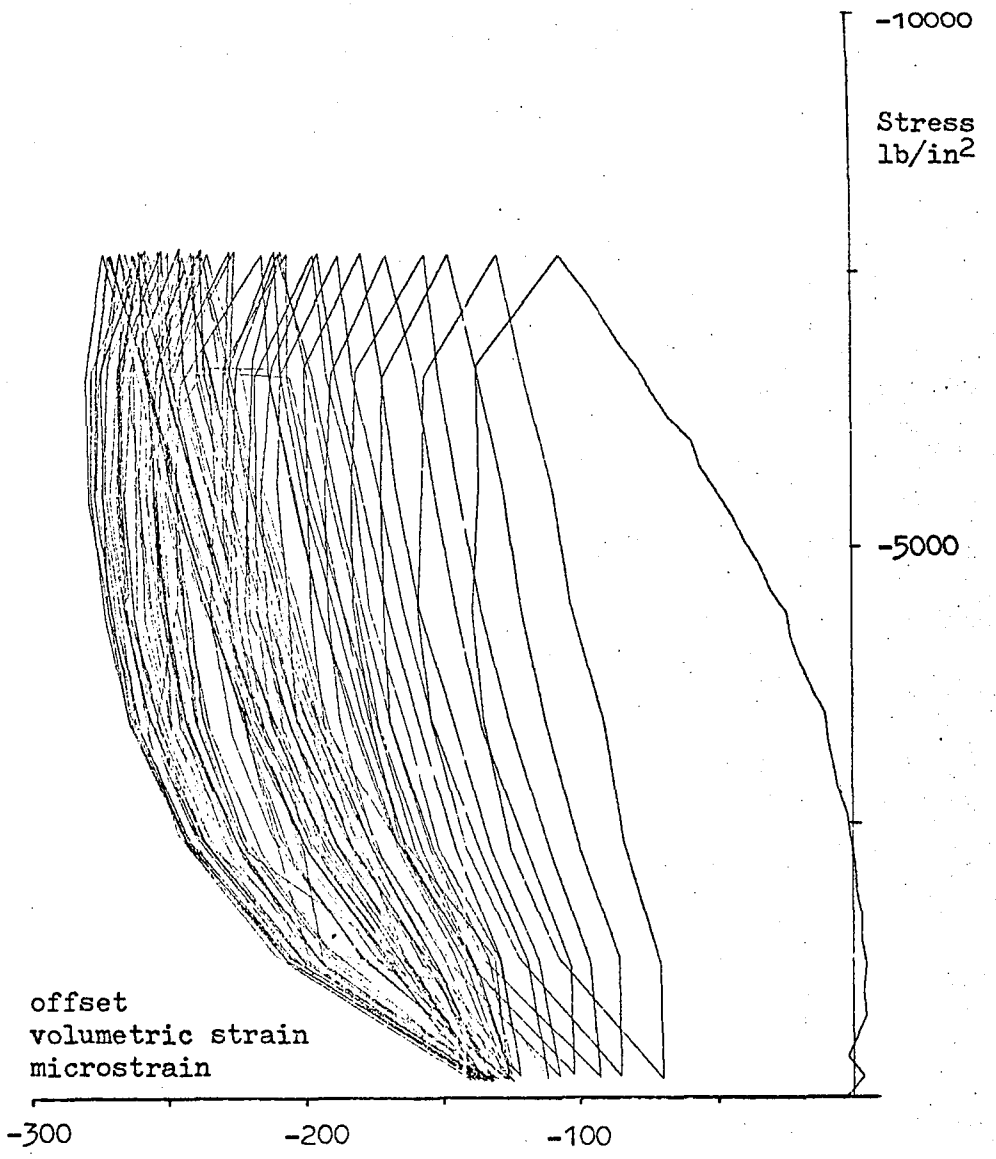


Figure 5.4. Variation of offset volumetric strain with cycles of stress for Specimen No. 8 of idealised concrete with Vca = 26%.

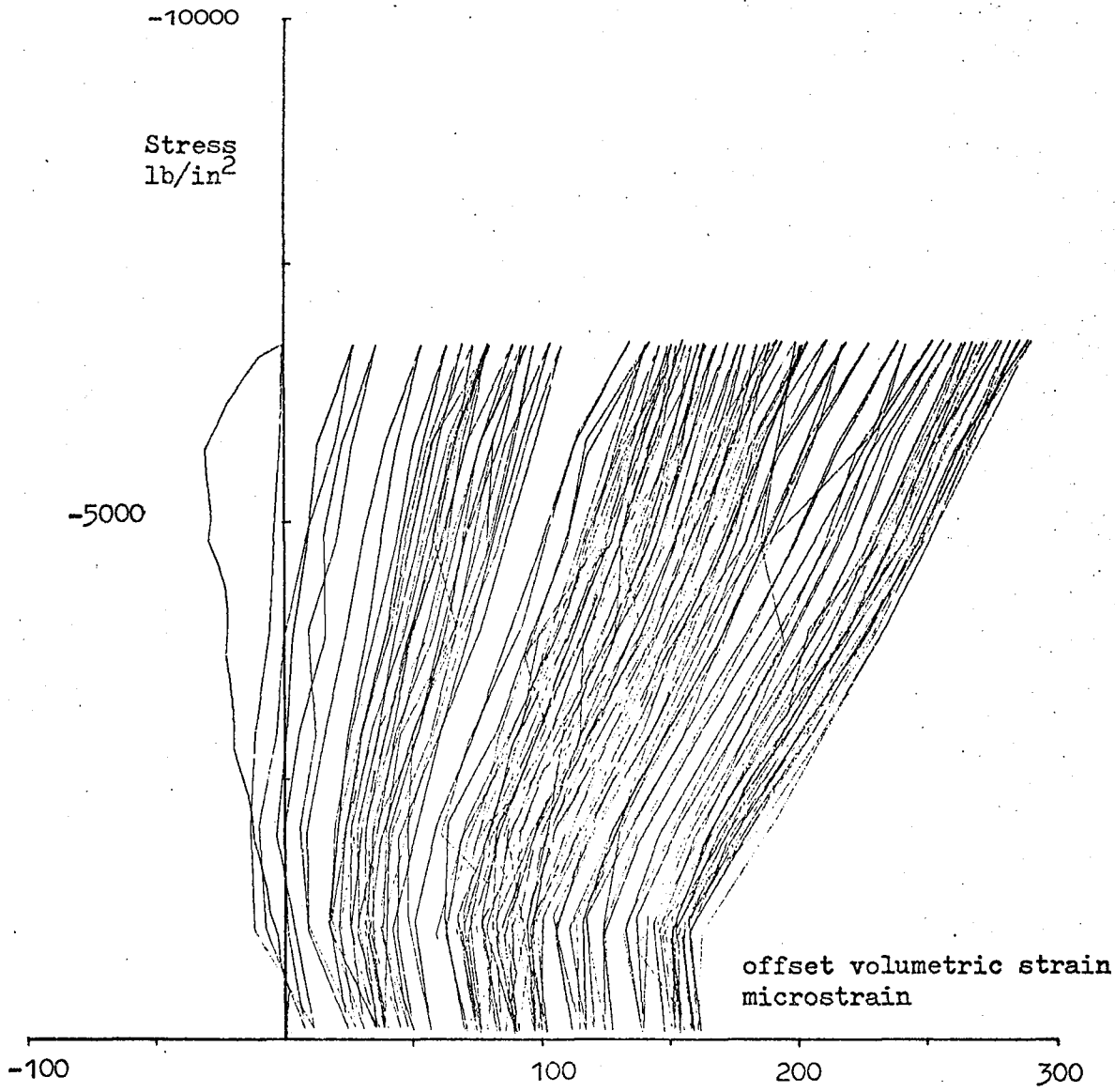


Figure 5.5. Variation of offset volumetric strain with cycles of stress for Specimen No. 5 of idealised concrete with Vca = 26%.

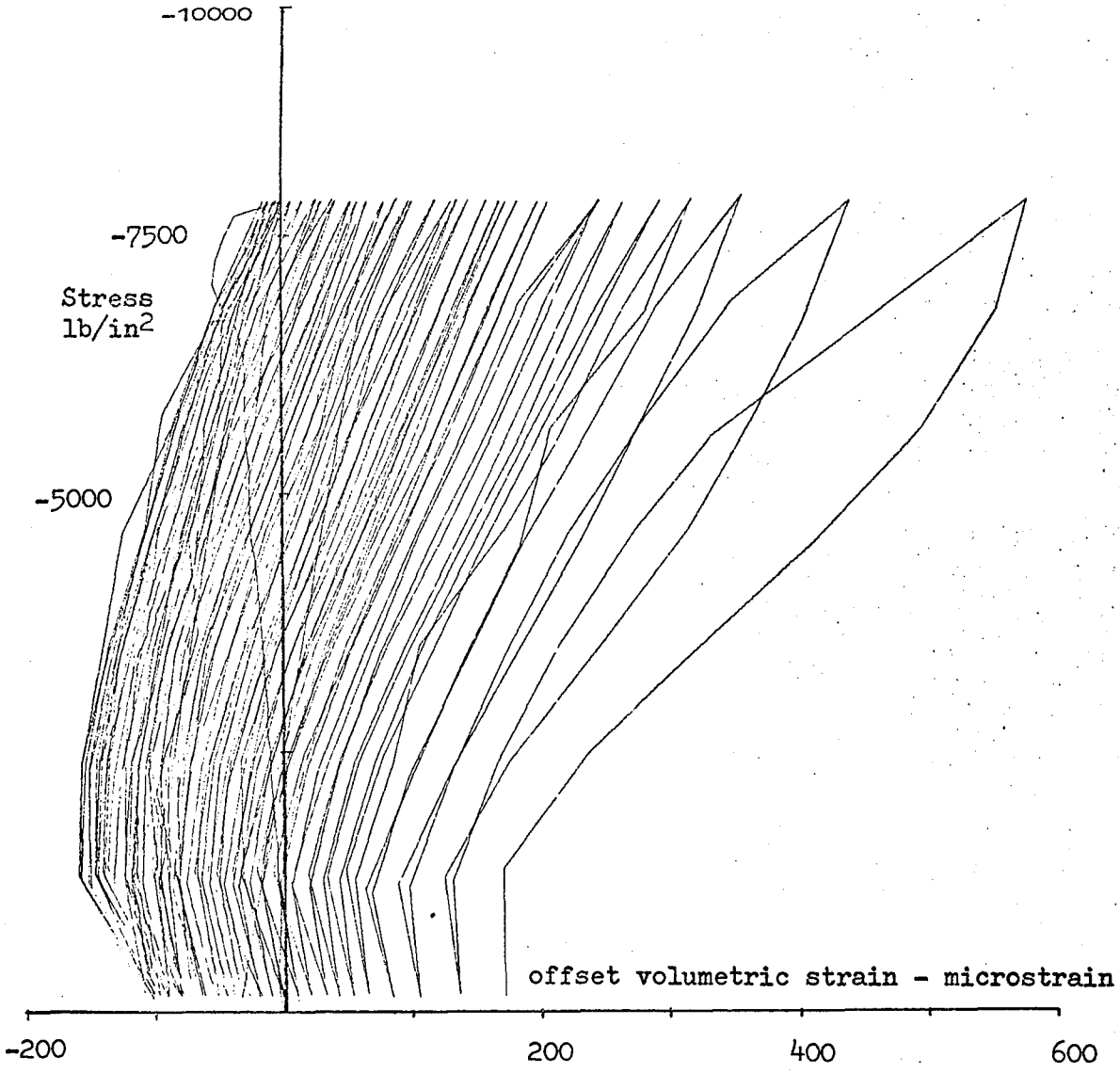


Figure 5.6. Variation of offset volumetric strain with cycles of stress for Specimen No. 9 of idealised concrete with Vca = 26%.

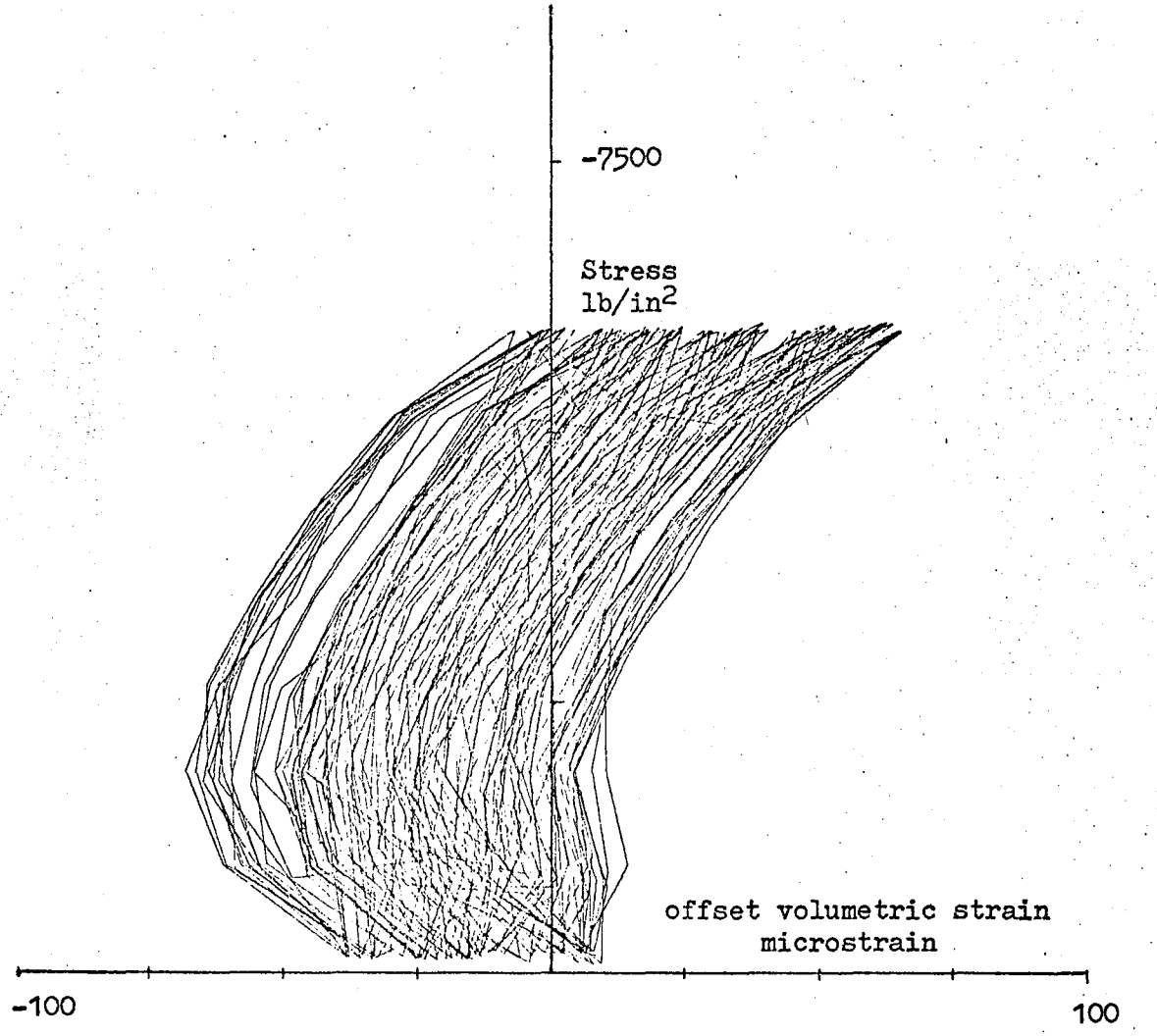


Figure 5.7. Variation of offset volumetric strain with cycles of stress for Specimen No. 6 of idealised concrete with Vca = 46%.

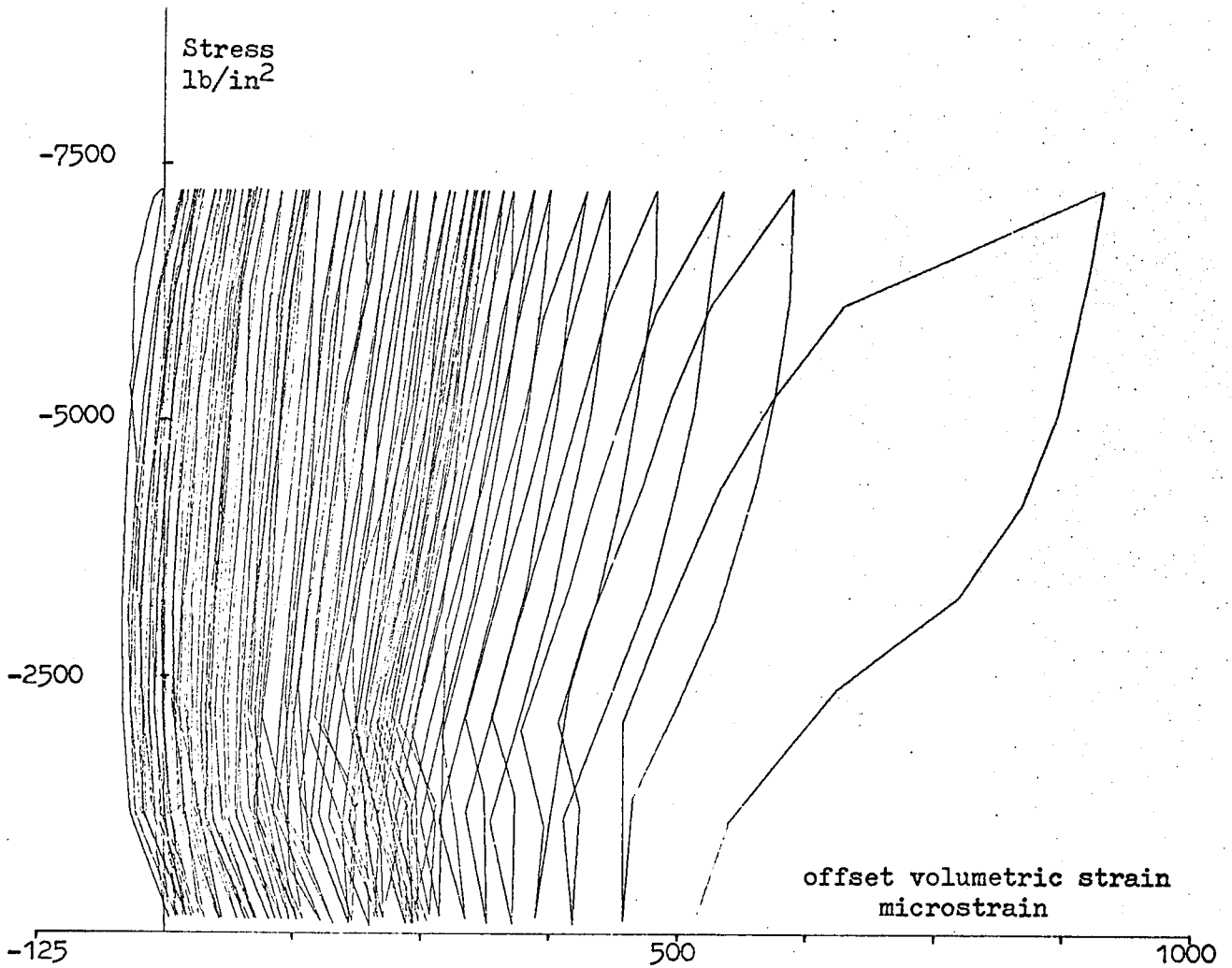


Figure 5.8. Variation of offset volumetric strain with cycles of stress for Specimen No. 4 of idealised concrete with Vca = 46%.

The specimens depicted have been selected to illustrate the typical modes of behaviour described in 5.3.7.

The summarised results showing the details of the loading regime for each test, and the resulting behaviour, are given in Tables 5.1. and 5.2. These Tables do not show the change in ultrasonic pulse velocity since, for all tests, this decreases continually with increasing number of cycles when measured both at the lower and upper limit of each cycle.

5.3.9. Discussion of Results

5.3.9.1. Stages of Behaviour evaluated from Short Term Uniaxial Tests

On Figures 5.9. and 5.10. the stages of behaviour for each mix are indicated in terms of the 95% confidence limits for the mean of the stress levels defining the boundaries of the stages, Comparison of these Figures shows that, for all the boundaries, the stress level decreases with increase in volume fraction of aggregate. This is due to the effect of heterogeneity and is discussed fully in Chapter 7.

An interesting point is that cracking is not detected by the ultrasonic technique until the stress almost reaches the o.u.f.p. level (minimum volume level). This behaviour confirms that noted for real concretes tested during a trial series [16], and demonstrates the influence of the sensitivity of the measuring technique.

5.3.9.2. Behaviour under Repetitive Loading

Deformational Characteristics

The main results for the mix containing a V_{ca} of 26% are shown on Figure 5.9. Although the number of specimens tested is insufficient to allow definite conclusions to be drawn, the Figure tends to indicate the following:-

1. For a maximum stress lying within Stage I, the zone within which the behaviour is considered to be quasi-elastic, successive cycles of stress cause the volume to continue to decrease to stability. Stability is indicated by the constant hysteresis loop formed by the strains which develop during the ascending and descending stress regime. This is indicated by Figures 5.3. and 5.4. which show the similarity between hysteresis loops formed after the first cycle of stress.

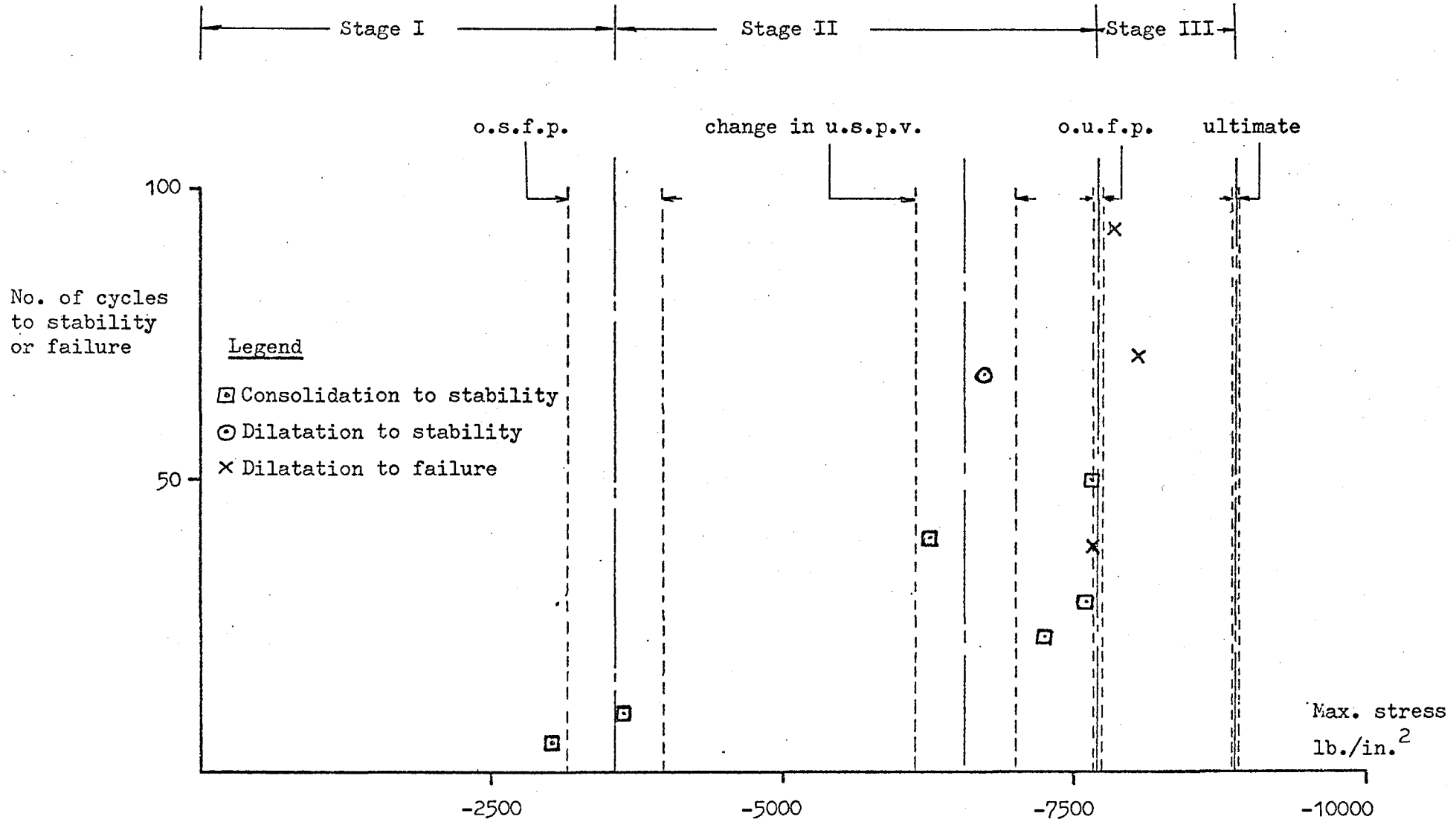


Figure 5.9. The significant changes in material behaviour for idealised concrete with V_{ca} = 26% under uniaxial compression and their relationship to the behaviour under repeated uniaxial load.

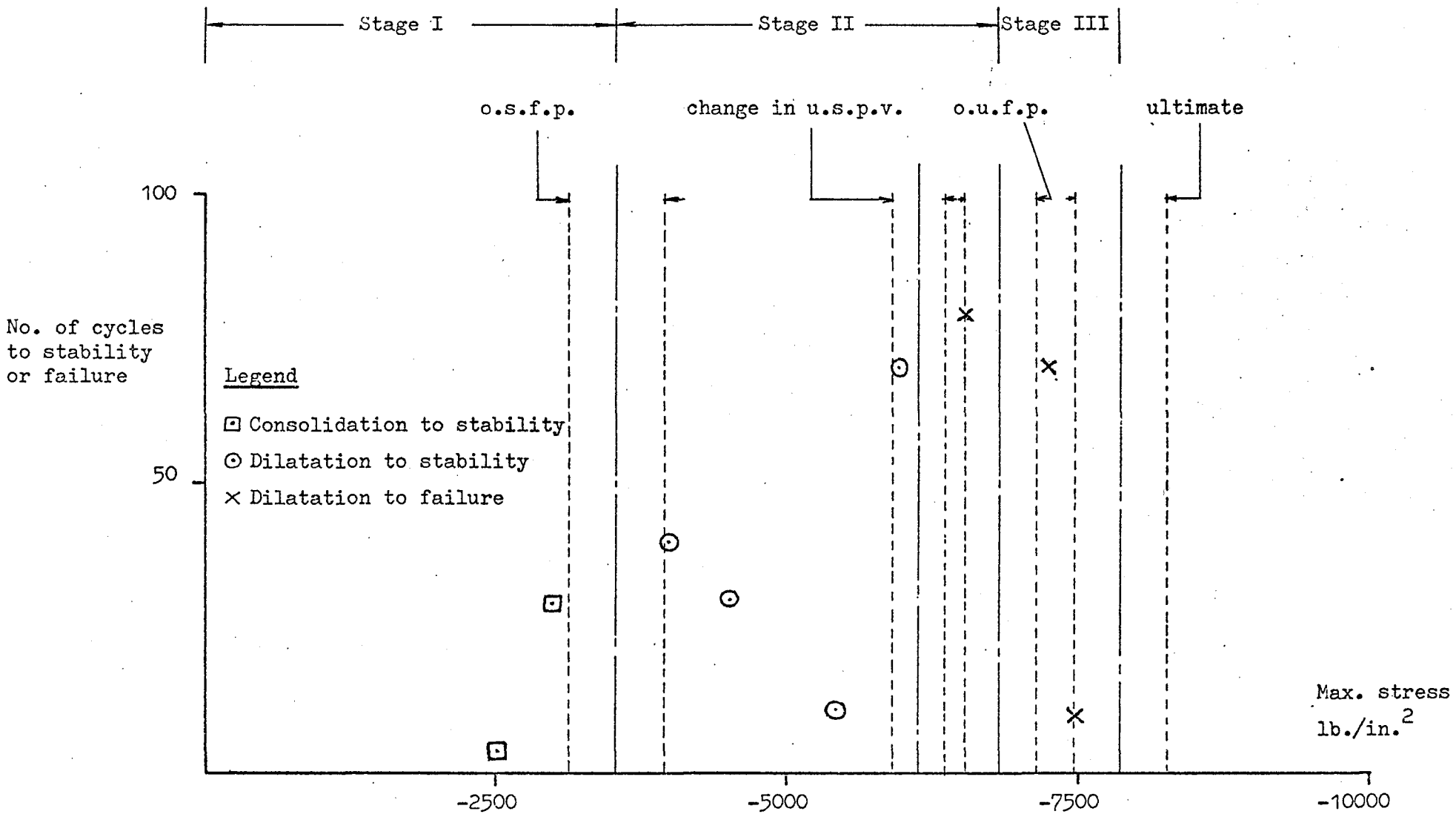


Figure 5.10. The significant changes in material behaviour for idealised concrete with V_{ca} = 46% under uniaxial compression and their relationship to the behaviour under repeated uniaxial load.

2. For a maximum stress lying within Stage III the zone within which the behaviour is considered to be unstable, failure is eventually caused after excessive dilatation. The typical form of the behaviour is shown in Figure 5.6. which demonstrates the gradual increase in hysteresis with each successive cycle of stress, particularly near failure.

3. For a maximum stress within Stage II the zone considered to be related to stable crack propagation, the behaviour is characteristic of either (a) dilatation to stability or (b) consolidation to stability. An example of the latter behaviour is shown in Figure 5.5. which shows the similarity of hysteresis loops after the first few cycles, culminating in a near-constant loop which indicates stability.

For the mix containing a V_{ca} of 46%, the principal results are shown in Figure 5.10. which indicates essentially the same trends as for the previous mix except that, for this case, the behaviour within Stage 2 is solely dilatation to stability.

In a similar investigation carried out concurrently by Shah and Chandra [138] the same behaviour was observed for a real concrete cyclically loaded to a maximum stress within Stage 3. However, no specimens were loaded at less than 60% of the short-term uniaxial compressive strength and so only that part of Stage 2 close to the upper boundary (minimum volume level) was investigated. The measured behaviour within this portion of Stage 2 indicated continuous volume increases with no tendency to stability even after 1000 cycles. From the work it was concluded that the minimum volume level marked the boundary between specimens which did and did not fail during repetitive loading.

Ultrasonic Pulse Transmission Characteristics

The most surprising result from the tests is that for all specimens the ultrasonic pulse velocity decreases with increasing number of cycles, irrespective of the maximum stress level. It is to be expected that the changes in ultrasonic pulse velocity would show the same trends as observed for the volumetric strains and such behaviour has, in fact, been observed in similar tests [138]. No satisfactory explanation can be found for the present behaviour except that, during the cycles of loading, the

transducers may have gradually detached from the surface of the specimens. In order to confirm this the tests must be repeated.

Modes of Failure

The specimens which eventually failed exhibit symmetrical fracturing in the axial splitting mode, which indicates uniform loading.

For those specimens loaded within Stage II, for which the strain measurements indicate dilatation to stability, no cracks are visible at the surfaces. However, lateral slices cut from some specimens when subjected to the ultra-violet dyeing technique show an extensive interconnected system of cracks through the mortar matrix and around the coarse aggregate particles.

Specimens loaded within Stage I also show internal cracks, but in such cases these are isolated within the mortar matrix and are not interconnected.

5.3.10. Conclusions

1. The structural stability of a concrete under repeated uniaxial compressive loading can be assessed accurately from a detailed study of the formation of voids during each successive load cycle. Such a study leads to the identification of one of the following modes of behaviour for a given test:-

   a) Consolidation to stability

   b) Dilatation to stability

   c) Continually increasing dilatation to eventual failure.

2. Each of the three principal stages of behaviour under short-term static stress corresponds closely with a characteristic deformational response of one of the above types, if the same concrete is repeatedly loaded at the same stress rate to induce a stress level within the stage, as follows:-

Maximum Stress	Characteristic Behaviour under Repeated Loading
within Stage I	Volumetric consolidation to stability. Isolated matrix cracking evident.

within Stage II — Consolidation or dilatation to stability. For the latter type of behaviour extensive interconnected cracking is evident.

within Stage III — Dilatation to failure.

3. In view of the above it can be assumed, with some degree of confidence, that the three stages of material behaviour identified for short-term static loading can be used to predict the likely response of a concrete under more complex loading regimes.

   This is of considerable importance if the levels of significant change in behaviour (o.s.f.p. and o.u.f.p.) are to be used as criteria for the design of concrete structures.

It should be emphasised that only relatively simple stress states have been considered in the test series, and the existence of the stages of behaviour must be confirmed for other more complex stress states. Such an attempt is made in the following Chapters for the cases of uniaxial tension, uniaxial compression and triaxial compression.

6. STRENGTH OF CONCRETE UNDER TRIAXIAL COMPRESSION - AN ANALYSIS OF PREVIOUS WORK

6.1. Introduction

Over many years a large number of criteria have been proposed for evaluating the combinations of stresses or strains which could cause the ultimate failure of various materials. These have been reviewed by Marin [158], Nadai [159], and Timoshenko [160]. Rocks have been adequately covered by Jaeger [161] and Hoek [162] while Newman [9] has dealt with concrete.

In the present and previous work [19, 20] the Author has presented the case for adopting criteria, not only to evaluate ultimate strength, but to describe conditions necessary for significantly changing the behaviour of a material such that may affect its future load carrying potential. These significant changes have been discussed in Chapters 4 and 5 for concrete and other brittle materials, and it is considered that it is essential to evaluate the criteria for such material changes for use in contemporary concepts of limit stage design [2, 20]. Unfortunately it is such data that are lacking, since more attention has been devoted to quantifying the conditions at ultimate.

In the light of the lack of data describing the process of breakdown of concrete under multiaxial stress it is useful to study the variation in ultimate strength envelopes for changes in material and environmental parameters, since this may provide an insight into the likely effects of changing these parameters on other critical behavioural levels which are the subject of the work described in Chapter 7.

To this end, ultimate strength data have been collected for tests in which triaxial 'compressive' stress states have been induced in specimens using a conventional hydraulic cell device. The data has been restricted to that obtained from such a device since it is considered that it produces the most reliable and definable stress state (see Chapter 2).

The results of tests on 123 different mixes reported during the period 1928-72 [67, 163 to 179] have been analysed to study the effect of the following main parameters on the characteristics of the strength envelopes:-

Condition of specimen at test (saturated or dry)
Maximum size of aggregate

Type of aggregate (lightweight or natural)
Volume fraction of aggregate
Water/cement ratio

For this purpose it has been necessary to obtain the following details for each mix:-

Aggregate Characteristics

Type, shape, surface texture, maximum size.

Mix Proportions by Weight

Water/cement ratio, fine aggregate/cement ratio, coarse aggregate/cement ratio.

Mix Proportions by Volume

Volume fraction of fine aggregate, volume fraction of coarse aggregate.

Curing Regime prior to Test

Treatment of specimen before, and degree of saturation at, test.

In some cases insufficient data is available to ascertain some of the above details. In such cases the data is inferred from the general context of the published work and/or a knowledge of similar materials or investigations.

The strength data, consisting of values for confining pressure and associated axial stress at ultimate for each mix, is stored in a form suitable for computer analysis.

It should be emphasised that the values of stress at ultimate relate to the maximum axial load which the specimen sustained during the test and are, therefore, nominal values uncorrected for the change in cross-sectional area of the specimen.

6.2. Representation of the Strength Envelope

Strength data may be represented in two main ways. The data can be either plotted directly in principal stress space or some function of the three principal stresses at failure can be presented. For the latter method the function is usually chosen in terms of the three invariants of the stress tensor, namely:-

$$I_1 = \sigma_1 + \sigma_2 + \sigma_3$$

$$I_2 = \sigma_1\sigma_2 + \sigma_2\sigma_3 + \sigma_3\sigma_1 \quad .. \quad .. \quad .. \quad (1)$$

$$I_3 = \sigma_1\,\sigma_2\,\sigma_3$$

The most common form of representation relates the octahedral shear stress (τ_{oct}) at failure to the value of the mean normal stress (σ_m) where:-

$$\tau_{oct} = \frac{1}{3}\sqrt{(\sigma_1 - \sigma_2)^2 + (\sigma_2 - \sigma_3)^2 + (\sigma_3 - \sigma_1)^2} \quad .. \quad (2)$$

$$\sigma_m = \frac{1}{3}(\sigma_1 + \sigma_2 + \sigma_3) \quad .. \quad .. \quad .. \quad (3)$$

The expression for τ_{oct}, equivalent to that for maximum distortional strain energy, is considered useful since it includes all three principal stresses. However, it has been shown that such a representation effectively desensitises the data since large variations in the intermediate principal stress are not evident (180).

This dependence on the method of data representation has been avoided in the present analysis by plotting absolute, or normalised, values of strength data as direct coordinates in principal stress space, and attempting to select an empirical relationship or model which adequately defines the resulting envelope.

An empirical relationship, rather than the actual experimental points, has been used as the basis for comparison since only through a mathematical procedure can the data be presented conveniently to designers. It is, therefore, the change in shape of the data envelope, expressed numerically with variation of particular parameters, that is required.

A mathematical relationship should, if possible satisfy the following requirements:-

(i) Express the envelope in a manner conducive to easy strength prediction for a given mix, or type of mix, by interpolation or extrapolation.

(ii) Conform to the generally accepted shape characteristics of the strength surface and provide a good fit with the data over the required range of values.

(iii) Enable comparison to be made between groups of concretes containing results obtained by different workers.

Regarding item (i) it is considered that a maximum of two parameters should be included in the expression relating principal stresses, since more would prove unwieldy.

Item (ii) has been discussed by Franklin [181], with particular reference to rocks, and the following expression was considered to be the most appropriate:-

$$(\sigma_{axial} - \sigma_{conf}) = A(\sigma_{axial} + \sigma_{conf})^B \quad .. \quad .. \quad .. \quad (4)$$

Such a relation, derived from the Mohr representation, passes through the origin of stress space and therefore cannot be said to satisfy item (ii). The same criticism can also be made of the following relation suggested by the Author [19] as a good fit for concrete data:-

$$\sigma_{axial} = \sigma_c + A\sigma_{conf}^B \quad .. \quad .. \quad .. \quad (5)$$

where σ_c = uniaxial compressive strength

Although the parabolic form of equation definitely appears to adequately represent concrete and rock triaxial strength data and satisfied item (i) in that it contains only two parameters, it must be improved in order to predict a finite tensile strength, and hence satisfy item (ii). This is achieved by effecting a transformation such that the curve passes through the tensile side of the confining pressure axis. Such a transformation leads to the following relationship:-

$$\sigma_{axial} = A(\sigma_{conf} + T)^B \quad .. \quad .. \quad .. \quad (6)$$

where T = intercept on tensile side of confining pressure axis.

In order to satisfy item (iii) a convenient form of representation is by normalising the data in some way.

Such a normalising procedure is generally expected to eliminate some, or all, of the effects due to different testing techniques employed between groups of specimens. The main assumption is that the effect of the testing technique will be the same for all specimens within a group, and hence will be

'cancelled out' by such a procedure. This line of reasoning is not strictly correct, as the effects of the testing technique will undoubtedly be different for specimens tested under differing conditions of stress. With concrete, for instance, the usual method is to normalise with respect to the uniaxial compressive strength σ_c, but under high confining pressures the testing machine/specimen interaction effects may be completely different from those operating on an unconfined specimen. Normalising is also expected to enable comparisons to be made between groups of specimens with different values of normalising parameter. For concrete, the use of σ_c as the parameter essentially means that the effects of differing water/cement ratio, age or curing conditions should be eliminated. This line of reasoning is also suspect but appears reasonable since the quality of the cement paste undoubtedly contributes to most of the properties of concrete under stress and is likely to be reflected in the performance of a concrete for all stress states. The effectiveness of normalising with respect to σ_c in removing of effects of water/cement ratio is demonstrated in 5.3.

Thus it would seem that although the effects of normalising may be more complex than expected, it nevertheless remains a powerful technique for comparative purposes and is used in the present analysis.

If normalised with respect to the unconfined compressive strength σ_c equation (7) becomes:-

$$\sigma_{axial}/\sigma_c = A(\sigma_{conf}/\sigma_c + T)^B \quad .. \quad .. \quad .. \quad (8)$$

This equation, however, contains three parameters and, to reduce the number, it would be convenient to replace the parameter T by the uniaxial tensile strength. Unfortunately such a substitution does not lead to a good fit with the experimental data, a fact also noted by Franklin [181] for rocks.

The equation can be reduced to two parameters by forcing the curve to pass through the point represented by:-

$$\sigma_{conf}/\sigma_c = 0 \qquad \sigma_{axial}/\sigma_c = 1$$

In this case the equation becomes:-

$$\sigma_{axial}/\sigma_c = \left[A(\sigma_{conf}/\sigma_c) + 1\right]^B \quad .. \quad .. \quad .. \quad (9)$$

It must be emphasised that the above equation relies on the adoption of an estimate for σ_c. If this estimate is taken as the axial stress at zero confining pressure, as abstracted from the data set under consideration, then this value will be unduly weighted. Although undesirable this is considered inevitable if a comparison between data groups is required. A representative value for σ_c for a particular set of triaxial strength values is extremely difficult unless performed by eye. Such a process is operator sensitive and is likely to lead to more errors than the use of the experimental value of uniaxial compressive strength. Thus, for comparison purposes, the stress values have been normalised with respect to the mean value of uniaxial compressive strength for each set of specimens tested.

As previously discussed, the parabolic form of equation is only one of a number of possible equations which adequately express the experimental data. For example, a hyperbolic equation transformed in a manner similar to that for the parabola leads to the following:-

$$\sigma_{axial}/\sigma_c = \left[A(\sigma_{conf}/\sigma_c)^2 + B(\sigma_{conf}/\sigma_c) + 1 \right]^{\frac{1}{2}} \quad .. \quad (10)$$

By comparing the parabola, hyperbola and other relationships for closeness of fit with the data, on the basis of the sums of squares, it is found that the parabola and hyperbola are considerably more efficient than other equations. Of these two, the parabola is slightly more efficient for most envelopes, although in some cases (including the data obtained in Chapter 7) the hyperbola is superior.

On the basis of this comparison of fit and the ability to satisfy the requirements outlined in Items (i) to (iii), the normalised parabolic representation has been adopted and a computer programme, based on a minimum neighbourhood least squares fitting routine has been developed to analyse the data. The results of the analysis are presented in the following sections. The upper and lower bound limits indicated on the strength envelopes are obtained by substituting the relevant upper and lower non-linear confidence limits [183] into the parabolic equation.

6.3. Effect of Water/Cement Ratio

As discussed in 6.2. the effect of normalising with respect to σ_c is generally intended to eliminate the effects of the strength of the mix tested on the

characteristics of the resulting failure envelope. As strength is synonymous with water/cement ratio, for a given aggregate type and content curing condition and age, this hypothesis is tested by comparing the envelopes exhibited by mixes containing water/cement ratios varies between certain limits.

For this purpose it is required to eliminate as many other variables as possible, and so only mixes containing $\frac{3}{4}$" maximum size of aggregate, the largest group tested, are used. The effect of the conditions of curing prior to test is found in 6.4. not to significantly affect the normalised failure envelope, and so both wet and dry specimens are included.

The mixes are divided into six groups, each group containing mixes having total water/cement ratios lying within a given range. These groups are shown in Table 6.1. Since, from considerations of workability, practical concrete mixes with a high w/c ratio tend to be those with a high aggregate content it is virtually impossible to eliminate the effect of simultaneous changes in V_a from the analysis. The mean value of V_a for each group is shown in the Table and it can be seen that this generally increases with water/cement ratio.

Table 6.1. also shows the coefficients defining the parabolic envelope for each group, together with the upper and lower non-linear confidence limits. The envelopes defined by these limits are shown in Figure 6.1. from which it can be seen that no definite trend exists between the shape of the envelopes and the water/cement ratio or aggregate content of the mixes.

Thus, although the results of the analysis cannot be considered conclusive, it would appear that normalising the strength data with respect to the uniaxial compressive strength σ_c has the effect of eliminating, or at least minimising, the influence of the water/cement ratio on the ultimate strength envelope, provided the aggregate content is allowed to increase with increasing water/cement in the generally accepted manner. This tends to support the assumptions made in 6.2. regarding the use of normalising for purposes of comparison.

Group	No. of Mixes in Group	Range of W/C ratio	Mean V_a for Group (%)	Coefficients by least squares estimation A	B
J	7	0.30 - 0.39	61.2	7.8010 (7.7835 - 7.8733)	0.7196 (.6855 - .7506)
K	6	0.40 - 0.49	68.5	3.0506 (2.7328 - 3.3631)	1.1081 (1.0335 - 1.1702)
L	19	0.50 - 0.59	70.3	7.0765 (6.8744 - 7.2817)	0.7739 (.7682 - .7792)
M	7	0.60 - 0.69	75.7	11.9958 (10.2567 - 13.9705)	0.6206 (.5893 - .6464)
N	7	0.70 - 0.79	76.2	6.8446 (6.0548 - 7.6909)	0.7327 (.7018 - .7585)
O	3	0.80 - 0.80	71.9	4.0161 (4.0012 - 4.0375)	0.9996 (.9364 - 1.0569)
P	4	70.89	78.0	10.7864 (9.4774 - 12.2323)	0.7165 (.6938 - .7347)

Table 6.1. Values of coefficients in the normalised ultimate strength relationship

$$\sigma_{axial}/\sigma_c = (A.\sigma_{conf}/\sigma_c + 1)^B$$

for concretes containing $\frac{3}{4}$" aggregate with various ranges of W/C ratio.

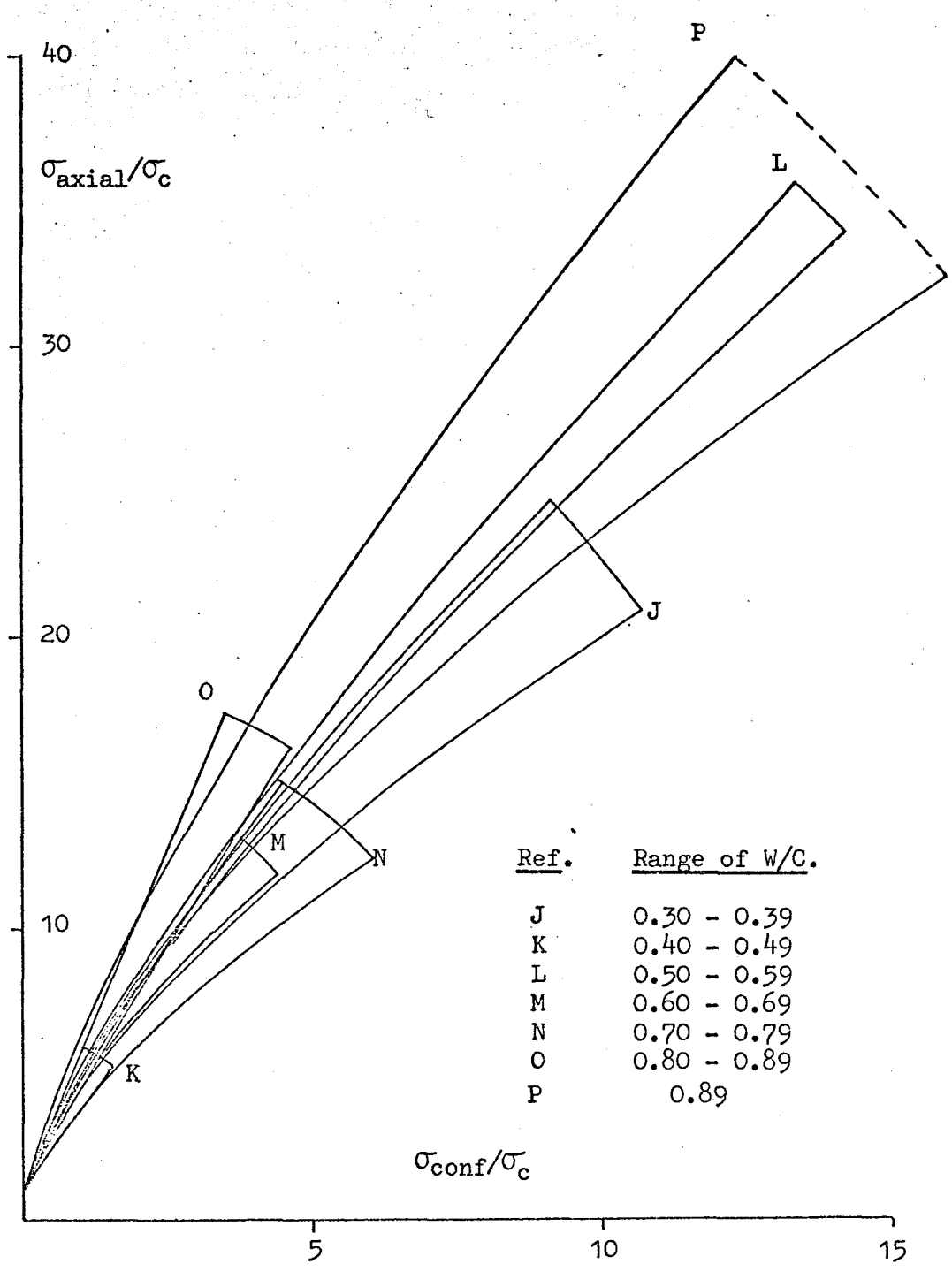


Figure 6.1. Confidence regions for parabolic relationships defining normalised ultimate strength envelopes for concretes containing $\frac{3}{4}$" natural aggregate with various ranges of W/C ratio.

6.4. Effect of Curing Regime Prior to Test

In general, the concretes tested are found to have been subjected to one of two main regimes prior to test. Either the specimens were cured in conditions of high humidity and tested in an 'undried' condition, or attempts at moisture removal were made and the specimens tested 'dried' or partly dried.

For the present purpose of comparison it has been assumed that the specimens were either tested 'wet' if no attempt at drying is indicated or 'dry' if the investigator has definitely reported such an attempt. All specimens about which no conclusive evidence of curing regime is indicated are eliminated from the analysis.

The results of the analysis are given in Table 6.2. and Figure 6.2. from which it can be seen that the condition of the specimen at test does not appear to have a significant effect on the normalised failure envelope. In fact the envelope for dry concretes would appear to be slightly lower than that for specimens tested wet, which contradicts the available evidence [169, 170]. However, this would be explained by the fact that the 'wet' concretes, in general, contained higher volume fractions of aggregate (see Table 6.2.) and it is shown in 6.6. that aggregate content is a factor which does influence the ultimate strength envelopes.

An attempt to remove the influence of V_a is made by only including in the analysis those mixes containing V_a between the limits 0.70 and 0.79. The results are shown in Table 6.3. and Figure 6.3., from which it can be seen that the range of confining pressures and variability of results for the 'dry' mixes now influences the envelopes. It can be concluded, however, that the effect of curing regime and moisture condition of specimen at test is not significant.

6.5. Effect of Mix Type and Maximum Size of Aggregate

Table 6.4. and Figure 6.4. show the results of analysing the following groups of mixes:-

Pastes - tested wet
tested air dried
tested oven dried
Mortars-with 3/16" maximum size of aggregate
Concretes-with 3/8" maximum size of aggregate
-with 3/4" maximum size of aggregate
-with $1\frac{1}{2}$" maximum size of aggregate
Lightweight aggregate concretes

Group	No. of Mixes in Group	Mean W/C	Mean V_{ca} (%)	Coefficients by least squares estimation A	B
Wet	21	0.71	73.6	6.4298 (6.0602 - 6.8064)	0.7968 (.7850 - .8078)
Dry	23	0.49	69.0	6.9408 (6.6540 - 7.2349)	0.7637 (.7551 - .7715)

Table 6.2. Values of coefficients in the normalised ultimate strength relationship

$$\sigma_{axial}/\sigma_c = (A.\sigma_{conf}/\sigma_c + 1)^B$$

for concretes containing $\frac{3}{4}$" aggregate tested wet or dry.

Group	No. of Mixes in Group	Mean W/C	Mean V_{ca} (%)	Coefficients by least squares estimation A	B
Wet	17	0.76	75.9	6.5706 (6.1421 - 7.0088)	0.7929 (.7795 - .8052)
Dry	9	0.58	75.0	16.0093 (14.2646 - 17.8971)	0.5995 (.5794 - .6172)

Table 6.3. Values of coefficients in the normalised ultimate strength relationship

$$\sigma_{axial}/\sigma_c = (A.\sigma_{conf}/\sigma_c + 1)^B$$

for concretes with $\frac{3}{4}$" aggregate containing volume fraction of aggregate between 0.70 and 0.79 tested wet or dry.

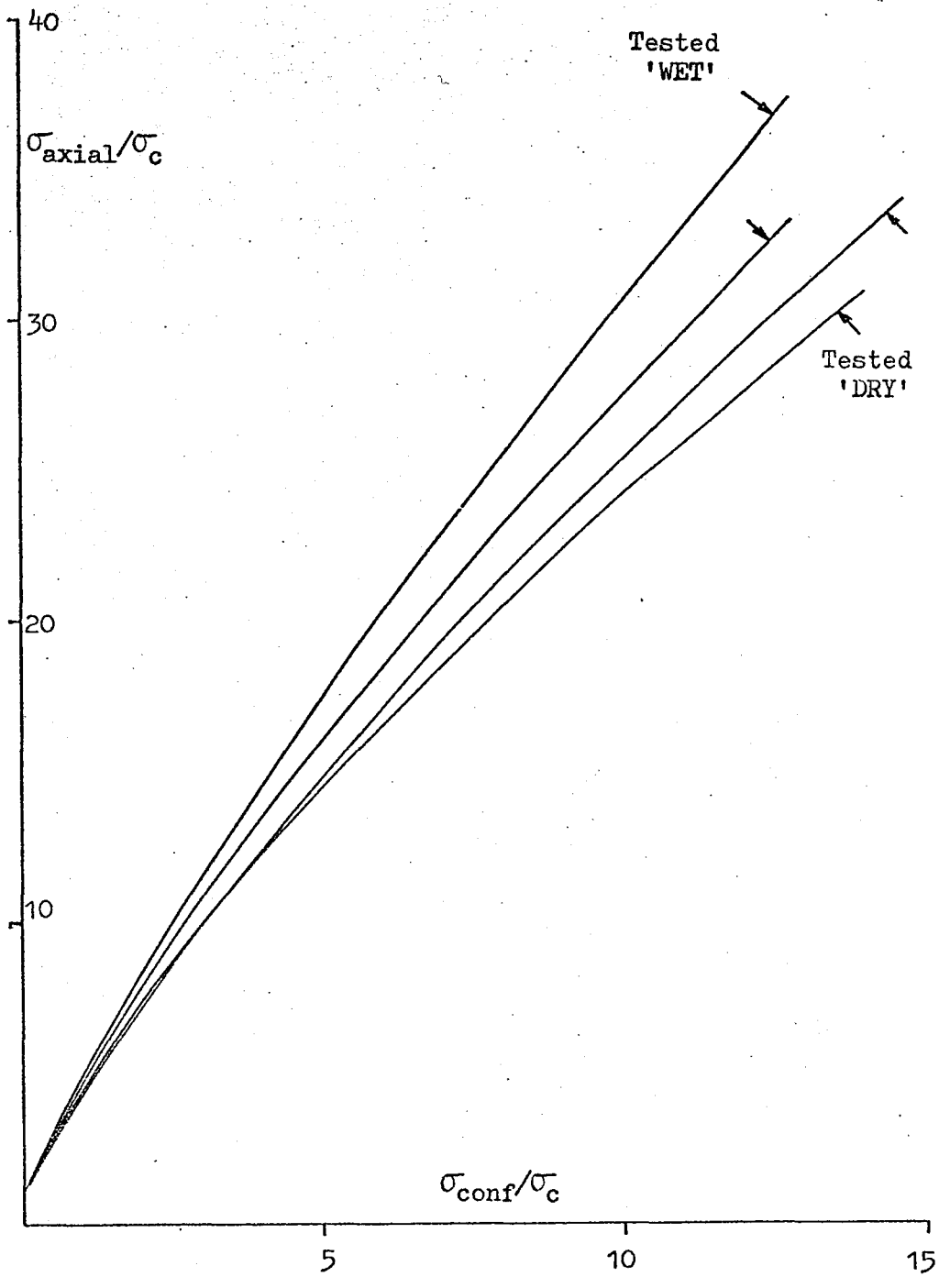


Figure 6.2. Confidence regions for parabolic relationships defining normalised ultimate strength envelopes for concretes containing $\frac{3}{4}$" natural aggregate tested in the 'wet' or 'dry' condition.

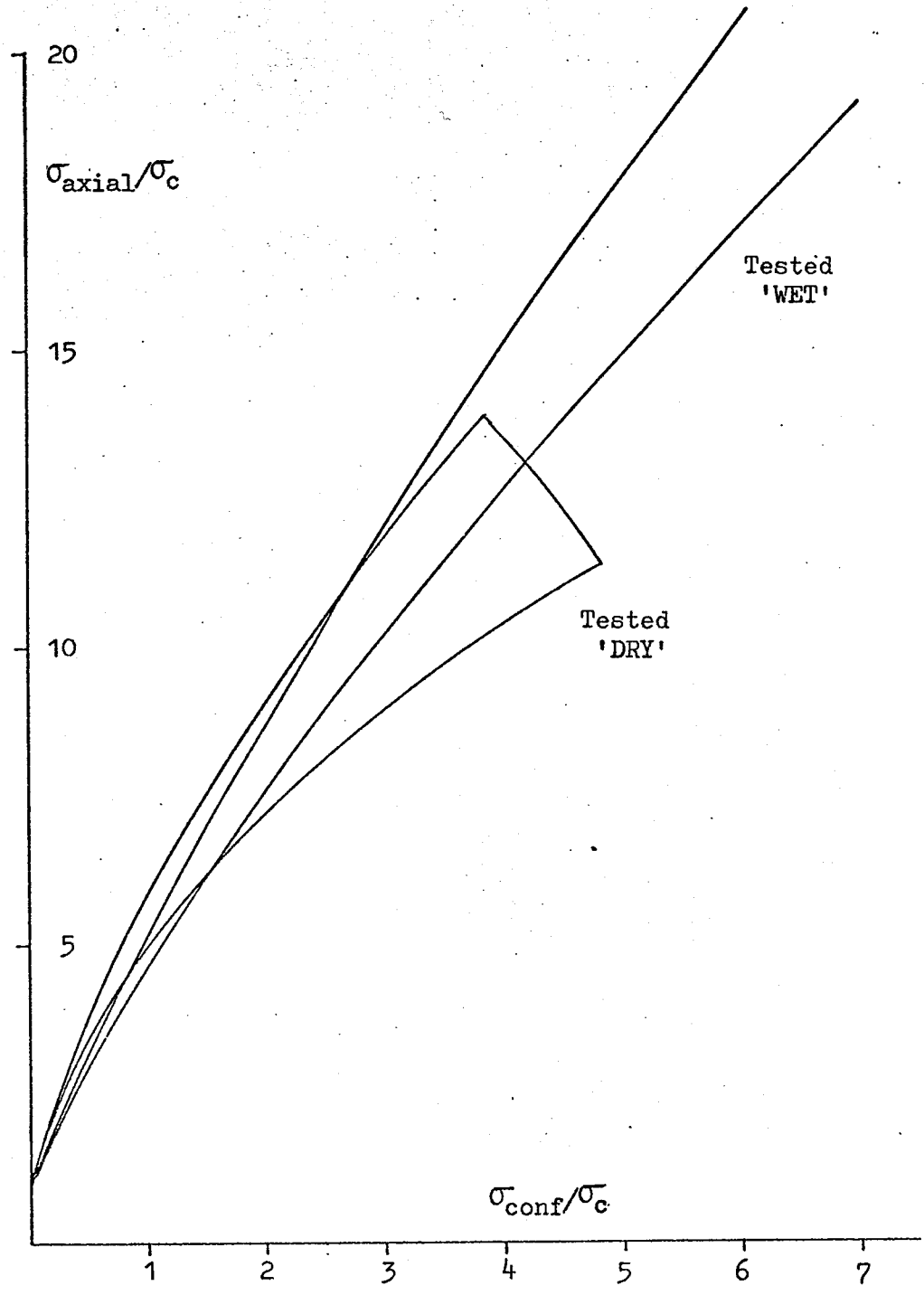


Figure 6.3. Confidence regions for parabolic relationships defining normalised ultimate strength envelopes for concretes containing a volume fraction of $\frac{3}{4}$" natural aggregate within the range 0.70 and 0.79 tested in the 'wet or 'dry' condition.

Group	No. of Mixes in Group	Mean W/C	Mean V_{ca} (%)	Coefficients by least squares estimation A	B
Pastes tested 'wet'	1	0.70	NIL	7709.4331 (5010.5071 - 12567.2382)	0.1809 (.1703 - .1914)
Pastes tested after air drying	3	0.35	NIL	37.3122 (32.2994 - 44.3277)	0.3581 (.3321 - .3805)
Pastes tested oven dry	1	0.35	NIL	55.3482	0.5076
Mortars (3/16" aggt.)	14	0.55	50.3	4.9314 (4.8229 - 5.0403)	0.9055 (.8987 - .9119)
Concretes (3/8" aggt.)	9	0.49	66.6	10.8405 (10.1853 - 11.5264)	0.6326 (.6117 - .6518)
Concretes (3/4" aggt.)	48	0.59	71.4	6.6426 (6.4410 - 6.8472)	0.7791 (.7729 - .7849)
Concretes ($1\frac{1}{2}$" aggt.)	23	0.56	73.8	5.4418 (5.1564 - 5.7321)	0.8407 (.8264 - .8536)
Lightweight aggt. concretes	14	0.65	59.4	7.6362 (6.9287 - 8.4705)	0.5455 (.5099 - .5761)

Table 6.4. Values of coefficients in the normalised ultimate strength relationship

$$\sigma_{axial}/\sigma_c = (A.\sigma_{conf}/\sigma_c + 1)^B$$

for various types of mixes.

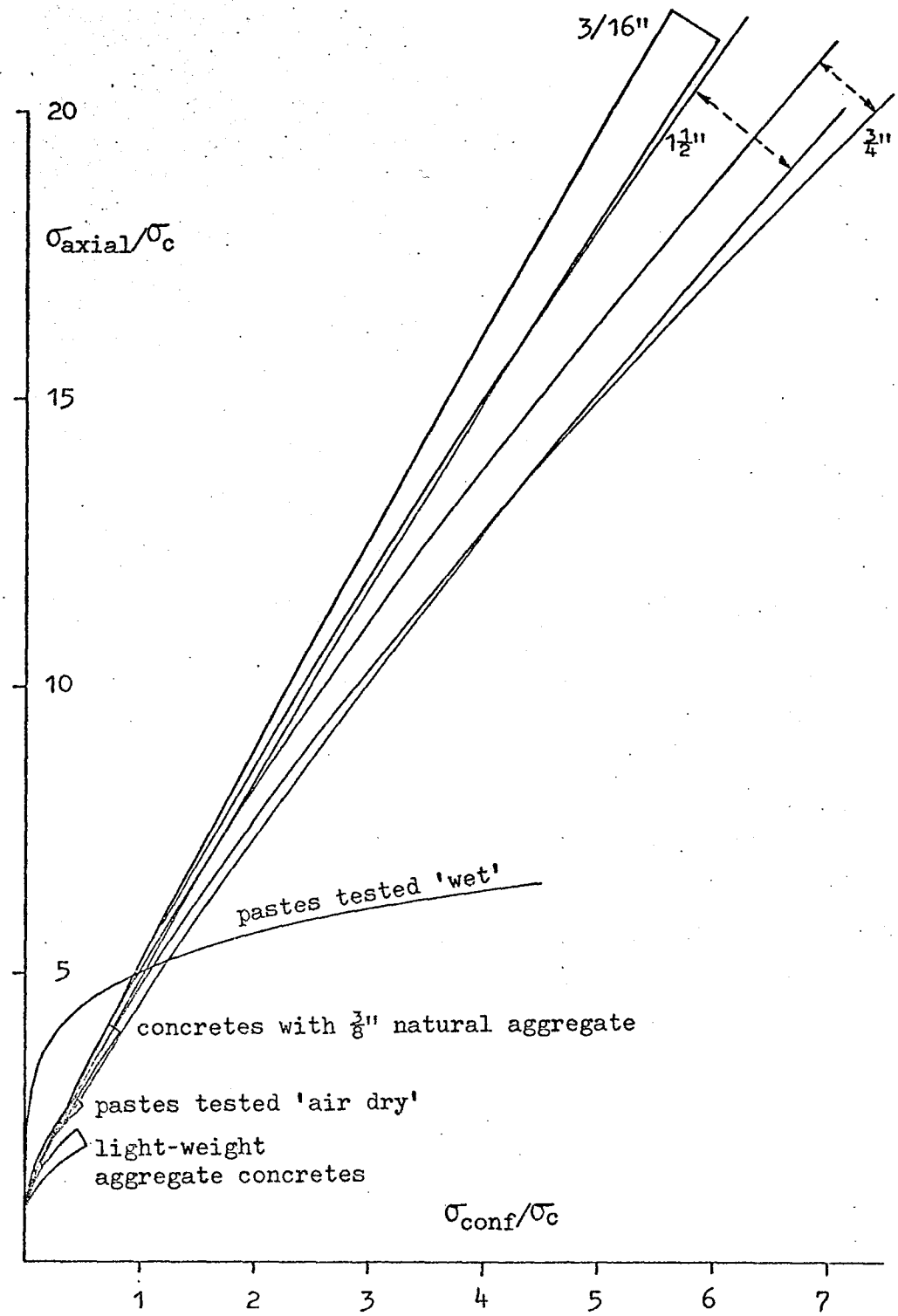


Figure 6.4. Confidence regions for parabolic relationships defining normalised ultimate strength envelopes for various types of concrete.

From the shape of the envelopes on Figure 6.4. the mixes appear to be grouped into the following classes:-

(i) Concretes or mortars containing natural aggregate with a maximum size of at least 3/16"

(ii) Concretes containing lightweight aggregate

(iii) Pastes

These will be discussed in turn in the following sections.

6.5.1. Mortars and Concretes

For this class of material, the strength increases continually with confining pressure. The envelopes indicate that this increase is largely independent of the aggregate size. It might be expected that the tendency would be for the mixes containing coarse aggregate to show greater strength increases under the influence of confining pressure due to their heterogeneity. The envelope for $\frac{3}{4}$" concretes, in fact, does lie slightly below that for $1\frac{1}{2}$" but the 3/16" mortar envelope lies above the $1\frac{1}{2}$". The displacement of the mortar envelope may be caused by the manner in which the ultimate state is defined. For all tests reviewed, the ultimate axial stress is based on the nominal maximum stress which each specimen sustains during the test with no account taken of the true cross-sectional area of the specimen. For coarse aggregate concretes the end point of a test is marked by a 'brittle' failure whereas, for mortars, considerable lateral deformation in the form of 'bulging' occurs which gives rise to 'ductile' behaviour at higher confining pressures. Such behaviour can lead to a considerable strength 'bonus' being given for mortars due to the significant increase in cross-sectional area of specimens.

6.5.2. Lightweight Aggregate Concretes

The rapid decrease in slope of the envelope with increase in confining pressure suggests the breakdown of the porous material under pressure. This phenomenon is discussed in more detail in Chapter 7.

6.5.3. Pastes

The strength of these materials is quite distinct from that exhibited by the natural aggregate concretes, but is similar to that for lightweight

aggregate mixes. The characteristic shape of envelope suggests strongly that the mechanism of failure is due to collapse of the porous paste structure under hydrostatic pressure (see Chapter 7).

The differences between the envelopes for the three classes of paste, namely moist, air dried and over dried, are emphasised in Figures 6.5. and 6.6. which show the strong influence of curing treatment on the behaviour under stress. The greatest increase in strength with confining pressure is given by the oven-dried paste. This is probably due to the tendency of the paste to crack extensively if placed in a drying environment. This cracking will reduce the uniaxial compressive strength and the paste will behave in a similar manner to granular materials. Under a confining pressure, however, the cracks will tend to close producing high strength increases until breakdown of the porous structure occurs.

6.6. Effect of Volume Fraction of Aggregate

If the true influence of the volume fraction of aggregate V_a on the shape of the ultimate strength envelope is to be studied it is necessary to eliminate the effects of other important variables. For the present analysis, only mixes containing $\frac{3}{4}$" maximum size of aggregate are considered although the curing conditions, found in 6.4. not to significantly affect the envelope, have not been restricted. However, as outlined in 6.3. it is extremely difficult to eliminate the influence of varying the water/cement ratio, since lean mixes tend to contain higher water contents than rich. This fact is evident from Table 6.5. which shows the division of the mixes into three groups, each defined by the range of volume fraction of aggregate, together with the mean water/cement ratio for each group. The Table also shows the parabolic coefficients and non-linear confidence limits, the envelopes defined by the latter also being shown on Figure 6.7.

Although the envelopes indicate a considerable degree of variability, the trend is for the lean mixes with high water/cement ratios to possess a higher normalised ultimate strength for a given value of normalised confining pressure than richer mixes with lower water/cement ratios.

Comparing the results of the analyses described in 6.3. with the present analyses, it would appear that the volume fraction of aggregate has a greater influence on the normalised ultimate strength envelope than the water/cement ratio.

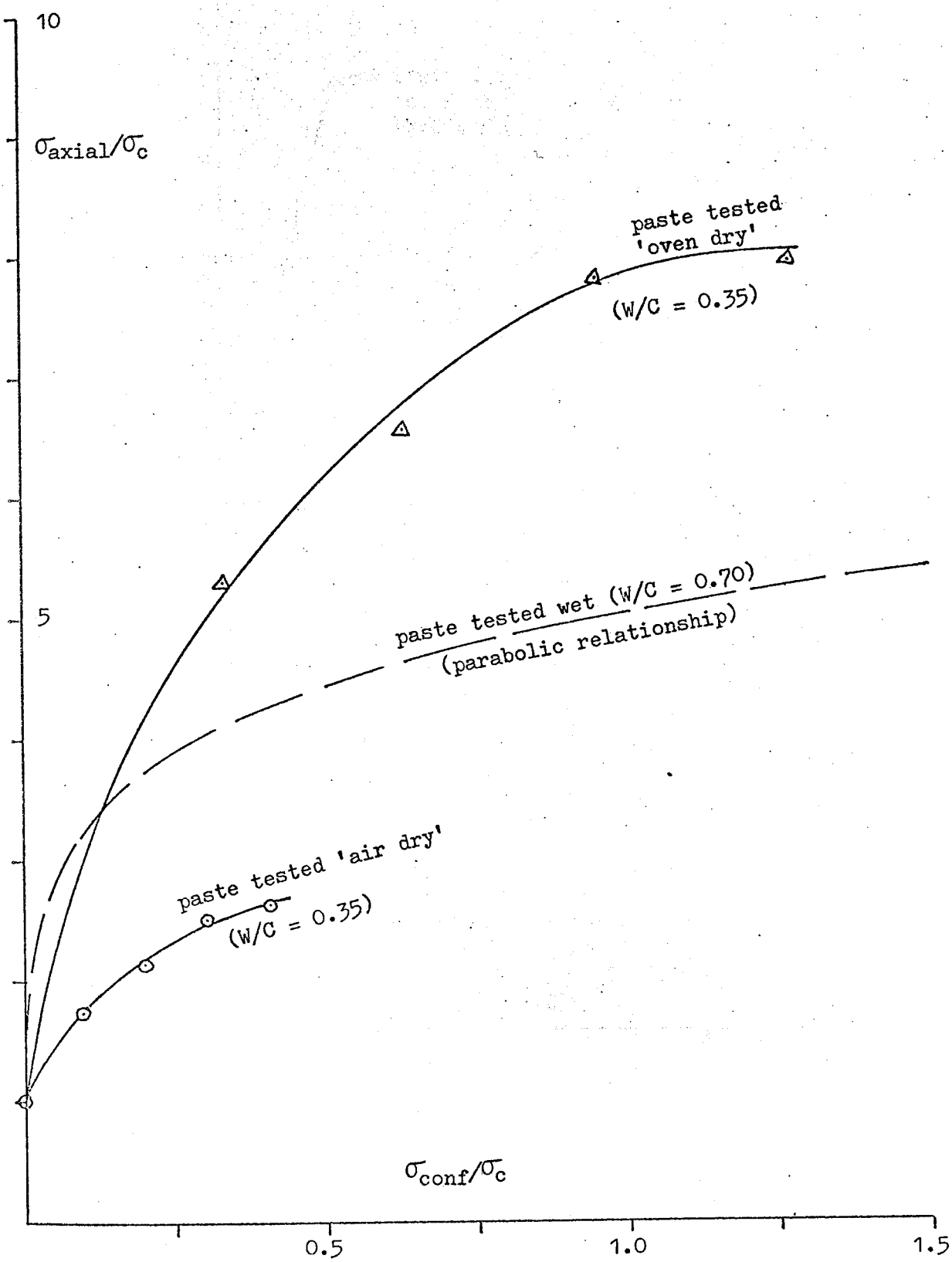


Figure 6.5. Normalised ultimate strength relationships for cement pastes subjected to various curing conditions.

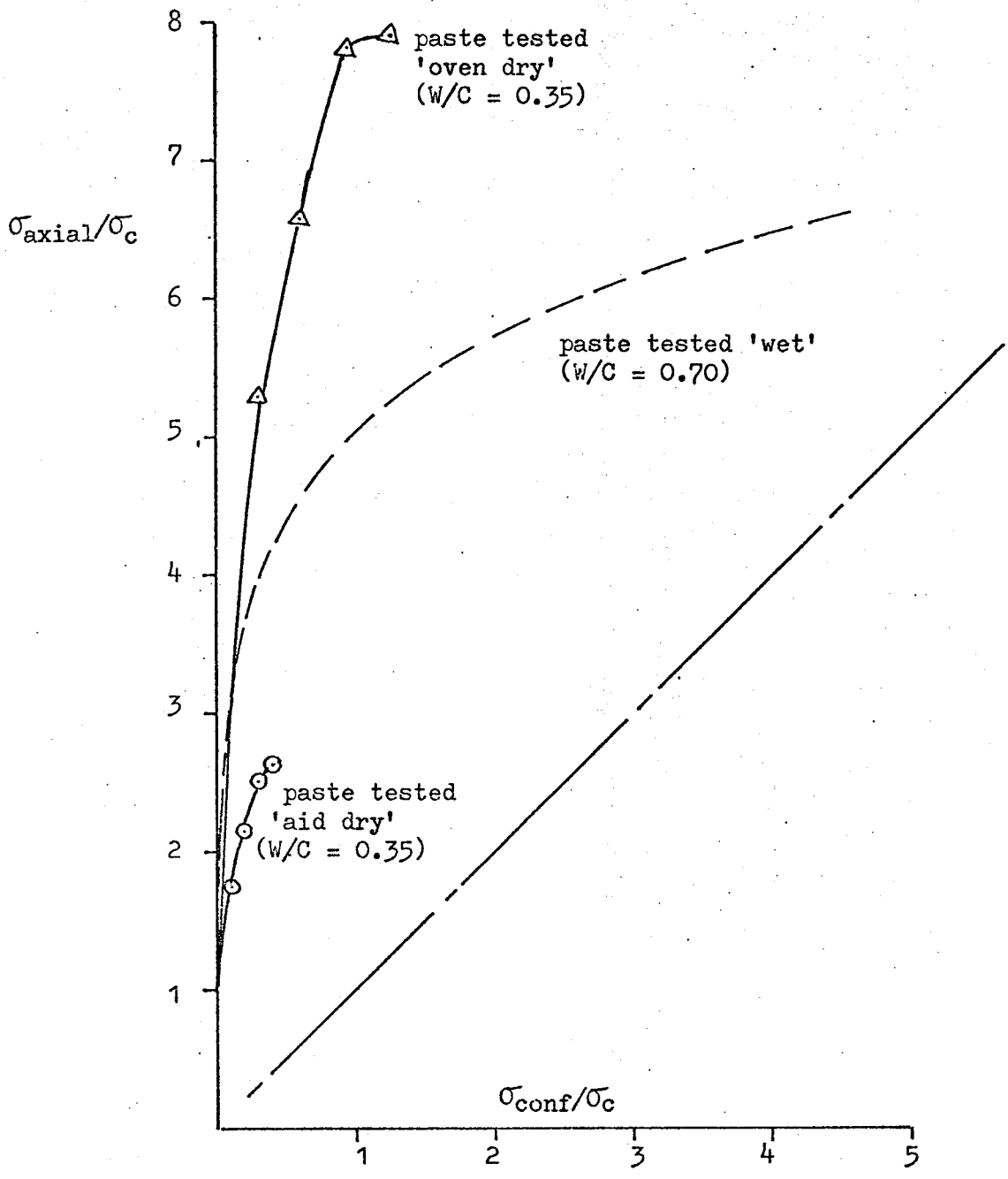


Figure 6.6. Normalised ultimate strength relationships for cement pastes subjected to various curing conditions.

Group	No. of Mixes in Group	Range of V_a (%)	Mean W/C for Group	Coefficients by least squares estimation A	B
F	6	54 - 63	.35	6.3155 (5.6065 - 7.0873)	.7635 (.7348 - .7861)
G	19	64 - 71	.51	6.8991 (6.6668 - 7.1362)	.7702 (.7635 - .7766)
H	27	72 - 80	.71	5.6865 (5.3703 - 6.0076)	.8168 (.8045 - .8282)

Table 6.5. Values of coefficients in the normalised ultimate strength relationship

$$\sigma_{axial}/\sigma_c = (A.\sigma_{conf}/\sigma_c + 1)^B$$

for concretes containing various ranges of volume fractions of $\frac{3}{4}$" natural aggregate.

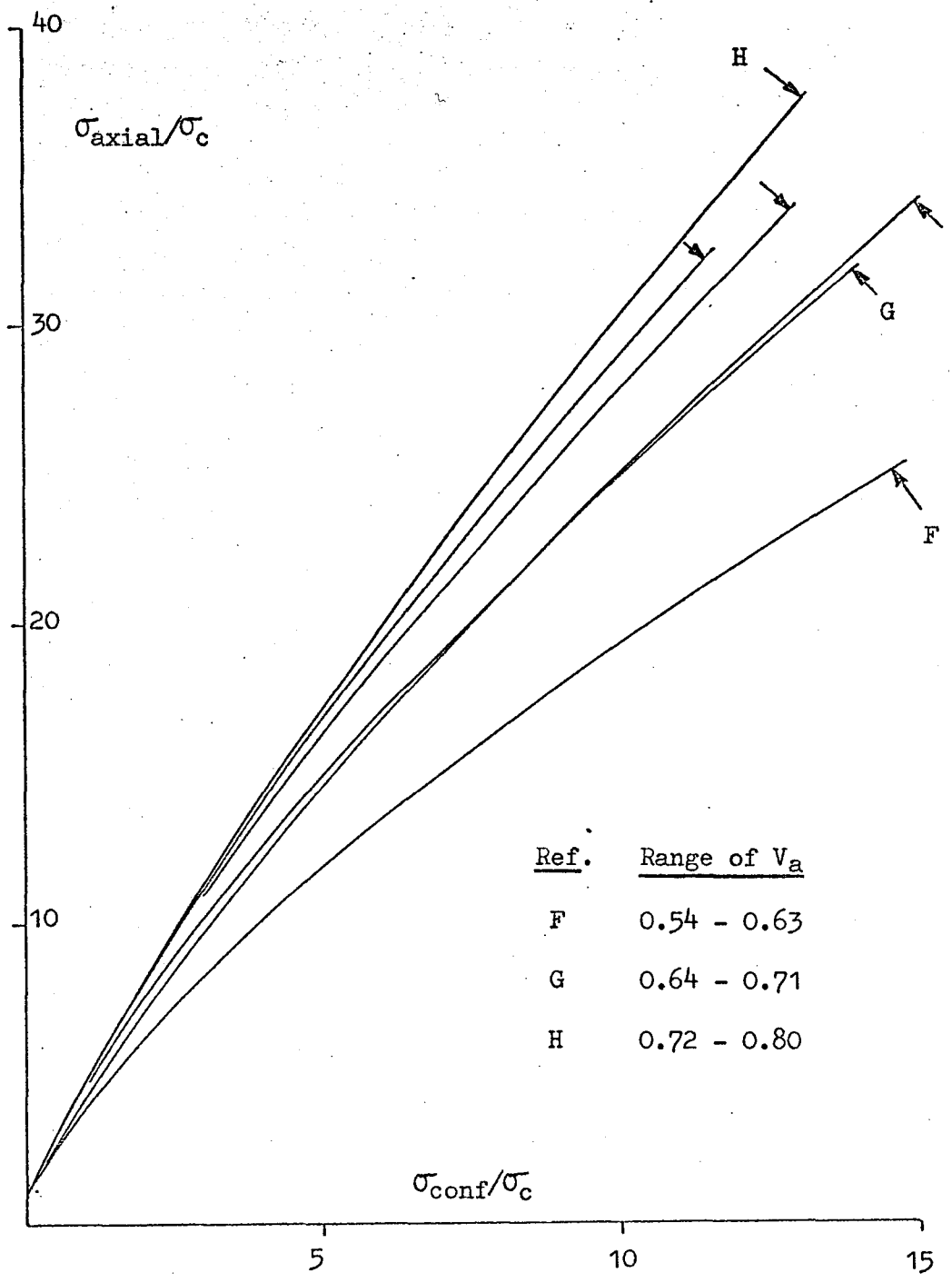


Figure 6.7. Confidence regions for parabolic relationships defining normalised ultimate strength envelopes for concretes containing various ranges of volume fractions of $\frac{3}{4}$" natural aggregate.

6.7. Conclusions

For the present analysis the data has been extracted from a large number of sources. A variety of types of loading apparatus and test procedures have been used and the mix parameters and curing procedures have, in many cases, been varied simultaneously. It has been assumed that the effects of testing are minimised by normalising the data with respect to the uniaxial compressive strength. The effects of the mix parameters, however, remain difficult to isolate.

Even accepting the above restrictions the analyses can provide an indication of likely trends, a knowledge of which will be of assistance in choosing parameters to be investigated in the triaxial test series described in Chapter 7. The main conclusions obtained are as follows:-

1. Normalising the ultimate strength envelopes with respect to the uniaxial compressive strength of each mix appears to effectively eliminate the influence of water/cement ratio for practical mixes containing natural coarse aggregate.

2. The strength envelope for all concretes containing aggregate is open-ended in stress space. For cement paste and lightweight concretes, however, the envelope tends towards an intersection with the hydrostatic axis. A possible explanation for this behaviour is given in Chapter 7.

3. The ultimate strength data for natural aggregate concretes can be adequately represented by a parabolic or hyperbolic function capable of allowing valid interpolation to be made for stress states in the proximity of uniaxial compression as well as for higher confining pressures.

4. Except for cement pastes, the conditions under which the specimen is cured prior to test appear to have an insignificant effect on the shape of the normalised ultimate strength envelope. For pastes, however, the strength envelope is significantly affected by the extent to which the paste is dried prior to test.

5. For a maximum aggregate size above 3/16", the shape of the ultimate strength envelope is largely independent of the size of aggregate.

6. Lean concretes (i.e. those with a high volume fraction of aggregate), with corresponding high water/cement ratios, give larger strength increases with increasing confining pressure than rich mixes with low water/cement ratios.

7. Following from (6) and (1) it would appear that a change in the aggregate content produces a greater effect on the normalised strength envelope than a change in the water/cement ratio. Since the two variables could not be isolated in the present analysis this conclusion is tentative.

Establishing, albeit in a general way, the influence of various mix characteristics and environmental conditions on the ultimate strength envelopes for various concretes under triaxial 'compression' facilitates the formulation of the investigation into the events leading to failure described in the following chapter.

7. DEFORMATIONAL BEHAVIOUR OF CONCRETES UNDER UNIAXIAL TENSION AND TRIAXIAL 'COMPRESSION' STRESS STATES

7.1. Introduction

The principal aim of the present project is to provide structural designers with data regarding the behaviour of concrete under complex states of stress (see Chapter 1). It is considered essential that any data obtained should be suitable for the following purposes:

(i) To provide information regarding the deformational response of the material suitable for use in conjunction with modern computational methods of structural analysis.

(ii) To provide information on the failure processes occurring under load in a form applicable to the limit state philosophy of design, with particular reference to the new Unified Code of Practice [2].

To fulfill the first of the above requirements it is necessary to subject representative elements of concrete to definable states of stress and to measure accurately the resulting complete deformational response.

The second requirement involves a detailed study of the deformational behaviour in order to identify significant levels of change in the internal structural characteristics under load (see Chapter 4) and to determine the way in which the failure process is modified for different stress states.

The results of analytical and experimental investigations to determine the stress state in specimens under load (see Chapter 2) have indicated the many difficulties associated with testing materials even under comparatively simple boundary loading configurations. For more complex configurations of load, the uncertainties regarding the stress state induced in specimens become intolerable unless boundary conditions are applied to specimens of an appropriate shape. Recommendations are made in Chapter 2 regarding suitable loading procedures.

Based on the above recommendations it has been decided to study the behaviour of cylindrical specimens of concrete under multiaxial stresses using a hydraulic cell arrangement, such that the boundary stresses are equal to the principal stresses induced in the specimen. The technique involves

subjecting cylindrical specimens to fluid (confining) pressure in two or three directions, with a load applied through rigid platens replacing, or superimposed upon, fluid pressure in the axial direction.

It is evident that such a system of loading enables only restricted sets of stress conditions to be attained, namely those where two principal stresses are equal (see Section 7.3.4.5.). It is, however, considered justifiable to sacrifice generality of loading in favour of inducing definable stress states.

Although the stress state restriction appears, to be unduly limiting, reference to the Chapters 7 and 8 will demonstrate the quantity of useful information which can be obtained, and inferred from, such tests.

The loading regime used for the tests is that of increasing the confining pressure to a given value and then increasing the axial stress to failure, the confining pressure remaining constant. A test programme, under the Author's direction, is being planned in which the regime of triaxial compressive loading is to be varied. Such variations in regime have been found by Bertacchi [184] not to affect the strength results significantly, but the tests were carried out using a rigid-platen loading device and no deformational behaviour was studied.

The loading arrangement developed for the present series of tests (from the recommendations of 2.7.) is capable of performing 'compression' tests where the axial stress is greater than the lateral (confining) pressure, and 'extension' tests where the axial stress is less than the lateral pressure. If a suitable shape of specimen is chosen, the 'extension' facility can be used to induce compression/compression/tension stress states. However, the present work is concerned solely with triaxial 'compression' states of stress although equal biaxial compression tests, being a special case of triaxial 'extension' have been conducted (see Chapter 4). The general cases of triaxial 'extension' and compression/compression/tension are covered by another investigation which is being carried out under the Author's direction [21].

In the tests, much emphasis is placed on the importance of obtaining the complete deformational behaviour of the concrete with apparatus sufficiently sensitive to detect significant changes in specimen response. As already stated in Chapter 4, the stress or strain levels at which these changes

occur are used as the bases of defining the failure of concrete.

In the test series, no pore pressure effects are studied, and the programme is conducted using undrained specimens. Undoubtedly, pore pressure, or the presence of pore fluid, produces significant reductions in strength of some rocks [91, 185 to 188] and concrete [169]. Brace and Byerlee [95] have concluded, however, that for the ductile or brittle/ductile region of triaxial compression, the strength is almost independent of the pore pressure for crystalline rocks, probably due to their low porosity.

The intention of the test programme is, however, to test mature air-dried specimens since it is considered that a knowledge of the behaviour of concrete in such a state is more useful for design purposes (particularly for such structures as prestressed concrete pressure vessels, dams, etc.) than information on the response of saturated specimens at an early age. The build-up of pore pressure in such mature specimens is likely to be insignificant, and hence the differences between drained and undrained tests are probably not measurable.

The philosophy behind the choice of curing conditions used, is given more fully in 7.2.2. together with the choice of mixes.

7.2. Choice of Concrete Mixes, Curing Conditions and Specimens

7.2.1. Concrete Mixes

Concrete is a heterophase material consisting of aggregates of various sizes and shapes, embedded in a matrix of cement paste. The structure of cement paste itself is complex, consisting of unhydrated cement particles surrounded by hydration products whose morphology is extremely varied. Various chemical and physical forms of gel, together with other materials formed during the hydration process, exist in conjunction with voids of various sizes and shapes. The voids are caused by (a) incomplete hydration or excessive initial water/cement ratio, (b) effects of segregation and (c) thermal or shrinkage movements due to the instability of cement paste.

Most aggregates, on the other hand, are generally considered to remain stable with time and environment. When particles of aggregate are included in cement paste they give rise to heterogeneities, in addition to those provided by the paste, due to the incompatibility of mechanical, physical and chemical properties.

The interaction between the two main phases prior to loading produces further voids or flaws, either within the body of the matrix due to relative movements or volume changes, or at the aggregate/paste boundary to segregation [130, 131]. These interactive processes also continue to affect the properties of the system when external stress or strain is applied.

The behaviour of the composite material before, and during, stressing is dependent not only on the properties but on the volume fractions of the various constituent phases present.

It is evident, therefore, that pastes, mortars or concretes are extremely complex if considered at the microscopic or interparticle levels. At the macroscopic, or overall, level the complexity of concrete and coarse mortar is still formidable, and simplifying assumptions must be made in order to attempt to understand the effect of mix characteristics on the response to load.

One method of simplifying the structure of pastes, mortars and concretes is by considering them as two-phase composite [189] as follows:-

Composite Material	Matrix Phase	Included Particle Phase
Paste	Gel	Unhydrated cement
Mortar	Paste	Fine aggregate
Concrete	Mortar	Coarse aggregate

For pastes, the above method of phase separation appears to be satisfactory since it distinguishes between materials of markedly differing properties.

For the case of mortars and concretes, however, the validity of the division is arguable for two main reasons. Firstly, the particle size distribution of most normal concreting aggregates is essentially continuous from about 100 micron, or less, to $\frac{3}{4}$" or above. To distinguish between fine and coarse aggregate is, therefore, a matter of personal choice. Secondly, the matrix phase does not contain materials exhibiting properties entirely distinct from those of materials in the included particle phase. For example, in the case of concretes, the matrix phase consists of mortar containing particles of fine aggregate and these particles may have properties identical, or at least similar, to those of the coarse aggregate which is considered to be the included particle phase.

The alternative to the above simplification is to revert to the traditional approach, where the effect of change of mix characteristics for concrete made with a given grading and type of aggregate is studied by varying the water/cement ratio and/or aggregate cement ratio and/or grading. It is considered, however, that such an approach will not lead to a fundamental understanding of the problem.

Thus, in spite of the apparent limitations, the choice of mixes for the present investigation is based on a simplification into two phases, as described above, with the mortar being defined as containing all material passing a 3/16" sieve.

Even assuming such a simplification, changes in the grading of aggregate which are unavoidable when changing the proportions of constituent in normal concretes, may tend to obscure the fundamental behaviour of the material. Therefore, in order to obtain clear patterns of response for different mixes, a series of realistic concretes with idealised gradings (hereafter referred to as 'idealised concretes') has been adopted. Such concretes, consisting of regularly shaped coarse aggregate particles embedded in a fine sand/cement matrix, are in fact examples of gap-graded mixes.

It has been shown [14, 15] that the fracture processes occurring within idealised two-dimensional models of such gap-graded concretes under stress are, for a given mortar matrix and type and shape of aggregate, mainly dependent on the volume fraction of aggregate.

It has also been demonstrated that the behaviour of these simplified two-dimensional models (containing various geometrical arrangements and concentrations of single-sized aggregate particles) accurately predicts the overall behaviour under uniaxial compression of the three-dimensional two-phase concretes [57]. A gap-graded concrete containing various volume fractions of a single-sized irregular aggregate (flint river gravel) in a fine mortar matrix also behaved in a similar manner, but with the fracture processes starting at a slightly earlier stage [15].

The above approach, using simplified models of concrete, has provided fundamental answers to many questions regarding the failure of concrete under uniaxial compression which would have been almost impossible to

answer using specimens of normal concrete.

As a result, it has been decided to use the same approach to investigate the fracture processes occurring when concrete is subjected to triaxial stress. To the Author's knowledge, these processes have, hitherto, not been examined in detail for concrete and, therefore, before testing real concretes with all their complexity it would seem logical to evaluate trends in behaviour using simplified models.

The idealised mixes, which have been chosen to complement the two-dimensional model tests which have been carried out in conjunction with the present programme [14, 15] are described in 7.5.1. and Appendix 3.

Having established patterns of behaviour for the idealised concretes, the work is extended to investigate the behaviour of concretes likely to be representative of the range of mixes which might be encountered in practice. The mixes (hereafter referred to as real concretes) have been chosen in order to examine as many parameters as possible in an efficient manner such that the behaviour of intermediate cases can be inferred by interpolation. The choice has been facilitated by consideration of the results obtained from the idealised concrete series. Full details of the mixes are given in 7.6.2.

7.2.2. Curing Conditions

In many investigations concerned with the behaviour of concrete under short-term loading, specimens in a saturated condition are tested after being cured under standard conditions. This regime of treatment prior to test is unlikely, however, to be representative of the conditions obtaining in most structures. The environment within which many structures, or parts of structures, are likely to be situated will probably lead to the concrete attaining a dehumidified state, in equilibrium with the normal ambient surroundings.

The curing conditions used for the specimens for the triaxial test series have been chosen to simulate, as far as possible, those in real structures. To achieve this the specimens are cured under B.S. conditions [62] for twenty-eight days and then allowed to slowly dry to laboratory ambient conditions in a further period of three weeks. After three weeks the specimens are stored in the laboratory atmosphere (approximately 20°C and 65% R.H.) for a period in excess of ten months until tested.

7.2.3. Specimens

Since the maximum size of aggregate in the mixes is $\frac{3}{4}$" it is considered that the following cross-sectional dimensions of specimens will provide representative volume elements of concrete:-

Test Specimen	Minimum Cross Section
Cube	4" x 4"
Direct Tensile	4" x 3"
Cylinder	4" diameter

For all specimens, it is ensured that the direction of maximum compressive, or minimum tensile stress coincided with the vertical direction as cast. Thus any anisotropy [130, 131] should result in the same relative effects for all states of loading. In order to achieve this, it is necessary to test the cubes without turning them on their sides as specified in B.S. 1881 [62].

The shape of the direct tensile specimens is identical to that adopted by Ward [6] which is based on a 4" x 4" x 20" flexural test piece. For the cylindrical specimens used in the uniaxial and triaxial test series a height/diameter ratio of 2.5 has been chosen, following the recommendations given in Chapter 2.

7.3. Apparatus and Methods of Testing

7.3.1. Measuring and Recording Systems for Stresses and Strains

As stated in 7.1. the main aims of the test programme are to study the complete deformational response of specimens of concrete when subjected to a given loading system or pattern, and to identify levels at which significant changes in material response occur. It is considered essential that to achieve the above aims (a) strain measurement should be made accurately with (b) a high degree of sensitivity, (c) in zones of specimens where the stress or strain state is uniform and definable and (d) that the strains, together with the conditions of applied boundary stress, should be recorded continually throughout the loading process.

To fulfill the above requirements, electrical resistance strain gauges have been used, with a gauge length of 60 mm. This length is more than adequate for measuring average, rather than local, strains for the maximum size of aggregate ($\frac{3}{4}$") used in the concretes tested (see 2.6.2.1.).

For tests in which large deformations are likely to occur, the post-yield type of gauge is adopted. This type of gauge is suitable for strains up to 25%. For low order strains (up to 2%) ordinary strain gauges are used.

At the outset of the programme it was thought essential to continuously record stress and strain data in analogue form, to enable any changes in behaviour to be identified. To this end a multi-channel pen recorder (Rikadenki Type B.641) was used, in which voltage changes are recorded on a strip chart moving at a given speed. The system was capable of a maximum sensitivity of 100 microstrain per inch with an available chart width of 10". The effective range of the recorder was extended above the 1000 microstrain equivalent to the available chart width, without sacrificing sensitivity, by feeding in a reverse voltage step, approximately equivalent to 1000 microstrain (10" of pen movement), when the pen had traversed the chart. 250 steps were provided, giving a total strain capacity of 250000 microstrain (25% strain).

A limited number of tests were carried out using the above system and these demonstrated the accuracy, sensitivity and rapid response of the apparatus when measuring large or small strains. In spite of the obvious advantages of such a method of data recording, difficulties were experienced in transcribing the data for further analysis and presentation. This proved to be an extremely time consuming process of scaling by hand and, as a result, a decision was taken to perform the remainder of the tests using a digital data logging system with its simpler form of presentation.

A Peekel automatic data logger using a.c. bridge energisation was available for the tests, and this system is capable of recording strains to a resolution of $\pm$ 1 microstrain. A high accuracy ($\pm$ 5 microstrain in 5000) is claimed by the manufacturers of the instrument, and checks prove that this can be achieved with excellent stability. The data is recorded digitally on printed paper strip at a maximum recording rate of 1 channel per second.

During the course of the test series the logger became subject to intermittent but frequent problems caused by faulty reed relays. The effects of the faults were generally such as to prevent any data being recorded, but did not impair the accuracy of any strains which were recorded between the periods of intermittent malfunctioning.

As a result of the continuing relay difficulties, which the manufacturers could not cure without a long-term redesigning of the system, it was decided to obtain a data logger of proven reliability.

After an extensive study of the available logging systems, the final choice was a Modulog manufacturered by Intercole Systems Ltd. The apparatus uses semi-constant current d.c. energisation and is, therefore, not subject to problems of capacitive unbalance as found in a.c. systems. The apparatus is capable of recording data simultaneously in printed and punched tape form, at a rate of 10 channels per second. Using high stability fixed bridge resistors, specified by the Concrete Materials Research Group, for the channels used for recording strain, the system is capable of reading to an accuracy of 2 microstrain in 5000, with a resolution of 1 microstrain. Such an accuracy can be guaranteed since the logger is calibrated before, and checked for drift after, each test.

7.3.2. Cube Tests

7.3.2.1. Apparatus

An Amsler 300 Tonf. testing machine and hydropacer control unit are used for the tests which are performed on 4" cubes (see Appendix 1). Proving tests were carried out on the spherical seating/upper platen unit of the loading frame using a device developed by Sigvaldason to measure slip in spherical seating units [4], and also a strain gauged 4" x 4" x 12" aluminium proving prism to assess eccentricity of loading. The results indicated serious deficiencies in the behaviour of the system in that the main requirements of a self-aligning loading device were not fulfilled [63], namely, that (a) the device did not align itself to the specimen surface after a small initial application of load and (b) it did not remain fixed throughout the loading regime, but appeared to slip at intervals.

In view of the above, a subsidiary platen/spherical seating unit was designed in order to test specimens of 4" x 4" cross section or 4" diameter and to overcome the above problems. Hardened steel subsidiary platens with a thickness of 1" and the same cross-sectional dimensions as the nominal cross-section of the specimen to be tested (see 2.6.), and a spherical seating unit whose male and female halves together formed a 4" diameter cylinder, are used. The lower subsidiary platen is accurately dowelled to the centre of the lower machine platen to facilitate setting-up. The upper platen and seating unit can be easily and accurately located using the

surface of the specimen itself. It should be noted that the same basic design is incorporated in the triaxial cell and used for 'compression' tests.

The general arrangement of the cube in the testing machine is shown in Figure 7.1.

7.3.2.2. Method of Tests

The cubes are aligned in the testing machine using the specially developed platens and spherical seating unit. Load is applied at a constant rate of stress of 2000 lb./in.^{2} per minute [62] using the Amsler control system fitted with a load-pacer unit. Three specimens are tested for each mix and the cube strengths calculated from the maximum load, recorded by a slave pointer on the load indicator dial, and the measured average cross-sectional dimensions of the specimens prior to test.

7.3.3. Direct Tensile Tests

7.3.3.1. Apparatus

The direct tensile testing machine developed by Ward [6] is considered fundamentally the most suitable loading device for the tests. However, trial tests using this apparatus demonstrated a number of operating difficulties liable to reduce the accuracy of any results obtained. These deficiencies, together with the remedial modifications carried out to minimise them, are summarised in the following:

(i) The hydraulic loading ram was pressurised by a two-cylinder pump via a needle-valve control circuit. This led to uneven loading rates. To improve control the complete system has been removed and the ram connected to an Amsler Hydropacer unit which enables accurately constant loading rates to be automatically maintained.

(ii) Load measurement was effected by a pressure gauge. This is not considered sufficiently accurate, or suitable, for continuous recording of load. For increased precision a sensitive load cell, incorporating an electrical resistance strain gauge bridge, has been designed and used to measure directly the axial load on the specimen. The output of the load cell is recorded by an automatic data logger.

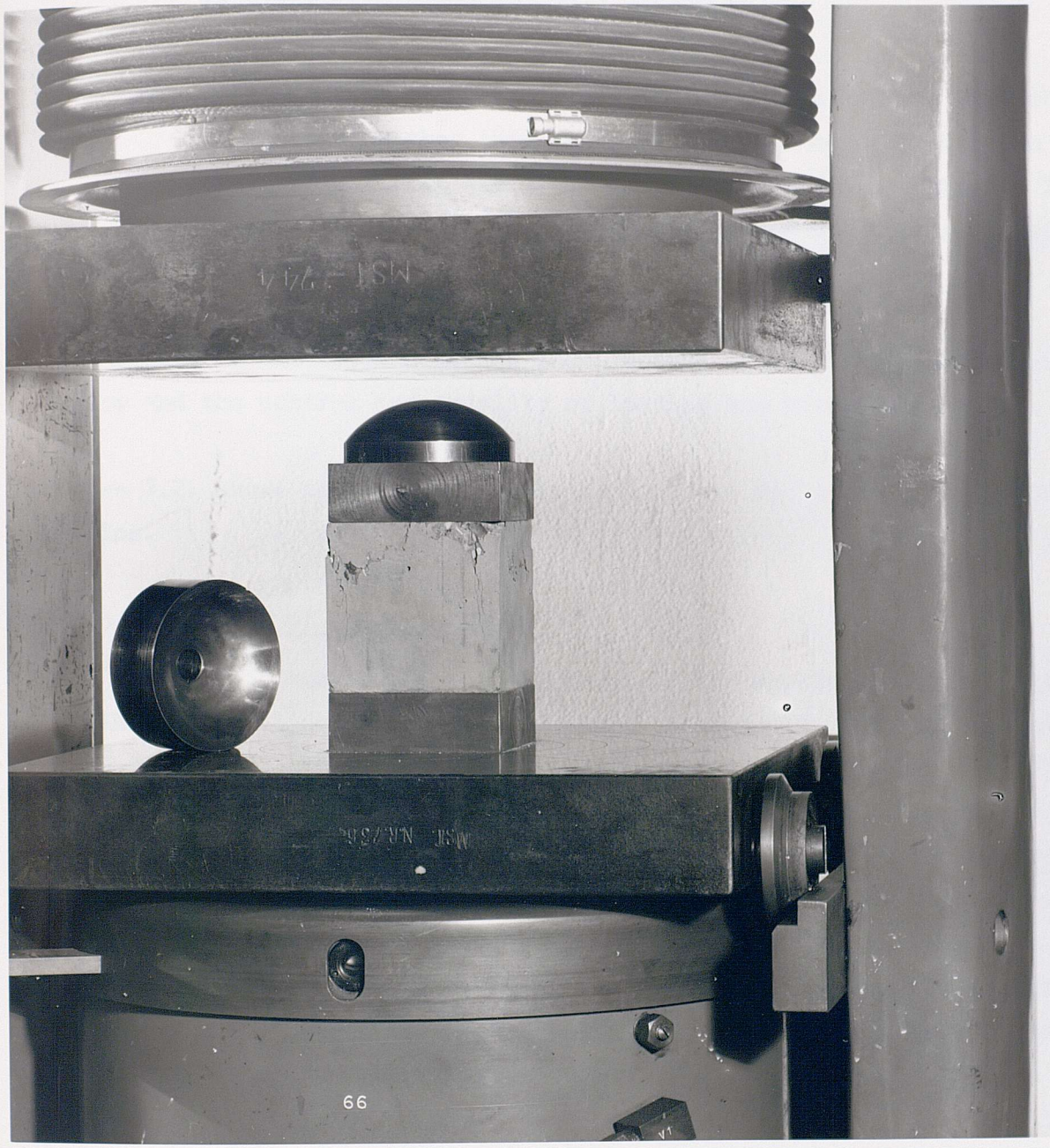


Figure 7.1. View showing arrangement of cube in testing machine.

(iii) Axiality of loading was extremely difficult to achieve due to general 'looseness' of the gripping devices. Alignment has been improved by fitting spacers and locating washers, where required, to reduce the excessive free movements.

(iv) Many specimen failures indicating eccentric loading were observed. It is thought that this could have been caused by slippage at the specimen/grip due to insufficient surface roughness. To remedy this series of parallel serrations has been machined on to the grips.

As a result of the above measures the specimen is more easily set up in the device and the control and axiality of loading has been improved.

Figure 7.2. shows the general arrangement of the specimen in the testing machine.

7.3.3.2. Method of Testing

Care is taken to ensure correct alignment of the specimen in the testing machine such that no significant eccentric loading is induced, the axiality of loading being checked by comparing the strain values measured on opposite faces of the test specimen. The load is applied automatically at a constant rate, equivalent to a rate of increase of tensile stress in the 'waisted' section of 100 lb./in.^{2} per minute. Readings of stress and strain are recorded by data logger at various intervals of time during each test. The failure load is measured in terms of the hydraulic pressure recorded at the Amsler control console, since the reading of the load cell directly measuring load might not be taken precisely at the instant of failure.

As a result of careful setting-up which is facilitated by improvements to the gripping devices (see 7.3.2.), relatively few specimens failed outside the 4" x 3" 'waisted' section (4 out of 51). Results for any specimens in which the failure plane was not entirely in this section have been discarded.

Stress values are calculated from the load cell readings, using a calibration equation obtained from a linear regression analysis, and the average measured cross-sectional dimensions of the 'waisted' section of the specimens. Ultimate strength is calculated from the load recorded by a slave pointer

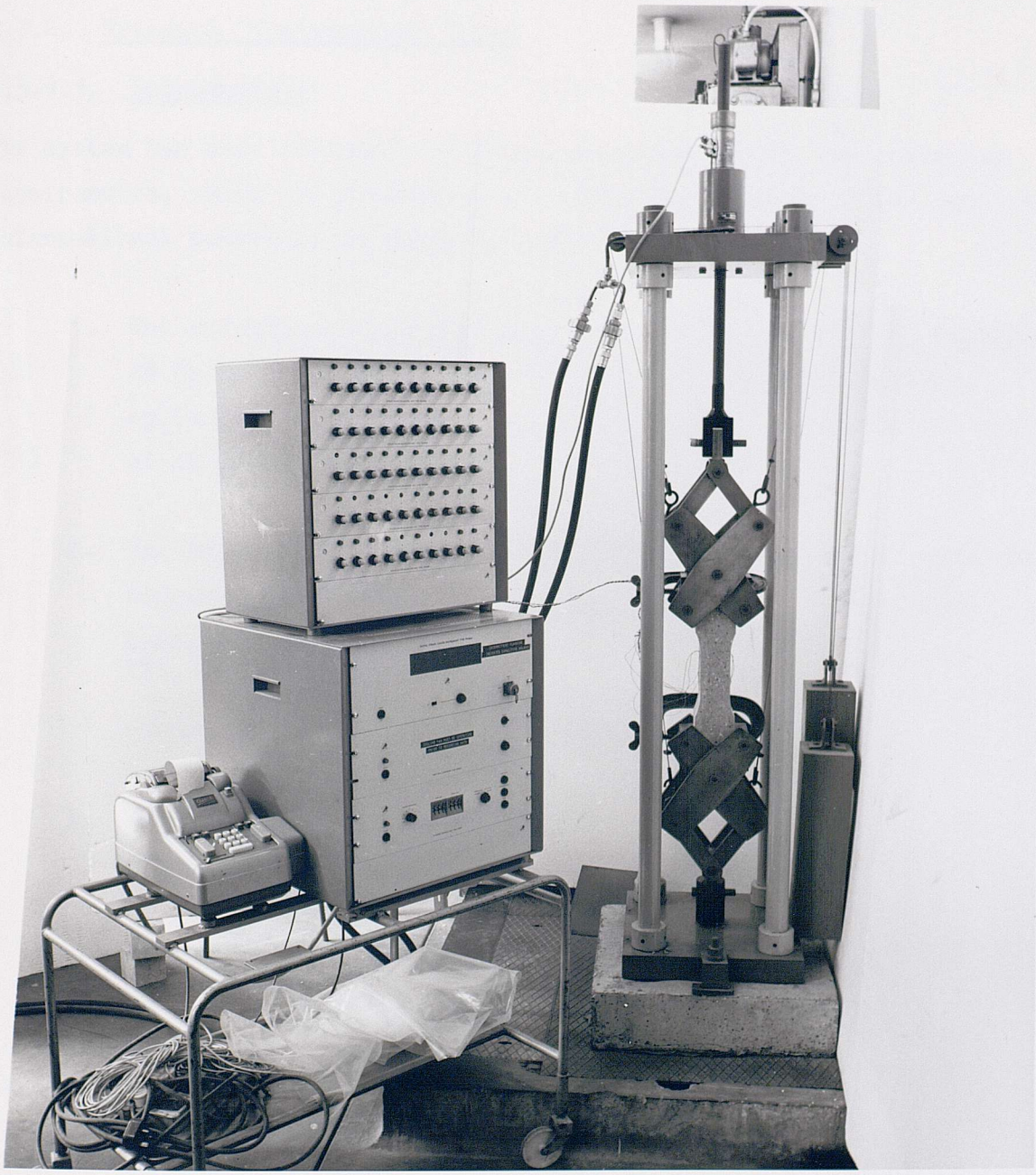


Figure 7.2. General view showing arrangement of direct tension specimen in testing machine.

on the load indicator of the pressure control console. Strain values are corrected for gauge factor.

7.3.4. Triaxial 'Compression' Tests

7.3.4.1. Introduction

The system has been designed and constructed to fulfill the following requirements, which are considered essential for a study of the complete deformational behaviour of concrete under triaxial stress:-

1. The ability to test cylinders of concretes containing aggregates of up to $\frac{3}{4}$" maximum size. This necessitates the use of cylinders of at least 4" diameter with a height/diameter ratio of at least 2.5.

2. The capability of applying confining pressures up to 20000 lb./in.^{2} together with a total axial stress of up to 100000 lb./in.^{2}, a load which previous data (67, 163 to 167, 171 to 173, 179) indicates that various types of concrete can sustain if subjected to this lateral pressure.

3. Facilities for the application and measurement of pore pressure within specimens.

4. Independence of control between the confining pressure and axial loading systems for ease and accuracy of operation.

5. Facilities for the attainment, and accurate measurement of large, as well as small, specimen deformations to a high degree of sensitivity. Previous work (67) indicates that axial and lateral strains of up to 20% can be expected to occur at confining pressures of up to 20000 lb./in.^{2}.

6. Facilities for accurately applying uniform rates of axial stress or axial deformation to specimens.

7. Ease of setting up the specimen and loading system prior to test, and subsequent ease of dismantling without damage to the specimen or apparatus.

The main features of the various units are outlined in the following sections and Appendix 1. Fully detailed working drawings are available from the Concrete Materials Research Group.

7.3.4.2. Triaxial Cell and Control System

The general arrangement of the cell is shown in Figure 7.3. The base unit of the cell contains ducts for drains, pore pressure application and measurement, and electrical leadouts. A barrel unit is attached to the base, by means of locking segments and a retaining ring. This ensures ease of assembly and dismantling since no screw thread is used which would be liable to distortion and subsequent seizure after being subjected to pressure. The barrel unit encloses as pressure chamber which can accommodate 4" diameter x 10" long specimens with associated subsidiary platens and a spherical seating unit. The subsidiary platens and spherical seating unit conform to requirements for loading devices for concrete which have been incorporated in a draft standard for testing machines by a Concrete Society working party of which the Author is a member [3].

An axial load piston of the 'balanced' type, is fitted to the barrel unit to ensure that no resultant force acts on it due to the fluid pressure in the cell. In this way the axial and lateral stresses can be varied independently.

The tests described in 7.4. and 7.5. are 'compression' tests in which the axial compression stress is greater, or equal to, the lateral (confining) pressure. However, the cell is also capable of performing 'extension' or 'tension' tests where the lateral pressure is greater than the axial stress. Details of the modifications to the cell necessary to achieve the latter stress states are described in Chapter 5 and Appendix 6.

The control system for applying and measuring the confining pressure within the cell is shown in Figure 7.4. It has been designed around a modified Budenberg deadweight piston and cylinder assembly. The deadweight assembly, which originally formed part of a pressure calibration unit, is capable of measuring pressure to an accuracy of within 0.5%.

The complete system can automatically maintain pressure to within $\pm$ 20 lb./in.^{2} which is considered permissible for pressures above 2000 lb./in.^{2}. For pressures of 2000 lb./in.^{2} and below, control is effected manually by means of a hand pump. Using this arrangement the pressure can be maintained

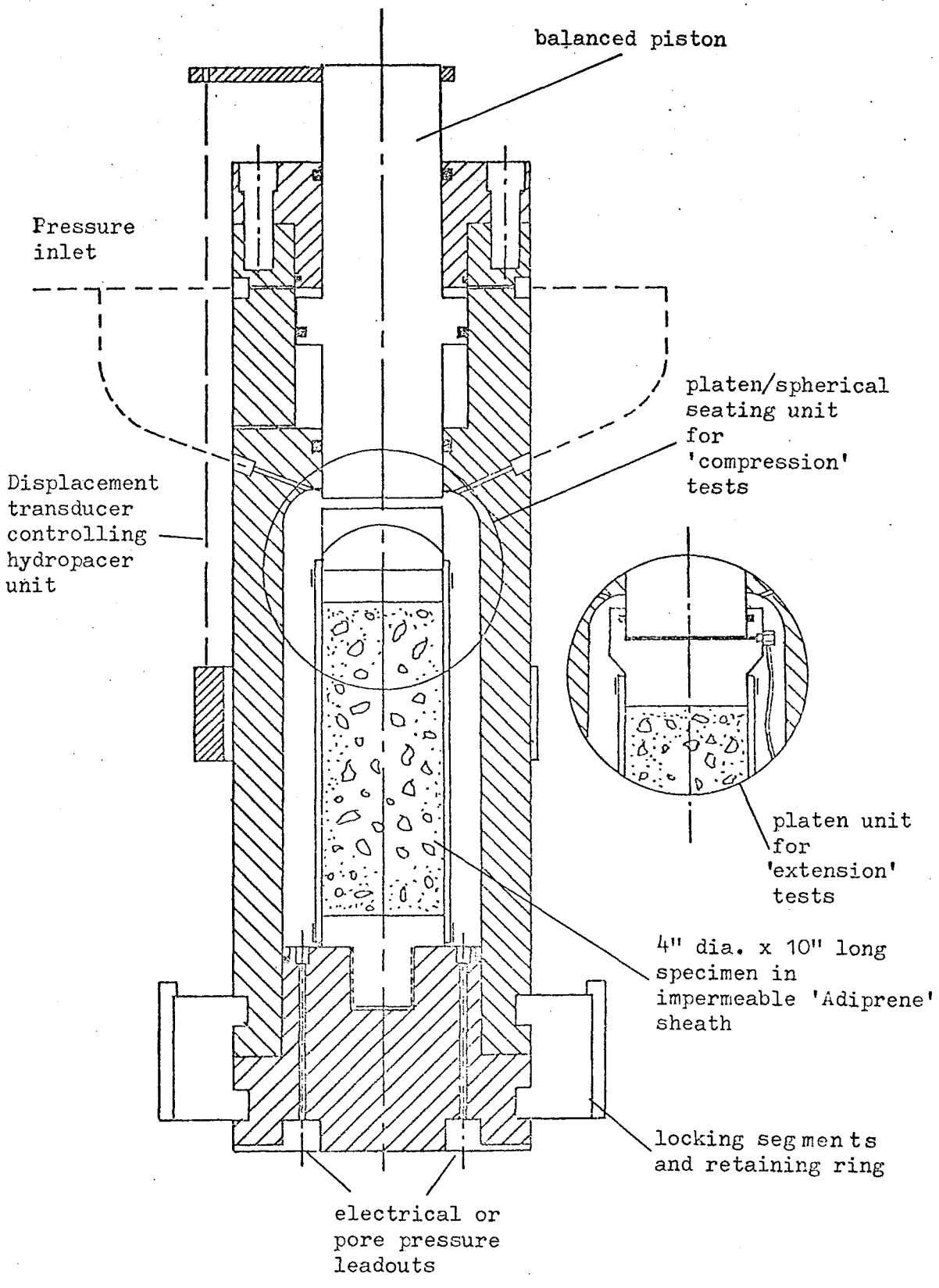


Figure 7.3. General arrangement of hydraulic triaxial cell.

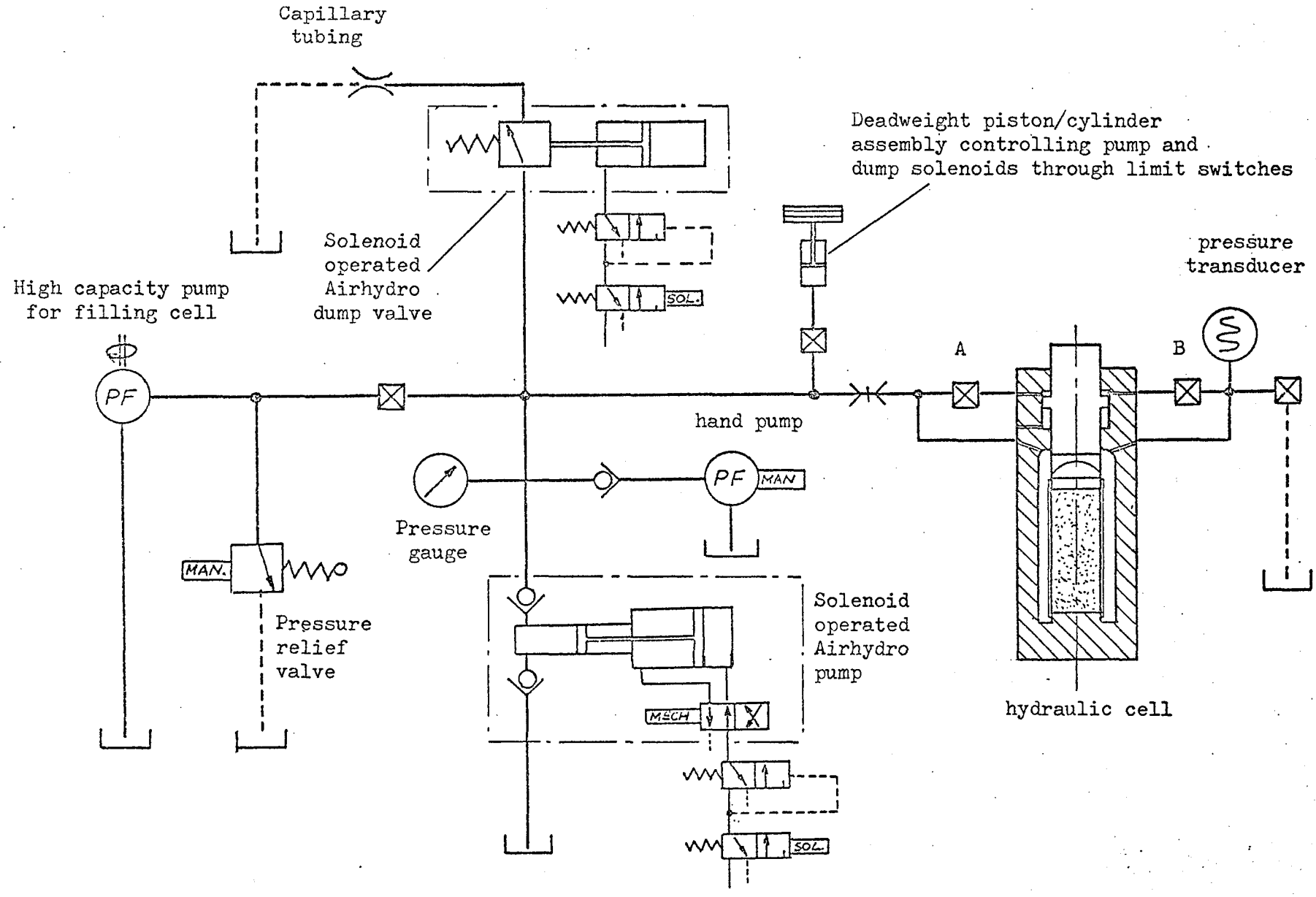


Figure 7.4. Confining pressure control system for triaxial 'compression' tests.

constant to the accuracy of the deadweight unit.

Continuous recording of pressure is possible with a pressure transducer fitted in the hydraulic circuit. The transducer contains an electrical resistance strain gauge bridge network, the output of which can be fed to a logging device.

7.3.4.3. Loading Frame and Control System

The three column loading frame and spherical seating unit, specially constructed to accommodate the triaxial cell, has been designed to have vertical and lateral stiffnesses in excess of those suggested by Sigvaldason [4]. Lifting facilities are incorporated to simplify assembling and dismantling the cell, and an important feature is the moveable lower platen unit which enables the cell to be set up outside the frame and then rolled into the loading position.

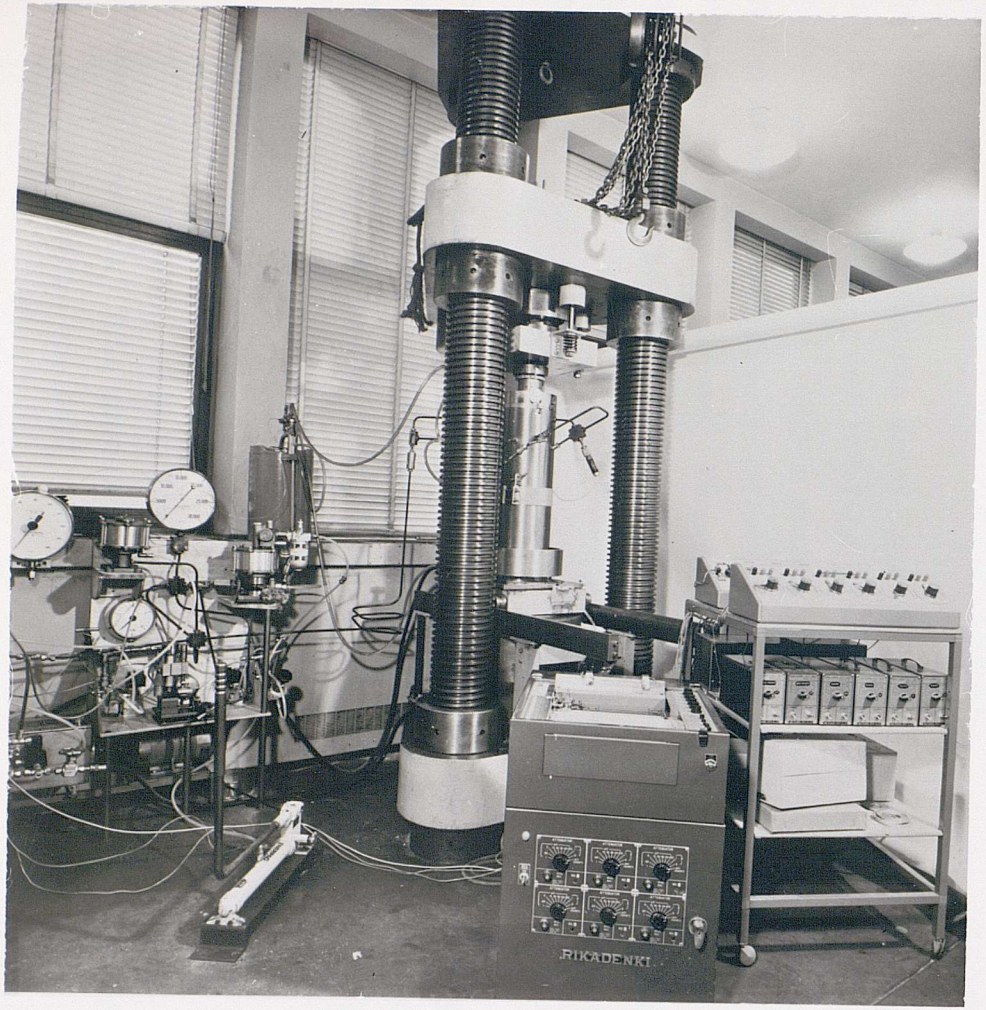
Load is applied through an Amsler Hydrospacer servo pressure unit connected to a 500 tonf. hydraulic ram fixed to the base of the loading frame, and is measured by a pressure transducer connected to the hydraulic circuit. The transducer contains an electrical resistance strain gauge network which can be connected to a data logger.

A general view of the cell assembled on the loading frame is shown in Figure 7.5 . which also shows the layout of the confining pressure and vertical load control system.

The rate of applied deformation to the specimen within the triaxial cell is controlled by the hydropacer unit, from information received from a displacement transducer mounted between the barrel of the cell and piston. This transducer and hydropacer control panel is shown in Figure 7.5(b). Full working drawings of the loading frame are available from the Concrete Materials Research Group.

7.3.4.4. Assembly Procedures

An important factor in the design of the cell is ease of setting-up prior to, and dismantling after, each test. This is achieved by making the specimen, loading platens and spherical seating a detachable unit. This unit, together with the Adiprene impermeable sheath to prevent ingress of oil to the specimen, can be accurately assembled and checked outside the



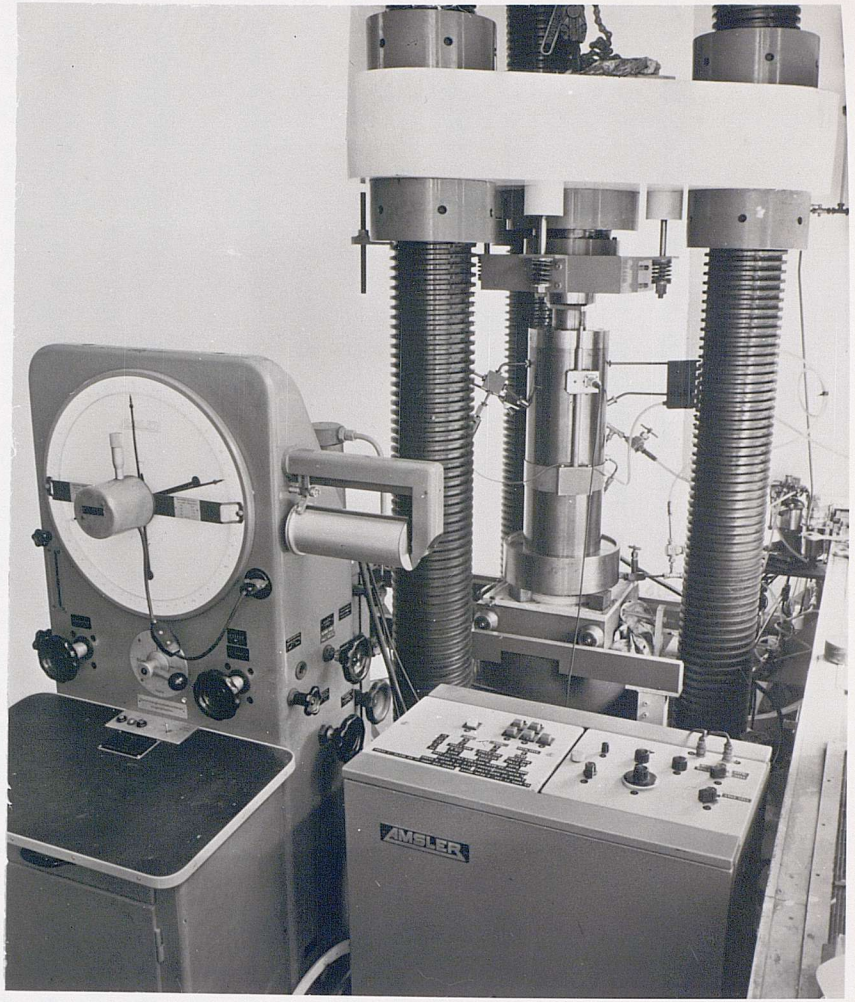


Figure 7.5. General views of hydraulic triaxial cell, loading frame and control system showing confining pressure control system (left) and displacement transducer and servo-control system for deviator load (right).

cell and full details of this process are given in Appendix 6. Figure 7.6. shows the arrangement after completion of the operations.

7.3.4.5. Method of Testing

The loading path used for the tests is shown in Figure 7.7. It is achieved by increasing the confining pressure at a rate approximately equivalent to an increase of strain of 200 microstrain per minute. The maintenance of a constant rate of strain is difficult since the apparatus is not fitted with an automatic servo-control system. After reaching the required maximum value, the confining pressure is maintained constant using the control system. A superimposed axial load is then applied monotonically to the specimen through the cell piston, using the loading frame. A constant rate of specimen deformation is automatically, and accurately, applied by means of a servo system and is equivalent to a rate of increase of axial strain, as measured at the centre of the specimen, of approximately 200 microstrain per minute. It should be noted that as the overall axial deformation of the specimen is monitored, the measured strain rate in the mid-zone of the specimen will vary slightly throughout the test, due to redistribution of strain.

Operation of the automatic axial load servo-control system is extremely difficult to initiate, and involves a lengthy and intricate process of pressure balancing. The process takes a number of minutes to complete and results, in some cases, in relatively large increases of specimen strain under the constant hydrostatic stress. These are particularly evident at high confining pressures for concretes exhibiting high creep rates (i.e. those containing small volume fractions of aggregate and/or high water/cement ratio).

Confining pressure, axial stress, axial and circumferential strains are measured and recorded continuously throughout the test. The test is terminated when the specimen deformation reaches the limit of the cell or when three of the four strain gauges have ceased to function.

After test the axial load is removed slowly and maintained at a low value. The confining pressure is then lowered to zero and the residual axial load completely removed. This procedure has been evolved so that the specimens can be removed from the cell without excessive damage.

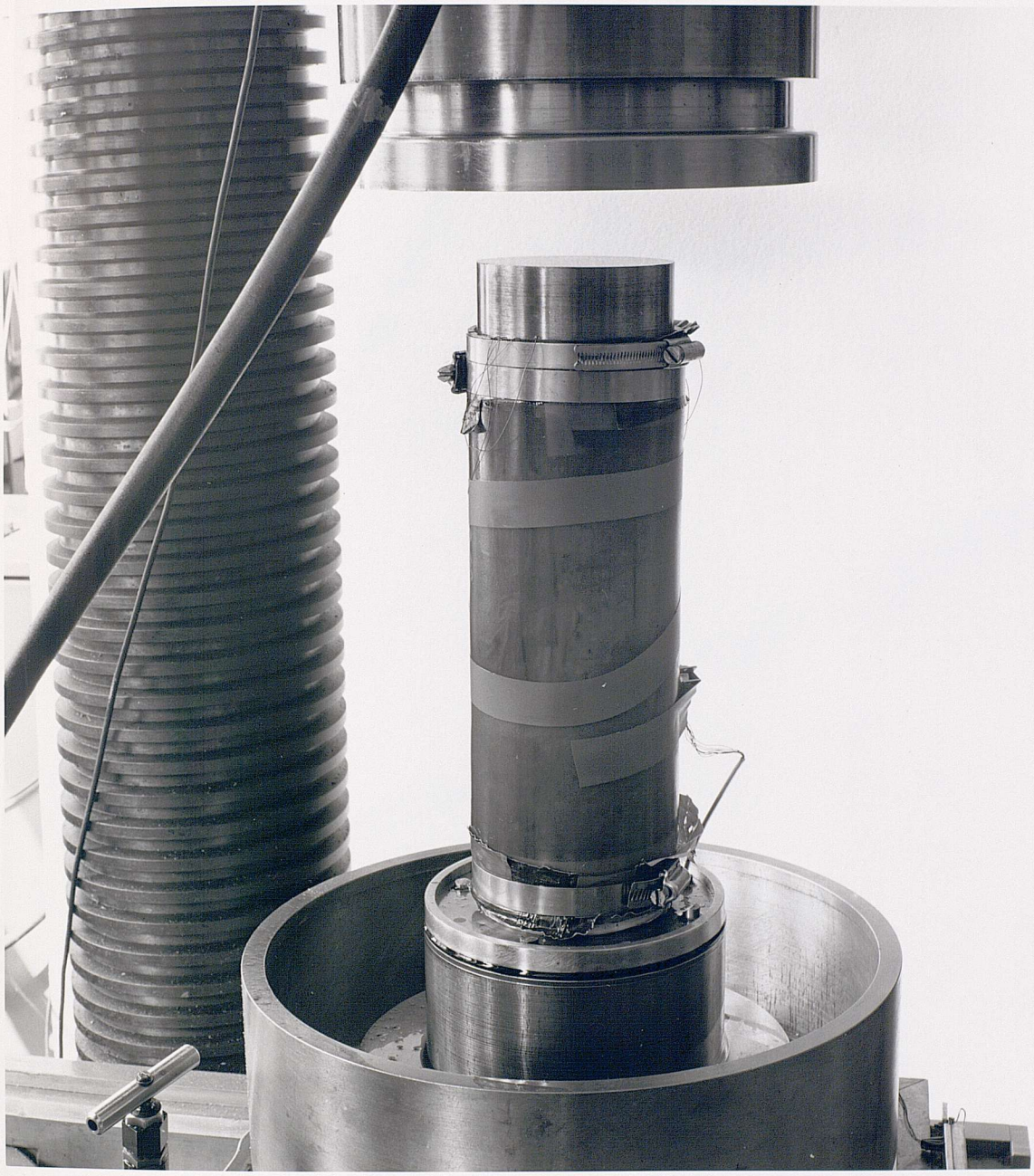


Figure 7.6. View showing arrangement of specimen/platen/sheath unit prepared for a triaxial 'compression' test in the hydraulic cell.

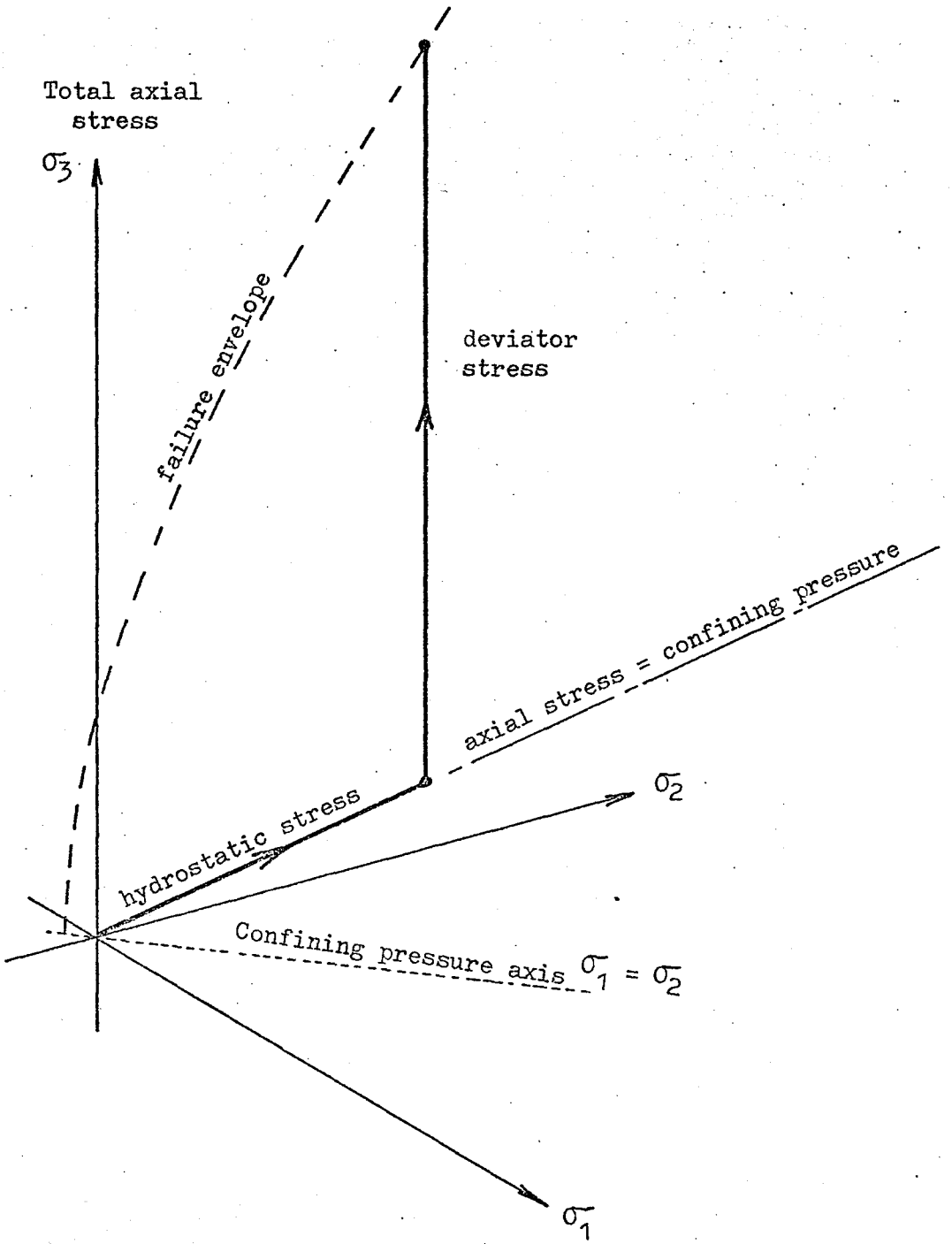


Figure 7.7. Loading path used for triaxial 'compression' tests

After dismantling the cell and specimen/platen assembly, the Adiprene sheath is removed using an extraction device specially developed to avoid damaging the specimen and sheath.

The values of confining pressure are calculated from the pressure transducer readings using a calibration equation obtained from a linear regression analysis.

Nominal values of superimposed axial stress are obtained from the pressure transducer calibration equation, again using the linear regression analysis, with a correction for frictional resistance of the cell piston. The value for friction depends mainly on the position of the piston and the value of applied cell (confining) pressure. Full details are given in Appendix 8.

The actual superimposed value of axial stress acting on the mid-zone of the specimens are calculated from the current cross-sectional dimensions of this zone, as measured by the circumferential strain gauges (see Appendix 5).

Strain values are corrected for gauge factor and also for non-linearity effects associated with a Wheatstone bridge type circuit. Full details of this latter correction, which assumes significance for strains above 10000 microstrain, are given in Appendix 5.

The influence of the confining pressure on the strain gauge readings has been checked by calibration against a material of known compressibility, and found to be negligible (see Appendix 9). No correction factor for this effect is, therefore, required.

7.4. Preparation of Specimens for Test

7.4.1. Introduction

A trial series of tests, in which specimens of a fine mortar were subjected to triaxial compressive loading, produced significant eccentricity of load as indicated by the strain differences across the diameter of some specimens which induced inclined fracture planes during failure [57]. Also, throughout this series, the incidence of early breakdown of the strain gauges reached unacceptable proportions due to the effects of implosion under pressure caused mainly by the presence of voids near the surface of the specimens.

It must be emphasised that a great deal of experimentation has been necessary before a reliable procedure evolved for preparing specimens for test such that these problems are minimised.

The main aims are to:-

(a) achieve uniform loading during each test;

(b) obtain accurate measurements of the axial and lateral strain within the central zone of specimens, from low values up to levels of 25%;

(c) complete each triaxial test without the specimen suffering any ingress of oil before, during or after ultimate failure.

The procedure finally adopted is described in the following.

7.4.2. Casting and Compaction

All specimens are cast in steel moulds conforming to the tolerance requirements of B.S. 1881 [2]. A 4" diameter by 10" long cylindrical specimen has been adopted for uniaxial and triaxial compression tests following the recommendations given in 2.6. Companion uniaxial tension tests are carried out using 4" x 4" x 20" 'waisted' tensile specimens of the type developed by Ward [6] and modified by Vile [8]. For control purposes 4" x 4" x 4" cubes are also cast from each mix.

Full compaction of the concrete in the specimens is attempted using a vibrating table. The cylindrical moulds are filled in three layers, and the cubes and tensile moulds in two layers, each layer being compacted to 'refusal' i.e. until no further significant quantities of air are expelled, or until the surface appearance indicates slight signs of bleeding. The efficiency of the compacting process is clearly demonstrated by reference to the air content of the mixes detailed in Appendix 3.

7.4.3. Curing

Details of the curing process are given in 7.4.3.

7.4.4. Surface Preparation

After removing the specimens from water, the surfaces subsequently to be loaded are ground accurately plane and parallel using a specially adapted surface grinding machine fitted with a diamond-impregnated lens polishing cup wheel. It should be noted that the cubes are tested in a direction parallel to the casting direction and hence the top and bottom surfaces, as cast, are ground. The grinding process is carried out using water as a coolant in sufficient quantities such that no significant thermal gradients are induced which would be liable to affect the properties of the material.

Prior to testing, and after the specimens have been in air for some time, the curved surfaces of the cylinders are sand-blasted to remove all laitence, and to expose all air voids near the surface which would be liable to implosion during the regime of hydrostatic loading.

For all other specimens the laitence is removed by abrasion from the areas to be covered by strain gauges.

Surface irregularities within the areas over which the strain gauges are placed, and over which the connecting wires run, are filled with epoxide resin. Any surplus hardened filler is removed by abrasion, to ensure that the irregularities contain resin only up to the surface of the specimen.

7.4.5. Strain Gauging

60 mm. long 120 ohm electrical resistance strain gauges are used for all specimens, to ensure the measurement of average rather than local material strain. Previous work [8] had indicated that, for concretes containing aggregate up to a maximum size of $\frac{3}{4}$", a 30 mm. gauge length should prove satisfactory and the Author considers that the use of longer gauges is an improvement.

For the triaxial and uniaxial compression test specimens, gauges of the post-yield type are used. These are aligned symmetrically about the centre circumference to measure axial and circumferential strain. Two gauges are used for each direction and placed diametrically opposite each other. The lacquer-covered copper connecting wires are guided along the prepared areas of the surface ensuring no 'kinking' and sufficient 'play'.

For the tensile specimens ordinary 60 mm. gauges are aligned axially and laterally on opposite faces to form crosses with their centres at the geometrical centre of each face.

After gauging, the system is checked for continuity, correct electrical resistance and insulation. For the latter a minimum value of 50 megohm, measured between the specimen and each gauge, is considered satisfactory. The checking process is repeated after the specimen has been assembled and placed in the apparatus with final connections made to the data logger.

7.4.6. Assembly Procedure for Specimen/Platen/Sheath Unit

A series of trial tests indicated that non-axial loading could be caused by the sheath being incorrectly sealed on to the loading platens. The problem was traced to the platens not making even contact with the surfaces of the specimen under load, due to the sheath being extruded during the sealing process.

The assembly procedure developed to overcome these difficulties is described in Appendix 6. Essentially the process involves clamping the platens on the specimen with a light pressure, prior to sealing the sheath on the platens using torque clips. Before the sealing process, the sheath is extruded slightly so that a small amount of prestress is developed which holds the platens in contact with the specimen after removal from the clamping jig, and before being loaded into the cell.

7.5. Triaxial Test Programme for Idealised Concretes

7.5.1. Concrete Mixes

As already discussed, the projects previously carried out by the Concrete Materials Research Group to study the fundamental behaviour of concrete under load have been concerned mainly with two-dimensional models [14, 15]. The idealised mixes designed for the present investigation are intended to be three-dimensional representations of mixes of the same type of gap-graded concrete, with the volume fraction of coarse aggregate being the only intentionally varied mix parameter.

The concretes contain single-sized ($\frac{3}{4}$") spheres of E-glass embedded in a fine mortar matrix, and full details of the constituent materials, mix proportions and fresh and hardened properties are given in Appendices 2 and 3 respectively.

For all concretes the matrix remains the same (and is identical to that used for the two-dimensional models tested in a complementary test programme [14, 15]). Various volume fractions of glass spheres are used, ranging from zero to that equivalent to the closest possible packing in the matrix (approximately 58%). A relatively large number (eight) of different volume fractions has been tested, since the primary object of the series is to evaluate general trends in hitherto unknown behaviour. The series is intended as a prelude to the test series concerned with real concretes. It is hoped that the patterns of behaviour noted for the idealised concrete will lead to (a) a clearer understanding of the mechanisms of failure for concrete, considered as a two-phase composite material and (b) a more efficient test programme from which design data for real concrete can be obtained. This subsequently is proved to be the case.

When received, the glass spheres possess extremely smooth surfaces. These are roughened by tumbling, for a given time, in a rotating cylindrical mill containing carborundum powder. The duration of the tumbling process is predetermined by trials in order to give a final surface finish approximately equivalent to that of normal river-gravel aggregates. After the tumbling process the spheres are carefully washed to remove all traces of dust, and dried.

7.5.2. Cube Tests

7.5.2.1. Results

Three cubes from each mix are tested and the detailed results are given in Appendix 3, and shown in Figure 7.8. in terms of the means and their 95% confidence limits.

The failure modes indicate uniform loading in all cases, with cracking extending up to the specimen/platen interface. Some specimens exhibit a few fractured coarse aggregate particles but in the main the cracking is almost entirely confined to the mortar phase.

7.5.2.2. Discussion of Results

Figure 7.8. indicates an increase in cube strength with volume fraction of aggregate, up to a volume fraction of approximately 34%, after which the cube strength remains essentially constant. This behaviour is similar to that observed by Erntroy and Shacklock [190] for normal concretes where, for a given mix, the strength increases with aggregate/cement ratio. It is to be compared with a reduction in the uniaxial compressive (cylinder) strength with volume fraction of aggregate. A full explanation of this phenomenon is given in 7.5.4., which deals with the results of triaxial 'compression' tests on the idealised concretes.

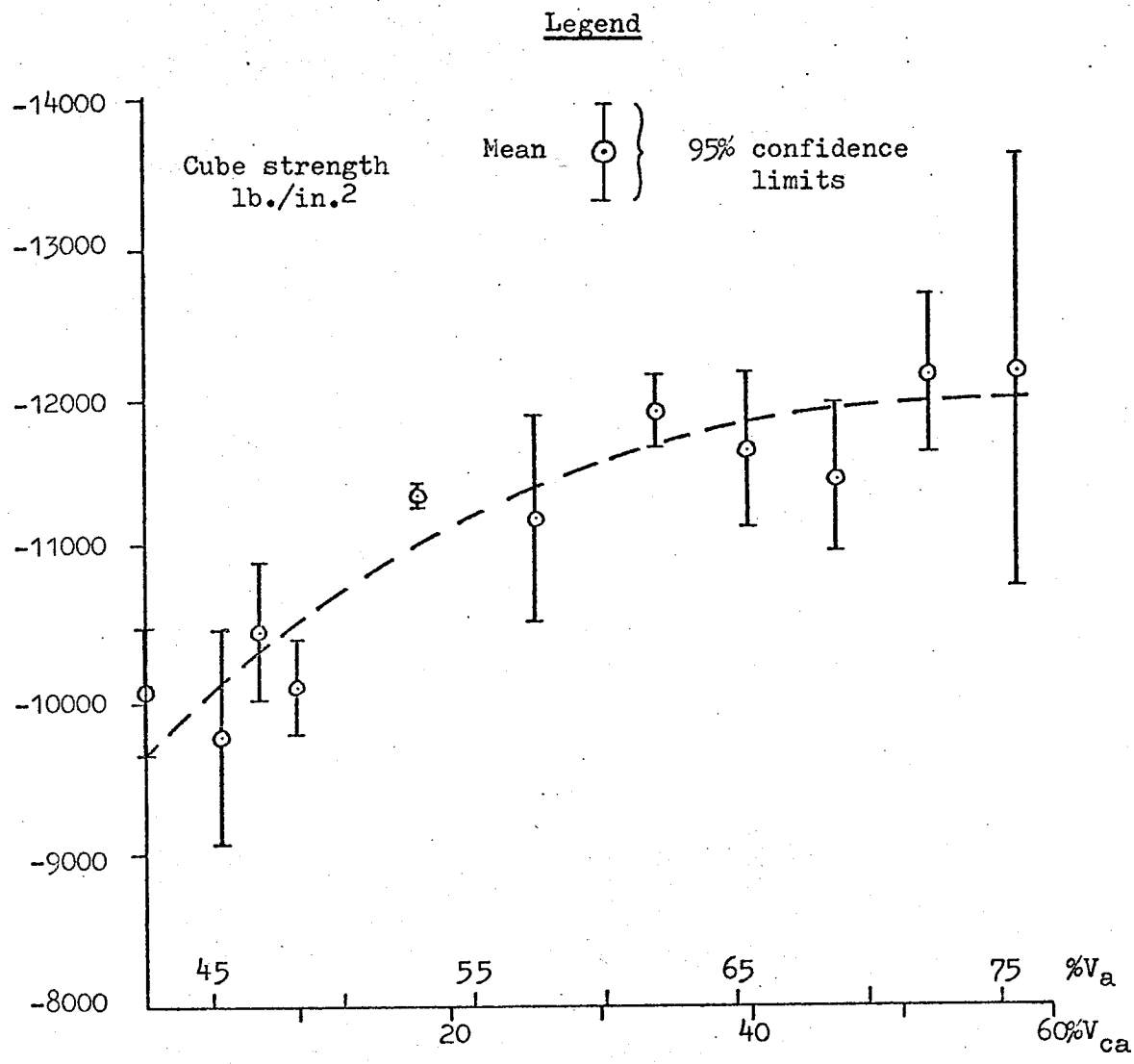


Figure 7.8. Relationship between strength of 4" cubes and volume fraction of aggregate for idealised concretes.

It is to be expected that the concretes containing low volume fractions of aggregate would be subject to a greater variation between samples of the material for those containing a high proportion. A statistical analysis proves this not to be the case, since no significant trends for the within-batch variation are observed. Thus it can be concluded that the aggregate is distributed evenly throughout all mixes, with no significant segregation having occurred during the casting and compacting process.

7.5.3. Direct Tensile Tests

7.5.3.1. Results

Three specimens were tested for each mix and the complete stress-strain relationships for all specimens are stored in the form of computer cards and printouts with the Concrete Materials Research Group where they are available for further analysis. The derived results are given in Appendix 7 and these will be described and discussed in the following sections.

7.5.3.2. Stress-strain Relationships

For all mixes, the axial stress-strain relationships are generally curvilinear throughout the complete stress range, as found by previous investigators (6, 8, 191, 192, 130, 193). No proportional limit, similar to that detected by Kaplan (119), is evident.

In some cases the axial strains increase more rapidly immediately prior to failure which, in all cases, was sudden and without warning. The lateral strains appear to vary almost linearly with stress up to failure, whereas Vile observed distinct non-linearity (8), but are subject to considerable variations of the type noted by Hughes and Chapman (191, 192).

Typical examples of deformational behaviour, for mixes containing low and high volume fractions of aggregate, are shown in Figure 7.9. This indicates the increasing curvature of the axial stress-strain relationship, and clearly demonstrates the increasing stiffness of the concrete, as the content of relatively stiff aggregate is increased. Similar behaviour has been noted by previous workers (6, 130).

This increasing stiffness is also illustrated by Figure 7.10. which shows the variation of secant 'E' value at $\frac{1}{3}$rd of ultimate stress with volume fraction of aggregate. The value increases from approximately 4×10^6 lb./in.^{2} for pure mortar matrix to about 7×10^6 lb./in.^{2} for the mix containing 58% of coarse aggregate by volume. Similar increases have been measured by Hobbs (194) for a concrete tested under uniaxial compression.

The variation of secant Poisson's ratio at $\frac{1}{3}$rd of ultimate stress with V_{ca} is also shown on Figure 7.10. In this case the value increases only

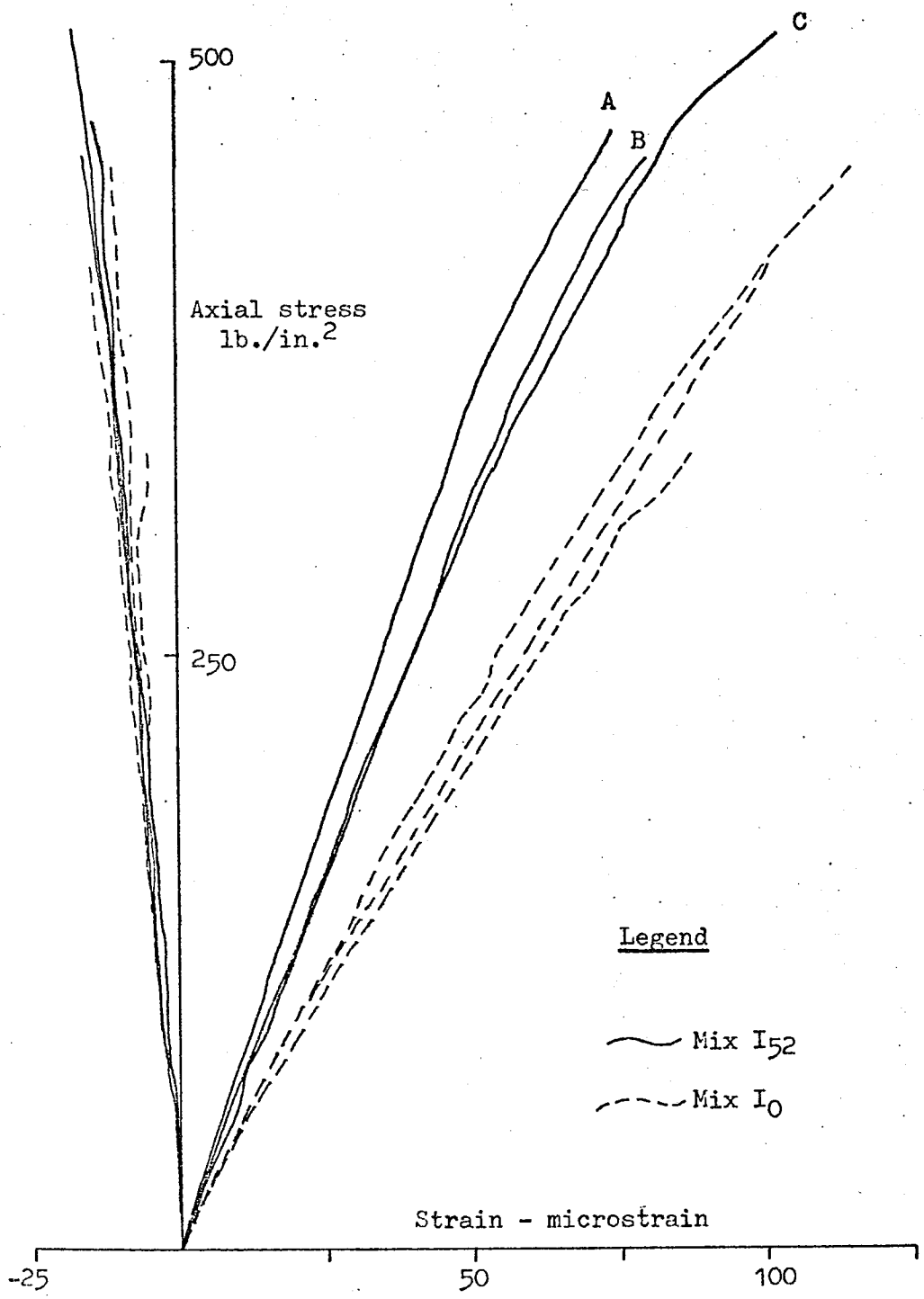


Figure 7.9. Variation of axial and lateral strains with axial stress for mixes I_0 and I_{52} under direct tension.

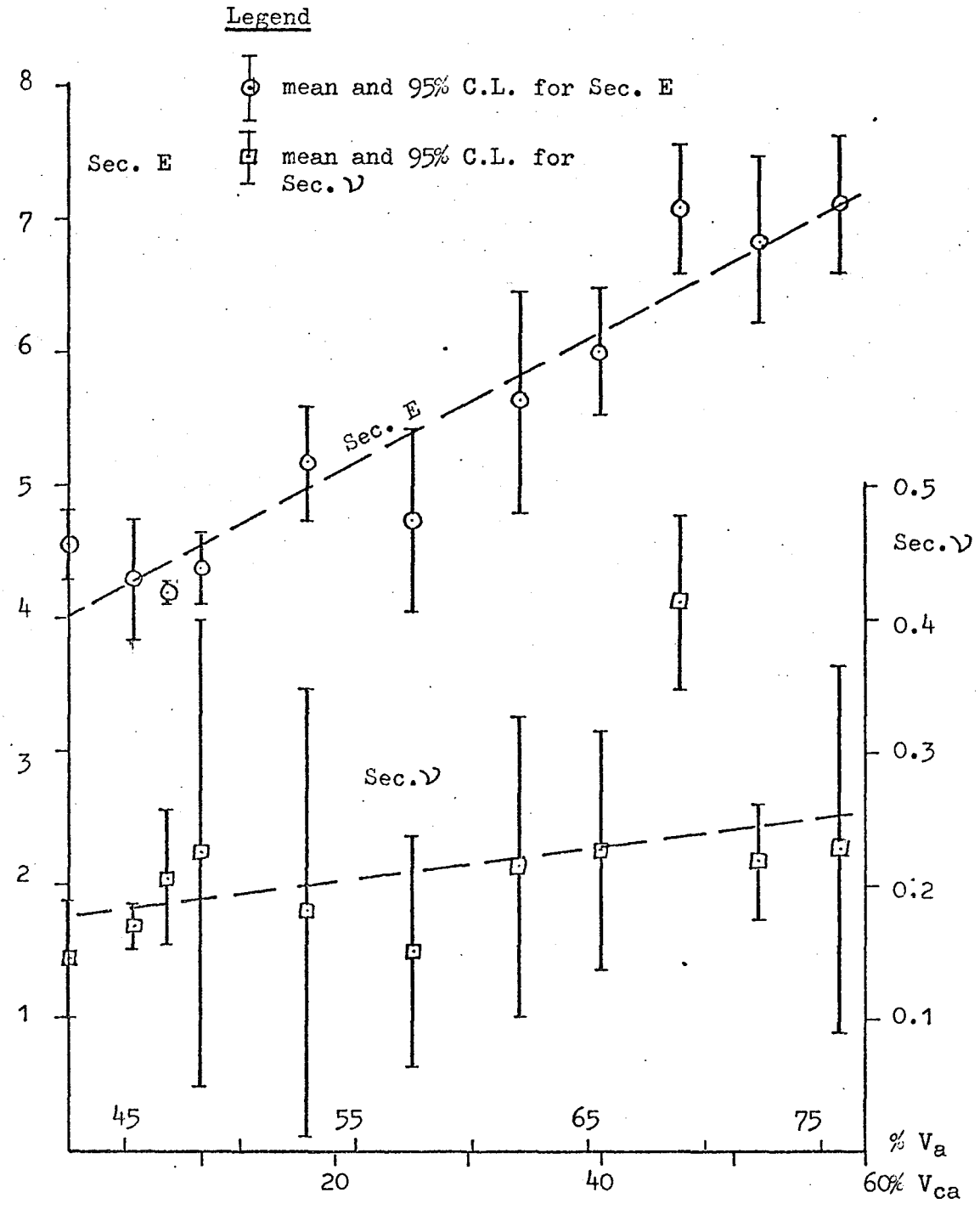


Figure 7.10. Relationships between secant E and ν values at a stress level of $\frac{1}{3}$rd ultimate with volume fraction of aggregate for idealised concretes under direct tension.

slightly with increasing coarse aggregate content, but the increase cannot be considered highly significant.

This observation is in conflict with the results of Anson [79] who measured a decrease in static Poisson's Ratio with volume fraction of aggregate for concretes loaded in uniaxial compression. Anson's results are supported by those given for the idealised concretes when loaded in uniaxial compression, or under triaxial compression with low confining pressures (see 7.5.4.3.). No explanation has been found to account for the reversal in trend for uniaxial tension since, as concluded by Anson for compressive loading, it would be expected that the relatively stiff particles of aggregate would restrain the lateral movement of the composite below that of either of the main constituents. It must be re-emphasised, however, that the lateral strains are of an extremely low order (between 3 and 7 microstrain at the level of stress considered) and the measuring system insufficiencly sensitive ($\pm$1 microstrain) for much significance to be attached to the variations in Poisson's Ratio (see Figure 7.10).

7.5.3.3. Onset of Stable Fracture Propagation (o.s.f.p.)

The procedure described in Section 4.5.3.1. is used to evaluate the onset of stable fracture propagation for the specimens. The technique, which for uniaxial loading is equivalent to detecting a change in the tangent value of 'Poisson's Ratio', indicates for the majority of cases significant void formation prior to ultimate failure. Figure 7.11. shows the variation of stress at this level, and indicates a slight increase in the stress with an increase in V_{ca}. For all mixes, however, the stress at onset of stable fracture propagation remains approximately 85% of the ultimate strength.

The variation of axial and lateral strains at o.s.f.p. is shown in Figure 7.12. A distinct decrease of the axial strain from about 85 microstrain for the pure mortar matrix, to approximately 59 microstrain for 58% of coarse aggregate is apparent, whereas the lateral strain remains essentially constant at -12 microstrain. As a result of the above strain changes, the value of volumetric strain at o.s.f.p. decreases with increasing V_{ca} as shown in Figure 7.13.

The above observations are to be compared with the results of other investigations [8, 119, 131, 195, 196] where the onset of cracking has been detected at stress levels of between 40% and 100% of ultimate depending on the volume fraction, size and type of aggregate and rate of loading.

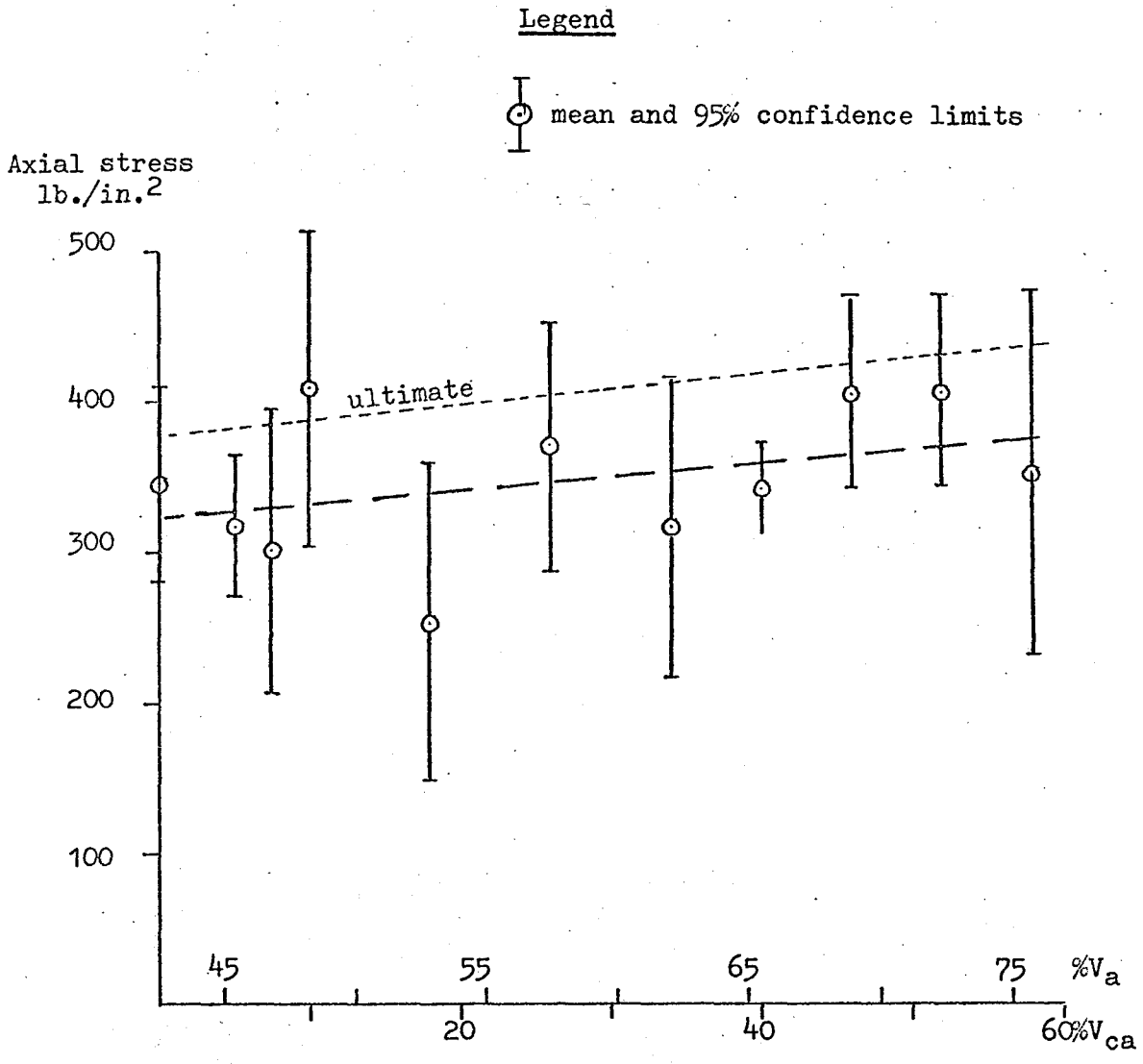


Figure 7.11. Variation of stress at o.s.f.p. with volume fraction of aggregate for idealised concretes under direct tension.

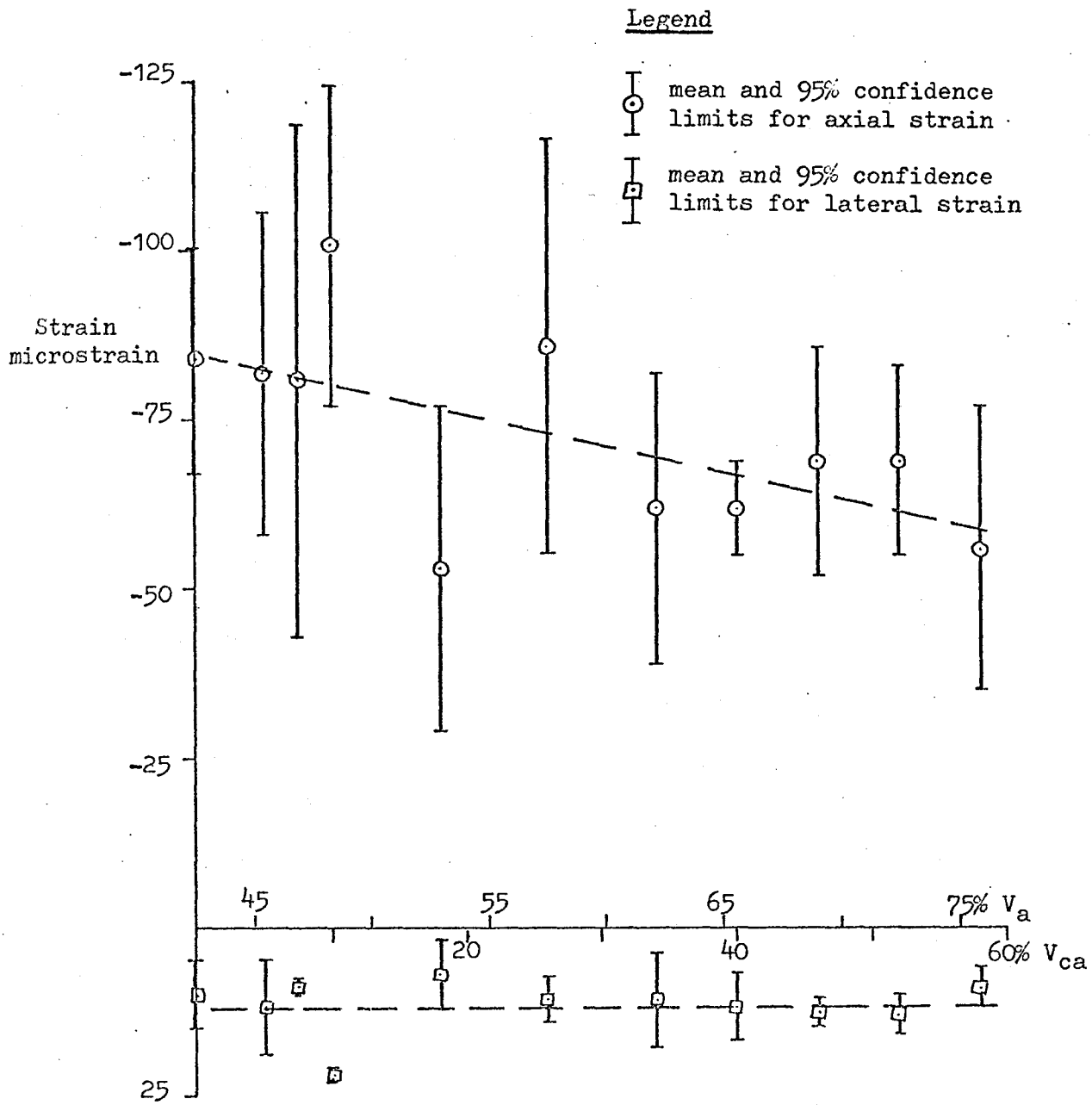


Figure 7.12. Variation of axial and lateral strains at o.s.f.p. with volume fraction of aggregate for idealised concretes under direct tension.

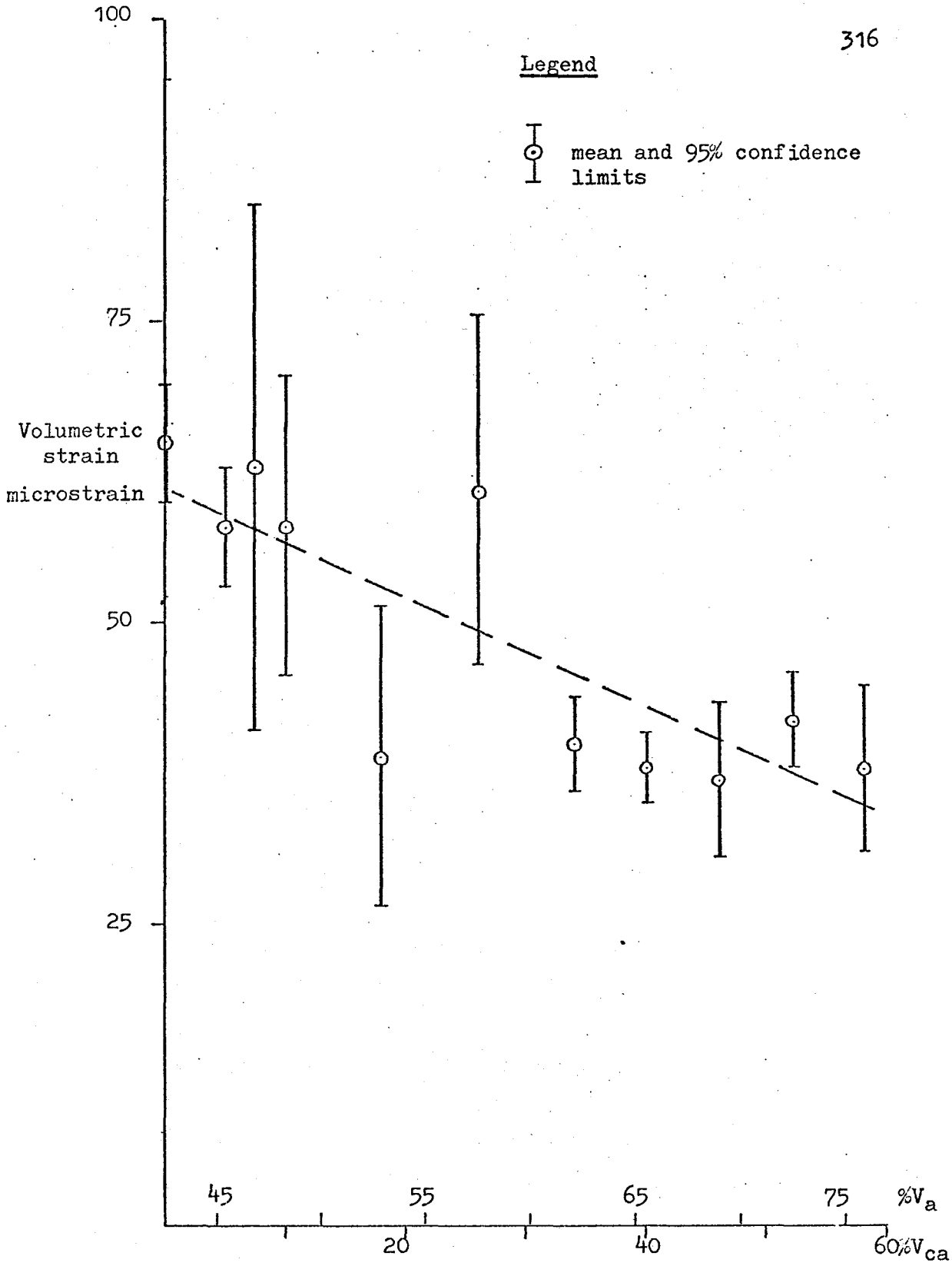


Figure 7.13. Variation of volumetric strain at o.s.f.p. with volume fraction of aggregate for idealised concretes under direct tension.

A summary of these investigations is given in Table 7.1.

7.5.3.4. Volume Changes

Figure 7.14. shows volume changes measured for typical mixes containing low and high volume fractions of aggregate. The curves show that the volume increases continually throughout the test (as compared with a decrease followed by a superimposed increase exhibited under compressive loading), and that smaller volume increases are given for the mix containing a higher proportion of relatively stiff aggregate.

Another feature of the curves is the increase in the rate of increase of volume as the load is increased. Similar behaviour has been noted by Stroeven [131], and by Cotsovos [21] for triaxial 'extension' tests.

7.5.3.5. Ultimate Stresses and Strains

Figure 7.15. shows the variation of ultimate strength with V_{ca}. A relatively insignificant trend is apparent, the strength increasing only slightly with increasing coarse aggregate content. It would be expected that the increasing heterogeneity of the mix would give rise to greater local interparticle strain concentrations which, in turn, would lead to cracking being induced at a lower stress level. Similar behaviour has been noted by Johnston [193] who noted that the tensile strengths of low workability mixes were essentially independent of the aggregate/cement ratio for constant workability. Tests carried out by other workers [119, 6, 8, 196] however, have indicated decreased stresses and strains at, or near, ultimate for increases in V_{ca} in a given mortar matrix. Figure 7.16. does, in fact, show a decrease in axial strain with V_{ca} from approximately 105 microstrain for the pure matrix, to about 77 microstrain for a V_{ca} of 58%. This is similar to behaviour previously noted [119, 8] where the strain varied from 100 to 50 microstrain for a similar variation of V_{ca}.

No significant conclusions can be drawn from the variation of lateral strains, also shown in Figure 7.16. since they are subject to wide variations due to the relative insensitivity of the strain measuring techniques compared with the extremely low strain levels measured.

It can be seen that the variability of stresses at ultimate is considerably greater than observed in the cube tests (see Figure 7.15.). This is probably due to the differences in the mechanism of failure for the two

Investigator	Method of Detection	Cracking Stress as a proportion of ultimate	Main Conclusions
Kaplan (119)	Proportional limit of axial stress/ strain curve	60 - 68%	σ cracking/σ ultimate decreases with increasing V_a
Vile (8)	USPV	60 - 84%	σ cracking/σ ultimate decreases with increasing V_{ca} for given s/c ratio. Cleavage strain at discontinuity varies from 40 to 100 microstrain.
Jones (195)	USPV	68 - 85%	σ cracking/σ ultimate increases with increasing rate of stressing.
Hughes and Ash (196)	USPV	40 - 100%	σ cracking/σ ultimate decreases with increasing size and roughness of aggregate. Cracking and ultimate coincident for cement paste.
Stroeven (131)	Increase in Poisson's Ratio	60 - 80%	No further details given.

Table 7.1. Summary of investigations into the behaviour of concrete under direct tension.

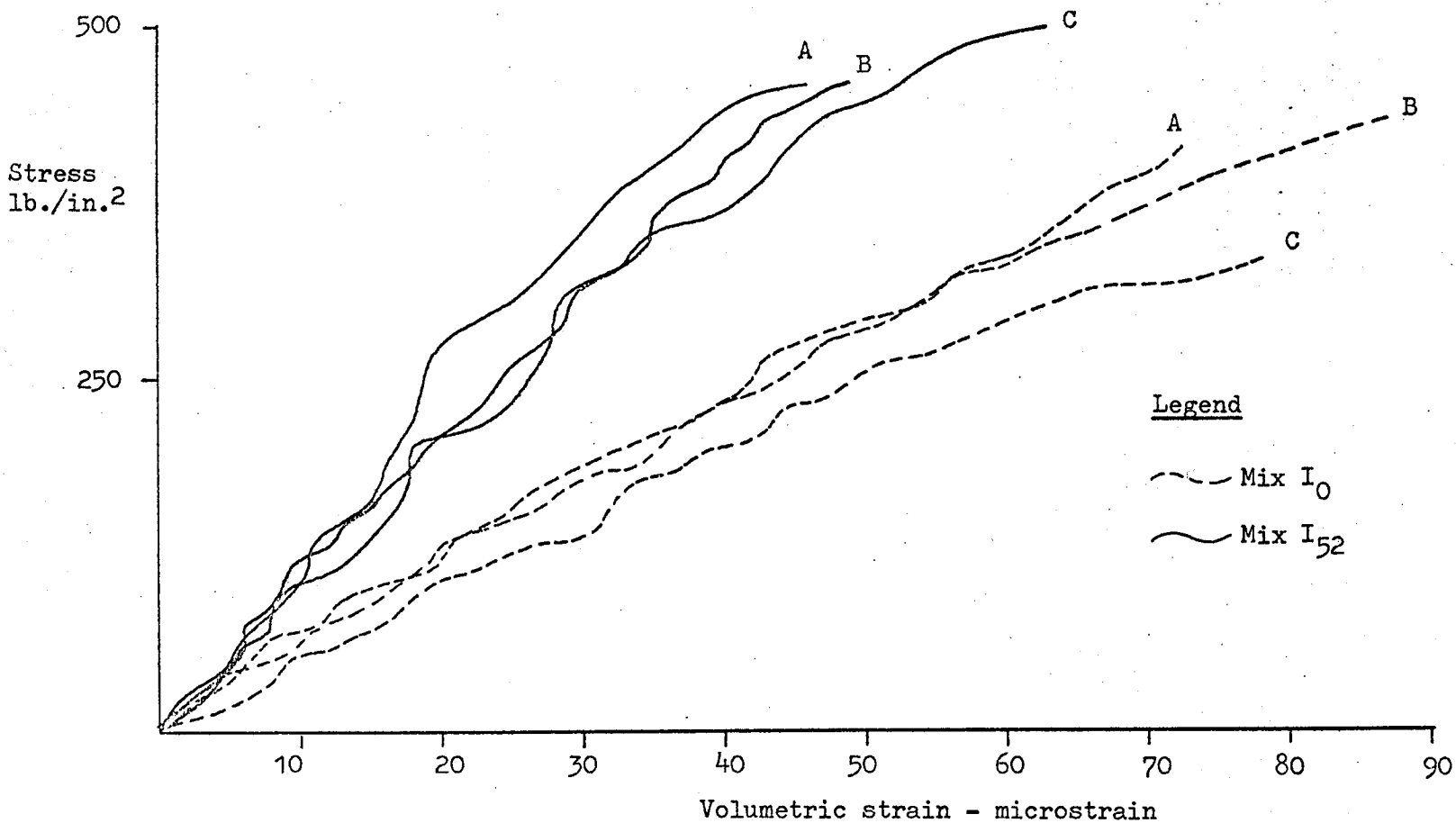


Figure 7.14. Variation of volumetric strain with axial stress for idealised concrete mixes I_0 and I_{52} under uniaxial tension.

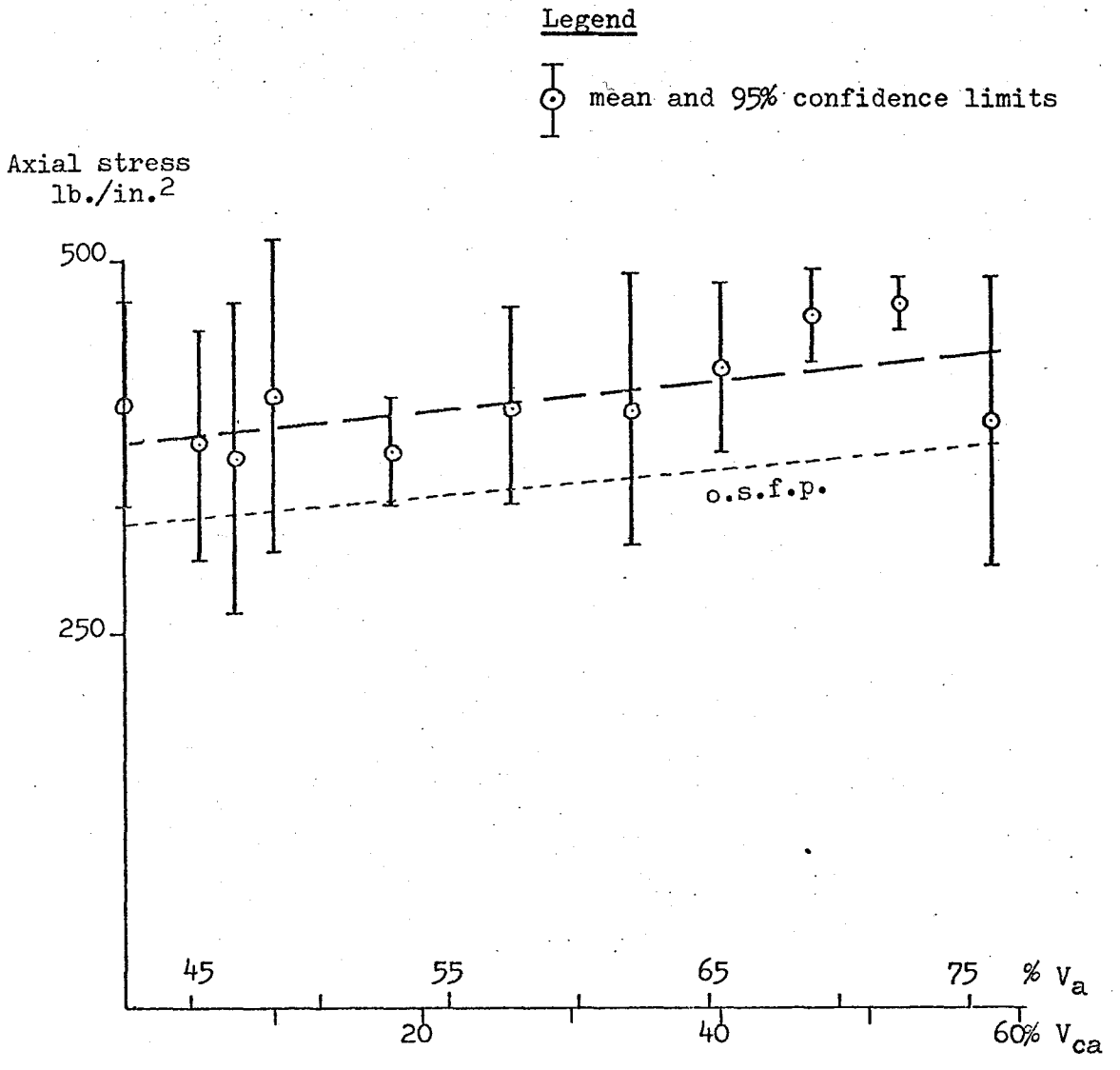


Figure 7.15. Variation of stress at ultimate with volume fraction of aggregate for idealised concretes under direct tension.

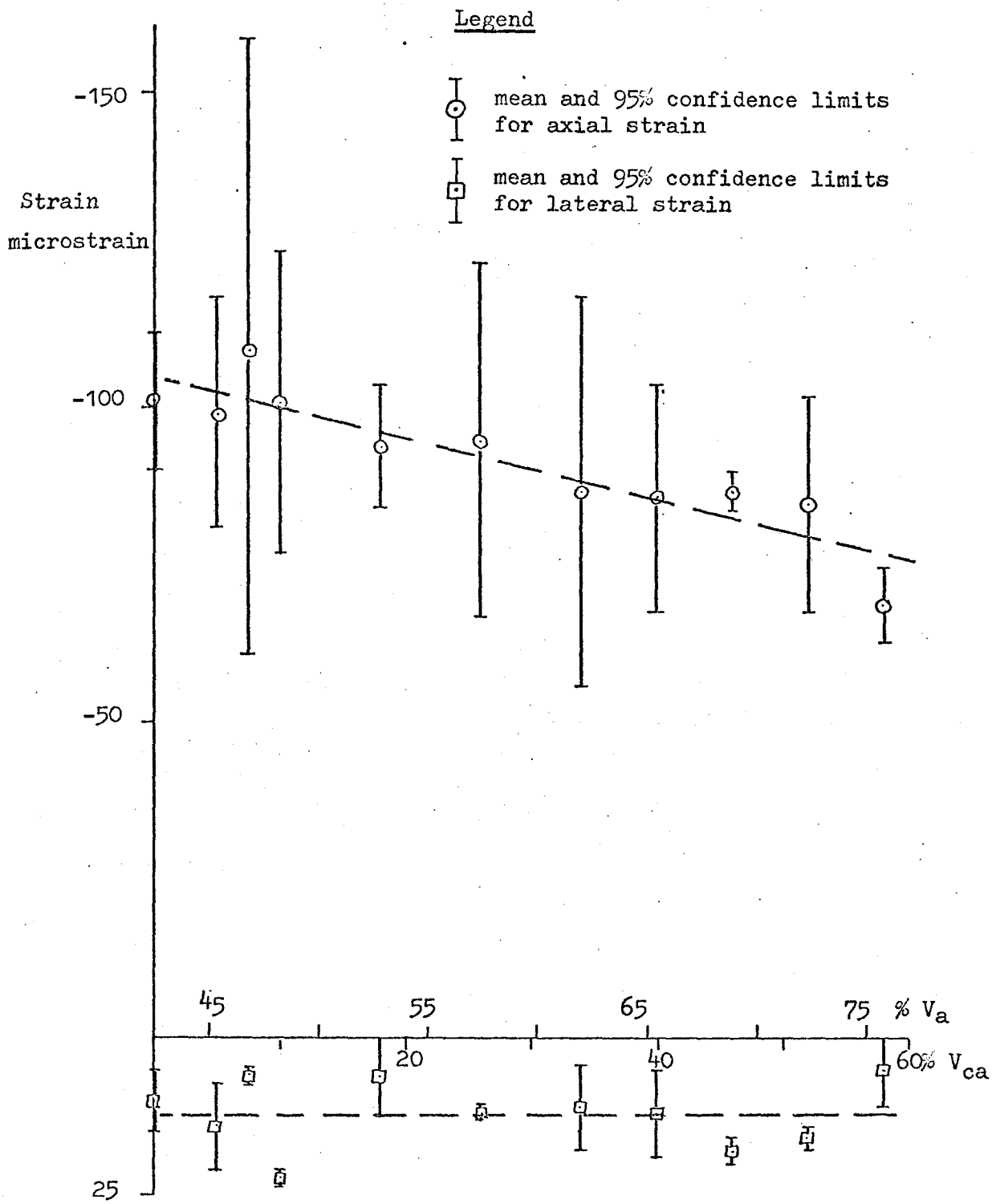


Figure 7.16. Variation of axial and lateral strains at ultimate with volume fraction of aggregate for idealised concretes under direct tension.

types of test. In the case of pure tension, failure occurs from a critical pre-existing flaw and propagates extremely rapidly causing complete disruption after only a small amount of strain redistribution. In a compression test, however, considerable strain redistribution is possible prior to failure. The dependence of the ultimate level is thus less dependent on the actual characteristics, or position, of critical flaws.

7.5.3.6. Mode of Failure

Figure 7.17. shows the fracture surfaces for typical specimens of the various mixes after failure under direct tension. The most significant feature of the appearance of these surfaces in the relatively large number of coarse aggregate particles which have been cleaved during the failure process, in addition to those which have 'debonded' due to the fracture path passing around their periphery. Similar patterns are exhibited by cylinders of the same concretes tested in direct tension under controlled rates of strain by Stroeven [235] except that slightly fewer fractured particles are evident.

Such failure characteristics are surprising, since the strength of the glass is considerably higher than that of the mortar matrix. It would be expected, therefore, that all fracturing would be confined to the matrix and aggregate/matrix interface. In fact, under uniaxial and near uniaxial compressive loading, fracturing of aggregate particles rarely occurs and is definitely not characteristic of the failure process (see 7.5.4.8.). The difference between the tensile and compressive failure modes is either fundamental, or due to the differences in the manner in which the two types of test are performed. It is considered that the latter may be the cause of the discrepancies for the following reasons.

Under uniaxial loading the process of failure is slow, being accompanied by considerable redistribution of strain. For normal short-term rates of loading, the fracture paths can, therefore, change direction and bifurcate. The process continues without the specimen experiencing any significant change in the effective area orthogonal to the direction of load. This results in complete disruption of the material, due to a form of buckling instability, after the formation of multiple failure surfaces.

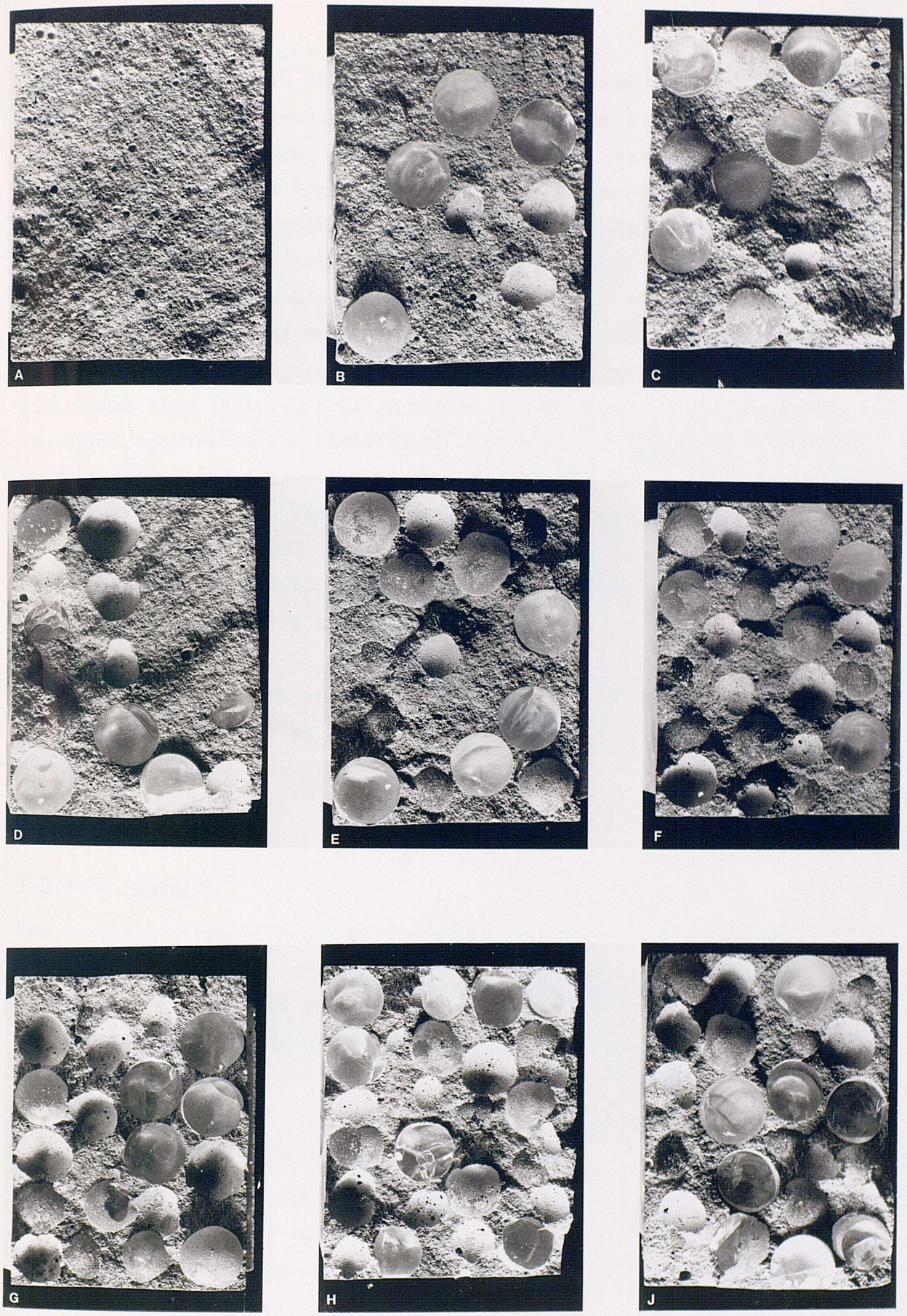


Figure 7.17. Typical failure surfaces exhibited by specimens of idealised concretes after loading under direct tension: (A) I_0, (B) $I_{7.5}$, (C) I_{18}, (D) I_{26}, (E) I_{34}, (F) I_{40}, (G) I_{46}, (H) I_{52}, (J) I_{58}.

Under tension, however, strain redistribution is not possible near ultimate since the effective cross-sectional area of the specimen is reduced as the failure process proceeds. For constant rates of loading this causes failure in an unstable manner, as evidenced by the abruptness of the final disruption, prior to which the specimen appears completely coherent. Thus, during the stages immediately preceding ultimate, the fracture front advances across the eventual failure plane at high velocity. From geometrical considerations, the tensile stress at the tip of the front will be extremely large compared with the field stress and will undoubtedly be much higher than that required to cleave the material of the aggregate. As the front approaches the vicinity of a particle of aggregate it has the possibility of (a) deflecting around the particle or (b) travelling straight through the particle. The energy requirements of the two processes for a given material and speed of fracture advancement will determine the eventual mode, and for relatively high loading rates the chances of the fracture path deflecting may not be high.

The failure mode of the specimens tested under constant rates of strain (235) suggests that there may be an increased likelihood of fracture deflection under such conditions.

7.5.4. Triaxial Compression Tests

7.5.4.1. Results

The complete stress-strain relationships for all specimens are stored in computer card and printout form with the Concrete Materials Research Group and will be the subject of a separate report (197). The principal derived results are given in Appendix 7 and these will be described and discussed in the following sections.

7.5.4.2. Stress-Strain Relationships

Figures 7.18. to 7.25. show the variation of axial and lateral strains with total axial stress for each of the idealised concrete mixes tested. Each relationship covers the entire loading regime, including hydrostatic as well as deviatoric, for a particular maximum level of confining pressure applied. All figures are plotted to the same scale to facilitate comparison.

The following main points arise from the relationships:-

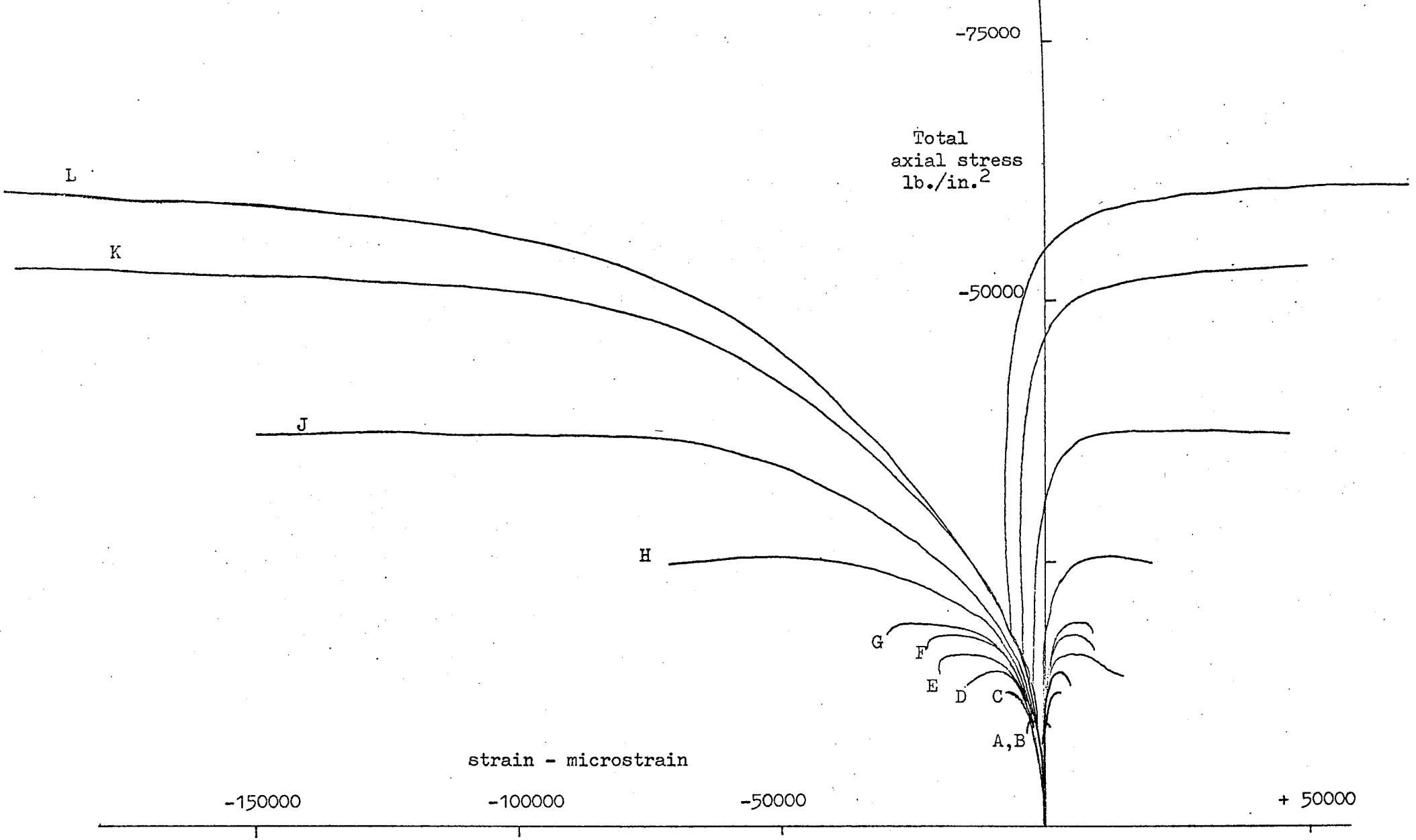


Figure 7.18. Variation of axial and lateral strains with total axial stress for cylinders of mix I_0 under triaxial compression with various values of confining pressure.

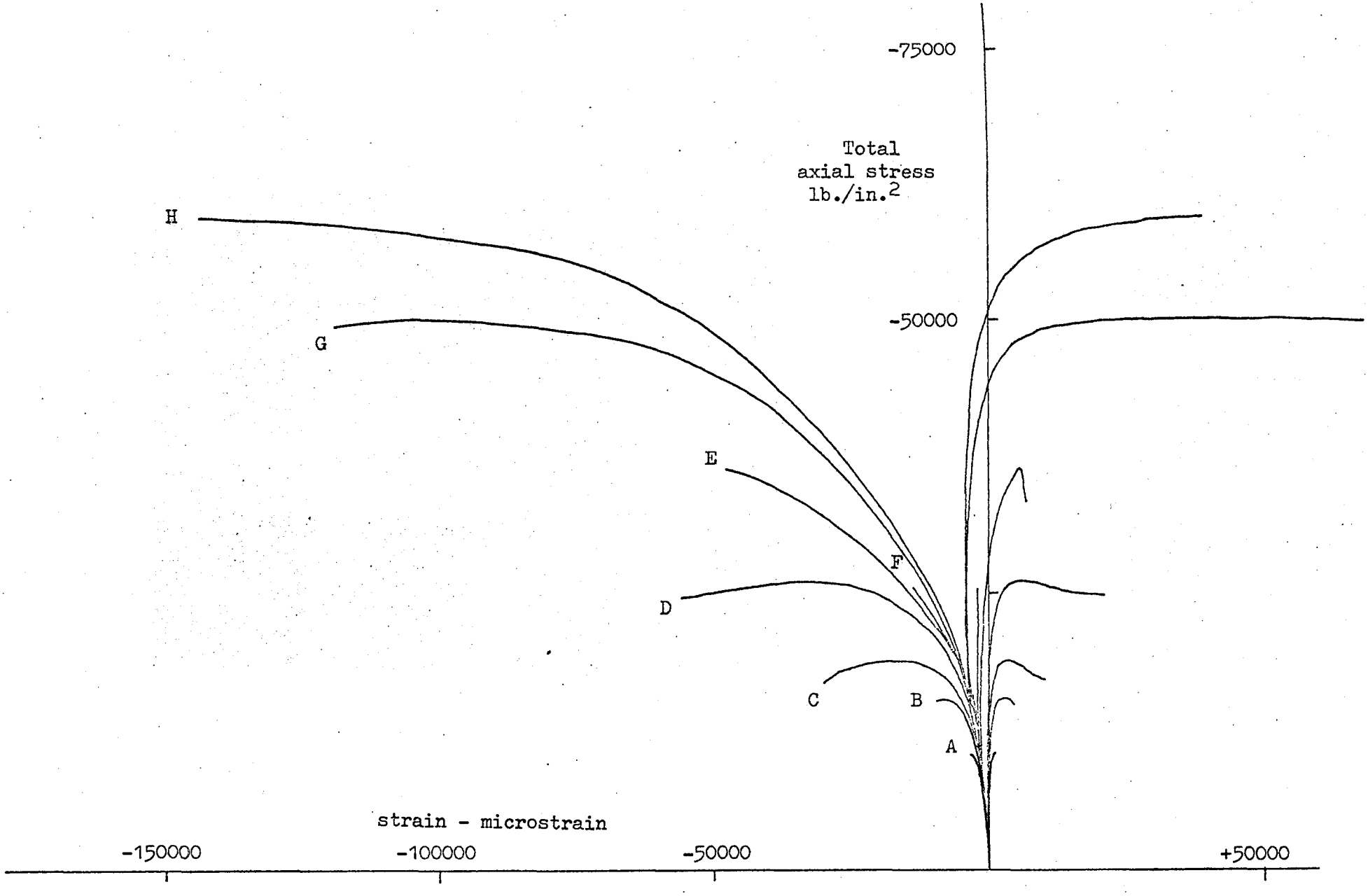


Figure 7.19. Variation of axial and lateral strains with total axial stress for cylinders of mix I_{10} under uniaxial compression with various values of confining pressure.

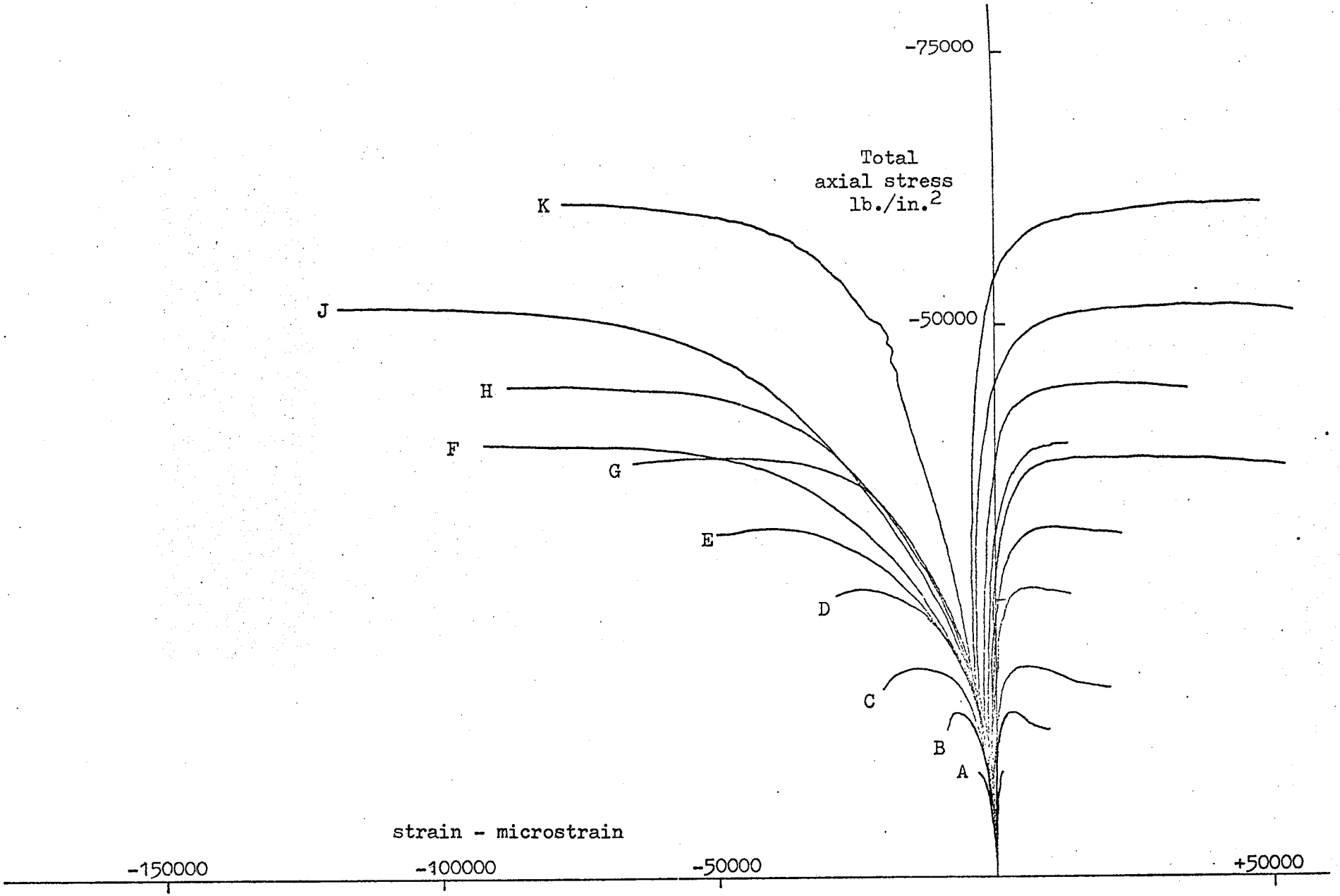


Figure 7.20. Variation of axial and lateral strains with total axial stress for cylinders of mix I_{18} under triaxial compression with various values of confining pressure.

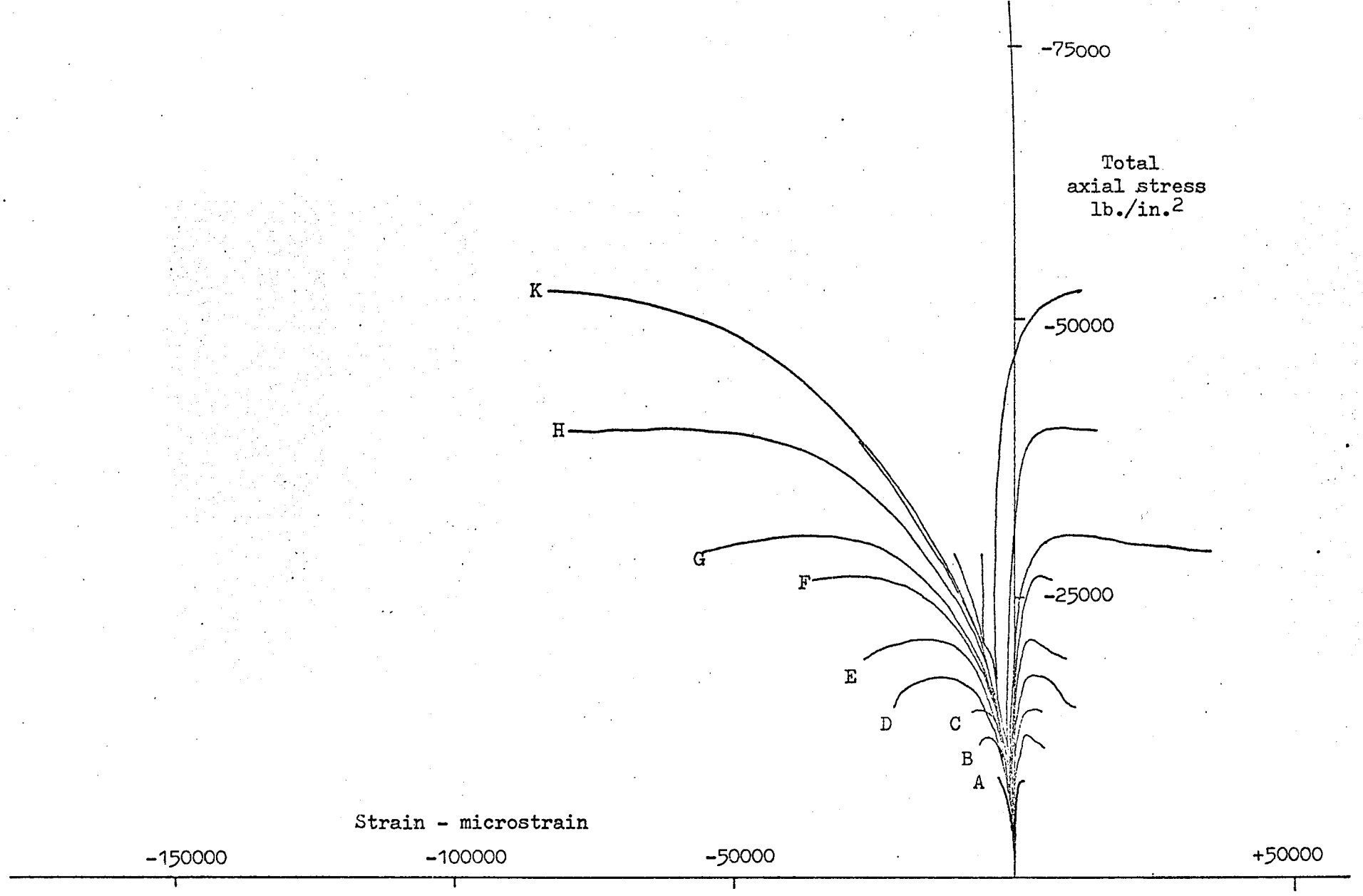


Figure 7.21. Variation of axial and lateral strains with total axial stress for cylinders of mix I_{26} under triaxial compressio with various values of confining pressure.

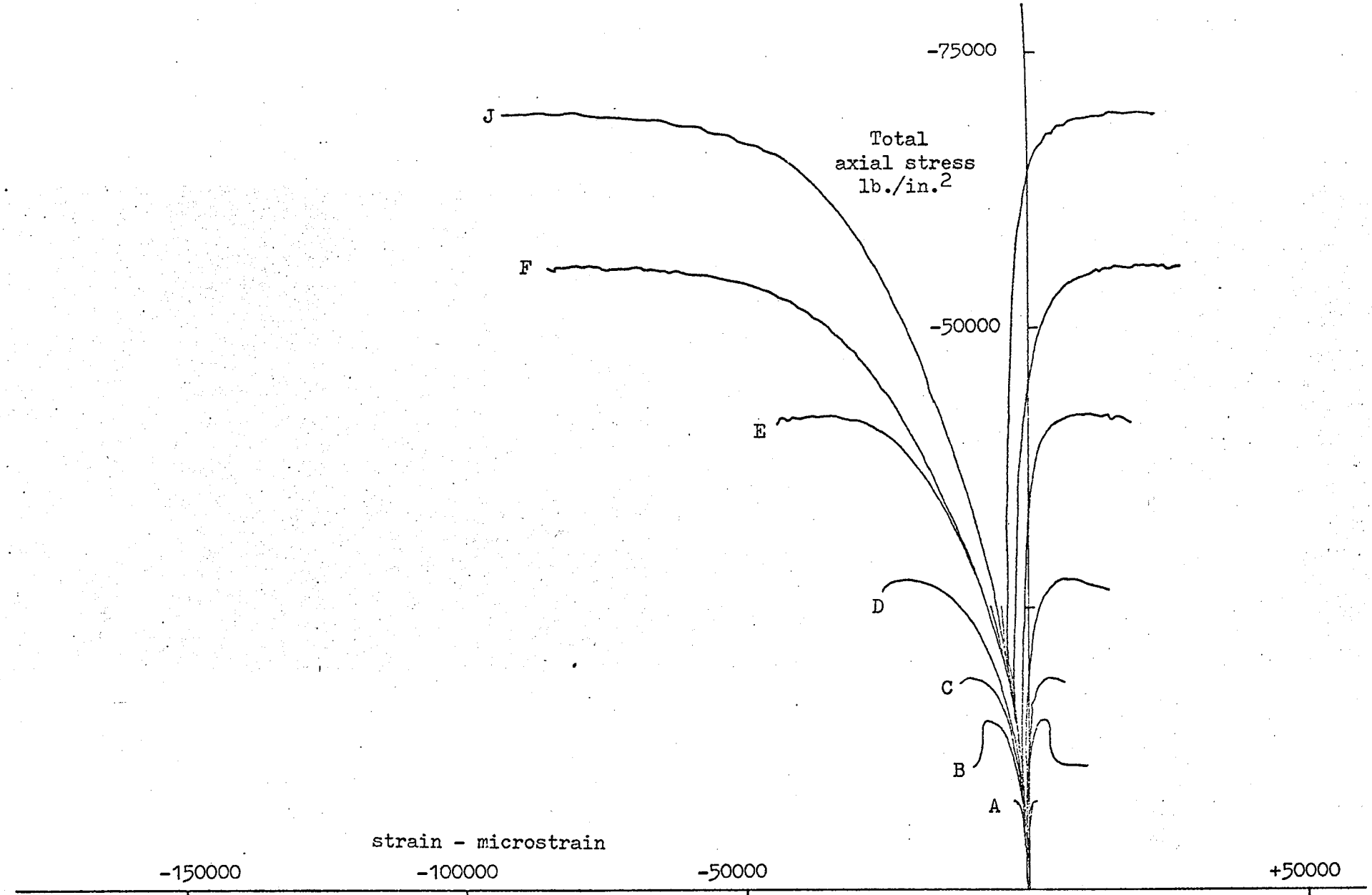


Figure 7.22. Variation of axial and lateral strains with total axial stress for cylinders of mix I34 under triaxial compression with various values of confining pressure.

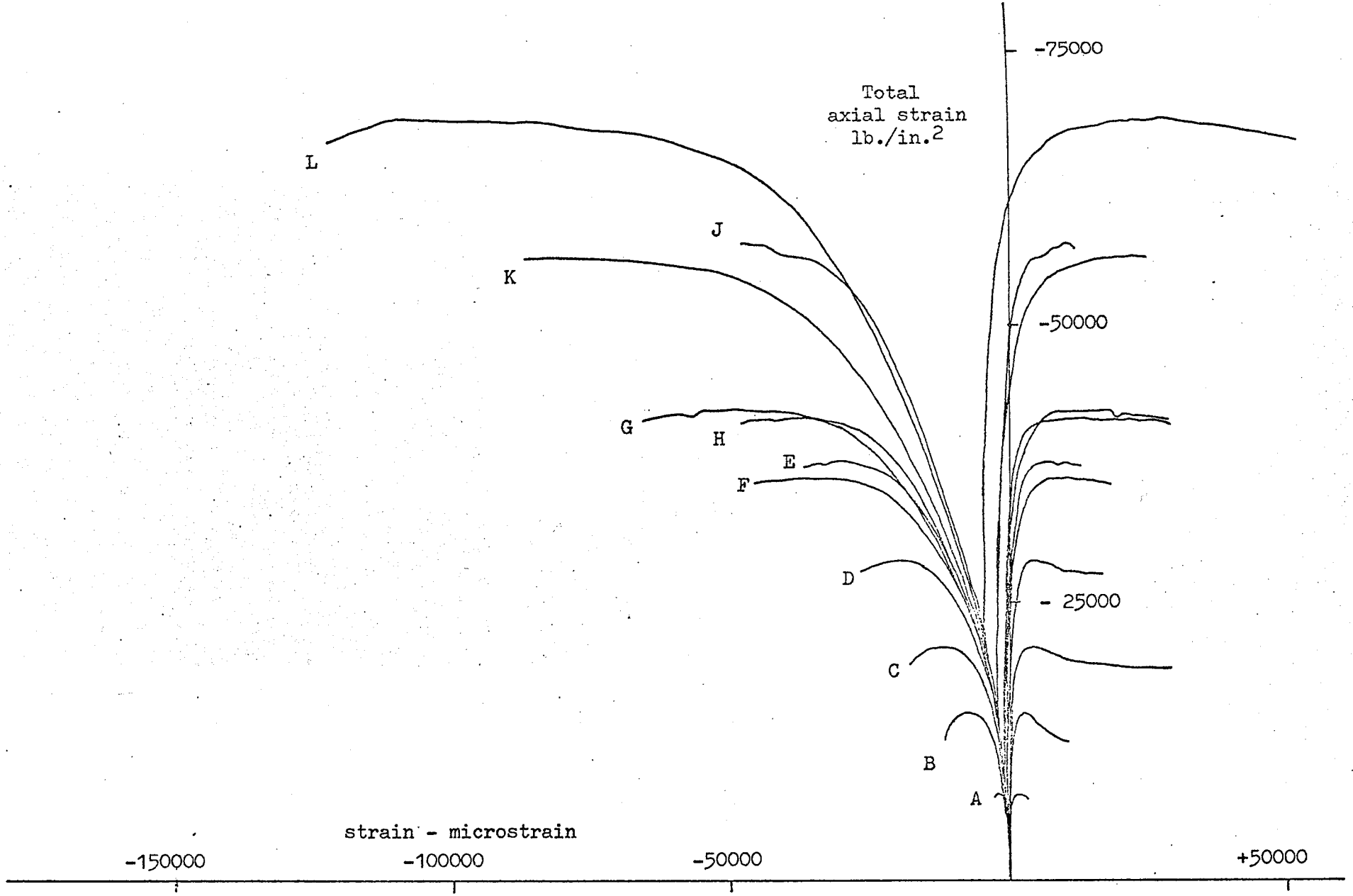


Figure 7.23. Variation of axial and lateral strains with total axial stress for cylinders of mix I_{40} under triaxial compression with various values of confining pressure.

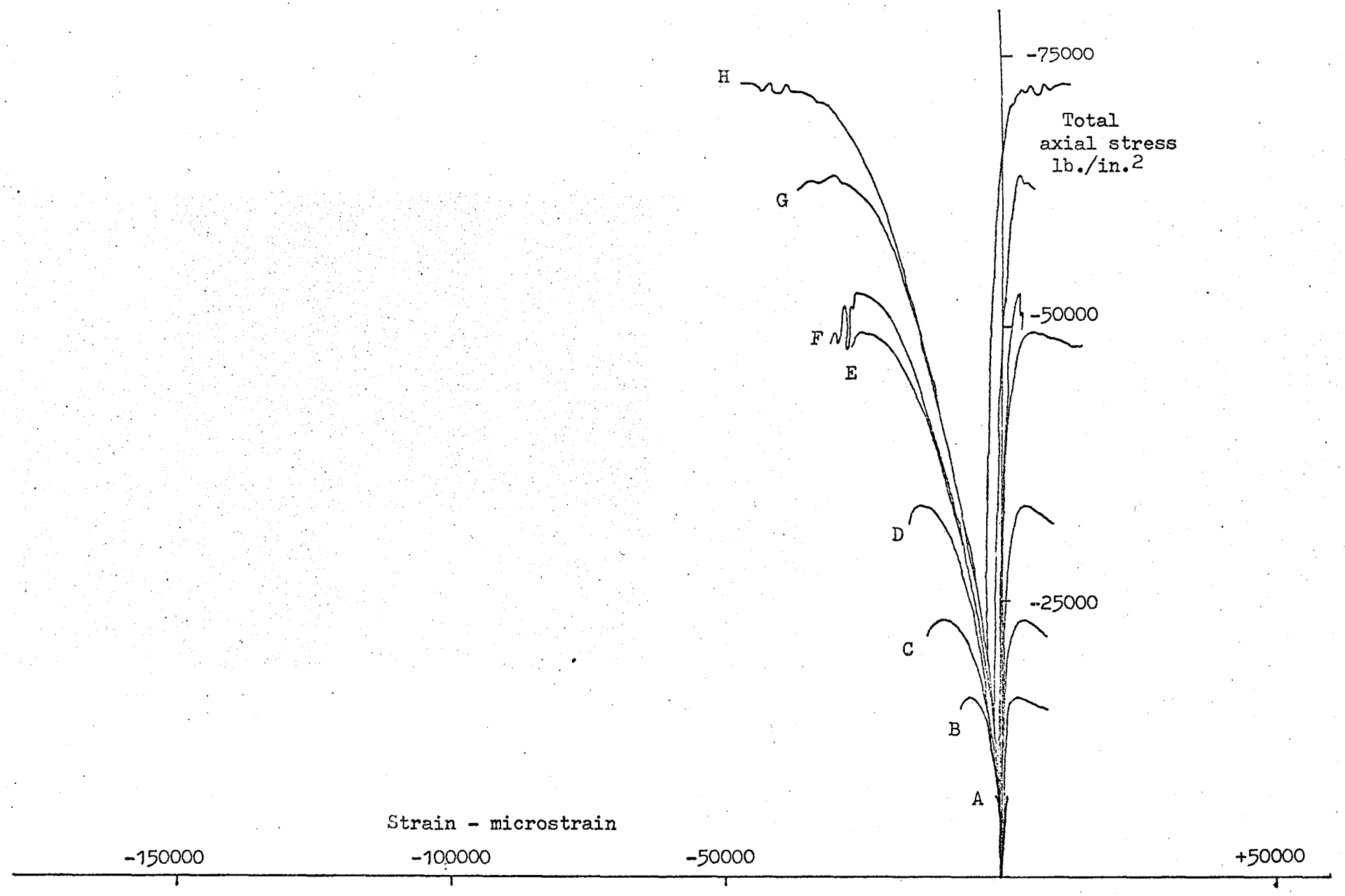


Figure 7.24. Variation of axial and lateral strains with total axial stress for cylinders or mix I_{52} under triaxial compression with various values of confining pressure.

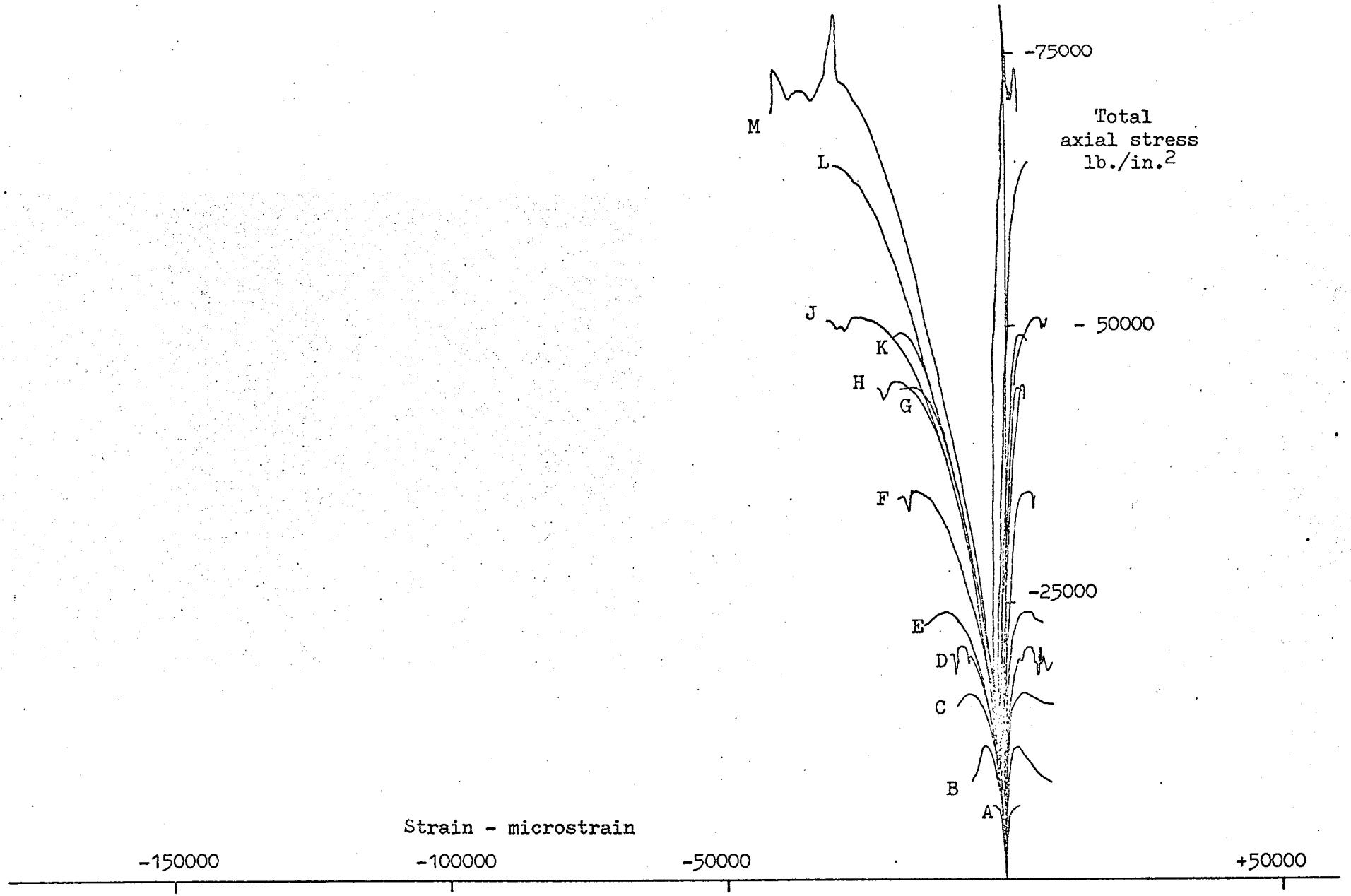


Figure 7.25. Variation of axial and lateral strains with total axial stress for cylinders of mix I_{58} under triaxial compression with various values of confining pressure.

(i) For a given mix and confining pressure the stress-axial strain relationship gradually increases in curvature with increasing stress. The corresponding stress-lateral strain relationship, however, exhibits marked increases in curvature only as ultimate failure is approached. This phenomenon can be attributed to the process of cracking and the alignment of the cracks for this type of loading, which will be discussed more fully in 7.5.4.3.

One important feature is that in all cases neither the axial stress-axial strain or axial stress-lateral strain relationship shows any linear portion or consequent 'limit of proportionality'.

(ii) For a given mix the material exhibits a transition from relatively 'brittle' to more 'ductile' behaviour as the maximum confining pressure for the test is increased. At low confining pressures, the slope of both the axial and lateral stress-strain curves reverses distinctly at ultimate. At higher confining pressures, this reversal is less obvious, particularly for the mixes containing low volume fractions of aggregate, when the relationships are aligned almost parallel to the stress axis indicating a high degree of plasticity. Such behaviour has been observed by previous workers for concrete and rocks for tests in which variation in the overall axial strain with the nominal applied stress was measured. Gvozdev [198] has suggested that the phenomenon may be due to the slipping of particles of material against each other during the loading process.

(iii) For a given confining pressure, increases in the volume fraction of aggregate cause the axial stress-axial strain relationship to become steeper, indicating increased stiffness (see 7.5.3.2.). This is clearly demonstrated by Figures 7.26. to 7.29. which show the variation of axial and lateral strains with deviatoric axial stress for the mixes, each figure referring to a given nominal confining pressure. Hobbs [199] also has detected a similar trend. The variation of axial strain indicates that the relative increase in stiffness with volume fraction of aggregate is greater for tests under applied confining pressure than for the uniaxial compressive case.

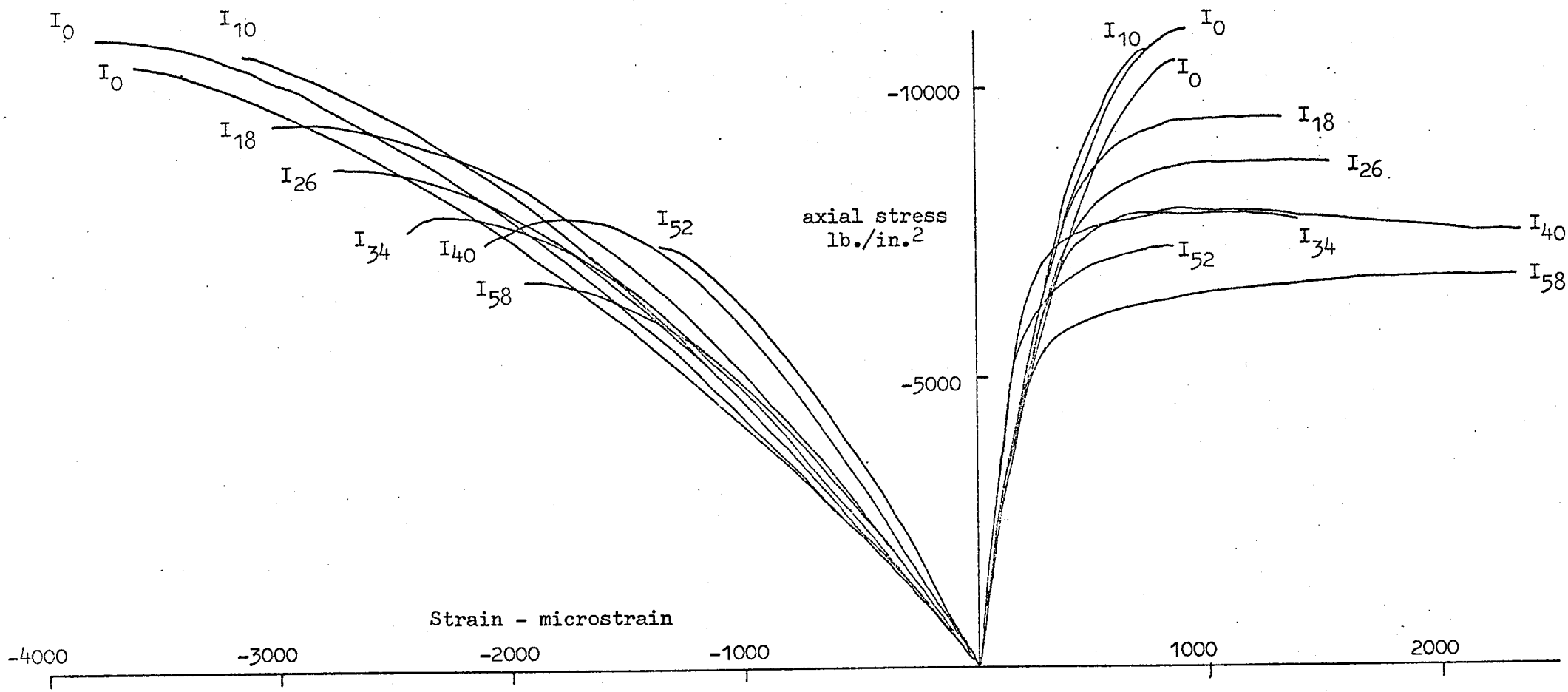


Figure 7.26. Variation of axial and lateral strains with axial stress for cylinders of idealised concretes under uniaxial compression.

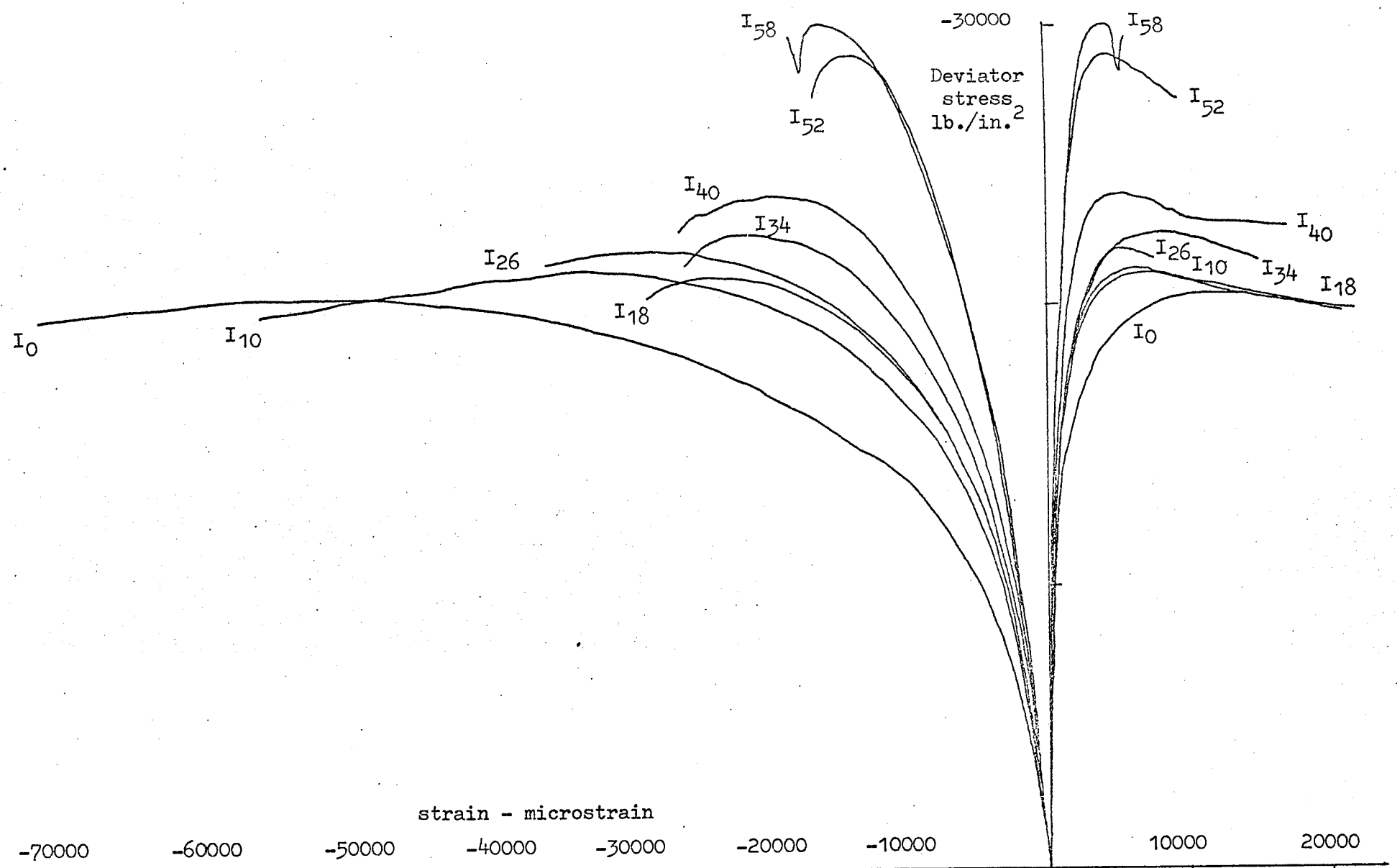


Figure 7.27. Variation of axial and lateral strains measured from the start of deviator loading with the deviator component of axial stress for cylinders of idealised concretes under a nominal confining pressure of 5000 lb./in

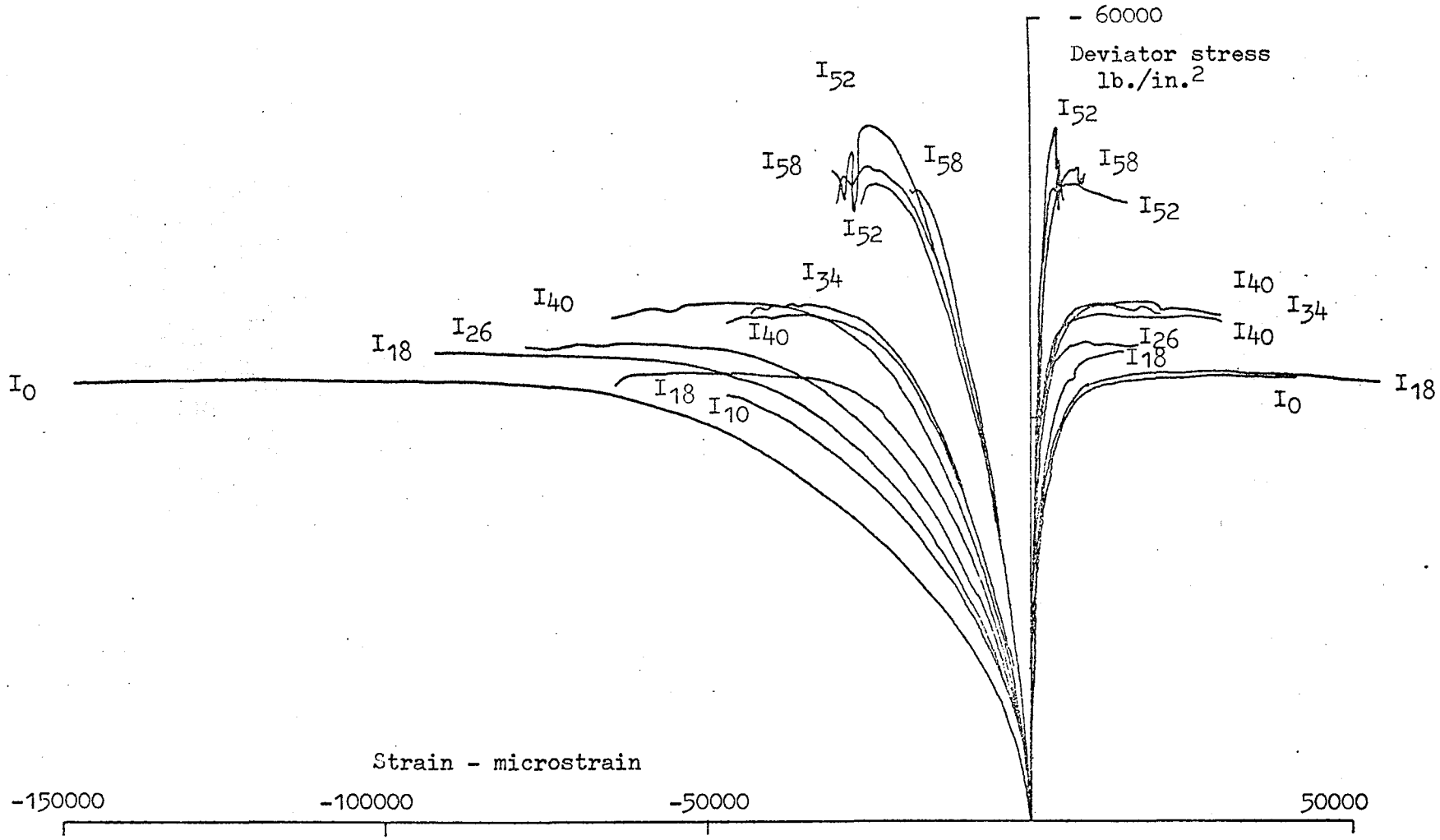


Figure 7.28. Variation of axial and lateral strains measured from the start of deviator loading with the deviator component of axial stress for cylinders of idealised concretes under a nominal confining pressure of 10000 lb./in.^{2}.

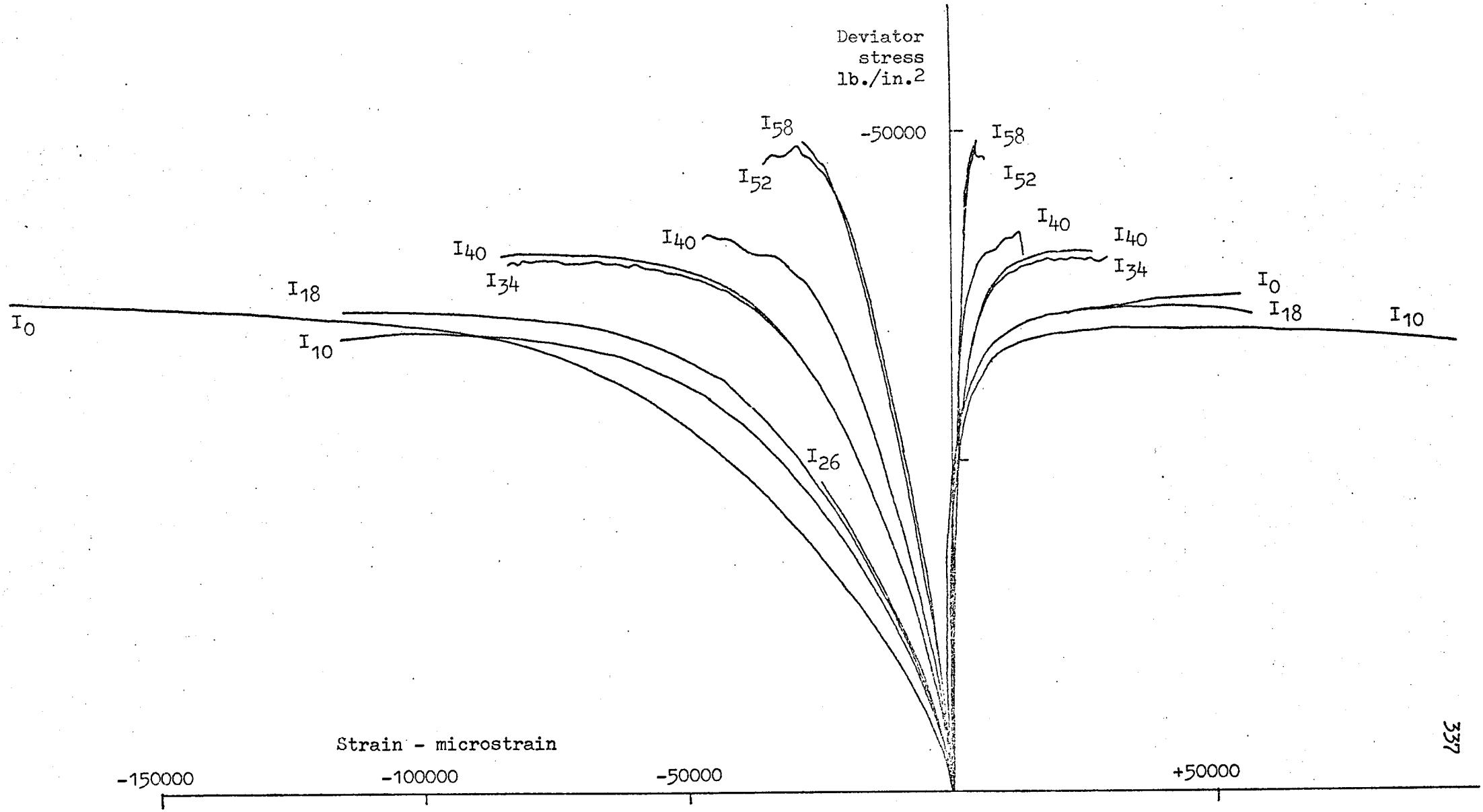


Figure 7.29. Variation of axial and lateral strains measured from the start of deviator loading with the deviator component of axial stress for cylinders of idealised concretes under a nominal confining pressure of 15000 lb./in.^{2}.

The variation of lateral strain, however, does not show such a trend until approaching ultimate. In fact, for a given applied confining pressure, the curves for the various mixes appear almost coincident during the initial stages of applied deviator stress.

The irregular behaviour at, or approaching, ultimate for the mixes containing higher volume fractions of aggregate subjected to relatively high confining pressures suggests disruption of individual aggregate particles. This is supported by the sounds emanating from the specimen coincident with the sharp changes in shape of the stress-strain curve.

7.5.4.3. Onset of Stable Fracture Propagation (o.s.f.p.)

Essentially, the onset of stable fracture propagation is defined as the level after which the lateral strain increases faster than the axial (see 4.5.). For each mix, the relationships between axial and lateral strains under various confining pressures are shown in Figures 7.30 to 7.33. For clarity, only the portion of the relationship covering the region up to just beyond the onset of fracture propagation is shown.

After the hydrostatic stress region, corresponding ideally to an equality of compressive strains, the curves generally indicate a linear portion prior to the lateral strain increasing, in a tensile mode, at an increasing rate.

For low confining pressures, the linear portions of the curves slope towards the positive (tensile) lateral strain axis which corresponds to a negative value of the incremental strain ratio. As the confining pressure is increased this ratio changes to become more positive.

The difficulty of assessing the limits of the linear portion from a stress axial strain-lateral strain relationship is apparent from the figures but it can be accomplished easily with the aid of the incremental strain ratio-stress plots. The onset of fracture propagation is, therefore, evaluated by detecting an increase in the incremental strain ratio as described in 4.5. The variations of the i.s.r. with the deviator component of axial stress and confining pressure for the mix are shown in Figures 7.34. to 7.37.

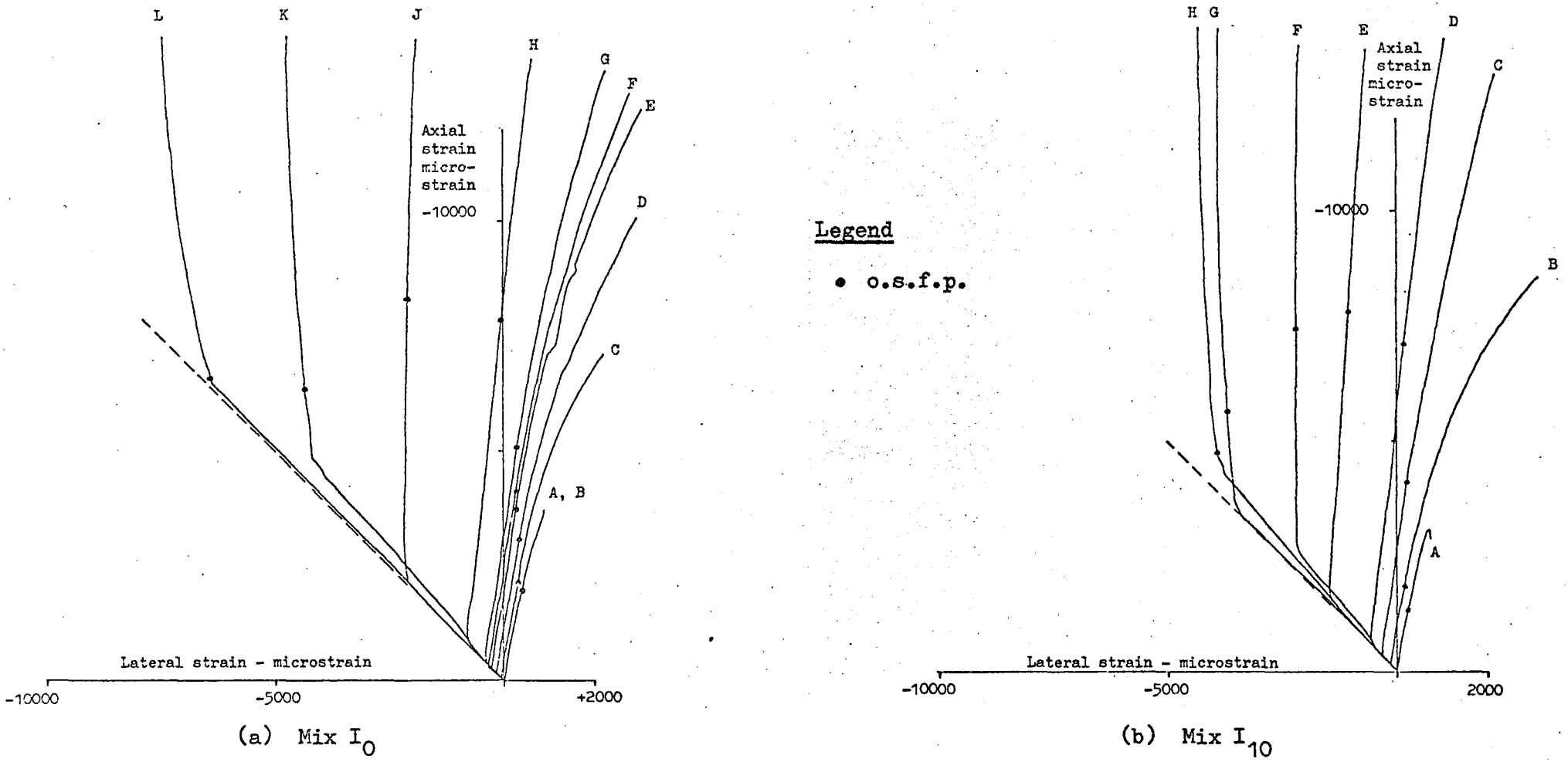
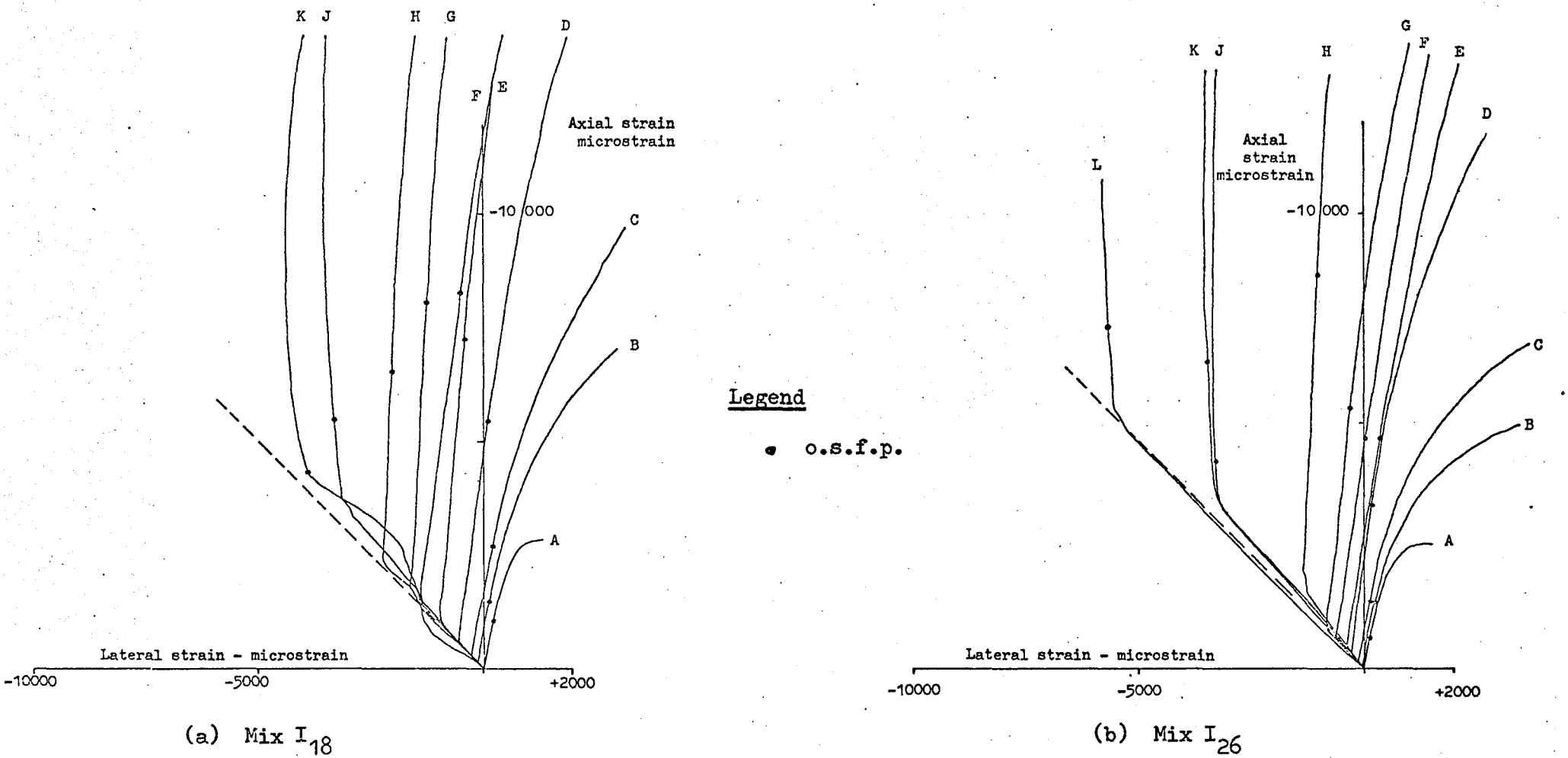


Figure 7.30 Relationships between axial and lateral strains for idealised concretes under triaxial compression with various values of confining pressure.



(a) Mix I_{18}

(b) Mix I_{26}

Figure 7.31. Relationships between axial and lateral strains for idealised concretes under triaxial compression with various values of confining pressure.

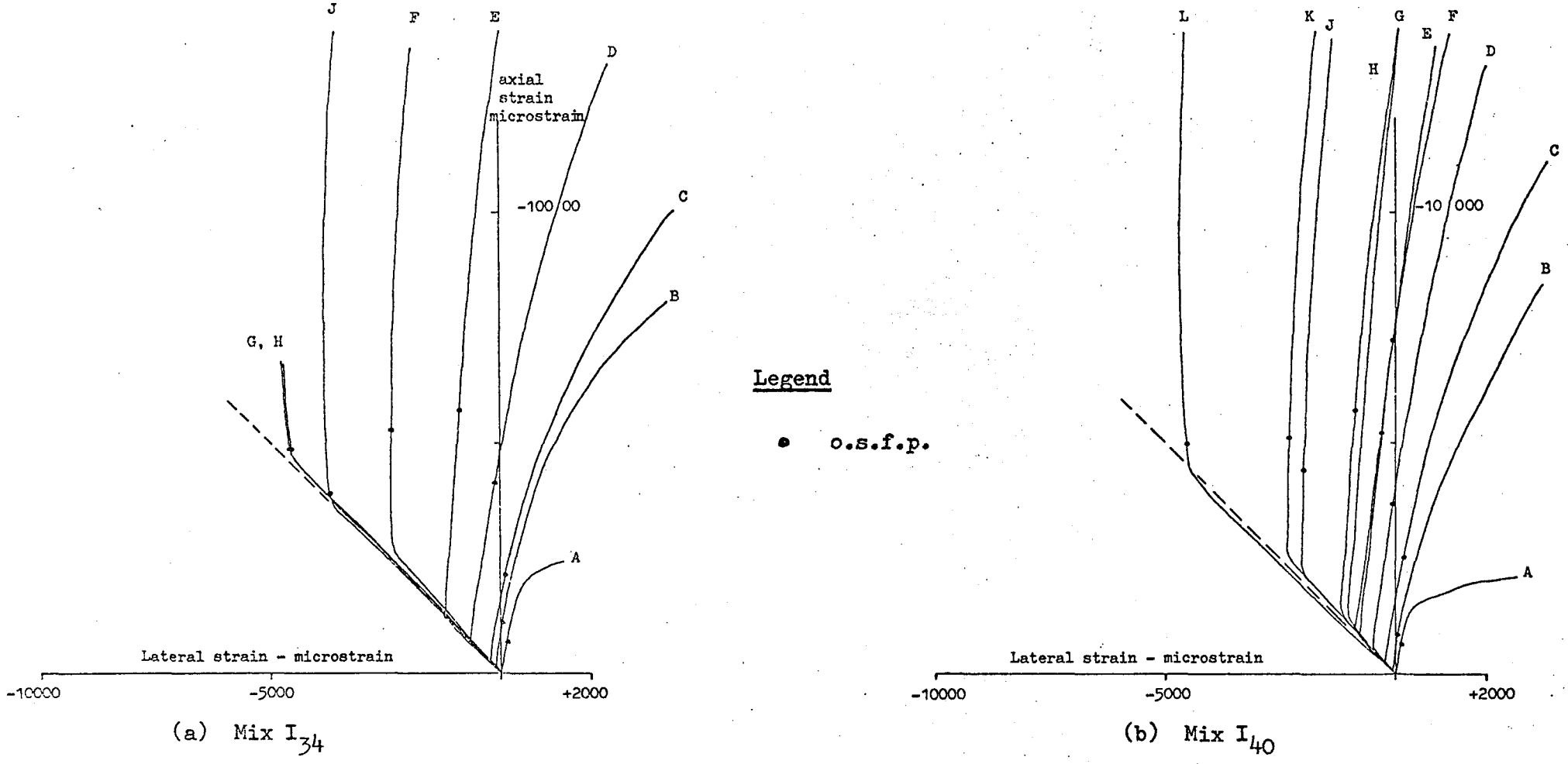
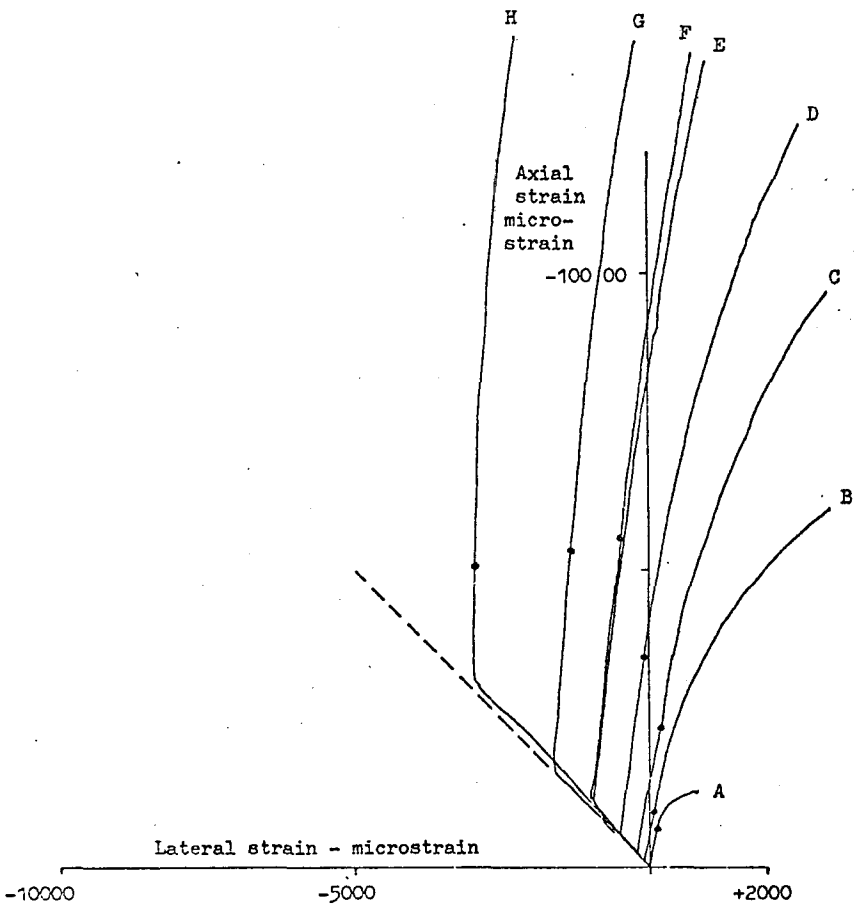
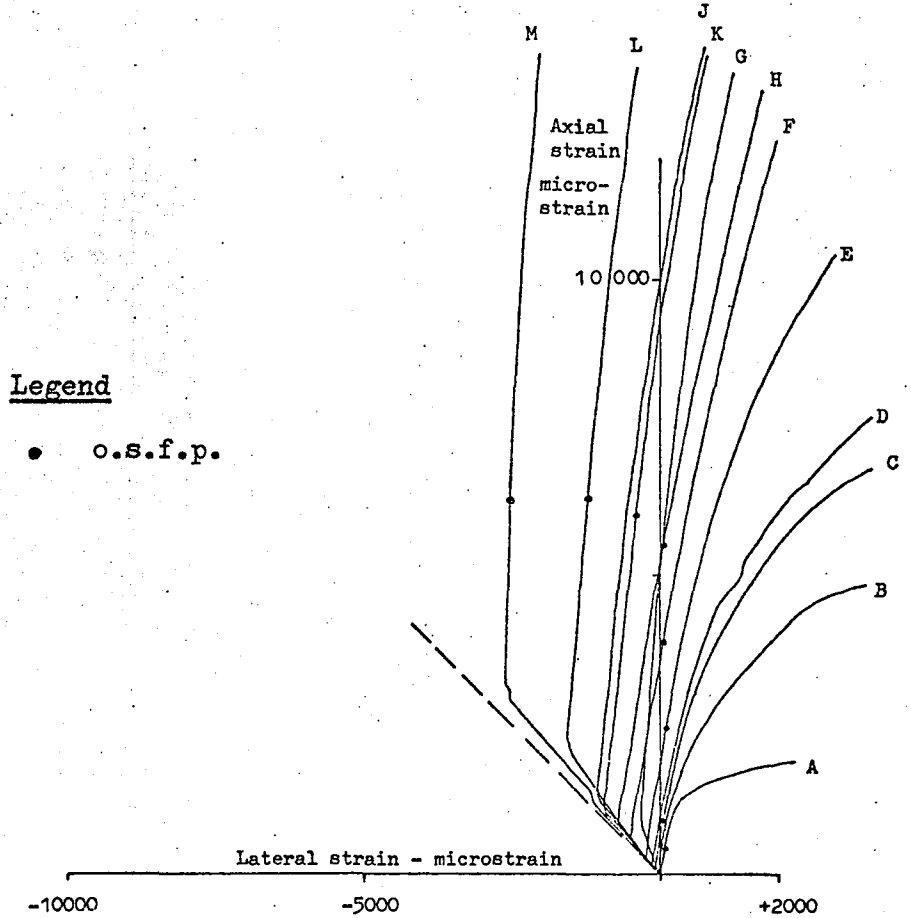


Figure 7.32. Relationships between axial and lateral strains for idealised concretes under triaxial compression with various values of confining pressure.

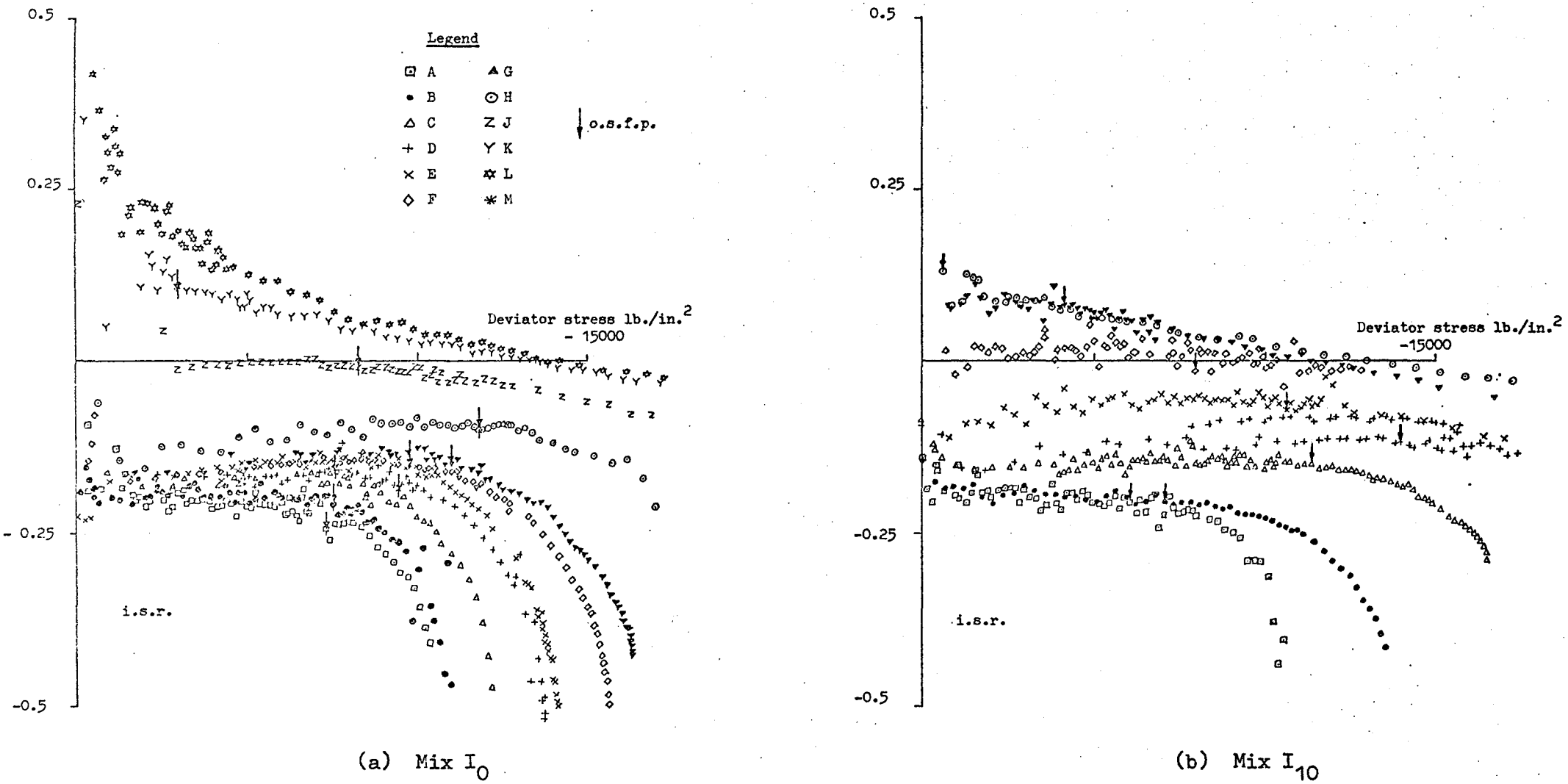


(a) Mix I_{52}



(b) Mix I_{58}

Figure 7.33. Relationships between axial and lateral strains for idealised concretes under triaxial compression with various values of confining pressure.



(a) Mix I_0

(b) Mix I_{10}

Figure 7.34. Variation of incremental strain ratio with deviator component of axial stress for idealised concretes under triaxial compression with various values of confining pressure.

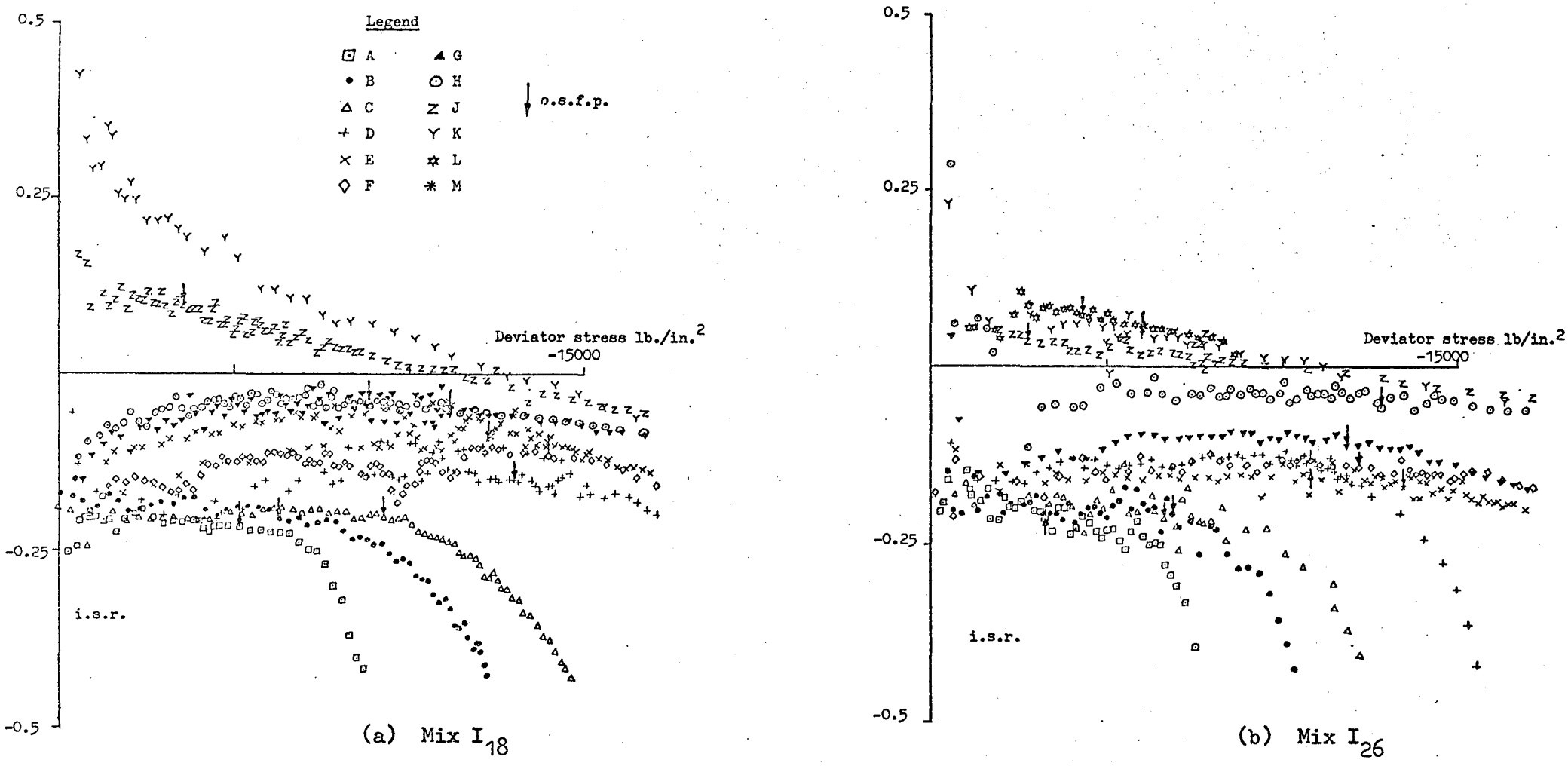


Figure 7.35. Variation of incremental strain ratio with deviator component of axial stress for idealised concretes under triaxial compression with various values of confining pressure.

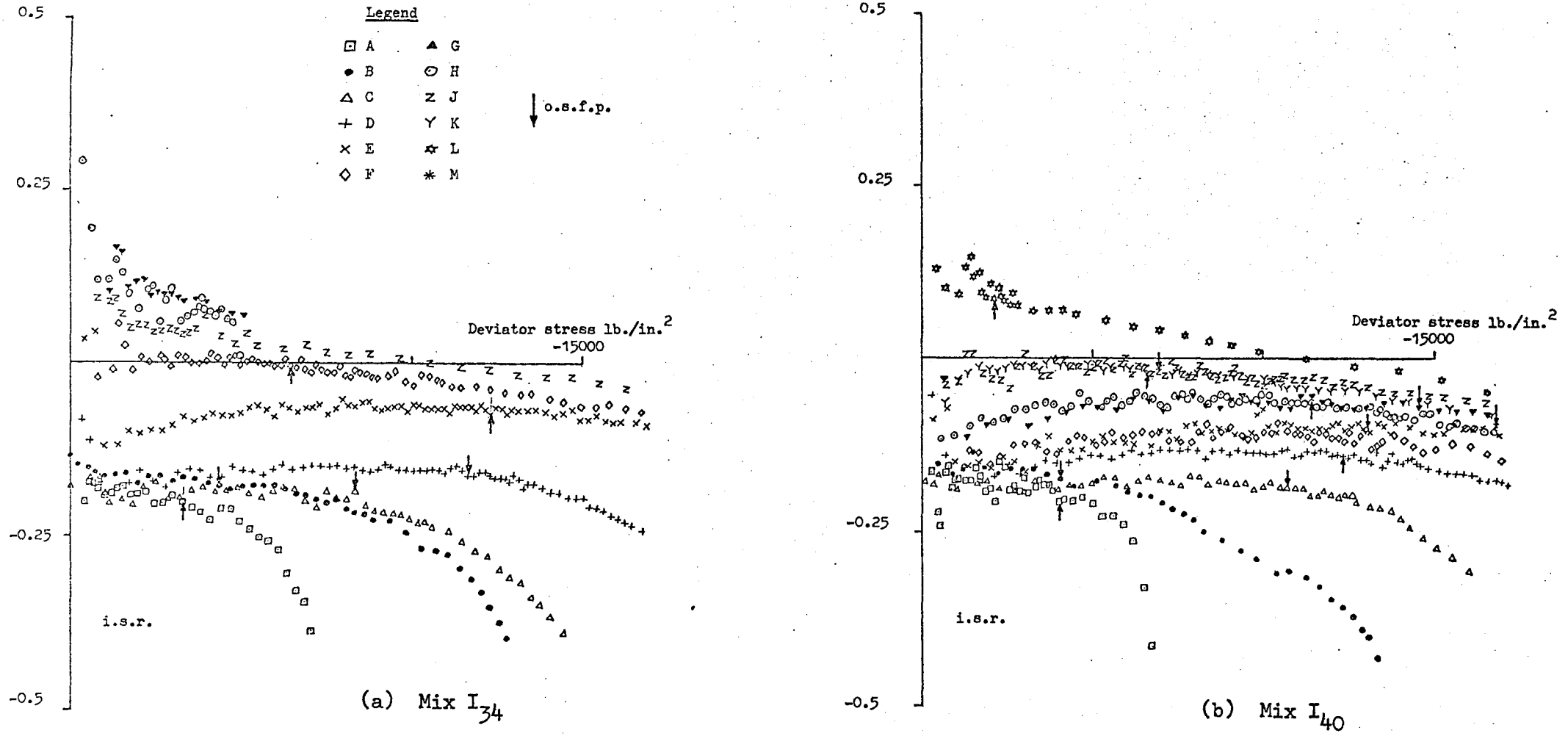


Figure 7.36. Variation of incremental strain ratio with deviator component of axial stress for idealised concretes under triaxial compression with various values of confining pressure.

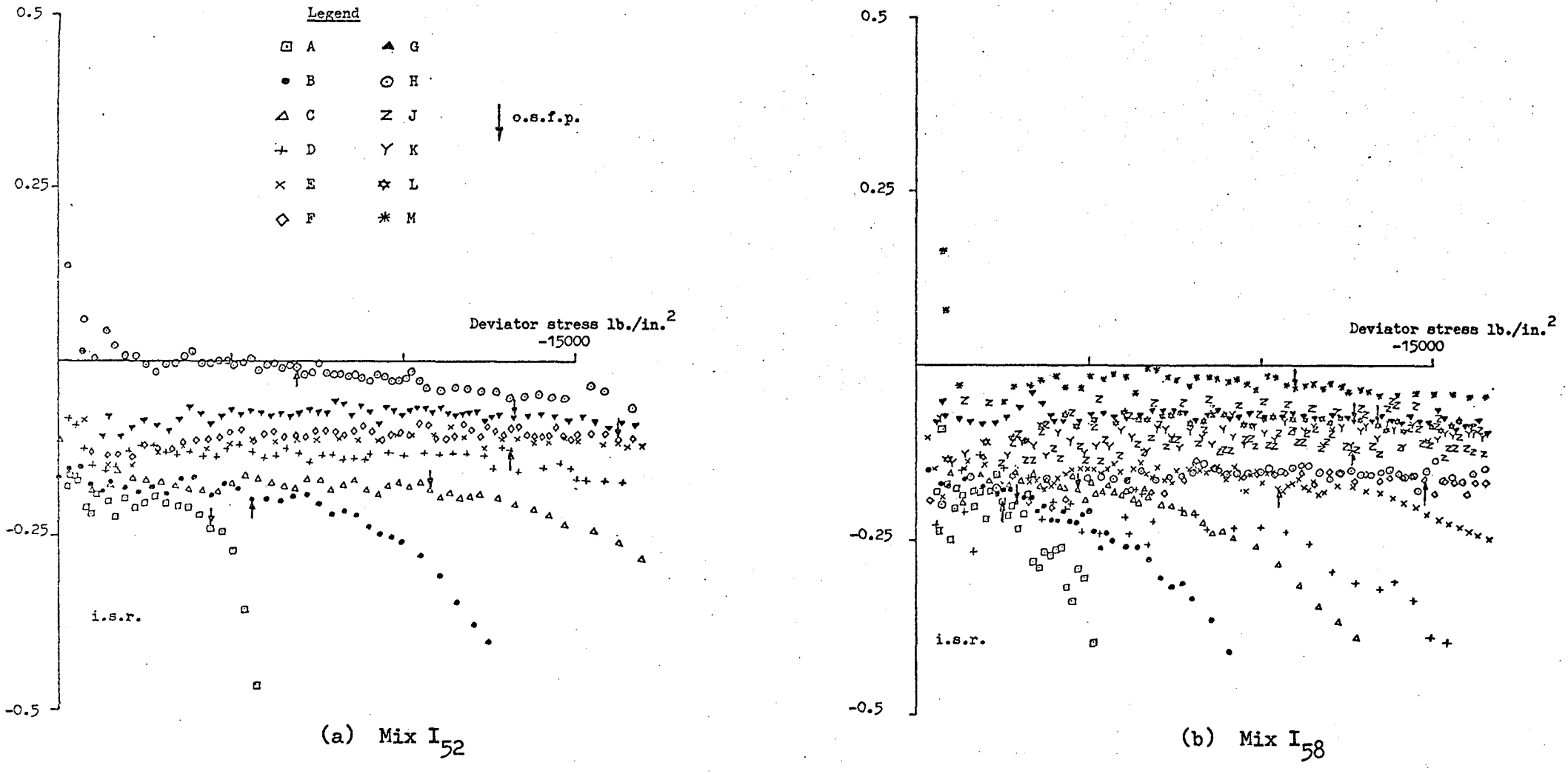


Figure 7.37. Variation of incremental strain ratio with deviator component of axial stress for idealised concretes under triaxial compression with various values of confining pressure.

For low confining pressures, the relationships are of the type described in 4.5.3. in that the i.s.r. decreases up to a certain critical stress level, probably due to crack closure, after which it remains essentially constant before increasing rapidly to ultimate.

Under intermediate values of confining pressure, the range of deviator stress over which crack closure is indicated increases and the near-constant portion is followed by a relatively low rate of increase of i.s.r. At high confining pressures, increases in i.s.r. from the start of deviator load are indicated for mixes containing low volume fractions of aggregate.

The mean value of the i.s.r. after flaw closure, and prior to the approximate critical stress level for typical mixes, is shown on Figure 7.38. This further illustrates the change in initial slope of the axial-lateral strain relationship from negative to positive with increasing confining pressure.

For uniaxial compression, where the i.s.r. concept is synonymous with that of 'Poisson's Ratio', the tendency is for the i.s.r. to decrease with volume fraction of aggregate. This trend, which persists for triaxial loading under very low confining pressures, is similar to that observed by Anson (200) who concluded that the relatively stiff aggregate particles reduced lateral expansion, and hence overall Poisson's Ratio, below that given by either of the principal constituents (mortar and aggregate).

The influence of confining pressure rapidly modifies this behaviour since, above pressures of approximately 3000 lb./in.^{2} the i.s.r. decreases with V_{ca}.

As described in 4.5., the mean values of i.s.r. after crack closure and before fracture propagation define the mean slope of the linear portion of the axial-lateral strain relationship which is used to detect o.s.f.p. The deviations of the measured lateral strains from this linear portion provide a clear indication of the start of continuous increase in i.s.r., and these deviations all show the expected rapid increase in strain deviation after the critical stress level for all tests. The onset of stable fracture propagation, defined as the level after which this increase starts, is indicated in Figures 7.34. to 7.37.

Strains at o.s.f.p.

The values of strain at o.s.f.p. given in Appendix 7, are indicated on the relationships between axial and lateral strains (Figures 7.30 to 7.33).

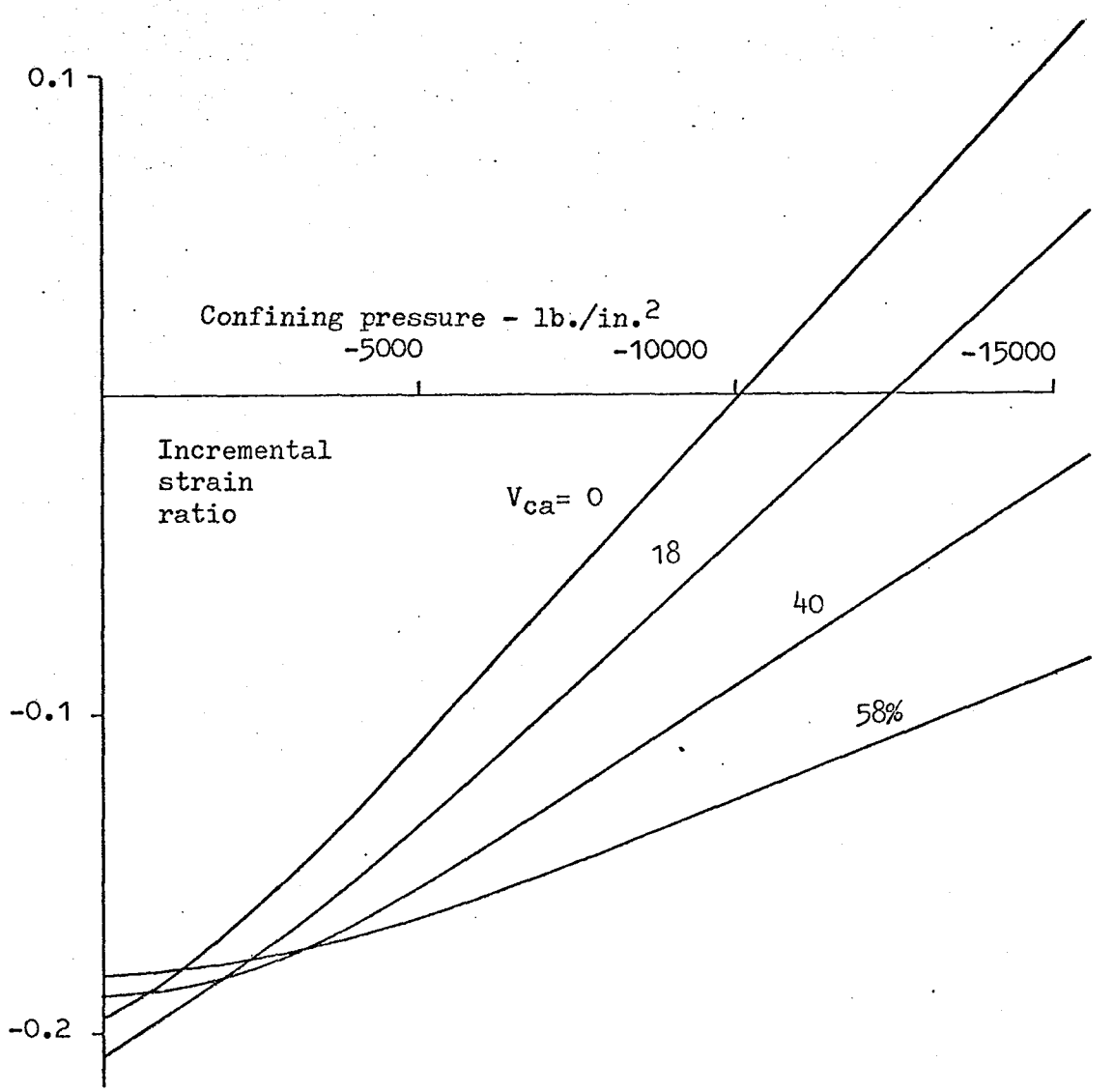


Figure 7.38. Variation of mean value of incremental strain ratio between end of crack closure and o.s.f.p. with confining pressure for typical idealised concretes under triaxial compression.

By plotting the strains at o.s.f.p. for each mix against the corresponding volume fraction of aggregate, and choosing suitable curves to represent the data, the typical envelopes of Figure 7.39. are obtained.

Each emvelope can be divided into three main regions as follows:-

Region I — For confining pressures up to approximately 4000 lb./in.^{2}.

o.s.f.p. occurs at increasing axial compressive strain, with the lateral tensile strain remaining approximately equal to that for a uniaxial compression test.

Region II — For confining pressures between approximately 4000 lb./in.^{2} and 10000 lb./in.^{2}.

The axial strain at o.s.f.p. continues to increase, but at a fast diminishing rate, reaching a maximum at the end of this region. The corresponding lateral strain gradually increases compressively.

Region III — For confining pressures above approximately 10000 lb./in.^{2}.

The axial strain becomes less compressive while the lateral strain continues to become more compressive. The region is terminated by the envelope intersecting the hydrostatic strain axis at 90°. Only in the case of the low volume fractions of aggregate is this intersection actually illustrated on Figure 7.39. since, for the concretes containing larger volumes of aggregate, the maximum confining pressure used is insufficient to produce this phenomenon.

The broken section of each envelope joins the strains corresponding to uniaxial compression to those at o.s.f.p. for uniaxial tension. This gives an indication of the shape of the envelope within the compression-tension-tension region of stress space. Strictly, the points representing the strains under uniaxial tension do not form part of the envelopes for the axisymmetric stress cases, and the strains at o.s.f.p. under equal biaxial tension should be used. It is likely, however, that the difference between the two sets of values will be small.

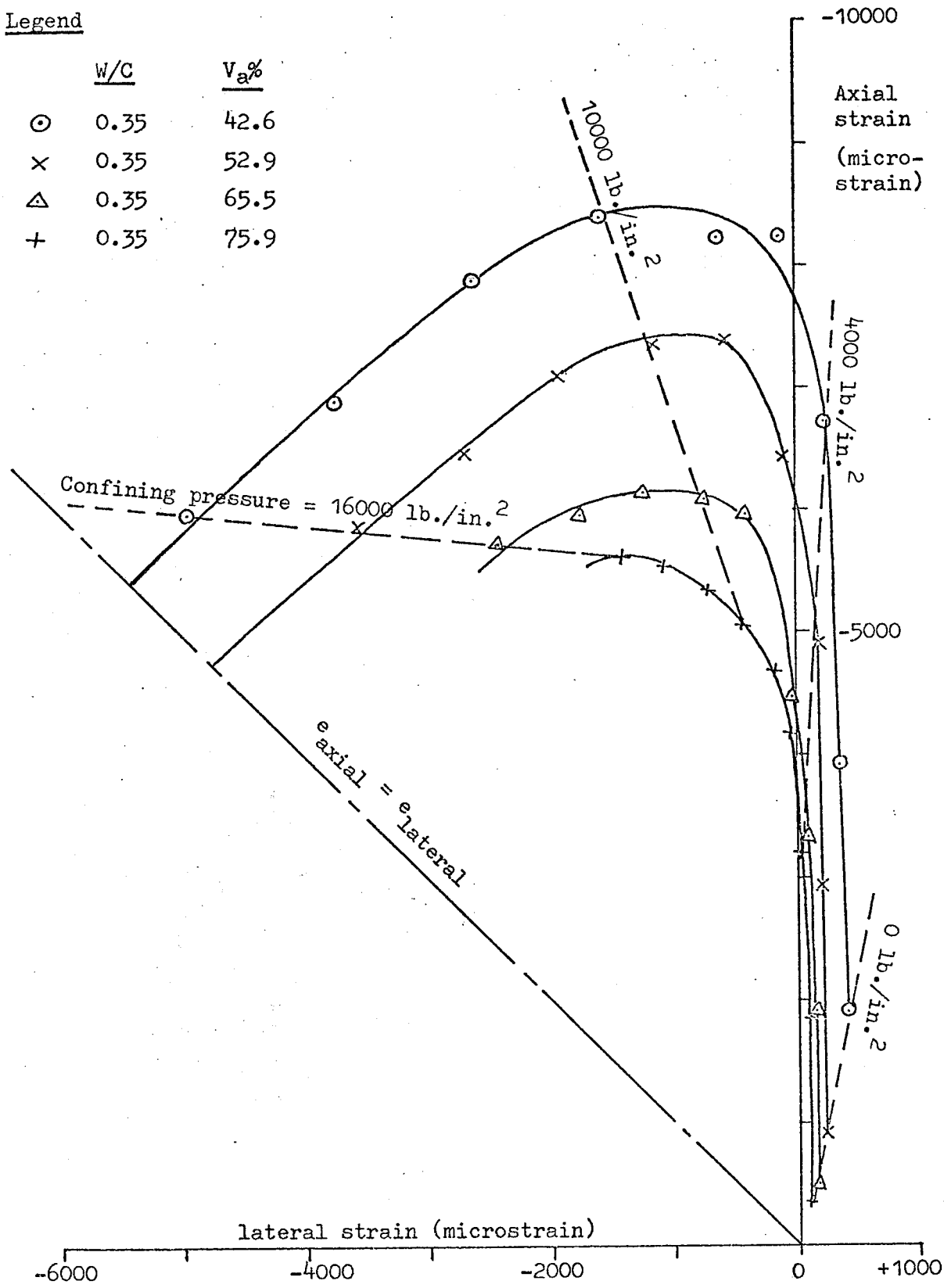


Figure 7.39. Relationships between axial and lateral strains at onset of stable fracture propagation under triaxial compression for typical idealised concretes.

The envelopes, therefore, are of closed form in strain space and, in this respect, are similar to those for stress at o.s.f.p. Possible mechanisms of failure which would produce envelopes exhibiting such characteristics are discussed in 7.5.4.4.

Comparison of the strain envelopes shows the decrease in magnitude of both axial and lateral strains, for given levels of confining pressure, as the volume fraction of aggregate is increased. The relative decrease is greater for increases in volume fraction at low aggregate contents than for corresponding increases at high volume fractions.

Stresses at o.s.f.p.

By plotting the stresses at o.s.f.p. for each mix (given in Appendix 7) against the corresponding volume fraction of aggregate, and choosing suitable curves to represent the data, the typical envelopes given in Figure 7.40. are obtained. As in the case of the strain envelopes (described in the preceding section), the curves are extended to pass through the uniaxial tensile value indicated on the confining pressure axis. Again, this is not fundamentally accurate - since the equal biaxial tension case should be represented - but should serve to indicate the characteristics in the C-T-T zone. Figure 7.41. shows the same data normalised with respect to the ultimate strength under uniaxial compression.

These curves again all show the same trend, namely that, as the confining pressure of the test is increased for a given mix, the envelope tends towards intersections with the hydrostatic axis in both the compression and tension zones such that a closed portion of stress-space is defined. This is to be contrasted with the ever-increasing stress at ultimate with increasing compressive confining pressure (described in 7.5.4.7.) which gives rise to the open-ended envelopes also shown in Figure 7.40. and is discussed in 7.5.4.4.

Niwa et Al [201] and Kobayashi and Koyanagi [74], defining the fracture initiation level as the onset of non-linear stress-overall deformation behaviour and consequent irrecoverable deformation on unloading, found this level to occur at stresses of between 60 and 70% of ultimate, giving rise to an open-ended envelope. This is in conflict with the present results but it is considered that the apparent disparity may be due to the

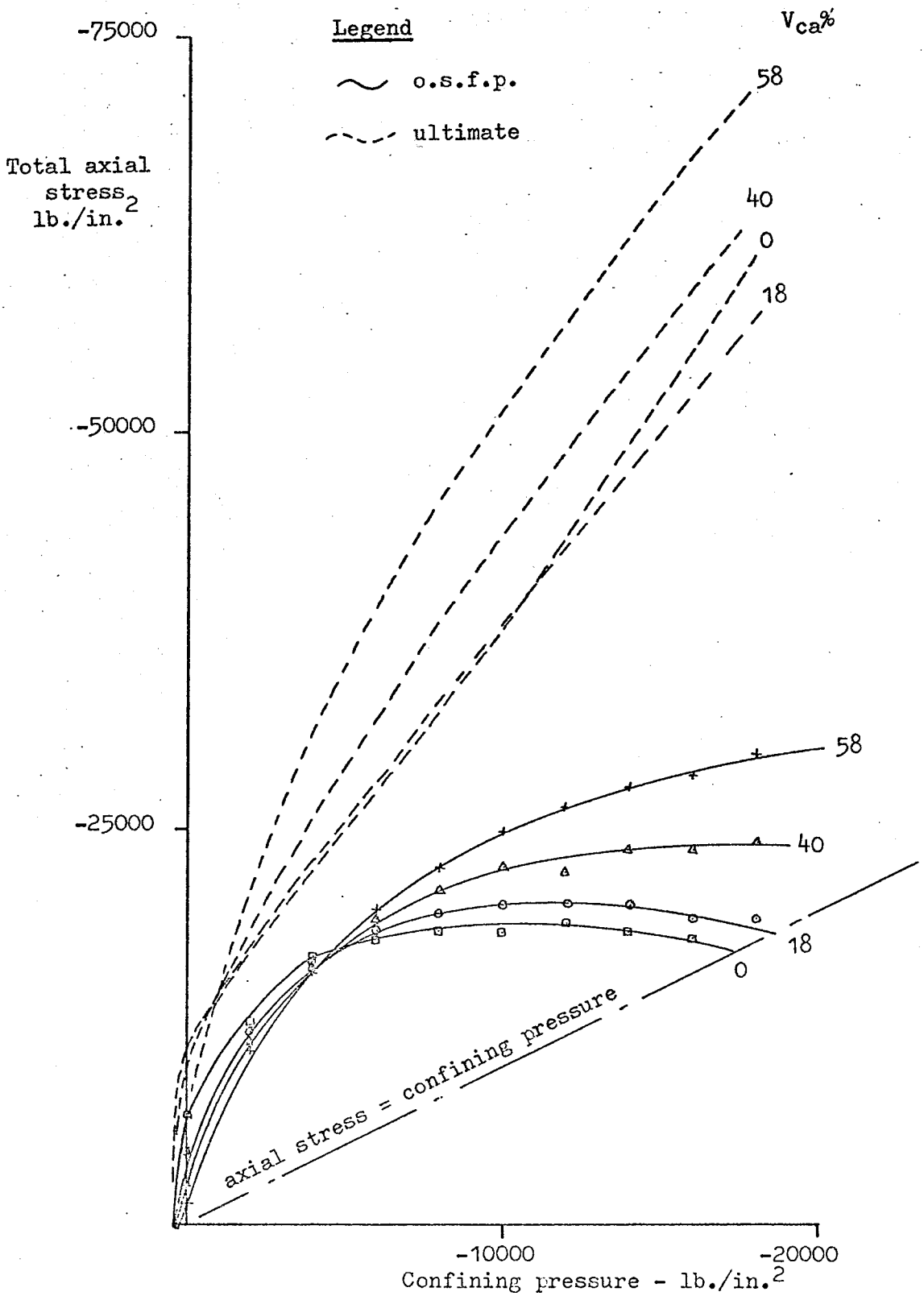


Figure 7.40. Relationship between total axial stress at o.s.f.p. and confining pressures for typical idealised concretes tested under triaxial compression (ultimate axial stress shown for comparison).

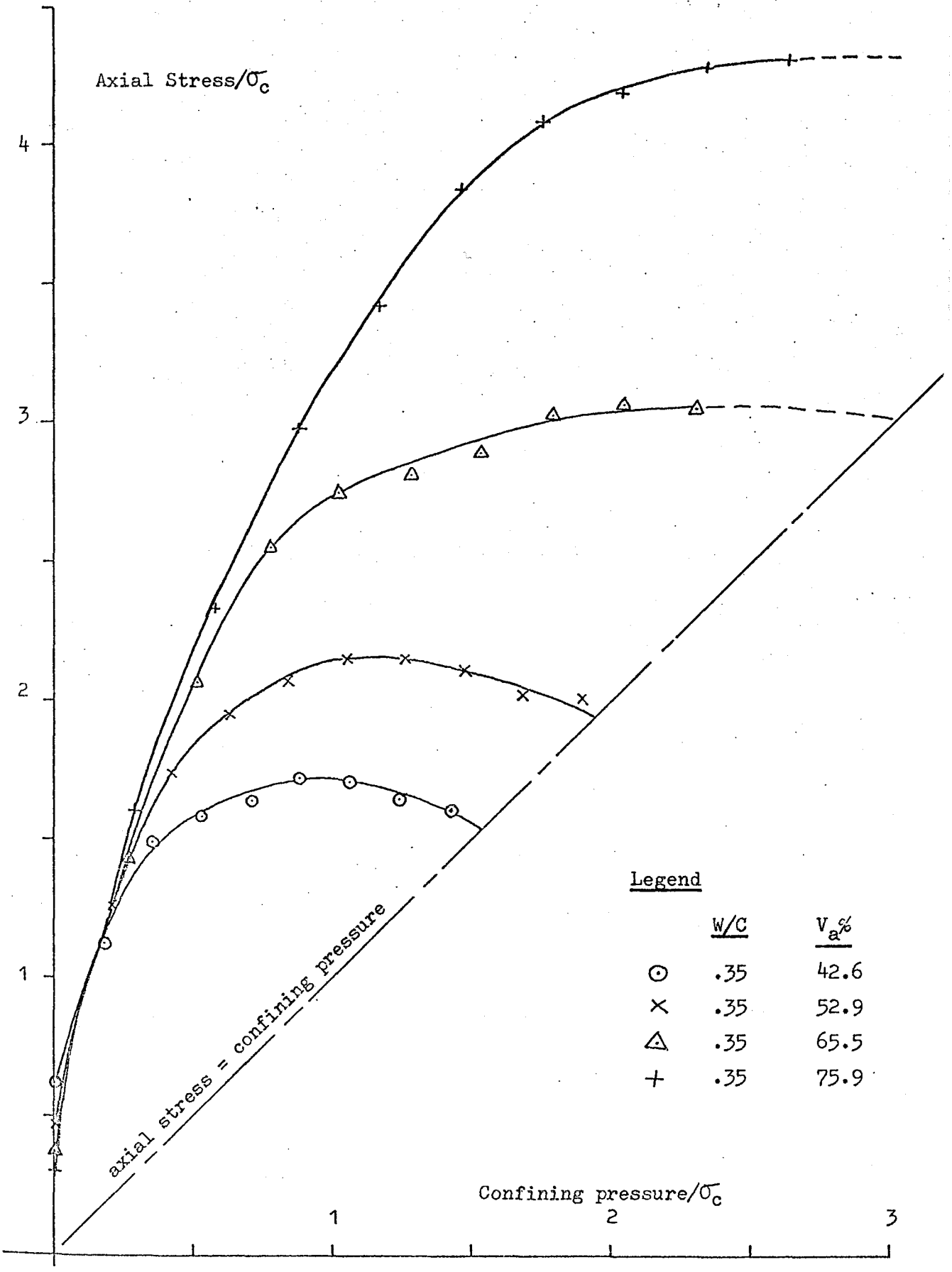


Figure 7.41. Relationship between normalised axial stress and confining pressure at onset of stable fracture propagation under triaxial compression for typical idealised concretes.

lack of sensitivity of the detection technique used by Niwa et Al, coupled with the effects of the rigid-platen method of loading used.

Undoubtedly, the apparent deformation behaviour of concrete is influenced by either the method of triaxial loading or deformation measurement since in the present tests, using surface-mounted strain gauges and hydraulic cell loading, no linear portion of the relationships between stress and axial or lateral strain is detected (see 7.5.4.). Other investigators have, however, observed distinct linearity or limits of proportionality for tests conducted using rigid-platen loading and, necessarily, measuring overall deformations [203, 204] or using conventional hydraulic cells by measuring overall, rather than local, deformations [205].

Another significant feature of Figure 7.40. is that up to a certain value of confining pressure (between 4000 and 5000 lb./in.^{2}) the axial stress at o.s.f.p. decreases with aggregate content, whereas after the level the reverse is the case. This critical level corresponds very closely to the level of confining pressure marking the end of the region of near-constant lateral tensile strain at o.s.f.p. (see Figure 7.39.) and this fact is discussed in 7.5.4.4.

This phenomenon is further demonstrated by Figure 7.42., which shows the variation of the axial stress at o.s.f.p. with V_{ca} for various values of confining pressure. For confining pressures below approximately 5000 lb./in.^{2}, the stress at o.s.f.p. decreases with V_{ca}, whereas above this pressure the trend reverses.

After this critical confining pressure level, the relative increase in the stress at o.s.f.p. with an increase in V_{ca} for a given value of confining pressure is greater between mixes containing high aggregate contents, than between those containing low volume fractions. This is to be compared with the opposite case for the strains, described in the preceding section.

The effect of aggregate content on the total axial stress and deviatoric stress at o.s.f.p. as proportions of total ultimate and deviator ultimate stress is shown in Figures 7.43. and 7.44. respectively. Both figures show a decrease in the ratios with V_{ca}, up to confining pressures of about 10000 lb./in.^{2} when total stresses are considered, and between 7500 lb./in.^{2} and 10000 lb./in.^{2} for deviator stresses. Thus at low confining pressures,

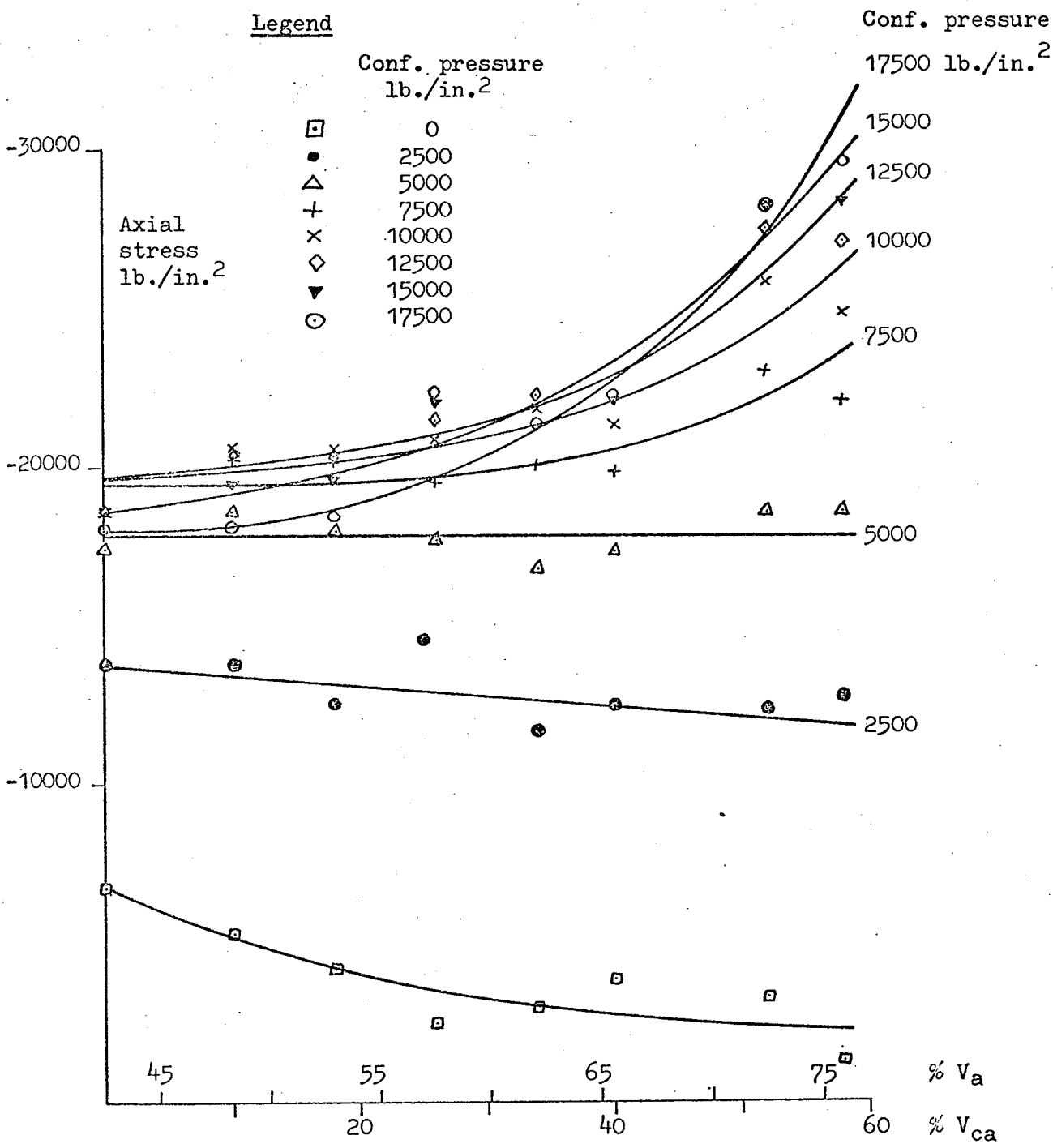


Figure 7.42 Variation of total axial stress at o.s.f.p. with volume fraction of aggregate for cylinder of idealised concretes tested under various confining pressures.

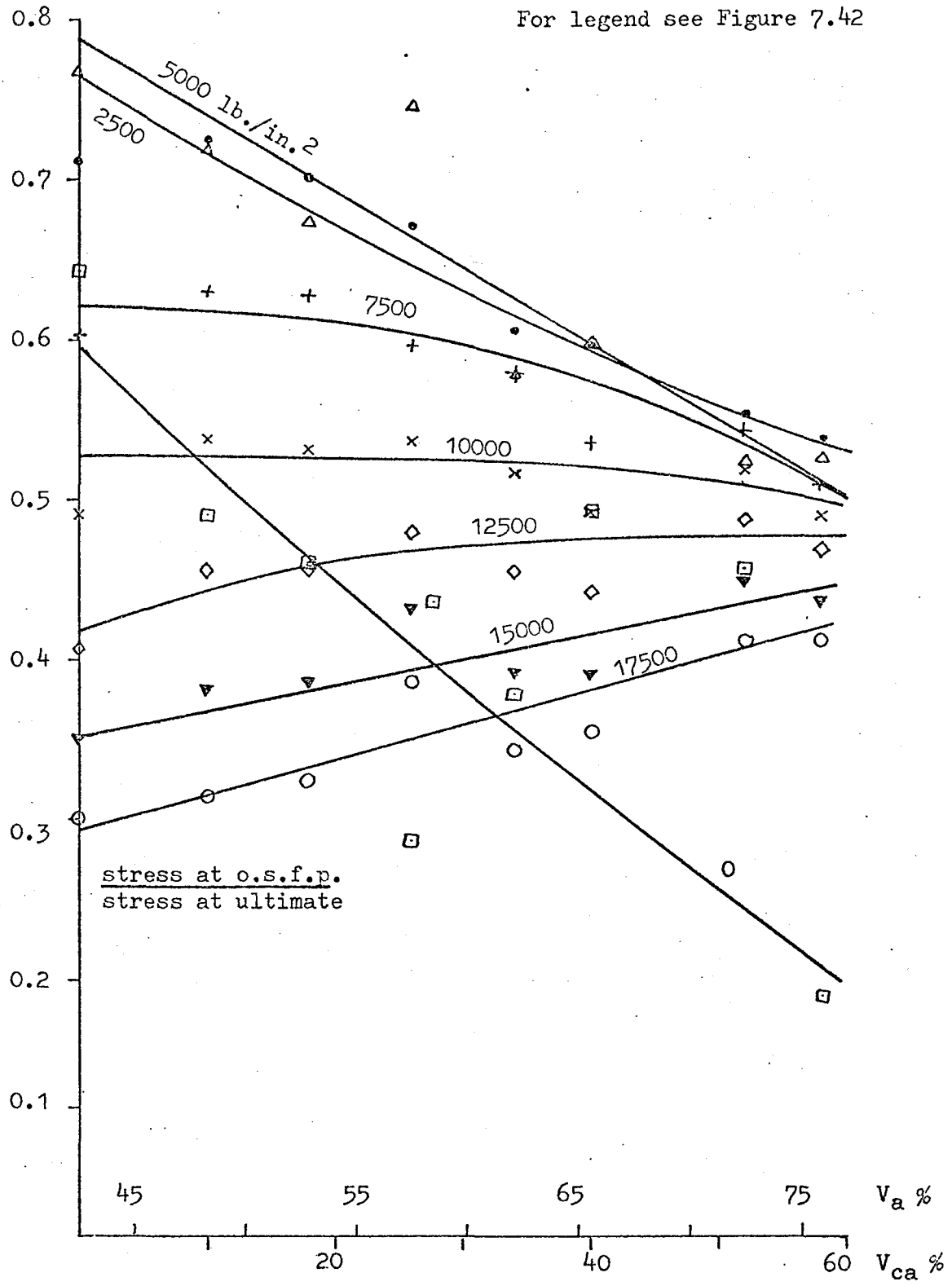


Figure 7.43. Variation of total axial stress at o.s.f.p. as a proportion of total ultimate stress for cylinders of idealised concretes tested under various confining pressures.

deviator stress at o.s.f.p.
deviator stress at ultimate

For legend see Figure 7.42.

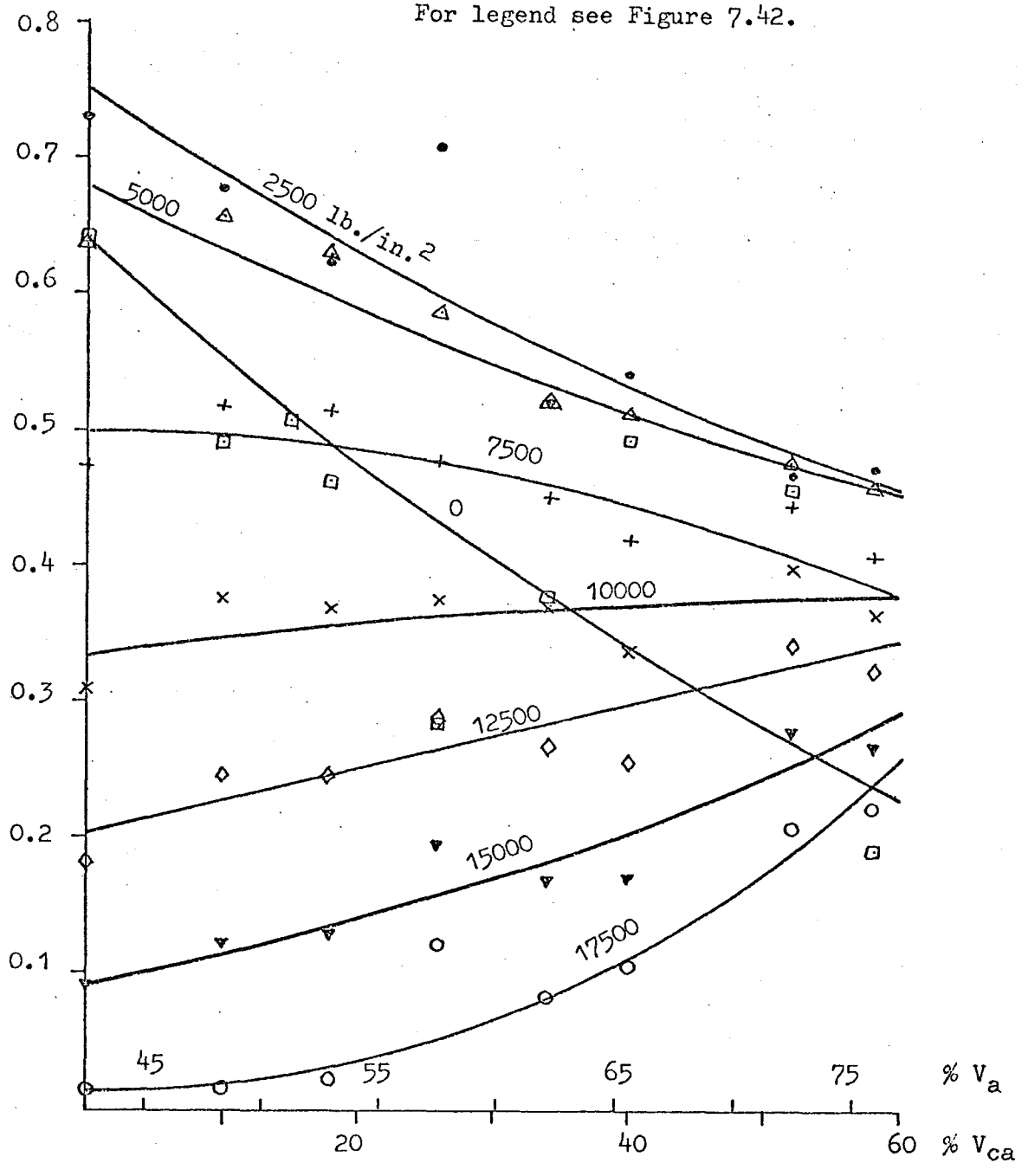


Figure 7.44. Variation of deviator axial stress at o.s.f.p. as a proportion of deviator stress at ultimate for cylinders of idealised concretes tested under various confining pressures.

increasing the heterogeneity of a mix causes significant fracture propagation to occur earlier in the loading regime, while the effect of increasing the confining pressure is to reverse this trend. A probable cause of such a reversal will be discussed in 7.5.4.4. but it is to be noted that the critical confining pressure range necessary to reverse the trend is higher when proportions of ultimate, as opposed to absolute values of stress, are considered.

Another feature of Figures 7.43. and 7.44. is the considerable scatter of results for the case of zero confining pressure, compared with that at higher pressures. This is probably due to the fracture propagation process starting from critically situated and orientated open cracks for an unconfined specimen, which will necessarily be highly dependent on the disposition of the cracks in a given specimen. If a confining pressure is imposed the cracks will tend to close, and thus the criticality of the cracks will tend to reduce, since friction across crack surfaces becomes an important factor.

7.5.4.4. Hypothesis for the Behaviour at o.s.f.p.

Envelopes defining some early changes in the structure of concrete under multiaxial load have also been found by other investigators to be of closed form in stress space [204, 205]. Thus it would appear from the results of these and the present tests, that concrete may be significantly disrupted even under a pure hydrostatic stress, if such a stress is above a critical level.

This view is supported by the work of Zimmerman [206] who noted a decrease in the uniaxial strength and reduction in stiffness of specimens of concrete tested after being unloaded from a state of hydrostatic compression.

This disruption may be caused by the following two effects acting either separately, or more likely concurrently, during the loading regime.

(i) Local Stress or Strain Concentrations

Such concentrations are caused by the heterogeneous nature of concrete, and their existence is supported by the work of Niwa, Kobayashi et Al [201, 207] who detected cracks on the underside of aggregate particles when specimens of concrete were unloaded from a state of hydrostatic compression.

These cracks apparently emanated from voids or flaws, and gave rise to bond cracks which increased with hydrostatic load. Only a relatively small number of mortar cracks were noted.

It was also found by Niwa et Al that testing a concrete under triaxial compression (using a rigid-platen loading device) induced no significant bond cracks until a stress mid-way between the hydrostatic and ultimate levels was attained. After this stage bond cracking increased, together with mortar cracking, the latter being more tortuous than that produced under uniaxial compression. For tests conducted under high confining pressures, these mortar cracks were difficult to detect but wide bond cracks were evident due, it was considered, to rotation and displacement of aggregate particles with the matrix behaving in a plastic manner.

(ii) Collapse of Paste Phase

Another factor contributing to the behaviour, apart from, or in addition to, the local stress concentrations may be the breakdown of the cement paste phase which is highly porous [208] at an early stage of deviator stress, or under a given value of confining pressure. This explanation is supported by the volume changes which concretes undergo when subjected to hydrostatic compression (see 7.5.4.5.). The confining pressure, however, prevents catastrophic crack propagation and, together with aggregate interlocking effects, causes the ultimate stress to attain a much higher value (see 7.5.4.5.).

An ultimate strength envelope for pure cement paste tested in triaxial compression, similar in shape to the o.s.f.p. envelopes derived in the present test series, has in fact been found by Palaniswamy and Shah [178]. This envelope, obtained for moist specimens of paste with a water/cement ratio of 0.7, is shown in Figure 7.45. Also shown on the figure are envelopes for a syntactic foam [209], the behaviour of which Palaniswamy and Shah have compared with that of paste, and lightweight aggregate concrete (see 6.5.), both being examples of highly porous materials.

The envelopes for paste and syntactic foam show the same

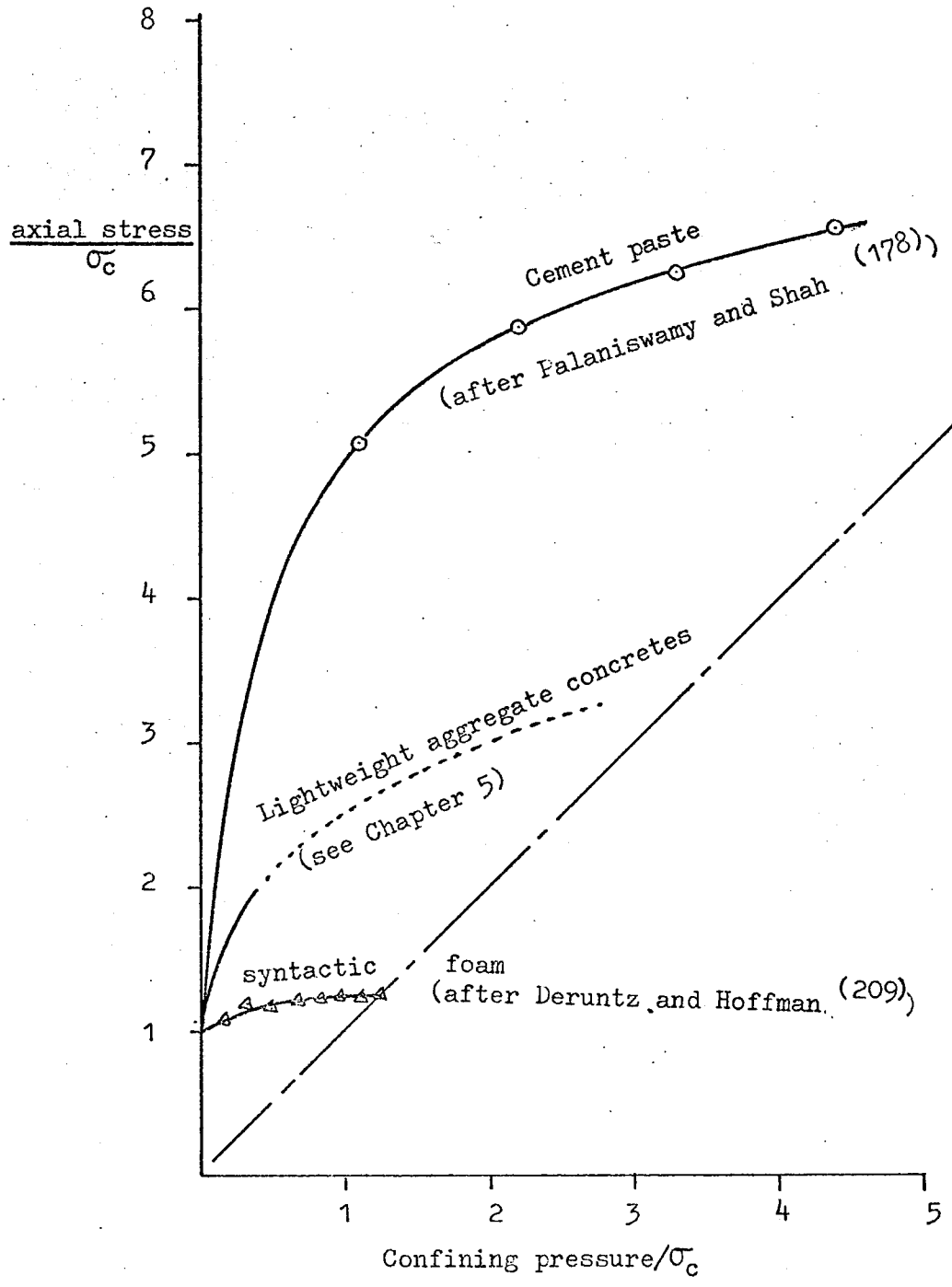


Figure 7.45. Relationships between ultimate axial stress and confining pressure both normalised with respect to the ultimate strength under uniaxial compression for cement paste, lightweight aggregate concretes and syntactic foam under triaxial compression.

characteristic of relatively high rate of increase in strength with first application of confining pressure and subsequent reduction in the rate of increase as the material collapses under hydrostatic stress. This reduction results in the material completely breaking down at a finite level of hydrostatic stress.

For lightweight concrete, the range covered by the results is insufficient to enable definite conclusions to be drawn but it would appear likely that with a sufficiently high confining pressure the curve would intersect the hydrostatic axis at

$$\sigma_{conf}/\sigma_c = 3.5 \text{ (approximately).}$$

The closed form of the o.s.f.p. envelopes, in strain terms, found for the concretes in the present series also tends to confirm the hypothesis of paste collapse since similar behaviour has been noted for the failure of pure cement paste under triaxial compression [178]. The graphical results reported in this latter work are re-plotted in Figure 7.46. in a form similar to that used for the present test series (see Figure 7.39.). The remarkable similarity between these two figures is at once apparent. For the pure paste the mode of failure up to, and including, confining pressures of 4000 lb./in.^{2} was described by Palaniswamy and Shah as 'tensile splitting' while those failures of above this pressure were said to be of a 'crushing' type.

Effect of Aggregate Content

Below a certain level of confining pressure, the axial stress at o.s.f.p. decreases with V_{ca}, while above this the reverse is the case. The fact that this pressure level is similar to that marking the end of the region of near-constant lateral tensile strain at o.s.f.p. suggests that below this level fracture propagation is caused mainly by the effects of heterogeneity, as opposed to paste collapse (c.f. 'tensile splitting' zone of Palaniswamy and Shah [178]. Above this pressure level paste collapse becomes the predominant factor. However, the aggregate framework can transmit part of the applied stress by acting as thrust rings [210], thus reducing the effective stress on the paste and raising the critical stress necessary to induce detectable paste collapse.

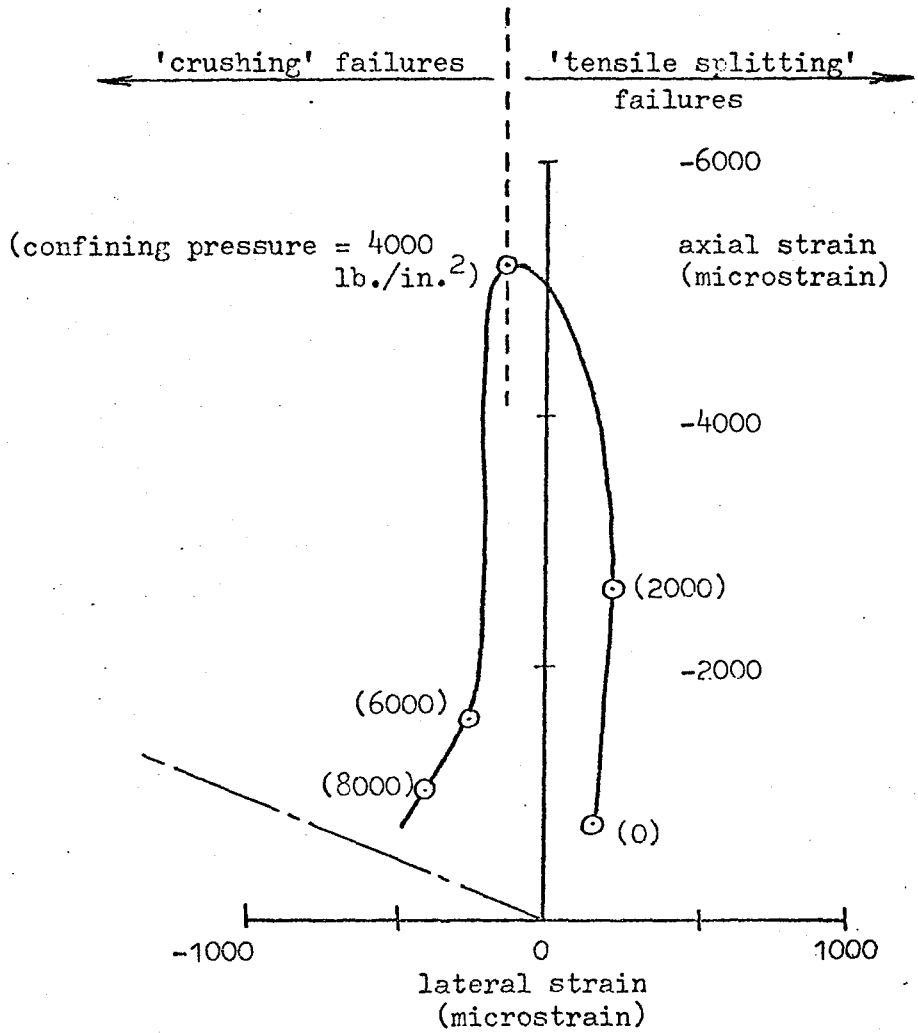


Figure 7.46. Relationship between axial and lateral strains at ultimate for a cement paste under triaxial compression.

(Derived from data obtained by Palaniswamy and Shah [178])

The relative rise in o.s.f.p. stress level with aggregate content may also be due, in some measure, to the sensitivity of the fracture detection technique, which relies on the measurement of relative changes in overall strain. As the volume fraction of aggregate increases, the volume fraction of paste decreases thus reducing the overall magnitude of the effects of collapse. As the sensitivity of the strain measuring technique remains constant it may be possible that such effects, although significant at the local level, will remain undetected phenomenologically. This latter reason is thought to effect the apparent behaviour only to a slight degree since the measured variation of i.s.r. (see Figures 7.34. to 7.37.) is such that in most cases a minimum value is being sought, with the 'damping' effects being in operation both before and after this value.

7.5.4.5. Volume Changes

Figures 7.47. to 7.50. show the relationships between volume changes and total axial stress at various confining pressures.

The curves generally show the following trends:-

i) a non-linear volume decrease for an increase in hydrostatic stress followed by -

ii) a further decrease in volume on application of deviator stress, and -

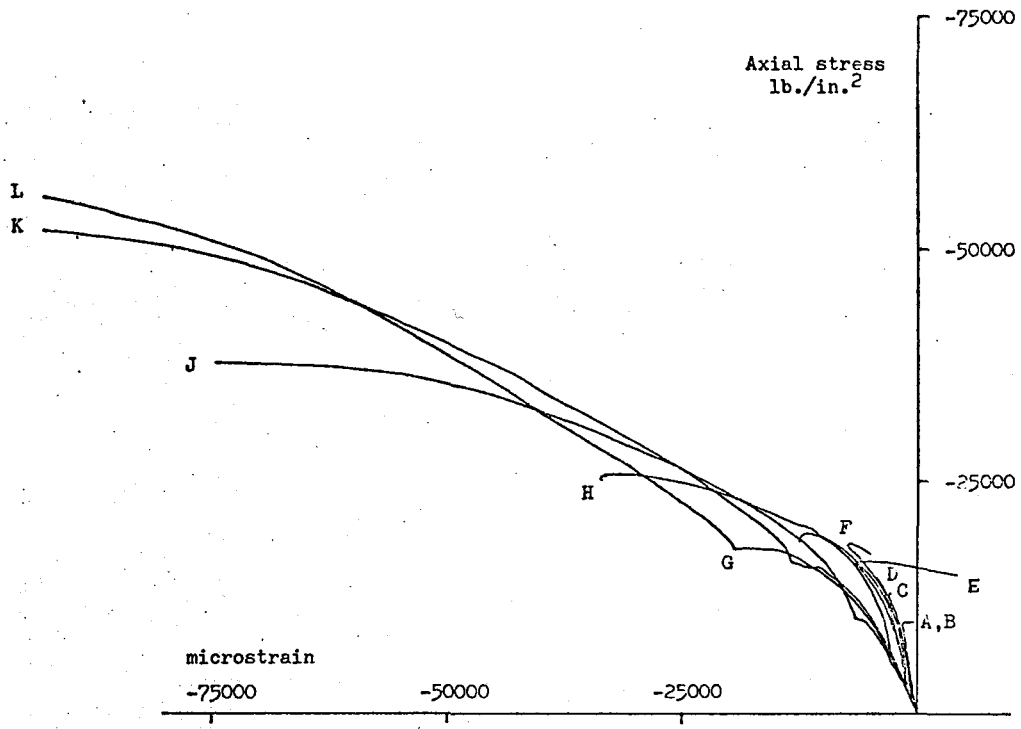
iii) a reversal of the volume change at a stress approaching ultimate, such that the volume attains a minimum value before increasing up to failure.

These characteristics will be discussed in turn in the following sections.

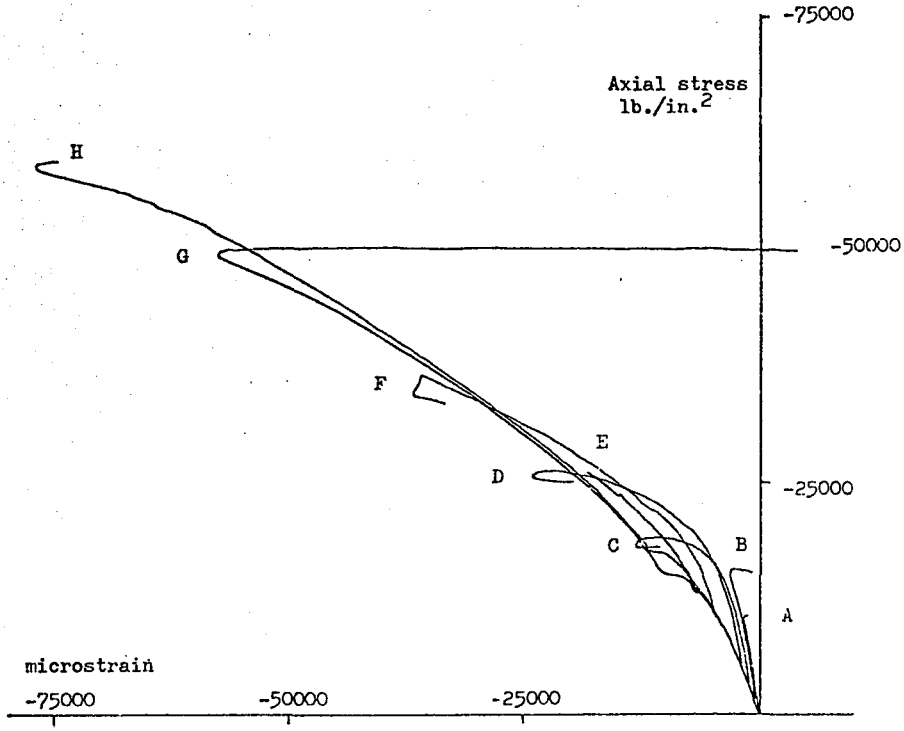
Hydrostatic Compressibility

Figures 7.51. to 7.54. show the relationship between volumetric strain and confining pressure for the various mixes, each figure containing results for all specimens of the mix.

For the initial application of confining pressure the relationship is very nearly linear. As the pressure is increased, however, the volume starts

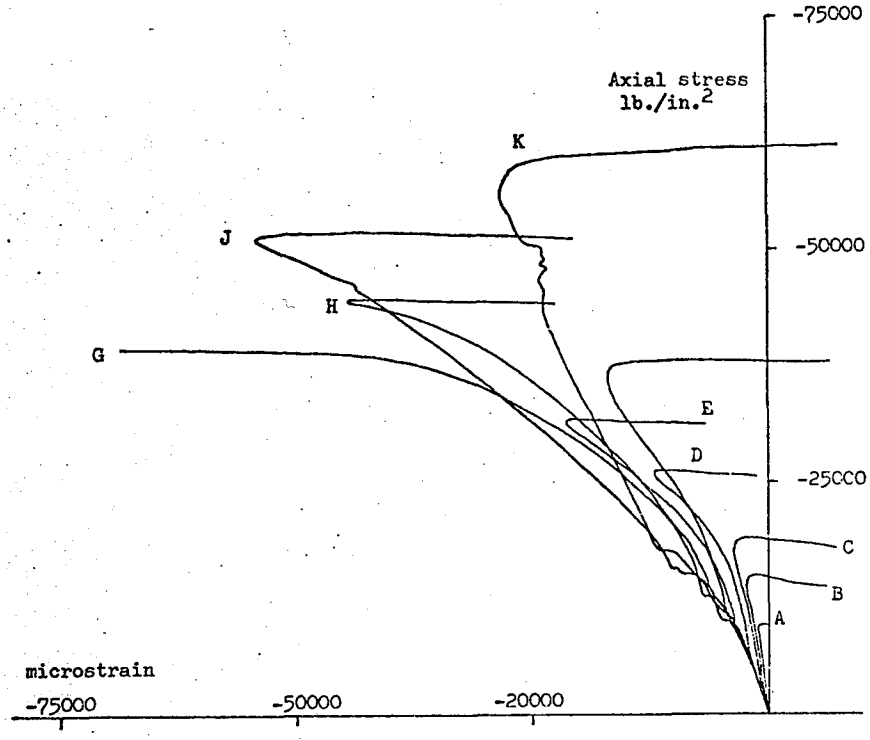


(a) Mix I_0

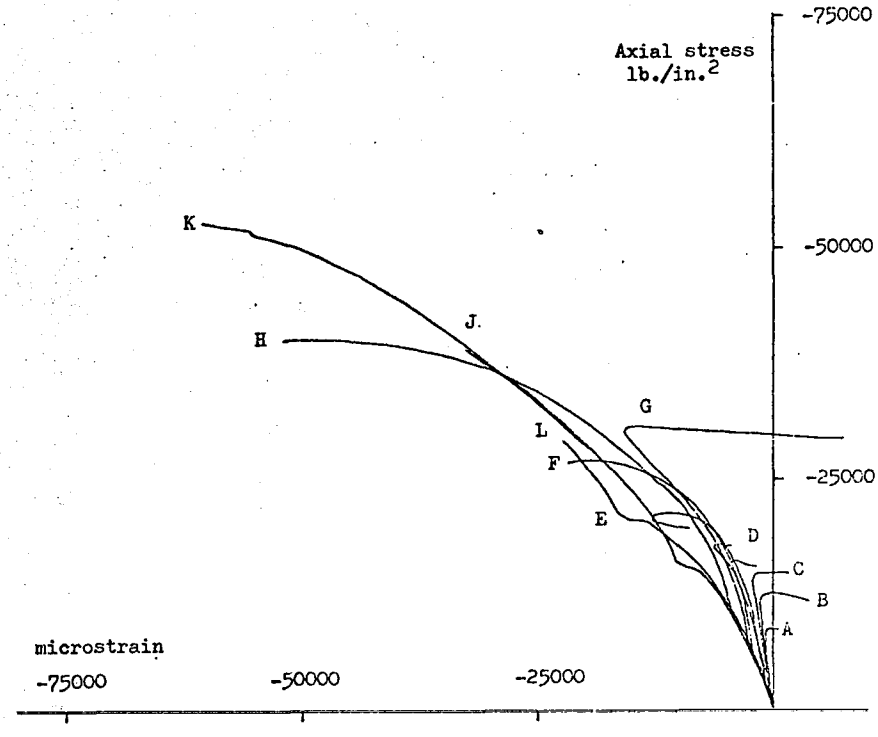


(b) Mix I_{10}

Figure 7.47. Variation of volumetric strain with total axial stress for idealised concretes under triaxial compression with various values of confining pressure.

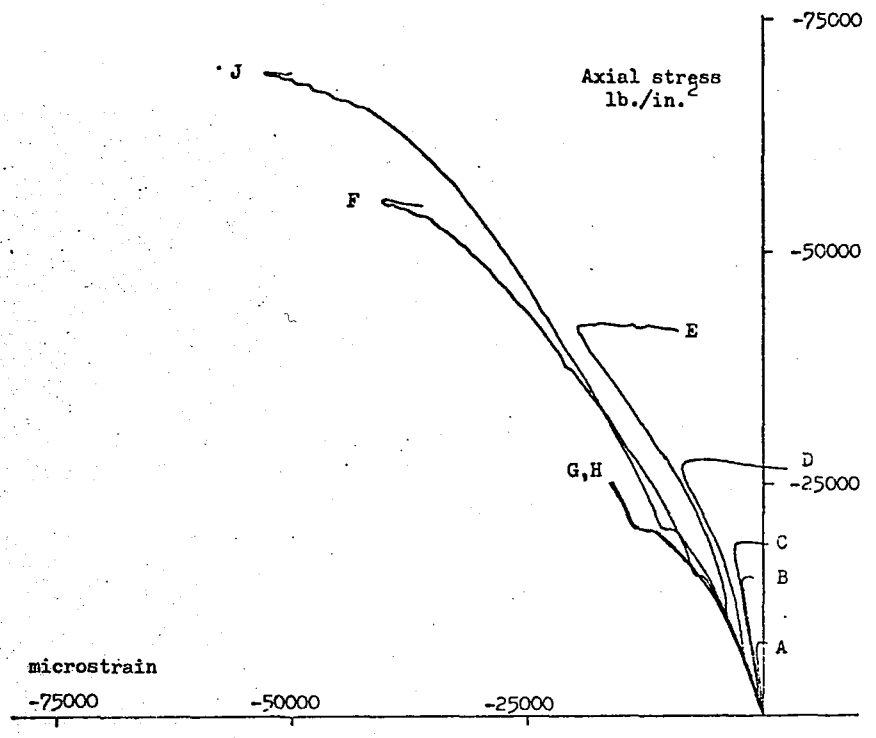


(a) Mix I_{18}

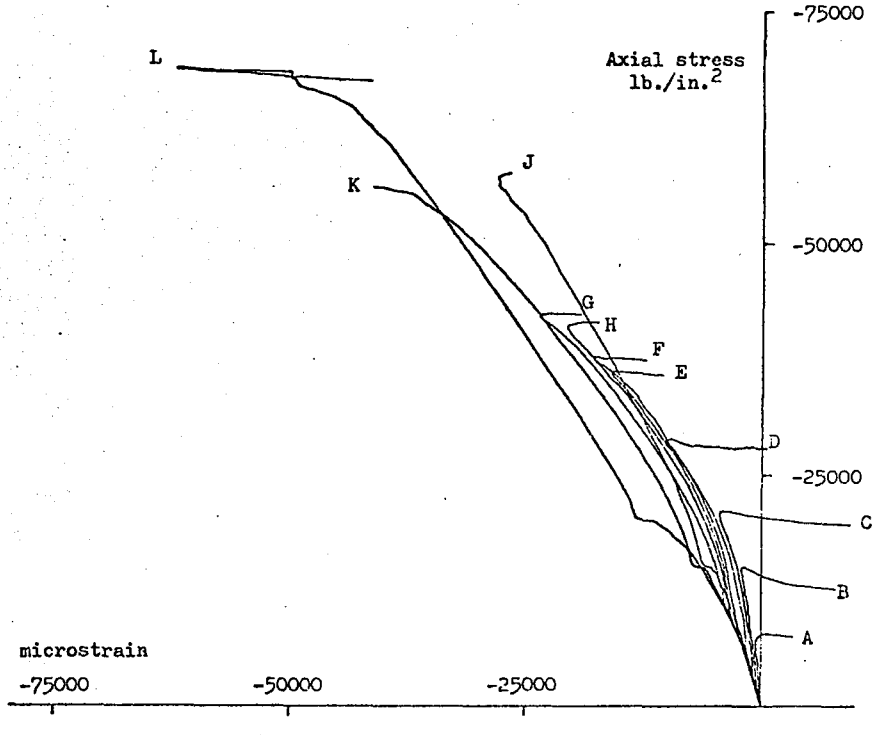


(b) Mix I_{26}

Figure 7.48. Variation of volumetric strain with total axial stress for idealised concretes under triaxial compression with various values of confining pressure.

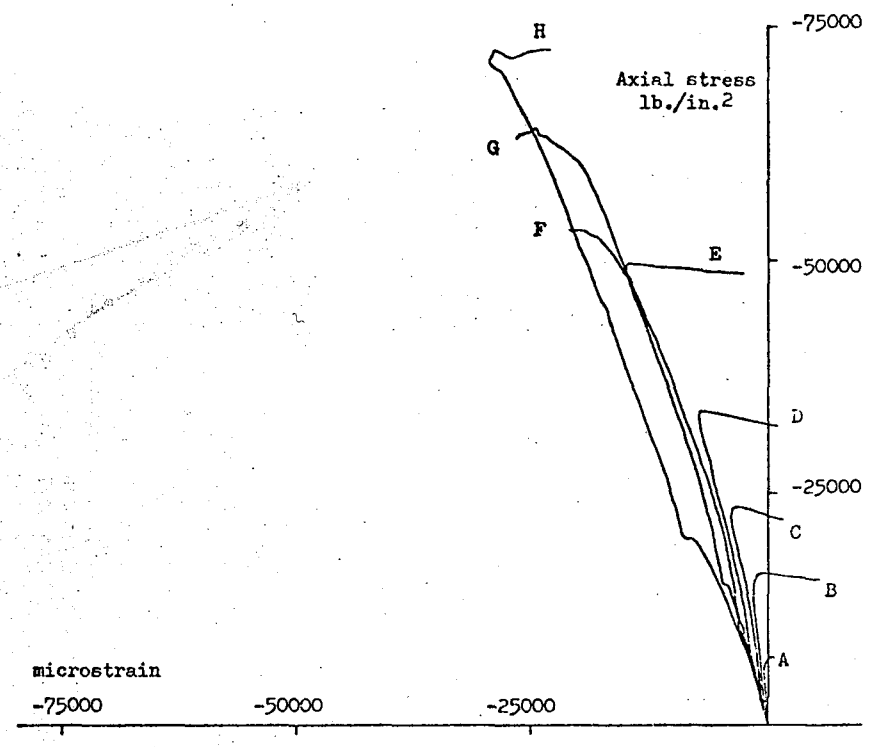


(a) Mix I_{34}

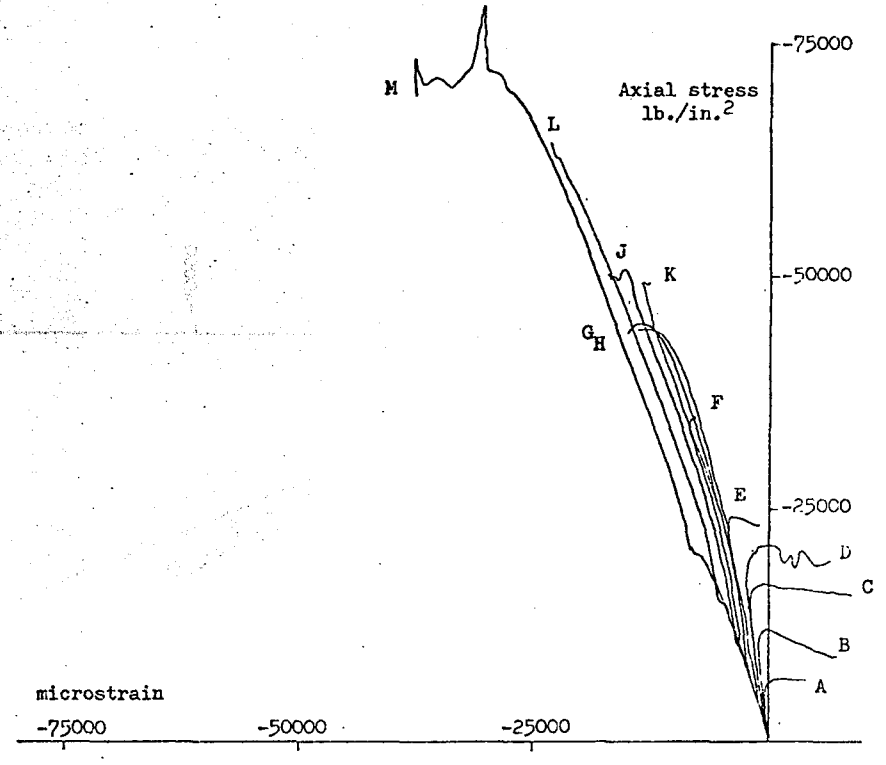


(b) Mix I_{40}

Figure 7.49. Variation of volumetric strain with total axial stress for idealised concretes under triaxial compression with various values of confining pressure.

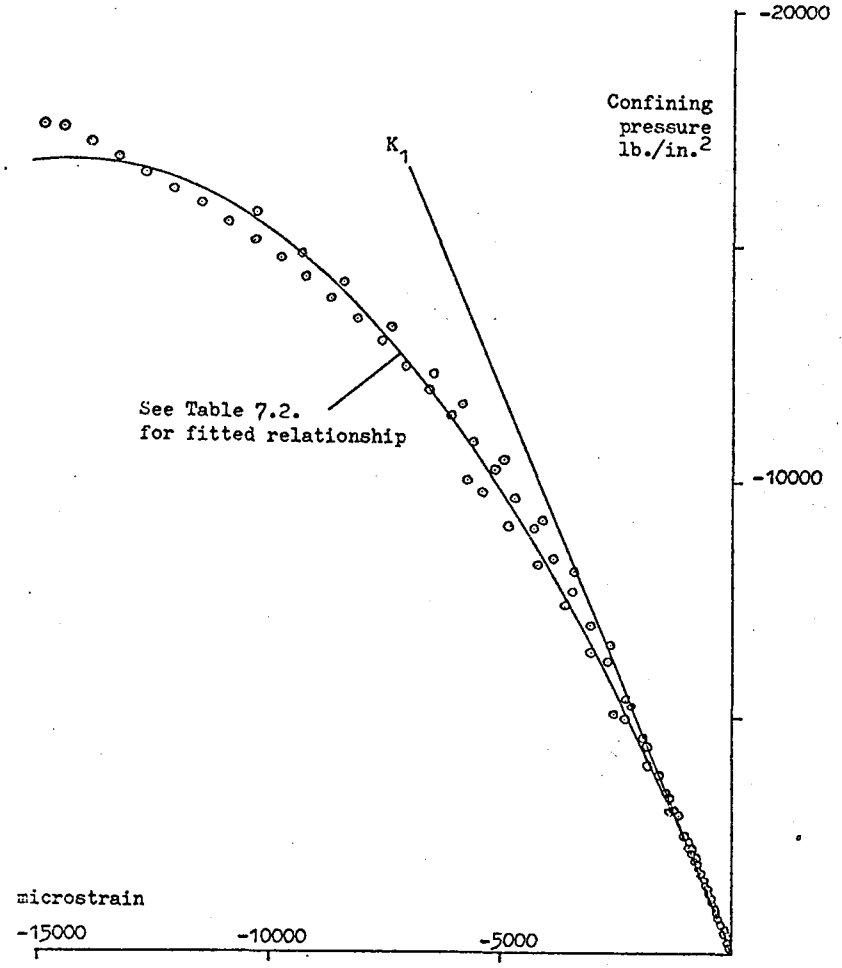


(a) Mix I_{52}

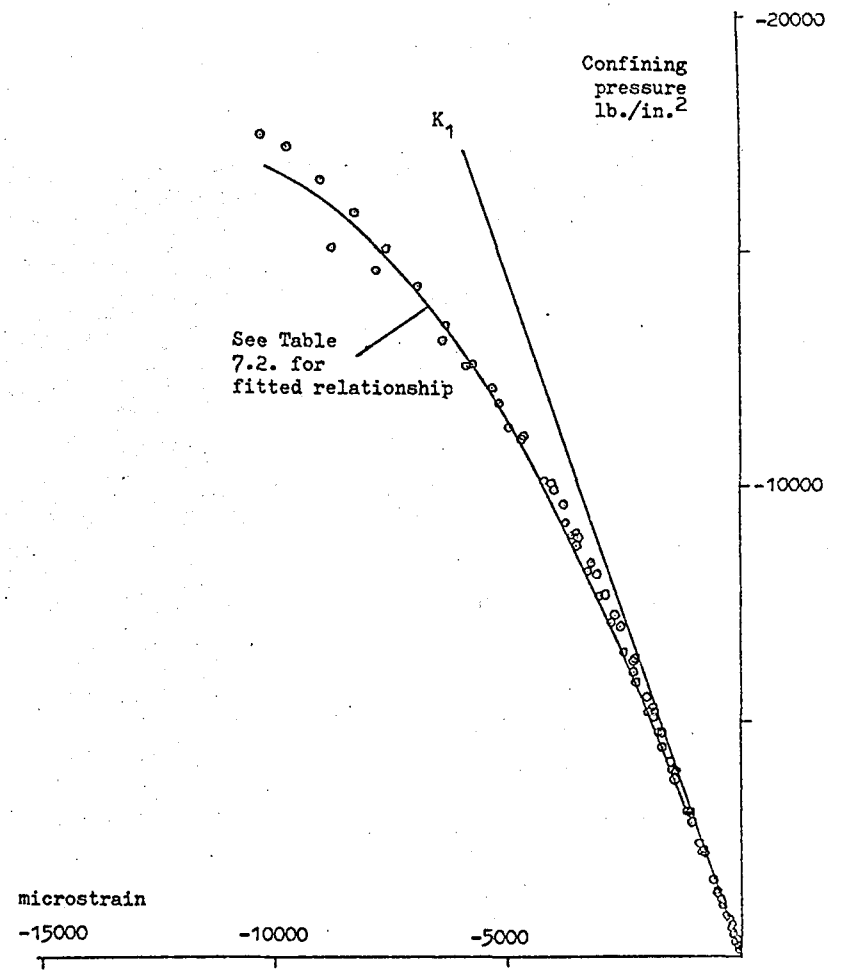


(b) Mix I_{58}

Figure 7.50. Variation of volumetric strain with total axial stress for idealised concretes under triaxial compression with various values of confining pressure.

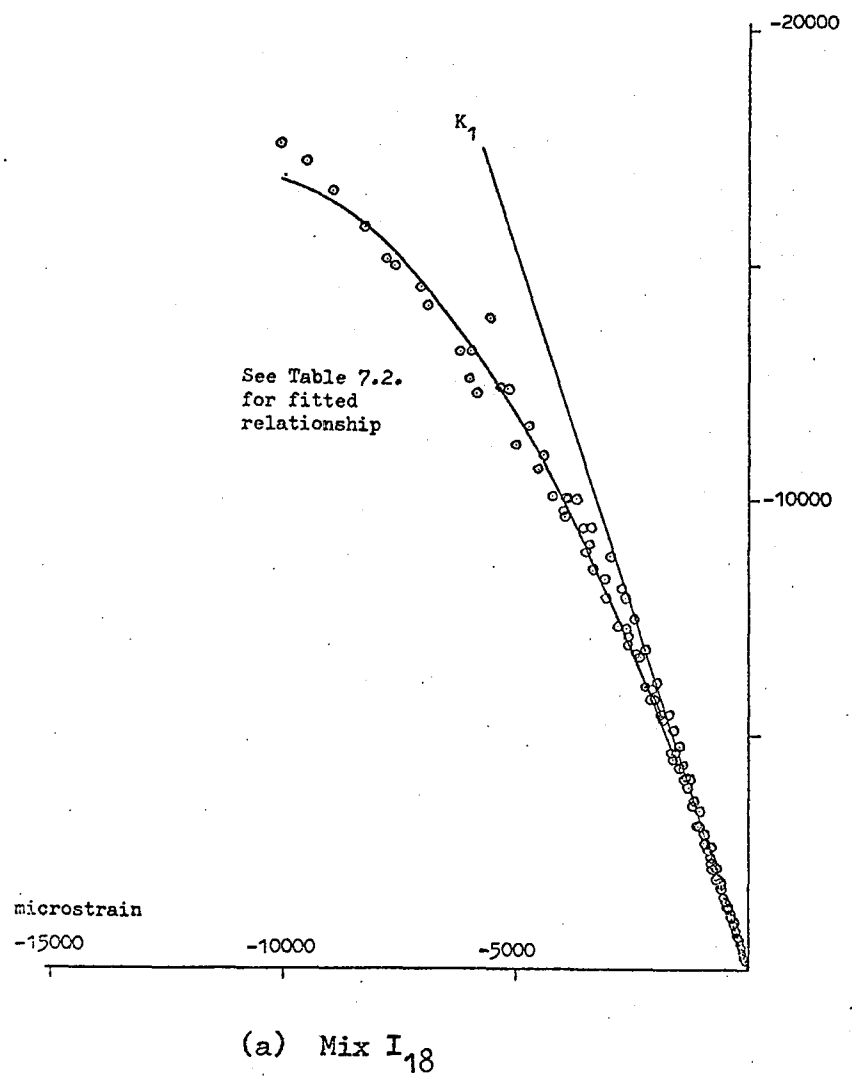


(a) Mix I_0

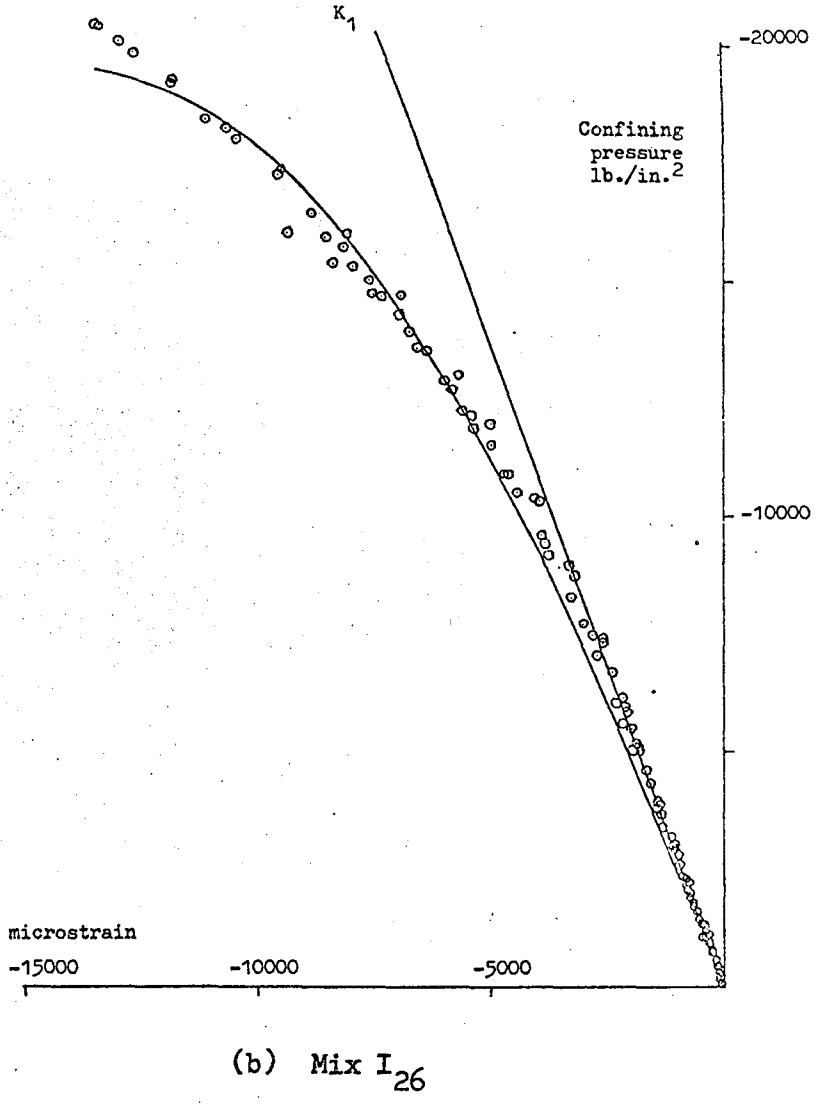


(b) Mix I_{10}

Figure 7.51. Variation of volumetric strain with confining pressure for idealised concretes during the hydrostatic portions of triaxial 'compression' tests.

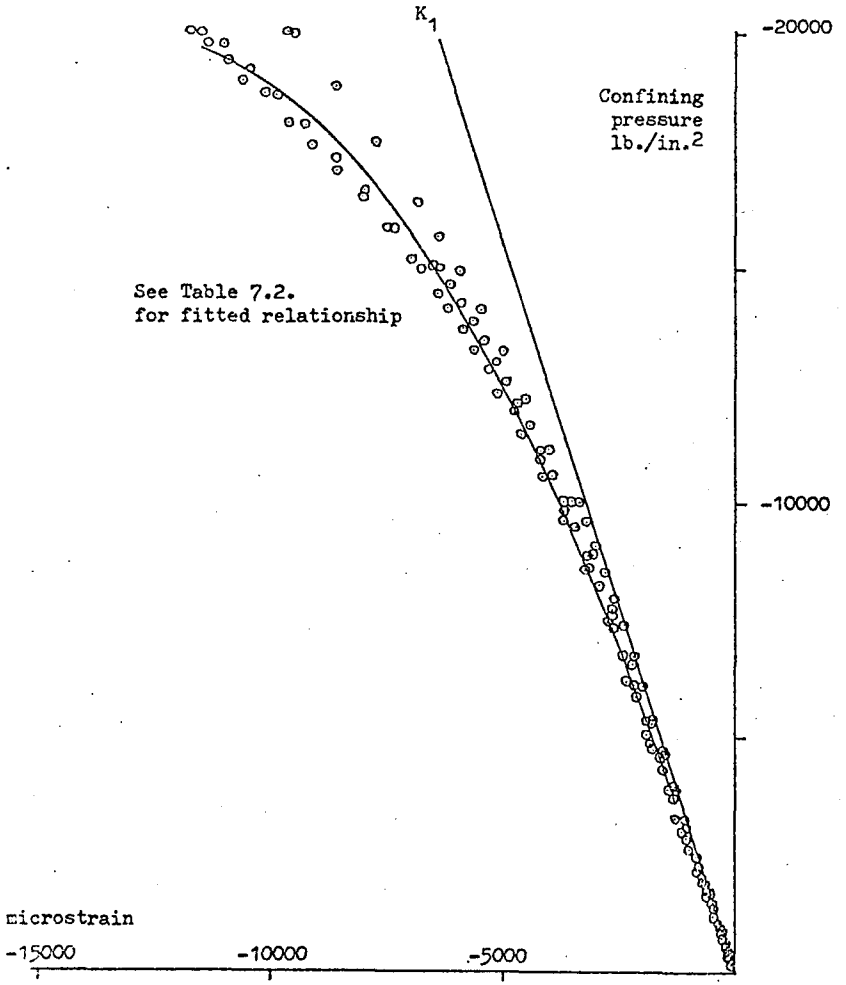


(a) Mix I_{18}

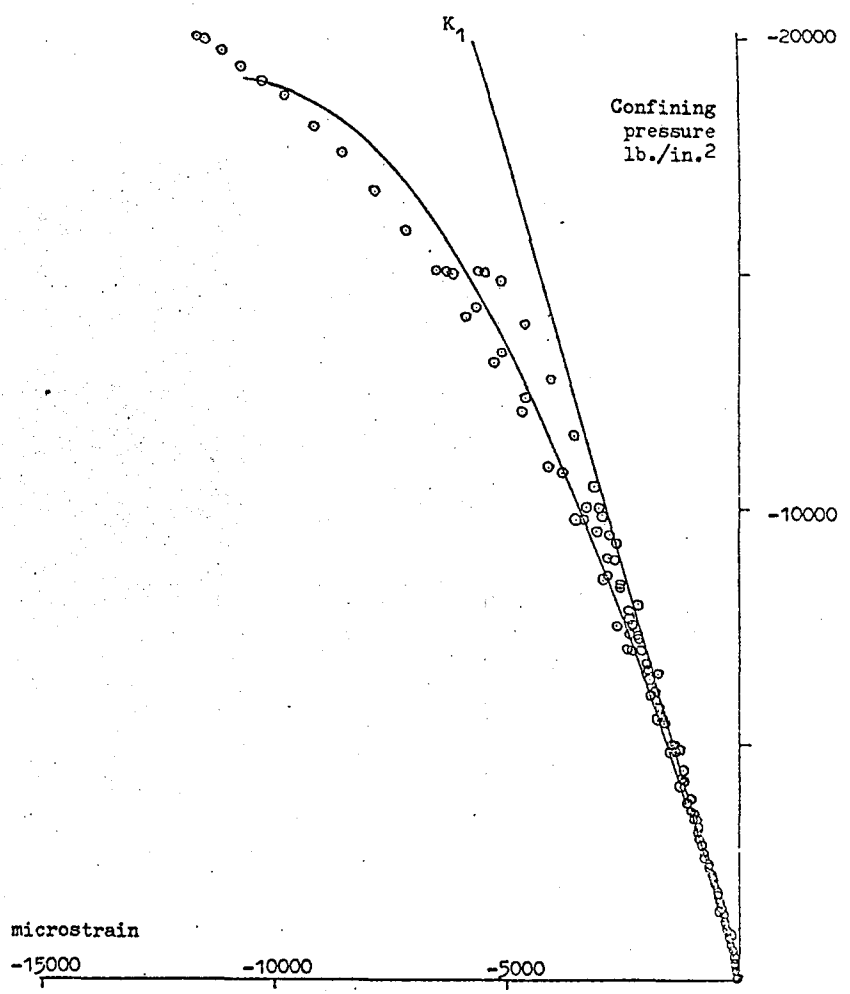


(b) Mix I_{26}

Figure 7.52. Variation of volumetric strain with confining pressure for idealised concretes during the hydrostatic portions of triaxial 'compression' tests.

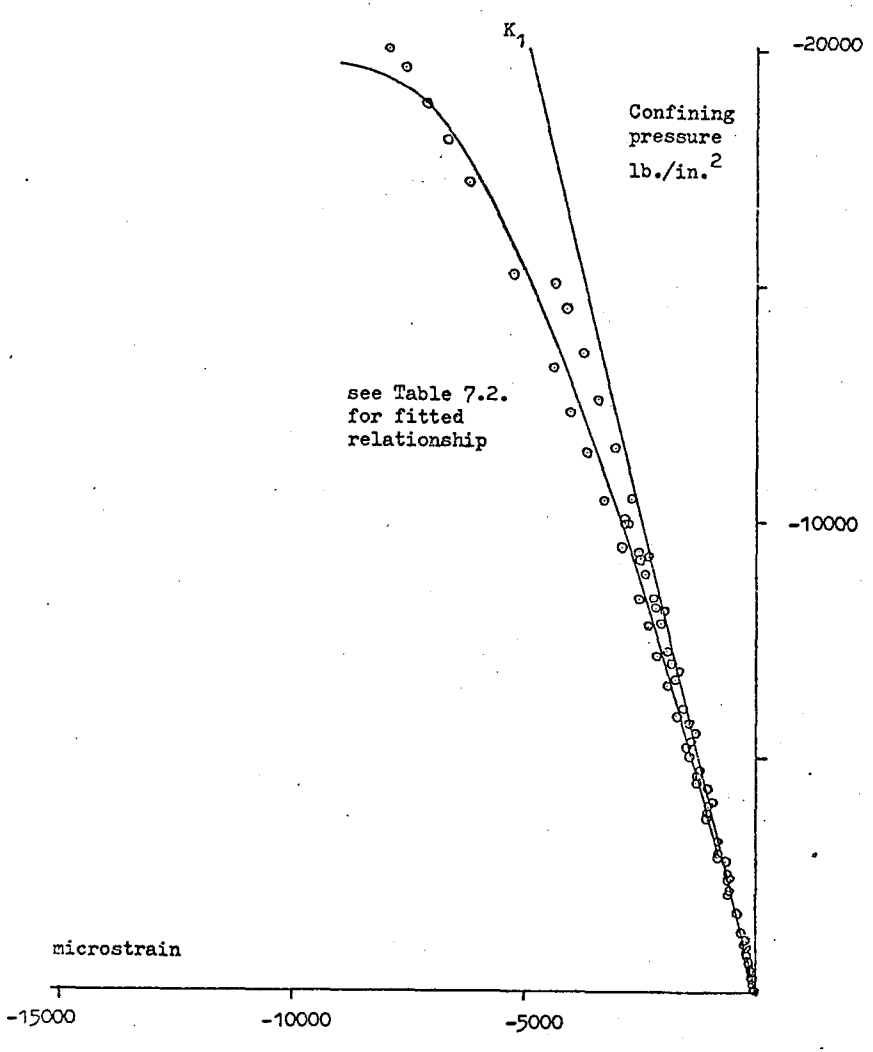


(a) Mix I_{34}

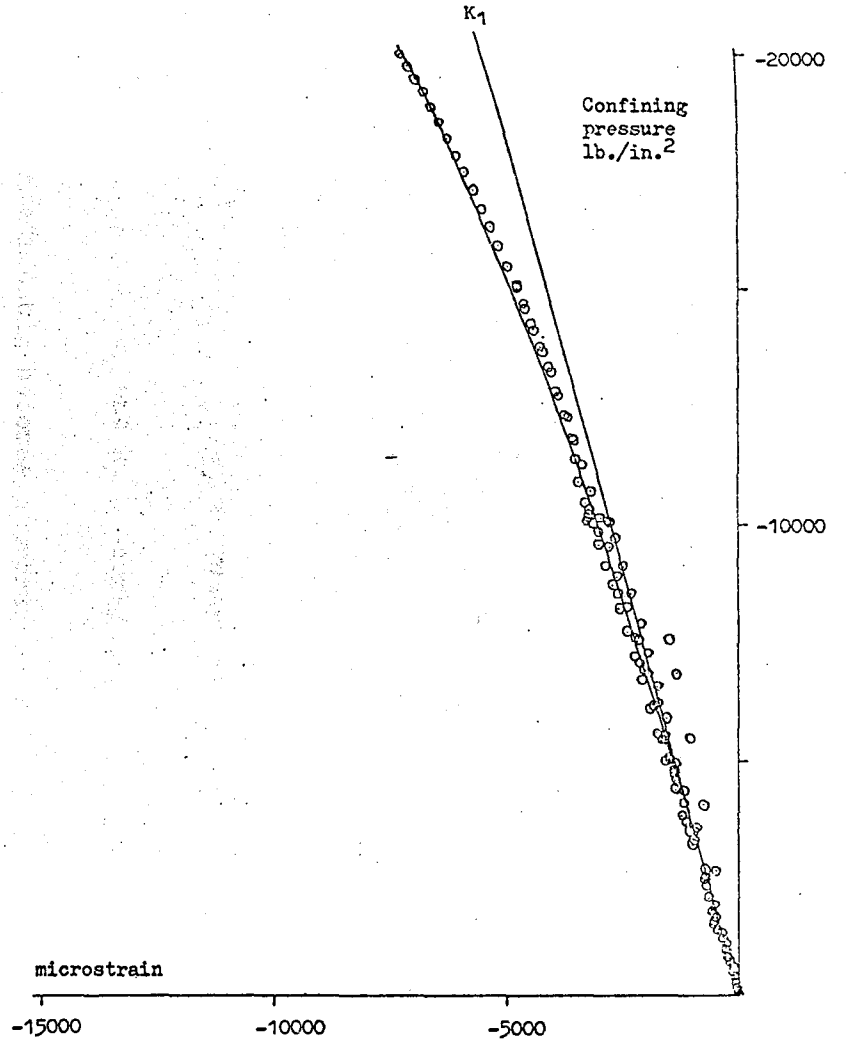


(b) Mix I_{40}

Figure 7.53. Variation of volumetric strain with confining pressure for idealised concretes during the hydrostatic portions of triaxial 'compression' tests.



(a) Mix I_{52}



(b) Mix I_{58}

Figure 7.54. Variation of volumetric strain with confining pressure for idealised concretes during the hydrostatic portions of triaxial 'compression' tests.

to decrease rapidly and the resulting curves become distinctly non-linear. The non-linearity is more marked for the mixes containing low V_{ca} and it is considered that it is due to the breakdown of the porous cement paste (see 7.5.4.4.). The characteristic shape of the curves can be closely approximated by a relationship of the form:-

$$\bar{\sigma}_{conf} = k_1 e_v + k_2 e_v^2$$

where $\bar{\sigma}_{conf}$ = confining pressure

e_v = volumetric strain

k_1 and k_2 = constants for a given mix

Such a relationship becomes approximately linear for small values of volumetric strain with an initial gradient of k_1. As the strain increases the relationship becomes increasingly more curved.

The best fit equations for the mixes, found using a minimum neighbourhood least squares method [182], are given in Table 7.2. The equations are superimposed on Figures 7.51. to 7.54. from which it can be seen that the fit is generally close except at high confining pressures where the curvature of the fitted relationships is excessive.

The line corresponding to the best fit value of k_1 is also shown on the figures and the variation of this constant, relating closely to initial compressibility, with V_{ca}, is shown in Figure 7.55. which shows the expected increase in stiffness with increasing aggregate content. Such an increase follows from the increasing content of relatively stiff glass aggregate (compressibility = 6.49×10^6 lb./in.^{2}) in the softer mortar matrix (initial compressibility = 2.5×10^6 lb./in.^{2} approximately).

Figure 7.55. also shows the upper and lower bounds based on the following 2-phase models:-

$$\text{Upper bound} \quad k_1 = (1 - V_{ca})k_m + V_{ca}k_a$$

$$\text{Lower bound} \quad 1/k_1 = (1 - V_a)/k_m + V_{ca}/k_a$$

V_{ca} %	V_a %	K_1 (lb./in.^{2} - microstrain units)	K_2
0	42.5	2.3879	0.0008447
10	48.3	2.9211	0.0001236
18	52.9	3.0605	0.0001382
26	57.5	2.7818	0.0000987
34	62.1	3.1335	0.0001234
40	65.5	3.5322	0.0001624
52	72.4	4.1111	0.0002046
58	75.9	3.6840	0.0001222

Table 7.2. Least squares values of K_1 and K_2 in the equation $\sigma_{conf} = K_1 e_v + K_2 e_v^2$ relating volumetric strain and confining pressure for idealised concrete mixes.

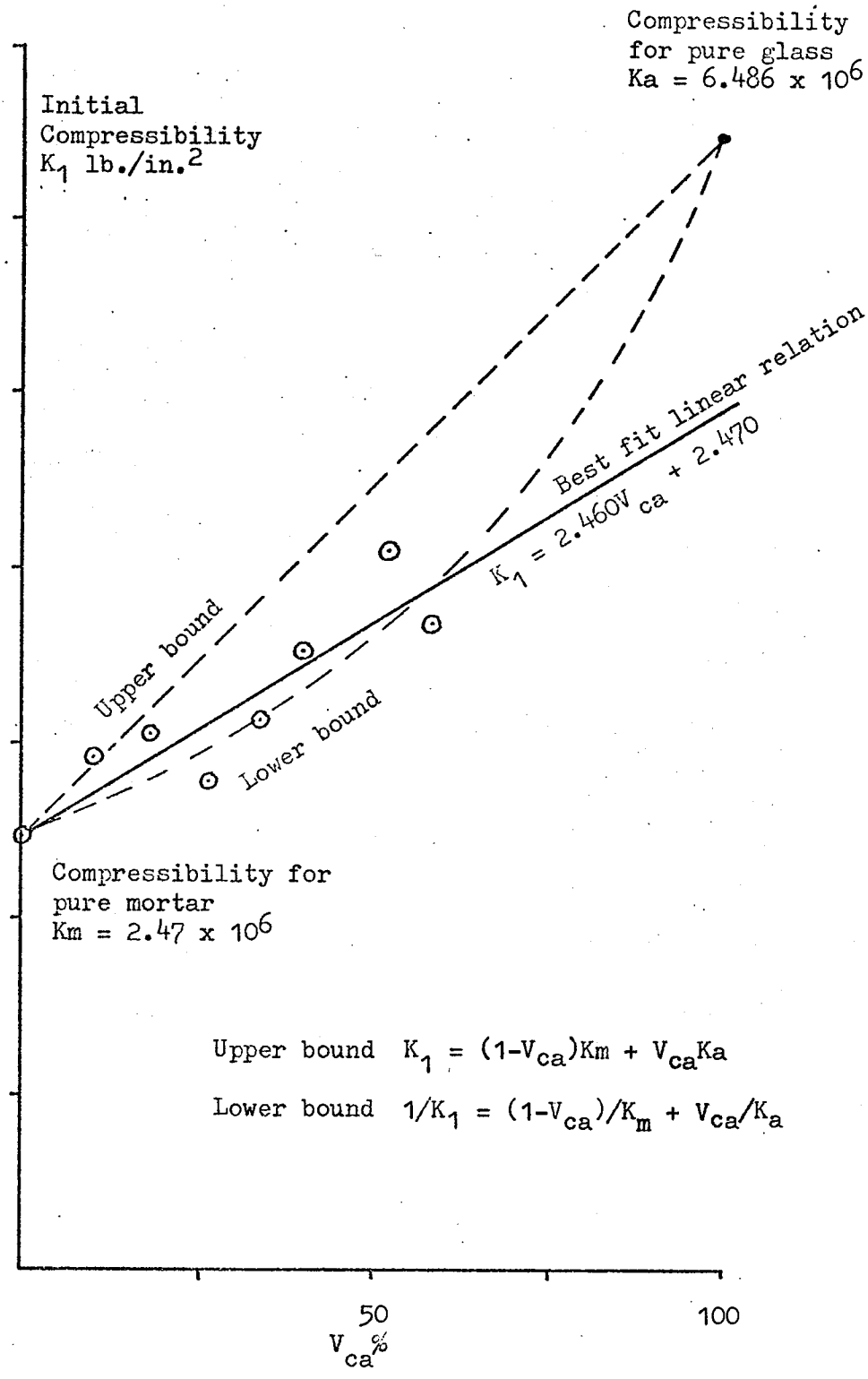


Figure 7.55. Variation of initial compressibility K_1 with V_{ca} for idealised concrete mixes.

where k_m = compressibility for pure matrix

k_a = compressibility for pure aggregate

k_1 = compressibility for composite

The compressibility data generally lie between the two bounds, showing that the materials can be considered to a good degree of approximation as two-phase materials consisting of mortar matrix with aggregate inclusions.

Volume Changes during Deviatoric Loading

These are shown in Figures 7.56. to 7.59. Only the volume changes occurring after the end of hydrostatic loading are represented, and each figure refers to the changes for the mixes tested under one nominal confining pressure.

For all confining pressures, the larger volume decreases are given for those mixes containing low volume fractions of aggregate. This is due to the decrease in the content of aggregate which is more volume stable than the mortar matrix. Hobbs [199] has also noted similar behaviour.

In all cases the rate of decrease of volume increases with increasing stress up to the stage when cracking significantly influences the process. After this stage, cracking induces a reversal in the trend due to a superimposed volume increase. This causes the volume change-stress relationship to pass through a minimum level after which the volume increases to failure.

This volume decrease followed by dilatation prior to failure has been observed for rocks [95, 94, 84, 85, 87] and concrete [131] under uniaxial and triaxial compression. Such a volume decrease followed by dilatation to failure has been observed not only for rocks and concrete but also for non-cementitieous materials [211] and cast iron [212], and is due to the massive opening of interstices or void formation within the material. Shah and Winter [127] consider this dilatation to be caused by increasingly extensive mortar matrix cracking.

7.5.4.6. Onset of Unstable Fracture Propagation (o.u.f.p.)

For a compression test the o.u.f.p. level is defined as that level of stress or strain at which the material attains a minimum volume (see 4.5.2.) and it will be seen from the preceding sections that the level is clearly

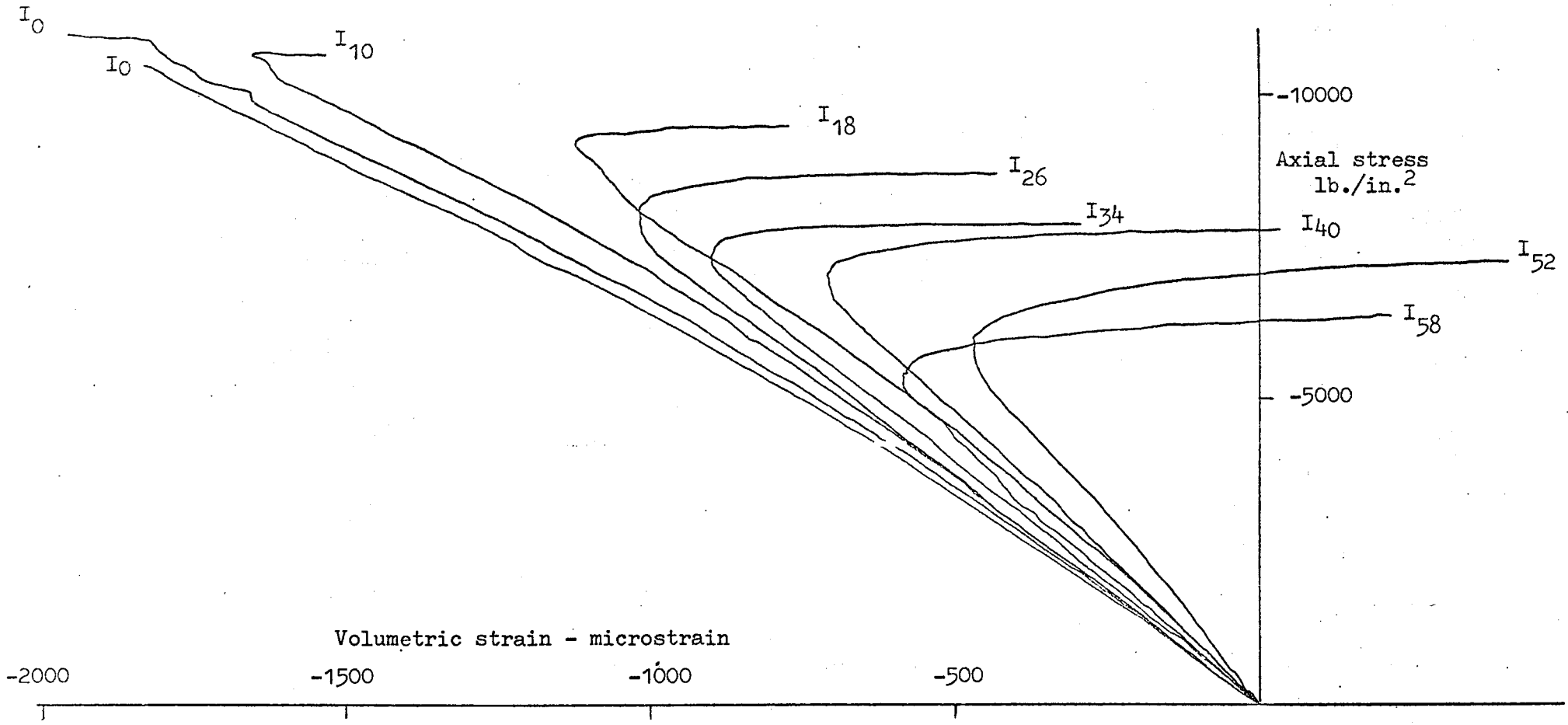


Figure 7.56. Variation of volumetric strain with axial stress for cylinders of idealised concretes under uniaxial compression.

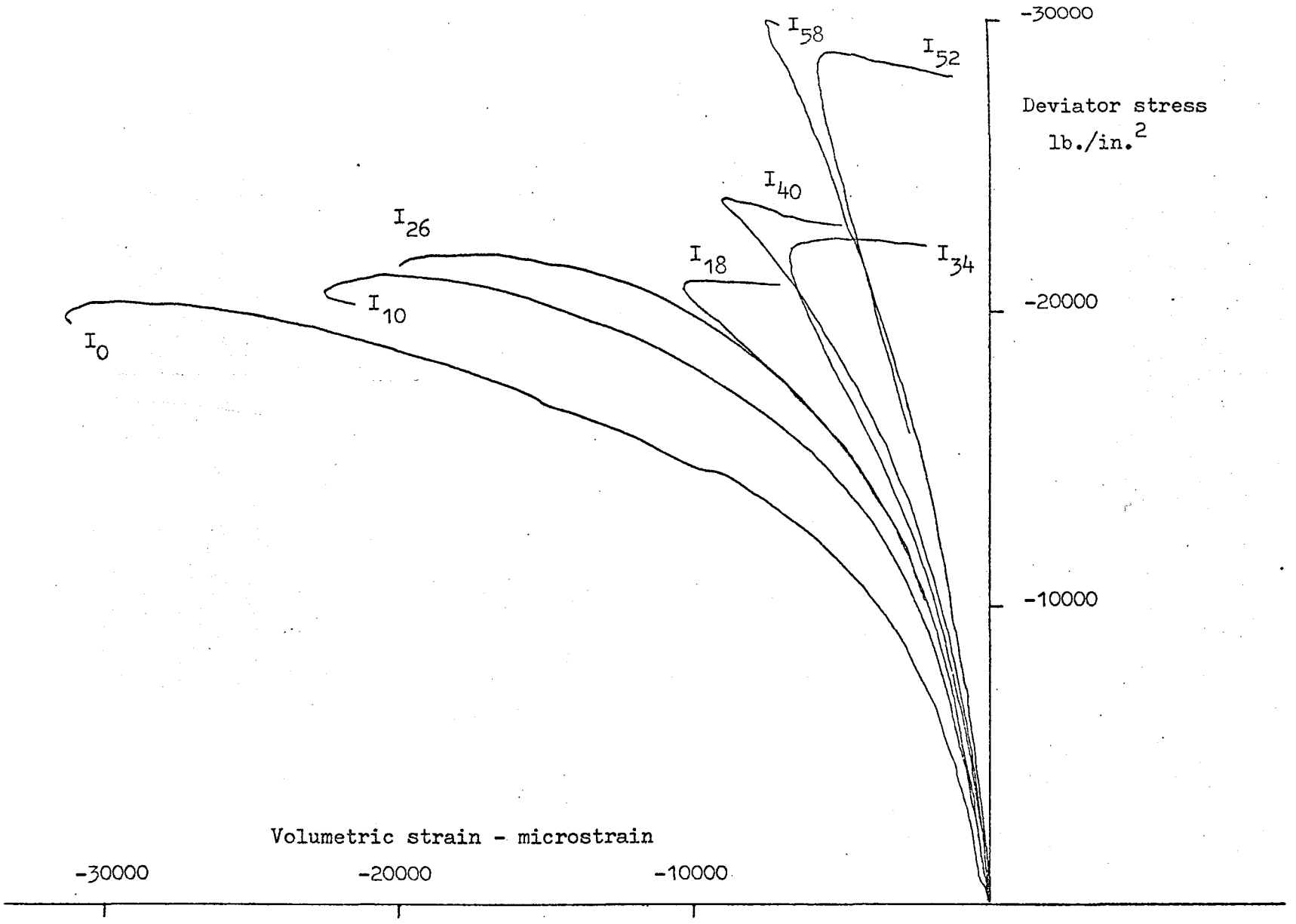


Figure 7.57. Variation of volumetric strain measured from the start of deviator loading with the deviator component of axial stress for cylinders of idealised concretes under a nominal confining pressure of 5000 lb./in.^{2}.

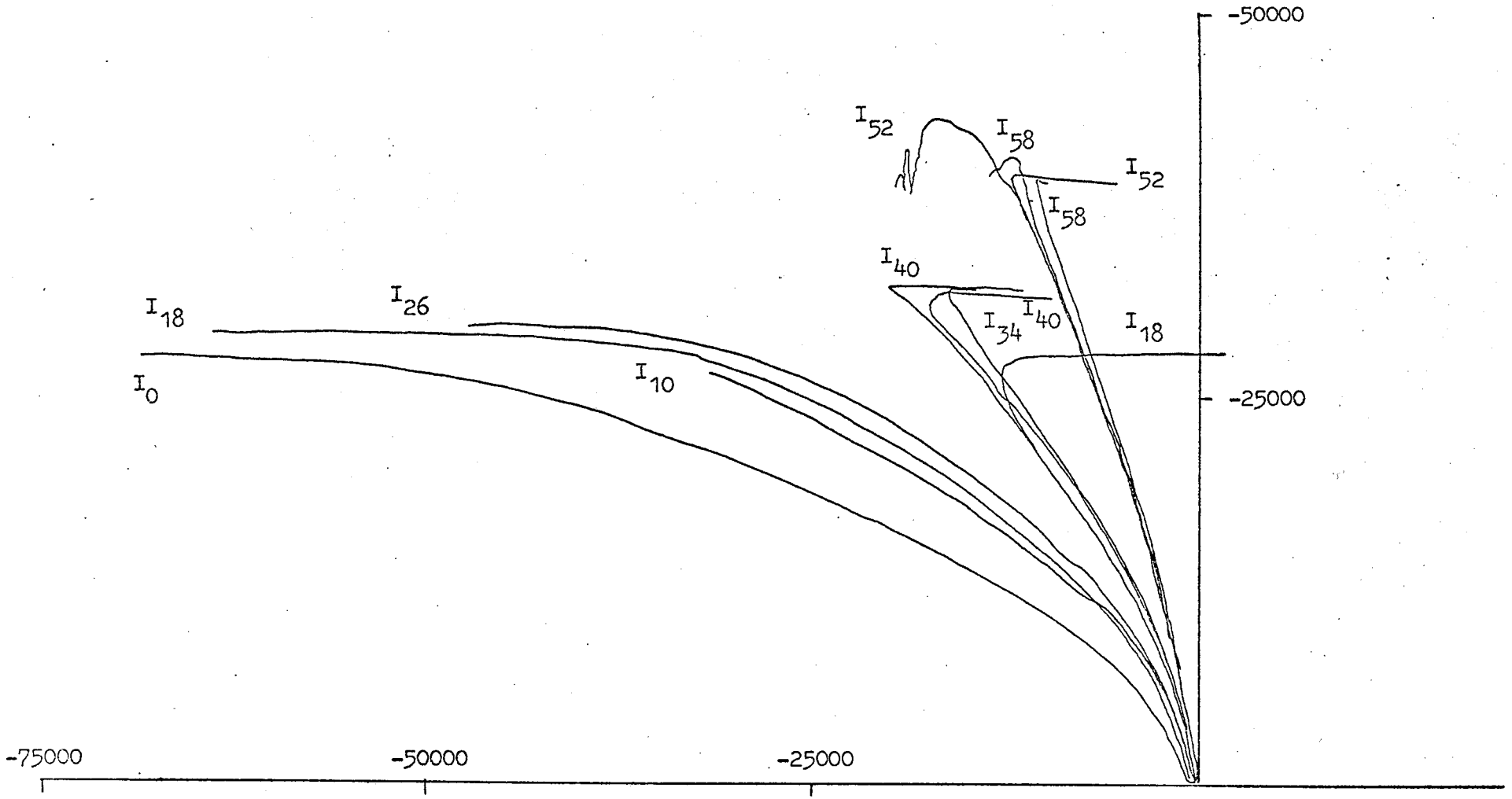


Figure 7.58. Variation of volumetric strain measured from the start of deviator loading with the deviator component of axial stress for cylinders of idealised concretes under a nominal confining pressure of 10000 lb./in.^{2}.

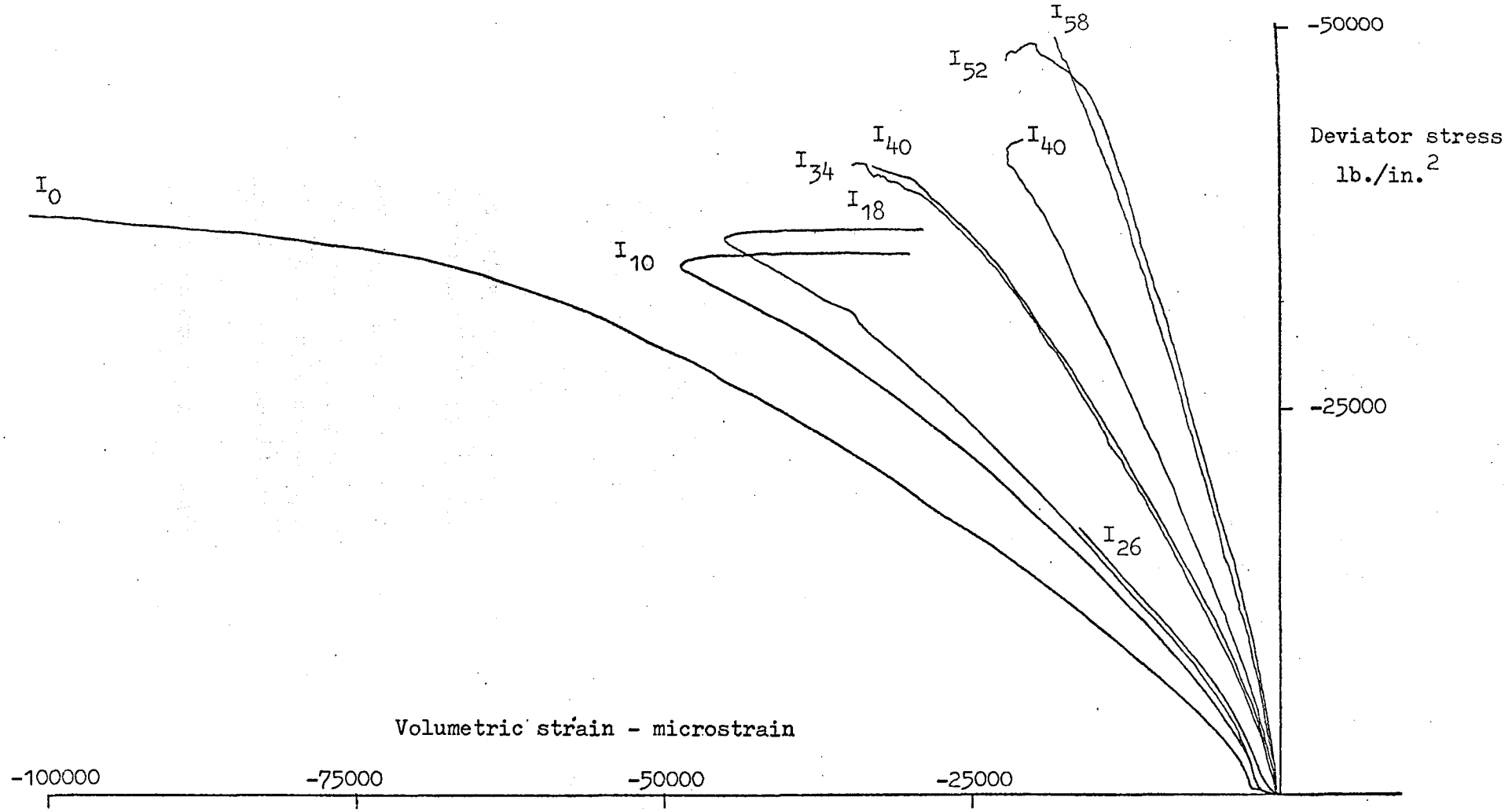


Figure 7.59. Variation of volumetric strain measured from the start of deviatoric loading with the deviator component of axial stress for cylinders of idealised concretes under a nominal confining pressure of 15000 lb./in.^{2}.

defined for all tests.

The stress and strain values at o.u.f.p. are given in Appendix 9 and discussed in the following sections.

Stress at o.u.f.p.

Figure 7.60. shows the variation of stress at o.u.f.p. with V_{ca} for various levels of confining pressure. The values shown on the figure corresponding to each level of confining pressure have been derived from the relationships between the stress at o.u.f.p. and confining pressure for each mix, suitable curves being chosen to represent such relationships. As mentioned in the previous section, in certain cases the minimum volume point defining the o.u.f.p. level occurs after ultimate. Where this has occurred the o.u.f.p. level has, for practical purposes, been taken as occurring at ultimate. For comparison the stresses at ultimate are also shown on the figure.

The figure shows that, for confining pressures up to and including 5000 lb./in.^{2}, the stress at o.u.f.p. as a proportion of ultimate stress, increases with V_{ca}. For zero confining pressure, the proportion reduces from 100% for the pure mortar to approximately 82% for V_{ca} = 58%. At confining pressures of 2500 and 5000 lb./in.^{2} the proportion reduces from 100% to 94% and 98% respectively. Above 5000 lb./in.^{2} the o.u.f.p. level occurs at, or after, ultimate except for some anomalous behaviour for volume fractions in the middle range of those tested.

At zero confining pressure, for low V_{ca}, the reversal in volume change is abrupt and is followed closely by ultimate failure. As the V_{ca} is increased, the reversal in trend occurs over a larger stress range and o.u.f.p. is reached at a stress level considerably before ultimate.

As the confining pressure is increased, the above characteristics are no longer evident. All reverses in volume occur abruptly immediately before and, in some cases, after ultimate (see below).

Hobbs [199] has detected the minimum volume stress to lie between 80% and 95% of ultimate for various concretes but found the proportion to be largely independent of the confining pressure.

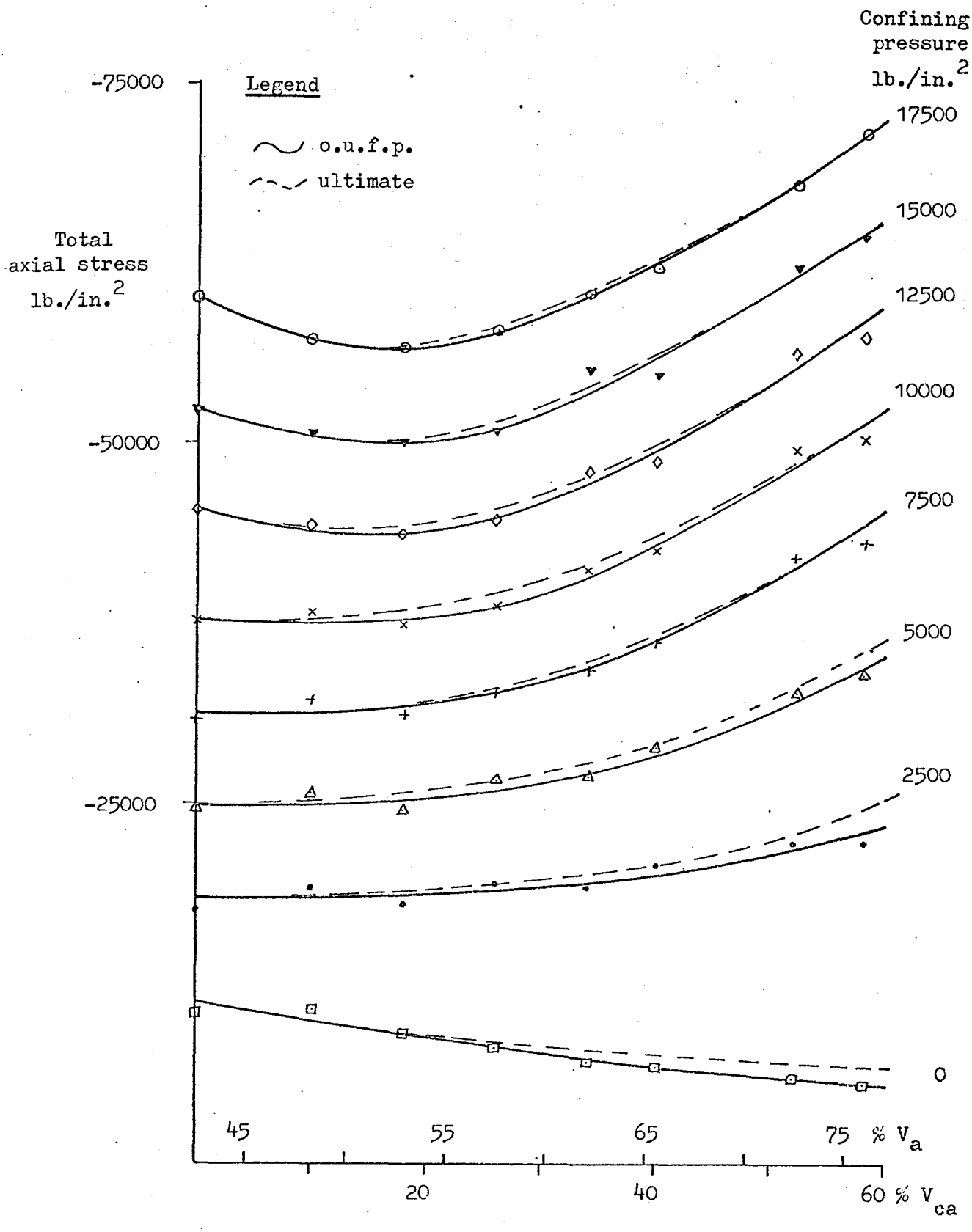


Figure 7.60. Variation of total axial stress at o.u.f.p. and ultimate with volume fraction of aggregate for idealised concretes tested under various confining pressures.

The trends exhibited by the figure can be compared with those shown by the corresponding figure for stresses at o.s.f.p. (Figure 7.40). In both instances the trend of decrease in stress with V_{ca} reverses as the confining pressure is increased, although the level of pressure at actual reversal differs.

Thus the two phenomena are undoubtedly linked closely and may provide an insight into the fracture process which is discussed in 7.5.4.7.

Strains at o.u.f.p.

Further evidence of the interdependence between the two levels of behaviour is given by Figure 7.61. which shows the relationship between axial and lateral strains at o.u.f.p. for typical idealised concrete mixes and, for comparison, the corresponding envelopes for o.s.f.p.

For high V_{ca}, the o.u.f.p. envelopes show the same trend as those corresponding to o.s.f.p. namely, a reversal in direction as the confining pressure is increased. For low V_{ca}, the maximum confining pressures attained in the tests are insufficient to cause this reversal but the trend is still apparent. The most striking feature of the figure is that the o.u.f.p. envelopes could be considered to be 'unfolded' and 'stretched' versions of the o.s.f.p. envelopes.

7.5.4.7. Ultimate Stresses and Strains

Figure 7.62. shows the relationships between total axial stress at ultimate and confining pressure for typical idealised concrete mixes. These relationships have been plotted from data obtained from the individual relationships for each mix. The curves have been shown passing through the point corresponding to the biaxial tensile strength which, as already discussed, has been represented by the uniaxial tensile strength. The data, normalised with respect to the uniaxial compressive strength of each mix is shown in Figure 7.63.

Each mix exhibits the anticipated characteristic increase in strength with confining pressure, the rate of increase being greater at low pressures (see Chapter 6). As the confining pressure is increased each curve, except that for the pure mortar, tends towards the slope:-

$$\sigma_{axial}/\sigma_{conf} = 2.6 \quad \text{(approximately)}$$

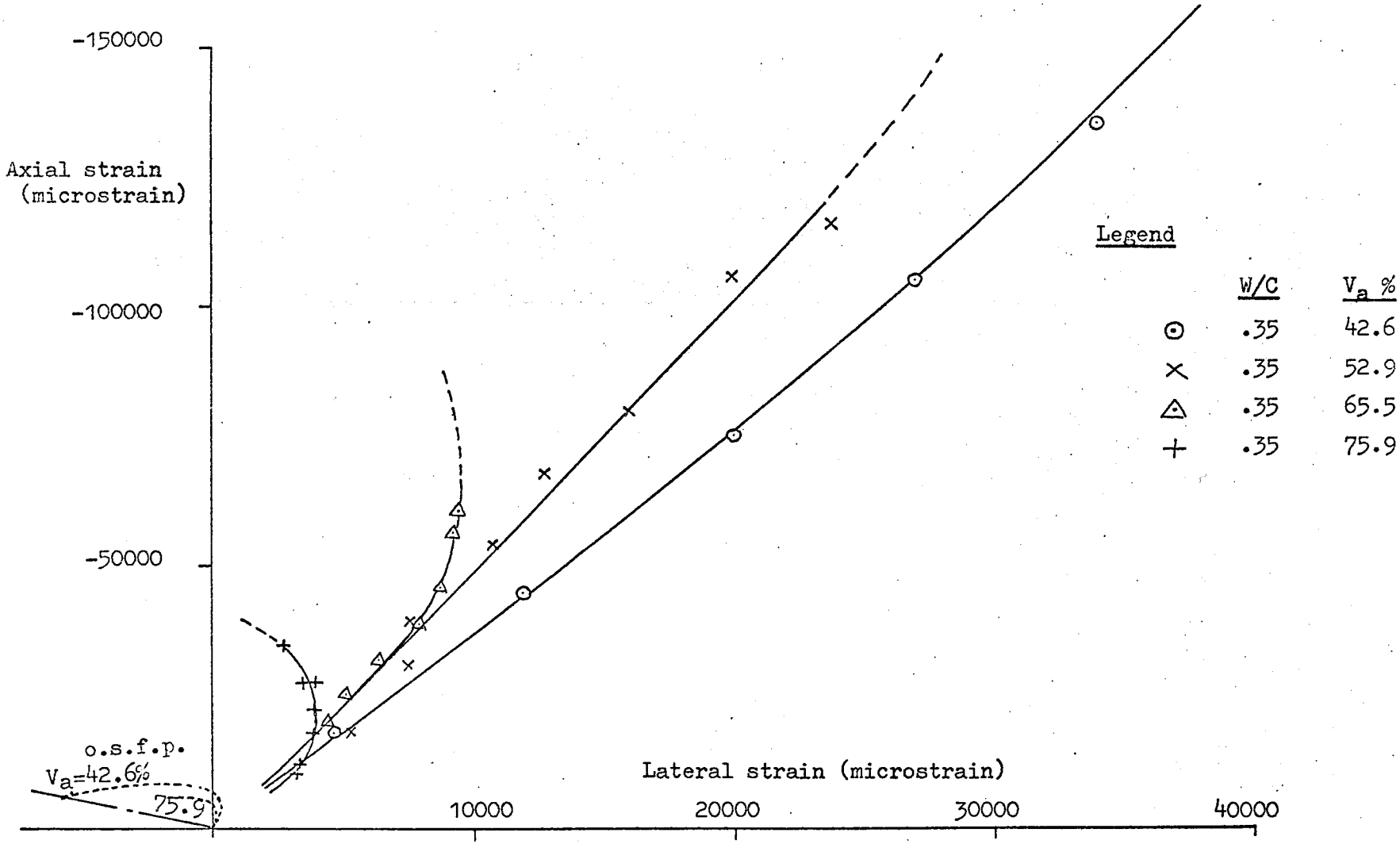


Figure 7.61. Relationships between axial and lateral strains at o.u.f.p. under triaxial compression for typical idealised concretes.

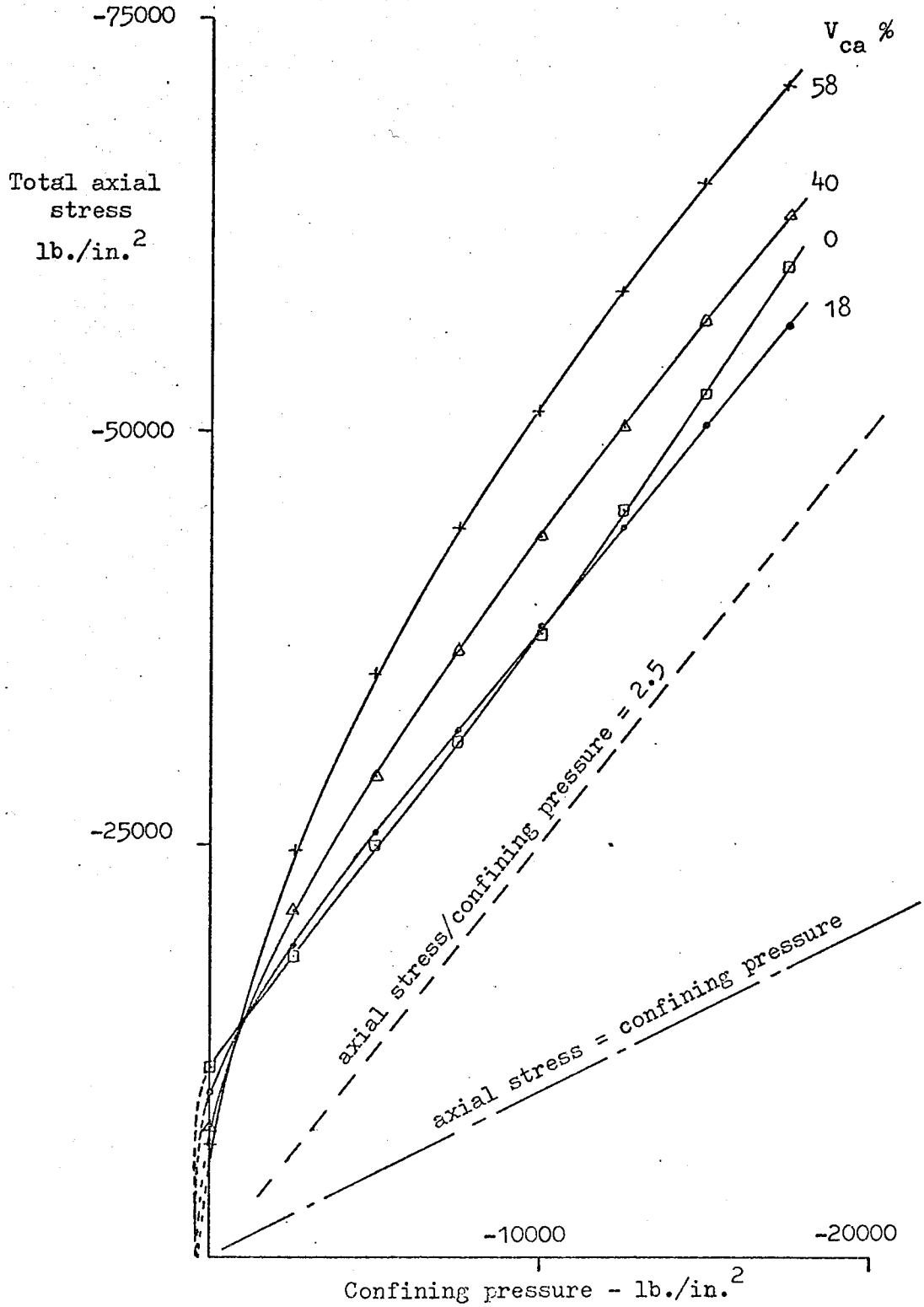


Figure 7.62. Variation of total axial stress at ultimate with confining pressure for typical idealised concretes under triaxial compression.

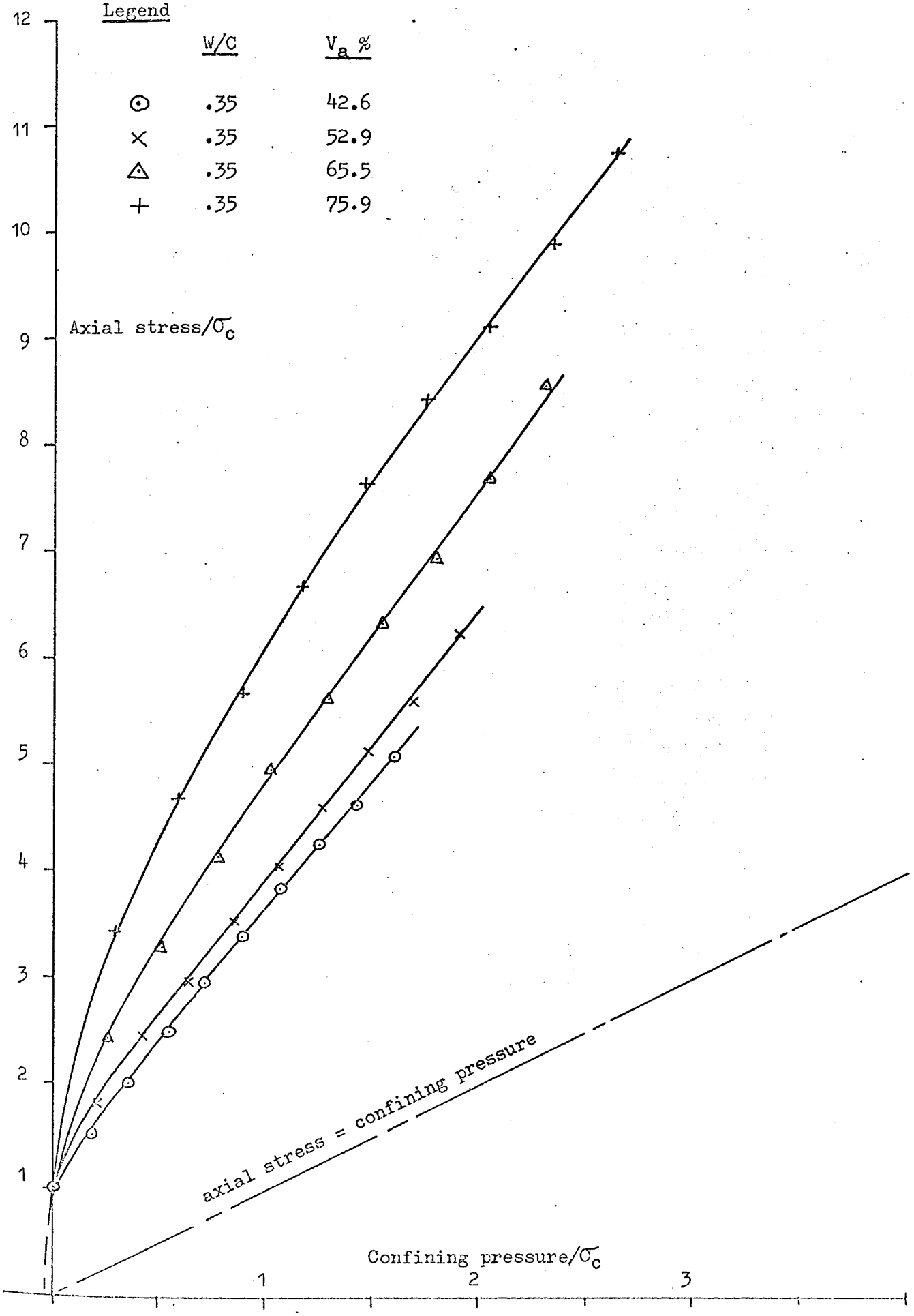


Figure 7.63. Relationships between normalised axial stress and confining pressure at ultimate under triaxial compression for typical idealised concretes.

In the case of the mortar (V_{ca} = 0) the strength relationship for values of confining pressure above 10000 lb./in.^{2} does not apparently exhibit the same tendency as the relationships for the concretes containing coarse aggregate, in that the rate of increase of strength increases rather than remains constant. No satisfactory explanation has been found for this phenomenon, but a similar tendency has been noted in Chapter 6 for the strength of mortars based on the nominal cross-sectional area as compared with coarse aggregate concretes (see Figure 6.4.).

The relationships demonstrate an extremely interesting and significant feature. Up to a confining pressure of approximately 1000 lb./in.^{2} the ultimate strength decreases with V_{ca}, while above this pressure the reverse is the case.

The reason for this behaviour may be explained by assuming the two opposing modes of behaviour as discussed in 7.5.4.4. to be in operation during compressive loading. Firstly, the inclusion of aggregate particles in a mortar matrix induces internal strain disturbances, and associated crack propagation and proliferation, which leads to disruption and eventual failure of the matrix at a stress level which decreases as the volume fraction of particles increases. This mode of behaviour may be termed 'brittle' fracture and give rise to failure in the 'tensile', 'splitting' or 'cleavage' mode. As the confining pressure is increased, the process of crack propagation is influenced mainly by the process of paste breakdown and the extension and proliferation of cracks, necessary for complete breakdown of the material, is inhibited by the confining pressure together with aggregate interlocking effects. Thus, at higher confining pressures the matrix can be considered as behaving as a 'plastic' mass. Under these conditions particle interference becomes the dominant resistive mechanism against increasing deviator stress, resulting in the failure stress of the concretes increasing with aggregate content. This mode of behaviour may be termed 'ductile' and will give rise to 'ductile' failures.

Such a division into two main modes of behaviour has been made by Cowan [213] who suggested 'tensile' failures, governed by a maximum tensile stress or strain, and 'cracking' failures in which internal friction caused by the aggregate played a part. This broad distinction has also been supported by other workers who have studied the behaviour of concrete under multiaxial stress. Avet-Flancart et Al [205] have suggested 'brittle' as

opposed to 'plastic' or 'microslipping' failures while Palaniswamy and Shah [178] have divided the behaviour into 'tensile' and 'crushing' types.

Workers in the field of rock mechanics have for some time studied a phenomenon which they term the 'brittle-ductile transition' [214]. Attempts have been made to define the confining pressure necessary to inhibit complete collapse of the material, but to allow a maximum stress to be maintained with a corresponding increase in deformation. In practice the transition appears to be gradual rather than occurring at a definite level.

The particle interference effect may explain the results of the cube tests for the idealised concrete (see 7.5.2.2.) where the cube strength is found to increase with V_{ca}. In cube tests, platen restraint effects are significant and tend to induce a state of triaxial compressive stress throughout the main body of the specimen due to its low height/width ratio (see Chapter 2). Thus it would appear, by comparing the magnitude of the increase in cube strength with V_{ca} with the strength relationships under triaxial compression, that the overall effect of this restraint is equivalent to an applied confining pressure of just above 1000 lb./in.^{2}.

Hughes and Bahramian [129] have also noted a decrease in the uniaxial compressive strength of cylinders but an increase in cube strength for concretes with increasing cement contents. They suggested the differences in testing techniques as one reason for the disparity in behaviour. After testing the cubes with a friction-reducing interface, the strength was observed to decrease slightly with increasing cement content at a given water/cement ratio.

The above observations are not supported by those of Pomeroy et Al [215] who have measured a reduction in the strength of cubes, prisms and cylinders or gap-graded concrete for increases in volume fraction of coarse aggregate (maximum size 3/8") from zero up to 30-40%. Above this value the trend for all specimens reverses.

The results for the real concretes also conflict with the observations on the idealised concretes, but probable causes of the apparent disparity in this case are discussed fully in 7.6.3. It is understood that a test programme is to be undertaken at the University of Surrey in an attempt to resolve this problem.

As discussed in Chapter 6 the ultimate strength data can be adequately represented by relationships of the following types:-

Parabolic equation $$\sigma_{axial}/\sigma_c = \left[A\,(\sigma_{conf}/\sigma_c) + 1\right]^B$$

Hyperbolic equation $$\sigma_{axial}/\sigma_c = \left[A(\sigma_{conf}/\sigma_c)^2 + B(\sigma_{conf}/\sigma_c) + 1\right]^{\frac{1}{2}}$$

Of the above relationships the hyperbolic equation gives a slightly superior fit and the values of the coefficients in the relationship, obtained by a non-linear least squares method, are plotted on Figure 7.64. which shows their variation with V_{ca}.

Figure 7.64. has been used to obtain typical values of A and B for various values of V_{ca} and the resulting relationships are shown on Figure 7.65. which favourably compare with the 'raw' data shown in Figure 7.62.

7.5.4.8. Mode of Failure

As discussed in 7.4.1., a trial series of tests using a fine mortar mix produced inclined fracture planes after failure in triaxial compression. These planes were considered to be caused by non-uniform loading due to specimen/platen interaction as evidenced by the disparity of strain across the specimens which is supported by the observations of Zimmerman [206]. In the present series of tests such eccentricity of loading is minimised by careful specimen preparation and setting-up. The resulting failure modes are shown in Figures 7.66. and 7.67. Some specimens exhibit a fracture plane orthogonal to the axis of the cylinder. This is caused by the process of removing the specimen from the sheath and is not characteristic of the method of test.

It can be seen that the failure mode changes from splitting, parallel to the direction of maximum compression at low confining pressures, to plastic bulging at higher pressures with no inclined fracture planes evident. This behaviour is particularly evident for mixes with low volume fractions of aggregate.

On the specimens exhibiting 'plastic' behaviour there is evidence of a large number of parallel failure planes inclined at angles on either side of the axis of maximum compressive stress. These planes are similar to the

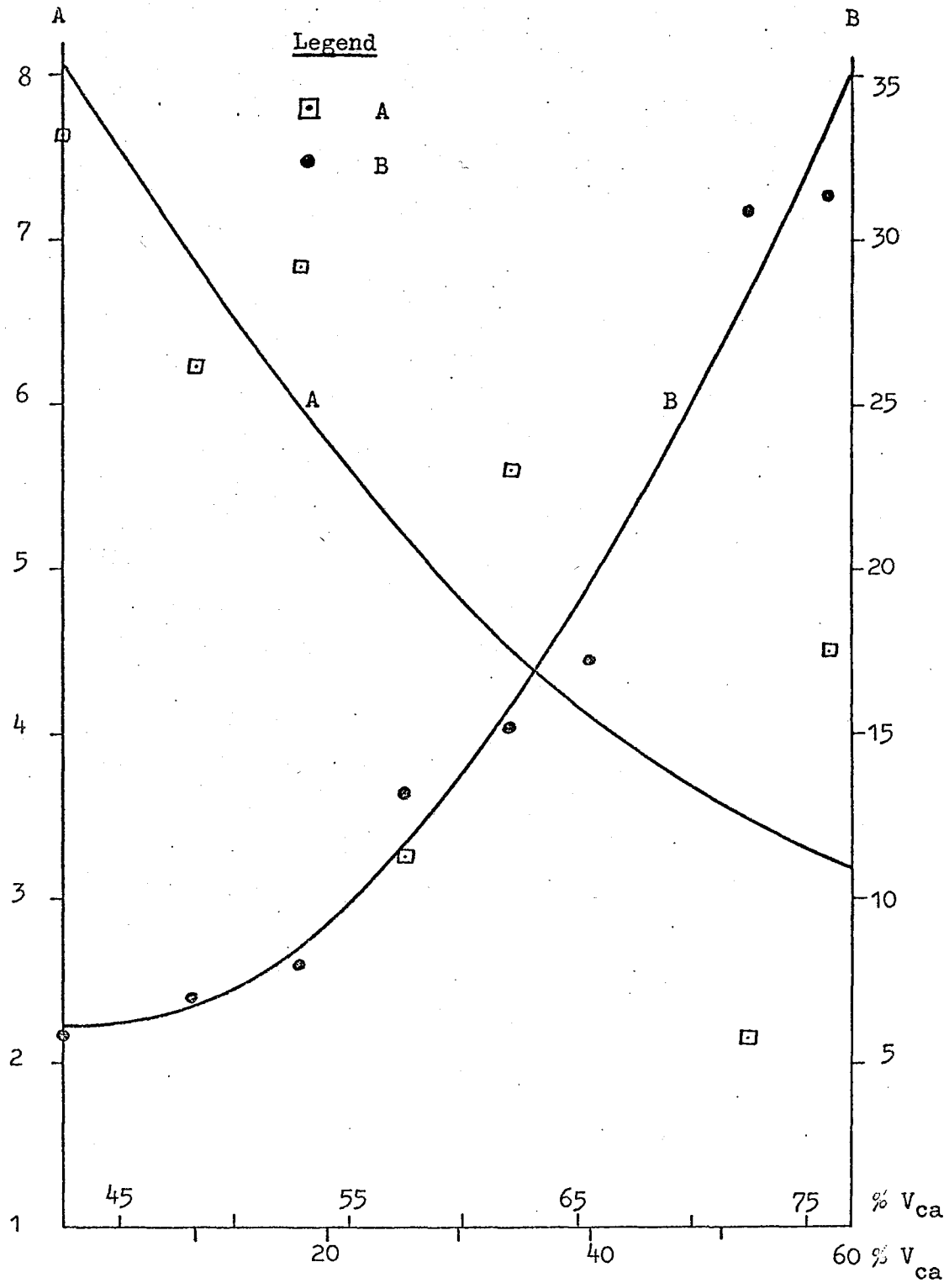


Figure 7.64. Variation of A and B in the ultimate strength relationship

$$\sigma_{axial}/\sigma_c = (A(\sigma_{conf}/\sigma_c)^2 + B(\sigma_{conf}/\sigma_c) + 10)^{\frac{1}{2}}$$

with volume fraction of aggregate for idealised concretes under triaxial compression.

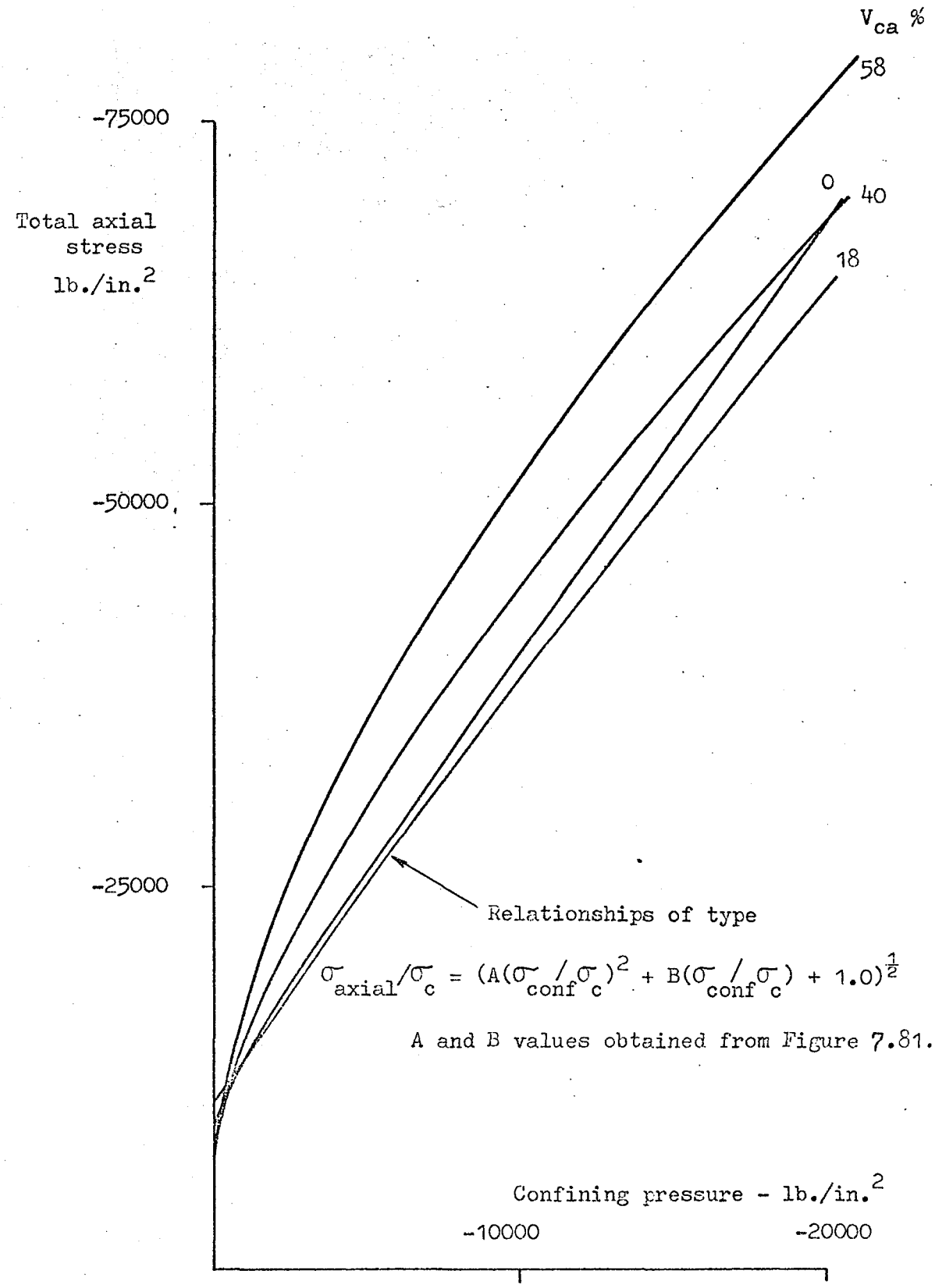


Figure 7.65. Relationships between total axial stress at ultimate with confining pressure for typical idealised concretes obtained by fitting data to a hyperbolic equation.

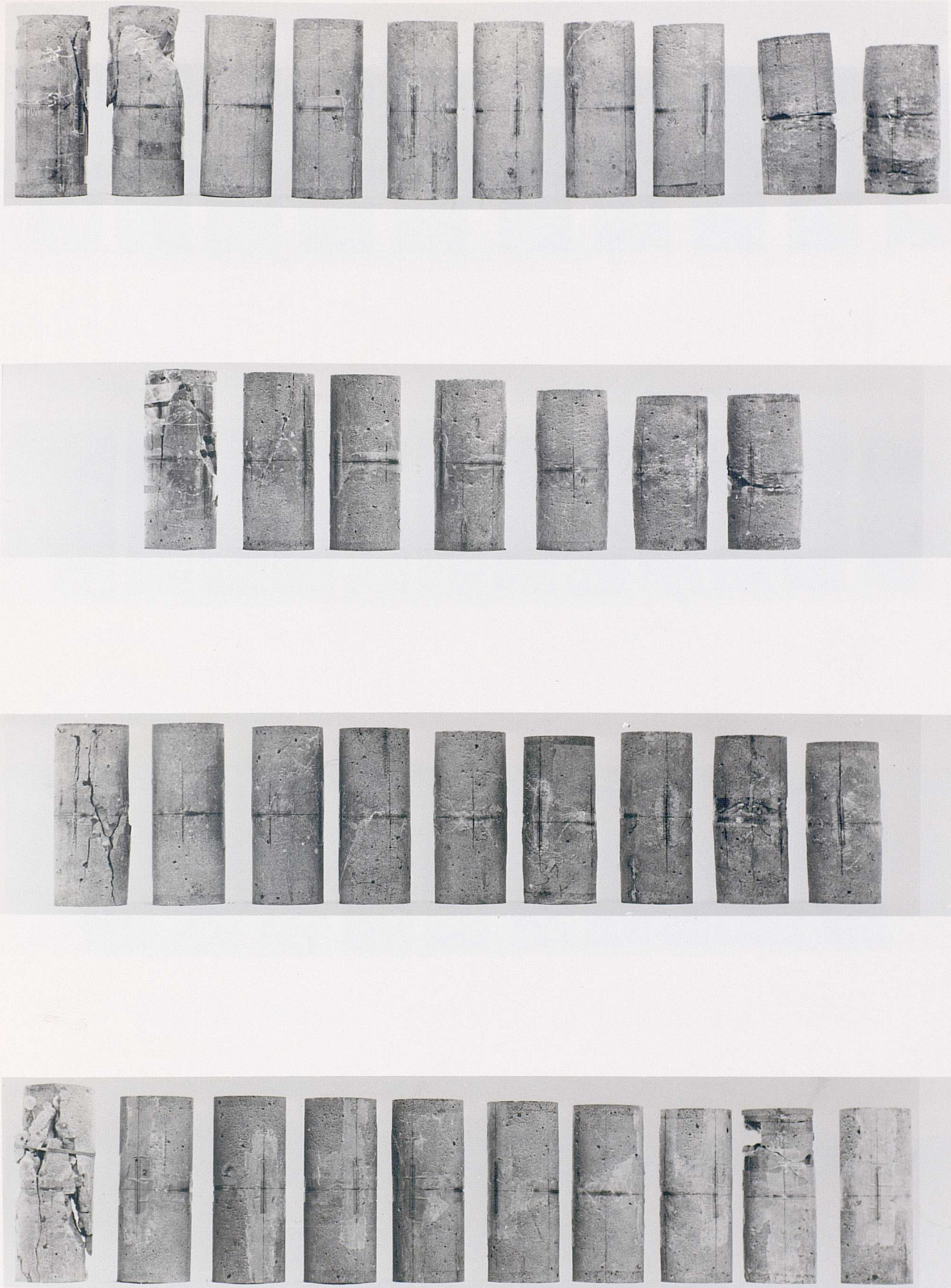


Figure 7.66. Specimens of idealised concretes after failure under triaxial 'compression': (top to bottom) I_0, I_{10}, I_{18}, I_{26}, with confining pressure increasing from left to right.

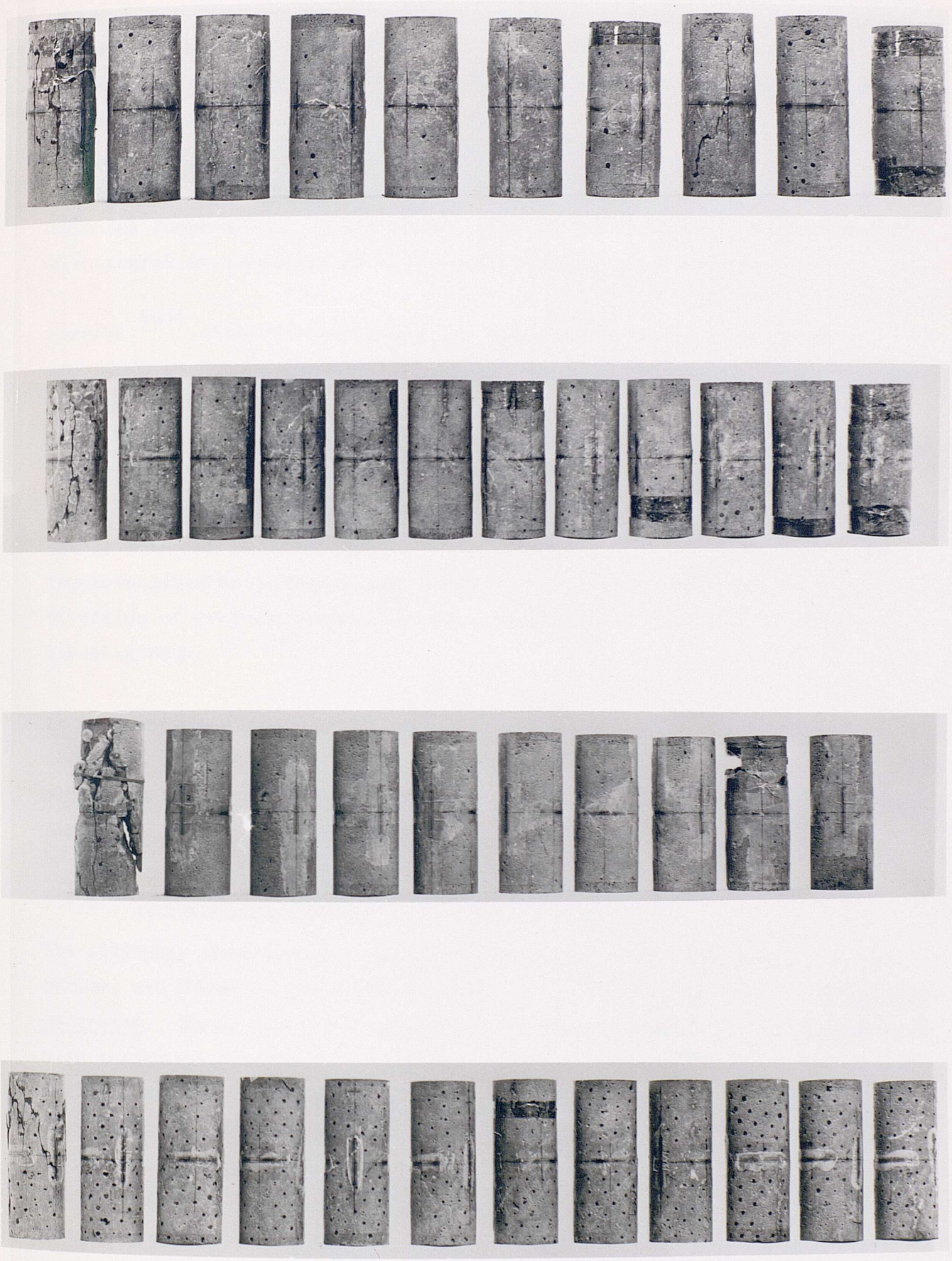


Figure 7.67. Specimens of idealised concretes after failure under triaxial 'compression': (top to bottom) I_{34}, I_{40}, I_{52}, I_{58}, with confining pressure increasing from left to right.

Luder's Lines often observed on deformed metals, and are undoubtedly evidence of slipping intensified by the confining pressure which inhibits microcrack proliferation [216].

Bellamy [217] observed 'shear' planes in cylinders of concrete tested under triaxial compression. These tended towards the horizontal and eventually disappeared at confining pressures of 6,000 lb./in.^{2} and above.

Murrell [91] noted that at confining pressures of between 16000 lb/in.^{2} and 20000 lb./in.^{2}, specimens of limestone fractured along inclined planes but the specimens remained coherent across the failure plane due, it was suggested, to a form of pressure welding. Above this pressure range 'slip bands' inclined at 45° to the axial direction where observed. For uniaxial tests and triaxial tests at low confining pressures there is very little evidence of fracturing the coarse aggregate. Typical 'cone' type fracture patterns surround each coarse aggregate particle and aligned in the direction of maximum compression are exhibited, as observed in other investigations [8, 19].

As the confining pressure increases this conical pattern becomes more difficult to distinguish, due to the extensive fracturing which has occurred within the 'plastic' region near ultimate, and a larger number of aggregate particles are found to be fractured.

7.5.5. Conclusions from Tests on Idealised Concretes

The following conclusions, considered to be the most significant for the series, are based on the results obtained for short-term tests on idealised concretes. These concretes consist of $\frac{3}{4}$" diameter spherical glass aggregate with roughened surfaces, suspended in a fine sand/ordinary Portland cement mortar matrix with a constant sand/cement and 'effective' water/cement ratio. The constant sand/cement ratio and complete imperviousness of the glass aggregate to water ensures that, for the constant 'effective' water/cement ratio, the total water/cement ratio also remains constant. All specimens are water-cured for twenty-one days and then allowed to gradually dry out before being stored in air for at least ten months prior to test.

7.5.5.1. Cube Tests

The cube strength increases with the volume fraction of aggregate (V_a) due to compressive restraint effects induced by the steel loading platens

(see Figure 7.8.). Fracturing is almost entirely confined to the mortar matrix.

7.5.5.2. Direct Tension Tests

(i) In the direction of loading both the stiffness and linearity of the stress-strain relationships increases with aggregate content. The sensitivity of the strain measuring technique is insufficient to detect differences in the behaviour of strains in the lateral direction (see Figure 7.9.).

(ii) The stress at o.s.f.p. and ultimate under direct tension both increase slightly with V_a, the o.s.f.p. stress being approximately 85% of ultimate. (see Figure 7.11.).

(iii) The tensile strain at both o.s.f.p. and ultimate decreases markedly with V_a, whereas the compressive strain remains significantly constant in both cases. (see Figure 7.12.).

(iv) The fracture paths travel both around and through the coarse aggregate particles. (see Figure 7.17.).

7.5.5.3. Triaxial Compression Tests

Stress-Strain Relationships

For a given confining pressure the stress-strain relationships indicate a marked decrease in stiffness, with respect to both axial and lateral strains and an increase in plasticity, for a decrease in V_a. For higher aggregate contents the stress-strain relationships show considerable irregularities approaching ultimate, undoubtedly caused by the disruption of individual particles (see Figures 7.26. to 7.29.).

Incremental Strain Ratio (see Figures 7.34. to 7.37.)

(i) For a given mix under confining pressures below a critical value the i.s.r. decreases (i.e. becomes more negative) with an initial increase in deviator stress due to crack closure, and then remains essentially constant up to o.s.f.p. before increasing to failure due to crack propagation and proliferation.

(ii) Above a critical confining pressure the i.s.r. increases continually from the start of application of deviator stress, indicating that

significant disruption of the material occurs during the hydrostatic loading regime.

(iii) Under uniaxial compression, the mean value of i.s.r. after crack closure and before o.s.f.p., increases (i.e. become less negative) with increases in the volume fraction of aggregate, due to the restraints imposed by the aggregate particles (see Figure 7.38.). This mean value, however, increases with applied confining pressure, the rate of increase being greater for mixes containing low contents of aggregate. Thus, above a critical range of confining pressure (1500 lb./in.^{2} to 3000 lb./in.^{2} approximately) the i.s.r. value decreases with V_a.

Onset of Stable Fracture Propagation (o.s.f.p.)

1. Strain Values (see Figure 7.39.)

(i) Under uniaxial compression the axial compressive and lateral tensile strains at o.s.f.p. both decrease with an increase in V_a reflecting the effect of heterogeneity.

(ii) For a given mix, as the confining pressure is increased up to a critical value (approximately 4000 lb./in.^{2}), o.s.f.p. occurs at increasing axial compressive strain and a near-constant value of lateral tensile strain. Above this critical confining pressure the lateral strain at o.s.f.p. becomes gradually more compressive while the axial compressive strain reaches a maximum and then decreases.

(iii) The above characteristic changes result in the envelope intersecting the hydrostatic axis at a finite value of strain, thus defining a closed relationship in strain space. This indicates that significant disruption can be induced by a hydrostatic strain field.

(iv) The closed form of strain envelope is characteristic of collapse of the porous cement paste structure under pressure.

(v) For increases in V_a the envelopes expand to enclose a larger portion of strain space, but remain approximately similar in shape. Thus

the effects of increases in heterogeneity in reducing the strains necessary to propagate fracturing persist for multiaxial strain states.

2. Stress Values (see Figures 7.40. and 7.41.)

(i) Under uniaxial compression, the stress at o.s.f.p. and the stress as a proportion of ultimate both decrease with V_a due to the effect of heterogeneity. For a given mix, increases in confining pressure cause the axial stress at o.s.f.p. to increase at a gradually diminishing rate such that the resulting envelope eventually intersects the hydrostatic axis.

(ii) The rate of increase in axial stress with confining pressure is less for mixes containing low volume fractions of aggregate, resulting in the envelopes intersecting at a confining pressure of approximately 4500 lb./in.^{2} after which the stress at o.s.f.p. increase with V_a for a given value of confining pressure.

(iii) The closed form of envelope defining stress at o.s.f.p. as in the case of the strain envelopes is characteristic of that obtained for failure of a porous material, such as cement paste, and suggests a process of collapse under pressure.

3. Volume Changes

(i) For a given mix under increasing hydrostatic stress the volume decreases at an increasing rate, indicating progressive collapse of the structure (see Figures 7.51. to 7.54.). The data fits closely to the relationship:-

$$\sigma_{conf} = K_1 e_v - K_2 e_v^2$$

where: e_v = volumetric strain

K_1 = initial compressibility

K_2 = term relating to non-linearity

(ii) For a given value of confining pressure, the volume changes decrease with an increase in V_a (see Figure 7.55) approximately in accordance with a relationship of the form:-

$$K_1 = 2.46\ V_{ca} + 2.47$$

where V_{ca} is in % and K_1 is evaluated for the lb./in.^{2} - microstrain system of units.

An equation of this type indicates the effect of diluting a compressible component (mortar matrix) with a relatively incompressible material (glass aggregate). The data, are insufficient, however, to enable the effects of strain concentrations due to heterogeneity to be evaluated.

(iii) Under uniaxial compression, and during the deviatoric stage of triaxial loading, the volume change relationships are all of the same form, namely, a decrease in volume at an increasing rate followed by a superimposed volume increase causing a level of minimum volume to be reached. After this level the volume increases to failure and indicates extensive void formation (see Figures 7.47. to 7.50.).

(iv) As for the case of hydrostatic loading, the volume changes for a given deviator stress under a given value of confining pressure are greater for mixes containing small aggregate contents (see Figures 7.56. to 7.59.).

Onset of Unstable Fracture Propagation (o.u.f.p.)

1. Stress Values (see Figure 7.60.)

(i) For uniaxial compression, the stress at o.u.f.p. decreases with volume fraction of aggregate. The stress as a proportion of ultimate also decreases with V_a from 100% for the mortar mix to 82% for the mix containing 58% of coarse aggregate.

(ii) As the confining pressure is increased the above trend reverses and the stress at o.u.f.p. as a proportion of ultimate tends to increase with V_a.

(iii) For a given mix the o.u.f.p. level as a proportion of ultimate increases with confining pressure.

2. Strain Values (see Figure 7.61)

The envelopes defining the state of strain at o.u.f.p. can be

considered as 'unfolded' versions of the corresponding o.s.f.p. envelopes, and the strains are less for mixes containing large aggregate contents.

Ultimate

(i) The ultimate strength under uniaxial compression decreases with V_a due to the effect of heterogeneity (see Figure 7.60.).

(ii) As the confining pressure is increased for a given ix the axial stress at ultimate increases at a diminishing rate until all envelopes tend to the slope:-

$$\sigma_{axial}/\sigma_{conf} = 2.5 \quad \text{(see Figure 7.62)}$$

(iii) The rate of increase in strength is lower for mixes containing low volume fractions of aggregate, being almost linear for the plain mortar. This is probably due to the influence of particle interference and results in the relationships intersecting at a certain value of confining pressure (1000 lb./in.^{2}), after which the strength increases with V_a.

(iv) The relationships can be adequately characterised by equations of the type:-

$$\sigma_{axial}/\sigma_c = (A\,\sigma_{conf}/\sigma_c + 1)^B$$

$$\sigma_{axial}/\sigma_c = (A(\sigma_{conf}/\sigma_c)^2 + B(\sigma_{conf}/\sigma_c) + 1)^{\frac{1}{2}}$$

(v) The mode of failure changes from brittle fracture in the axial splitting mode at low confining pressures, to ductile deformation accompanied by a large number of inclined failure planes visible on the surface at high pressures (see Figures 7.66. and 7.67.).

7.6. Triaxial Test Programme for Real Concretes

7.6.1. Introduction

It is the object of this section of the research programme to measure the deformational behaviour, under triaxial compression, of concretes representative of those used in practice and (a) to compare such data with those obtained for the idealised concretes and (b) after such a comparison

to use the data in the formulation of design charts capable of being interpolated to obtain representative measures of the behaviour for intermediate cases.

The testing procedure used is identical to that for the idealised concretes and it will be seen that the results obtained for individual mixes, in most cases, follow closely the pattern already established for idealised concretes and described in 7.5. Accordingly, the following section will not discuss the results in detail, unless it is required to comment on the influence of changes of parameters not considered in 7.5., or if the observed behaviour does not correspond to that exhibited by the idealised concretes.

7.6.2. Concrete Mixes

From the tests on the idealised concrete (7.5.) and the review of previous work (Chapter 6), the main characteristics of mixes likely to influence the behaviour of concrete under load are considered to be (i) the quality of the cement paste (water/cement ratio) and (ii) the volume fraction of the aggregate. Accordingly, mixes have been chosen to contain water/cement ratios and aggregate contents at each end of the range likely to be used in practice, and designed using data given in Road Note No. 4 [202] in accordance with C.P. 110 [2].

A rich mix, designated C1 with an 'effective' water/cement ratio of 0.35 and containing river gravel aggregate is chosen to correspond to the idealised mixes in respect of paste quality. A lean mix, also containing river gravel aggregate, is represented by concrete C2 with an 'effective' water/cement ratio of 0.60. To study the effect of varying V_a, the mortar fractions of the concrete mortar mixes C1 and C2, designated M1 and M2 respectively, are also tested.

In order to determine the effect of the changes in the type of aggregate used the deformational behaviour of concrete under multiaxial compression, about which little data has previously been published, concretes based on the mix proportions of Mix C2, but containing limestone (designated Mix C3) and granite (designated Mix C4) fine and coarse aggregate are tested.

The complete details of the constituent materials and their proportions in the real concrete mixes, are given in Appendices 2 and 3 respectively.

7.6.3. Cube Tests

7.6.3.1. Results

Detailed results are given in Appendix 3. As in the case of the idealised concretes the failure mode indicates uniform loading, with cracking visible at the specimen/platen interface. Fracturing is mostly confined to the mortar phase with few aggregate particles being affected.

7.6.3.2. Discussion of Results

Figure 7.68. shows the variation in cube strength with total volume of aggregate for the mixes. It is to be noted that for an increase in the total volume fraction of aggregate (V_a) the strength decreases for mixes with the same 'effective' water/cement ratio and type of aggregate. This is in conflict with the results obtained by Erntroy and Shacklock for normal concretes [190], and with the results obtained for the idealised concretes described in 7.5.2.2.

The reason for the apparent discrepancy may lie in the definition of 'effective' water/cement ratio. For the present work, it has been assumed to be the water added to the mix in excess of that capable of being absorbed into the aggregate. The determination of this 'effective' water is based on a knowledge of the water absorbtion capacity of the various types and size ranges of aggregates used in the mix as assessed by the method described in B.S. 812 [1] and it is ensured that the aggregate in the mix is, in fact, fully saturated by using pre-soaked aggregates following the technique suggested by Newman [218].

It is assumed that this 'effective' water is the only water contributing to the hardening process of the cement paste and that the water originally within the aggregate boundaries (in the case of saturated aggregates) or capable of being absorbed into the aggregate (in the case of unsaturated aggregates) is not, at any time, available for hydration. The decrease in cube strength with an increase in V_a for the real concretes with a given 'effective' water/cement ratio and containing a given type of aggregate may, therefore, be due to the fact that some water which is considered to be confined at all times within the aggregate particle boundaries is available for the hydration process. Thus the truly effective water/cement ratio, with respect to the quality of the cement paste at a given age, may have a value lying somewhere between the 'effective' and total water/cement ratios in accordance with a relationship of the following type:-

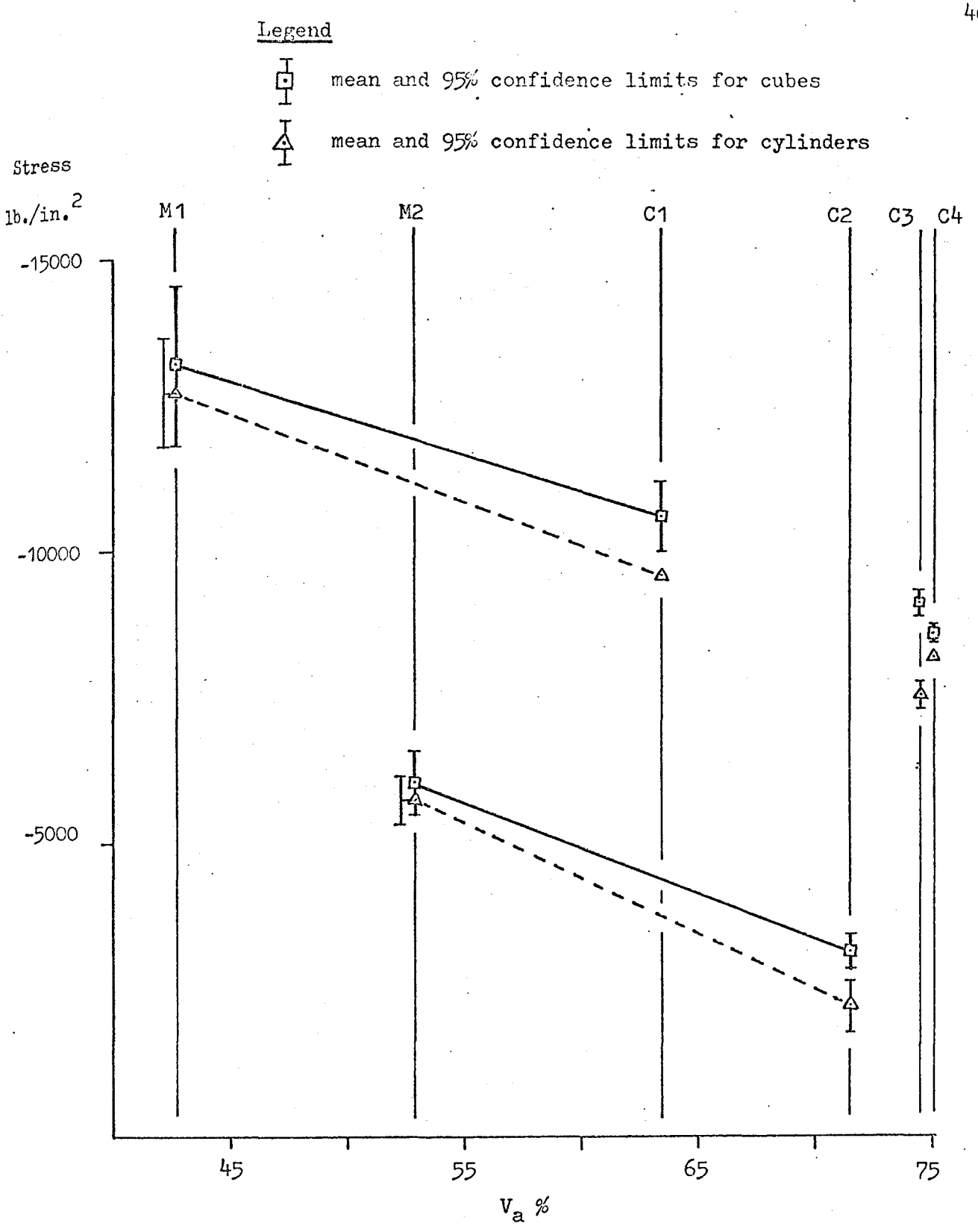


Figure 7.68. Variation of ultimate strength of 4" cubes and 4" diameter cylinders with volume fraction of aggregate for real concrete mixes tested under simple compression.

Truly effective w/c = 'effective' w/c + K x total w/c

= 'effective' w/c + K ('effective' w/c + w x A/C)

where K = a constant

w = water absorbtion capacity of aggregate

A/C = aggregate/cement ratio

Mixes containing aggregates which have a capacity for absorbing water will tend to increase in truly effective water/cement ratio for a given 'effective' water/cement ratio. This is clearly seen by referring to the mix details in Appendix 3, which show the appreciable difference between total and 'effective' water/cement ratio, particularly for those mixes containing large volume fractions of aggregates which have a relatively high water absorbtion.

Such a view is supported by the results obtained by Newman and Teychenné[219]. They found that relationships between cube strength and total water/cement ratio, for various types of mix, indicated an increase in cube strength with aggregate content for a given total water/cement ratio, but could be resolved to a single curve by replotting in terms of total water/cement ratio minus k x A/C .

The data fitted remarkably well to one curve for the following values of K:-

For O.P.C. K = 0.035

For R.H.P.C. K = 0.030

It should be pointed out that the choice of final transposed curve is entirely arbitrary.

Newman [218], following a similar technique, showed cube strength data for concretes made with saturated gravel aggregates to lie on one curve using the 'reduced' water/cement ratio (= 'effective' w/c - 0.008 x A/C) as abscissa. Significantly, the corresponding curve for concretes made with dry aggregates lay below that for saturated, the difference reducing with the value of 'reduced' water/cement ratio.

The dependence of paste quality on some function of 'effective' water/cement ratio and water absorbtion capacity of the aggregate is also confirmed by the results of the direct tension tests described in 7.6.4.

For the idealised concrete mix the problem does not arise, since both the 'effective' and the total water/cement ratios remain constant throughout the range of aggregate contents due to the constant sand/cement ratio used and the zero water absorption of the spherical glass coarse aggregate.

The reduction in cube strength with increase in V_a for the real concrete is not, however, as great as that measured by the uniaxial cylinder tests the results of which are shown on Figure 7.68. for comparison. Although the differences are marginal, this trend is similar to that found for idealised concrete (see 7.2.1.) where the differences are significant.

The influence of the water/cement ratio on the strength is clearly seen when comparing the results for mixes M1 and C1 with those for Mixes M2 and C2.

Further evidence of the dependency of the behaviour under load on the definition of 'effective' water/cement ratio is given in Chapter 5, where the mixes are designed on the assumption that water equivalent to only 50% of the absorption capacity of the aggregate is retained throughout the hydration process. Cube strength values are found in this case to increase with V_a, whereas the uniaxial strengths decrease.

7.6.4. Direct Tensile Tests

7.6.4.1. Results

Complete stress-strain relationships for all specimens tested are stored in computer card and printout form with the Concrete Materials Research Group where they are available for further analysis. The principal derived results are given in Appendix 7. These results are described in the following.

7.6.4.2. Stress-Strain Relationships

The relationships between axial stress and strain are of the form found for the idealised concretes and described in 7.5.3.2.

The effect of the aggregate content in increasing the stiffness of the mixes is shown by the variation of secant E value at $\frac{1}{3}$rd ultimate with V_a in Figure 7.69. The trends exhibited are similar to those found for idealised concretes. The reduction in stiffness caused by increasing the

'effective' water/cement ratio is demonstrated by comparing the changes in E value for mixes M1 and C1 with those for mixes M2 and C2.

As for the idealised mixes, the changes in secant Poisson's ratio value remain insignificant with changes in V_a.

7.6.4.3. Onset of Stable Fracture Propagation (o.s.f.p.)

As for the case of the idealised concretes, the procedure outlined in 4.5. is used to estimate the onset of fracture propagation under direct tension.

Figure 7.70. shows the stress level at o.s.f.p. for the mixes and clearly indicates the sharp decrease in this level for increases in V_a at given values of 'effective' water/cement ratio and type of aggregate. This demonstrates the effects of heterogeneity since, for the mortars M1 and M2, the o.s.f.p. level coincides with ultimate, whereas for the concrete mixes C1 and C2 o.s.f.p. occurs earlier at 65% and 54% of ultimate respectively. This is to be compared with the case of the idealised concretes where the o.s.f.p. stress level increased with V_a but remained constant at about 85% of ultimate for all aggregate contents.

This difference in behaviour between the real and idealised concretes is similar to that indicated by the cube strength tests as described in 7.6.3.2. The larger decrease in strength with increase in V_a for mixes M2 and C2 compared with mixes M1 and C1 does, in fact, appear to be related in some degree to changes in total water/cement ratio and 'effective' water/cement ratio for the mixes rather than the 'effective' water/cement ratio alone.

This effect is also demonstrated by the variation of axial and lateral strains at o.s.f.p. shown in Figure 7.71. As for the idealised mixes the axial strain, although subject to a large degree of scatter, decreases significantly with V_a for a given 'effective' water/cement ratio, this decrease being greatest for the leaner mixes. The lateral strain also shows a significant increase in V_a, whereas for the idealised mixes it remains essentially constant. The resulting volumetric strain at o.s.f.p. is shown in Figure 7.72.

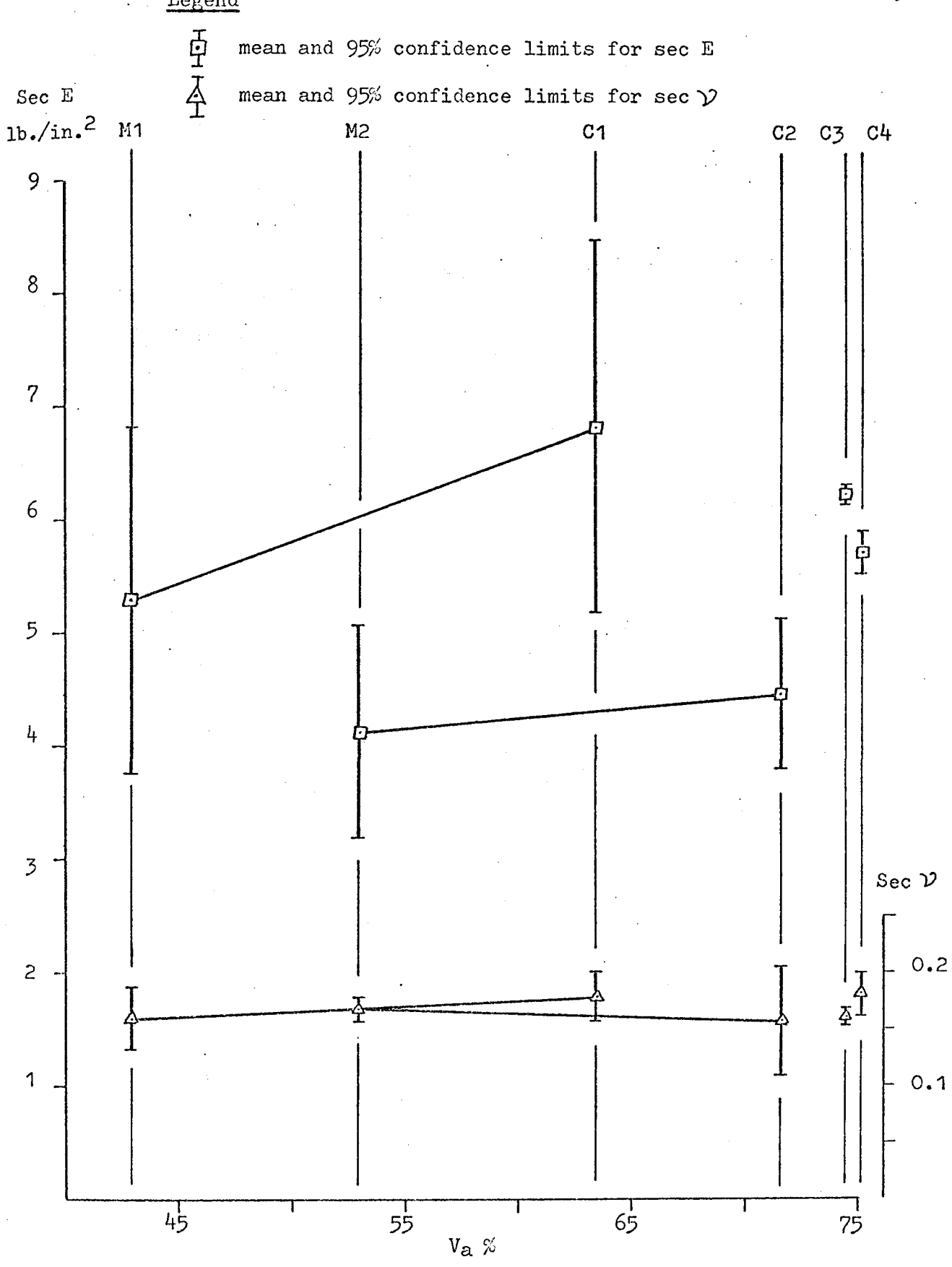


Figure 7.69. Variation of Sec E and Sec ν at a stress level of $\frac{1}{3}$rd ultimate with volume fraction of aggregate for real concretes under direct tension.

Legend

mean and 95% confidence limits

see Figure 7.73 for confidence limits for ultimate

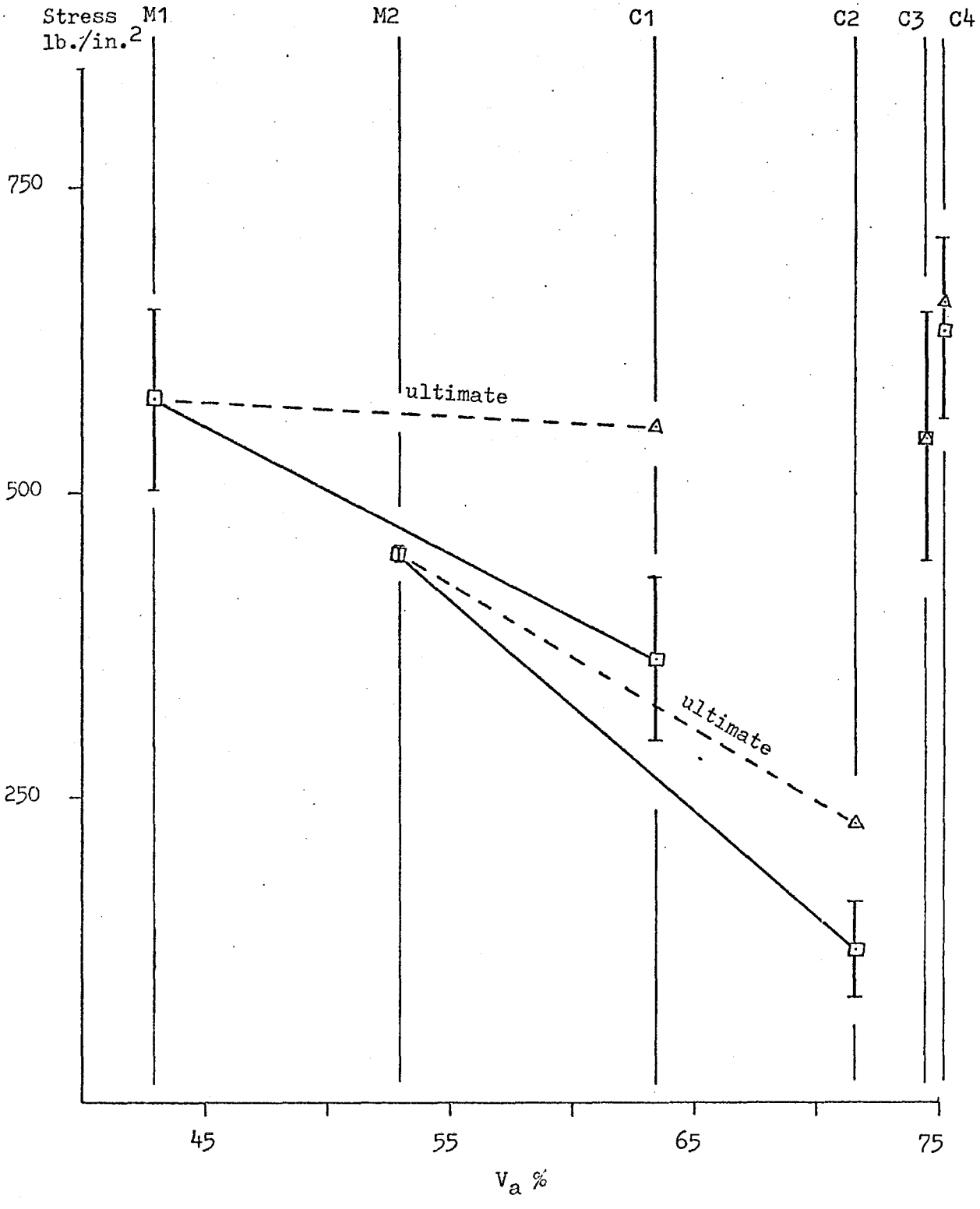


Figure 7.70. Variation of stress at o.s.f.p. with volume fraction of aggregate for real concretes under direct tension.

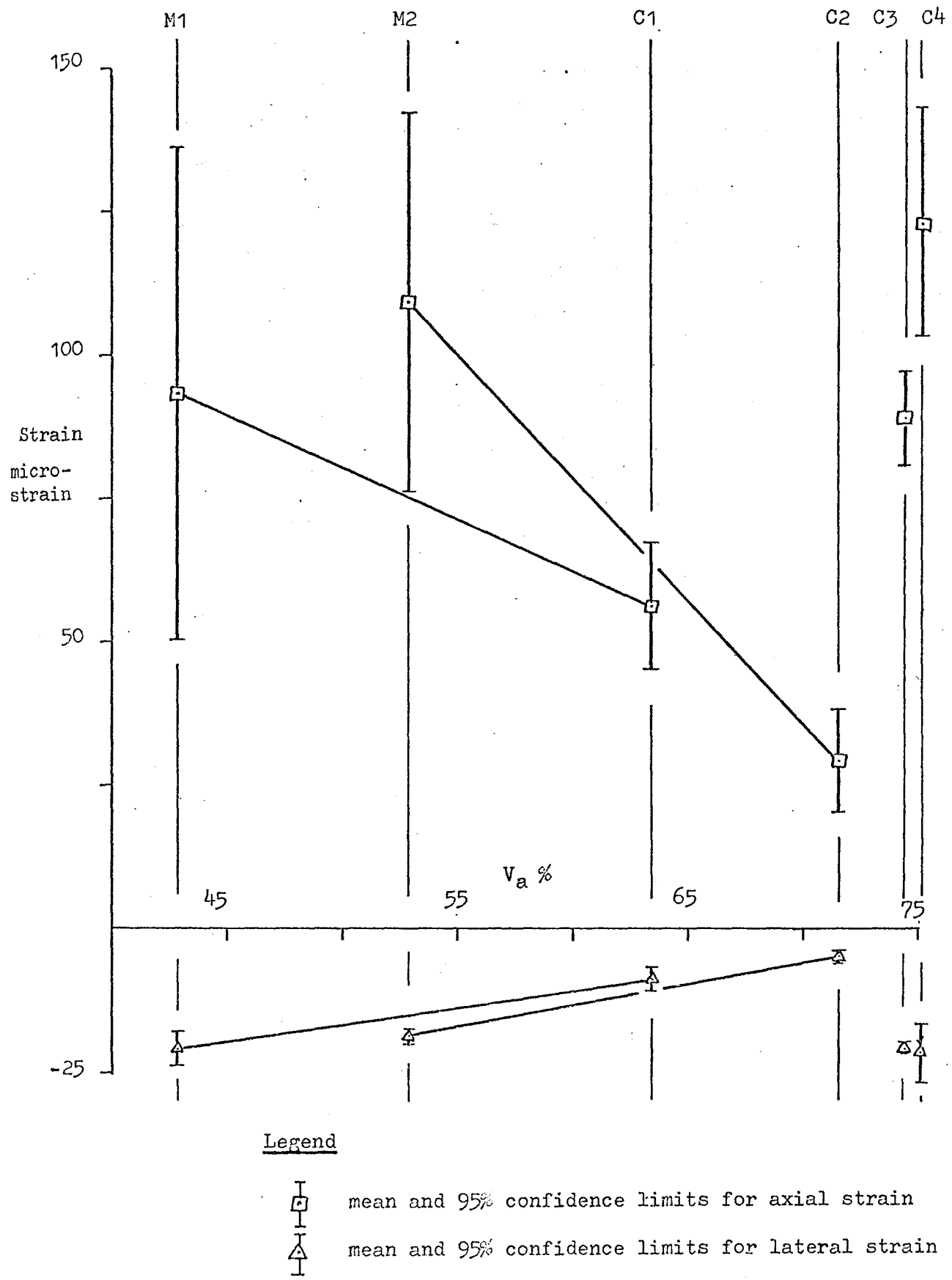


Figure 7.71. Variation of axial and lateral strain at o.s.f.p. with volume fraction of aggregate for real concretes tested under direct tension.

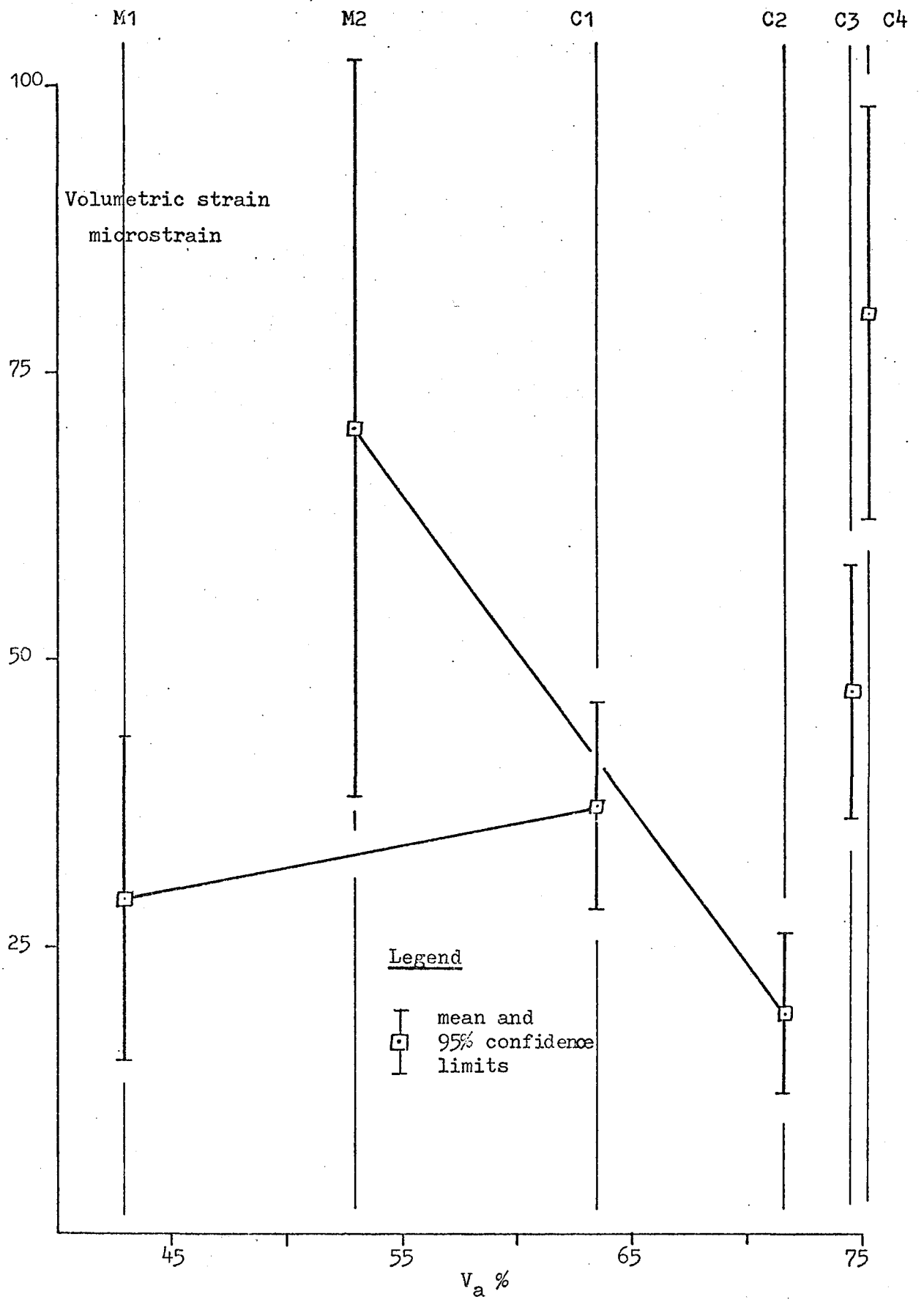


Figure 7.72. Variation of volumetric strain at o.s.f.p. with volume fraction of aggregates for real concretes under direct tension.

7.6.4.4. Volume Changes

For all mixes the volume increases continuously with load as in the case of the idealised concretes (see 7.5.3.4.).

No clear pattern emerges regarding the effect of the various mix parameters on this process.

7.6.4.5. Ultimate Stresses and Strains

Figure 7.73. shows the variation of ultimate strength with V_a for the various mixes. It is to be noted that the strength for the low 'effective' water/cement ratio mixes M1 and C1 does not vary significantly with V_a. Similar behaviour is noted for the idealised concretes which show a slight, but insignificant, increase in strength with increase in V_a (see 7.5.3.5.) and is in agreement with the work reported by Johnston [193]. However, the mixes M2 and C2, with a high 'effective' water/cement ratio, exhibit a clear reduction in strength with V_a, and these results agree with those reported by other workers [119, 6, 8, 196].

Thus, it would appear that in common with the stresses at o.s.f.p., the influence of the degree of heterogeneity on strength for a given type of aggregate is closely related to the characteristics of the hardened cement paste which, in turn, is related to some function of both the 'effective' and total water/cement ratios.

The axial and lateral strains at ultimate, shown in Figure 7.74. also indicate this effect although the degree of scatter is too great to allow definite conclusions to be drawn.

7.6.4.6. Failure Modes

Figure 7.75. shows the failure surfaces for specimens of the various mixes. For the concrete mixes, as in the case of the idealised concretes, the fracture path passes directly through a large number of aggregate particles as well as travelling along the aggregate/matrix interface.

7.6.5. Triaxial Compression Tests

7.6.5.1. Results

The complete stress-strain relationships are stored in computer card and printout form with the Concrete Research Group and will be published as a

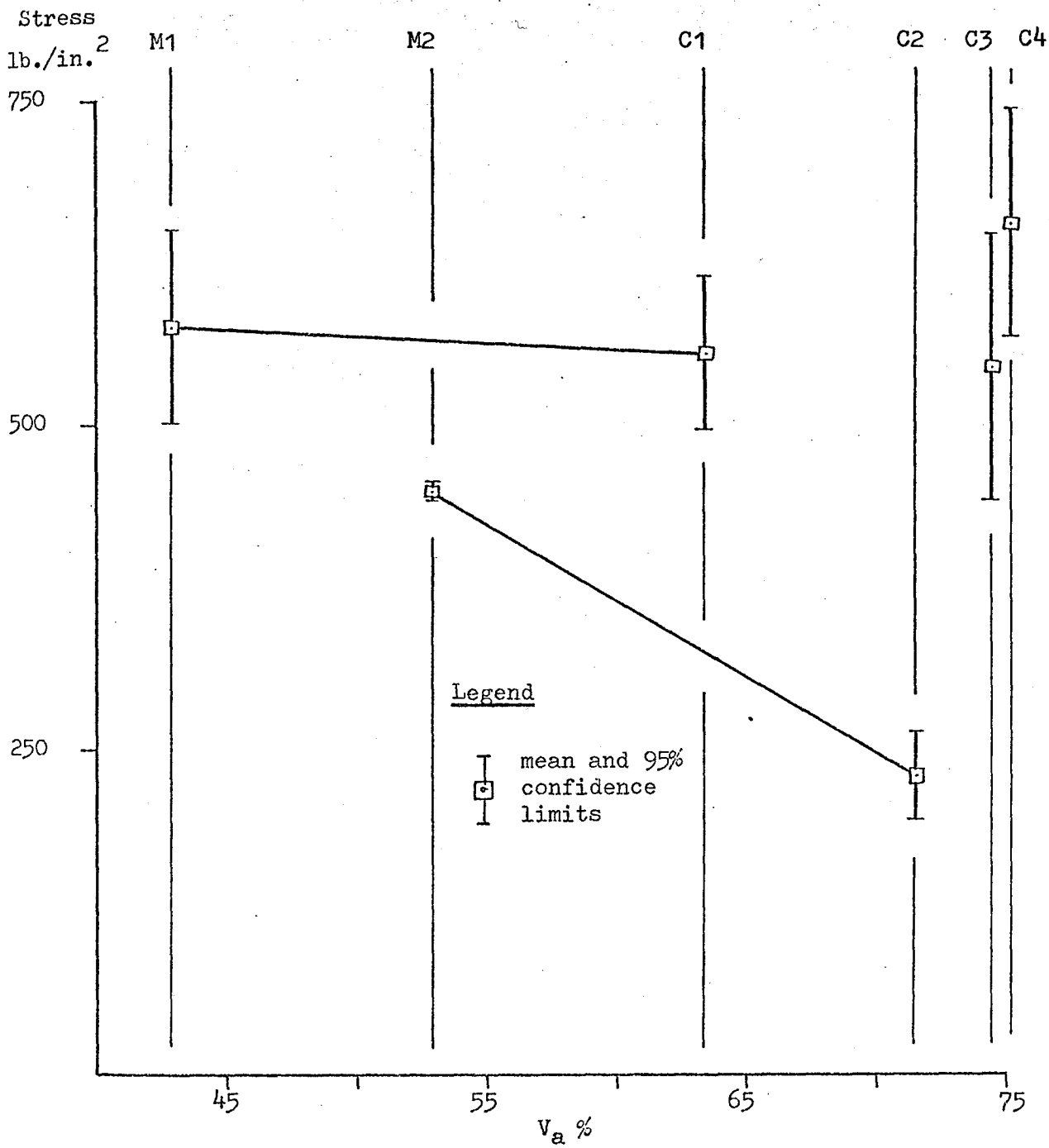


Figure 7.73. Variation of ultimate strength with volume fraction of aggregate for real concretes tested under direct tension.

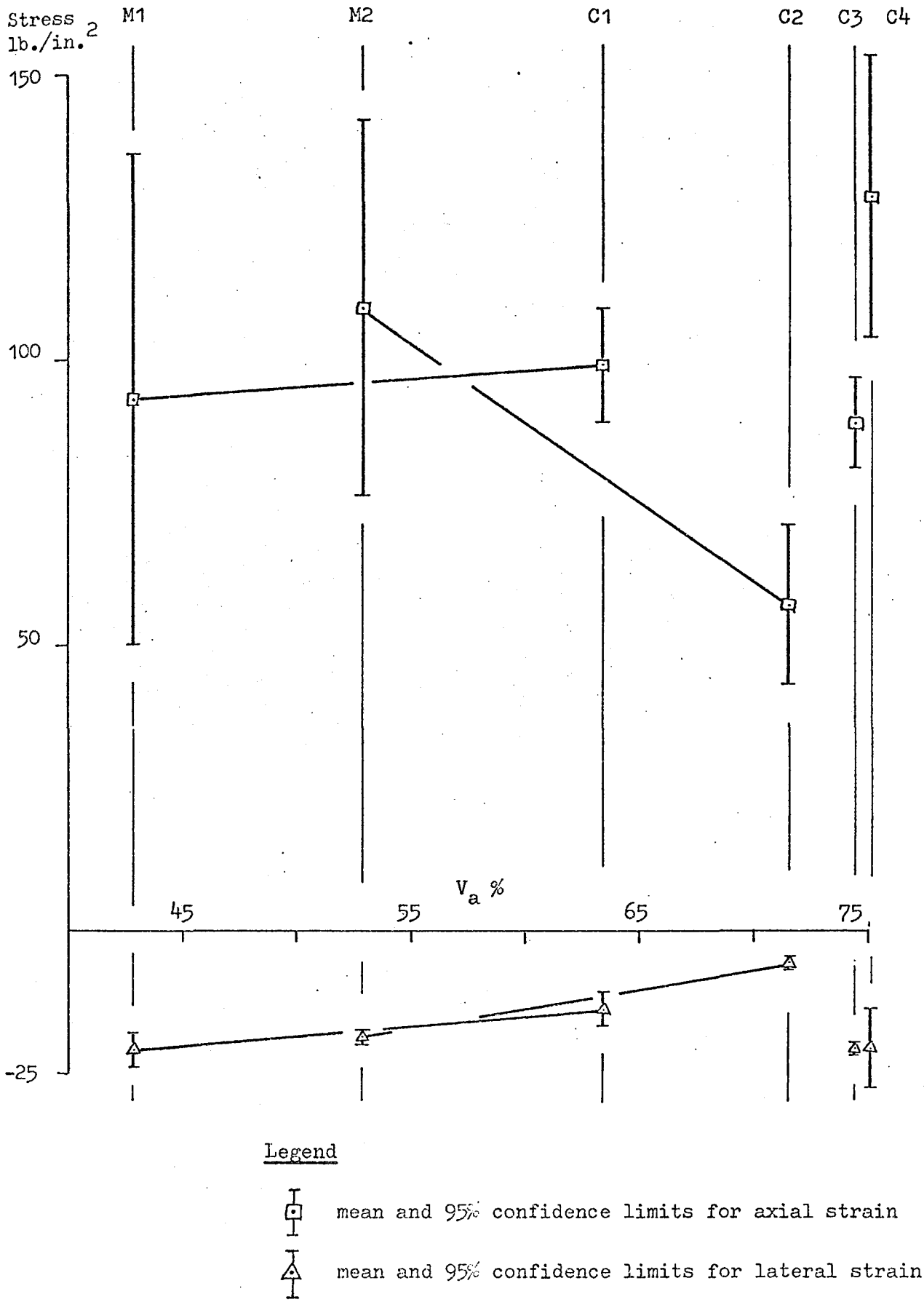


Figure 7.74. Variation of axial and lateral strains at ultimate with volume fraction of aggregate for real concretes under direct tension.













Figure 7.75. Typical failure surfaces exhibited by specimens of real concretes after loading under direct tension: (A) M1, (B) C_1, (C) M2, (D) C2, (E) C3, (F) C_4.

separate report [197]. The principal derived results for all specimens are given in Appendix 7. These results will be discussed in the following sections.

7.6.5.2. Stress-Strain Relationships

For each of the real concretes the variations of axial and lateral strains with total axial stress for given values of confining pressure, are shown in Figures 7.76. to 7.81. All relationships are plotted to the scale used for the idealised concretes (Figures 7.18. to 7.25.) for ease of comparison.

The stress-strain relationships exhibit the same general characteristics, with respect to the change in shape of the curves with change in confining pressure and change in V_a for a given 'effective' water/cement ratio, as those for the idealised mixes. However, in addition to these characteristics, already described in 7.5.4.2., the following points are of interest:-

(i) Influence of Changes in 'effective' Water/cement Ratio

Comparing the relationships of mix M1 with M2 and Mix C1 with C1 clearly demonstrates the considerable decrease in 'stiffness' and increase in 'ductility' with an increase of 'effective' water/cement ratio for all values of confining pressure. It should be noted that the comparisons are not strictly valid since the volume fraction of aggregate is not constant in each case.

(ii) Influence of Changes in Aggregate Type

Comparing the curves for mix C3 (limestone) and mix C4 (granite) with those for C2 (river gravel) shows the change in characteristics associated with varying the aggregate type, for mixes with the same 'effective' water/cement ratio containing the same volume fraction and grading of aggregate.

For given values of confining pressure the granite and limestone mixes are stiffer than those containing river gravel aggregate. This may be due to differences in aggregate stiffness and angularity which are both greater for limestone and granite than gravel (see Appendices 2 and 3), but is more likely to be due to the increased water absorption capacity of the gravel

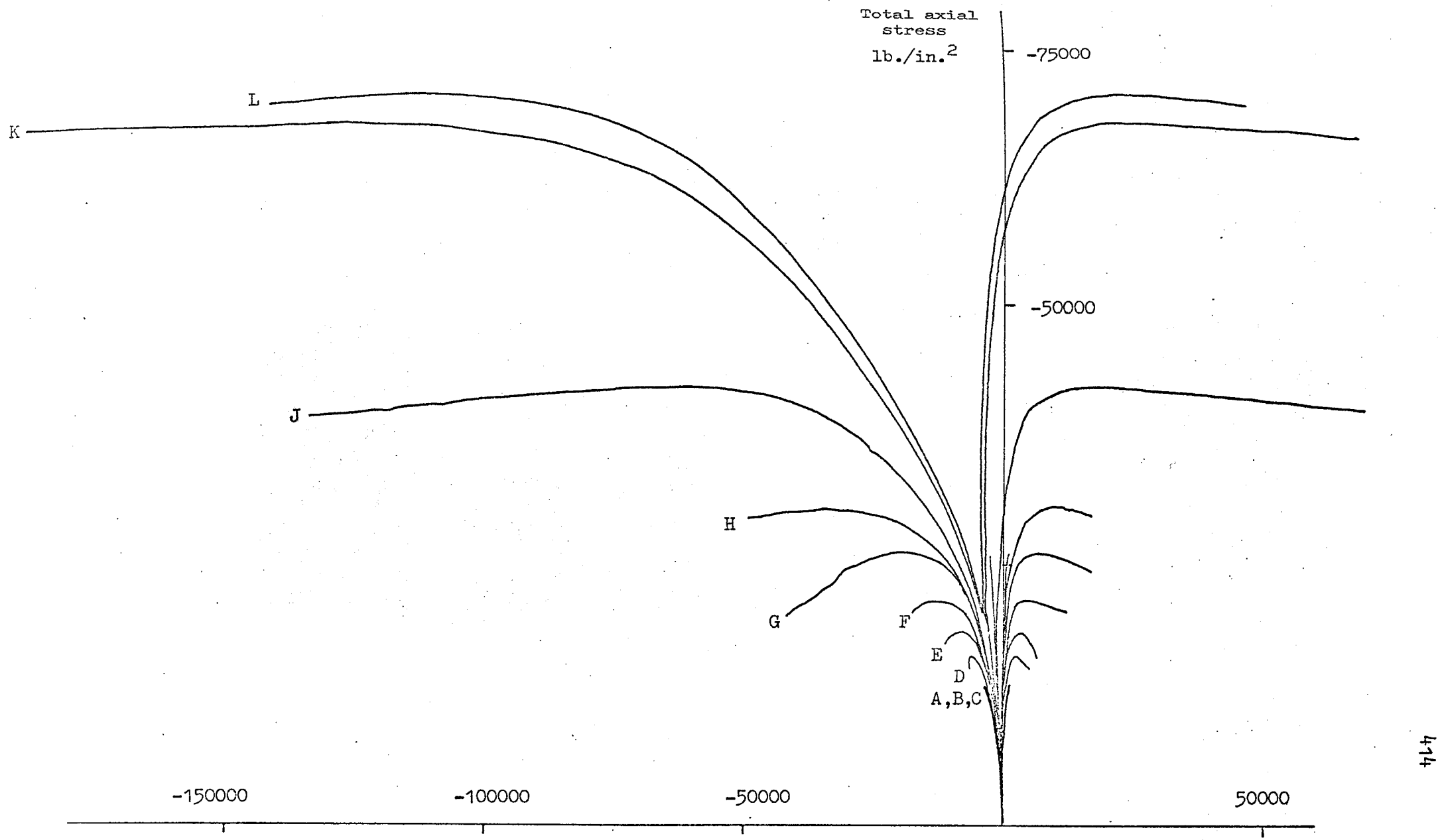


Figure 7.76. Variation of axial and lateral strains with total axial stress for cylinders of mix M1 under triaxial compression with various values of confining pressure.

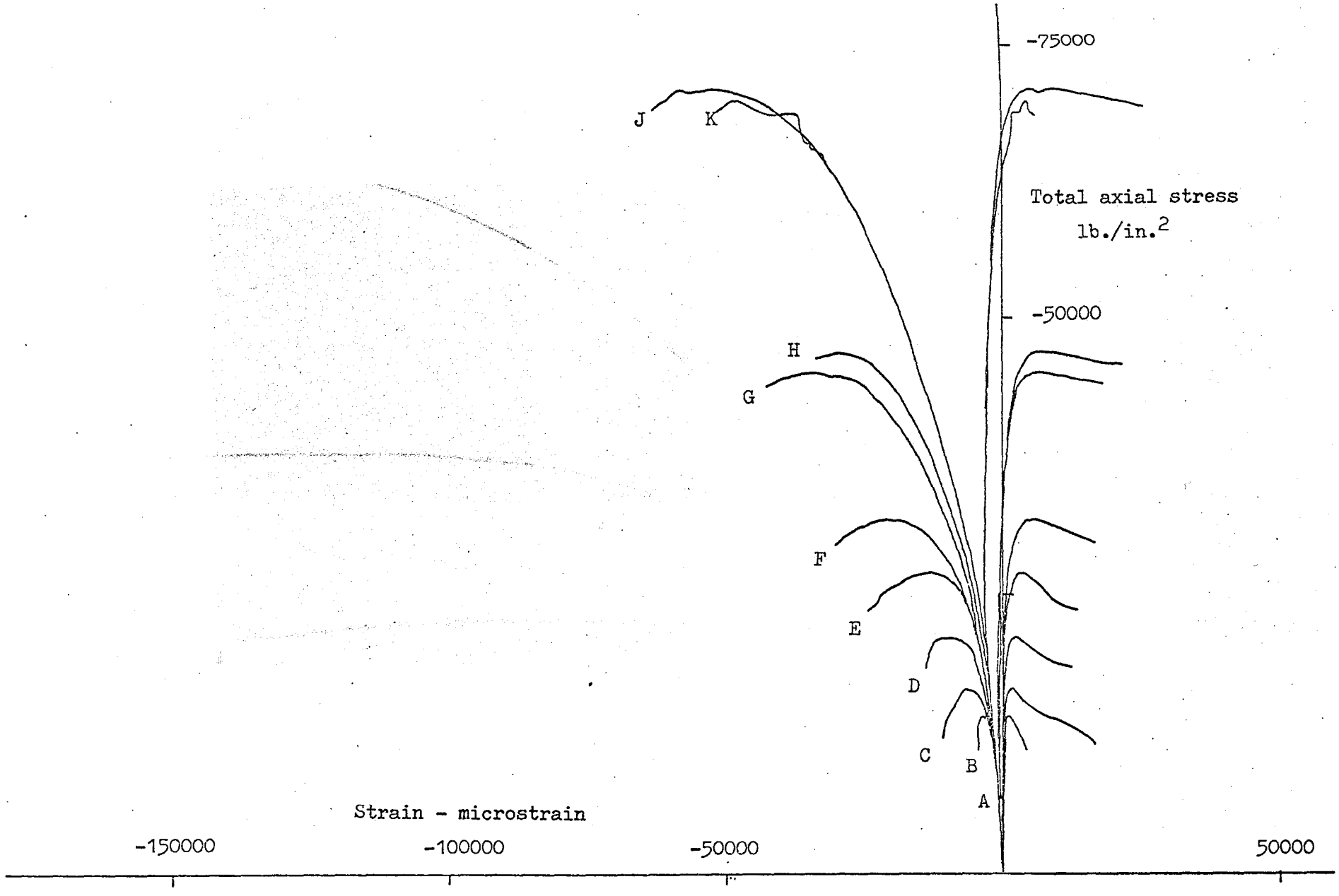


Figure 7.77. Variation of axial and lateral strains with total axial stress for cylinders of Mix C1 under triaxial compression with various values of confining pressure.

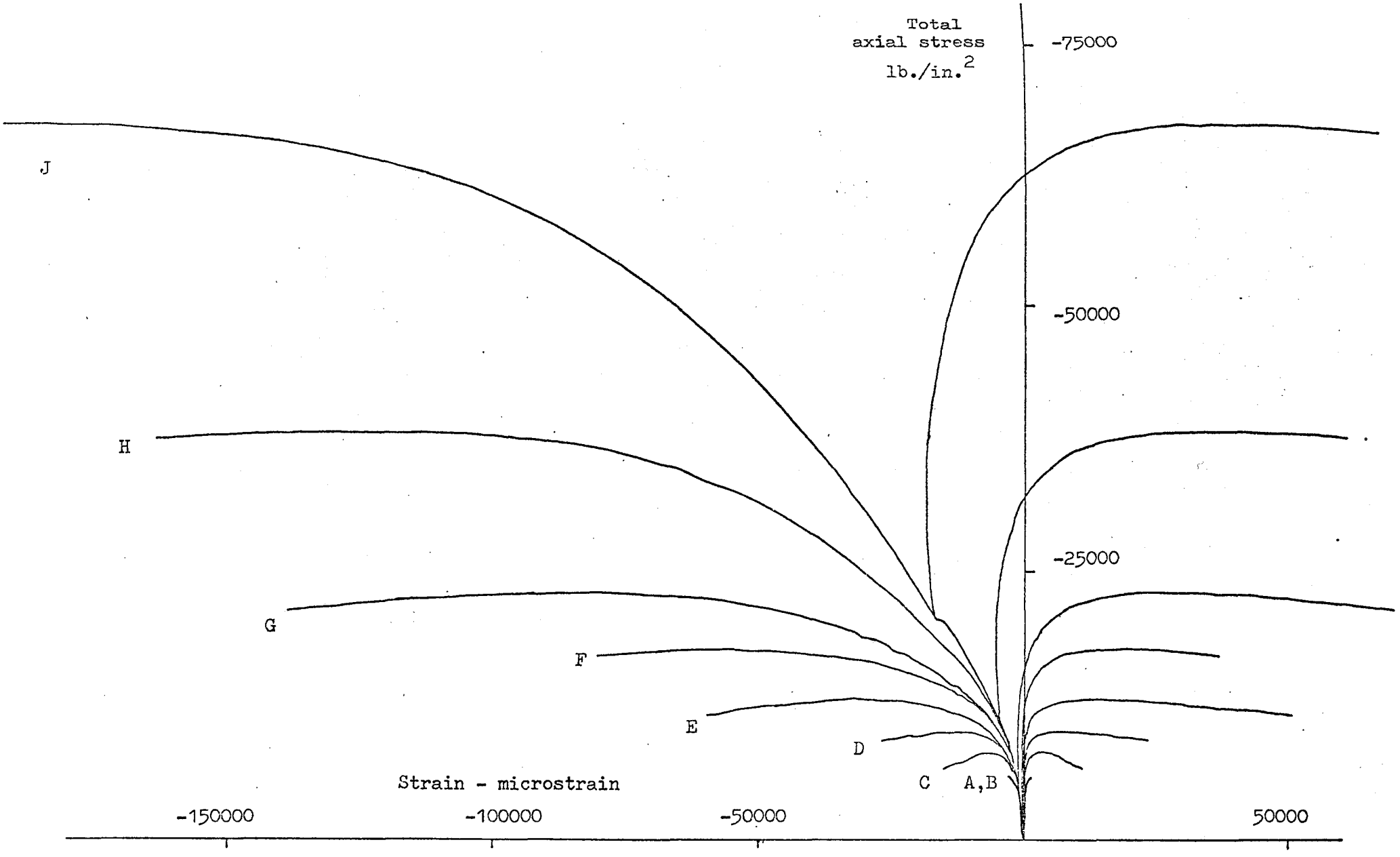


Figure 7.78. Variation of axial and lateral strains with total axial stress for cylinders of Mix M2 under triaxial compression with various values of confining pressure.

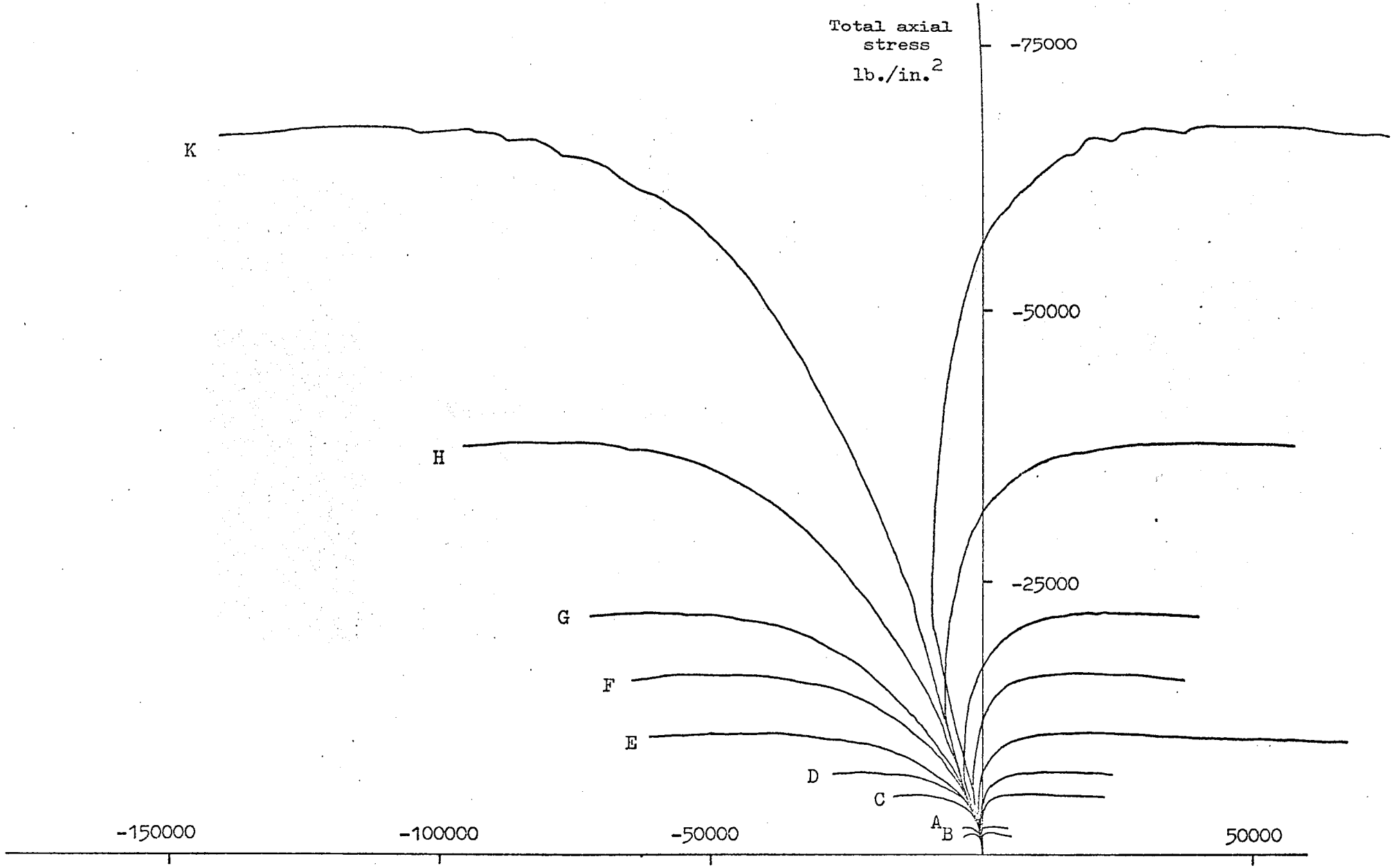


Figure 7.79. Variation of axial and lateral strains with total axial stress for cylinders of Mix C2 under triaxial compression with various values of confining pressure.

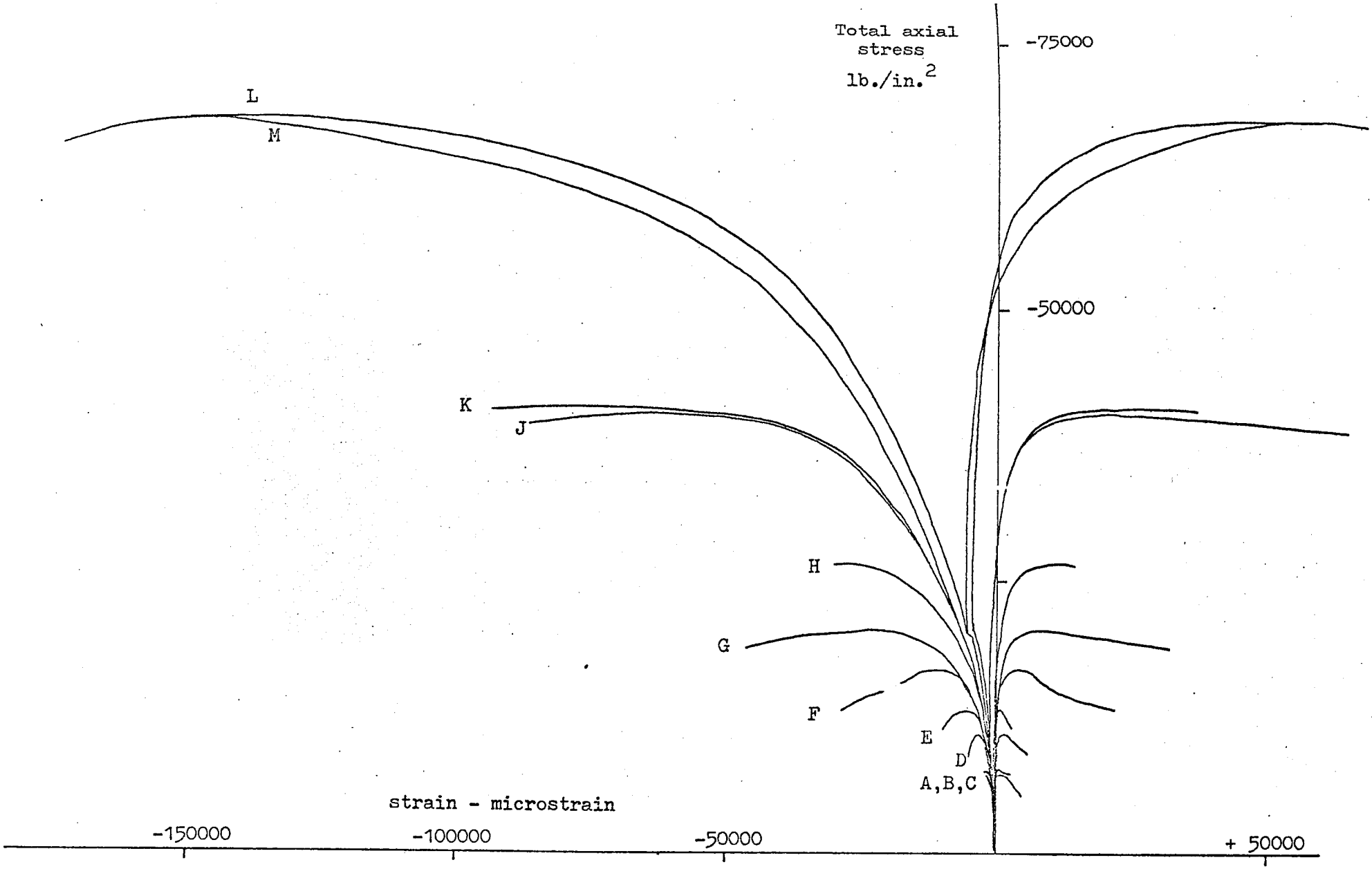


Figure 7.80. Variation of axial and lateral strains with total axial stress for cylinders of Mix C3 under triaxial compression with various values of confining pressure.

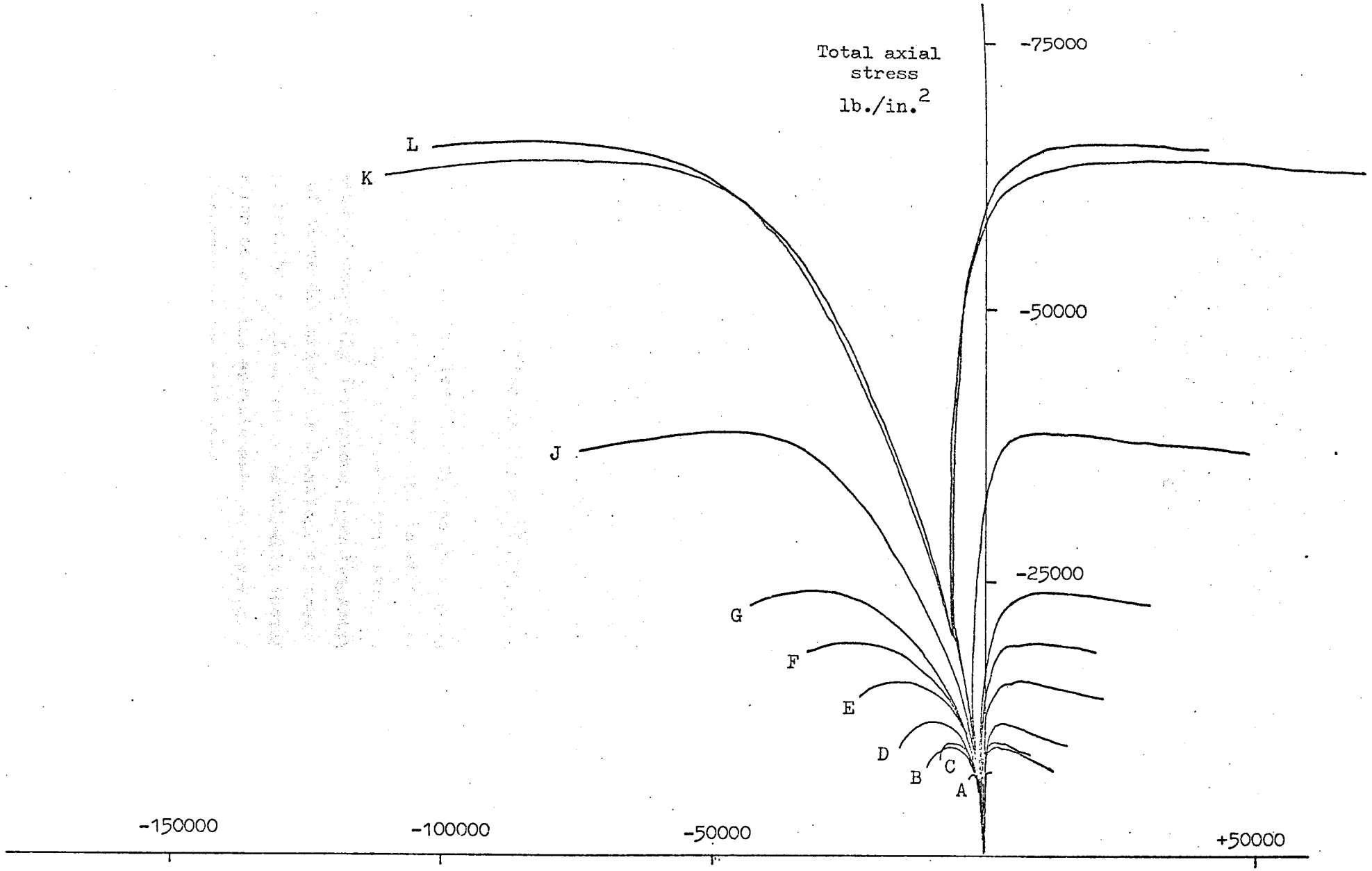


Figure 7.81. Variation of axial and lateral strains with total axial stress for cylinders of Mix C4 under triaxial compression with various values of confining pressure.

and its effect in increasing the total water/cement ratio necessary to attain a given 'effective' water/cement ratio (see 7.6.3.).

7.6.5.3. Onset of Stable Fracture Propagation (o.s.f.p.)

The method of assessing o.s.f.p., based on the relationship between axial and lateral strain is described in 4.5. Figures 7.82. to 7.84. show the axial strain-lateral strain relationships for the various mixes. The basic characteristics of these with respect to variations due to changes in confining pressure and volume fraction of aggregate for a given 'effective' water/cement ratio are similar to those observed for the idealised concretes, and described in 7.5.4.3.

A measure of the slope of the tangent to the above relationships is given by the value of the incremental strain ratio (i.s.r.) as defined in 4.5., at a given stress level. For the various mixes the variation of i.s.r. with level of deviator stress is shown in Figures 7.85. to 7.87.

These relationships again exhibit the same characteristics as those corresponding to the idealised concretes. In all cases the increase in the numerical value of i.s.r., which indicates fracture propagation, can be clearly seen. The level of stress at which this increase starts (o.s.f.p.) however, is difficult to assess from the curves except in the case of some tests conducted at low confining pressures.

The determination of the level of stress at o.s.f.p. is facilitated by using the technique described in 4.5., in which the mean slope of the linear portion of the axial strain-lateral strain relationships is used as the basis of computing deviations from linearity of the lateral strain. The form of these deviations is identical to those given by the idealised concretes, and the o.s.f.p. level is clearly indicated in all cases. The variation of strains and stresses at o.s.f.p. for the various mixes will be discussed in the following:-

Strains at o.s.f.p.

Figure 7.88. shows the relationship between axial and lateral strains for the mixes containing river gravel aggregate. The closed form of these envelopes in strain space is similar to that found for the idealised concretes, as is the decrease in the size of the envelope for an increase

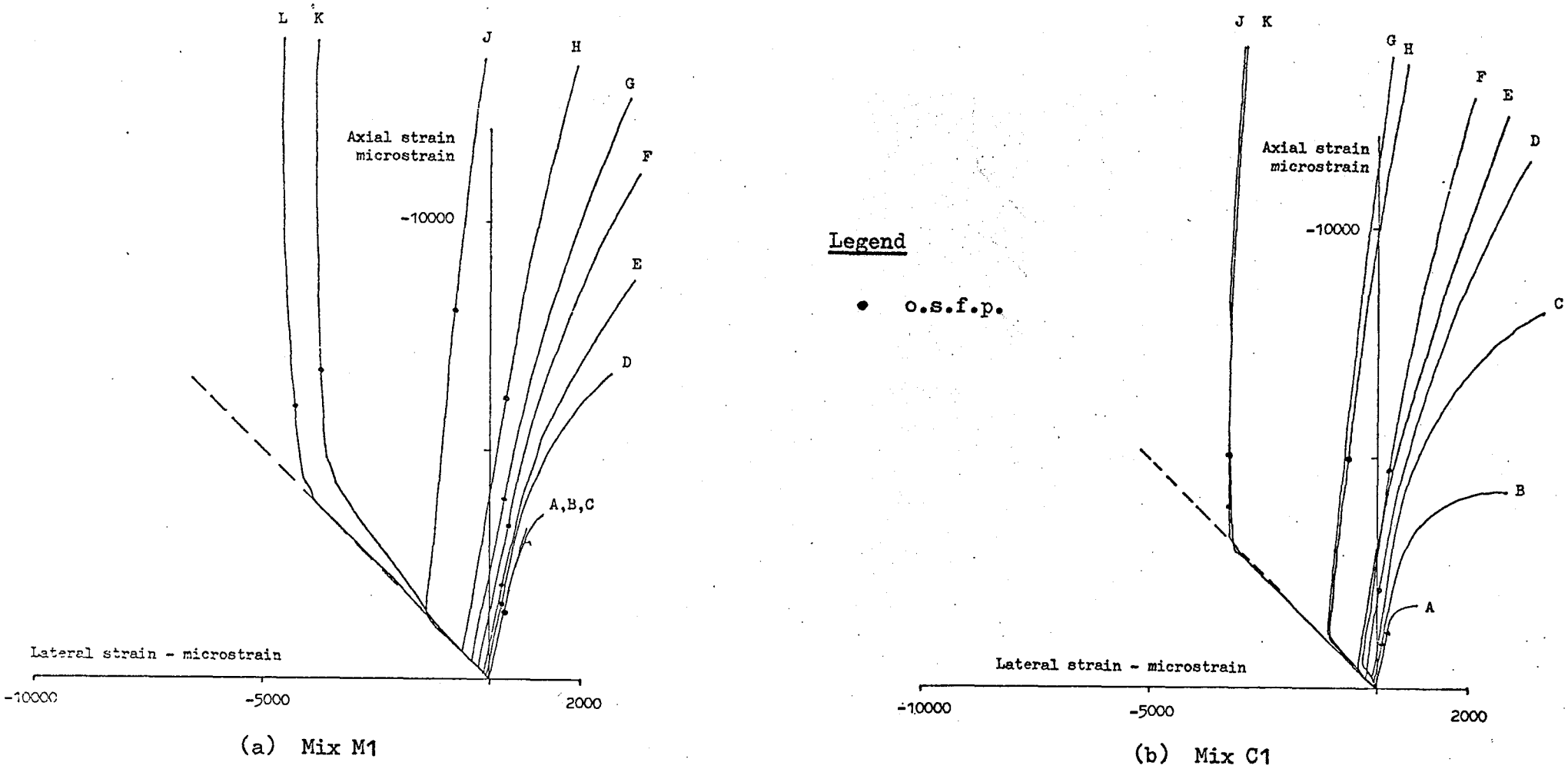
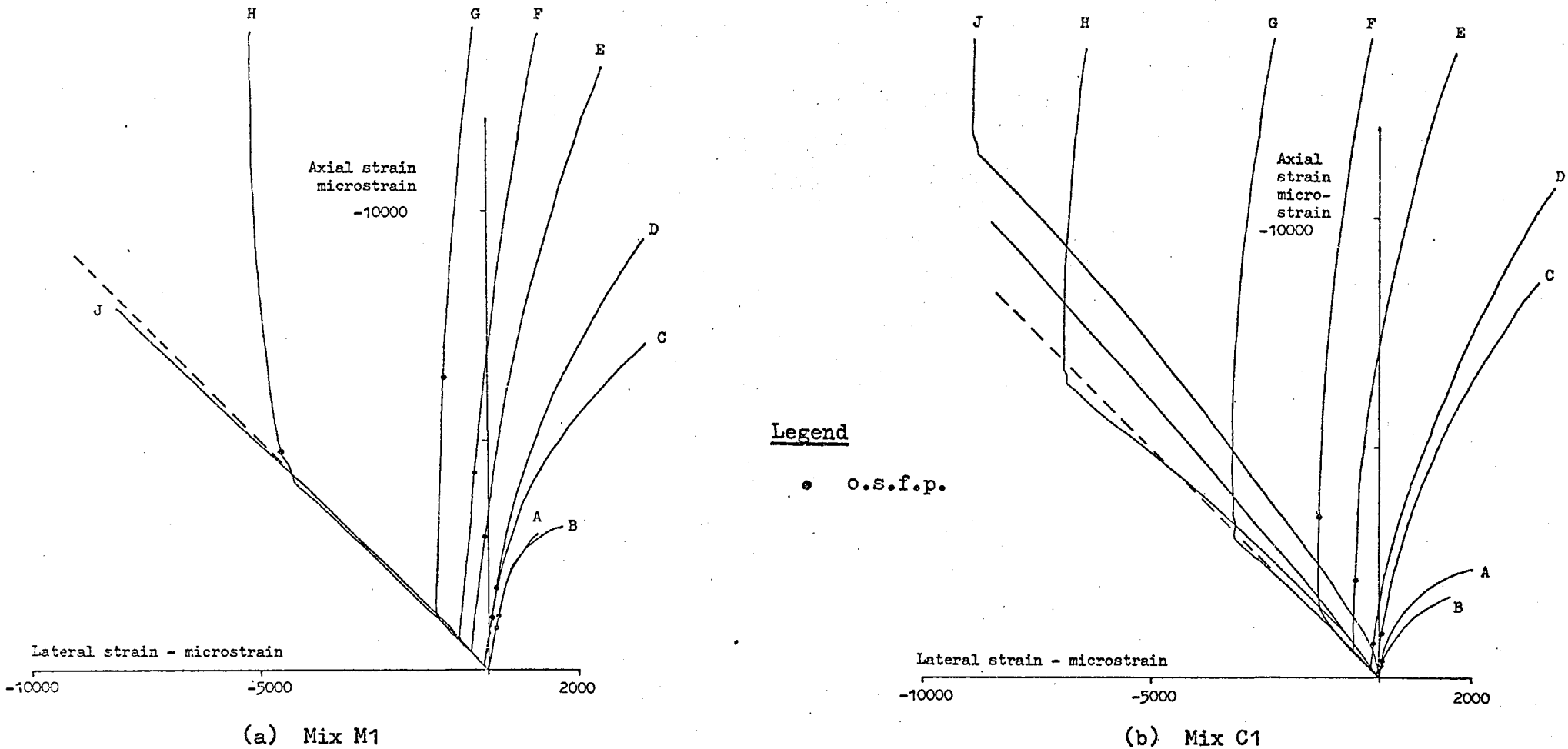


Figure 7.82. Relationships between axial and lateral strains for real concretes under triaxial 'compression' with various values of confining pressure.



(a) Mix M1

(b) Mix C1

Figure 7.83. Relationships between axial and lateral strains for real concretes under triaxial 'compression' with various values of confining pressure.

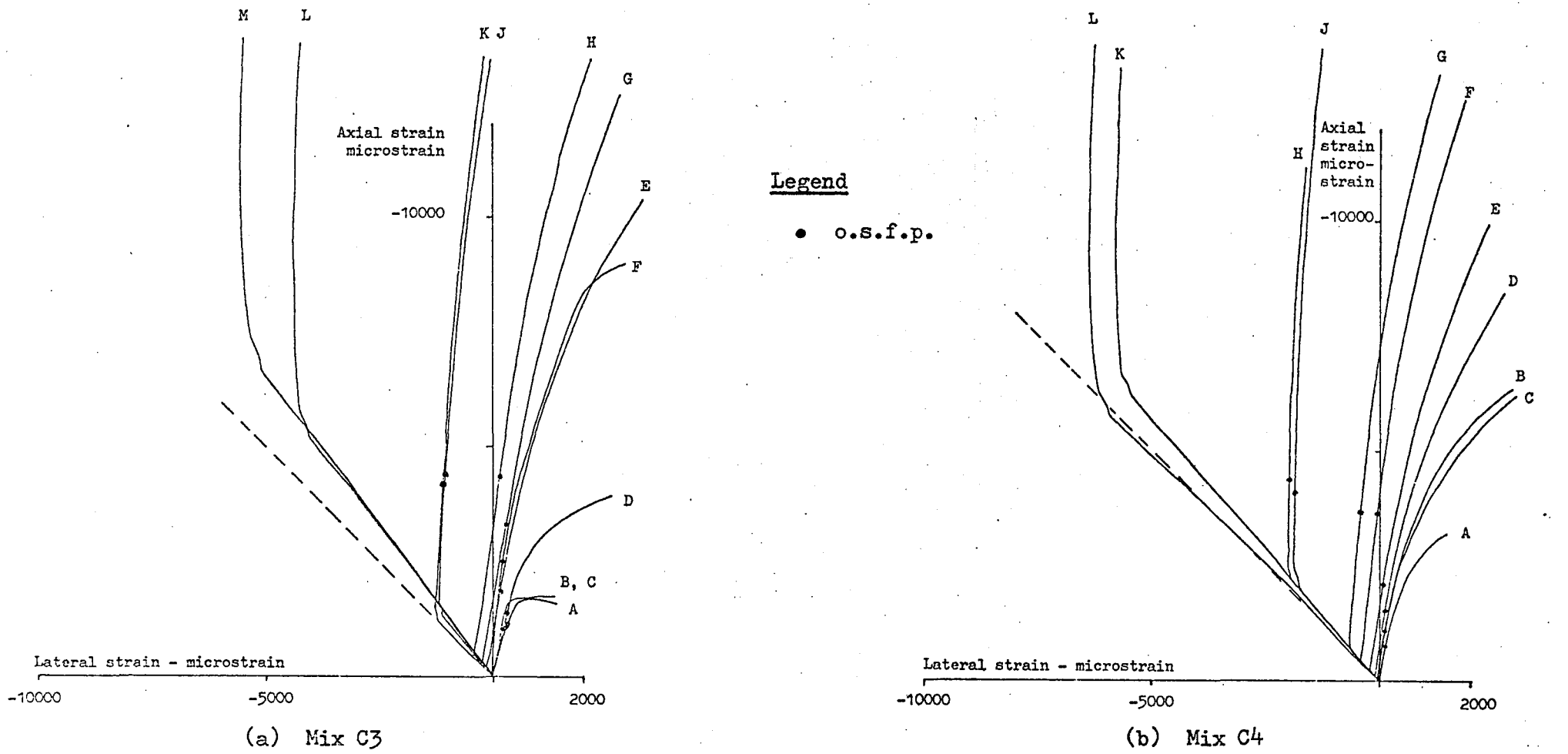


Figure 7.84. Relationships between axial and lateral strains for real concretes under triaxial 'compression' with various values of confining pressure.

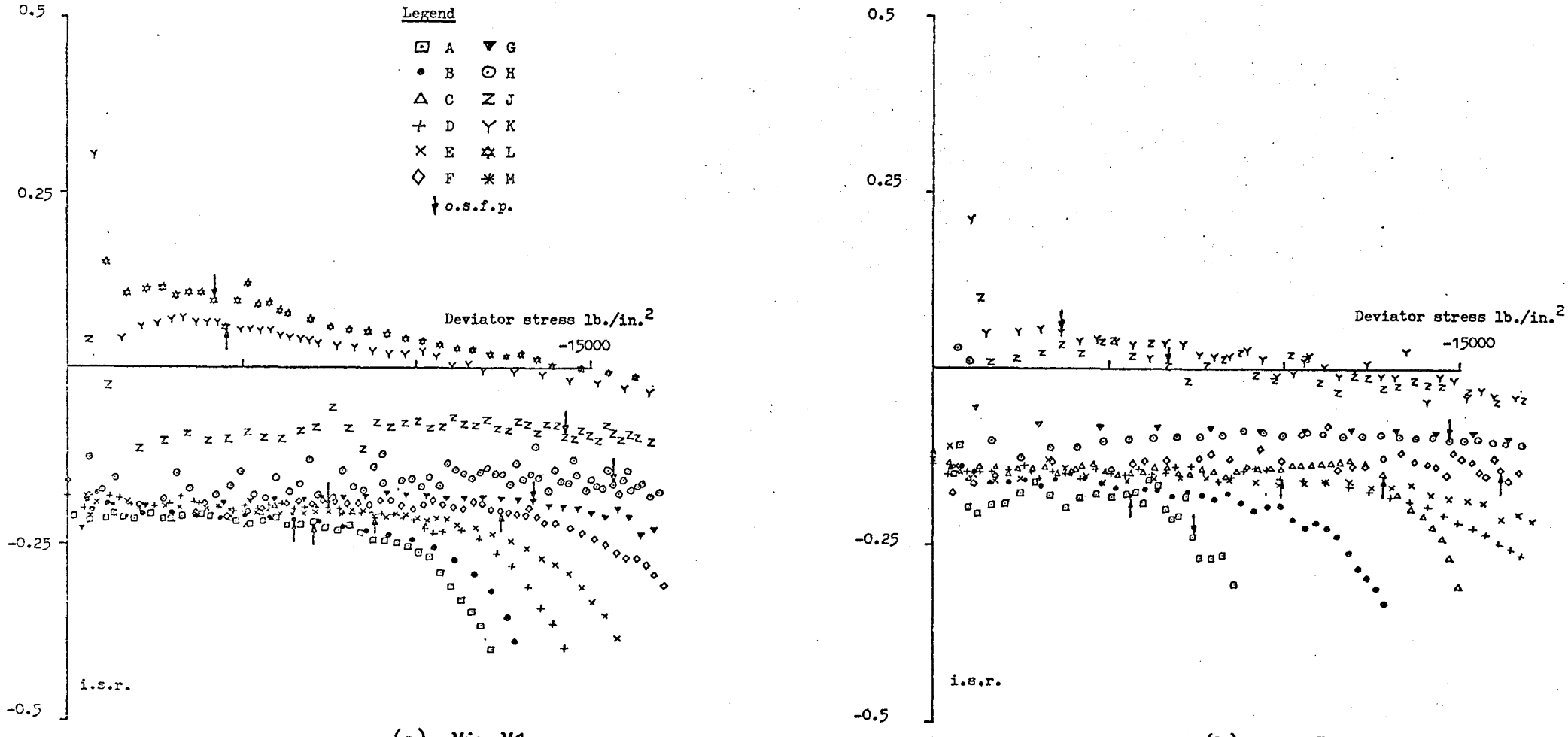


Figure 7.85. Variation of incremental strain ratio with deviator component of axial stress for real concretes under triaxial compression with various values of confining pressure.

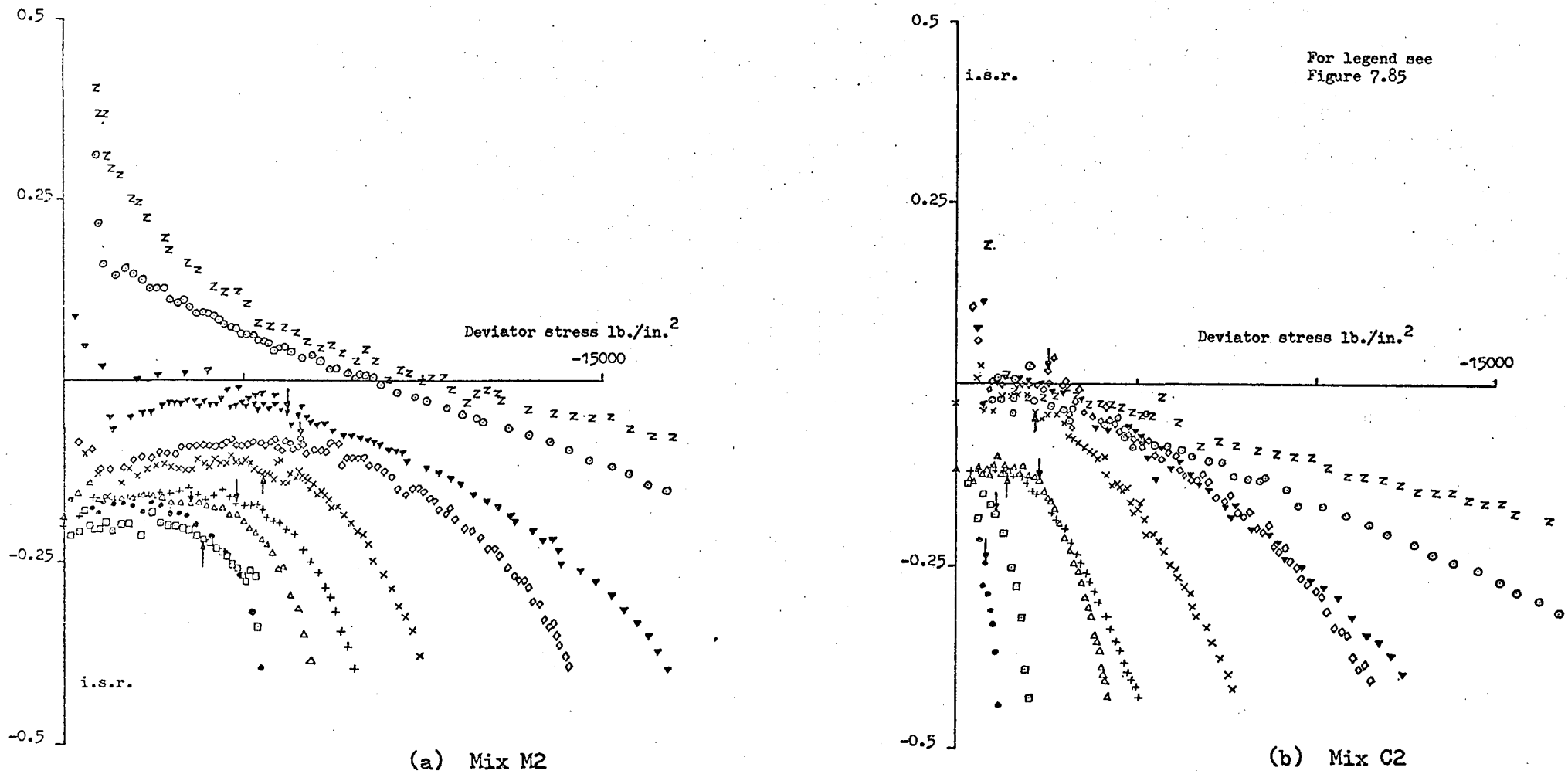


Figure 7.86. Variation of incremental strain ratio with deviator component of axial stress for real concretes under triaxial compression with various values of confining pressure.

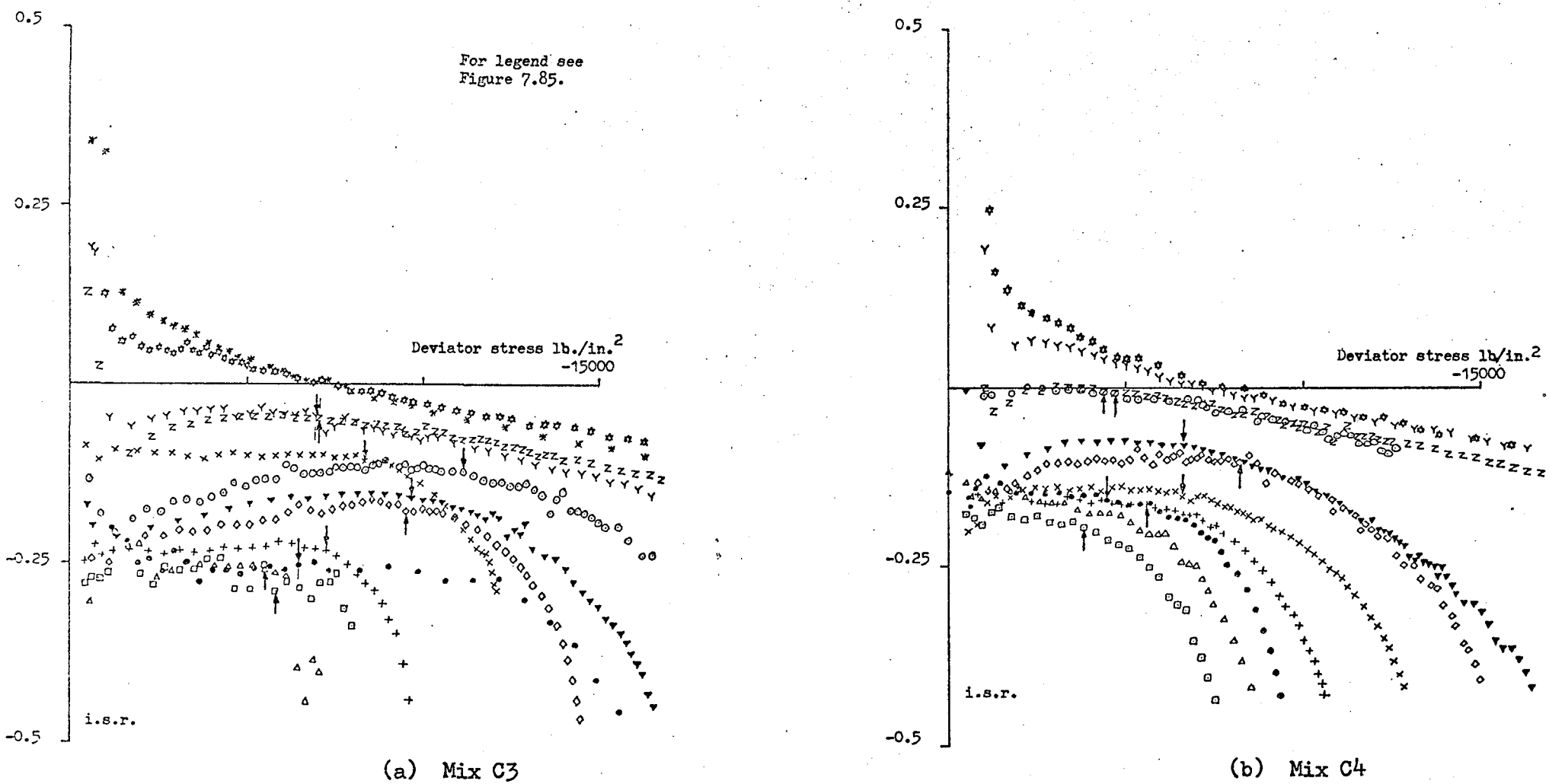


Figure 7.87. Variation of incremental strain ratio with deviator component of axial stress for real concretes under triaxial compression with various values of confining pressure.

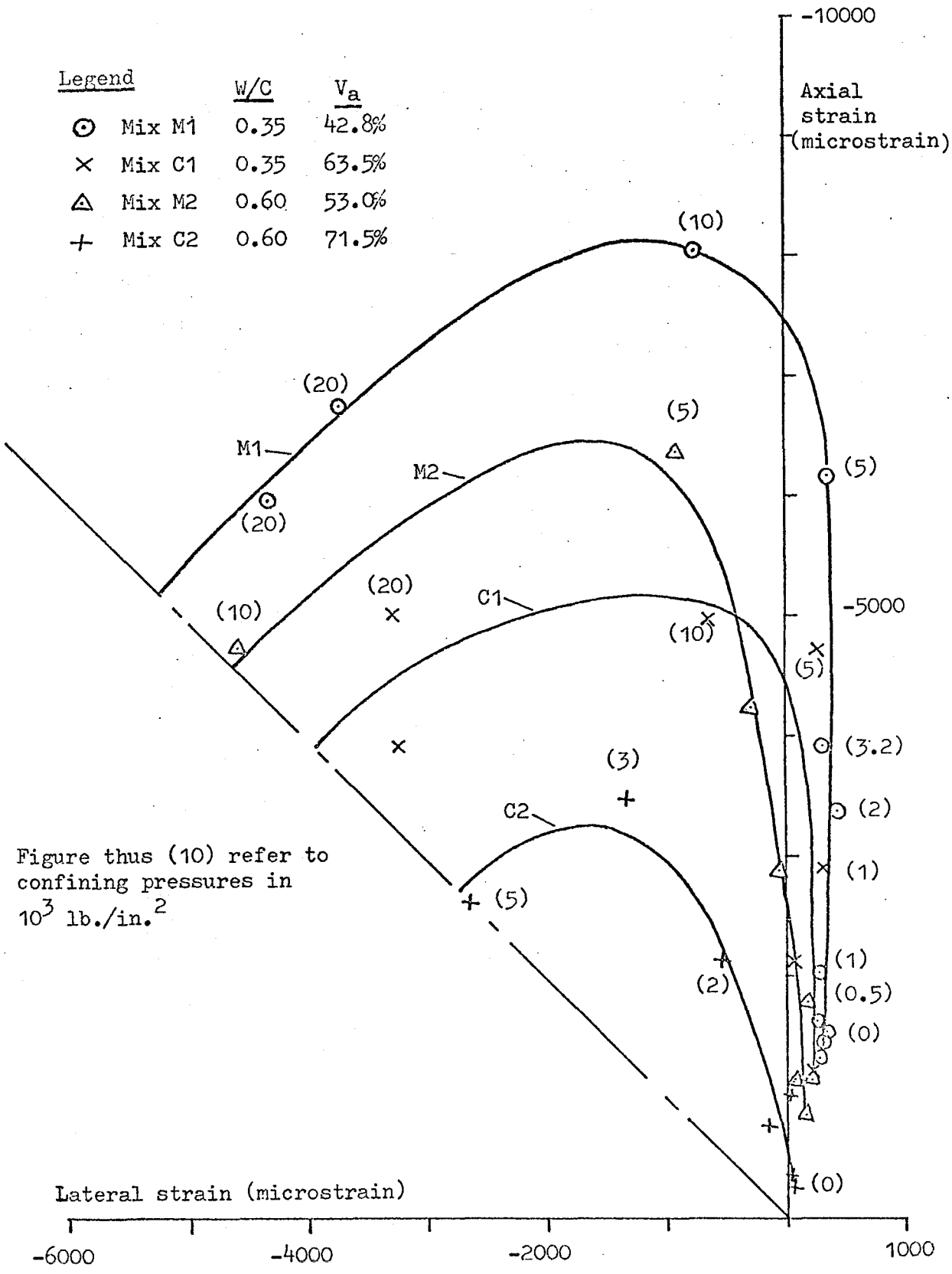


Figure 7.88. Relationships between axial and lateral strains at onset of stable fracture propagation under triaxial compression for mortars and concretes containing river gravel aggregates.

in the volume fraction of aggregate at a given 'effective' water/cement ratio.

Although mixes with the same volume fraction and type of aggregate, but with varied water/cement ratio, are not available for comparison it would appear from Figure 7.88. that the envelopes are also functions of the water/cement ratio of the mix. The fact that those for mixes M2 and C2 form a separate family to those for mixes M1 and C2 suggests that a lowering of paste quality, by increasing the water/cement ratio, will reduce of magnitude of the o.s.f.p. envelope. This is discussed more fully when dealing with the stresses at o.s.f.p.

The envelopes defining strain at o.s.f.p. for the concretes containing limestone and granite aggregates (mixes C3 and C4 respectively) are shown in Figure 7.89. Both envelopes are significantly less critical than that for the corresponding mix containing the same grading of river gravel aggregate (C2). As discussed previously, this may be due to the change in shape or stiffness of the aggregates or, more likely, to the lower absorption capacities of the granite and limestone requiring less total water for a given 'effective' water content (see Appendices 2 and 3).

Stresses at o.s.f.p.

Figures 7.90. and 7.91. show the envelopes of stress at o.s.f.p. for the real concrete mixes made with gravel aggregates, together with the ultimate strength envelopes for comparison. As for the idealised mixes, all envelopes are of closed form in stress space.

For mixes M1 and C1, with an 'effective' water/cement ratio of 0.35, the o.s.f.p. envelope for the concrete is marginally, but not significantly, above that for the mortar. For mixes M2 and C2 the envelope for the concrete lies significantly below that for the mortar. This behaviour is to be compared with that for idealised concretes where, for the same 'effective' water/cement ratio, increases in the volume fraction of aggregate tended to expand the envelopes.

As for the case of strains at o.s.f.p. this may be due mainly to the effect of the water absorbtion capacity of the aggregate on the total water required for a given 'effective' water content.

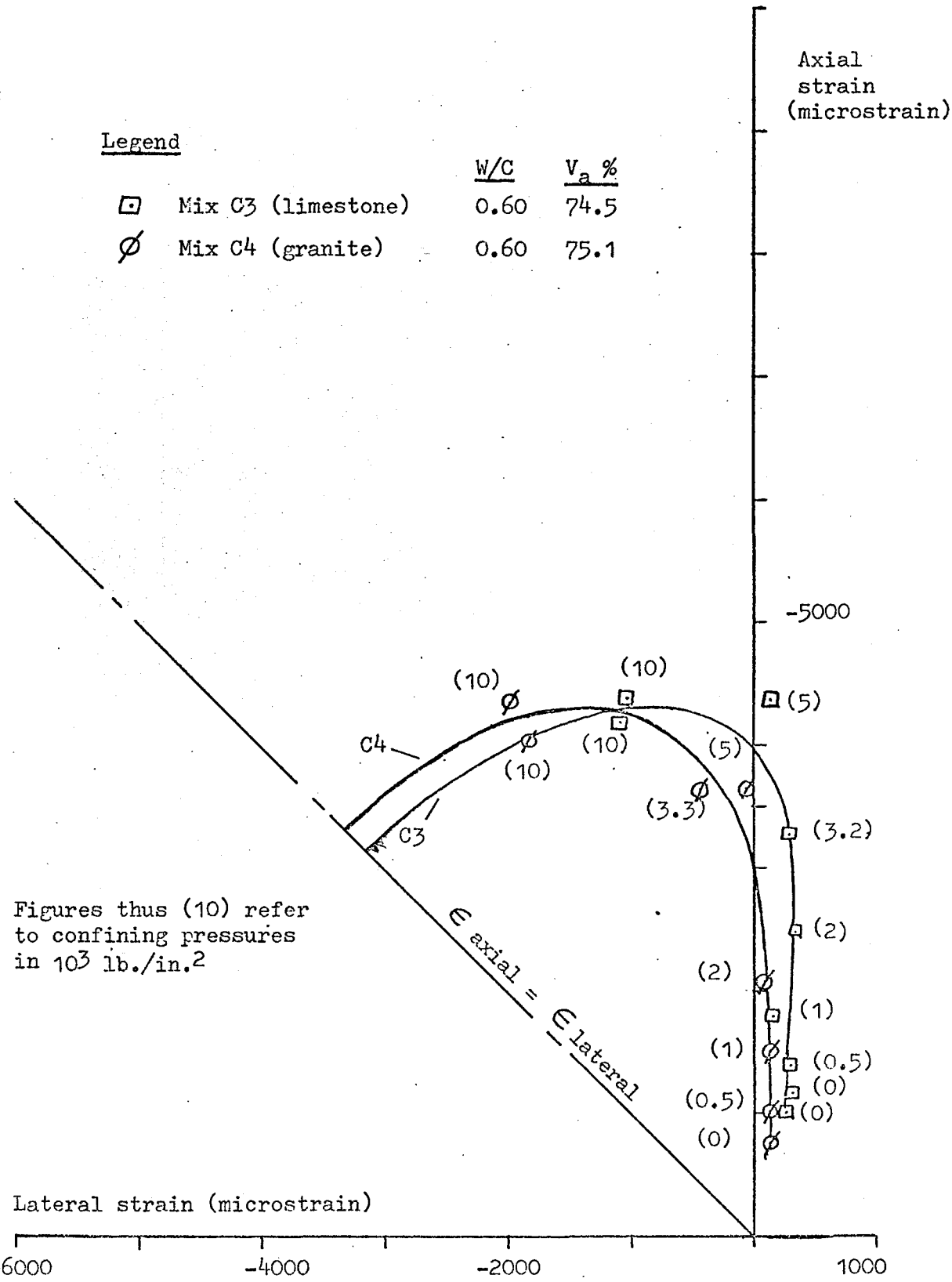


Figure 7.89. Relationships between axial and lateral strains at onset of stable fracture propagation under triaxial compression for concretes containing limestone and granite aggregates.

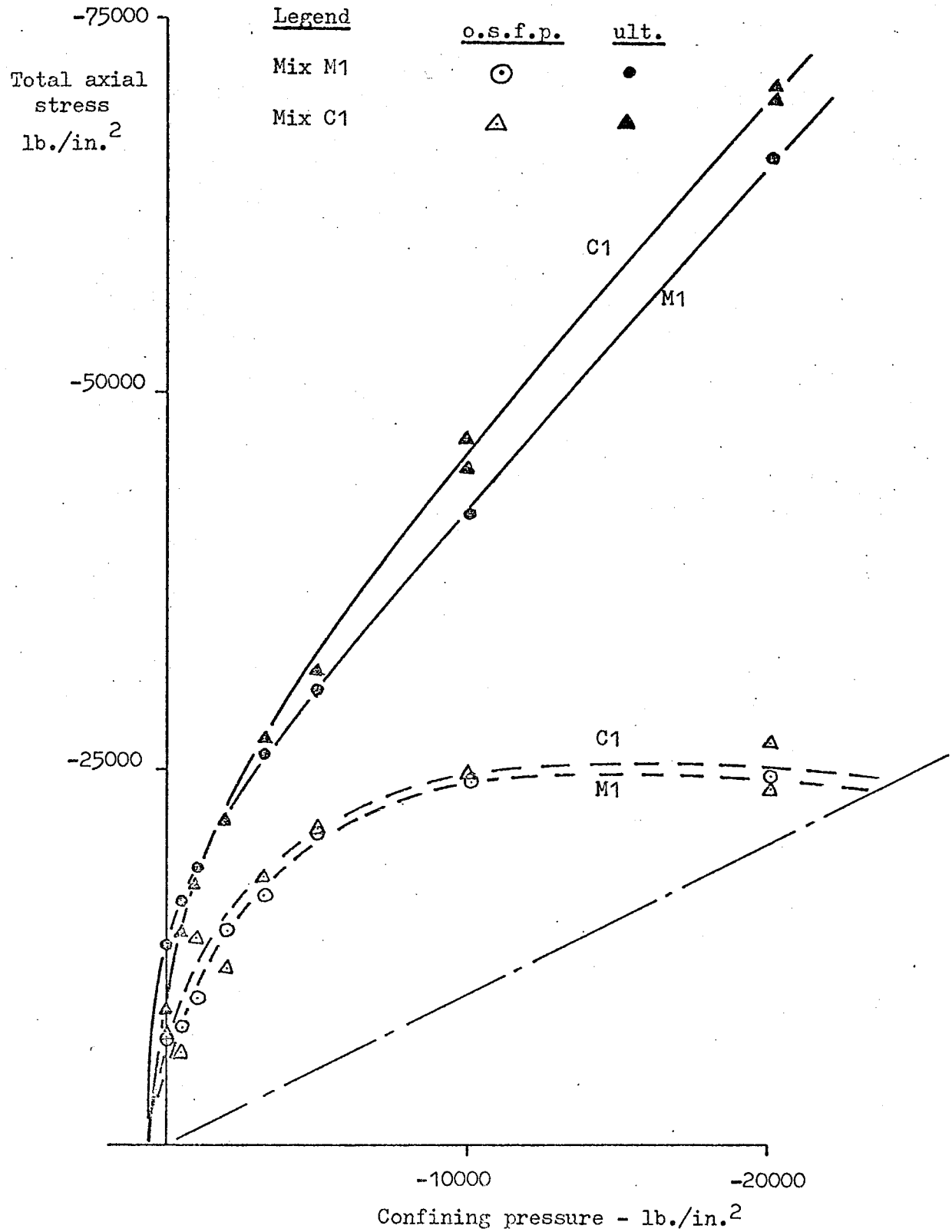


Figure 7.90. Variation of total axial stress at o.s.f.p. and ultimate with confining pressure for mixes M1 and C1 under triaxial compression.

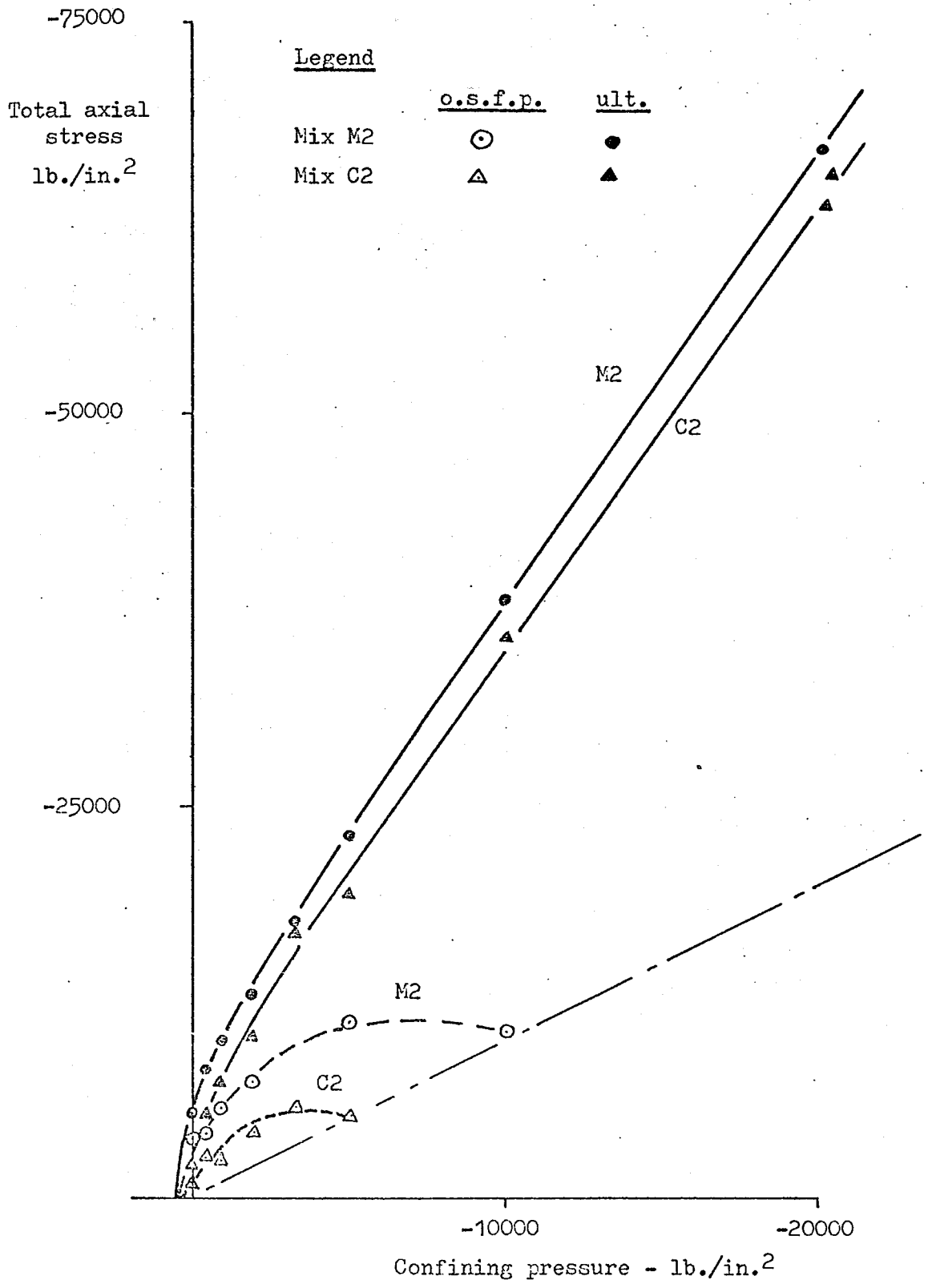


Figure 7.91. Variation of total axial stress at o.s.f.p. and ultimate with confining pressure for Mixes M2 and C2 under triaxial compression.

The criticality of the water/cement ratio of the mixes in affecting the magnitude of the envelopes is clearly demonstrated when comparing the envelopes for mixes M1 and C1 with those for M2 and C2. An increase in the 'effective' water/cement ratio dramatically reduces the size of the envelopes and this cannot be ascribed to the effect of the volume fraction of aggregate since, between the two sets of mixes, values of the volume fractions overlap (see Appendix 3).

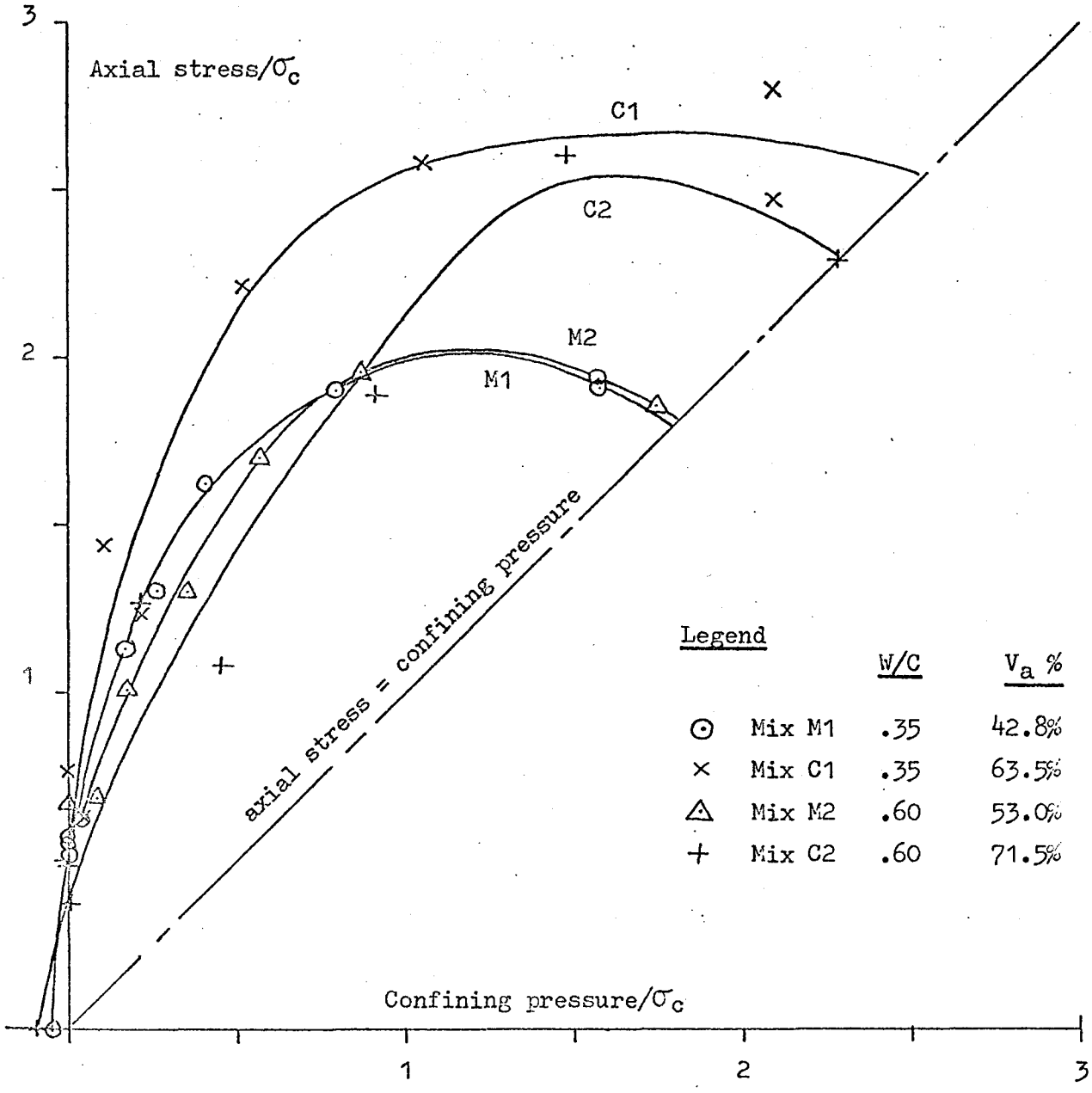
Thus it would appear that the water/cement ratio is the predominant factor influencing the magnitude of stress at o.s.f.p. This tends to confirm the hypothesis described in 7.5.4.4., in which the level of stress at o.s.f.p. is considered to be linked with collapse of the relatively porous cement paste matrix under hydrostatic load. An increase in the water available for hydration of the cement which, it is suggested, is a function of the total water/cement ratio as well as the 'effective' water/cement ratio, will produce a lower quality paste with an increased porosity [208]. This porosity will cause the hardened paste to collapse more readily under hydrostatic compression.

The envelopes of stress at o.s.f.p. for the gravel aggregate mixes, normalised with respect to the corresponding values of uniaxial compressive (cylinder) strength, are shown in Figure 7.92.

Figure 7.93. shows the envelopes of stress at o.s.f.p. for the concretes made with limestone (C3) and granite (C4) aggregates.

As for the case of strains at o.s.f.p. both envelopes are considerably less critical than that for mix C2 which contains the same 'effective' water/cement ratio and same grading of river gravel aggregate. This, again, appears to confirm the contribution of the water absorbed by the aggregate to the paste hydration, although the effects of the change in shape and stiffness of aggregate may be significant (see Appendix 2).

Figure 7.94. shows the normalised envelopes for mixes C3 and C4, and comparison with Figure 7.92. indicates that the limestone mix (C3) is slightly less critical than that for the gravel (C2), except at higher values of normalised confining pressure. The granite mix (C4) is considerably more critical for all values.



7.92. Relationships between normalised axial stress and confining pressure at onset of stable fracture propagation under triaxial compression for mortars and concretes containing river gravel aggregate.

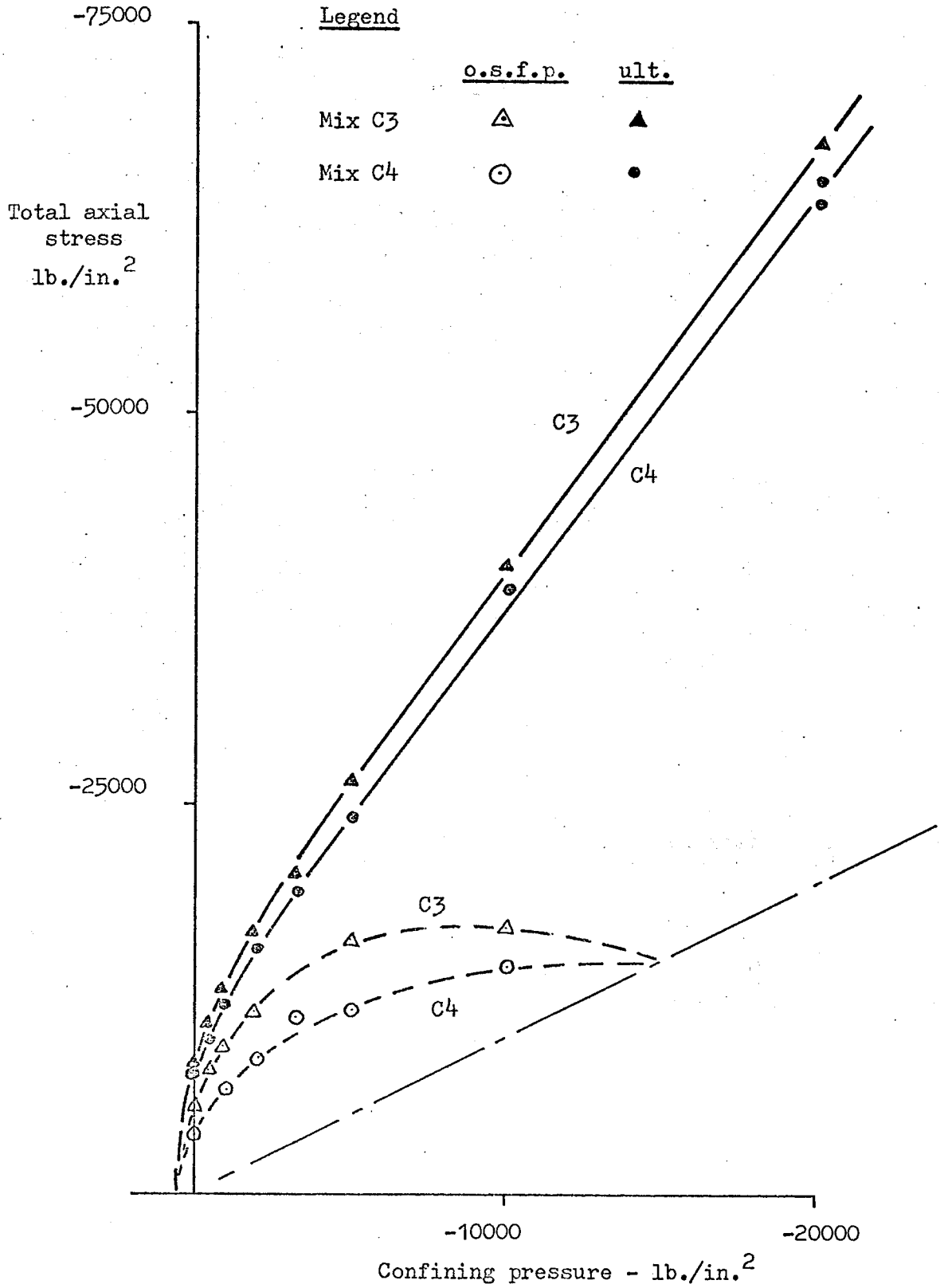


Figure 7.93. Variation of total axial stress at o.s.f.p. and ultimate with confining pressure for mixes C3 and C4 under triaxial compression.

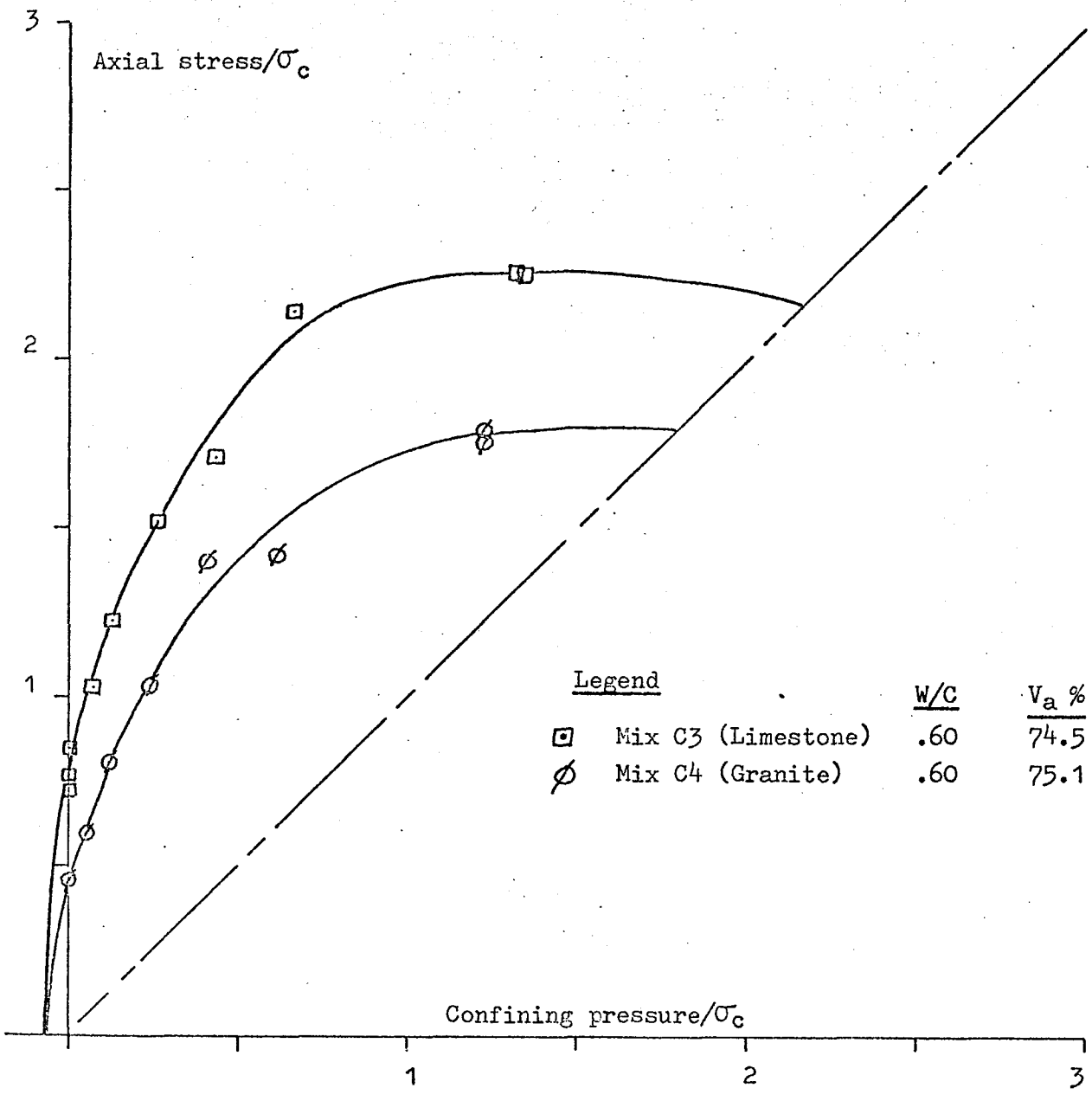


Figure 7.94. Relationships between normalised axial stress and confining pressure at onset of stable fracture propagation under triaxial compression for concretes containing limestone and granite aggregates.

7.6.5.4. Volume Changes

Figures 7.95. to 7.97. show the relationships between volume changes and total axial stress for various levels of confining pressure.

As for the idealised concretes the relationships for all mixes exhibit the same basic characteristics as follows:-

i) a non-linear volume decrease as the hydrostatic stress is applied up to the required level.

ii) A further decrease in volume during application of the deviator component of axial stress.

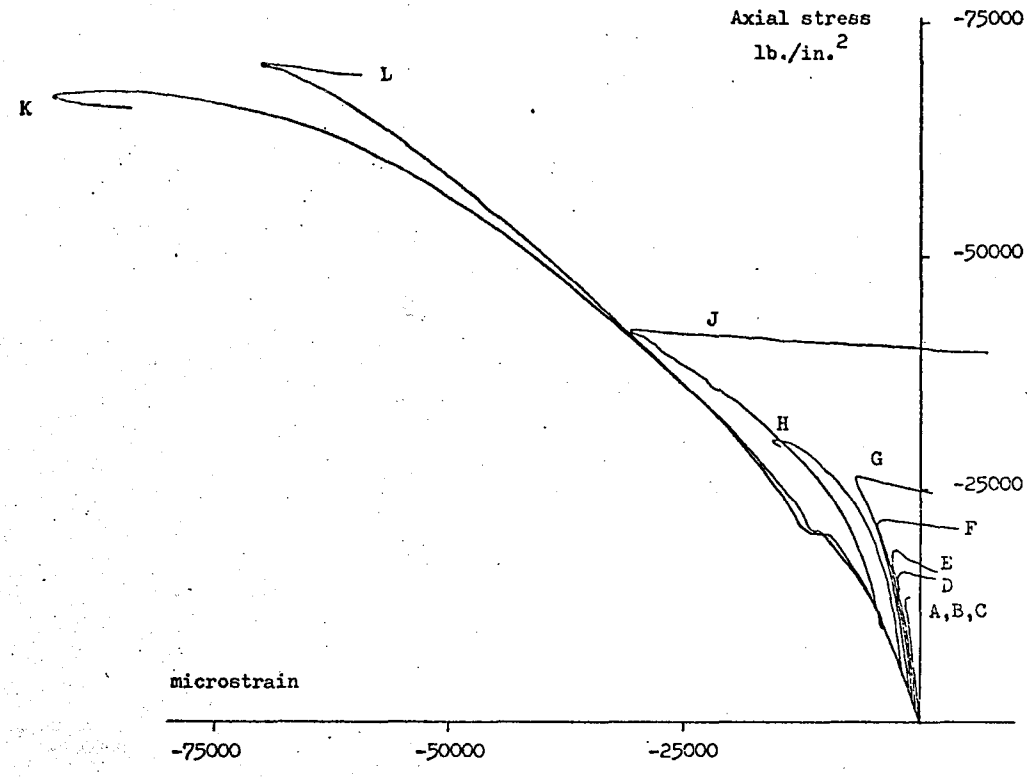
iii) attainment of minimum volume at an axial stress level approaching ultimate, after which the volume increases rapidly to ultimate failure.

These characteristics will be discussed in the following:-

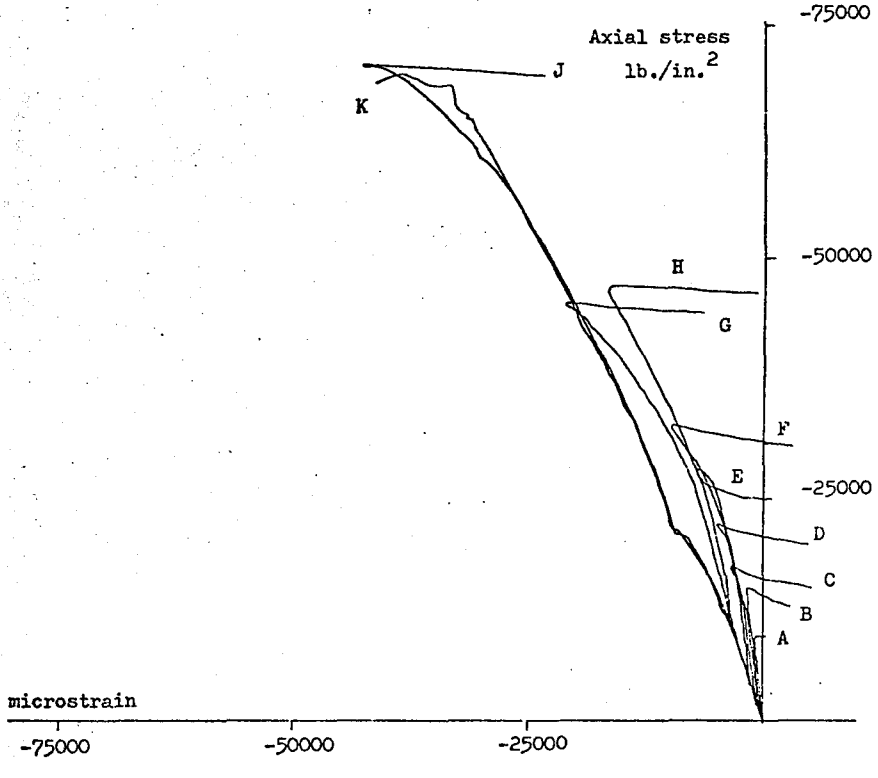
Hydrostatic Compressibility

Figures 7.98 to 7.100 show in detail the relationships between volumetric strain and confining pressure for the hydrostatic portion of each test. Each figure contains results for all specimens of a given mix tested, and where possible the figures have been plotted to the same scale as used for the idealised concretes for comparison. Where the volume change becomes too large for the complete curve to be represented (mixes M2 and C2) this is shown to a reduced scale.

Except for mix M2 and C2, the mixes show the initial volume change to vary almost linearly with pressure, as found for the idealised concretes. After the initial application of pressure, however, the volume decreases at an increasing rate for all mixes which indicates progressive breakdown of the paste matrix. This is particularly the case for mixes M2 and C2 where the extremely large strains reflect the low quality cement paste matrix. It is interesting to note that for mix C2, the mix with apparently the lowest quality paste, the rate of decrease in volume tends to decrease after a certain level of confining pressure. This behaviour may be caused by particle interference effects which follow the collapse of the porous paste structure and is similar to that exhibited by syntactic

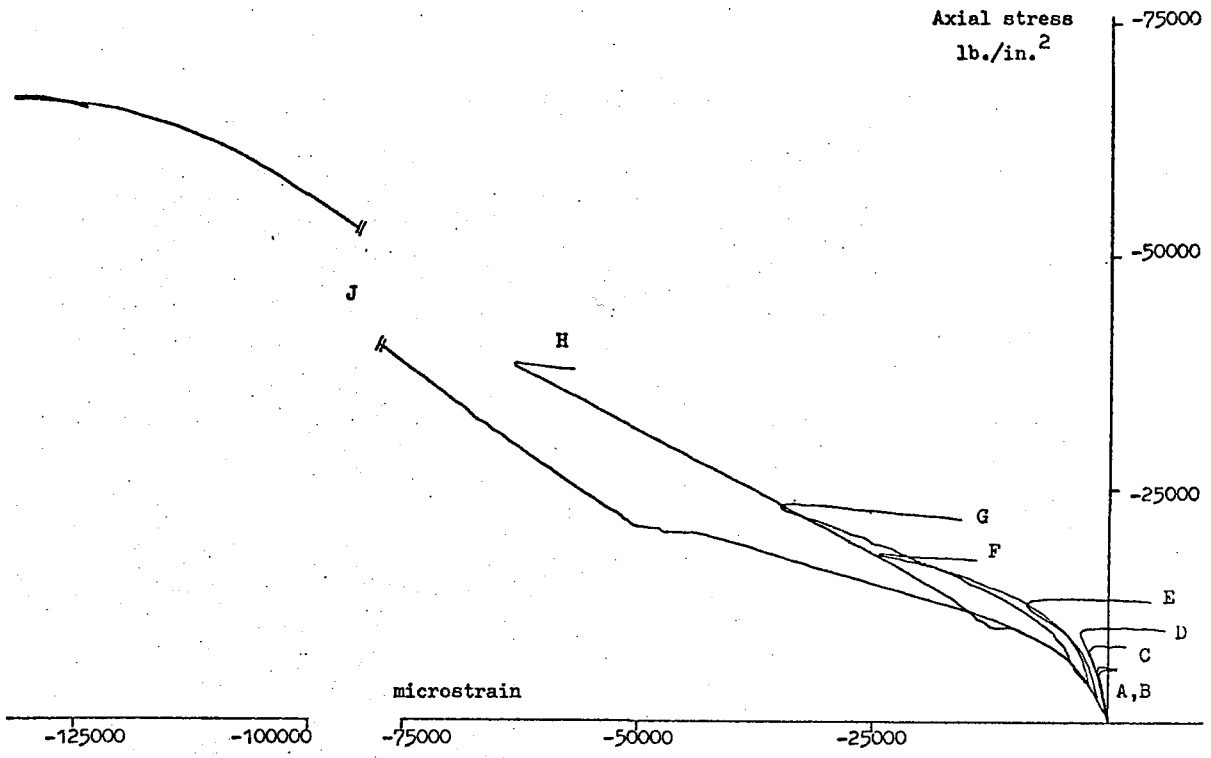


(a) Mix M1

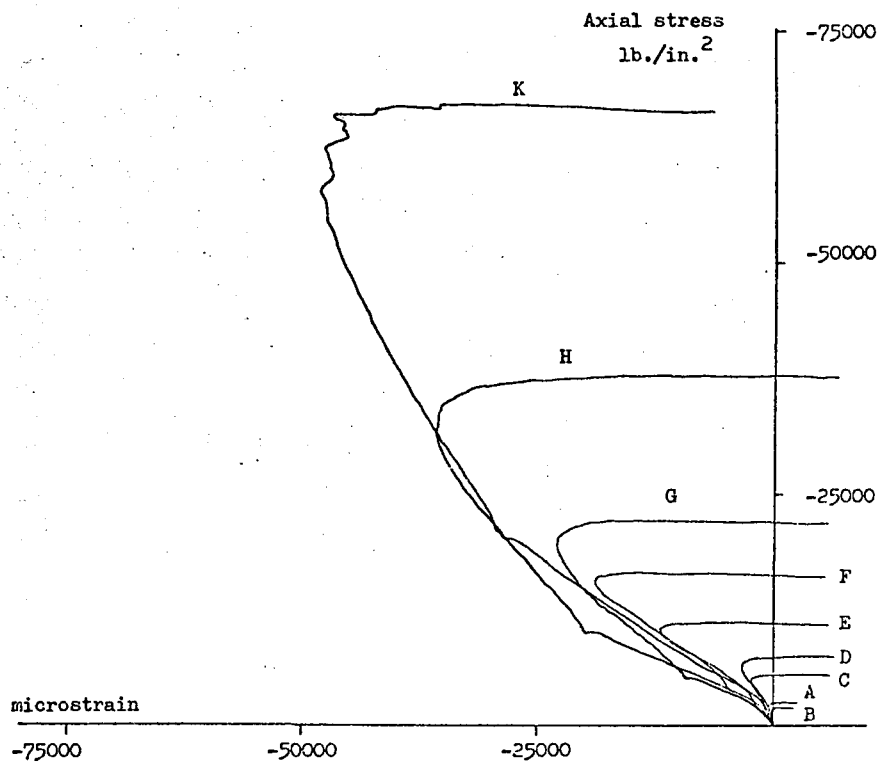


(b) Mix C1

Figure 7.95. Variation of volumetric strain with total axial stress for real concretes under triaxial compression with various values of confining pressure.

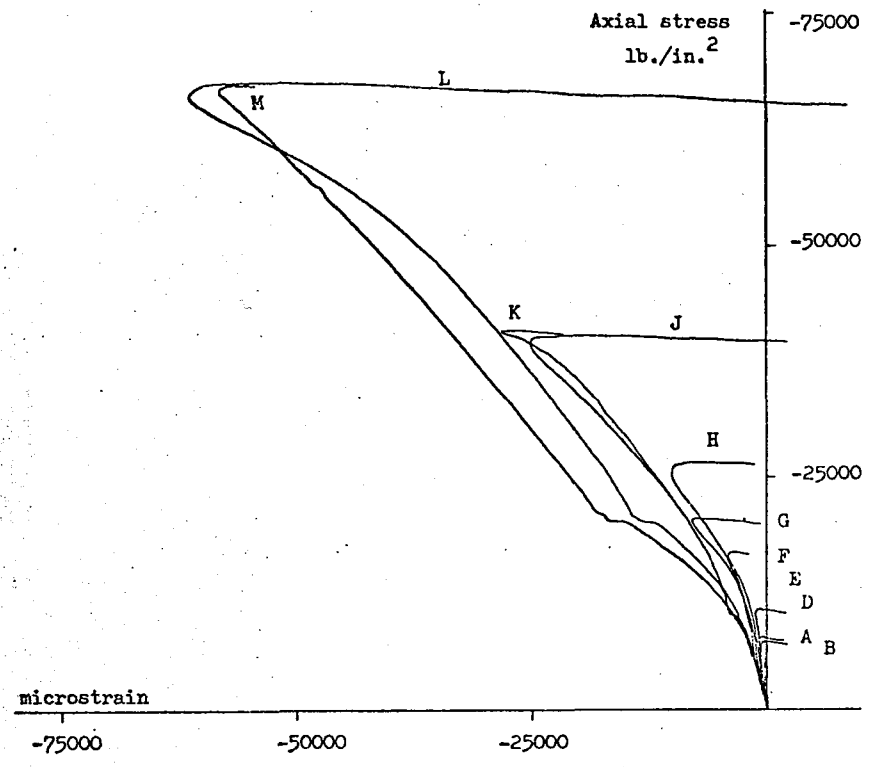


(a) Mix M2

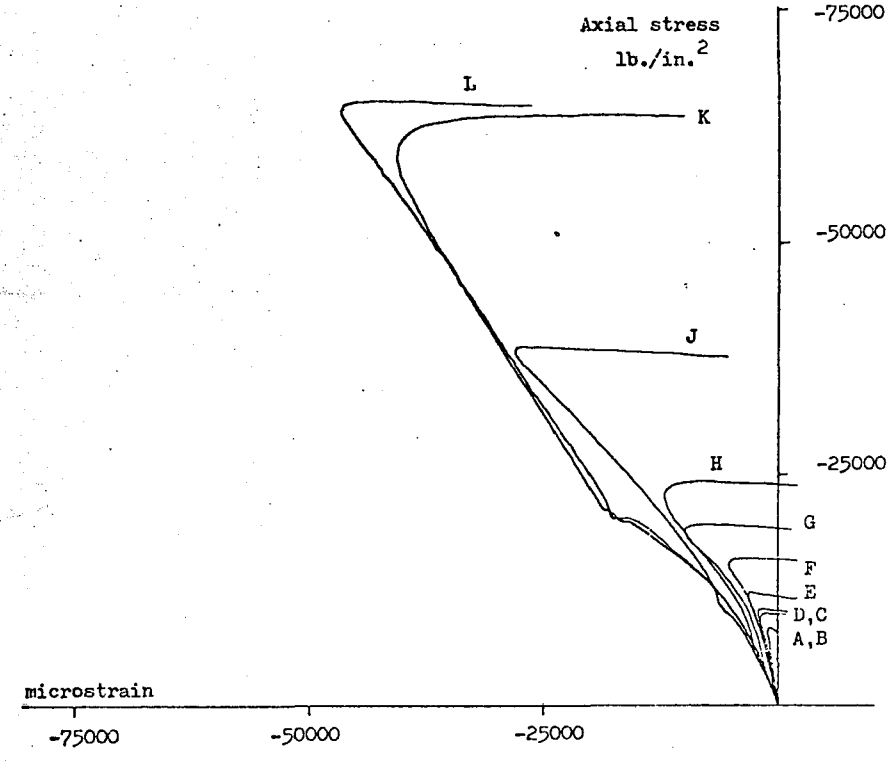


(b) Mix C2

Figure 7.96. Variation of volumetric strain with total axial stress for real concretes under triaxial compression with various values of confining pressure.

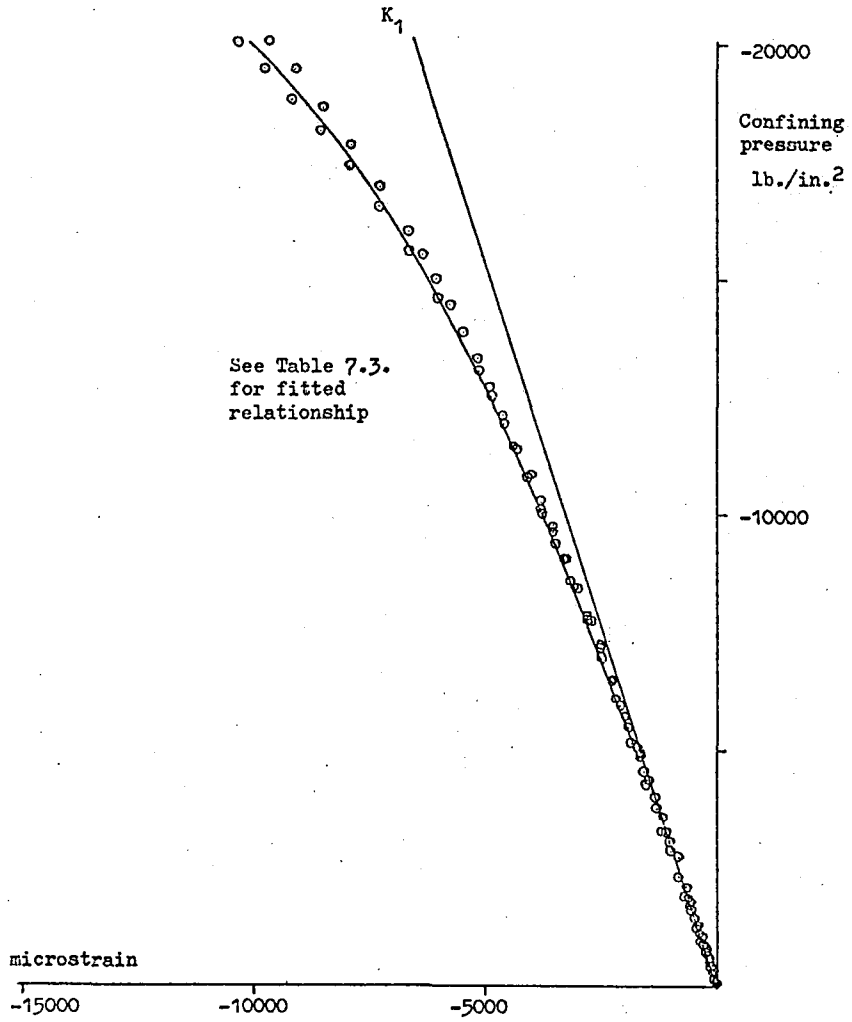


(a) Mix C3

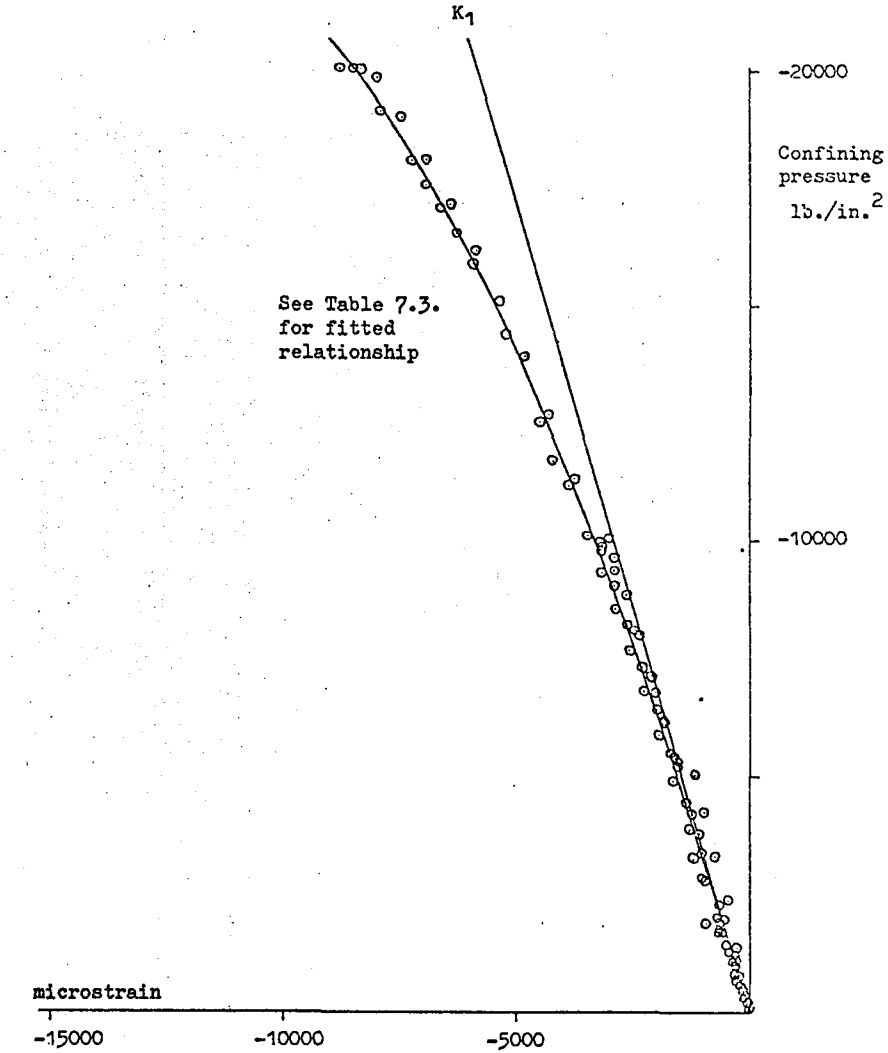


(b) Mix C4

Figure 7.97. Variation of volumetric strain with total axial stress for real concretes under triaxial compression with various values of confining pressure.

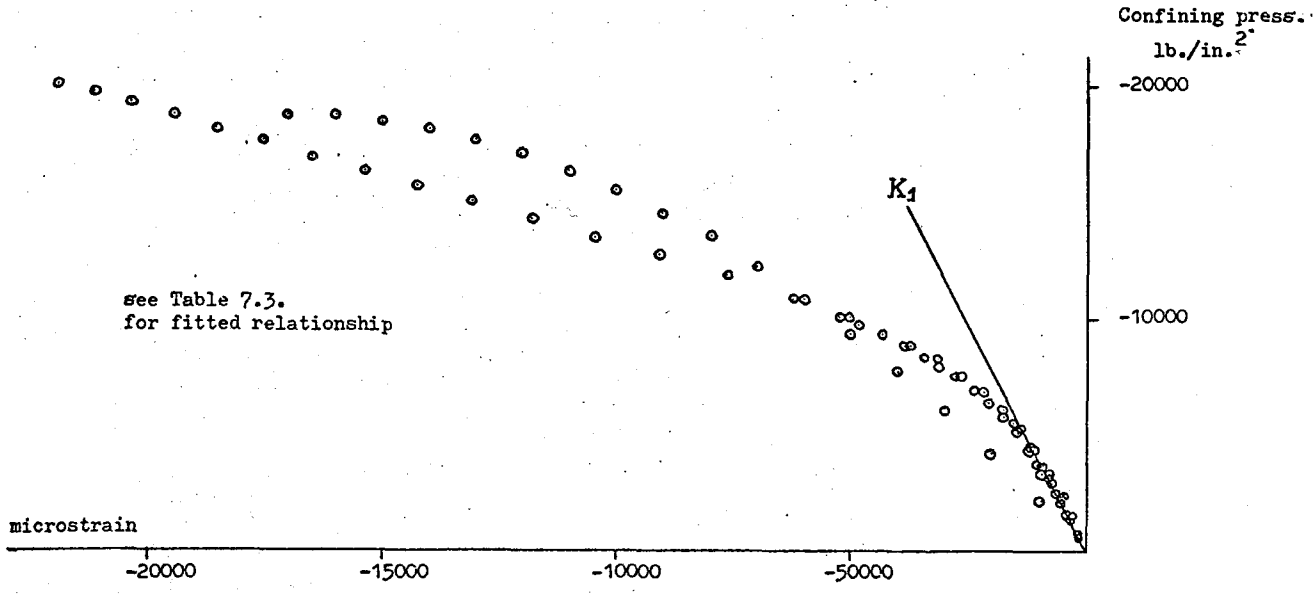


(a) Mix M1

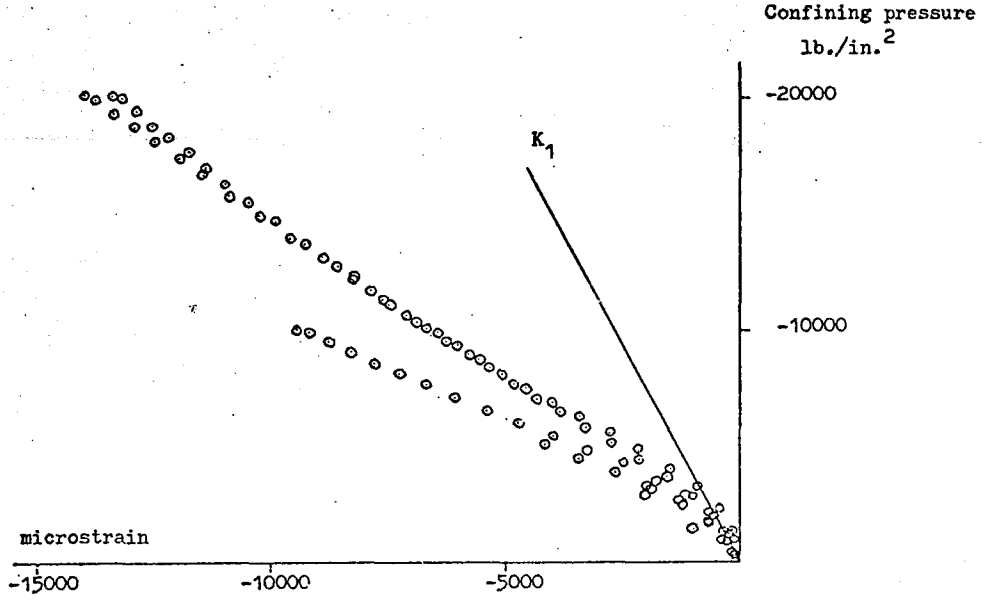


(b) Mix C1

Figure 7.98. Variation of volumetric strain with confining pressure for real concretes during the hydrostatic portions of triaxial 'compression' tests.

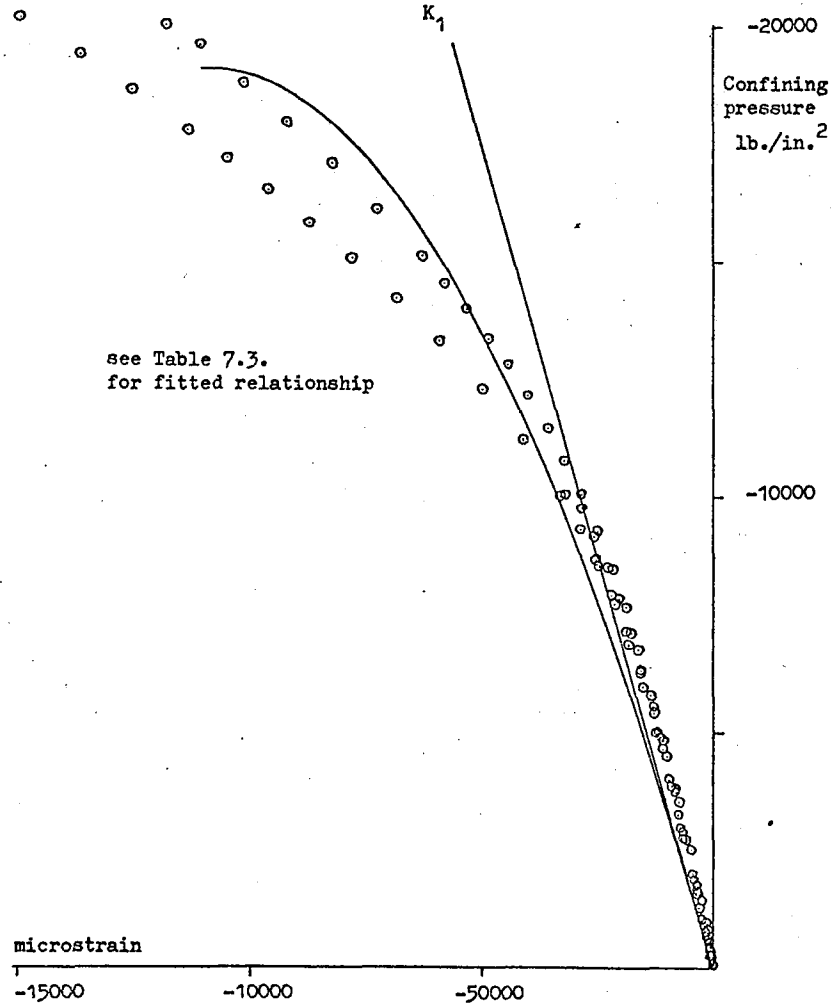


(a) Mix M2

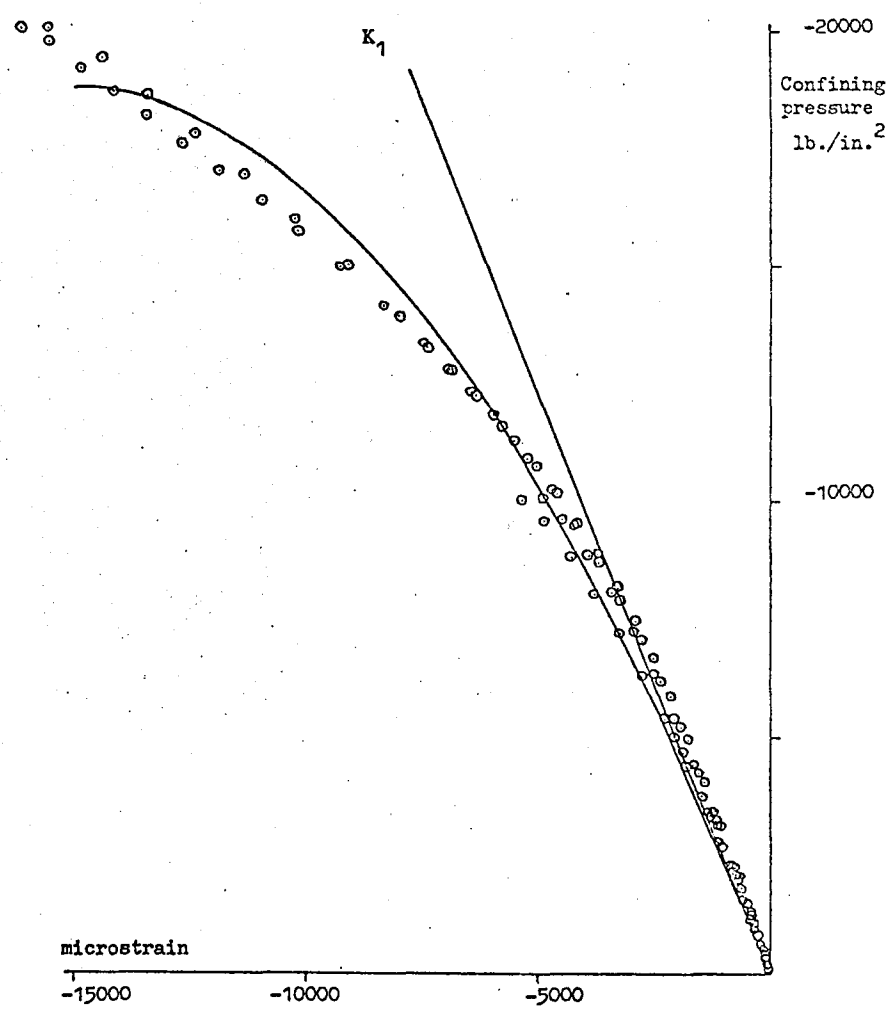


(b) Mix C2

Figure 7.99 Variation of volumetric strain with confining pressure for real concretes during the hydrostatic portions of triaxial 'compression' tests.



(a) Mix C3



(b) Mix C4

Figure 7.100. Variation of volumetric strain with confining pressure for real concretes during the hydrostatic portions of triaxial 'compression' tests.

foams under hydrostatic consolidation.

As for the idealised concretes the shape of most of the relationships can be represented closely by an equation of the form:-

$$\sigma_{conf} = K_1 e_v - K_2 e_v^2$$

where σ_{conf} = confining pressure
e_v = volumetric strain
K_1 and K_2 = constants for a given mix

The above equation, however, does not provide a good fit to the data for M2 and C2.

Values of K_1 and K_2, determined by a least squares method as described in 7.5.4.5., are shown in Table 7.3. for all mixes except M2 and C2. For these two mixes the K_1 value, representing the initial compressibility, is evaluated graphically.

For mixes M1 and C1 the increase in stiffness with increasing aggregate content for a given value low 'effective' water/cement is apparent from Table 7.3. This behaviour is found for the idealised concretes (which have a similar 'effective' water/cement ratio). For mixes M2 and C2, where the paste quality is extremely low due to the high water/cement ratio, the initial stiffness is also low and apparently not significantly affected by the aggregate content. In fact, the K_1 value for mix C2 is marginally lower than that for mix C_1 which may reflect the effect of the water absorbed by the aggregate. For mixes C3 (limestone) and C4 (granite) the initial compressibility K_1 is considerably higher than that for the corresponding mix C_1 containing gravel aggregate, again probably due to the low water absorption capacity of the aggregates.

Volume Changes during Deviatoric Loading

Comparing the volume changes given by mix M1 with mix C1 and mix M2 with mix C2 it is apparent that, as for the idealised concretes, mixes of a given 'effective' water/cement ratio containing a higher volume fraction of aggregate give rise to smaller volume changes at a given value of confining pressure.

Mix	K_1 (in lb./in.^{2} - microstrain units)	K_2
M1	3.0822	0.0001081
C1	3.4229	0.0001249
M2	1.973 *	-
C2	1.898 *	-
C3	3.5224	0.0001618
C4	2.4627	0.00008032

* Values estimated graphically

Table 7.3. Least squares values of K_1 and K_2 in the equation $\sigma_{conf} = K_1 e_v - K_2 e_v^2$ relating volumetric strain and confining pressure for real concrete mixes.

It is also evident, by comparing the gravel aggregate mixes with an 'effective' water/cement ratio of 0.35 with those having an 'effective' water/cement ratio of 0.60, that the volume change for a given value of confining pressure increases with water/cement ratio. As for the volume changes under hydrostatic pressure, the quality of cement paste appears to be the overriding factor.

7.6.5.5. Onset of Unstable Fracture Propagation (o.u.f.p.)

Stress at o.u.f.p.

Figures 7.101. and 7.102. show the variation of stress at o.u.f.p. (minimum volume) as a proportion of the ultimate total axial stress with confining pressure, for the real concrete mixes made with river gravel aggregate. For mixes M1 and C1 the proportion increases as the confining pressure is increased up to between approximately 5000 to 6000 lb./in.^{2}, after which the minimum volume level essentially coincides with ultimate. This behaviour is also noted for the idealised concretes which have a similar 'effective' water/cement ratio.

However, the decrease in the above proportion with an increase in volume fraction of aggregate found for the idealised mixes is not apparent. In fact, the reverse appears to be the case, with the proportion for the concrete at a given confining pressure being slightly less than that for the mortar.

For mixes M2 and C2, the o.s.f.p. stress as a proportion of ultimate also increases with confining pressure. Unlike mixes M1 and C1 it also decreases with increasing volume fraction of aggregate. The excessive scatter of results given by Mix C2 precludes drawing any definite conclusions, but the behaviour may be governed largely by the extremely low quality paste matrix of mix C2 which results from the water absorption capacity of the aggregate and its effect on the water available for hydration.

Figure 7.102. also shows the axial stress at o.s.f.p. as a proportion of ultimate for mixes containing limestone (C3) and granite (C4) aggregates. The scatter of results is large but the proportion of ultimate is distinctly higher, and thus less critical, than for the equivalent mix made with gravel aggregate (C2). This is undoubtedly due to the effect of the relatively low water absorption capacity of the limestone and granite and its effect on the paste quality.

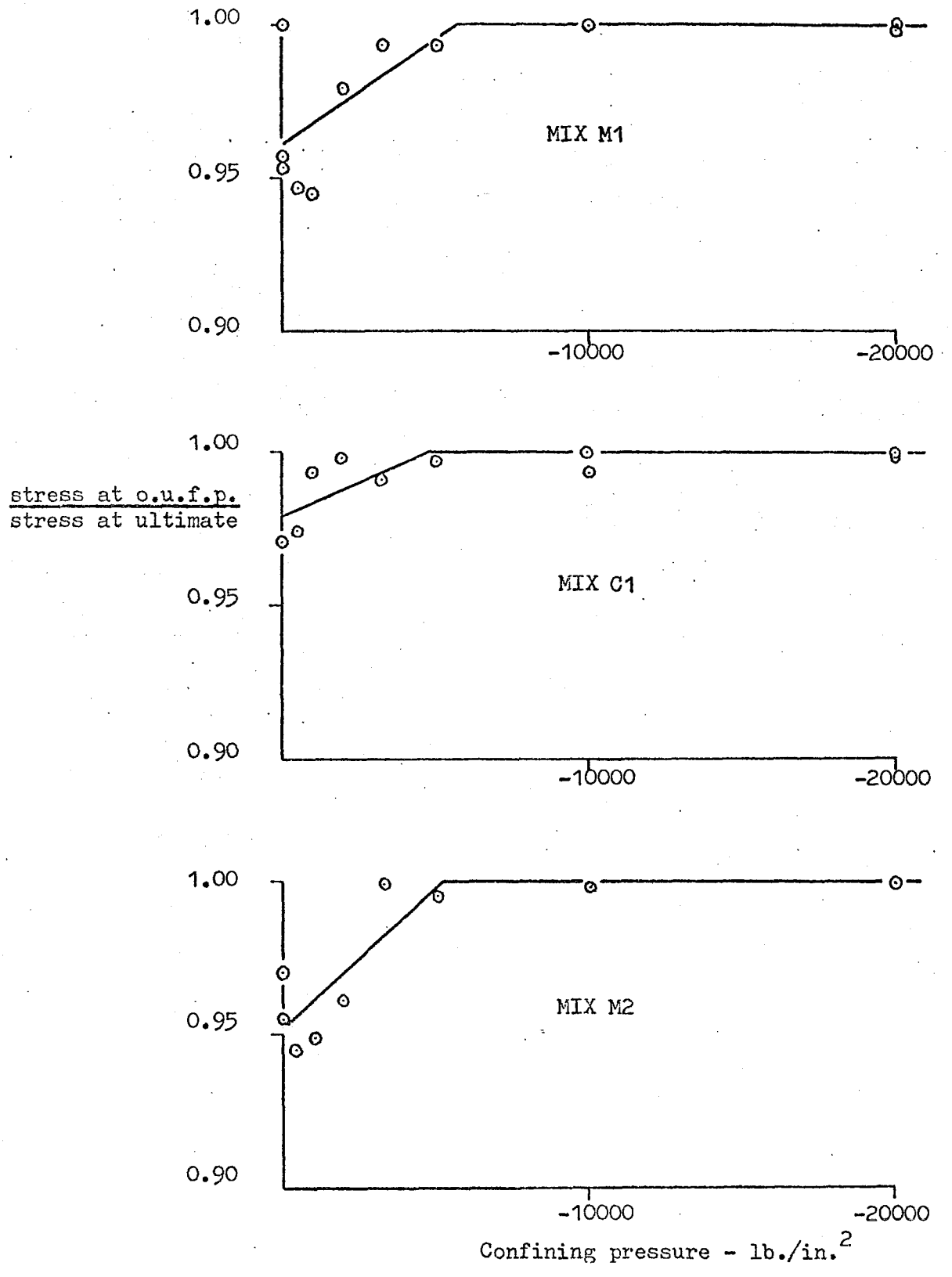


Figure 7.101. Relationships between the stress at o.u.f.p. as a proportion of ultimate and confining pressure for cylinders of Mixes M1, C1 and M2 under triaxial compression.

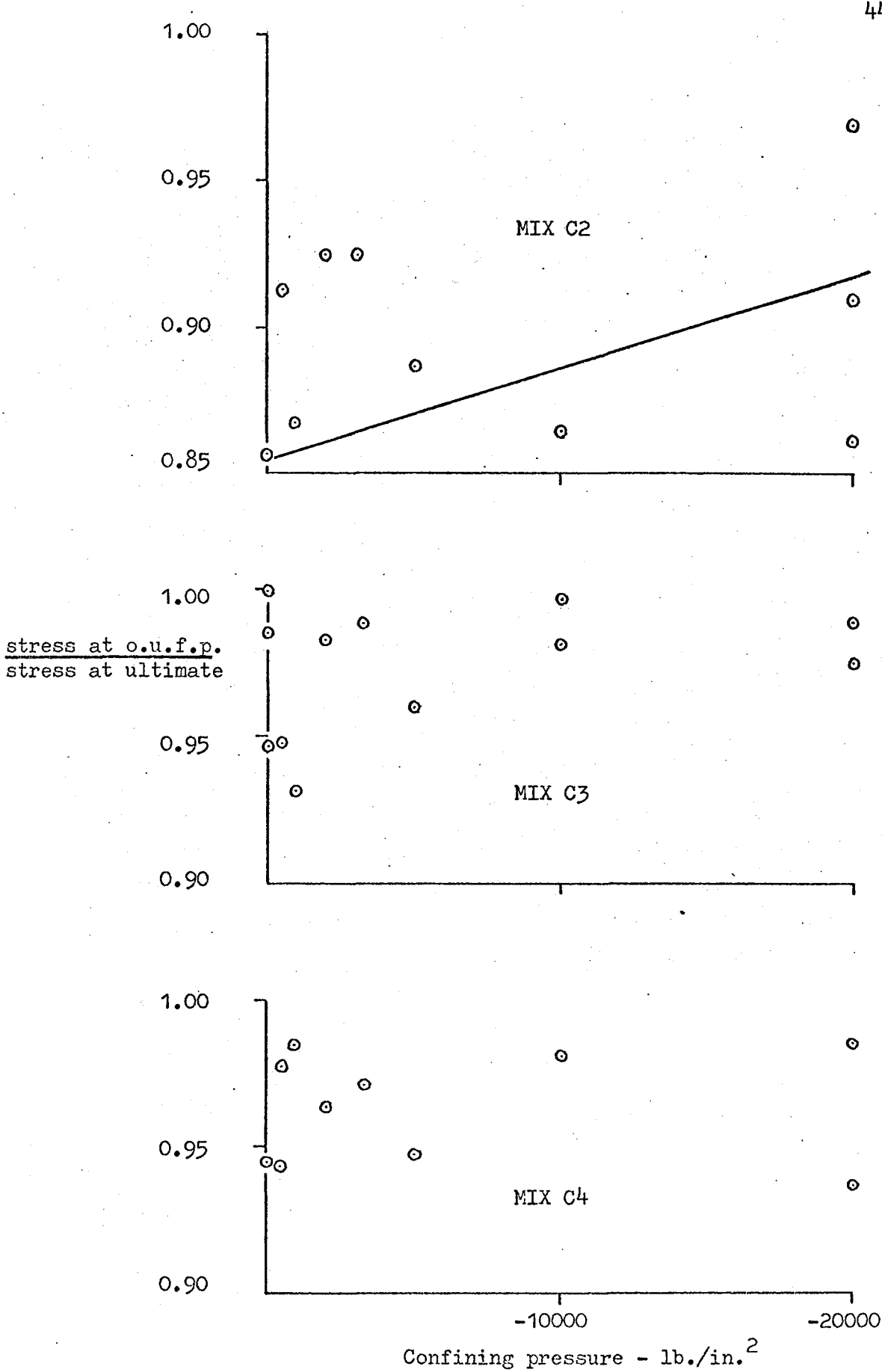


Figure 7.102. Relationships between the stress at o.u.f.p. as a proportion of ultimate and confining pressures for cylinders of Mixes C2, C3 and C4 under triaxial compression.

Strains at o.u.f.p.

Envelopes relating the axial strain to the lateral strain at the minimum volume level for the gravel aggregate mixes are shown in Figure 7.103. The shapes of the envelopes are similar to those found for the idealised mixes (see Figure 7.61) with the mixes containing high volume fractions of aggregate (C1 and C2) exhibiting much smaller strains than those given by the mortar mixes (M1 and M2) with lower aggregate contents. As noted for the idealised mixes the envelopes defining the minimum volume level can be considered to be 'unfolded' versions of those defining strain at o.s.f.p., although the large scatter of results for the concrete mixes renders it difficult to represent the data by curves.

The corresponding envelopes for the limestone (C3) and granite (C4) mixes are shown in Figure 7.104. Although the granite mix gives an envelope similar in magnitude and shape to that given by the corresponding gravel mix C2, the envelope for the limestone is more related to the gravel mortar M2 and is thus less critical.

7.6.5.6. Ultimate Stresses and Strains

Figure 7.90. shows the variation of total axial stress at ultimate with confining pressure for the real concrete mixes M1 and C1 containing gravel aggregate. As for the idealised concretes with a similar 'effective' water/cement ratio the rate of increase of axial stress with confining pressure is initially greater for the concrete with a high aggregate content than the mortar. As the uniaxial strength of the mortar is greater than the concrete the result of this is that up to a value of confining pressure of approximately 1500 lb./in.^{2} (c.f. 1000 lb./in.^{2} for the idealised concretes) the ultimate strength decreases with V_a, while the reverse is the case above this value. The probable cause of this phenomenon is discussed in 7.5.4.7.

As the confining pressure is increased above approximately 10000 lb./in.^{2} both envelopes tend towards a slope of:-

$$\sigma_{axial}/\sigma_{conf} = 2.36 \quad \text{(approximately)}$$

This value compares closely with that of 2.50 for the idealised concretes with a similar 'effective' water/cement ratio.

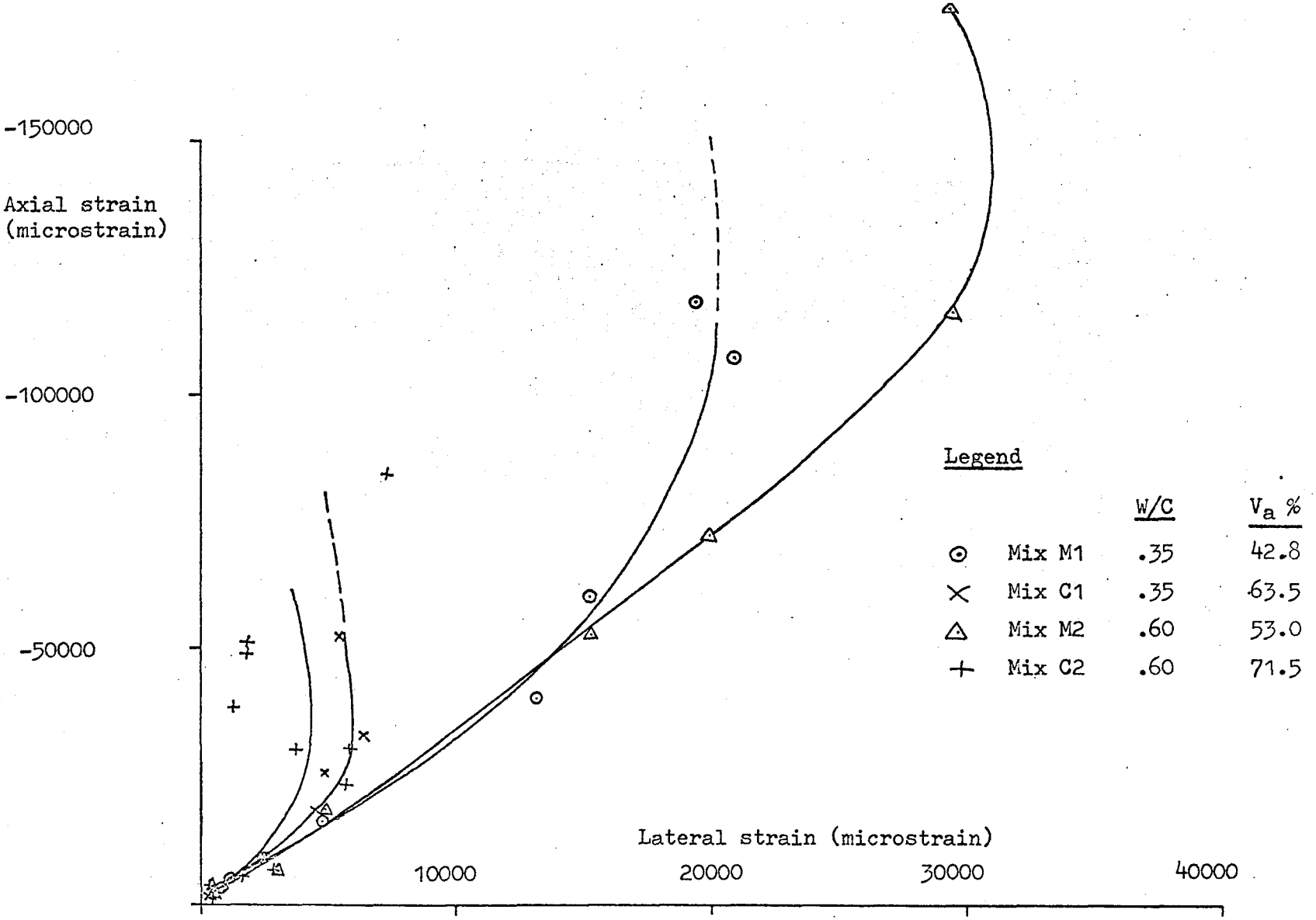


Figure 7.103. Relationships between axial and lateral strains at minimum volume under triaxial compression for mortars and concretes containing river gravel aggregate.

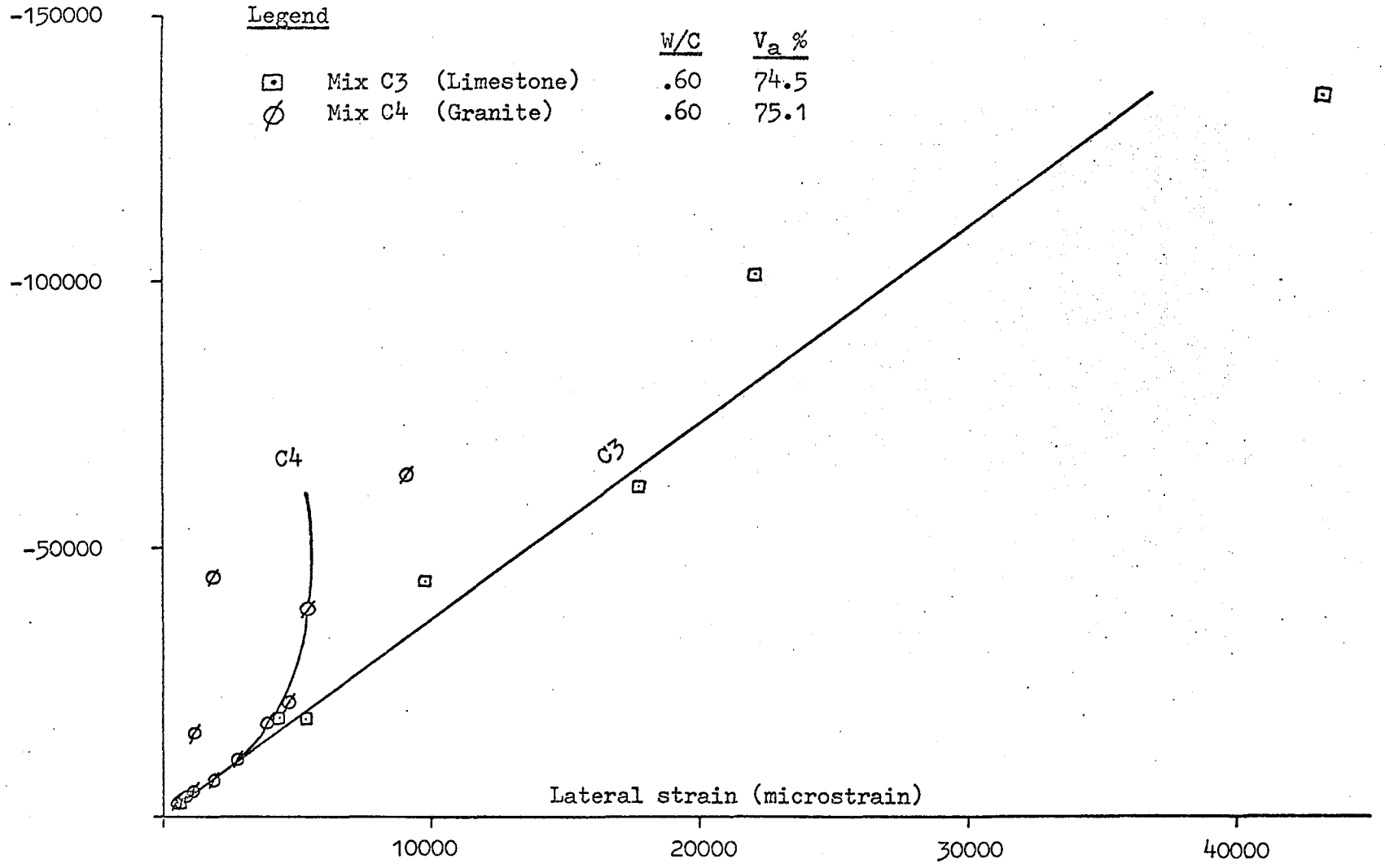


Figure 7.104. Relationships between axial and lateral strains at minimum volume under triaxial compression for concretes containing limestone and granite aggregates.

The ultimate strength envelopes for mixes M2 and C2 with a higher 'effective' water/cement ratio containing gravel aggregates are shown in Figure 7.91. In this case the rates of increase of axial stress with confining pressure are similar for both mixes. Since the uniaxial strength of the mortar is greater than for the concrete the mortar (M2) envelope, as a result, always lies above that for the concrete (C2). For confining pressures above approximately 7500 lb./in.^{2} the rate of strength increase is :-

$$\sigma_{axial}/\sigma_{conf} = 2.84 \quad \text{(approximately)}$$

This value is considerably higher than that for the mixes with an 'effective' water/cement ratio of 0.35 and the trend agrees with that observed for the uniaxial strength results analysed in Section 6 and with those obtained by Hobbs [199] who found that weaker (and leaner) concretes benefit from the confining pressure more than stronger (and richer) mixes.

Thus for the weak mixes the strength at a given confining pressure decreases with aggregate content for all levels of confining pressure, whereas with the stronger mixes this is only the case up to a relatively low level of pressure. This phenomenon is probably linked with the behaviour observed in the cube and direct tensile tests where the reduction in strength with an increase in V_a is most marked for the weaker mixes M2 and C2.

For the limestone (C3) and granite (C4) mixes the ultimate strength envelopes are shown in Figure 7.93. The envelope for Mix C3 lies slightly above that for C4 but both tend towards a slope of:-

$$\sigma_{axial}/\sigma_{conf} = 2.74 \quad \text{(approximately)}$$

This slope is slightly less than that for the gravel mixes with the same 'effective' water/cement ratio.

Figure 7.105. shows the envelopes for the gravel mixes normalised with respect to the uniaxial compressive strength. Each envelope has been fitted to a hyperbolic relationship of the type:-

$$\sigma_{axial}/\sigma_{conf} = (A\,(\sigma_{conf}/\sigma_c)^2 + B\,(\sigma_{conf}/\sigma_c) + 1.0)^{\frac{1}{2}}$$

As for the case of the idealised concretes such a relationship has been chosen in preference to the parabolic representation since it appears to

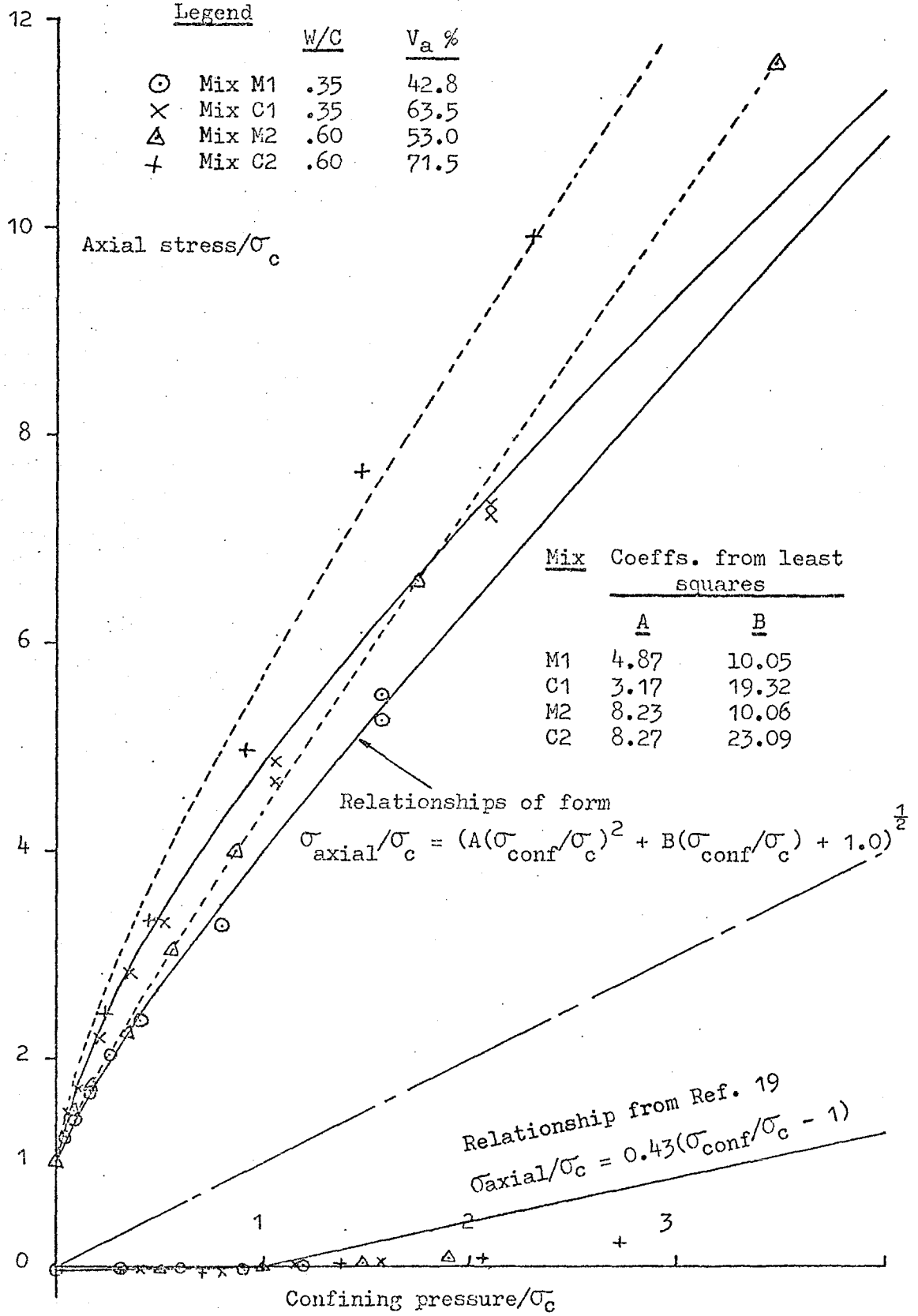


Fig. 7.105. Relationships between normalised axial stress and confining pressure at ultimate under triaxial compression and extension for gravel mortars and concretes.

('Extension' results after Cotsovos [21])

provide a slightly closer and more realistic fit to the data.

A non-linear technique is used to estimate the coefficients A and B (see 7.5.3.5.) and the values for the coefficients, and the form of the resulting relationships, are shown in Figure 7.105. The figure clearly shows the influence of (a) increasing the aggregate content and (b) increasing the effective water/cement ratio, in increasing the normalised strength for a given value of normalised confining pressure.

The corresponding relationships for the limestone (C3) and granite (C4) mixes are shown in Figure 7.106. and comparison with Figure 7.105. shows the envelopes to be lower than for the gravel aggregate mix with the same 'effective' water/cement ratio. Again, this is probably due to the low water absorption capacity of the aggregates giving a higher quality paste which results in the concretes not gaining as much benefit from the confining pressure as a concrete with a lower quality paste.

7.6.5.7. Modes of Failure

Figures 7.107. and 7.108. show the modes of failure for the specimens of the various mixes. Some specimens exhibit a fracture plane orthogonal to the axis of the cylinder. This is caused by the process of removing the specimen from the sheath and is not characteristic of the method of test.

As for the idealised concretes the failure mode changes from 'splitting' to 'plastic bulging' as the confining pressure is increased, particularly for the mixes with low aggregate contents or high water/cement ratios. The lack of evidence of inclined failure planes suggests concentricity of loading, which is confirmed by the similarity of strains across the diameter of specimens for load stages close to ultimate.

7.6.6. Conclusions from Test Series on Real Concretes

In this series, mixes are compared on the basis of constant 'effective' water/cement ratio, i.e. that water in the mix in excess of that absorbed into the aggregates. The total water/cement ratio is adjusted to achieve this for the different aggregate contents of the mixes.

The conclusions drawn from the series are based on tests carried out on concretes with 'effective' water/cement ratios of 0.35 and 0.60, chosen to

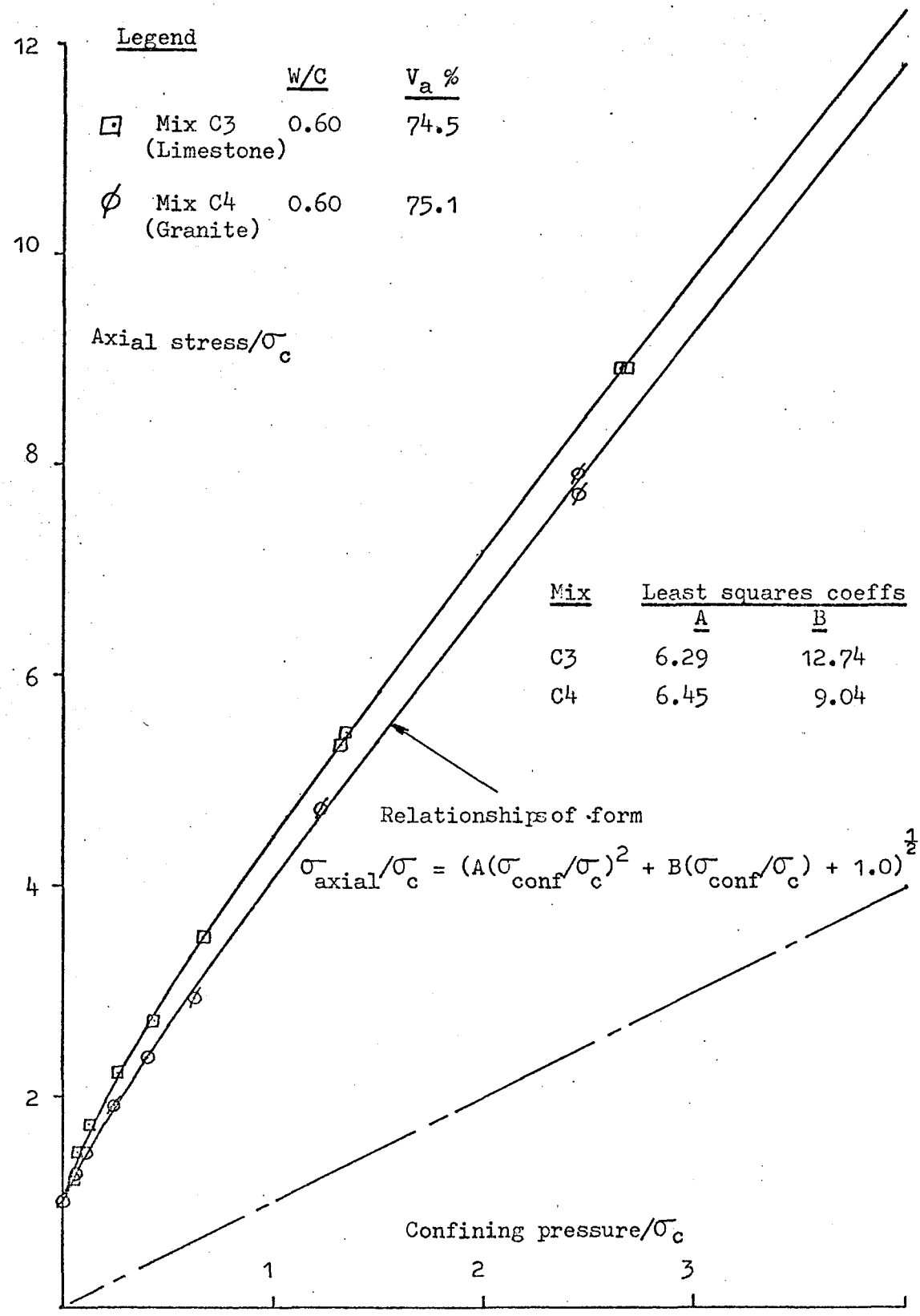


Figure 7.106. Relationships between normalised axial stress and confining pressure at ultimate under triaxial compression for limestone (C3) and granite (C4) concretes.

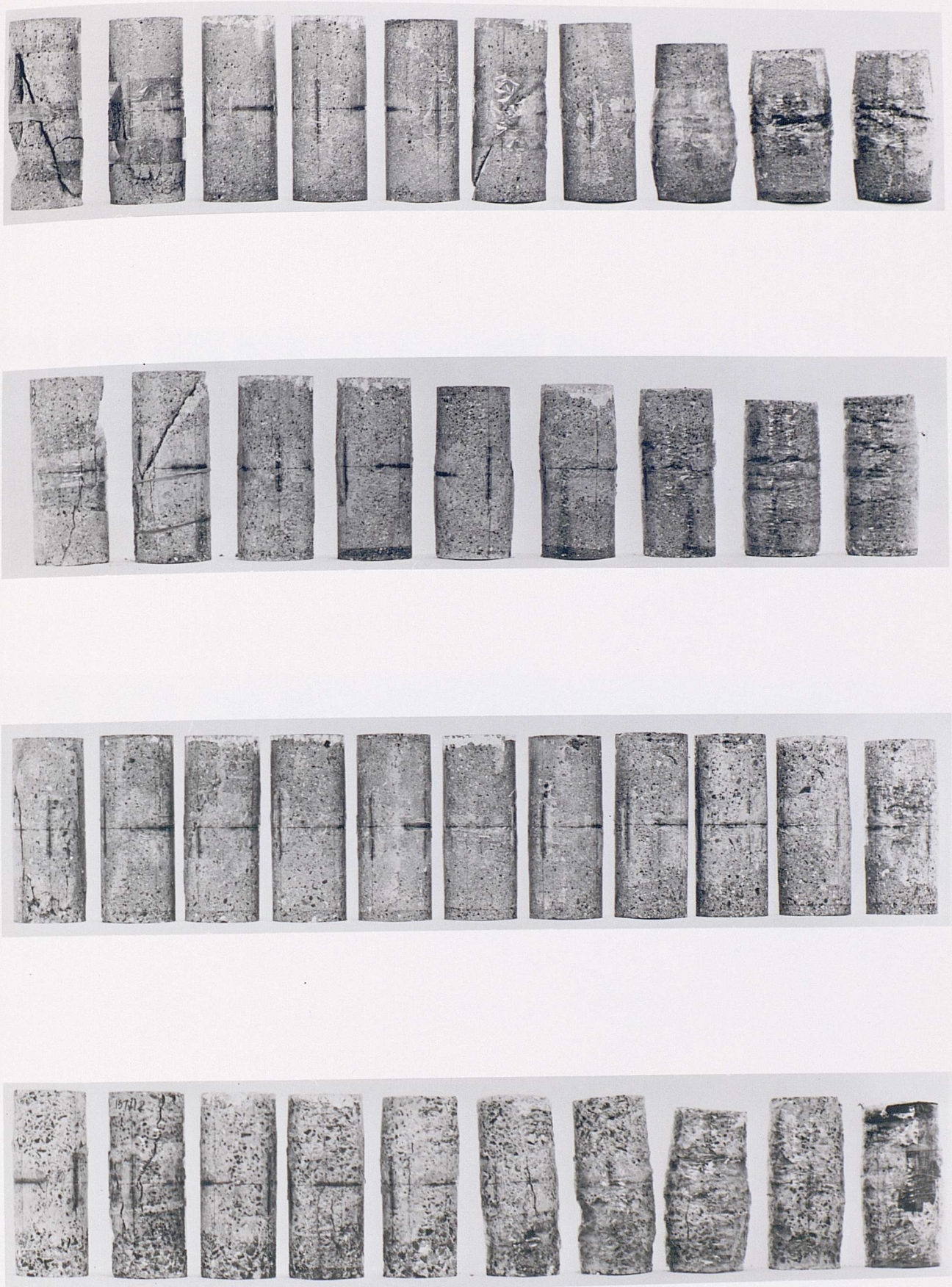


Figure 7.107. Specimens of real concretes after failure under triaxial 'compression': (top to bottom) M1, C1, M2, C2, with confining pressure increasing from left to right.

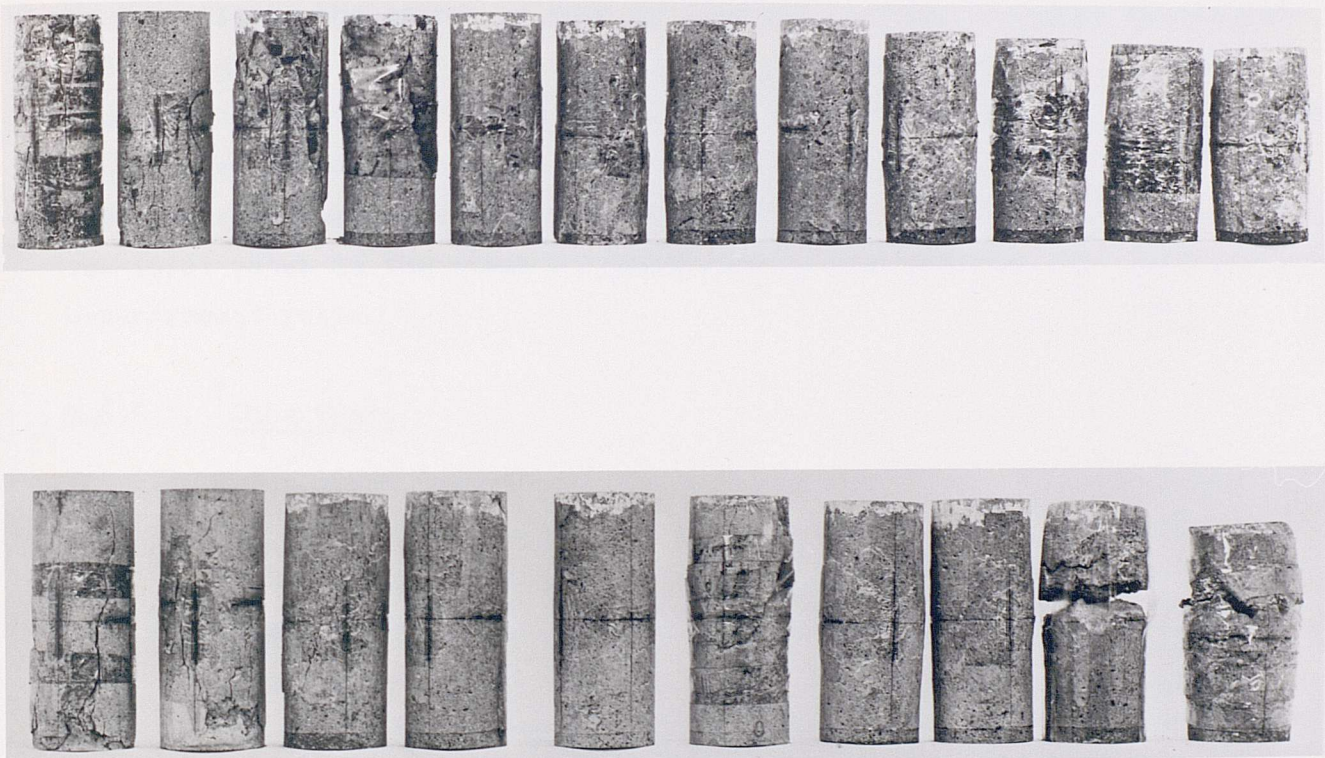


Figure 7.108. Specimens of real concretes after failure under triaxial 'compression'. (Top) C3, (bottom C4, with confining pressure increasing from left to right.

represent mixes at each end of the range of practical mixes. For each value of 'effective' water/cement ratio two mixes containing river gravel aggregate have been tested namely, a mix containing coarse and fine aggregate, and a mortar mix in which any aggregate above a maximum size of 3/16" is omitted. This mortar mix contains the same sand/cement ratio as the coarse aggregate concrete.

To investigate the effect of type of aggregate on the behaviour of concrete under triaxial stress two mixes, containing limestone and granite coarse and fine aggregate, have been tested. These concretes contain dry materials in the same proportions as the river gravel coarse aggregate mix containing the higher of the two values of 'effective' water/cement ratio (0.60), and the total water in the mixes is again adjusted to maintain this 'effective' water/cement ratio.

7.6.6.1. Cube Tests

(i) For a given 'effective' water/cement ratio, the cube strength of the river gravel aggregate mixes decreases with V_a (see Figure 7.68.). This decrease (compared with the increase found for the idealised concretes) may be due to the water absorption capacity of the aggregates requiring a larger total water/cement ratio for a given 'effective' value at higher aggregate contents. The water/cement ratio actually available for hydration of the cement paste probably has a value between the 'effective' and the total values and thus the mixes with a high V_a may have a lower quality paste component. These effects apparently mask the effects of platen restraint, which should increase with aggregate content. The fracturing is confined entirely to the mortar matrix (as for the idealised mixes).

(ii) The limestone and granite mixes have a cube strength higher than the corresponding river gravel mix (see Figure 7.68.) probably due to the low absorption capacity of those aggregates and its effect in reducing the total water/cement ratio necessary to achieve a given value of 'effective' water/cement ratio.

7.6.6.2. Direct Tension Tests

(i) The stiffness (see Figure 7.69.) and linearity of the axial stress-strain relationships for the gravel aggregate concretes

increase with V_a for a given 'effective' water/cement ratio (as for the idealised concretes). The stiffness of limestone and granite mixes is higher than for the corresponding gravel mix which may reflect the increased stiffness and/or angularities of these materials.

(ii) The stress at o.s.f.p. for the gravel aggregate mixes decreases markedly with V_a for a given 'effective' water/cement ratio (see Figure 7.70.), compared with the slight increase detected for the idealised concretes. For both effective water/cement ratios, this stress as a proportion of ultimate decreases with aggregate content from 100% for the mortars to 65% and 54% for the mixes with low and high water/cement ratios respectively.

(iii) For the limestone and granite mixes, the stress at o.s.f.p. and this stress as a proportion of ultimate is considerably higher than the corresponding gravel mix.

(iv) The tensile and compressive strains at o.s.f.p. decrease with aggregate content for both types of gravel aggregate mix, but those for the limestone and granite mixes are substantially higher than for the corresponding gravel mix (see Figure 7.71.).

(v) The stress at ultimate remains essentially constant with V_a for the gravel mixes with a low 'effective' water/cement ratio, but decreases significantly for mixes with a high ratio (see Figure 7.73.). This behaviour may reflect the influence of the water absorption of the aggregate which is further substantiated by the high strengths exhibited by the limestone and granite mixes compared with the corresponding gravel mix.

(vi) The compressive strain at ultimate decreases with aggregate content for both types of gravel mix, as does the tensile strain for the mixes containing a high 'effective' water/cement ratio. For the mixes containing a low 'effective' water/cement ratio the tensile strain remains essentially constant (see Figure 7.74.).

(vii) The limestone and granite mixes attain considerably higher strains at ultimate than those for the corresponding gravel mix.

7.6.6.3. Triaxial Compression Tests

Stress-Strain Relationships (see Figures 7.76. to 7.81.)

(i) The relationships for the gravel mixes indicate a decrease in stiffness and increase in plasticity under all values of confining pressure for a decrease in V_a at a given 'effective' water/cement ratio (as for the idealised mixes).

(ii) For the limestone and granite mixes the stiffness is greater, and the plasticity less, than the corresponding gravel mix, due probably to the low water absorption capacity of the crushed aggregates.

(iii) For the gravel mixes, the stiffness and plasticity both decrease with an increase in 'effective' water/cement ratio.

Incremental Strain Ratio (i.s.r.) (see Figures 7.85. to 7.87)

(i) For all mixes under confining pressures below a critical value, the i.s.r. decreases with initial increase in deviator stress, due to crack closure, and then remains essentially constant up to o.s.f.p. before increasing to failure due to crack propagation (as for the idealised concretes).

(ii) For confining pressures above a critical value, the i.s.r. increases continually from the initial application of deviatoric stress. This indicates that the material is already significantly disrupted under the given value of hydrostatic pressure (as for the idealised concretes).

(iii) For the gravel mixes containing high 'effective' water/cement ratios, however, the increases in i.s.r. due to fracture propagation follow almost immediately the decreases due to crack closure, and are much greater than for the low water/cement ratio mixes. For the limestone and granite mixes this trend is not so evident.

Onset of Stable Fracture Propagation (o.s.f.p.)

1. Strain Values (see Figures 7.88. and 7.89.)

(i) The shape of the envelopes defining the state of strain at o.s.f.p.

are closed in strain space and for all mixes, except the gravel concretes with a high water/cement ratio, indicate a region of near constant tensile strain for low confining pressures.

(ii) The strain envelopes for the gravel concretes expand in strain space with decreases in V_a for a given 'effective' water/cement ratio (as for the idealised concretes). The envelopes for the limestone and granite are larger than for the corresponding gravel mix.

(ii) For a given V_a, the envelopes for the gravel mixes expand in strain space with a decrease in 'effective' water/cement ratio.

2. Stress Values

(i) For all mixes, the shape of the envelope defining the states of stress at o.s.f.p. indicates an increase in axial stress at o.s.f.p. at a diminishing rate as the confining pressure is increased. This results in an intersection with the hydrostatic axis, (see Figures 7.92. and 7.94.) and, in this respect, shows essentially the same trends as for the idealised concretes.

(ii) No clear trend is evident regarding the effect of increasing V_a on the initial rate of increase in axial stress with confining pressure for gravel mixes with a given 'effective' w/c ratio (see Figures 7.90. and 7.91.). For idealised mixes the rate of increase is greater for mixes with a high V_a (see Figure 7.40.).

(iii) The envelopes for the gravel mixes containing high 'effective' water/cement ratios enclose a smaller portion of stress space than those for the low water/cement ratio mixes (see Figures 7.90. and 7.91.).

(iv) The envelopes for the limestone and gravel mixes enclose a larger portion of stress space than that for the corresponding gravel mix (see Figure 7.93.).

Volume Changes

1. Under Hydrostatic Pressure (see Figures 7.98. to 7.100.)

(i) The volume decreases at an increasing rate with increasing stress (as for the idealised concretes).

(ii) For the gravel mixes containing the low 'effective' water/cement ratio the compressibility for mixes containing a high V_a is greater than for the low V_a mixes.

(iii) The gravel mixes containing high 'effective' water/cement ratios exhibit considerably higher compressibility than those containing a low water/cement ratio. Collapse of the cement paste is evident from the extremely large volume decreases measured. This collapse mechanism completely masks the effect of aggregate concentration, due undoubtedly to the influence of the water/cement ratio on the paste quality, for the different values of V_a

(iv) The limestone and granite mixes exhibit compressibilities considerably higher than the corresponding gravel mix. This is also probably due to the low water absorption capacity of the crushed aggregates.

2. Under Deviatoric Loading (see Figures 7.95. to 7.99.)

(i) For most mixes the volume changes during deviatoric loading follow the pattern characteristic of a compression test, namely an initial decrease in volume, at an increasing rate, followed by a superimposed volume increase which results in a level of minimum volume. After this minimum volume level the volume increases at a rapid rate. The gravel aggregate mix with a high 'effective' water/cement ratio and high V_a, however, exhibits the tendency for the volume to increase from the start of deviatoric loading under high values of confining pressure.

(ii) For gravel mixes of a given 'effective' water/cement ratio, smaller volume changes are induced at a given confining pressure for a high V_a.

Onset of Unstable Fracture Propagation (o.u.f.p.)

1. Stress Values

(i) The stress at o.u.f.p. as a proportion of ultimate increases with confining pressure for all mixes containing gravel aggregate. For the mixes containing limestone and particularly granite aggregates this increase is not so apparent (see Figures 7.101. and 7.102.).

(ii) For the gravel mixes under a given confining pressure, the stress at o.u.f.p. as a proportion of ultimate decreases with an increase in 'effective' water/cement ratio. This reflects the early disruption of an inferior quality cement paste.

2. Strain Values (see Figures 7.103 and 7.104.)

(i) The envelopes defining the strain state at o.u.f.p. are 'unfolded' versions of the o.s.f.p. envelopes (as for the idealised concretes).

(ii) For gravel aggregate mixes containing the same 'effective' water/cement ratio higher aggregate contents significantly reduce the size of the envelope.

(iii) For the gravel mixes containing a high V_a, the envelope for the mix with a low 'effective' water/cement ratio mix lies within that for the mix with a high water/cement ratio. The reverse is the case for the mixes containing low V_a. This may be due to the influence of the water absorption capacity of the aggregates.

(iv) For the granite mix the envelope defining the strain state at o.u.f.p. is similar to that for the corresponding gravel mix. However, the envelope for limestone mix encloses a larger portion of strain space than even the mortar mixes.

Ultimate

(i) The uniaxial compressive strength for gravel mixes of a given 'effective' water/cement ratio decreases with increasing V_a (see Figure 7.68.). This behaviour (also noted for idealised concretes) is caused by the change in heterogeneity of the concretes.

(ii) As the confining pressure is increased the axial stress at ultimate increases at a faster rate for mixes containing high V_a probably due to particle interlock effects (see Figures 7.90, 7.91 and 7.93).

(iii) For the gravel mixes with the same V_a, the increase in axial stress at ultimate with confining pressure is greater for mixes with a high 'effective' water/cement ratio (see Figures 7.90 and 7.91.).

(iv) The limestone and granite mixes have a higher uniaxial compressive strength than the corresponding gravel mix, due to the effect of the low water absorption of the crushed aggregates (see Figure 7.68.). The rate of increase of ultimate axial stress with confining pressure is lower (see Figure 7.93.) and this behaviour also suggests the influence of a high quality paste.

(v) For all mixes, the relationships between the axial stress at ultimate and confining pressure can be characterised by hyperbolic equations of the form:-

$$\sigma_{axial}/\sigma_c = \left[A(\sigma_{conf}/\sigma_c)^2 + B(\sigma_{conf}/\sigma_c) + 1 \right]^{\frac{1}{2}}$$

(see Figures 7.105. and 7.106.).

8. DESIGN CRITERIA FOR CONCRETE UNDER COMBINED STATES OF STRESS

8.1. Introduction

The main programme of work described in this thesis consists of a comprehensive investigation to determine the deformational and strength characteristics of various idealised and real concrete mixes when subjected to short-term triaxial 'compression' states of stress (see Chapter 7). Accurate strain gauge techniques are used to measure axial and lateral strains throughout these loading regimes. Significant changes are detected in the principal and volumetric strains under increasing stress, from which it is possible to identify critical levels of behaviour occurring prior to ultimate and defined as onset of stable fracture propagation (o.s.f.p.) and onset of unstable fracture propagation (o.u.f.p.).

Proposals are made for considering these levels as lower and upper criteria for practical structural design. This hypothesis is strongly supported by the results of tests under repeated uniaxial compressive loading (see Chapter 5) in which a close correlation has been obtained between:-

(i) the lower bound level and the start of significant, but stable, cracking;

(ii) the upper bound level and the onset of unstable cracking.

On the basis of this work, design criteria are proposed for concrete subjected to combined states of stress. For a given state of stress, the factors which affect the lower and upper bound criteria are likely to include the characteristics of the concrete (including the volume fraction of aggregate or cement paste and water/cement ratio) the maturity, age, moisture and temperature conditions of the specimen and the method, rate and sequence of applying the load. Comprehensive design charts are presented for concrete containing gravel aggregates which enable an assessment to be made as to whether any particular concrete will satisfactorily withstand a given state of multiaxial compression.

As far as the limit states in C.P. 110 [2] are concerned, it is proposed that the lower bound criterion (defined as o.s.f.p.) is a suitable

serviceability limit state related to that for cracking (see Clause 2.2.3.2.) and the upper bound criterion (o.u.f.p.) is related to the ultimate limit state (see Clause 2.2.2.).

This thesis contains the main results of the experimental programme together with information on the experimental techniques. Full details of the experimental data, including the complete stress-strain curves, are given in a further Report to be published [197].

8.2. Application of Test Results

Although the test data and design criteria can be applied to a wide range of states of stress, concrete mixes and conditions, there are certain limitations which must be appreciated when the data are used.

8.2.1. Concrete Characteristics

Recent research has shown clearly that, when considering different concrete mixes, the characteristics of these which influence the deformational behaviour must be expressed more specifically in terms of the internal structure of the material and the properties of the constituents. The most important parameters which need to be defined are:-

Volume fraction of aggregate or volume fraction of cement paste.
Maximum aggregate size.
'Effective' water/cement ratio of the mix.
Secant modulus of elasticity of the aggregate.
Secant modulus of elasticity of the cement paste.

Two separate groups of the tests were performed, one with so-called 'idealised' concretes and the second with concretes representing a range of practical mixes. The idealised mixes which contained $\frac{3}{4}$" (20 mm.) single-sized spheres of E-glass embedded in a fine mortar matrix, can be considered as two-phase composite materials. Volume fractions of glass spheres ranged from 0 to the equivalent of the closest possible packing in the matrix (approximately 58%). A total of eleven different volume fractions were used to establish comprehensive trends of behaviour. The surface of the glass spheres was roughened by rotating in a small mill containing carborundum powder until the surface finish approximated that of normal river gravel aggregate. Significant patterns of behaviour were obtained from the idealised concretes which enabled a more efficient

test programme to be planned for the real concretes. These mixes comprised mortars and concretes containing river gravel, granite and limestone aggregates. Full details of the materials used and the concrete characteristics in the fresh and hardened states are given in Appendices 2 and 3.

8.2.2. States of Stress and Method of Loading

In practice, it is extremely difficult to obtain test results which are independent of machine or testing effects, due mainly to the interaction between the testing machine used to apply the load and the specimen under test. All evidence suggests that there are severe practical difficulties in obtaining a uniform and definable multiaxial stress state in specimens loaded by rigid systems, whether or not the load is applied through interfacial materials which attempt to reduce secondary restraints (see Chapter 2).

For this reason, it was decided to adopt a hydraulic cell arrangement to apply triaxial stresses to concrete cylinders. In this cell, equal hydrostatic stresses are applied to the cylinder in the lateral direction by fluid pressure while the third axial stress is applied mechanically through rigid platens. The boundary conditions of loading, therefore, approximate to a combination of near-uniform stress produced by the lateral confining pressure and near-uniform strain induced by the axial load. With this system, the undesirable interaction effects of the rigid loading platens on the specimen can be minimised by adopting a height/diameter ratio of 2.5 for the cylinder (see Chapter 2). Experiments show that, under these conditions, the central zone of the specimen is effectively uniformly stressed. All strain measurements were made in this region.

In the so called 'compression' type of triaxial test, which forms the main part of the experimental investigation, the axial stress throughout the test is always greater or equal to the confining lateral pressure applied hydraulically. This is to be compared to the case of triaxial 'extension' where the axial stress is always less than or equal to the confining pressure.

In the 'compression' tests the cell pressure was increased to the desired value and then maintained constant while the axial stress was applied to

ultimate failure. The axial load was increased in a manner which induced a constant rate of increase of average strain over the length of the specimen, which corresponded to an increase in strain in the central zone of the specimen of approximately 200 micro-strain per minute. This rate of loading is similar to that specified for standard compressive strength tests [62].

During the loading, the values of axial stress, confining pressure, axial and lateral strain were recorded continuously using an automatic data logger capable of resolving to 1 microstrain. Although such a high sensitivity is not necessary to establish the shape of the stress-strain curve, it is essential if changes in specimen response are to be detected. The stress or strain levels at which significant changes occur are used as the basis of the definition of failure of concrete (see 4.5.).

8.2.3. Specimens and Environmental Characteristics

The cylindrical concrete specimens 10" (250 mm.) long and 4" (100 mm.) diameter were cast vertically and cured initially in water at 20°C for twenty-eight days. Then both ends of the specimens were ground plane and parallel before the cylinders were placed under initially wet hessian and allowed to dry slowly in air at 20°C and 65% R.H. for a further twenty-one days. The specimens were then uncovered and stored in the laboratory at 20°C and 65% R.H. for a minimum of ten months until testing.

The specimens were tested at ages ranging from ten to twelve months, by which time the concrete had dried out and hydration effectively ceased. This condition can be considered equivalent to the condition of concrete in-situ during service. In structures such as dams and prestressed concrete pressure vessels, it is unlikely that the concrete will be fully loaded until twelve months after casting.

8.2.4. Validity of Test Results

All the factors affecting the mechanical behaviour of concrete are listed in Table 8.1. which gives comprehensive details of the scope covered by the present investigation and probable range of validity of the results. The Table indicates that, although the test results and design data must be considered in the context of the experiments, the results can be applied to a wide range of concretes made with different materials and subjected

Parameter	Values in Current Test Programme	Validity of Results	
		Range	Basis for Assumption
Concrete Characteristics			
Volume fraction of aggregate V_a %	43, 53, 63, 72 and 75.	40 - 75.	From patterns exhibited by idealised concretes within range of V_a % from 43 to 76.
Maximum size of aggregate	20 mm ($\frac{3}{4}$") and 5 mm (3/16").	5 - 20 mm (3/16" - $\frac{3}{4}$").	Comparison of test results
Aggregate grading	5 mm - 150 um (3/16" - No. 100 Sieve) and 20 mm - 150 um ($\frac{3}{4}$" - No. 100 Sieve)	All practical gradings	Comparison of test results for real concrete series with those obtained for gap-graded idealised concretes.
Degree of maturity	Assumed fully hydrated.	Fully hydrated.	By assumption *
Type of cement	Ordinary Portland cement.	Any type of hydraulic cement.	Non-dimensional strength data presented.
Type of aggregate	River gravel, limestone and granite.	All types of natural aggregate.	Comparison of test results.
Specimen and Environmental Characteristics			
Moisture conditions within specimen	Air dried to constant weight.	Air dried to constant weight	By definition *

Table 8.1. Factors affecting the behaviour of concrete and the scope of the present investigation.

(contd. over)

Parameter	Values in Current Test Programme	Validity of Results	
		Range	Basis for Assumption
Specimen and Environmental Characteristics (contd.)			
Environment	Normal temperatures (20°C) and humidity (65% RH).	Normal temperatures and humidity.	By definition *
Ratio of minimum specimen dimension to maximum size of aggregate	5 to 21	Value of 5 and above	Previous experimental data
States of Stress or Strain			
Type	Axisymmetric triaxial 'compression' (Confining pressure with superimposed axial stress)	All stress states with at least 2 principal stresses compressive	Assumptions based on knowledge of behaviour under triaxial 'extension' and compression-compression-tension
Magnitude	Up to ultimate	Up to ultimate	By definition
Boundary conditions	Combination of uniform boundary stress and uniform boundary strain	Uniform boundary stress	Shape of specimen chosen to minimise restraint effects *
Method of Loading			
Type of loading - Rate of increase of strain	200 microstrain per minute	Short term ** static loading 0.07 - 7.0 N./mm.^{2}/sec. (10 - 10^3 lb./in.^{2}/sec.)	Previous experimental data
Pattern of loading	Increased monotonically to failure	Increased ** monotonically to failure	By definition

Notes: * More data required before range of validity can be extended.

** The range of validity may be extended provided stresses are kept below the initial cracking level.

Table 8.1. (Contd.) Factors affecting the behaviour of concrete and the scope of the present investigation.

to different states of stress. The method of data presentation is designed to facilitate such an application.

8.3. Definitions of Failure

The formation and propagation of small microscopic cracks or micro-cracks (3-5 microns) are now accepted as the causes of fracture and failure of concrete. Research has shown that there are at least three stages in the process of crack initiation and propagation (see Chapter 4). In the first stage, localised cracks are initiated at the microscopic level at isolated points throughout the specimen where the tensile strain concentrations are the largest. These strain or stress concentrations, which can be produced by loading or by shrinkage or thermal movements, are due to the incompatability of the elastic properties of the aggregate and cement paste components of concrete. Crack formation relieves the strain concentrations and, at this load stage, cracks do not propagate but remain stable. This produces stable crack initiation and the concrete specimen exhibits quasi-elasticity.

As the applied load is increased, a second stage is reached when these initially stable cracks begin to propagate. There is now a distribution of crack propagation superimposed on that for stable crack initiation. The crack system multiplies and propagates but in a slow stable manner since if loading is stopped and the stress maintained at that level, crack propagation ceases. This stage can be described therefore as stable crack propagation.

The degree of cracking eventually reaches a more severe level, which is easily detected by volume change, pulse velocity and acoustic measurement, when the crack system becomes unstable. Within this third stage, ultimate failure occurs whether or not the load is continued to be applied. This further stage of unstable crack propagation results in a dilatation of the structure, as indicated by a reversal in the volume change behaviour (see Chapter 4). The end of this stage marks the ultimate strength of the material.

On this basis, two definitions of failure are proposed:-

(i) Lower bound criterion for failure

Onset of stable fracture propagation (o.s.f.p.) which can be

considered as the limit state for cracking.

(ii) Upper bound criterion for failure

Onset of unstable fracture propagation (o.u.f.p.) which can be considered as the ultimate limit state.

These criteria of failure are related to two significant stress levels. Firstly, o.s.f.p. occurs at the stress at which more severe cracking or void formation begins. There is a certain analogy between this stress level and the yield point in metals for, below this, concrete can be considered to act as a quasi-elastic material. Provided stresses are kept below this level, which occurs at a certain proportion of ultimate strength, depending on the mix characteristics, type of stress, etc., concrete specimens are unlikely to fail under any state of stress or regime of loading.

Secondly, o.u.f.p. occurs at the stress at which the crack system becomes unstable and self-propagates until complete disruption occurs. The beginning of this stage can be defined by the minimum volume level and corresponds probably to the long-term strength of concrete. Once this level is reached, failure is inevitable and the structure completely disrupts.

The suitability of these lower and upper bound definitions of failure has been confirmed by tests under repeated loading (see Chapter 5). As long as the stress levels were kept below the lower bound criterion (i.e. o.s.f.p.) no volume increases in specimens were detected. However, once the upper bound criterion (i.e. o.u.f.p.) was exceeded, severe dilatation occurred and the specimen failed after relatively few cycles of loading. The methods of defining the upper and lower bound criteria from principal and volumetric strain measurements are shown in 4.5. which also shows the method of assessing the ultimate level.

8.4. Test Results

The stress-strain relationships obtained from the test series (see Figures 7.18. to 7.25 and 7.76 to 7.81) show that the material exhibits a transition from relatively 'brittle' to more 'ductile' behaviour as the confining pressure increases above about 2000 lb./in.^{2} (14 N./mm.^{2}). For a given confining pressure, increases in the volume fraction of aggregate

cause the axial stress-axial strain relationships to become steeper, reflecting the increased stiffness of these mixes, while increases in water/cement ratio reduce the stiffness.

The variation of volume change with applied stress (see Figures 7.47. to 7.50 and 7.95. to 7.97.) shows the overall dilatation of the material above a critical stress level (o.u.f.p.). As the confining pressure is increased, the decreases in volume become larger and, for a given confining pressure, increasing the aggregate content or decreasing the water/cement ratio reduces the rate of volume decrease.

8.5. Stress Data as a Basis for Design

8.5.1. Introduction

Throughout this work, the triaxial stress is the actual stress acting on the central cross-section of the specimen corrected from the circumferential strain gauge measurements (see 4.5.). To aid in the production of design charts, all stresses have been 'normalised' by dividing by the stress at ultimate of the concrete when tested under uniaxial compression. Most researchers in concrete agree that the results from triaxial compression tests can be compared on the basis of normalised data. Such a procedure is intended to eliminate, or at least minimise, the effects due to testing technique, differing water/cement ratios, age and curing conditions. Although this is probably an oversimplification of a complex situation (see Chapter 6), the method remains a useful technique since it facilitates comparison between different concrete mixes.

8.5.2. Ultimate

8.5.2.1. Idealised Concretes

When relationships are plotted between the combinations of normalised axial stress at ultimate and confining pressure, a pattern of curves for different volume fractions of aggregate is obtained (see Figure 7.63). These show:-

(i) For a given aggregate content, the axial stress at ultimate increases with confining pressure and all relationships can be adequately represented by a hyperbolic function (see 7.5.4.7.) of the form:-

$$\sigma_{axial}/\sigma_c = \left[A(\sigma_{conf}/\sigma_c)^2 + B(\sigma_{conf}/\sigma_c) + 1\right]^{\frac{1}{2}}$$

(ii) The initial rate of increase of axial stress at ultimate with confining pressure is greater for mixes with higher aggregate contents.

(iii) For a given confining pressure, the axial stress at ultimate is greater for mixes with higher aggregate contents.

(iv) Irrespective of the aggregate content, the relationship tends to a slope of:- $\sigma_{axial}/\sigma_{conf} = 2.5$ approximately

8.5.2.2. Real Concretes

The relationships between normalised axial stress at ultimate and confining pressure for mortars and concretes containing gravel, limestone and granite aggregates are shown in Figures 8.1., 8.2., 7.105. and 7.106. These curves exhibit trends similar to those for idealised concretes in that:-

(i) The axial stress at ultimate increases with the confining pressure.

(ii) For a given confining pressure, higher axial stresses at ultimate are obtained for mixes containing higher volume fractions of aggregates.

(iii) The normalised strength data for all concrete mixes can be fitted to the hyperbolic relationship shown in Equation (1).

In Figure 8.1. the best fit curve for the mix with the lowest volume fraction of aggregate (Mix M1) is shown to be a suitable lower limit. This curve, in which the constants of Equation (1) are A = 4.87 and B = 10.05, has also been drawn on Figure 8.2. It will be seen that this particular relation can be considered to be a lower limit curve for ultimate strength for all the real concretes tested.

The best fit hyperbolic relations for all the mixes tested are given in Figures 7.105. and 7.106. These may be used, if required, for more accurate design purposes.

8.5.3. Onset of Unstable Fracture Propagation (Minimum Volume)

The determination of the onset of unstable fracture propagation (o.u.f.p.) was made from volume change measurements using the method described in 4.5. The relationships between normalised axial stress at the onset of unstable cracking and confining pressure are very similar to the relationships at ultimate (see 8.5.2.) and exhibit the following general trends:-

(i) The normalised axial stress at o.u.f.p. is a higher proportion of the axial stress at ultimate as the confining pressure is increased.

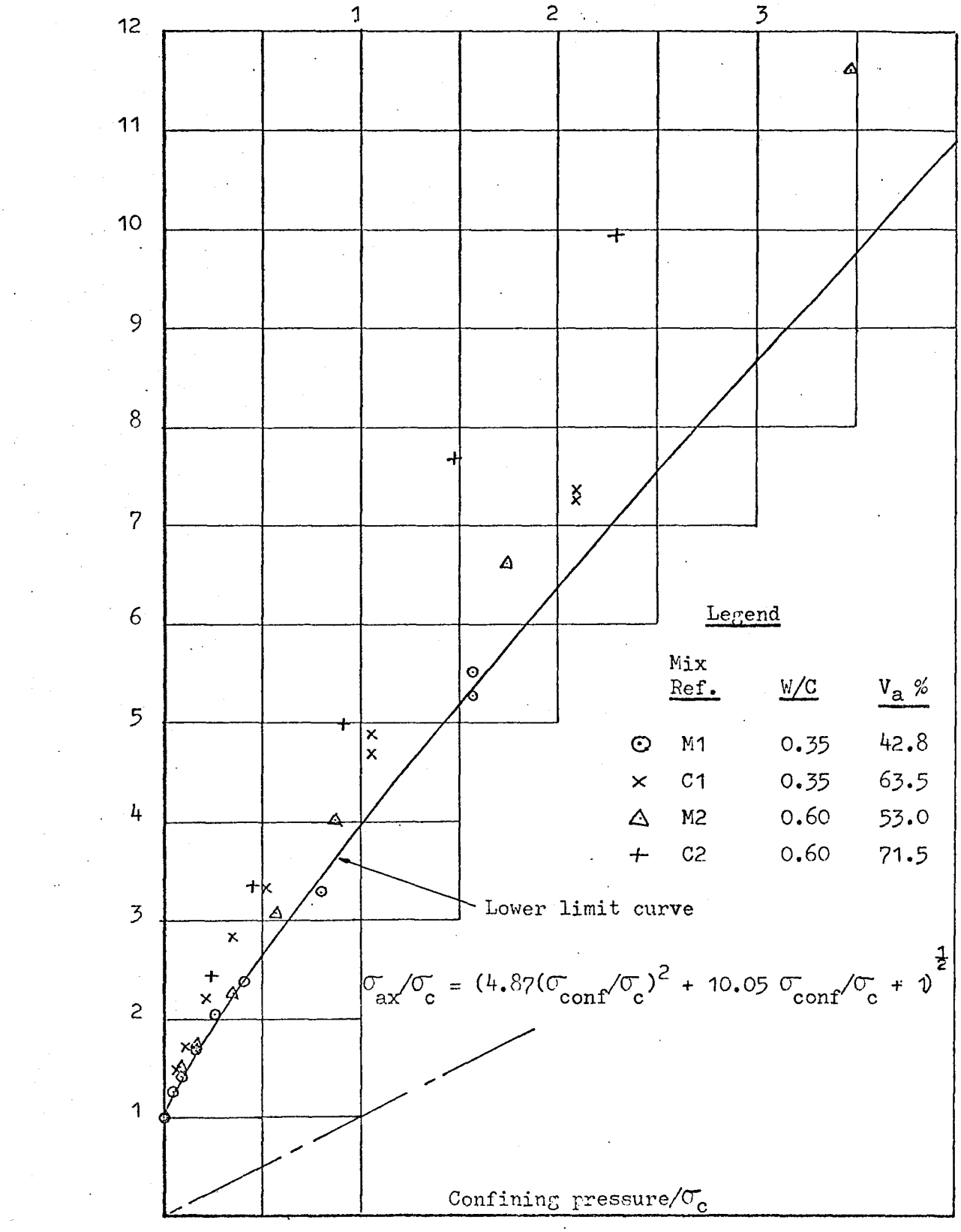


Figure 8.1. Variation of normalised axial stress with confining pressure at ultimate under triaxial compression for gravel mortars and concretes.

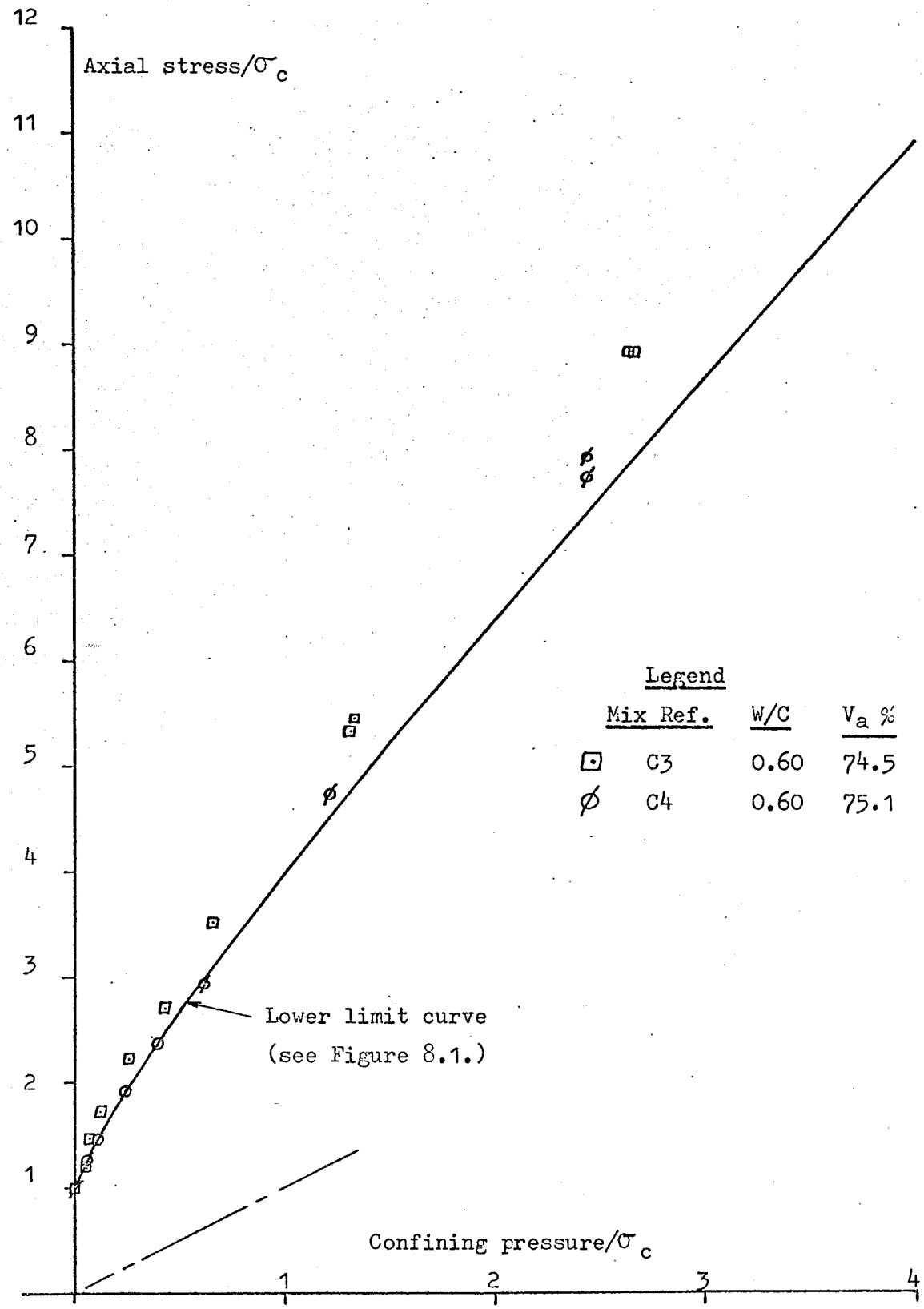


Figure 8.2. Variation of normalised axial stress with confining pressure at ultimate under triaxial compression for limestone (C3) and granite (C4) concretes.

(ii) For concretes containing gravel aggregates, the axial stress at o.u.f.p. becomes a higher proportion of the axial stress at ultimate with a decrease in the volume fraction of aggregate or a decrease in the water/cement ratio. In fact, for mixes with a water/cement ratio as low as 0.35, the axial stress at o.u.f.p. is almost equivalent to the axial stress at ultimate.

The normalised axial stress at o.u.f.p. is apparently closely related to the value at ultimate. Using the data from concretes containing gravel aggregates, relationships were established between the ratio between the normalised axial stresses at o.u.f.p. and ultimate for various values of confining pressure (see Figure 8.3.). The figure refers basically to mixes with water/cement ratios of 0.60, the values for mixes with a water/cement ratio of 0.35 being coincident with the envelope for a volume fraction of aggregate of 0.50 for all aggregate contents. Figure 8.3. can be used, together with the relationships established between normalised axial stress at ultimate and confining pressure, to establish the upper bound criterion of failure (o.u.f.p.).

8.5.4. Onset of Stable Fracture Propagation (o.s.f.p.)

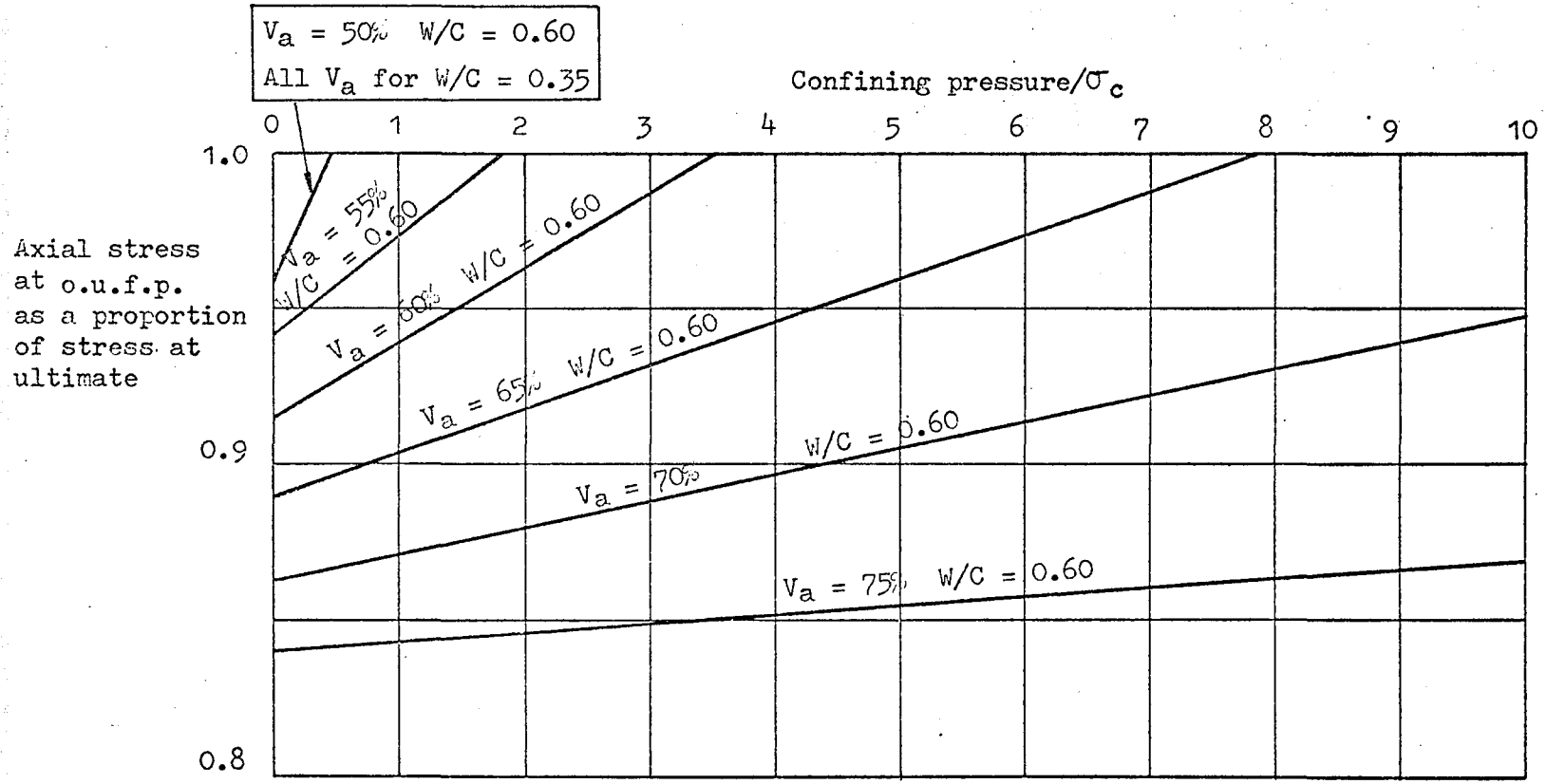
8.5.4.1. Idealised Concretes

The relationships between combinations of normalised axial stress at initial cracking and confining pressure indicate a pattern of curves for different volume fractions of aggregate (see Figure 7.41.). These show:-

(i) For a given confining pressure, higher axial stresses are required to cause o.s.f.p. as the volume fraction of the aggregate is increased.

(ii) For a given mix, as the confining pressure is increased, the o.s.f.p. envelope tends towards an intersection with the hydrostatic axis so defining a closed portion of stress-space. This implies that concrete can be significantly disrupted even under pure hydrostatic stress if this is above a critical level. Possible explanations for this are:-

(a) The composite structure of concrete, with hard aggregate particles embedded in a softer mortar



N.B. Chart refers to Mixes with W/C = 0.60. Values for Mixes with W/C = 0.35 are coincident with the envelope for V_a = 50% for all aggregate contents.

Figure 8.3. Relationships between axial stress at o.u.f.p. as a proportion of the ultimate stress under triaxial compression with normalised confining pressure for river gravel concretes.

matrix can give rise to local internal strain concentrations even under hydrostatic boundary stresses. This could result in fracture initiation and propagation.

(b) The collapse under pressure of the highly porous cement paste matrix.

8.5.4.2. Real Concretes

Figures 7.92. and 7.94. show the relationships between normalised axial stress at initial cracking and confining pressure for mortars and concretes containing gravel aggregates, limestones and granite aggregates. Despite the increased variation in particle size distribution in real concretes, these produced a pattern of curves which bear a strong similarity to those for the idealised concretes. Other trends which can be detected include:-

(i) At low confining pressures, mortars containing small maximum sized aggregate require a higher axial stress to cause o.s.f.p. than coarse aggregate concretes. However, at higher confining pressures, coarse aggregate mixes can sustain much higher axial stresses before o.s.f.p. occurs.

(ii) For concrete containing coarse aggregate particles, a decrease in water/cement ratio increases the axial stress to cause o.s.f.p. for a given confining pressure.

(iii) Although of the same basic pattern, different curves are obtained for concretes containing different types of coarse aggregate. For the mixes with the same volume fraction of aggregate, the normalised axial stress required to cause o.s.f.p. for a given normalised confining pressure, is highest for gravel concrete and lowest for granite. Comparison with Figure 7.41. shows that the envelope for the corresponding idealised concrete mix, containing spherical aggregate, is considerably higher than for the real concrete mixes. This suggests that the variation may be due to differences between the shape of the aggregate particles probably coupled with differences in their elastic moduli. The angularities and elastic moduli of the various types of aggregate

are given in Appendix 2. This shows that, in general, the angularity of the particles becomes greater and the stiffness of the aggregate diverges from that of the paste matrix, through the progression glass - gravel - limestone - granite.

8.6. Design Charts for Stresses

8.6.1. Methods of Representing Test Data

There are various ways in which the data from tests on concrete can be represented. Figures such as 8.1. and 8.2. are two-dimensional principal stress plots. However, on such plots, it is not possible to demonstrate the effect of varying the third principal stress. Representations of the lower and upper bound failure criteria must include the influence of all three principal stresses and their invariants. To this end, several investigators have produced plots in terms of normal and octahedral shear stresses which, in turn, are related to the first and second invariants of the stress tensor. These methods do not take account of the third stress invariant and furthermore are insensitive to changes in the intermediate principal stress [180].

Any state of stress in terms of the three principal values can be expressed as a single point in three-dimensional stress space. If the combinations of principal stresses causing o.s.f.p. and o.u.f.p. are known, three-dimensional plots of these values produce limiting surfaces of o.s.f.p. and o.u.f.p. These failure surfaces can be represented by solid bodies, the axes of which lie along the line $\sigma_1 = \sigma_2 = \sigma_3$. The shape of the cross-sectional contour lines may range from triangular to almost circular.

The overall shape of these failure surfaces can be represented by two-dimensional stress plots of particular sections through the surface, viz:

(i) The Rendulic stress curves produced by meridian sections of the surface cut by a plane containing the space diagonal ($\sigma_1 = \sigma_2 = \sigma_3$) and one of the principal stress axes (see Figures 8.4., 8.6.).

(ii) The right sections or equivolumetric stress planes, i.e. planes of constant volumetric stress which lie normal to the axis $\sigma_1 = \sigma_2 = \sigma_3$ (see Figure 8.14.).

The advantage of using the Rendulic and equivolumetric stress planes was first shown in 1967 by Niwa and Kobayashi [220]. Since then, these and similar concepts have been used by the author [19] and others [221, 222, 223] to provide design criteria for concrete under combined stresses.

The method of constructing Rendulic and equivolumetric stress envelopes for o.s.f.p. and o.u.f.p. for gravel aggregate concretes is described below. The fundamental concept of separating a state of stress into its volumetric and deviatoric components is adopted, since this simplifies the use of such envelopes for design purposes.

8.6.2. Ultimate

The relationships between the normalised axial stress at ultimate and confining pressure for the gravel mixes (Figure 8.1.) show the same trends as the corresponding curves for the idealised concretes at a given water/cement ratio (Figure 7.6.3.). Both sets of data can be adequately fitted to hyperbolic relationships of the form of Equation (1), i.e.:-

$$\sigma_{axial}/\sigma_c = \left[A(\sigma_{conf}/\sigma_c)^2 + B(\sigma_{conf}/\sigma_c) + 1\right]^{\frac{1}{2}}$$

This fact has been used as the basis for interpolating between volume fractions of aggregate (V_a) for each value of water/cement ratio as follows:-

(i) The normalised data for each idealised concrete mix is fitted to the basic hyperbolic relationship to obtain the best fit values of A and B for the idealised concretes.

(ii) For the idealised mixes, the relationships between A and V_a, and B and V_a, when plotted are found to be approximately linear.

(iii) The normalised data for each gravel mix is fitted to the basic hyperbolic relationship to obtain the corresponding value of A and B for these real concretes.

(iv) On the basis of step (ii), linear interpolation is used to obtain values of A and B at intermediate rounded-off values of V_a for each group of gravel mixes.

(v) The equations resulting from step (iv) are shown represented on the Rendulic plane in Figure 8.4. on which is also indicated the equivolumetric stress planes.

As well as the ultimate envelopes within the triaxial 'compression' zone, Figure 8.4. shows a lower envelope which can be used for triaxial 'extension' and compression - compression - tension. This envelope is based on the relation:-

$$\sigma_{axial}/\sigma_c = 0.43\ \sigma_{conf}/\sigma_c - 1 \qquad (2)$$

which has been derived from data from other investigations [2]. Results from a recent preliminary series of tests on the same range of gravel mixes [21] have shown this to be a safe lower limit which will be modified as more information is obtained.

8.6.3. Onset of Unstable Fracture Propagation (o.u.f.p.)

For gravel mixes, Figure 8.3. shows the relation between the ratio of the stress at o.u.f.p. to the stress at ultimate and values of normalised confining pressure. Figure 8.5. shows this relation represented on a Rendulic plane, which can be used to evaluate the o.u.f.p. envelope in terms of a known ultimate envelope for any value of confining pressure.

Within the triaxial 'extension' and compression - compression - tension zone, data available for the same range of mixes show that the lower envelope in Figure 8.4. can be safely assumed to be coincident with the lower limit for ultimate.

8.6.4. Onset of Stable Fracture Propagation (o.s.f.p.)

The normalised envelopes for the gravel mixes (Figure 7.92) show the same trends as the corresponding curves for the idealised concretes (Figure 7.41). The pattern of relationships for the idealised concretes at a constant water/cement ratio has been used as the basis for interpolating the values of axial stress at various values of confining pressure for intermediate rounded-off values of V_a.

The resulting envelopes for each group of gravel concretes, represented on the Rendulic plane, are shown in Figure 8.6. Again, values of

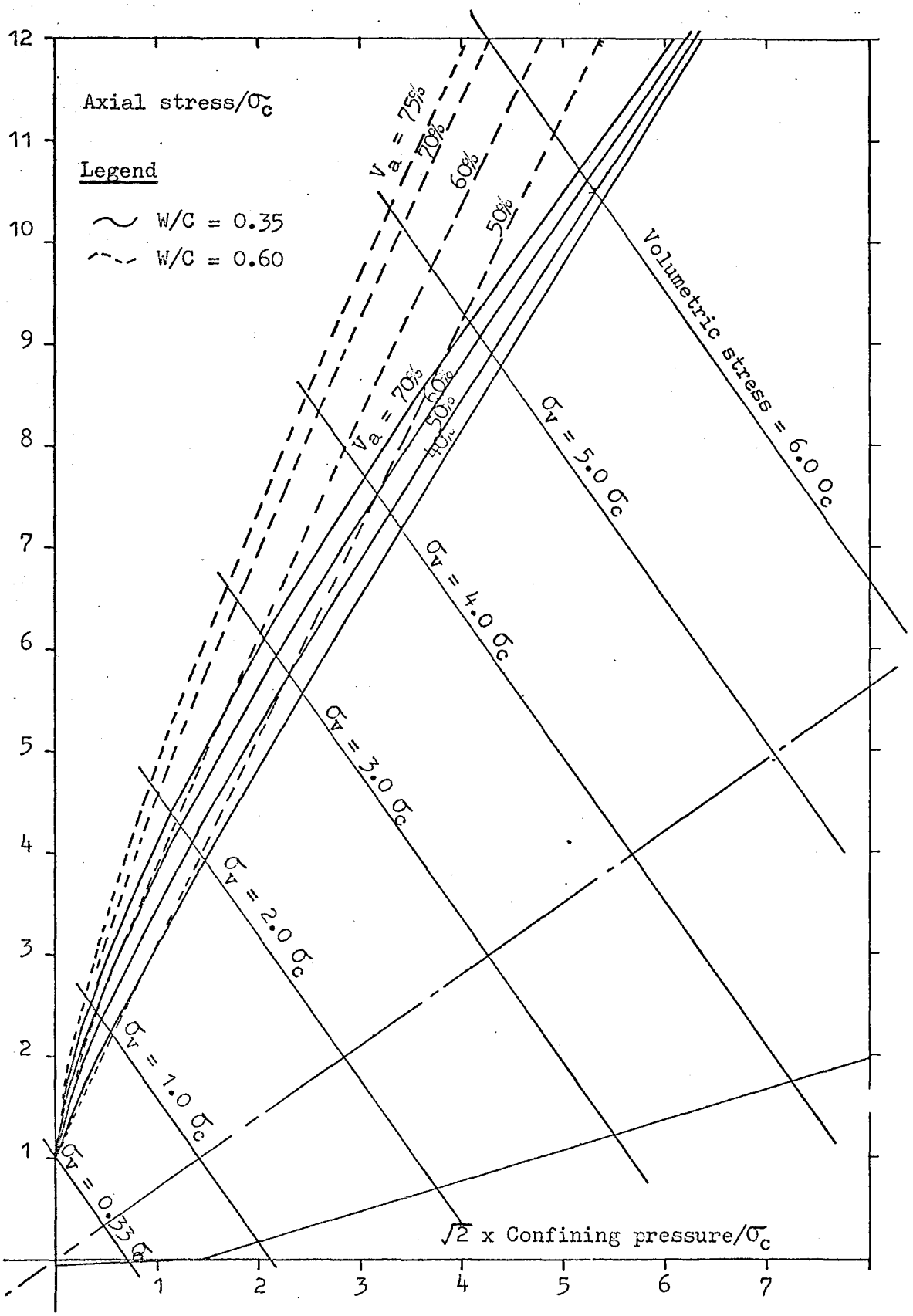


Figure 8.4. Design chart represented on Rendulic plane for determining combinations of normalised stress at ultimate.

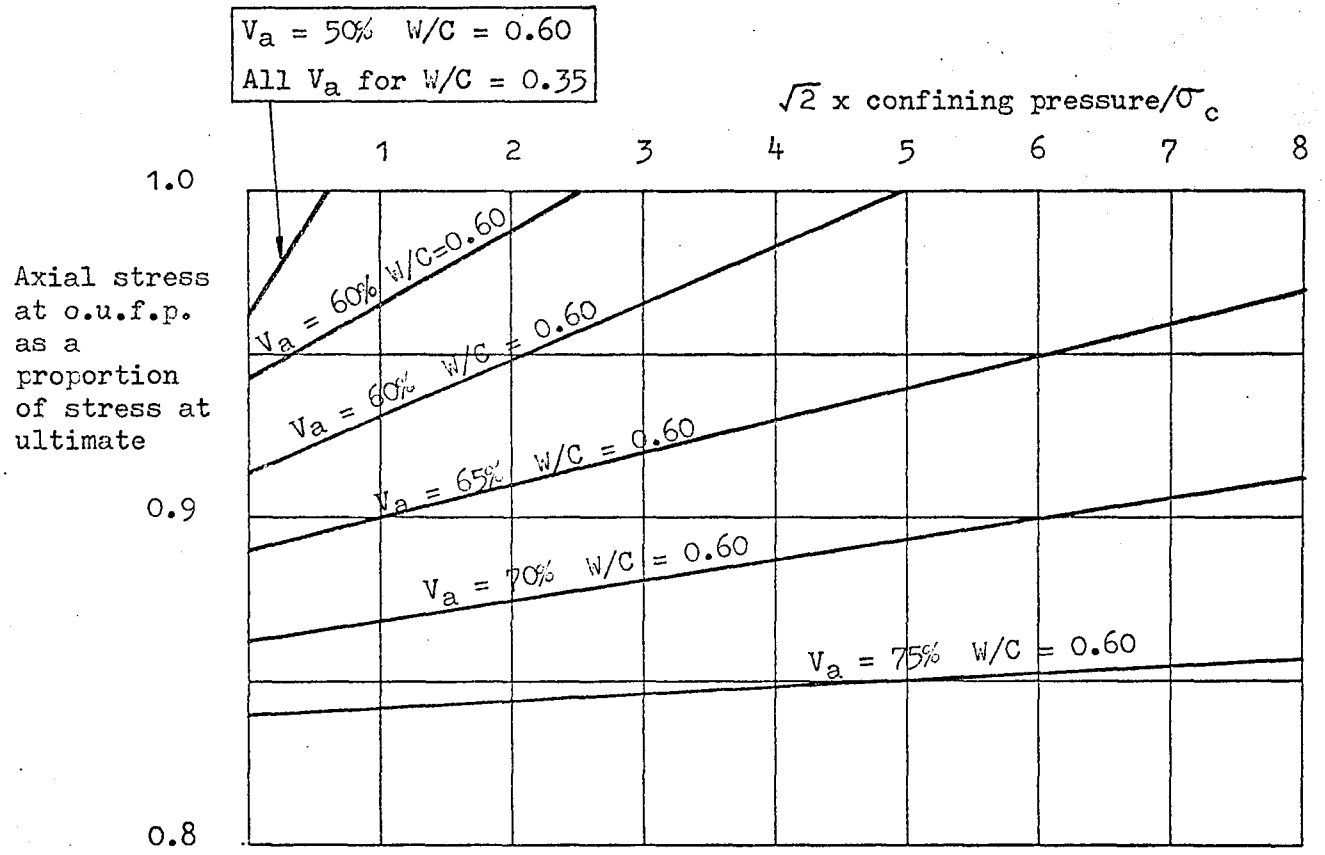


Figure 8.5 Design chart represented on Rendulic plane for determining the axial stress at o.u.f.p. as a proportion of the ultimate stress under triaxial compression.

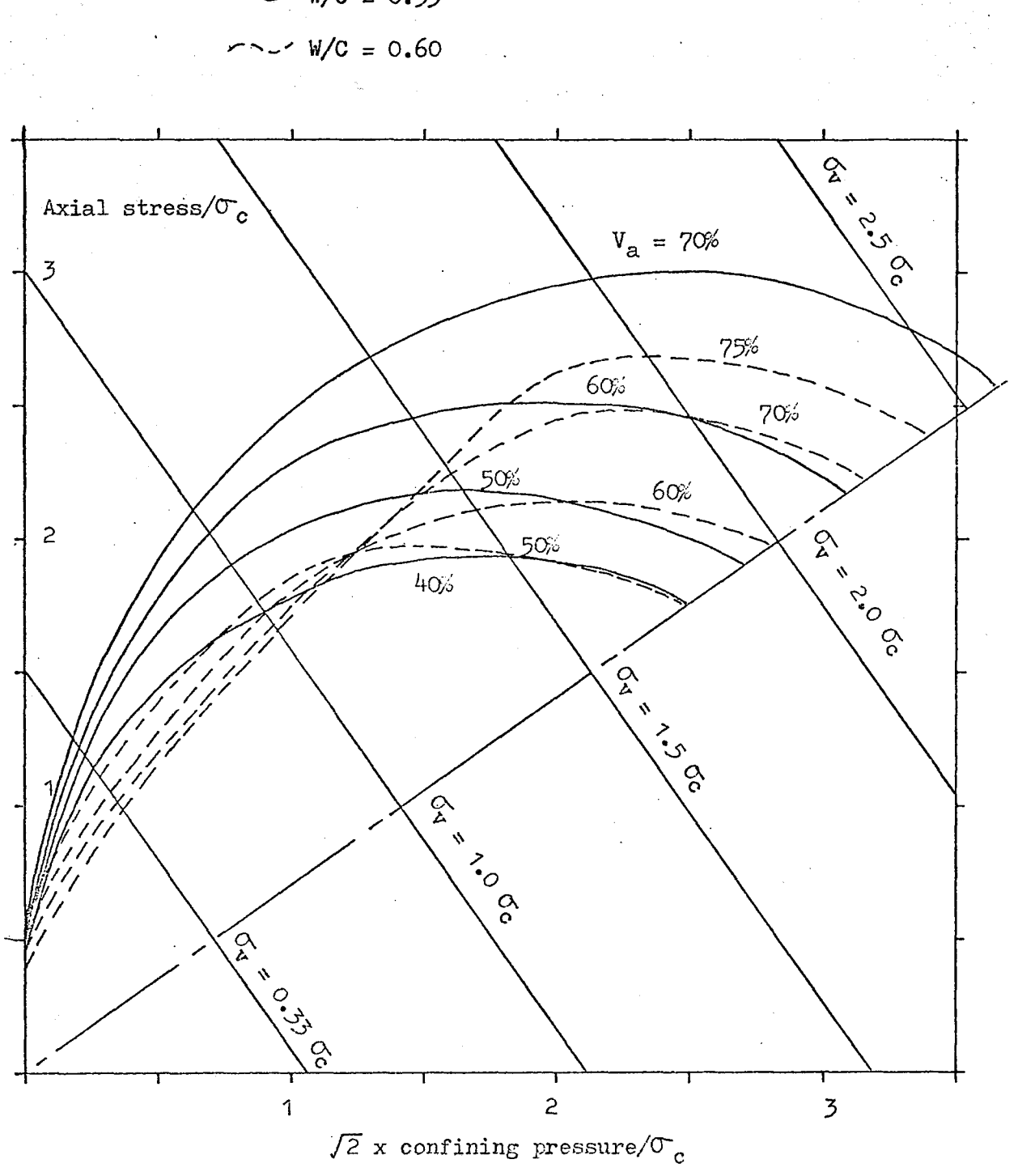


Figure 8.6. Design chart represented on the Rendulic plane for determining combinations of normalised stress necessary to cause onset of stable fracture propagation.

equivolumetric stress are indicated.

An approximate method of extending the o.s.f.p. envelopes into the triaxial 'extension' and compression - compression - tension zone is to multiply the offsets along the equivolumetric stress planes in Figures 8.6. by a factor of 0.67 (see 8.6.5. Design Example). This factor has been evaluated following the results of preliminary tests carried out within the latter zones on the same range of gravel mixes [21]. As more information is obtained, the design charts will be suitably modified.

8.6.5. Design Example

8.6.5.1. The Problem

It is required to assess whether a volume element made from a particular concrete mix, with a characteristic strength at twenty-eight days of 40 N/mm^2, will satisfactorily withstand the state of multiaxial compression defined by σ_1 = 82 N/mm^2, σ_2 = 70 N/mm^2, σ_3 = 50 N/mm^2.

Mix Proportions (by weight of dry materials)

	Kg/m^3	Water absorption %
Ordinary Portland Cement	450	
Thames Valley gravel aggregate		
Sand 5 mm. max. size	575	1.3
Coarse agg. 20 mm. max. size	1155	1.5

Total water/cement ratio	0.47
Specific gravity of cement	3.12
Specific gravity of aggregate	2.60

8.6.5.2. Design Procedure

1. Calculate the 'effective' water/cement ratio

'effective' w/c = total w/c - water absorbed by aggregates
= 0.47 - 0.055
= 0.415

2. Calculate the volume fraction of aggregate

On the basis of proportions and specific gravities of materials

V_a = 66%

3. Convert the characteristic strength to uniaxial (i.e. cylinder) strength of concrete σ_c at the required maturity

(i) Assume the strength development of the concrete in the structure is equivalent to that of cubes initially water-cured for twenty-eight days and then air-cured for eleven months.

C.P. 110 Table 2 suggests that the cube strength at one year for a 40 N/mm^2 mix may be taken as 50 N/mm^2, i.e. an increase of 25%. For the conditions in the structure, assume as reasonable a slightly smaller increase - say 20%.

Strength of concrete in structure at 12 months $= 1.2 \times 40$ N/mm^2
$= \underline{48 \text{ N/mm}^2}$

(ii) Assume cylinder/cube strength ratio of 0.80 for concrete made with 20 mm. ($\frac{3}{4}$") coarse aggregate:-

Uniaxial strength of concrete at 1 year $\sigma_c = 48 \times 0.80$ N/mm^2
$= \underline{38.4 \text{ N/mm}^2}$

4. Calculate the normalised volumetric and deviatoric components of applied stress

$$\sigma_1 = 82/38.4 = 2.13\ \sigma_c$$
$$\sigma_2 = 70/38.4 = 1.82\ \sigma_c$$
$$\sigma_3 = 50/38.4 = 1.30\ \sigma_c$$

Volumetric Stress Component

$$\sigma_v = \frac{\sigma_1 + \sigma_2 + \sigma_3}{3} = \underline{\underline{1.75\ \sigma_c}}$$

This value defines the equivolumetric stress plane.

Deviatoric Stress Components

$$\sigma_{D1} = \sigma_1 - \sigma_v = \underline{\underline{+ 0.38\ \sigma_c}}$$

$$\sigma_{D2} = \sigma_2 - \sigma_v = \underline{\underline{+ 0.07\ \sigma_c}}$$

$$\sigma_{D3} = \sigma_3 - \sigma_v = \underline{\underline{- 0.45\ \sigma_c}}$$

5. Establish the ultimate, o.u.f.p. and o.s.f.p. envelopes

(i) Ultimate

Use the appropriate design charts (Figures 8.7. and 8.8.) and linear interpolation to obtain the ultimate envelopes in the 'compression' zone on the required equivolumetric stress plane as shown on Figure 8.9.

Firstly, from Figure 8.7. obtain the envelope for V_a = 66%, w/c = 0.35. From Figure 8.8. obtain the envelope for V_a = 66%, w/c = 0.35. Plot these envelopes representing V_a = 66%, w/c = 0.415. The intersection of this envelope and the equivolumetric stress plane $\sigma_v = 1.75\ \sigma_c$ gives the point U_c on Figure 8.9.

In the 'extension' zone, use the lower limit envelope indicated on Figure 8.7. to give point U_e.

Points U_c and U_e define the envelope for ultimate for this particular concrete.

(ii) o.u.f.p.

Use the design chart (Figure 8.5.) to obtain the o.u.f.p. envelope as a proportion of the ultimate stress envelope within the compression zone.

Firstly, from Figure 8.5. interpolate to obtain the two straight line relations representing V_a = 66%, w/c = 9.35 and V_a = 66%. w/c = 0.60. Plot these relations on Figure 8.10. and interpolate for the straight line relation representing V_a = 66%, w/c = 0.415.

This relation indicates that the o.u.f.p. stress as a proportion of ultimate varies linearity from 94% at $\sqrt{2}\ \sigma_{conf}/\sigma_c = 0$ to 100% at $\sqrt{2}\ \sigma_{conf}/\sigma_c = 2.8$. From this, the o.u.f.p. envelope can be

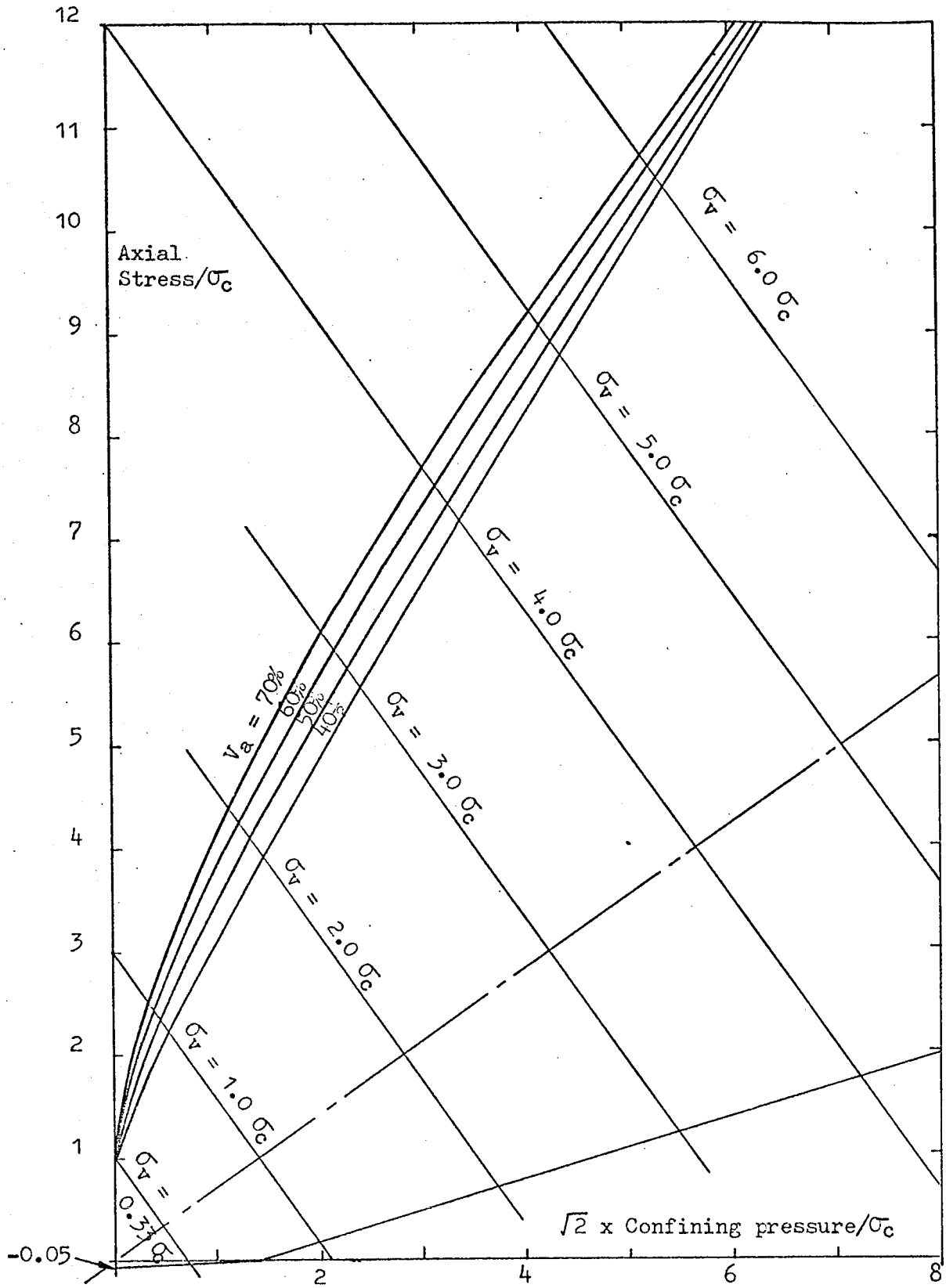


Figure 8.7. Design chart represented on Rendulic plane for determining combinations of normalised stress at ultimate for concretes with W/C = 0.35.

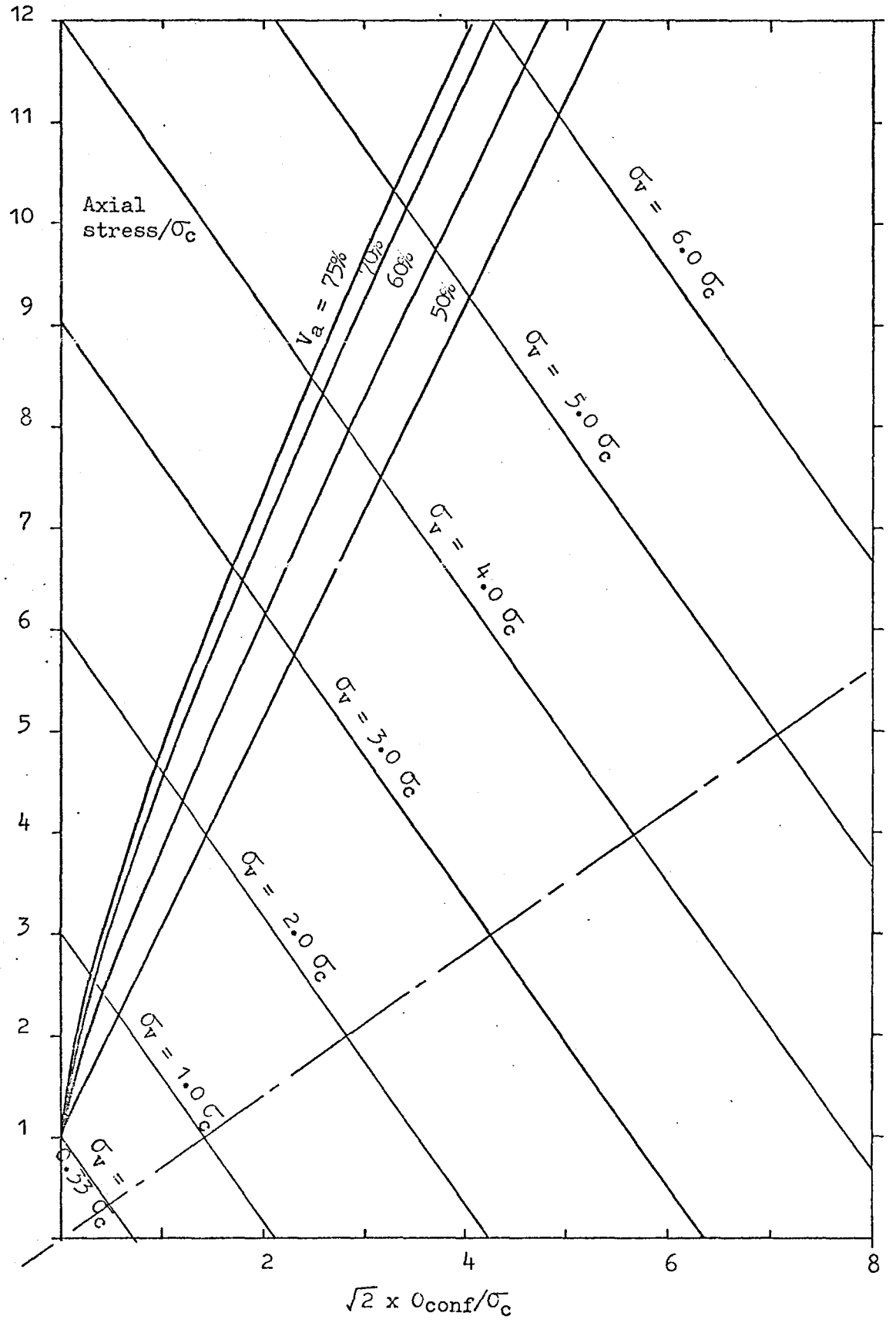


Figure 8.8. Design chart represented on Rendulic plane for determining combinations of normalised stress at ultimate for concretes with W/C = 0.60.

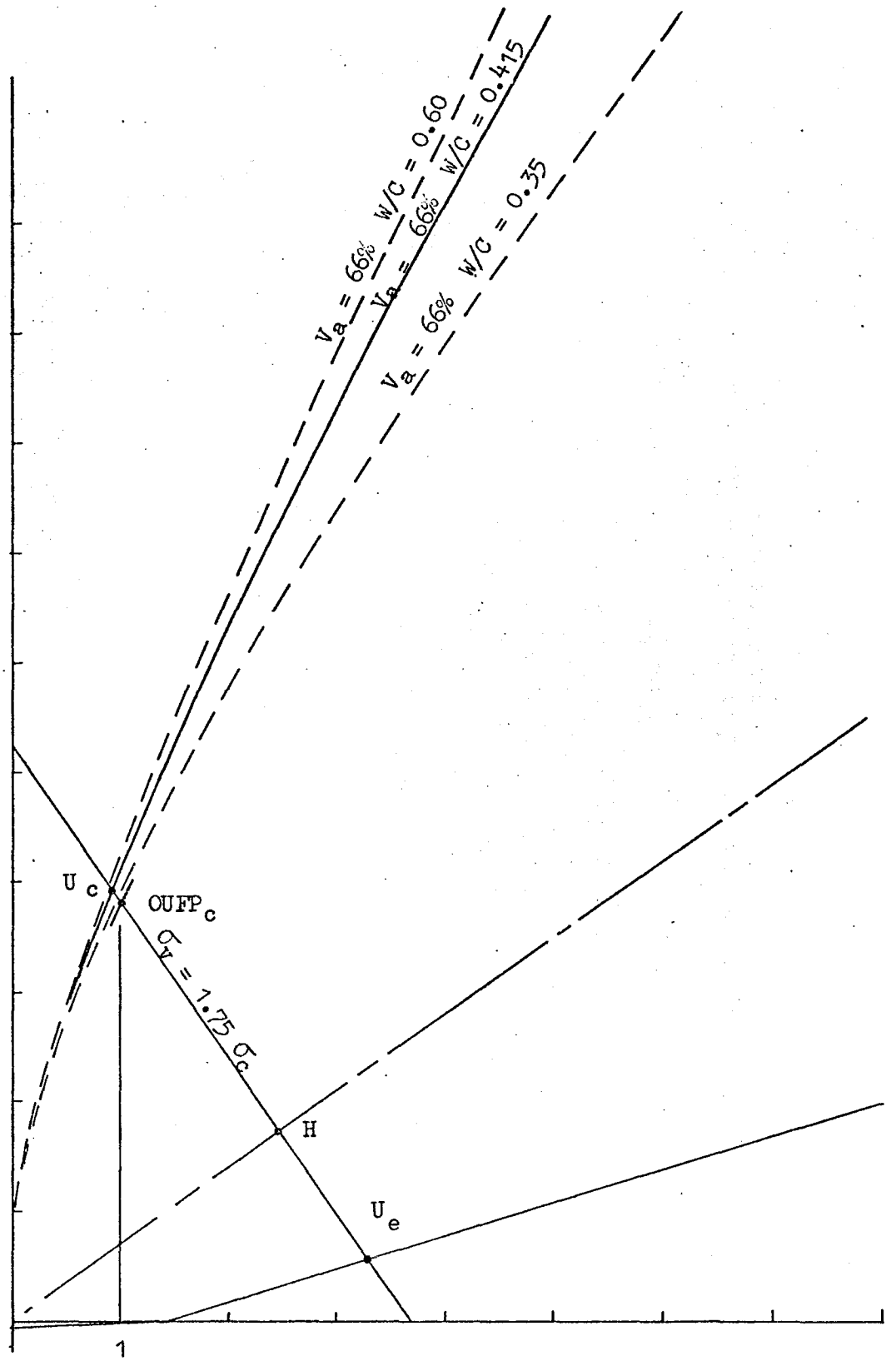


Figure 8.9. Interpolated ultimate and onset of unstable fracture propagation envelopes on Rendulic plane.

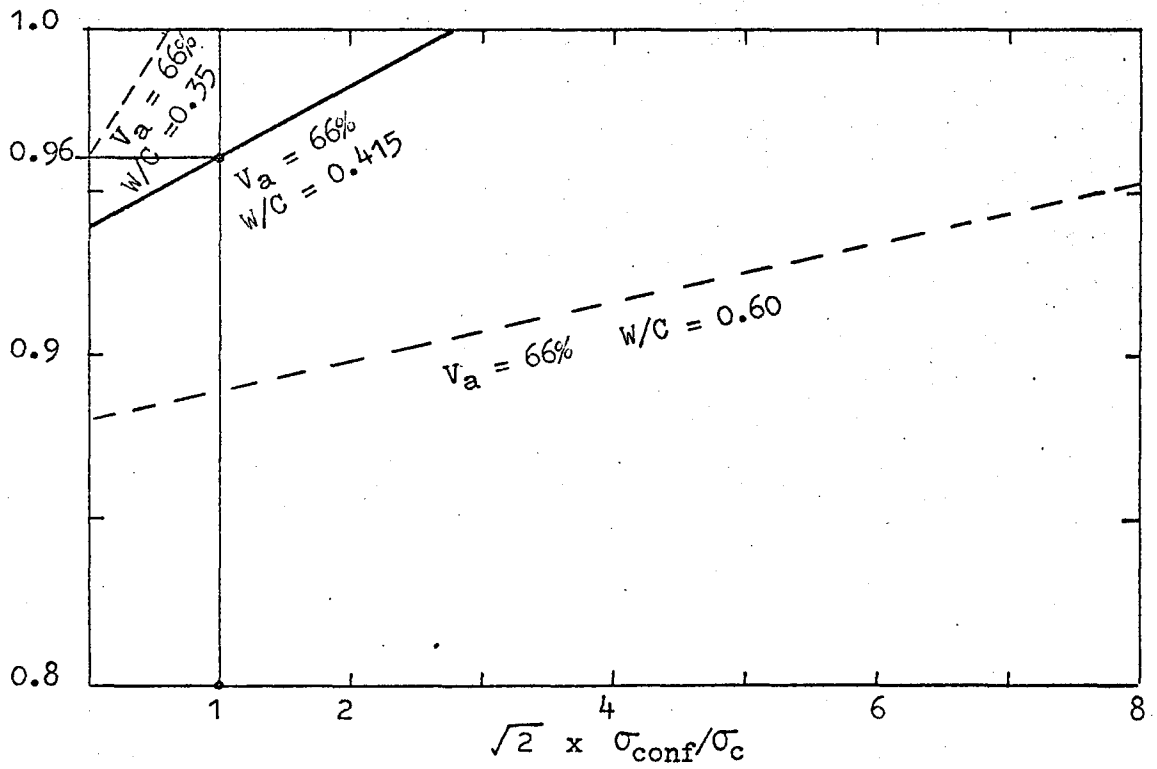


Figure 8.10. Interpolated values of stress as onset of unstable fracture propagation as a proportion of ultimate.

plotted on Figure 8.9. for various values of $\sqrt{2}\,\sigma_{conf}/\sigma_c$ and o.u.f.p. stress (plotted in terms of axial stress/σ_c). It will be seen that the o.u.f.p. envelope intersects the equivolumetric stress plane $\sigma_v = 1.75\,\sigma_c$ at the point $OUFP_c$ which corresponds to the value of 96% ultimate stress and $\sqrt{2}\,\sigma_{conf}/\sigma_c = 1.0$ on Figure 8.10.

In the 'extension' zone, assume the o.u.f.p. envelope to be coincident with the safe lower limit for ultimate (i.e. point U_e on Figure 8.9.).

Points $OUFP_c$ and U_e (= $OUFP_e$) define the o.u.f.p. envelope for this particular concrete.

(iii) o.s.f.p.

Use the appropriate design charts (Figures 8.11. and 8.12.), and a similar interpolation procedure to that used for (i) ultimate, to obtain the o.s.f.p. 'compression' envelope on the equivolumetric stress plane $\sigma_v = 1.75\,\sigma_c$ as shown in Figure 8.13.

Firstly, obtain the envelopes for V_a = 66%, w/c = 0.35 from Figure 8.10. and V_a = 66%, w/c = 0.60 from Figure 8.12. Plot these envelopes on Figure 8.13. and interpolate for the envelope representing V_a = 66%, w/c = 0.415. The intersection of this envelope and the equivolumetric stress plane $\sigma_v = 1.75\,\sigma_c$ gives the point $OSFP_c$ on Figure 8.13.

In the 'extension' zone, assume values of 0.67 x 'compression' values for the appropriate offsets along the equivolumetric stress planes. This gives the point $OSFP_e$ on Figure 8.13.

Points $OSFP_c$ and $OSFP_e$ define the envelope for o.s.f.p. for this particular concrete.

6. Construct o.s.f.p., o.u.f.p. and ultimate envelopes on the required equivolumetric stress plane $\sigma_v = 1.75\,\sigma_c$

From Figures 8.9. and 8.13. measure the offsets to each envelope on the equivolumetric stress plane $\sigma_v = 1.75\,\sigma_c$

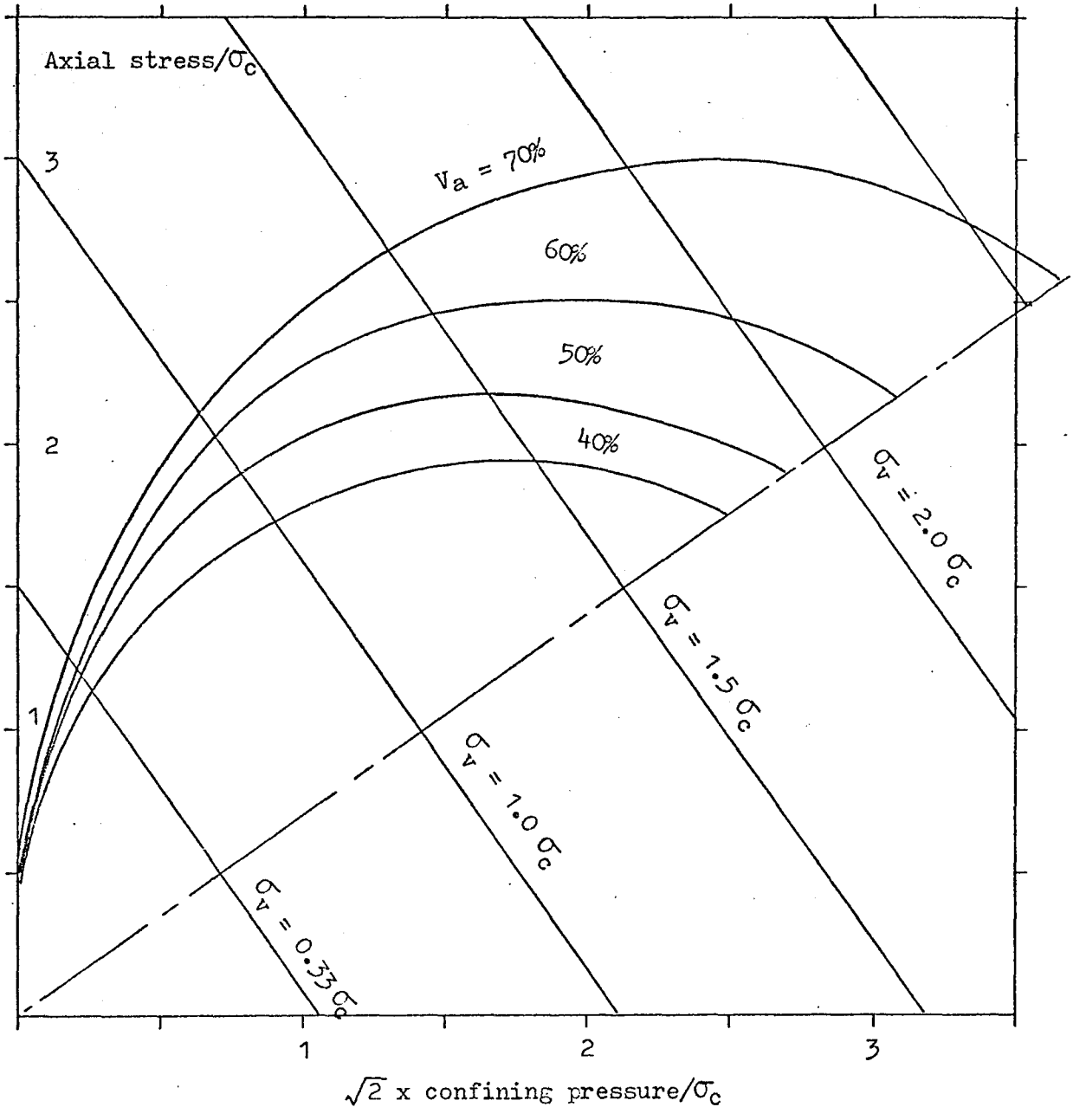


Figure 8.11. Design chart represented on Rendulic plane for determining combinations of normalised stress necessary to cause onset of stable fracture propagation for concretes with W/C = 0.35.

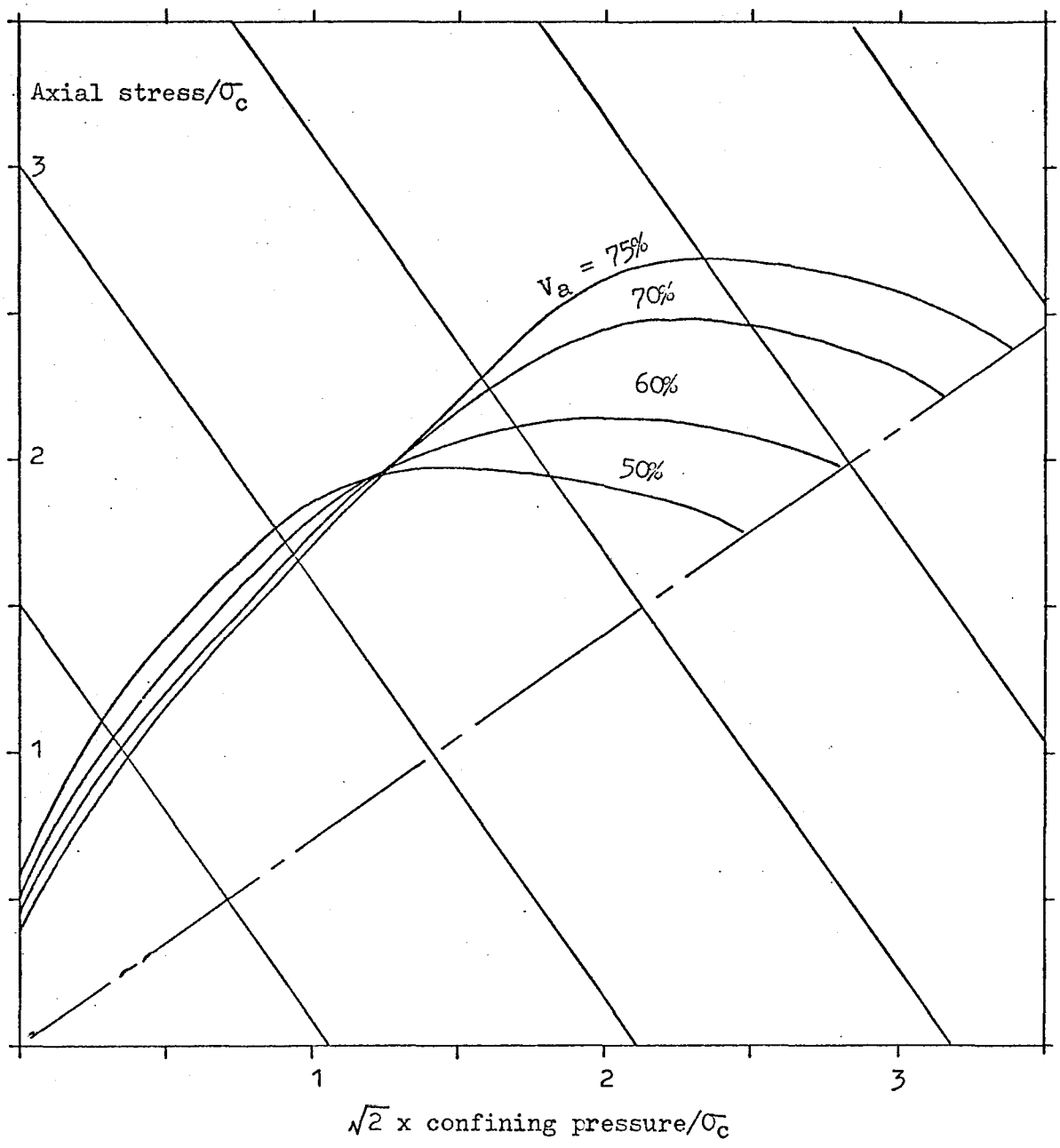


Figure 8.12. Design chart represented on Rendulic plane for determining combinations of stress necessary to cause onset of stable fracture propagation for concretes with W/C = 0.60.

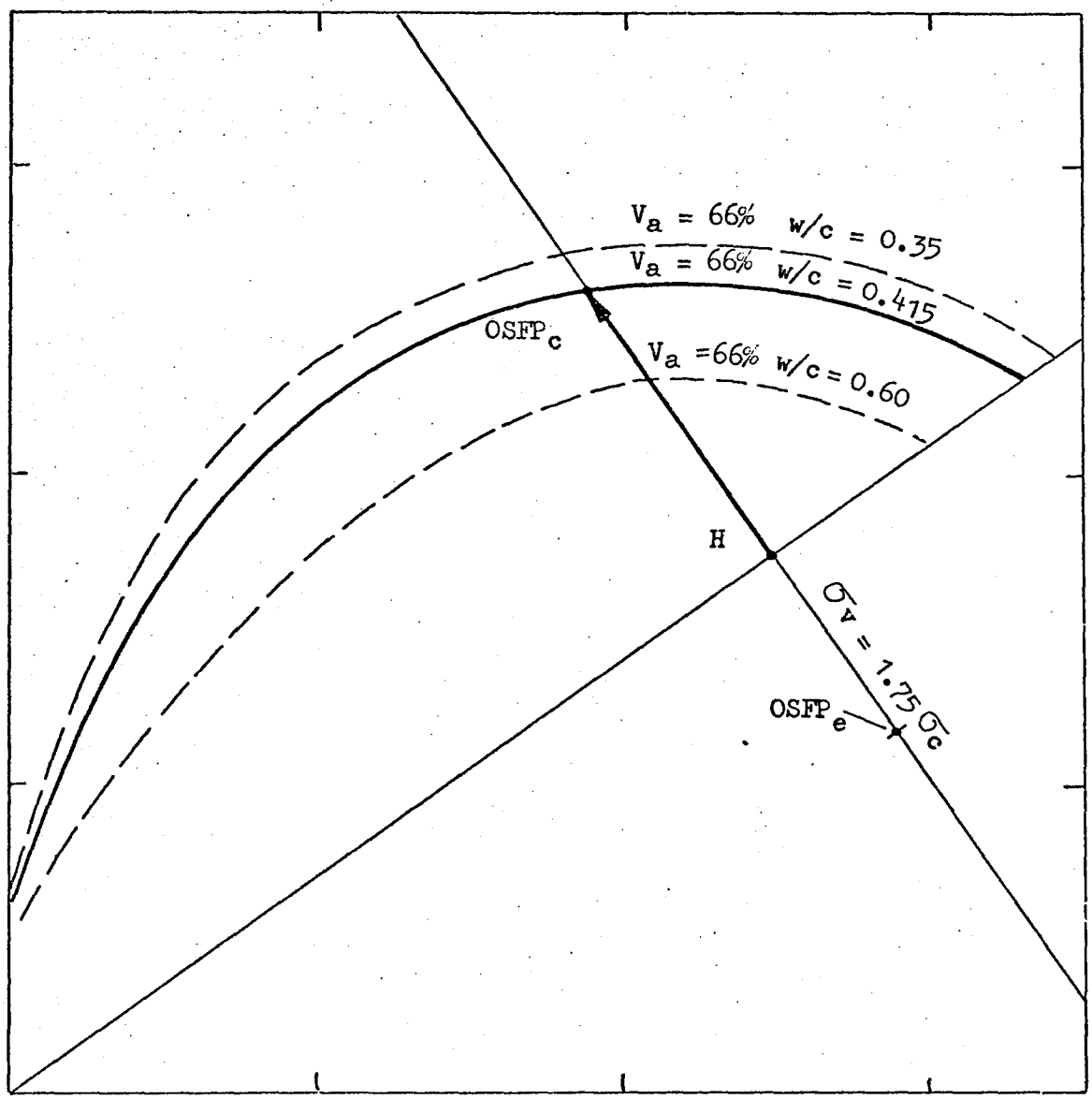


Figure 8.13. Interpolated envelopes for onset of stable fracture propagation on Rendulic plane.

H to U_c = 2.68)
) These define the ultimate envelope
H to U_e = 1.42)

H to $OUFP_c$ = 2.54)
) These define the o.u.f.p. envelope
H to $OUFP_e$ (or U_e) = 1.42)

H to $OSFP_c$ = 1.04)
) These define the o.s.f.p. envelope
H to $OSFP_e$ = 1.04 x 0.67 = 0.70)

On Figure 8.14. represent these points on the 'compression' or 'extension' axes of principal stress $\bar{\sigma}_1$, $\bar{\sigma}_2$ and $\bar{\sigma}_3$. Join these points by straight lines to produce the contours of the failure surfaces at the cross section representing the equivolumetric stress plane $\bar{\sigma}_v = 1.75\ \bar{\sigma}_c$.

7. Plot the deviatoric stress components on equivolumetric stress plane

In comparison to the scale of unity for principal stress axes $\bar{\sigma}_1/\bar{\sigma}_c$ etc., the equivolumetric stress planes have dimensions of $\sqrt{3}\ (\bar{\sigma}_1/\bar{\sigma}_c)$ and the projections of the principal stresses on the $\bar{\sigma}_1/\bar{\sigma}_c$ etc., axes must be plotted in Figure 8.14. to the scale $\sqrt{2}/\sqrt{3}\ (\bar{\sigma}_1/\bar{\sigma}_c)$ etc.

Plot the deviatoric stress components $\bar{\sigma}_{D1}$, $\bar{\sigma}_{D2}$ and $\bar{\sigma}_{D3}$ as distances $\sqrt{2}/\sqrt{3}\ \bar{\sigma}_{D1}$, $\sqrt{2}/\sqrt{3}\ \bar{\sigma}_{D2}$ and $\sqrt{2}/\sqrt{3}\ \bar{\sigma}_{D3}$ parallel to the $\bar{\sigma}_1$, $\bar{\sigma}_2$ and $\bar{\sigma}_3$ axes taking care to account for the sign of the deviatoric stress component), to give the resultant point P.

Compare P with the various envelopes to assess the degree of criticality.

8. Assessment of criticality of stress state

Point P lies outside the o.s.f.p. envelope but within the o.u.f.p. envelope.

If the applied stress state is likely to remain constant then the concrete should withstand this stress level without undue distress. If the stresses are liable to fluctuations up to this level then it would be advisable to consider one of the following alternatives to ensure that the o.s.f.p. level is not exceeded.

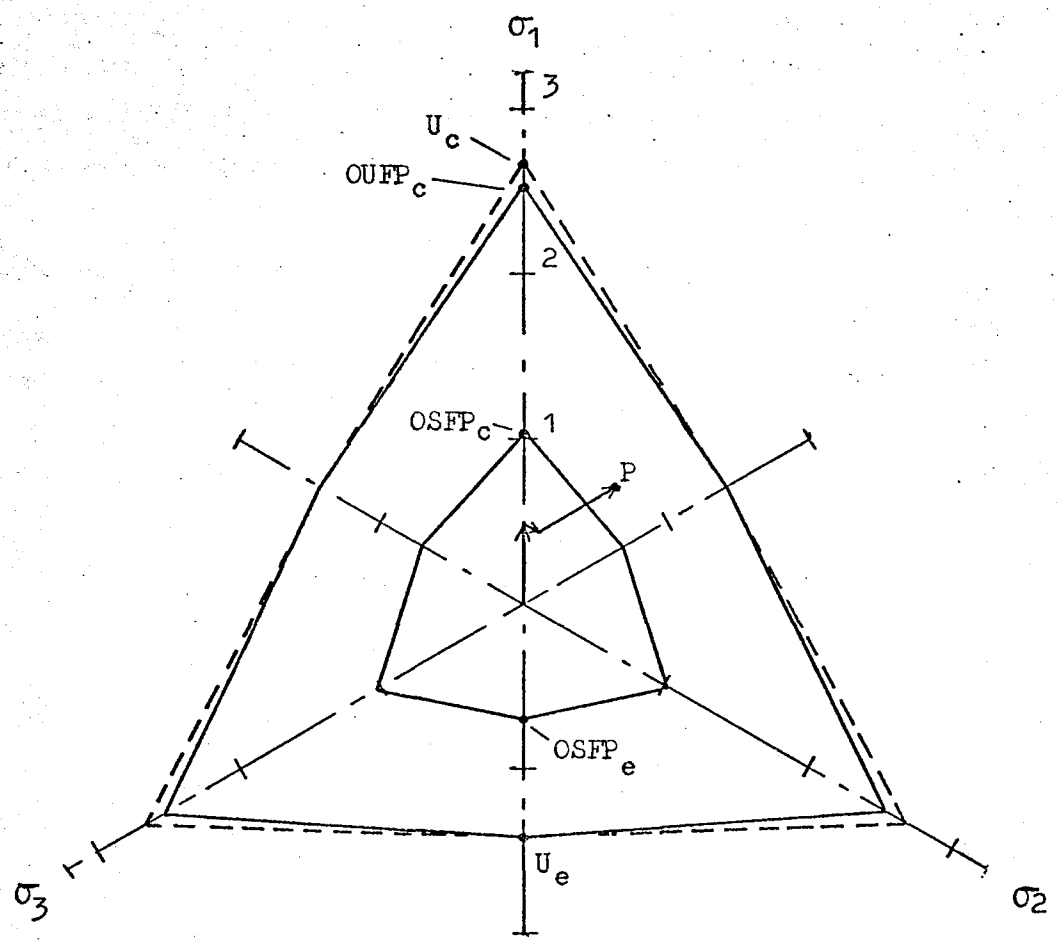


Figure 8.14. Envelopes on equivolumetric stress plane $\sigma_v = 1.75\ \sigma_c$ defining ultimate, onset of unstable fracture propagation and onset of stable fracture propagation for the given concrete.

(i) Use a concrete mix with a higher characteristic strength.

(ii) Alter the confining pressure or volumetric stress component.

(iii) Reduce the applied state of stress on the element.

It should be noted that in this problem only the criticality of the final stress state has been checked. For an actual case the development of the stress state should be investigated to ensure that a critical state is not reached by an interim condition [19].

8.6.5.3. Concretes with Other Aggregates

The design example and the charts given in Figures 8.4. to 8.8. apply only to gravel aggregate concretes. However, the information in Figures 7.106. and 7.94. can be used in conjunction with the design charts to provide a reasonable estimate of the criticality of any stress state for concretes made with limestone and granite aggregates.

8.7. Strain Data as a Basis for Design

8.7.1. Onset of Stable Fracture Propagation (o.s.f.p.)

8.7.1.1. Idealised Concretes

The relationships between axial and lateral strains at o.s.f.p. for idealised concrete are shown in Figure 7.39. Again a pattern of envelopes emerges and each envelope can be divided into three main regions.

Region 1 Confining pressures up to approximately 4000 lb./in.^{2} (28 N./mm.^{2}). o.s.f.p. occurs at values of axial compressive strain which increase with confining pressure. The lateral tensile strain remains approximately equal to that for a uniaxial compression test.

Region 2 Confining pressures from 4000 - 10000 lb./in.^{2} (28 - 70 N./mm.^{2}) approximately. The axial strain at o.s.f.p. continues to increase with confining pressure but at a diminishing rate, reaching a maximum near the end of this region.

The corresponding lateral strain gradually increases compressively.

Region 3 Confining pressures above approximately 10000 lb./in.^{2} (70 N./mm.^{2}). The axial strain becomes less compressive whilst the lateral tensile strain

continues to become more compressive. The region is terminated by the envelope intersecting the hydrostatic axis at 90°. The envelopes, therefore, are of a closed form in strain space and in this respect are similar to those for the corresponding stresses at o.s.f.p.

As the volume fraction of aggregate is increased the envelopes remain similar in shape but enclose a smaller portion of strain space.

8.7.1.2. Real Concretes

Figures 7.88 and 7.89. show the axial and lateral strains at initial cracking for concretes containing gravel, limestone and granite aggregates. These curves show the following features:-

(i) Each envelope exhibits the same three main regions as shown by the idealised concretes, with the possible exception of the gravel mix C2 with a high water/cement ratio and aggregate volume fraction V_a.

(ii) For mixes with a given water/cement ratio, the envelopes remain similar in shape as V_a is increased but enclose a smaller portion of strain space.

(iii) For a given V_a, the envelopes enclose a smaller portion of strain space as the water/cement ratio is increased.

(iv) For a given water/cement ratio, the envelopes for the concretes made with limestone and granite aggregates are similar but enclose a larger portion of strain space than the corresponding gravel mix.

It is considered that although the envelopes have been obtained under only one type of loading regime, they are valid for other regimes, provided the o.s.f.p. level is not exceeded by any interim stress or strain condition.

8.7.2. Onset of Unstable Fracture Propagation (o.u.f.p.)

8.7.2.1. Idealised Concretes

Figure 7.61. shows the relationships between axial and lateral strain at o.u.f.p. (minimum volume). The appearance of the envelopes suggests that they are 'unfolded' and 'stretched' versions of the corresponding o.s.f.p.

envelopes, of which examples are shown on the Figure. Apart from the lack of distinct regions for each envelope, these envelopes exhibit similar features to the o.s.f.p. envelopes.

8.7.2.2. Real Concretes

The axial strain-lateral strain relationships for the gravel mixes shown on Figure 7.103. conform to the same pattern as the idealised concretes, the main features being:-

(i) For mixes with a given water/cement ratio, the envelopes enclose a smaller portion of strain space as V_a is increased.

(ii) For a given V_a, the envelopes enclose a smaller portion of strain space as the water/cement ratio is increased.

The envelopes for the limestone and granite concretes shown on Figure 7.104. indicate that the behaviour of the granite mix is similar to that of the corresponding gravel concrete but that the limestone mix exhibits considerably different characteristics.

At such a high level of stress and advanced stage of cracking, it is almost certain that the strain relations at o.u.f.p. will depend markedly on the particular loading regime and sequence of applying the stresses. For this reason, the o.u.f.p. envelopes must be considered as unique to the particular loading system used in this investigation.

8.8. Design Charts for Strains

8.8.1. Introduction

Since the strain data for stresses applied above the o.s.f.p. limit are unlikely to be valid for loading regimes other than those used in the current test programme, their use as general design criteria is strongly discouraged. It is also possible that even the data obtained up to the o.s.f.p. level may have to be modified for stress states other than axi-symmetrical.

For these reasons only design data for o.s.f.p. are proposed and no attempt is made to represent these data in three-dimensional strain space.

8.8.2. Onset of Stable Fracture Propagation (o.s.f.p.)

The envelopes for the gravel mixes (Figure 7.88.) show the same trends as

those corresponding to the idealised concretes (Figure 7.39.). The pattern of relationships for the idealised concrete of a given water/cement ratio shows that, for a given value of confining pressure, linear interpolation can be used to obtain points on the envelope corresponding to any given volume fraction of aggregate.

This has been used to obtain the envelopes for each group of gravel mixes at rounded-off values of V_a. The resulting design chart is shown in Figure 8.15.

8.9. Influence of Thermal, Shrinkage and Creep Effects on the Design Criteria

In addition to designing structural elements to resist loads and deformations applied directly to the boundaries, in many cases it is necessary to take account of additional factors which may contribute to the overall or total state of stress or strain. These factors include:-

Thermal movement	-	caused by heat of hydration of the cement or external environmental conditions.
Shrinkage	-	caused by a drying environment.
Creep or relaxation	-	caused by sustained load or deformation.

Although the failure criteria proposed in this report have been derived from tests in which only the external loading configuration has been varied, they can be used to provide an estimate of the behaviour of concrete under a total state of stress. The environmental and other conditions for this investigation are defined in Table 8.1. Any stresses induced by additional factors would be superimposed upon the applied stress system.

In assessing the criticality of a particular state of strain, however, it must be recognised that the total strain state under some conditions may not result in a serviceability limit state being exceeded even though the same strains would be critical when induced by a system of applied stresses. Nevertheless the use of the design chart shown in Figure 8.15 should give a good indication of the criticality of an element with regard to the limit state of cracking under any conditions when the total superimposed state of strain is considered.

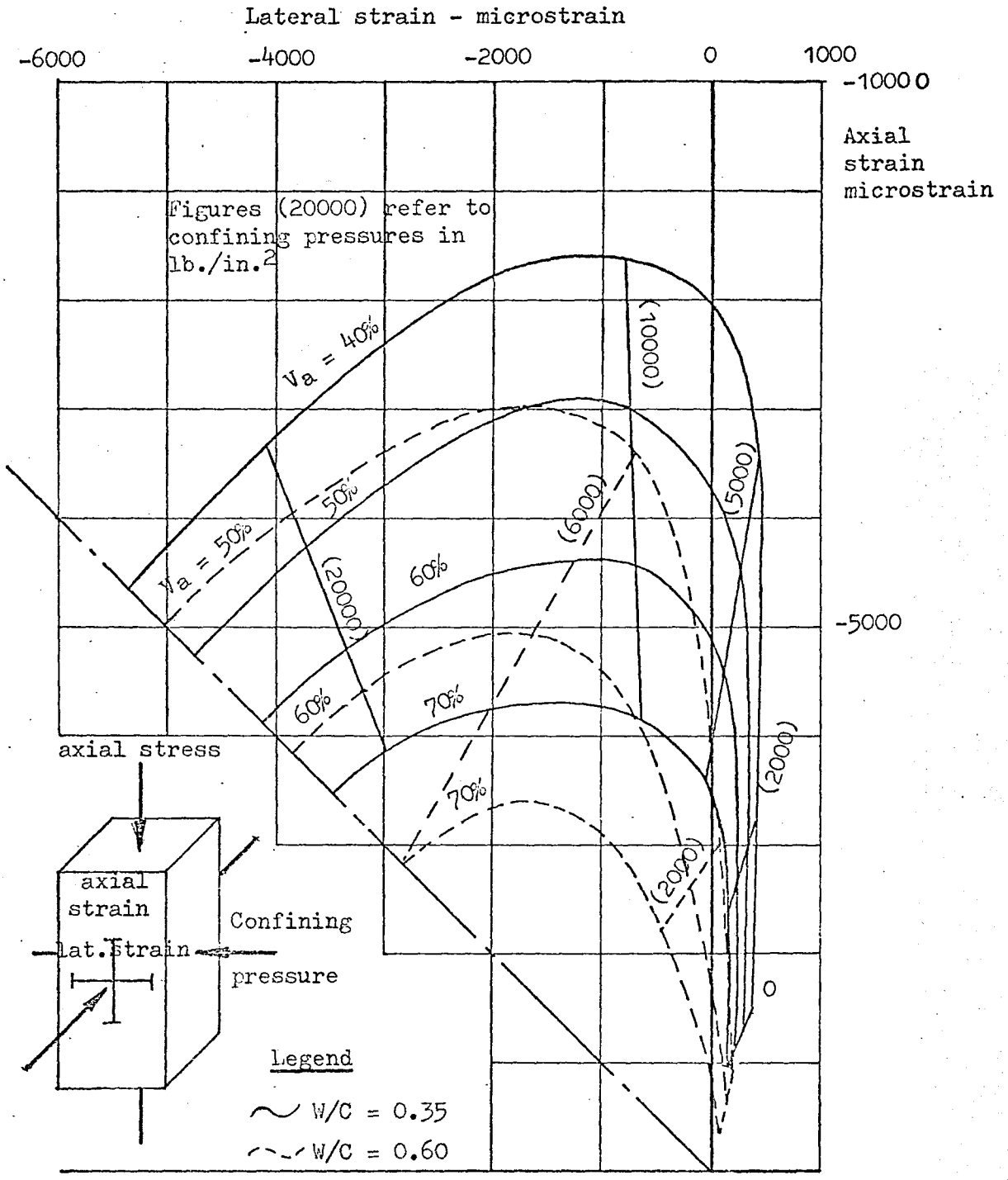


Figure 8.15. Design chart for determining combinations of axial and lateral strain necessary to cause onset of stable fracture propagation under triaxial compression for gravel mortars and concretes.

8.10. Test Programme to establish Design Criteria for a Particular Concrete

The design criteria have been based on a practical range of concrete mixes, and the results are valid within the scope of the experimental data (see Table 8.1.).

In certain cases, more detailed information may be required, or one or more of the various factors affecting the behaviour of concretes under load may be outside the range of validity of the present investigation. Then it could be advantageous to carry out a more detailed test programme in order to establish in detail the behaviour of a particular mix under a special set of conditions and loading regimes. The triaxial equipment and other facilities of the Concrete Materials Research Group at Imperial College are available for this purpose. A typical test programme suitable for providing design criteria for a given set of conditions using monotonically applied load is outlined below.

8.10.1. Specimens

Twenty-one 100 mm. (4") diameter and 250 mm. (10") long suitably prepared cylinders or cores with electrical resistance strain gauges attached to the cylindrical surface to measure axial and circumferential strains.

Three 100 mm. (4") x 100 mm. (4") x 500 mm. (20") 'waisted' prisms for testing under uniaxial tension. (If suitable tensile specimens are not available, then the required data can be estimated by extrapolation from triaxial 'extension' test data.)

8.10.2. Test Details

1. Test three cylindrical specimens under uniaxial compression to obtain the complete deformational behaviour and the ultimate strength σ_c.

2. Test three prisms under uniaxial tension to obtain the complete deformational behaviour and the ultimate strength.

3. Test three cylindrical specimens under triaxial 'compression' and three under triaxial 'extension', using a confining pressure of σ_c, to obtain the complete deformational behaviour and ultimate strength.

4. Repeat (3) using confining pressures of 2 σ_c and 3 σ_c.

Using the analytical techniques described in this thesis, the information obtained from the above tests would be used to determine the envelopes for stresses and strains at onset of stable fracture propagation, onset of unstable fracture propagation and ultimate.

9. PRINCIPAL CONCLUSIONS AND RECOMMENDATIONS FOR FUTURE WORK

9.1. Introduction

The conclusions drawn from the various parts of the analytical and experimental programme have already been given in detail in the appropriate sections of the thesis, and have been used in the formulation of design criteria in Chapter 8. At this stage, it is proposed, therefore, only to summarise the more important conclusions but, in addition to indicate any further work which may be required for their better substantiation.

9.2. Principal Conclusions

9.2.1. Conclusions from Part I

1. A restraint-free state of uniform compressive boundary stress can only be satisfactorily attained using a 'hydraulic' loading technique, provided problems such as extrusion can be overcome.

2. A boundary condition of near-uniform compressive strain, as produced by rigid-platen systems, may induce considerable secondary compressive restraints, particularly in specimens subjected to multiaxial loading conditions.

3. For the case of uniaxial compressive loading, a theoretical analysis of the stress state within specimens loaded through fully restrained boundaries indicates stress disturbances of a lower order than those obtained from experimental methods.

4. Experimental assessment of the stress-state within specimens indicates that the secondary restraint effects under rigid-platen loading may be reduced by:-

   (i) Inserting a suitable intermediate material at the platen/specimen interface of a type which does not tend to extrude under load. The investigations indicate that a 'bedding-down' material, i.e. one which deforms in the axial direction but not significantly laterally, will be most effective in this respect in that it produces a stress state closest to that desired. The use of non-rigid platen systems does not appear to significantly improve conditions. A grease-based friction-reducing material, however, induces a critical condition which

may lead to onset of fracture within the material at an early stage of load.

(ii) Choosing a suitable shape of specimen such that any stress disturbances are dissipated outside the zone within which deformational measurements are made. At the present time it is considered that such an approach will induce the most uniform and definable state of stress within specimens compared with the techniques outlined above.

4. Results from an experimental investigation suggest that rigid-platen loading systems, as used in practice, may also produce a disturbed state of stress or strain within specimens due to:-

(i) lack of flexural stiffness of the platen unit or inability of the spherical seating unit to accommodate initial geometrical imperfections and subsequently lock under load;

(ii) uneven contact between the specimen and platen.

More uniform conditions of stress or strain may be attained provided that (a) the platen/spherical seating unit is correctly designed for overall rigidity; (b) all contact surfaces of both platen and specimen are accurately ground plate and parallel, and (c) the platen cross-sectional area is equal to that of the specimen.

9.2.2. Conclusions from Part II

1. Increasing the degree of heterogeneity of a concrete mix significantly increases the differences in response of material to the conditions of near-uniform boundary stress and near-uniform boundary strain.

2. For the case of concretes with a high degree of heterogeneity under equal biaxial compression, the uniform boundary stress condition induces more critical stress and strain conditions within a specimen. These conditions lead to earlier fracture initiation and propagation, and subsequent loss in strength, than does the case of uniform strain.

For concretes with a low degree of heterogeneity, the differences in behaviour are much less significant.

3. The differences in response of specimens of practical concrete mixes under the two conditions of loading make it essential that these differences be taken into consideration when test data is used for design purposes.

9.2.3. Conclusions from Part III

1. For brittle materials, such as concrete and rocks, distinct stages in the behaviour under load can be detected, the level of stress or strain defining the boundaries to the stages depending on the sensitivity of the detection technique employed.

2. For concrete, three stages of behaviour are evident namely:-

Stage I Stable crack initiation

Localised cracks are initiated at isolated points within the specimen to relieve tensile strain concentrations.

Stage II Stable crack propagation

The initially stable cracks start to propagate in a slow stable manner such that, if the stress is maintained constant, the propagation ceases.

Stage III Unstable crack propagation

The crack system becomes unstable and is terminated by complete disruption of the material even if the stress is maintained constant.

3. The boundaries to the above stages of behaviour can be assessed from an examination of the detailed deformational behaviour of specimens of concrete as follows:-

(i) Onset of Stable fracture propagation (o.s.f.p.)

Defined as the level of stress or strain at which the ratio : increase of maximum principal tensile strain/increase of maximum principal compressive strain (for small increments of applied stress) starts to increase continuously.

(ii) Onset of Unstable fracture propagation (o.u.f.p.)

Defined as the level of stress or strain at which the overall

volumetric strain reaches a minimum value.

4. The above levels of behaviour are proposed as lower and upper definitions of failure. The validity of this approach has been confirmed by tests on concrete under repeated uniaxial compressive loading in which stress levels kept below the lower bound criterion (o.s.f.p.) resulted in no void formation within the material. If the stresses exceeded the upper bound criterion (o.u.f.p.) dilatation occurred and the material completely disrupted after a limited number of loading cycles. For maximum stress levels between the two bounds void formation increased to a certain level and then remained stable with increasing cycles of load.

9.2.4. Conclusions from Part IV

1. The apparatus and techniques developed for testing concretes under triaxial compression enable the complete deformational behaviour of specimens to be measured accurately and with relative simplicity.

2. The testing of concretes with idealised gradings facilitates the determination of patterns of behaviour which assist in the interpretation of results obtained from more practical and hence more complex mixes.

3. The lower and upper bound definitions of failure, as well as the ultimate level, can be easily evaluated for concretes under uniaxial tension, uniaxial compression and triaxial 'compression' stress states. A convenient method of comparing the envelopes defining these levels is by normalising with respect to the uniaxial compression strength.

Stress-strain Relationships

4. The measured stress-strain relationships show concrete to exhibit a gradual transition from relatively 'brittle' to more 'ductile' behaviour as the confining pressure increases.

5. For a given confining pressure, increases in the volume fraction of aggregate cause the axial stress-strain relationships to become steeper.

Volume Changes

6. The variation in volumetric strain with applied stress shows overall

dilatation of the material above a critical stress level (o.u.f.p.). As the confining pressure increases, the decreases in volume prior to the minimum volume (o.u.f.p.) level become larger.

7. For a given confining pressure, increasing the aggregate content, or decreasing the 'effective' water/cement ratio, reduces the rate of volume decrease.

Ultimate

8. The normalised axial stress at ultimate increases with confining pressure, and the relationships for mixes can be adequately represented by a hyperbolic function of the form:-

$$\sigma_{axial}/\sigma_c = \left[A(\sigma_{conf}/\sigma_c)^2 + B(\sigma_{conf}/\sigma_c) + 1\right]^{\frac{1}{2}}$$

where A and B are constants for each mix.

9. For a given volume fraction of aggregate the rate of increase of axial stress with confining pressure is greater for mixes containing larger 'effective' water/cement ratios.

10. The initial rate of increase of axial stress at ultimate is greater for mixes with higher volume fractions of aggregate.

Onset of Unstable Fracture Propagation (o.u.f.p.)

11. The envelopes for strains at o.u.f.p. can be considered as 'unfolded' and 'stretched' versions of the o.s.f.p. envelopes (see 11, 12 and 13 below) except in the case of the limestone concretes.

12. The normalised envelopes for stress at o.u.f.p. are of a form similar to the normalised ultimate envelopes. The axial stress at o.u.f.p., as a proportion of the axial stress at ultimate, increases with confining pressure and decreases with an increase in volume fraction of aggregate or 'effective' water/cement ratio.

13. Onset of Stable Fracture Propagation (o.s.f.p.)

The envelopes for o.s.f.p. are of closed form in stress or strain space, implying that concrete can be significantly disrupted even

under a pure hydrostatic stress if this is above a critical level.

14. For gravel mixes of a given 'effective' water/cement ratio, the envelopes for strains at o.s.f.p. essentially expand in strain space for decreases in volume fraction of aggregate. A decrease in the 'effective' water/cement ratio for a given volume fraction of aggregate also tends to expand the envelopes, but this trend diminishes at low aggregate contents.

15. For gravel mixes normalised envelopes for stress at o.s.f.p. tend to expand in stress space for decreases in 'effective' water/cement ratio for a given volume fraction of aggregate. For a given 'effective' water/cement ratio, increases in the volume fraction of aggregate for rich mixes cause the normalised envelopes to expand in stress space. For lean mixes, however, the behaviour is more complex since an increase in the volume fraction of aggregate increases the normalised axial stress at higher confining pressures but decreases for pressures below a critical value.

16. The shape of the envelopes for stress at o.s.f.p. is of the same basic pattern for concretes containing granite and limestone aggregates as for those containing gravel aggregates. For a given volume fraction of aggregate the normalised axial stress at o.s.f.p., for a given normalised confining pressure, is highest for gravel and lowest for granite, probably due to the differences in shape and elastic moduli of the aggregates. The corresponding strains at o.s.f.p. are essentially the same for both limestone and granite concretes but are slightly higher than for the corresponding gravel mix.

9.2.5. Conclusions from Part V

1. It is proposed that the lower bound criterion for failure (o.s.f.p.) level be considered as the limit state for cracking and the upper bound (o.u.f.p.) as the ultimate limit.

2. Using the information for triaxial 'compression' tests obtained in Part V, together with preliminary data on the behaviour under triaxial 'extension' states of stress, design charts have been

constructed to enable the criticality of any multiaxial stress state to be assessed with reference to the upper and lower bound failure criteria.

9.3. Recommendations for Future Work

9.3.1. Introduction

As is inevitable with a project of this nature, many questions have been answered in a relatively superficial manner. The resulting answers have led to the production of yet more queries which require further investigation. These main areas which would benefit from more detailed studied are outlined in the following.

9.3.2. The Stress State induced within Specimens under Load

9.3.2.1. Analytical Investigations (see 2.5.)

The analyses have been carried out using conditions of plane strain (or plane stress) and assumptions of linear elasticity. Such a restrictive approach has led to the production of apparently unrealistic solutions when compared with experimental data, and has suggested only general trends in behaviour. A more realistic approach could be made by the use of a non-linear, three-dimensional computational method. Such a technique is, in fact, at the development stage [224] following suggestions made by the Author, and could be employed to analyse the effect of differing degrees of boundary restraint and discontinuous behaviour of the material.

9.3.2.2. Experimental Investigation (see 2.6)

Surface-mounted strain gauges have been used to evaluate the stress state within specimens and such a technique has necessitated the use of a relatively homogeneous mortar specimen. The results, therefore, need to be verified for a concrete containing coarser aggregate, since it is likely that such a heterogeneous material will respond in a different way to the various boundary conditions considered. This will preclude the use of surface mounted gauges which may not, in any case, accurately reflect conditions within the material, and other techniques of measurement must be considered. One technique, which may help to solve the problem, is that developed at Cambridge [225, 226] based on the radiographic detection of points located at various positions within the material, provided small deformations can be monitored with such a system.

If such a technique does not prove suitable then, in the short-term, recourse must be made to directly comparing the deformational response and strength characteristics of specimens under given loading conditions using different testing methods (see 9.3.3.). This will indicate the extent of the problem and allow the effect of the difference in data to be evaluated with regard to their use as design information.

9.3.3. Response of Concretes of Different Degrees of Heterogeneity to Boundary Conditions of Near-Uniform Stress and Near-Uniform Strain (see Chapter 3)

The investigation has been carried out using only one type of loading configuration, namely equal biaxial compression. Such a stress state has been adopted since it is considered that no satisfactory apparatus has been developed to induce more general states of near-uniform boundary stress with the same degree of precision as the hydraulic cell available.

It is recognised that other loading systems exist which are claimed to apply more generalised but definable states of near uniform boundary stress and strain. The Author has suggested (at the RILEM International Conference at Cannes in 1972) that it would be valuable to initiate a comprehensive testing programme in which these systems could be compared. As a result, details of such a programme have been proposed by the University of Colorado [227] in which it is intended to use the following types of apparatus:

Hydraulic Triaxial Cell	-	Concrete Materials Research Group, Imperial College, London, S.W.7.
Fluid Cushion Cubical Test Cell	-	University of Colarado, Boulder, U.S.A.
Rigid Platen Cubical Test Apparatus	-	New Mexico State University, Las Cruces, U.S.A.
Brush Platen Cubical Test Apparatus	-	Technical University, Munich.

The Concrete Materials Research Group has agreed to cooperate in this work which will include measurement of the complete deformational behaviour of a given type of concrete under various states of multiaxial compression.

9.3.4. Detection of Fracturing Events (see 4.5.4.3.)

A pilot series of tests performed in order to detect discrete cracking events occurring within concrete specimens under load using an ultrasonic translator detector proved extremely successful, even with the limited amount of development work which could be carried out.

It is considered that, if more information is available from the use of such techniques, it would provide a clearer understanding of the distribution of fracturing events which would be of assistance in the formulation of statistical theories of failure [228, 229].

9.3.5. Influence of Loading Pattern on Various Stages of Material Behaviour (see Chapter 5)

In a series of pilot tests a link has been established between the stages of behaviour of concrete under short-term monotonic and repetitive loading for the case of uniaxial compression. For design purposes it is necessary to extend such an investigation in order to establish similar relationships for other loading regimes. Under the Author's direction work is already in progress to study the behaviour under triaxial 'compression' and 'extension' states of stress [21].

9.3.6. Behaviour of Concrete under Multiaxial Stress States (see Chapter 7)

The behaviour of mature concretes has been investigated under short-term monotonically increasing triaxial 'compressive' states of stress, using idealised mixes as well as mixes at each end of a range of practical concretes to enable interpolation to be used for assessing the behaviour of intermediate cases. Although a considerable amount of data has been obtained it is necessary to extend the work to conditions of triaxial 'extension' and compression-compression-tension in order to more fully define the various design envelopes postulated. Under the Author's direction a test programme to achieve this has already started [21] and preliminary results have been introduced into the proposed design criteria.

The necessity of investigating the influence of more mix and environmental parameters in order to improve the validity of the design data has been outlined in Chapter 8. It is considered that the most important of these are: degree of maturity of the concrete, moisture conditions within specimens, and temperature and humidity of the environment.

REFERENCES

1 BRITISH STANDARDS INSTITUTION. Methods for Sampling and Testing of Mineral Aggregates, Sands and Fillers. B.S. 812 : 1967.

2 BRITISH STANDARDS INSTITUTION. The Structural Use of Concrete. C.P. 110 Part 1 1972.

3 LACHANCE L. The Effect of End Restraint, Shape and Size on the Elastic Properties and Failure Characteristics of Concrete Specimens under Compression. M.Sc. Thesis. University of London 1962.

4 SIGVALDASON O.T. Failure Characteristics of Concrete. Ph.D. Thesis University of London 1965.

5 ANSON M. An Investigation into a Hypothetical Deformation and Failure Mechanism for Concrete. Ph.D. Thesis. University of London 1962.

6 WARD M.A. The Testing of Concrete Materials by Precisely Controlled Uniaxial Tension. Ph.D. Thesis. University of London 1964.

7 ROBINSON G.S. The Failure Mechanism of Concrete with Particular Reference to the Biaxial Compressive Strength. Ph.D. Thesis. University of London 1964.

8 VILE G.W.D. Behaviour of Concrete under Simple and Combined Stresses Ph.D. Thesis. University of London 1965.

9 NEWMAN K. The structure and engineering properties of concrete. Proceedings of International Symposium on Theory of Arch Dams. Southampton 1964.

10 BROWNE R.D. Properties of concrete in reactor vessels. Conference on Prestressed Concrete Pressure Vessels. Institution of Civil Engineers. London 1968.

11 THORP D.E. Elastic analysis of Dungeness B vessel. Conference on Prestressed Concrete Pressure Vessels. Institution of Civil Engineers. London 1968.

12 LANGAN D. Correlation between theory and experiment - Wylfa Vessel. Conference on Prestressed Concrete Pressure Vessels. Institution of Civil Engineers, London 1968.

13 CEMENT AND CONCRETE ASSOCIATION The Structure of Concrete and its Behaviour under Load : Proceedings of an International Conference. London 1965. Cement and Concrete Association. London 1968.

14 McCREATH D.R. The Fracture Mechanisms of Concrete. Ph.D. Thesis. University of London 1968.

15 PIGEON M. The Process of Crack Initiation and Propagation in Concrete. M.Phil. Thesis. University of London 1969.

16 NEWMAN J.B. and NEWMAN K. Interim Report on Civil Engineering Research Association Contract 1965-1967. Concrete Materials Research Group, Concrete Structures and Technology Section, Imperial College. London. May 1967.

17 NEWMAN J.B. and NEWMAN K. Progress Report on C.I.R.I.A. Contract 1968-1970. Concrete Materials Research Group, Concrete Structures and Technology Section, Imperial College, London. September 1968.

18 NEWMAN J.B. and NEWMAN K. Progress Report on C.I.R.I.A. Contract 1968-1970. Concrete Materials Research Group, Concrete Structures and Technology Section, Imperial College, London. May 1970.

19 NEWMAN K. and NEWMAN J.B. Failure Theories and Design Criteria for Plain Concrete. Proceedings of the International Conference on Structure, Solid Mechanics and Engineering Design, Southampton 1969. pp. 963-995.

20 NEWMAN J.B. and NEWMAN K. The Cracking and Failure of Concrete under Combined Stresses and its Implications for Structural Design. R.I.L.E.M. International Symposium on the Deformation and the Rupture of Solids subjected to Multiaxial Stresses. Cannes 1972.

21 COTSOVOS M. Failure Criteria for Concrete under Generalised Stress States. Ph.D. Thesis (to be published) University of London.

22 FILON L.N.G. On the Elastic Equilibrium of Circular Cylinders under certain Practical Systems of Load. Phil. Trans. of Royal Society. Series A Vol. 798 1902. pp. 147-233.

23 CONWAY J.C. An Investigation of the Stress Distribution in a Circular Cylinder under Static Compressive Load for Varying Boundary Conditions. M.Sc. Thesis. Pennsylvania State University, Department of Mining. September 1963. pp. 1-201.

24 GOODIER J.N. Compression of Rectangular Blocks, and the Bending of Beams by Non-Linear Distributions of Bending Forces. Trans. A.S.M.E. Vol. 54. 1932. pp. 173-183.

25 TIMOSHENKO S.P. and GOODIER J.N. Theory of Elasticity. McGraw-Hill 3rd Edition 1970. pp. 567.

26 PICKETT G. Application of the Fourier Method to the Solution of Certain Boundary Problems in the Theory of Elasticity. Journal of Appl. Mech. Vol. 11 No. 3, September 1944. pp. A176-A182.

27 D'APPOLONIA E and NEWMARK N.M. A Method for Solution of the Restrained Cylinder under Axial Compression. Proc. First U.S. Nat. Congress of Appl. Mech. A.S.M.E. Chicago 1951. pp. 217-226.

28 GREENBERG H.J. and TRUELL R. On a Problem in Plane Strain. Quart. of Appl. Math. Vol. 6 1948. pp. 53-62.

29 EDELMAN F. On the Compression of a Short Cylinder between Rough End Blocks. Quart. of Appl. Math. Vol 7, No. 3 1949. pp. 334-337.

30 PRENTIS J.M. On the Compression of a Cube between Rigid Rough End Plates. Quart. J. Mech. and Appl. Math. Vol. 5 Part 2 1952. pp. 253-256.

31 LISOWSKI A. Failure Types of Rock Cubic Specimens in the Light of the Theory of Elasticity. Bull. de L'academie Polonaise des Sciences Sene des Sciences Techniques. Vol. 7, No. 5 1959. pp. 341-351.

32 BALLA A. Stress Conditions in Triaxial Compression. Journ. of the Soil Mechs. and Foundns. Div. Proc. A.S.C.E. Vol. 86 SM6 December 1960. pp. 57-84.

33 BALLA A. A New Solution of the Stress Conditions in Triaxial Compression. Acta Technica Academiae Scientianum Hungaricae Vol. 28 No. 3-4 1960. pp. 349-387.

34 HODGKINS W.R. A Numerical Solution of the End Deformation Problem of Cylinders. U.K.A.E.A. The Reactor Group T.R.G. Report 294 (S) 1962.

35 HILSDORF H. Versuchstechnische Probleme beim Studium der Zweiachsigen Festigkeit des Betons (Testing Technique Problems in the Study of the Biaxial Strength of Concrete). Bericht Nr. 41 1965. Materialprufungsamt fur das Bauwesen de Technischen Hochschule, Munchen.

36 NIWA Y. and KOBAYASHI S. Stresses in Rectangular Blocks Compressed between Rough Plates. Kyoto University, Memoirs of the Faculty of Engineering, Vol. 28, Part 3 1966. pp. 244-253.

37 NIWA Y., KOBAYASHI S. and NAKAGAWA K. The Influence of End Frictions on Stresses in Compressed Specimens. Memoirs of the Faculty of Engineering, Kyoto University, Vol. XXXI, Part 1. January 1969. pp. 1-11.

38 KOSAKA Y., TANIGAWA Y. and HAYASHI C. Effect of End Condition of Concrete Specimen on Stress-Distribution under Uniaxial Compression. Personal communication.

39 GIRIJAVALLABHAN C.V. and MEHTA K.C. Stress-Strain Relationship from Compression Tests on Non-linear Materials. Proc. of Symposium on Applications of Finite Element Methods in Civil Engineering. A.S.C.E. November 1969. pp. 457-480.

40 PENG S.D. Stresses within Elastic Circular Cylinders loaded Uniaxially and Triaxially. Int. Journ. of Rock Mechs. and Min. Science. Vol. 8 1971. pp. 399-432.

41 BRADY B.T. Effects of Inserts on the Elastic Behaviour of Cylindrical Materials loaded between Rough End-Plates. Int. Journ. Rock Mechs. and Min. Science. Vol. 8 1971. pp. 357-369.

42 GREEN G.E. Strength and Compressibility of Granular Materials under generalised strain conditions. Ph.D. Thesis. University of London 1969.

43 BRADY B.T. Initiation of Failure in a Radially End-constrained Circular Cylinder of Brittle Rock. Int. Journ. Rock Mechs. and Min. Science. Vol 8, No. 5 1971. pp. 371-387.

44 McCLINTOCK F.A. and WALSH J.B. Friction on Griffith Cracks in Rock under Pressure. Proc. 4th Inter. Cong. Appl. Mechs. Berkeley, 1962. A.S.M.E. 1963. pp. 1015-1021.

45 COKER E.G. Polarised Light and its Applications to Engineering. Proc. Roy. Inst. of G.B. Vol. 21 1914-1916. pp. 573-599.

46 COKER E.G. and FILON L.N.G. Revised by JESSOP H.T. A Treatise on Photoelasticity - 2nd Edition. Cambridge Univ. Press 1957. 720 pp.

47 FROCHT M.M. Photoelasticity - Volume II. Wiley 1948. 505 pp.

48 DURELLI A.J. Distribution of Stresses in Partial Compression and a New Method of Determining the Isostatics in Photoelasticity. Proc. 13th Semi-Annual Photoelasticity Conf. Mass. Inst. Tech. 1941. pp. 25-50.

49 PARROTT L.J. An Improved Apparatus for Biaxial Loading on Concrete Specimens. Journ. of Strain Analysis. Vol. 5 No. 3 1970. pp. 169-176.

50 SELDENRATH T. and GRAMBERG J. Stress-Strain Relations and Breakage of Rocks. Mech. Props. of Non-Metallic Brittle Materials. Ed. Walton Interscience Inc. 1958. pp. 79-105.

51 HUGHES B.P. and BAHRAMIAN B. Cube Tests and the Uniaxial Compressive Strength of Concrete. Mag. of Conc. Res. Vol. 17 No. 53. Dec. 1965. pp. 177-182.

52 JORDAAN I.J. and ILLSTON J.M. A Creep Rig for Testing Concrete under Multiaxial Compressive Stress. Mag. of Conc. Res. Vol. 20 No. 65 Dec. 1968. pp. 235-239.

53 BEAK M. Steel Brush Platens for Elimination of Lateral Restraint on Compressive Strength Specimens. Min. of Pub. Buildings and Works. B.R.S. Internal Note ZN 43/70.

54 ROBINSON G.S. and VILE G.W.D. Investigation into the Restraint Effects of Loading Platens with Various Low Friction Materials. Concrete Structures and Technology, Report No. 15, Imperial College, London, (unpublished).

55 UNIVERSITY OF WALES, SWANSEA. Finite Element Solution System (FESS) Centre for Numerical Methods in Engineering, Dept. of Civil Engineering. November 1967. Personal Communication.

56 HOGGER C.J. A General Contouring Package for the CALCOMP Plotter. D.I.C. Thesis. Dept. of Computing and Control, Imperial College, 1971.

57 McCREATH D.R., NEWMAN J.B. and NEWMAN K. The Influence of Aggregate Particles on the Local Strain Distribution and Fracture Mechanism of Cement Paste During Drying Shrinkage and Loading to Failure. R.I.L.E.M. Colloquium, Munich, April 1968.

58 STAYNES B.W. Epoxide Resin Concrete as a Structural Material with special reference to the Limit State Design Philosophy. Ph.D. Thesis Univ. of London, 1972.

59 GRASSAM N.S.J. and FISHER D. Tests on Concrete with Electrical Resistance Strain Gauges. Engineering, Vol. 172 No. 4469. September 1951. pp. 356-358.

60 BINNS R.D. and MYGIND H.S. Use of Electrical Resistance Strain Gauges, and Effect of Aggregate Size on Gauge Length in connection with Testing of Concrete. Mag. of Conc. Res. Vol. 1, No. 1. January 1949. pp. 35-39.

61 COOKE R.W. and SEDDON A.E. The Laboratory Use of Bonded-wire Electrical Resistance Strain Gauges at the Building Research Station. Mag. of Conc. Res. No. 22, March 1956. pp. 31-38.

62 BRITISH STANDARDS INSTITUTION. Methods of Testing Concrete for Strength. B.S. 1881. Part 4, 1970.

63 CONCRETE SOCIETY. Main Clauses for inclusion in a Standard for Concrete Cube Compression Testing Machines. 3rd Report of a Concrete Society Working Party 1972. 10 pp.

64 BISHOP A.W. and HENKEL D.J. The Measurement of Soil Properties in the Triaxial Test. Arnold. 2nd Edition. London 1962.

65 BELLAMY C.J. Strength of Concrete under Combined Stress. Journ. Amer. Conc. Inst. October 1961.

66 RICHART F.E., BRANDTZAEG A. and BROWN R.L. A Study of the Failure of Concrete under Combined Compressive Stresses. Univ. of Illinois Eng. Expt. Stn. Bulletin No. 185, November 20th 1928.

67 CHINN J. and ZIMMERMAN R.M. Behaviour of Plain Concrete under Various High Triaxial Compression Loading Conditions. Res. and Tech. Div. Air Force Weapons Lab. Air Force Systems Command, Kirtland A.F.B., New Mexico. Tech. Rep. No. WLTR 64-163.

68 WASTLUND G. Nya ron Angaende Betongens Grundlaggande Hall fast Hetsegenskaper (New Evidence regarding the Basic Strength Properties of Concrete). Betong, Heft 3, 1937. pp. 189-205.

69 WEIGLER H. and BECKER B. Uber das Bruck-und Verformungsverhalten von Beton bei Mehrachsiger Beanspruchung. Bauingenieur. Vol. 36, Heft. 10. October 1961. pp. 390-396.

70 WEIGLER H. and BECKER B. Untersuchungen uber das Bruch-und Verformungsoerhalten von beton bei Zweichsiger Beanspruchung. (Investigation into Strength and Deformation Properties of Concrete subjected to Biaxial Stresses). Deutscher Ausschus fur Stahlbeton. Heft 157. Berlin 1963.

71 OPITZ H. Festigkeit und Verformungseigenschaftendes Betons bei Zweiachsiger Druckbeanspruchung (Strength and Deformation Properties of Concrete under Biaxial Compressive Loading). Proc. of Inter. Colloquium Festigkeitsprobleme des Betons, Dresden, June 1968. pp. 1520-1523.

72 KUPFER H., HILSDORF H.K. and RUSCH H. Behaviour of Concrete under Biaxial Stresses. Journ. Amer. Conc. Inst. Proc. V 66 No. 8. Aug. 1969. pp. 656-666.

73 MILLS L.L. and ZIMMERMAN R.M. Compressive Strength of Plain Concrete under Multiaxial Loading Conditions. Journ. Amer. Conc. Inst. Proc. Vol. 67 No. 10. October 1970. pp. 802-807.

74 KOBAYASHI S. and KOYANAGI W. Fracture Criteria of Cement Paste, Mortar and Concrete subjected to Multiaxial Compressive Stresses. R.I.L.E.M. Int. Symp. The Deformation and the Rupture of Solids subjected to Multiaxial Stresses. Cannes, October 1972. Vol. I. pp. 131-148.

75 STEGBAUER A. and LINSE D. Comparison of Stress-Strain Behaviour of Concrete and other Materials under Biaxial Loading. Proc. R.I.L.E.M. Int. Symp. The Deformation and the Rupture of Solids subjected to Multiaxial Stresses. Cannes, October 1972, Vol. I. pp. 229-243.

76 VILE G.W.D. Combined Stress Testing Machine for Concrete. The Engineer, July 1965.

77 SABNIS G.M. and ARONI S. Size Effects in Material Systems and the State of the Art. Proc. Int. Conf. Structure Solid Mechs. in Eng. Design. Southampton 1969. pp. 131-142.

78 HUGHES B.P. and ASH J.E. Some factors Influencing the Long-Term Strength of Concrete. R.I.L.E.M. Materiaux et Constructions. No. 14, Vol. 3. March/April 1970. pp. 81-84.

79 ANSON M. and NEWMAN K. The Effect of Mix Proportions and Methods of Testing on Poisson's Ratio for Mortars and Concretes. Mag. Conc. Res. Vol. 16, No. 47. June 1964. pp. 73-82.

80 NELISSEN L.J.M. Biaxial Testing of Normal Concrete. Heron (Delft) Vol. 18, No. 1. 1972.

81 ADAMS L.H. and WILLIAMSON E.D. The Compressibility of Minerals and Rocks at High Pressure. Journ. Franklin Inst. No. 195. 1923. pp. 475-529.

82 WALSH J.B. The Effect of Cracks on the Compressibility of Rock. Journ. Geophys. Res. Vol. 70, No. 2. January 1965. pp. 381-389.

83 BIRCH F. The Velocity of Compression Waves in Rocks to 10 Kb. Journ. Geophys. Res. No. 65, 1960. pp. 1083-1102. Journ. No. 66 1961. pp. 2199-2224.

84 BRIDGMAN P.W. Volume Changes in the Plastic Stages of Simple Compression. Journ. Applied Phys. Vol. 20, December 1949. pp. 1241-1251.

85a MATSUSHIMA S. On the Flow and Fracture of Igneous Rocks. Kyoto Univ. Disaster Prevention Res. Inst. Bull. 36. 1960. pp. 2-9

85b MATSUSHIMA S. On the Deformation and Fracture of Granite under High Confining Pressure. Kyoto Univ. Disaster Prevention Res. Inst. Bull. No. 36. 1960. pp. 11-20.

86 HANDIN J., HAGER R.V., FRIEDMAN M. and FEATHER J.N. Experimental Deformation of Sedimentary Rocks under Confining Pressure - Pore Pressure Tests. Bull. Amer. Assn. Petrol. Geologists. No. 47, 1963. pp. 717-735

87 MATSUSHIMA S. Variation of the Elastic Wave Velocities of Rocks in the Process of Deformation and Fracture. Kyoto Univ. Disaster Prevention Res. Inst. Bull. No. 32, 1960. pp. 1-8.

88 BRACE W.F. and BOMBOLAKIS E.G. A Note on Brittle Crack Growth in Compression. Journ. Geophys. Res. 68, No. 12. 1963. pp. 3709-3713.

89 COOK N.G.W. and HODGSON K. Some Detailed Stress-Strain Curves for Rock. Journ. Geophys. Res. Vol. 70, No. 2. June 1965. pp. 1883-2888.

90 HOEK E. Rock Fracture under Static Stress Conditions. Nat. Mech. Res. Inst. C.S.I.R.O. Pretoria, South Africa. Report MEG 383, October 1965.

91 MURRELL S.A.F. The Effect of Triaxial Stress Systems on the Strength of Rocks at Atmospheric Temperatures. Geophys. Journ. Royal Astr. Soc. No. 10. 1965. pp. 231-281.

92 BRACE W.F., ORANGE A.S. and MADDEN T.R. The Effect of Pressure on the Electrical Resistivity of Water-Saturated Crystalline Rocks. Journ. Geophys. Res. Vol. 70, No. 22. November 1965. pp. 5669-5678.

93 BRACE W.F. and ORANGE A.S. Electrical Resistivity Changes in Saturated Rock under Stress. Science Vol. 153, No. 3742. Sept. 1966. pp. 1525-1526.

94 BRACE W.F., PAULDING B.W. and SCHOLZ C. Dilatency in the Fracture of Crystalline Rocks. Journ. Geophys. Res. Vol. 71, No. 16. August 1966. pp. 3939-3953.

95 BRACE W.F. and BYERLEE J.D. Recent Experimental Studies of Brittle Fracture of Rocks. Failure and Breakage of Rock - Proc. 8th Symp. on Rock Mechanics. Minnesota, September 1966. pp. 58-81.

96 BIENIAWSKI Z.T. Mechanism of Brittle Fracture of Rock - Parts 1, 2 and 3. C.S.I.R.O. Pretoria, South Africa. Reports MEG 520, 521, 522. January 1967.

97 SCHOLZ C. Microfracturing and the Inelastic Deformation of Rock in Compression. Journ. Geophys. Res. 73. 1968. pp. 1417-1432.

98 BARRON K. The Fracture of Brittle Rocks around Mine Openings. Canadian Dept. of Energy, Mines and Mineral Reserves, Mining Res. Centre Int. Rep. MR/69/25 LD. November 1969.

99 RICHART F.E., BRANDTZAEG A. and BROWN R.L. The Failure of Plain and Spirally Reinforced Concrete in Compression. Univ. of Illinois, Eng. Expt. Stn. Bull. No. 190, April 2nd 1929.

100 RICHART F.E. and BROWN R.L. An Investigation of Reinforced Concrete Columns. Univ. of Illinois, Eng. Expt. Station Bull. No. 267. June 1934.

101 THOMAS F.G. Cracking in Reinforced Concrete. The Structural Engineer Vol. 14, No. 7. 1936. pp. 298-320.

102 CARLSON R.W. Attempts to Measure the Cracking Tendency of Concrete. Proc. A.C.I. Vol. 36, 1940. pp. 533-537.

103 EVANS R.H. Extensibility and Modulus of Rupture of Concrete. The Structural Engineer, Vol. 24, No. 12. 1946. pp. 636-659.

104 BERG O.Y. The Problem of Strength and Elasticity of Concrete. Proc. Acad. of Sci. of U.S.S.R. Vol. 70, No. 4. 1950. pp. 617-620.

105 HOGNESTAD E. A Study of Combined Bending and Axial Load in Reinforced Concrete Members. Univ. of Illinois, Eng. Expt. Stn. Bull. No. 399, November 1951. pp. 62.

106 HOGNESTAD E., HANSON N.W. and McHENRY D. Concrete Stress Distribution in Ultimate Strength Design. Journ. Amer. Conc. Inst. Proc. Vol. 52, No. 4. Dec. 1955. pp. 455-479.

107 JONES R. A Method of Studying the Formation of Cracks in a Material subjected to Stress. Brit. Journ. App. Phys. Vol. 3, No. 7. July 1952. pp. 229-232.

108 BLAKEY F.A. and BERESFORD F.D. Tensile Strains in Concrete: Parts 1 and 2. Aust. Div. Build. Res. Reports C2.2-1 1953. C2.2-2 1955

109 BLAKEY F.A. and BERESFORD F.D. A Note on Strain Distribution in Concrete Beams. Civ. Eng. and P.W.R. Vol. 50, No. 586, April 1955. pp. 415-416.

110 TODD J.D. The Determination of Tensile Stress-Strain Curves for Concrete. Proc. I.C.E., Vol. 4, Part 1, No. 2. March 1955. pp. 201-211.

111 JONES R. and KAPLAN M.F. The Effect of Coarse Aggregate on the Mode of Failure of Concrete in Compression and Flexure. Mag. Conc. Res. Vol. 9, No. 26. August 1957. pp. 89-94.

112 DANTU P. Etude des Contraintes dans les Milieux Heterogenes. Application au Beton. (Study of the Stresses in Non-Homogeneous Materials and its Application to Concrete). Annales de l'Institut Technique du Batiment et des Travaux Publics. Vol II, No. 121, January 1958. pp. 55-77.

113 DANTU P. A Study of the Distribution of Stresses in a Two-Component Heterogeneous Medium. Symp. on Non-Homogeneity and Plasticity in Concrete, Warsaw. September 1958. pp. 443-451.

114 RUSCH H. Physical Problems in the Testing of Concrete. Zement-Kalk-Gips. Vol. 12, No. 1. January 1959. pp. 1-9. (C. and C.A. Lib. Trans. No. 86, 1960).

115 GLUCKLICH J. The Influence of Sustained Loads on the Strength of Concrete. R.I.L.E.M. Bull. No. 5. December 1959. pp. 14-17.

116 HANSEN T.C. Creep and Stress Relaxation of Concrete (Chapter 6 - Plastic Flow and Creep of Concrete at High Overload). Proc. Swedish Cem. and Con. Res. Inst. Stockholm. No. 31, 1960. pp. 90-97.

117 HSU T.T.C., SLATE F.O., STURMAN G.M. and WINTER G. Microcracking of Plain Concrete and the Shape of the Stress - Strain Curve. Journ. Amer. Conc. Inst. Proc. Vol. 60, NO. 2. February 1963. pp. 209-224.

118 SLATE F.O. and OLSEFSKI S. X-Rays for Study of Internal Structure and Microcracking of Concrete. Journ. Amer. Conc. Inst. Proc. Vol. 60, No. 5. May 1963. pp. 575-588.

119 KAPLAN M.F. Strains and Stresses of Concrete at Initiation of Cracking and Near Failure. Journ. Amer. Conc. Inst. Proc. Vol. 60, No. 7. July 1963. pp. 853-879.

120 OLADAPO I.O. Cracking and Failure in Plain Concrete Beams. Mag. of Conc. Res. Vol. 16, No. 47. June 1964. pp. 103-110.

121 YOKOMICHI H., MATSUOKA K. and TAKADA N. Some Tests on Cracking of Concrete (On elastic wave of cracking of concrete). J.C.E.A. Review of XIX Gen. Meeting 1964. pp. 246-249. (Review of XVIII Gen. Meeting 1964. pp. 163-166).

122 RJETZ W. The Two Different Physical Mechanisms of Creep in Concrete. Proc. Int. Conf. on the Structure of Concrete and its Behaviour under Load, London, September 1965. pp. 146-153.

123 ILLSTON J.M. The Creep of Concrete under Uniaxial Tension. Mag. of Conc. Res. Vol. 17, No. 51. June 1965. pp. 77-84.

124 ISENBERG J. A Study of Cracks in Concrete by X-Radiography. R.I.L.E.M. Bull. No. 30, March 1966. pp. 107-115.

125 DESAYI P. and SEN B.R. An Investigation on the Prediction of Creep and True Ultimate Strength of Concrete. Indian Conc. Journal, Vol. 40, Nos. 4 and 6. April/June 1966. pp. 134-141, 248-256.

126 DESAYI P. and VISWANATHA C.S. True Ultimate Strength of Plain Concrete R.I.L.E.M. Bull. Series No. 36. September 1967. pp. 163-173.

127 SHAH, S.P. and WINTER G. Inelastic Behaviour and Fracture of Concrete. Journ. Amer. Conc. Inst. September 1966. Proc. V.63, No. 9. pp. 925-930.

128 BERES L. Investigation on Structural Loosening of Compressed Concrete. R.I.L.E.M. Bulletin No. 36, September 1967, pp. 185-190.

129 HUGHES B.P. and BAHRAMIAN B. Some Factors Affecting the Compressive Strength of Concrete. Mag. of Conc. Res. Vol. 19, No. 60. Sept. 1967. pp. 165-172.

130a HUGHES B.P. and ASH J.E. The Effect of Water-Gain on the Behaviour of Concrete in Tension, Torsion and Compression. The Concrete Society Technical Paper PCS 54, November 1969. 17 pp.

130b HUGHES B.P. and ASH J.E. Water Gain and its Effects on Concrete. Concrete. December 1969. pp. 494-496.

131 STROEVEN P. Poisson's Ratio in Uniaxial Tension and Anticlastic Bending of Microconcrete and Perspex. Heron (Delft). Vol. 17, No. 3. 1970. 23 pp.

132 STEPHEN R.M. and PIRTZ D. Application of Birefringent Coating to the Study of Strains around Circular Inclusions in Mortar Prisms. Proc. S.E.S.A. Vol 20, No. 1. pp. 91-97.

133 KEETON J.R. Photoelastic Determination of Strain Distribution in Cement Paste, Mortars and Concrete. U.S. Naval Civ. Eng. Lab. Port Hueneme. California. Tech. Rep. No. R.404. November 1965.

134 SWAMY R.N. Aggregate-Matrix Interaction in Concrete Systems. Int. Conf. on Struct., Solid Mechs. and Eng. Design. Southampton 1969. Wiley 1971. pp. 301-315.

135 GRIFFITH A.A. The Phenomena of Rupture and Flow in Solids. Phil. Trans. Roy. Soc. Series A. Vol. 221. 1921. pp. 163-198.

136 COOK J. and GORDON J.E. A Mechanism for the Control of Crack Propagation in All-Brittle Systems. Proc. Royal Soc. Series A. No. 1391, Vol. 282. Dec. 1964. pp. 508-520.

137 RUSCH H. Researches toward a General Flexural Theory for Structural Materials. Journ. Amer. Conc. Inst. Proc. Vol. 57, No. 1. July 1960. pp. 1-27.

138 SHAH S.P. and CHANDRA S. Fracture of Concrete Subjected to Cyclic and Sustained Loading. Univ. of Illinois, Dept. of Materials Eng., Rep. No. 69-4. June 1969.

139 De JOLY. Cited in:- Mills R.E. and Dawson R.F. 'Fatigue of Concrete' Proc. 7th Annual Meeting, Highway Res. Board. December 1927. pp. 160-172.

140 VAN ORNUM J.L. Fatigue of Concrete. Trans. A.S.C.E. Vol. 58, 1907. pp. 294-320.

141 GRAF. O. and BRENNER E. Versuch zur Ermittlung der Widerstandsfahigkeit von Beton gegen Oftmals Wiederholte Druckbelastung. (Studies of the Resistance of Concrete to frequently repeated Compressive Loads). Deutscher Ausschuss fur Eisenbeton. Bull. No. 76. 1934.

142 ANTRIM J. de C. and McLAUGHLIN J.F. Fatigue Study of Air Entrained Concrete. Journ. of Amer. Conc. Inst. Proc. Vol. 55, No. 11. May 1959. pp. 1173-1182.

143 GRAY W.H., McLAUGHLIN J.F. and ANTRIM J. de C. Fatigue Properties of Lightweight Aggregate Concrete. Journ. Amer. Conc. Inst. Proc. Vol. 58, No. 2. August 1961. pp. 149-162.

144 L'HERMITE R. What do we know about the Plastic Deformation and Creep of Concrete? R.I.L.E.M. Bull. No. 1, March 1969. pp. 21-51.

145 BENNET E.W. and RAJU N.K. Cumulative Fatigue Damage of Plain Concrete in Compression. Int. Conf. on Structure, Solid Mechs. and Engineering Design. Southampton 1969, Wiley 1971. pp. 1089-1102.

146 YOKOMICHI H., MATSUOKA K. and NOBUKUKI T. Some Tests on Cracking of Concrete. J.C.E.A. Review of XIX General Meeting 1964. pp. 246-249.

147 BERES L. Relationship of Deformational Processes and Structure Changes in Concrete. Int. Conf. on Struct. Solid Mechs. and Eng. Design. Southampton 1969. Paper No. 60.

148 HILSDORF H. and KESLER C.E. The Behaviour of Concrete in Flexure under Varying Repeated Loads. Univ. of Illinois T. and A.M. Report No. 172. 1960. pp. 147.

149 SHAH S.P. and WINTER G. Response of Concrete to Repeated Loading. Proc. R.I.L.E.M. Int. Symp. on the Effects of Repeated Loading on Materials and Structural Elements, Mexico City. September 1966.

150 CLEMMER H.F. Fatigue of Concrete. Proc. A.S.T.M. Vol. 22, II. 1922. pp. 408-418.

151 CREPPS R.B. Fatigue of Mortar. Proc. A.S.T.M. Vol. 23, II. 1923. pp. 329-337.

152 HATT W.K. Fatigue of Concrete. Proc. 4th Annual Meeting of Highway Res. Board. Dec. 1924. pp. 47-60.

153 HATT W.K. Researches in Concrete. Purdue Univ. Bull. 24. 1921. pp. 44-55.

154 KESLER C.E. Effect of Speed of Testing on Flexural Fatigue Strength of Concrete. Proc. Highway Res. Board. Vol. 32. 1953. pp. 251-258.

155 MURDOCK J.W. and KESLER C.E. The Mechanism of Fatigue Failure in Concrete. Univ. of Illinois T. and A.M. Rep. No. 587. 1960. pp. 138.

156 NEAL J.A. and KESLER C.E. The Fatigue of Concrete. Int. Conf. on Struct. of Concrete. London, September 1965. Paper E.2. pp. 1-12.

157 PROBST E. The Influence of Rapidly Alternating Load on Concrete and Reinforced Concrete. The Structural Engineer. Vol. 9, Dec. 1931. pp. 410-432.

158 MARIN J. Failure Theories of Materials Subjected to Combined Stresses. Trans. Amer. Soc. Civ. Eng. 1935. pp. 1162-1178.

159 NADAI A. Theory of Flow and Fracture of Solids. Vol. 1. 1950. McGraw-Hill, New York. 572 pp.

160 TIMOSHENKO S.P. History of Strength of Materials. McGraw-Hill, New York. 1953. 445 pp.

161 JAEGER J.C. Brittle Fracture of Rocks. Failure and Breakage of Rock. Proc. 8th Symp. on Rock Mechs. Minnesota, September 1966. Amer. Inst. of Min. Metall. and Petrol Engrs. Ed. Fairhurst. pp. 3-57.

162 HOEK E. Brittle Failure in Rock. Rock Mechanics in Engineering Practice. Eds. Stagg and Zienkiewicz. pp. 99-124.

163 RICHART F.E., BRANDTZAEG A. and BROWN R.L. A Study of the Failure of Concrete under Combined Compressive Stresses. University of Illinois Eng. Expt. Stn. Bull. No. 185, November 20th 1928.

164 SMITH F.C. and BROWN R.Q. The Shearing Strength of Cement Mortar. Univ. of Washington Eng. Expt. Stn. Bull. No. 106, Feb. 1941.

165 U.S. BUREAU OF RECLAMATION. Determination of Boundary Porosity by Triaxial Tests on Concrete. Res. and Geol. Div. Struct. Res. Lab. Report SP 15. 1947.

166 BALMER G.G. Shearing Strength of Concrete under High Triaxial Stress - Computation of Mohr's Envelope as a Curve. U.S. Dept. of Interior, Bureau of Reclamation. Res. and Geology Div., Struct. Res. Lab. Rep. No. Sp-23. October 1949.

167 FABRY J.W. Triaxial Strength Tests of Neat Cement and Mortar Cylinders. U.S. Dept. of Interior, Bureau of Reclamation. Lab. Report No. C-779. November 1954.

168 SHIDELER J.J. Lightweight Aggregate Concrete for Structural Use. Journ. Amer. Conc. Inst. Vol. 29, No. 4. October 1957. pp. 299-329.

169 AKROYD T.N.W. Failure Mechanism of Saturated Concrete. Engineering. May 1961. pp. 658-659.

170 AKROYD T.N.W. Concrete under Triaxial Stress. Mag. of Conc. Res. Vol. 13, No. 39. November 1961.

171 HANSON J.A. Strength of Structural Lightweight Concrete under Combined Stress. Journ. P.C.A. Vol. 5, No. 1. January 1963. pp. 39-46.

172 CORDON W.A. and GILLESPIE H.A. Variables in Concrete Aggregates and Portland Cement Paste which influence the Strength of Concrete. Journ. Amer. Conc. Inst. Proc. Vol. 60, No. 8. August 1963. pp. 1029-1050.

173 NOLI A. Prove Trassiali su Calcestruzzi di Cemento e Curve Intrinsiche Relative. Giornale del Genio Civile, Anno 103. Fasc. 9, 10/11. September 1965. pp. 483-495. Oct./Nov. 1965. pp. 528-537.

174 KRAHL N.W., VICTORY S.P., ERKMAN E. and SIMS J.R. The Behaviour of Plain Mortar and Concrete under Triaxial Stress. Proc. A.S.T.M. Vol. 65, 1965. pp. 695-711.

175 SMEE D.J. The Effect of Aggregate Size and Concrete Strength on the Failure of Concrete under Triaxial Compression. Civil Engineering Transactions. Inst. of Engineers, Australia. October 1967. pp. 339-344.

176 GARDNER N.J. Triaxial Behaviour of Concrete. Journ. Amer. Conc. Inst. Proc. Vol. 66, No. 2. February 1969. pp. 136-146.

177 HOBBS D.W. Strength and Deformation Properties of Plain Concrete subject to Combined Stress. Part I : Strength Results obtained on one Concrete. London C. and C.A. Tech. Rep. 42.451. November 1970. pp. 12.

178 PALANISWAMY R. and SHAH S.P. Deformation and Failure of Hardened Cement Paste subjected to Multiaxial Stresses. R.I.L.E.M. Int. Symp. The Deformation and the Rupture of Solids subjected to Multiaxial Stresses. Cannes, October 1972. Vol. I. pp. 169-179.

179 U.S. BUREAU OF RECLAMATION. Unpublished Triaxial Strength Data for Concrete. Personal communication.

180 HENDRON A.J. Failure Criteria for Concrete and Rock. Univ. Illinois Interim Rep. 1965. pp. 1-21.

181 FRANKLIN J.A. Classification of Rock according to its Mechanical Properties. Ph.D. Thesis. Univ. of London, January 1970.

182 MARQUARDT D.W. Least Squares Estimation of Nonlinear Parameters, a Computer Programme in FORTRAN IV Language. I.B.M. SHARE Program. Library. Distribution No. 309401. August 1966.

183 MARQUARDT D.W. An Algorithm for Least Squares Estimation of Nonlinear Parameters. Journ. Soc. Indust. and Appl. Math. Vol. II, No. 2. 1963. pp. 431-441.

184 BERTACCHI P. Behaviour of Concrete under Combined Loads: A Comparison of the Concrete Shearing Strength Values obtained from Direct Tests with the Values determined from Triaxial Tests. Trans. 8th Int. Cong. on Large Dams, Edinburgh. May 1964. Vol. 3. pp. 279-294.

185 REHBINDER P.A., SCHREINER L.A. and ZHIGACH K.F. Hardness Reducers in Drilling. Moscow Acad. of Science (1944). Trans. by C.S.I.R.O. Melbourne 1944. pp. 7-21.

186 ROBINSON L.H. The Effect of Pore and Confining Pressure on the Failure Process in Sedimentary Rock. Quart. of Colarado Sch. of Mines. Vol. 54, No. 3. July 1959. (3rd Symp. on Rock Mechs.).

187 MURRELL S.A.F. A Criterion for Brittle Fracture of Rocks and Concrete under Triaxial Stress, and the Effect of Pore Pressure on the Criterion. Rock Mechanics. Proc. 5th Symp. on Rock Mechs. Minnesota 1963. pp. 563-577.

188 BOOZER G.D., HILLER K.H. and SERDENGECTI S. Effects of Pore Fluids on the Deformation Behaviour of Rock subject to Triaxial Compression. Rock Mechanics. Proc. 5th Symp. Ed. Fairhurst, Pergamon, 1963. pp. 579-626.

189 HANSEN T.C. Theories of Multi-Phase Materials applied to Concrete, Cement Mortar and Cement Paste. Int. Conf. on the Struct. of Conc. London, September 1965. Paper A2.

190 ERNTROY H.C. and SHACKLOCK B.W. Design of High-Strength Concrete Mixes. Proc. Symp. on Mix Design and Quality Control of Concrete. C. and C.A. London, 1954. pp. 55-73.

191 HUGHES B.P. and CHAPMAN G.P. The Deformation of Concrete and Micro-Concrete in Compression and Tension with Particular Reference to Aggregate Size. Mag. Conc. Res. Vol. 18, No. 54. March 1966. pp. 19-25.

192 HUGHES B.P. and CHAPMAN G.P. The Complete Stress-Strain Curve for Concrete in Direct Tension. R.I.L.E.M. Bull. No. 30, March 1966.

193 JOHNSTON C.D. Strength and Deformation of Concrete in Uniaxial Tension and Compression. Mag. Con. Res. Vol. 22, No. 70. March 1970. pp. 5-16.

194 HOBBS D.W. The Dependence of the Bulk Modulus, Youngs Modulus, Shrinkage and Thermal Expansion of Concrete upon Aggregate Volume Concentration. C. and C.A. Tech. Rep. T.R.A. 437. December 1969. pp. 16.

195 JONES R. Cracking and Failure of Concrete Test Specimens under Uniaxial Quasi-Static Loading. Proc. Int. Conf. on the Struct. of Conc. and its Behaviour under Load. London, September 1965. pp. 125-130.

196 HUGHES B.P. and ASH J.E. Short-Term Loading and Deformation of Concrete in Uniaxial Tension and Pure Torsion. Mag. of Conc. Res. Vol. 20, No. 64. September 1968. pp. 145-154.

197 NEWMAN J.B. Deformational Behaviour of Concrete under Short-Term Multiaxial Loading - Detailed experimental Data. C.I.R.I.A. Contract : Criteria of Concrete Strength - Report 3. Imperial College. 1973.

198 GVOZDEV A.A. Some Mechanical Properties of Concrete particularly important for the Structural Mechanics of Reinforced Concrete Structures. Trans. of Scientific Res. Inst. for Reinf. Conc. (N.I.I. Zh.B.) No. 5 Gosstroiizdat. Moscow 1959 (in Russian).

199 HOBBS D.W. The Strength and Deformation Properties of Plain Concrete under Combined Stress. R.I.L.E.M. Int. Symp. The Deformation and the Rupture of Solids subjected to Multiaxial Stresses. Cannes, Oct. 1972. Vol. 1 pp. 97-111.

200 ANSON M. An Investigation into a Hypothetical Deformation and Failure Mechanism for Concrete. Mag. of Conc. Res. Vol. 16, No. 47. June 1964. pp. 73-82.

201 NIWA Y. KOBAYASHI S. and MIYAJI A. Some Considerations on Fracture Criteria of Cement Mortar subjected to Multiaxial Compression. Personal Communication.

202 ROAD RESEARCH LABORATORY Design of Concrete Mixes - Road Research Note No. 4, 2nd ed. London, H.M.S.O. 1950. 16 pp.

203 BERTACCHI P. and BELLOTTI R. Experimental Research on Deformation and Failure of Concrete under Triaxial Loads. R.I.L.E.M. Int. Symp. The Deformation and the Rupture of Solids subjected to Multiaxial Stresses. Cannes, October 1972. Vol. 1. pp. 37-52.

204 GACHON H. Comportement d'un Beton en Sollicitation Triaxiale (in French). R.I.L.E.M. Int. Symp. The Deformation and the Rupture of Solids subjected to Multiaxial Stresses. Cannes, October 1972. pp. 53-70.

205 AVET-FLANCART R. BERGUES J. COSTES D. Determination de la Limite Elastique d'Ecrouissage d'un Beton Humide Soumis a des Sollicitations Triaxiales (in French). R.I.L.E.M. Int. Symp. The Deformation and the Rupture of Solids subjected to Multiaxial Stresses. Cannes, October 1972. Vol. 1. pp. 7-22.

206 ZIMMERMAN R.M. Major Factors affecting the Multiaxial Compressive Strength of Plain Concrete. R.I.L.E.M. Int. Symp. The Deformation and the Rupture of Solids subjected to Multiaxial Stresses. Cannes, October 1972. Vol 1. pp. 257-272.

207 NIWA Y., KOBAYASHI S., KOYANAGI W. and NAKAGAWA K. Microcracks of Concrete under Triaxial Compression. Personal Communication.

208 POWERS T.C. Structure and Physical Properties of Hardened Portland Cement Paste. P.C.A. Res. and Dev. Labs. Bull. No. 94. March 1958.

209 DERUNTZ J.A. and HOFFMAN O. The Static Strength of Syntactic Foam. Journ. Appl. Mech. September 1969. pp. 551-557.

210 BAKER A.L.L. An Analysis of Deformation and Failure Characteristics of Concrete. Mag. of Conc. Res. Vol. II, No. 33. November 1959. pp. 119-128.

211 BORG I., FRIEDMAN M., HANDIN J. and HIGGS. D.V. Experimental Deformation of St. Peter Sand - a Study of Cataclystic Flow. Geol. Soc. Am. Mem. Vol. 79. 1960. pp. 133-191.

212 GILBERT G.N.J. The Components of Strain due to Deformation of the Matrix and due to Volume Changes in a Flake Graphite Cast Iron under Uniaxial Stress. Journ. B.C.I.R.A. Vol. II No. 4. July 1963. pp. 512-524.

213 COWAN H.J. The Strength of Plain, Reinforced and Prestressed Concrete under the Action of Combined Stresses, with particular reference to the Combined Bending and Torsion of Rectangular Sections. Mag. of Conc. Res. No. 14. December 1953.

214 MOGI K. Pressure Dependence of Rock Strength and Transition from Brittle Fracture to Ductile Flow. Bull. Earthquake Res. Inst. Tokyo. V.44. pp. 215-232.

215 POMEROY C.D., SPOONER D.C. and HOBBS D.W. The Dependence of the Compressive Strength of Concrete on Aggregate Volume Concentration for Different Shapes of Specimen. C. and C.A. Departmental Note No. DN/4016. March 1971.

216 AKHVERDOV I.N. and LUKSHA L.K. The Character of Concrete Failure under Various Stress Conditions. Beton i Zhelezobeton. 1964 (7). pp. 297-302. (Min. of Tech. B.R.S. Lib. comm. No. 1361, July 1966).

217 BELLAMY C.J. The Strength of Concrete under Combined Stress. Personal Communication.

218 NEWMAN K. The Effect of Water Absorption by Aggregates on the Water/ Cement Ratio of Concretes. Mag. of Conc. Res. Vol II, No. 53. November 1959. pp. 135-142.

219 NEWMAN A.J. and TEYCHENNE D.C. A Classification of Natural Sands and its use in Concrete Mix Design. Proc. Symp. on Mix Design and Quality Control of Concrete, London 1954. C. and C.A. 1955. pp. 175-194.

220 NIWA Y. and KOBAYASHI S. Failure Criterion of Cement Mortar under Triaxial Compression. Memoires of Fac. of Eng. Kyoto Univ. Vol. XXIX Part 1. January 1967. pp. 1-15.

221 HANNANT D.J. and FREDERICK C.O. Failure Criteria for Concrete in Compression. Mag. of Conc. Res. V.20, No. 64. Sept. 1968. pp. 133-144.

222 BREBBIA C.A. and FREDERICK C.O. A Failure Surface for Concrete. Central Electricity Generating Board. Central Elec. Res. Labs. Lab. Note No. RD/L/N.9/69.

223 LEWIS D.J. and CARMICHAEL D.G.T. A Multiaxial Failure Diagram for Concrete. Central Elec. Gen. Board. Res. and Dev. Dept. Berkeley Nuclear Labs. Report No. RD/B/N.1355. February 1969.

224 DAY A. Ove Arup and Partners. Personal Communication.

225 ROSCOE K.H. Some Soil Mechanics Concepts and the Possibility of their Wider Application. Proc. Int. Conf. Structure Solid Mechs. and Eng. Design. Southampton, 1969. pp. 923-949.

226 WROTH C.P. Engineering Dept. Univ. of Cambridge. Personal Communication.

227 GERSTLE K.H. and KO H.Y. Proposals for a Co-operative Programme for Triaxial Testing of Concrete. Dept. of Civil and Environmental Eng. Univ. of Colorado, U.S.A. Personal communication.

228 DOUGILL J.W. Further consideration of a Mathematical Model for Progressive Fracture of a Heterogeneous Material. Mag. of Conc. Res. Vol. 23, No. 74. March 1971. pp. 5-10.

229 HOBBS D.W. The Compressive Strength of Concrete - a Statistical Approach to Failure. Mag. of Conc. Res. Vol. 24, No. 80. Sept. 1972. pp. 127-138.

230 LIU T.C.Y., NILSON A.H. and SLATE F.O. Stress-Strain Response and Fracture of Concrete in Uniaxial and Biaxial Compression. Journ. of Amer. Conc. Inst. Proc. V.69. No. 5. May 1972.

231 GLOMB J.A. and PATAS P.J. Experimental Analysis of the Determination of a Test Specimen as a Method of Verifying the Compressing Conditions while Testing Concrete in Multi-way Stress Conditions. R.I.L.E.M. Int. Symp. The Deformation and the Rupture of Solids subjected to Multiaxial Stresses. Cannes, October 1972. pp. 79-91.

232 ATKINSON R.H. and KO H.Y. A Multiaxial Device for Testing Rock Materials. R.I.L.E.M. Int. Conf. The Deformation and the Rupture of Solids subjected to Multiaxial Stresses. Cannes, October 1972. pp. 33.

233 PANDIT G.S. Discussion of 'Behaviour of Concrete under Biaxial Stresses' by Kupfer H., Hilsdorf H.K. and Rusch H. Journ. Amer. Conc. Inst. Proc. V. 67. No. 2. February 1970. pp. 194-195.

234 TAYLOR M.A., JAIN A.K. and RAMEY M.R. Path Dependent Biaxial Compressive Testing of an All-Lightweight Aggregate Concrete. Journ. Amer. Conc. Inst. Prov. V. 69. No. 12. Dec. 1972. pp. 758-764.

235 STROEVEN P. Stevin-Laboratorium Technische Hogeschool, Delft. April 1971. Personal communication.

236 BRITISH STANDARDS INSTITUTION B.S. 12 : 1958. Portland Cement (Ordinary and Rapid Hardening).

237 GRIFFITH A.A. The Phenomena of Rupture and Flow in Solids. Phil. Trans. Roy. Soc. Series A. Vol. 221. 1921. pp. 163-198.

238 GRIFFITH A.A. The Theory of Rupture. Proc. 1st Int. Congress for Appl. Mechs. Delft 1924. pp. 55-63.

APPENDIX 1

Loading and Measuring Devices Used in the Test Series

Loading Device	Load Control	Load Measuring Device
Uniaxial Compression		
Amsler 300 Tonf. frame with subsidiary spherical seating unit.	Amsler cabinet with Amsler Hydropacer constant load/ deformation rate control unit.	Maximum load by Amsler dial. Intermediate loads by Bell and Howell pressure transducer (0-5000 lb./in.^{2}) Type 4-306 Serial No. L 21394 incorporating unbonded strain gauge sensor unit.
Uniaxial Tension		
Modified Ward 5 Tonf. tension frame.	Amsler control cabinet with Hydropacer unit.	Maximum load by Amsler dial. Intermediate loads by specially designed 10000 lbf. aluminium load cell incorporating 8 electrical resistance strain gauges.
500 Tonf. Frame for applying Deviator Load to Triaxial Specimens		
Specially designed 3-column 500 Tonf. frame.	Amsler Control cabinet with Hydropacer unit.	Maximum load by Amsler dial. Intermediate loads by one of the following - i) Intersonde pressure transducer (0-7500 lb./in.^{2}) Type PR 15-350 Serial No. 389 incorporating bonded electrical resistance strain gauges. ii) S.E.L. inductive type pressure transducer (0-6000 lb./in.^{2}) Type S.E. 1165/2/D Serial No. 54552 measured in conjunction with Peekel data logger and signal conditioning unit Type B.50.

iii) Bell and Howell pressure transducer (0-5000 lb./in.^{2}) Type 4-306 Serial No. L 21394 incorporating unbonded strain gauge sensor unit.

Triaxial Cell (for 'compression' tests)

Specially developed balanced piston 0-20000 lb./in.^{2} type triaxial cell manufactured by Messrs. Wykham Farrance Ltd.	Specially developed high pressure control system using Madan Airhydro pump with servo system based on Budenberg deadweight piston/cylinder assembly for maintaining pressures above 2500 lb./in.^{2}. Hand pump control for pressures lower than 2500 lb./in.^{2}.	Budenberg deadweight piston and cylinder assembly used for control. Continuous monitoring by Intersonde pressure transducer (0-20000 lb./in.^{2}) Type PR 15-350 Serial No. 775 incorporating bonded electrical resistance strain gauges.

Triaxial Cell (for equal biaxial compression tests)

Hydraulic Cell as for 'compression' tests with specially developed piston extension unit.	Cell pressure control system as for 'compression' tests. Specially developed balance pressure control system based on Amsler load maintainer valve.	Cell pressure measurement as for compression tests. Balance pressure monitored by 0-1000 lb./in.^{2} Bourdon type Budenberg pressure gauge. Serial No. 8742426.

Complex Stress Machine

Modified and stiffened Vile loading frame.	Specially developed control systems based on Amsler load maintainer valves.	Bell and Howell pressure transducers (0-10000 lb./in.^{2}) Type 4-366 incorporating unbonded strain gauge sensor unit - Serial No. L 26551 for vertical pressure. Serial No. L. 23643 for horizontal pressure.

Full detailed drawings of the above apparatus are available from the Concrete Materials Research Group, Civil Engineering Department, Imperial College. All the measuring devices were calibrated under conditions similar to those of an actual test and checked prior to each main test series. Full calibration details are available from the Concrete Materials Research Group.

APPENDIX 2

Materials for Concrete Mixes

A2.1. Ordinary Portland Cement

Supplied from Northfleet Works, Kent.

Prior to use the cement was blended in a cyclone blender.

Vibrated mortar cube strengths

Mix Proportions 1:3/0.40 in accordance with B.S. 12 (236).

3 day	7 day	28 day
4750	6860	8280
4770	6770	8370
4380	6920	8700
4630 lb./in.^{2}	6850 lb./in.^{2}	8450 lb./in.^{2}

Specific Surface - 3300 cm^3/gm.

A2.2. Spherical Glass Aggregate

Supplied by Redfearn Bros.

Type of glass	'E' glass
Nominal maximum size	3/4"single sized
Apparent specific gravity	2.66
24 hour water absorption	NIL
Modulus of elasticity - lb./in.^{2}	10.59 x 10^6
Poisson's Ratio	0.22
Bulk Modulus - lb./in.^{2}	6.486 x 10^6
Angularity number (1)	6

A2.3. Thames Valley Flint Gravel

Supplied by Thorney Mill Pit, Iver, Bucks.

Nom. size range (in.)	3/4-3/8	3/8-3/16	3/16-No.25 (Coarse sand)	No.25-No.100 (Fine sand)
Grading (1)				
Sieve Size	**Percentage Passing**			
3/4	100			
3/8	4	100		
3/16	Nil	1	100	
No. 7		Nil	85	
No. 14			61	
No. 25			34	100
No. 52			4	43
No. 100			Nil	6
Dust				Nil
Flakiness Index (1) - %	24.6	31.6		
Elongation Index (1) -%	17.2	17.7		
Angularity Number (1)	8			
Apparent Specific Gravity	2.61	2.61	2.67	2.67
24 hr. Water Absorption (1) - %	2.10	3.90	2.30	2.30
Modulus of elasticity lbf/in.^{2}	10 x 10^6 (approx.) in flawless condition. This is likely to be reduced for the size ranges used due to defects caused by processing.			

A2.4. Crushed Limestone

Supplied from Topley Pike, Derbyshire.

Nom. size range (in.)	3/4-3/8	3/8-3/16	3/16-No.25 (Coarse sand)	No.25-No.100 (Fine sand)
Grading (1)				
Sieve Size	**Percentage Passing**			
3/4	100			
3/8	1	100		
3/16	Nil	1	100	
No. 7		Nil	90	
No. 14			49	
No. 25			4	100
No. 52			Nil	37
No. 100				2
Dust				Nil
Flakiness Index (1) - %	31.6	31.1		
Elongation Index (1) -%	13.2	8.5		
Angularity Number (1)	9			
Apparent Specific Gravity	2.7	2.7	2.7	2.7
24 hr. Water Absorption (1) - %	0.3	0.2	0.2	0.2
Modulus of elasticity	10 x 10^6 lb./in.^{2} (approx.).			

A2.5 Crushed Granite

Supplied from Kirkmabreck, Creetown, Kirkcudbrightshire.

Nom. size range (in.)	3/4-3/8	3/8-3/16	3/16-No.25 (Coarse sand)	No.25-No.100 (Fine Sand)
Grading [1]				
Sieve size		**Percentage Passing**		
3/4	100			
3/8	1	100		
3/16	Nil	1	100	
No. 7		Nil	79	
No. 14			33	
No. 25			4	100
No. 52			Nil	43
No. 100				1
Dust				Nil
Flakiness Index [1] - %	22.9	25.4		
Elongation Index [1] - %	23.5	16.5		
Angularity number [1]	11			
Apparent Specific Gravity	2.68	2.67	2.51	2.51
24 Hr. Water Absorption [1] - %	0.28	0.45	0.18	0.18
Modulus of elasticity lb./in.^{2}	14×10^6 (approx.)			

APPENDIX 3

Details of Concrete Mixes

A3.1. Mixes MA, MBC and 6 IC

Mix Reference	Mortar MA	Mortar MBC	Concrete 6IC
Aggregate type -			
Fine	Irregular Thames Valley flint sand in proportions 70% coarse sand 30% fine sand		
Coarse	3/4" and 3/8" Thames Valley flint gravel		
Proportions by weight			
Cement (OPC)	1.00	1.00	1.00
Fine aggregate	2.40	2.40	2.40
3/8" aggregate	nil	nil	nil
3/4" aggregate	nil	nil	5.10
'Effective' water	0.42	0.52	0.46
Total water	0.47	0.57	0.62
Volume fractions %			
Fine aggregate	53.3	50.2	23.9
Coarse aggregate	nil	nil	51.0
Total aggregate	53.3	50.2	74.9
Properties in fresh state (62)			
Slump - in.	Collapse	Collapse	$\frac{1}{2}$"
Compacting factor	0.91	0.95	0.81
Properties in hardened state (62)	(mean of 3 specimens)		
Cube strength at time of testing - lb./in^2	-	6170	7002

3.2. Idealised Concrete Mixes

Mix. Ref.	I_0	I_5	$I_{7.5}$	I_{10}	I_{18}	I_{26}	I_{34}	I_{40}	I_{46}	I_{52}	I_{58}
Aggregate type -											
Fine	No. 25 - No. 100 Irregular Thames Valley river sand										
Coarse	3/4 in. dia. roughened spheres of E - glass										
Proportions by weight											
Cement (OPC)	1.00	1.00	1.00	1.00	1.00	1.00	1.00	1.00	1.00	1.00	1.00
Fine aggregate	1.40	1.40	1.40	1.40	1.40	1.40	1.40	1.40	1.40	1.40	1.40
Coarse aggregate	Nil	0.17	0.26	0.35	0.70	1.11	1.63	2.11	2.70	3.44	4.38
'Effective' water	0.36	0.36	0.36	0.36	0.36	0.36	0.36	0.36	0.36	0.36	0.36
Total water	0.39	0.39	0.39	0.39	0.39	0.39	0.39	0.39	0.39	0.39	0.39
Volume fractions %											
Fine aggregate	42.55	40.42	39.36	34.87	31.49	28.08	25.08	25.53	22.98	20.42	17.87
Coarse aggregate	Nil	5.00	7.50	10.00	18.05	26.01	34.00	40.01	46.01	52.00	58.01
Total aggregate	42.55	45.43	46.86	48.30	52.92	57.49	62.09	65.54	68.08	72.43	75.88
Properties in fresh state (62)											
Slump - in.	1/8	1/4	3/8	1	1/2	1/2	1/4	0	0	0	0
Compacting factor	*	*	*	0.924	*	*	*	0.786	0.765	0.765	0.786
VB - sec.	3.0	2.5	3.0	3.0	3.0	3.0	5.5	6.5	6.5	9.0	7.0
Air content %	5.0	5.0	4.5	4.1	3.6	2.8	2.8	2.4	1.7	1.8	1.6
Properties in hardened state (62) (mean of 3 specimens)											
Wet density - lb./ft.^{3}	138.9	138.6	139.7	141.2	141.6	143.9	144.8	146.0	147.5	147.0	147.9
Cube strength at time of testing - lb./in.^{2}	10085	9777	11475	10103	11387	11235	11935	11667	11489	12161	12192

* Mix too cohesive for apparatus

A3.3. Real Concrete Mixes

Mix Ref.	M1	C1	M2	C2	C3	C4
Aggregate type	Irregular Thames Valley river sand				Crushed Limestone	Crushed Granite
Proportions by weight						
Cement (OPC)	1.00	1.00	1.00	1.00	1.00	1.00
Sand (30% fine, 70% coarse)	1.40	1.40	2.96	2.96	2.96	2.96
$\frac{3}{8}$ in. aggregate	NIL	0.70	NIL	1.48	1.48	1.48
$\frac{3}{4}$ in. aggregate	NIL	1.40	NIL	2.96	2.96	2.96
'Effective' water	0.35	0.35	0.60	0.60	0.60	0.60
Total water	0.38	0.44	0.67	0.79	0.62	0.62
Volume fractions %						
Fine aggregate	42.82	25.33	52.96	28.55	29.80	31.17
Coarse aggregate	NIL	38.14	NIL	42.98	44.70	43.96
Total aggregate	42.82	63.47	52.96	71.53	74.49	75.13
Properties in fresh state (62)						
Slump - in.	3/4	1/4	Collapse	3/4	NIL	NIL
Compacting factor	0.981	0.852	0.993	0.935	0.851	0.733
VB - sec.	6.0	5.0	Collapse	3.0	6.0	6.0
Air content %	3.0	1.75	1.6	1.4	1.4	1.75
Properties in hardened state (62)						
Wet density - lb./ft.^{3}	141.0	176.6	132.6	146.2	154.0	151.7
28 day cube strength - lb./in.^{2}	10033	8778	5031	3202	7285	5885
Cube strength at time of testing - lb./in.^{2}	13226	10631	6085	3369	10164	8643

APPENDIX 4

Derived Results for Mortar Mix MA

A4.1. Onset of Stable Fracture Propagation (o.s.f.p.) and Ultimate Strength Levels for Mortar Mix Type MA under Uniaxial Compression and Tension

Age of Specimens : 16 weeks

Specimen Reference	o.s.f.p. Stress Level ($lb./in.^2$)	Ultimate Strength Level ($lb./in.^2$)
Uniaxial Compression Tests		
1	4830	10080
2	4423	9805
3	4941	10363
Mean	4731	10083
Standard deviation	273	279
Uniaxial Tension Tests		
1	576	576
2	532	532
3	494	494
Mean	534	534
Standard deviation	41	41

A4.2. Values for Elastic Constants for Mortar Mix Type MA tested under Uniaxial Compression after conditioning for 50 cycles of load

Age of Specimens : 16 weeks

Specimen Reference	Secant values for elastic constants at 3000 $lb./in.^2$	
	E $lb./in.^2$	
1	4.738×10^6	0.159
2	4.762×10^6	0.152
3	4.751×10^6	0.154
Mean	4.751×10^6	0.155
Standard deviation	0.012×10^6	0.004

APPENDIX 5

Reduction of Stress and Strain Data

A5.1. Calibration of Equipment and Analysis of Data

All stress measuring devices used in the present tests (see Appendix 1) were calibrated immediately prior to, and checked after, each main series. Full details of the calibrations are available from the Concrete Materials Research Group, and are incorporated in the following computer programmes, which contain routines for the comprehensive reduction of stress-strain data.

Programme Reference	Type of Test	Equipment Used
CYCFIT	Uniaxial tension	Ward machine
	Uniaxial compression	Amsler 300 Tonf. loading frame
	Triaxial compression	500 Tonf. loading frame and hydraulic cell
CELFIT	Equal biaxial compression	Hydraulic cell
VILFIT	Biaxial compression	Complex Stress machine

The strain measuring devices used in the test series were calibrated against a calibration resistor immediately before and after each individual test.

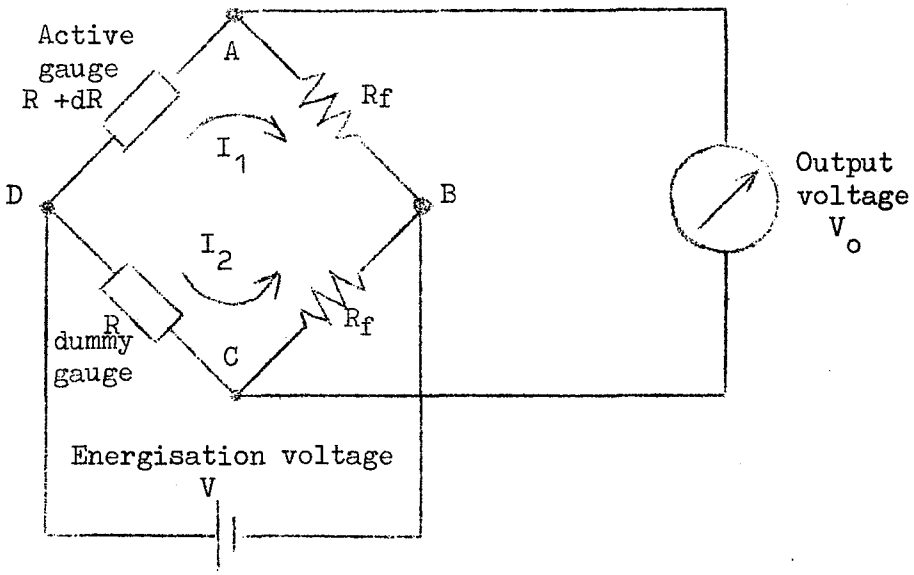
A5.2. Calculations of True Strain on Electrical Resistance Strain Gauges from Output of Wheatstone Bridge Circuits

All strain measuring systems incorporating electrical resistance strain gauges consist essentially of Wheatstone bridge circuits. One arm of each bridge comprises a matched pair of stable fixed resistors (of nominal resistance Rf) forming part of the measuring device while the other arm, provided by the user, incorporates a 'dummy' and an 'active' strain gauge (both of nominal resistance R).

The 'dummy' gauge is attached to an unloaded sample of the same material as under test, while the 'active' gauge is attached to the specimen. It is assumed that the effects of any changes in resistance of these gauges due to environmental changes (such as temperature) cancel out, and that the only resistance change affecting the bridge circuit is that due to elongation

or contraction of the 'active' gauge caused by deformation of the specimen under load.

Let this resistance change be dR and consider its effect on the voltage output of an energised Wheatstone Bridge circuit ABCD as shown below:



From Ohm's Law

$$V = I_1(R + dR + Rf) \quad \ldots\ldots\ldots\ldots\ldots\ldots (1)$$

$$V = I_2(R + Rf) \quad \ldots\ldots\ldots\ldots\ldots\ldots (2)$$

Similarly

$$\text{Voltage at A}, V_A = I_1(R + dR) \quad \ldots\ldots\ldots\ldots\ldots\ldots (3)$$

$$\text{Voltage at C}, V_C = I_2R \quad \ldots\ldots\ldots\ldots\ldots\ldots (4)$$

Substitute (1) in (3)

$$V_A = V(R + dR)/(R + dR + Rf)$$

Substitute (2) in (4)

$$V_C = V.R/(R + Rf)$$

but $V_O = V_A - V_C$

$$V_O = V\,(R + dR)/(R + dR + Rf) - R/(R + Rf)$$

which rearranges to -

$$V_O = V.RfdR/\,(R + Rf)^2 + (R + Rf)dR \quad \ldots\ldots\ldots\ldots\ldots\ldots (5)$$

In general, for small strains dR is small with respect to R and the term (R + Rf)dR is neglected in order to simplify the calculation.

For the present test series, however, such a simplification is not justified since strains of up to 25% can be attained:

By definition -

$$dR/R = F.e \qquad \ldots\ldots\ldots\ldots\ldots (6)$$

or $$dR = F.e.R \qquad \ldots\ldots\ldots\ldots\ldots (6)$$

where F = gauge factor

e = strain on gauge

Substitute (6) in (5)

$$V_0 = V.Rf.R.F.e/ (R + Rf)^2 + (R + Rf)R.F.e$$

which reduces to -

$$e = V_0.R/(R + Rf)^2/F(V.Rf - V_0(R + Rf) \qquad \ldots\ldots\ldots\ldots\ldots (7)$$

$$= \underline{\underline{A.V_0/F(V.Rf - B.V_0)}} \qquad \ldots\ldots\ldots\ldots\ldots (8)$$

where $A = R/(R + Rf)^2$

$B = (R = Rf)$

For the strain measuring equipment used in the present test series the system is calibrated before each test using a precision shunt resistor (Vishay type supplied by Welwyn Electric Co.), giving a resistance change which simulates a known value of strain. The energisation voltage V is adjusted until the given strain value is displayed, and V is generally not known.

As specified by the manufacturers of the calibration resistors the gauge factor is 2, and the equivalent value of strain is undoubtedly based on assumptions of small strain with dR small in comparison with R.

With these assumptions Equation 5 becomes -

$$V_0 = V.Rf.dR/(R + Rf)^2 \qquad \ldots\ldots\ldots\ldots\ldots (9)$$

Substitute (6) in (9) with F = 2

$$V_0 = 2.e.V.Rf/A \qquad \ldots\ldots\ldots\ldots\ldots (10)$$

after calibration $V_0 = e$

(10) becomes - $V.Rf = A/2 \qquad \ldots\ldots\ldots\ldots\ldots (11)$

Substitute (11) in (8)

$$e = \underline{\underline{A.V_0/F(A/2 - B.V_0)}} \qquad \ldots\ldots\ldots\ldots\ldots (12)$$

Equation (12) is used throughout the test series for calculating true strain on the strain gauges from the strains indicated as voltage outputs V_0.

A5.3. Triaxial Compression Test - Correction for Influence of Circumferential Strain on Axial Stress

In general, the effect of the change in lateral dimension on the axial stress induced in a specimen is neglected since the deformation is normally relatively small. Under triaxial 'compression' the lateral strain can attain values of up to 25% and must be taken into account. The correction used throughout the present test series is as follows:-

$$\text{True axial stress} = \underline{\underline{\text{nominal axial stress}/(1 + e_c)^2}}$$

where e_c is the measured mean circumferential strain at the given stress level.

A5.4. Equal Biaxial Compression Test in Hydraulic Cell - Calculation of Stresses

Consider the test arrangement shown diagrammatically in Figure A5.1., in which the curved surface of a 'waisted' specimen is subjected to a hydraulic pressure O .

Total tensile force on 'waisted' portion of specimen due to confining pressure $= \sigma\pi(D_3^2 - D_1^2)/4$ ... (1)

Total downward axial force due to 'balance' pressure P applied to annulus $= P\pi(D_4^2 - D_3^2)/4$ ... (2)

To nullify the axial force in order to achieve a state of equal biaxial compression the above forces must be equated:

$$P = \sigma(D_3^2 - D_1^2)/(D_4^2 - D_3^2) \qquad \ldots\ldots (3)$$

Let the frictional resistance against the extension of the specimen due to the piston seals (See Figure A5.1.) be equivalent to an effective downward pressure P_f on annulus, i.e. P must be reduced to compensate. Equation (3) becomes:

$$P = \sigma(D_3^2 - D_1^2)/(D_4^2 - D_3^2) - P_f \quad \ldots\ldots (4)$$

Let calibration of pressure gauge used to measure P be:

$$C = \text{gauge pressure } P_g / \text{actual pressure } P$$

$$Pg = C.P \quad \ldots\ldots (5)$$

Substitute (5) in 4

$$\underline{Pg = C(\sigma(D_3^2 - D_1^2)/(D_4^2 - D_3^2) - \sigma f)} \quad \ldots\ldots (6)$$

The estimated tolerances for the above quantities which may effect the accuracy of P_g are as follows:

Quantity	Tolerances
D_1	$\pm$0.001" for machine tolerance together with $\pm$0.001" for movements after machining giving a total of $\pm$0.002".
D_3	$\pm$0.0002"
D_4	$\pm$0.0002"
σ	$\pm$100 lb./in.^{2}
σf	+5lb./in.^{2}, -1 lb./in.^{2}
C	$\pm$1%

In order to eliminate, as far as possible, the effect of the above tolerances three types of equal biaxial tests have been performed as follows:

A 'Null' test - in which the tolerances have been taken as zero.

A 'Compression' test - in which the tolerance limits have been chosen as below to give the highest resultant compressive force in the axial direction -

Quantity	Tolerances
D_3	+0.0002"
σ	+100 lb./in.^{2}
C	+0.01
D_1	-0.002"
D_4	-0.002"
σ_f	-1 lb./in.^{2}

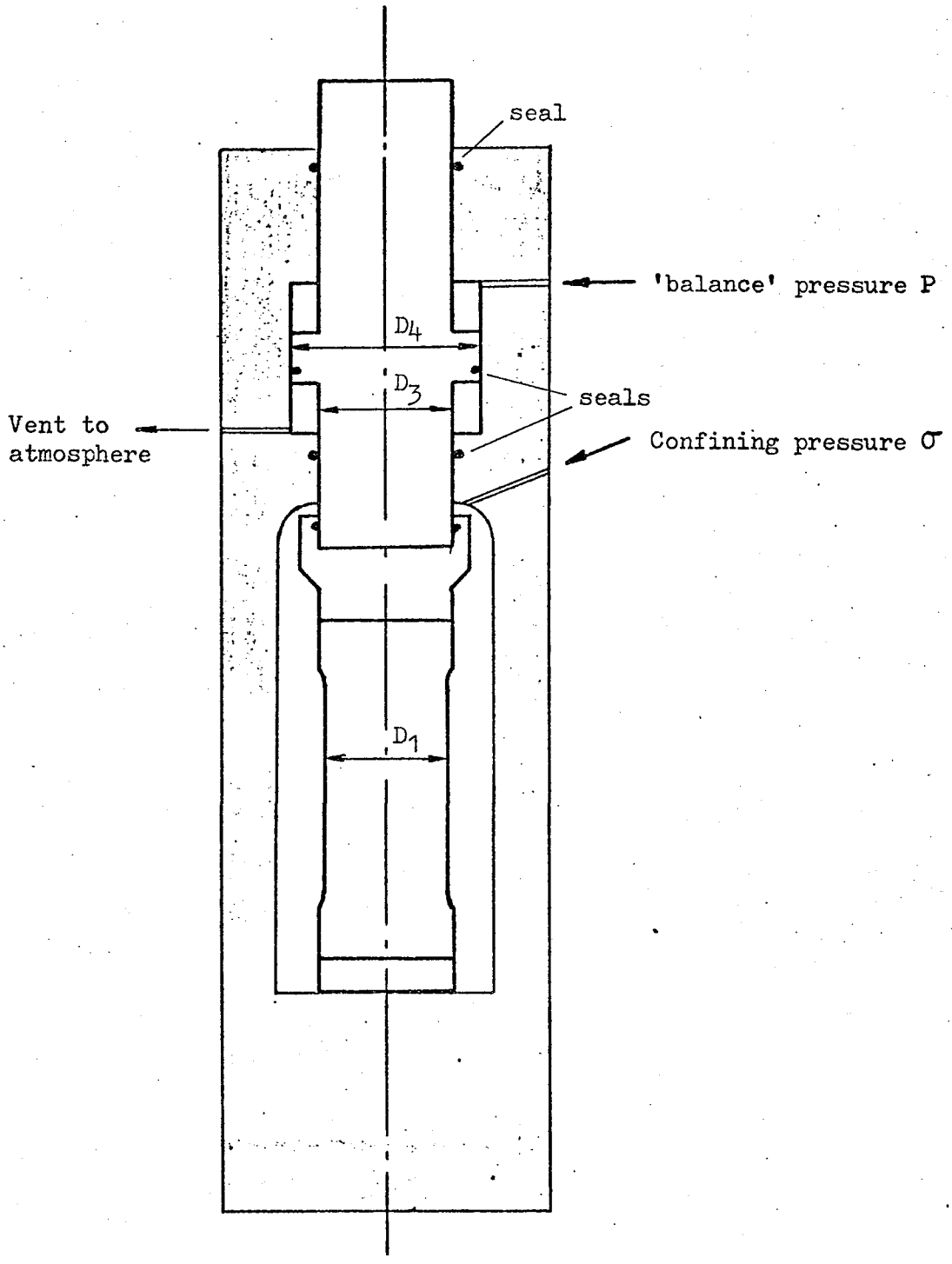


Figure A5.1. Schematic diagram showing method of load application for an equal biaxial compression test in the hydraulic cell.

A 'Tensile' test - in which the tolerance limits have been chosen as below to give the highest resultant tensile force in the axial direction -

Quantity	Tolerance
D_3	-0.0002"
$\bar{\sigma}$	-100 lb./in.^{2}
C	-0.01
D_1	+0.002"
D_4	+0.0002"
$\bar{\sigma}_f$	+5lb./in.^{2}

APPENDIX 6

Testing Machine and Specimen Alignment Procedures

A6.1. Complex Stress Machine

A6.1.1. Alignment of Frame End Platens

(i) The reaction plates on each main loading frame are set parallel to within $\pm$0.001" using a specially designed distance gauge incorporating a dial gauge reading to 0.0001".

(ii) The vertical loading rams are positioned along a common axis by means of a plumb-bob suspended from the centre of a dowel located in the centre of the upper ram, and pointing over a mark at the centre of the lower ram.

(iii) The lower platen block, which is constructed without a spherical seating unit, is fixed at the correct height by placing accurately machined distance pieces between the underside of the block and the body of the ram. The dimensions of these distance pieces were determined with the aid of an aluminium block machined to dimensions 10" x 10" x 4" gripped between the platens.

(iv) With the distance pieces inserted under the lower platen, the aluminium block clamped in position, and the two parts of each of the three spherical seating units locked flush and square using clamping plates, the lateral loading frame is aligned using reference marks scribed at the centre lines of the aluminium block and platens.

The above procedure is repeated periodically during a test series if checks disclose significant movement of the machine components.

A6.1.2. Setting-up Procedure for Slab Specimens

Prior to placing the specimen in the machine the distance pieces used for alignment of the complex stress machine are placed under the lower platen and the jig which maintains the lower platen square with the horizontal loading frame inserted. Under this system the lower platen block acts as

an immovable, and accurate, reference guide. The spherical seating units on the remaining platen blocks are clamped against rotation for the setting-up procedure.

The specimen is then placed on the lower platen block and clamped in the vertical direction by applying a small load through the vertical main frame. The alignment of the upper platen on the specimen is checked during this process.

The two side platens are then brought into contact with the specimen and a small load maintained. All jigs and spherical seating clamps are then removed, after checking the complete alignment of the system.

A6.2. Equal Biaxial Compression Test in Hydraulic Cell

A6.2.1. Assembly of Platen/Specimen/Sheath Unit

The procedure developed for this test has been adopted to fulfil the following requirements -

(a) To prevent ingress of oil during the test.

(b) To ensure that the sheath cannot intrude between the specimen and platens under pressure.

(c) To allow the loading piston in the hydraulic cell to enter the recess in the upper platen easily, and to ensure an effective seal against the confining pressure.

The procedure is essentially the same as for the triaxial compression test specimen with the addition of steel shims at the specimen/platen interface to prevent intrusion of the sheath. Local stress concentrations which might be caused by the sharp edges of the shim are minimised by bedding the shims on a number of layers of adhesive tape.

Sequence of Operations (see Figure A 6.1.)

(1) Assemble the lower and upper platens on the specimen using 1" x 0.010" steel shim and adhesive tape in the positions indicated.

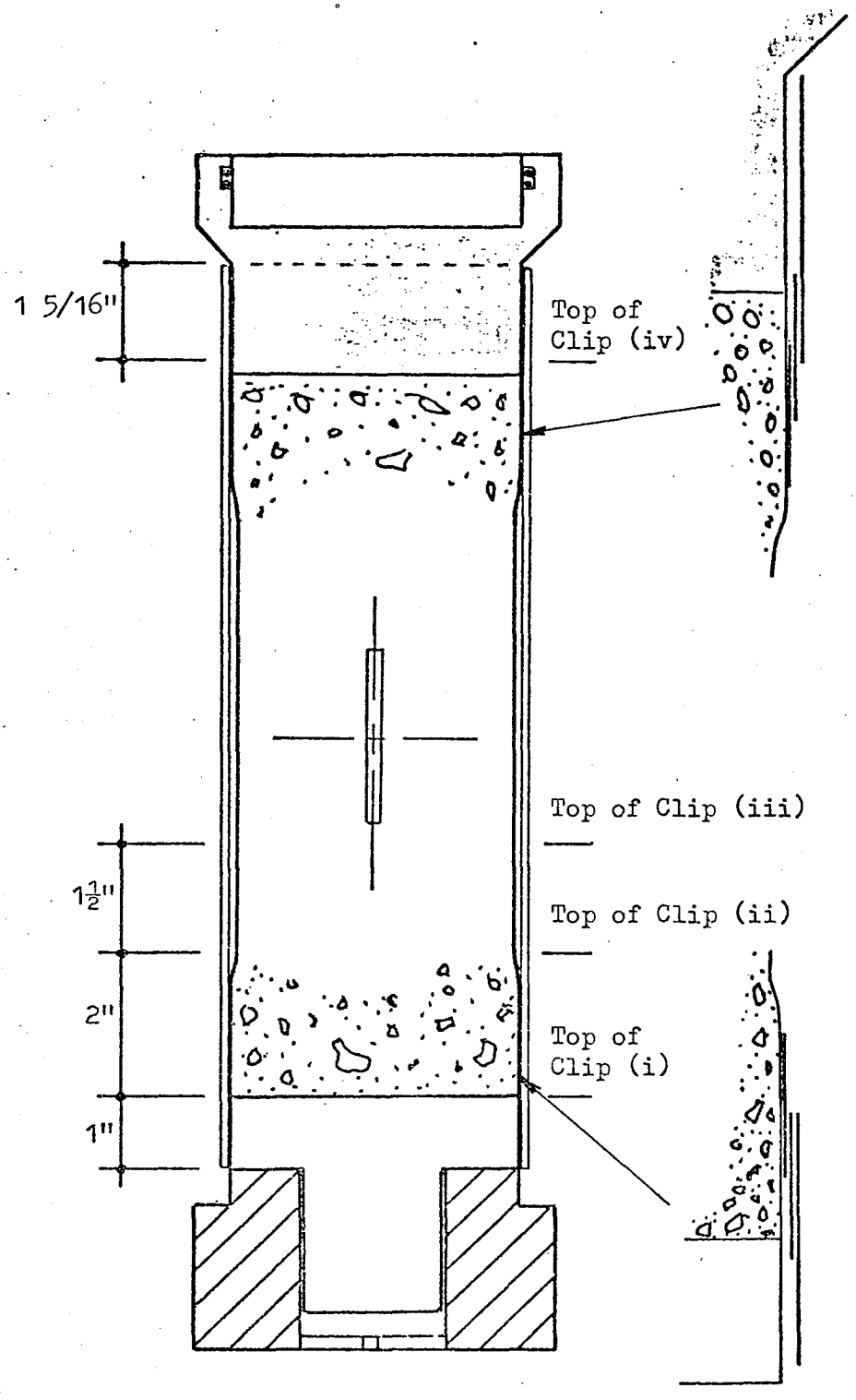


Figure A6.1. Schematic diagram showing details for assembly of platen/specimen/sheath unit for an equal biaxial compression test.

(2) Attach the strain gauge connecting wires to the face of the specimen and top platen using adhesive tape, ensuring that the wires do not cross or contact each other and also ensuring sufficient 'play'.

(3) Locate the assembly jig at the centre of a compression loading frame and place the adiprene sheath over the shoulder of the jig.

(4) Carefully slide the specimen and platen assembly into the sheath and pull the sheath over the specimen until the top edge of the sheath is level with the start of the shoulder on the upper platen. Check that no wires are 'kinked' or crossed.

(5) Place hose clips on the specimen as follows -

(i) 5/8" 'Hi-Torque' clip with buckle to RH Side at 90° to gauge wires.

(ii) 5/8" 'Hi-Torque' clip with buckle to LH Side at 90° to gauge wires.

(iii) 5/8" 'Hi-Torque' clip with buckle to RH Side at 90° to gauge wires.

(iv) 5/8" 'Hi-Torque' clip with buckle to LH Side at 90° to gauge wires.

(v) 3/8" modified 'Jubilee' clip with buckle to RH Side at 90° to gauge wires.

(6) Apply slight compression to the assembly.

(7) Place p.t.f.e. strip under clip (iv), with at least 1/2" protruding above the clip, and ensure that the joint in the strip is at 180° to the buckle. Position clip (iv) such that its lower edge is $1\frac{3}{8}$" below the start of the shoulder on the upper platen, and tighten to a torque of 140 lb.in.

(8) Position clip (v) such that the cut-out portion is adjacent to the buckle of clip (iv), and tighten.

(9) Place the temporary clip (iii) with its upper edge approximately 1/4" below the lower edge of the axial strain gauges, and tighten to a torque of 140 lb.in.

(10) Place temporary clip (ii) mid-way between clip (iii) and the lower edge of the specimen and tighten to a torque of 140 lb.in.

(11) Place p.t.f.e. strip under clip (i) and position the clip such that the top edge is not higher than the top edge of the lower platen, and tighten to a torque of 140 lb.in.

(12) Remove temporary clips (ii) and (iii) release the clamping load and remove the assembly from the assembly jig. Check that the sheath has not extruded below the lower edge of the lower platen and trim if necessary.

The assembly is now ready for attaching to the base of the hydraulic cell as described in A6.2.2.

A6.2.2. Procedure for Setting-Up Specimen

(1) The lower platen of the assembled platen/specimen/sheath unit is screwed into the base of the cell, the base being already located in the centre of the lower platen of the 500 Tonf. loading frame by means of a dowel.

(2) Hydraulic connection is made between the capillary tube venting the recess in the upper subsidiary platen, and the base of the cell. Final electrical connections are made to the data logger from the confining pressure transducer and strain gauges on the specimen, and the system is checked for stability, etc.

(3) The barrel unit is lowered on to the base of the cell, using the lifting equipment on the 500 Tonf. loading frame, and clamped by means of the locking segments and retaining ring.

(4) The lower platen of the loading frame, with assembled cell, is rolled into position and hydraulic connection is made to the cell pressure application and control system, and the balance pressure application and control system.

(5) The space above the axial piston annulus is filled with non-conducting oil, using the high pressure pump, and bled of all air.

(6) The axial piston is forced into the recess in the upper subsidiary platen, using a screw jack inserted between the top face of the piston and the upper platen of the 500 Tonf. loading frame. Correct location is checked by measurement.

(7) The cell is filled with a non-conducting transformer oil using the high capacity low-pressure pump, discharging into the base of the cell to ensure the displacement of all air.

A6.3. Triaxial Compression Test

A6.3.1. Assembly of Platen/Specimen/Sheath Unit

The sequence of operations described below for assembling the platen/specimen/sheath unit outside the hydraulic cell has evolved after a long period of development and should be strictly adhered to in order to prevent ingress of hydraulic fluid during a test, and to ensure the minimum of loading eccentricity.

Sequence of Operations (see Figure A6.2)

(1) Attach the lower subsidiary platen to the specimen using $1\frac{1}{2}$" wide adhesive tape around the cylindrical surface, leaving an approximately 3/32" gap between the lower edge of the tape and the lower edge of the platen.

(2) Attach the upper subsidiary platen and male seating unit to the specimen using 2" wide adhesive tape around the cylindrical surface, leaving an approximately 3/32" gap between the upper edge of tape and the upper edge of seating unit.

(3) Attach strain gauge wires to the face of the specimen and seating unit using adhesive tape, ensuring that wires do not cross or contact each other and also ensuring that there is sufficient 'play'.

(4) Locate assembly jig at the centre of a compression loading frame and place the 'adiprene' sheath over the shoulder of the jig.

(5) Carefully slide the specimen and platen assembly into the sheath and pull the sheath over the specimen until the top edge of the sheath is level with the top edge of the adhesive tape. Check that no wires are 'kinked' or crossed.

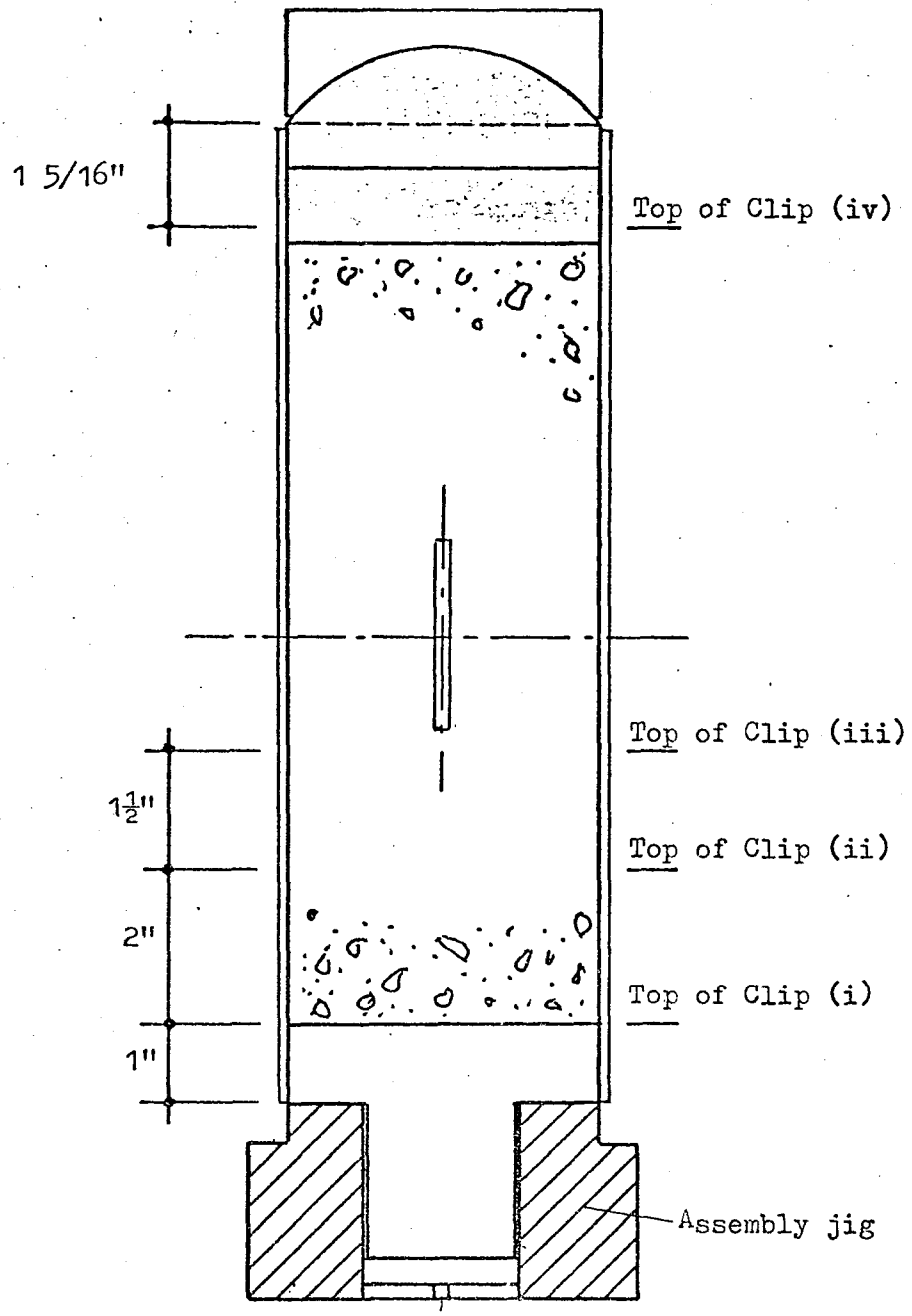


Figure A6.2. Schematic diagram showing details for assembly of platen/specimen/sheath unit for a triaxial 'compression' test.

(6) Drop hose clips over the sheath in the following order:

(i) 5/8" 'Hi-Torque' clip with buckle to R.H. side at 90° to gauge wires.

(ii) 5/8" 'Hi-Torque' clip with buckle to L.H. side at 90° to gauge wires.

(iii) 5/8" 'Hi-Torque' clip with buckle to R.H. side at 90° to gauge wires.

(iv) 5/8" 'Hi-Torque' clip with buckle to L.H. side at 90° to gauge wires.

(v) 3/8" modified 'Jubilee' clip with buckle to R.H. side at 90° to gauge wires.

(7) Place the female seating unit on the male unit and apply a slight compression to the assembly.

(8) Place p.t.f.e. strip under clip (iv), with at least $\frac{1}{2}$" protruding above the clip, and ensure that the joint in the strip is at 180° to buckle. Position clip (iv) such that its lower edge is 1 5/16" below the upper edge of male seating unit and tighten to a torque of 140 lb.in.

(9) Position clip (v), such that the cut-out portion is adjacent to the buckle of clip (iv) and tighten.

(10) Place temporary clip (iii) with its upper edge approximately $\frac{1}{4}$" below lower edge of axial strain gauges and tighten to a torque of 140 lb.in.

(11) Place temporary clip (ii) mid-way between clip (iii) and the lower edge of the specimen, and tighten to a torque of 140 lb.in.

(12) Place p.t.f.e. strip under clip (i) and position clip so that the top edge is not higher than the top edge of the lower subsidiary loading platen, and tighten to a torque of 140 lb.in.

(13) Remove temporary clips (ii) and (iii), release the load and remove the assembly from the assembly jig. Check that the sheath has not extruded below the lower edge of the lower subsidiary platen and trim if necessary.

The assembly is now ready for attaching to the base of the hydraulic cell (see A6.3.2.).

A6.3.2. Procedure for Setting-up Specimen

The step-by-step procedure for preparing the apparatus for test is described below -

(1) Screw the lower platen of the assembled platen/specimen/sheath unit into the base of the cell, the base being already located in the centre of the lower platen of the 500 Tonf. loading frame by means of a dowel.

(2) Make final electrical connections to the data logger from the confining pressure and loading frame ram pressure transducers and strain gauges on the specimen. Check the system for stability, etc.

(3) Lower the barrel unit on to the base of the cell, using lifting equipment provided on the 500 Tonf. loading frame and clamp by means of locking segments and a retaining ring.

(4) Roll the lower platen of the loading frame, and assembled cell, into position in the 500 Tonf. frame using the guide rails provided. Correct location is achieved by a pre-set buffer stop. Make hydraulic connections to the cell pressure application and control system.

(5) Fill the cell with the non-conducting transformer oil used for applying confining pressure, by means of the high-capacity low-pressure pump discharging into the base of the cell to ensure the displacement of all air.

(6) Isolate the low pressure circuit and make connections to the high pressure, low capacity pump and control system.

APPENDIX 7

Derived Results for Biaxial and Triaxial Test Series

Comprehensive information regarding the stress-strain data obtained in the main part of the experimental programme described in Chapters 5 and 7 is available from the Concrete Materials Research Group and will be the subject of a separate report [197]. The principal results derived from these data are shown in the following Tables:-

Table

A7.1. Values of stress and strain at o.s.f.p., o.u.f.p. and ultimate for specimens of Mix MBC under uniaxial compression.

A7.2. Values of stress and strain at o.s.f.p., o.u.f.p. and ultimate for specimens of Mix 6IC under uniaxial compression.

A7.3. Values of stress and strain at o.s.f.p., o.u.f.p. and ultimate for specimens of Mix MBC under equal biaxial compression.

A7.4. Values of stress and strain at o.s.f.p., o.u.f.p. and ultimate for specimens of Mix 6IC under equal biaxial compression.

A7.5. Values of stress and strain at o.s.f.p. and ultimate and E and ν at 33% of ultimate for specimens of idealised concrete Mixes I_0 to I_{26} under uniaxial tension.

A7.6. Values of stress and strain at o.s.f.p. and ultimate and E and ν at 33% of ultimate for specimens of idealised concrete Mixes I_{34} to I_{58} under uniaxial tension.

A7.7. Values of stress and strain at o.s.f.p., o.u.f.p. and ultimate for specimens of Mix I_0 under triaxial compression.

A7.8. Values of stress and strain at o.s.f.p., o.u.f.p. and ultimate for specimens of Mix I_{10} under triaxial compression.

A7.9. Values of stress and strain at o.s.f.p., o.u.f.p. and ultimate for specimens of Mix I_{18} under triaxial compression.

A7.10 Values of stress and strain at o.s.f.p., o.u.f.p. and ultimate for specimens of Mix I_{26} under triaxial compression.

A7.11. Values of stress and strain at o.s.f.p., o.u.f.p. and ultimate for specimens of Mix I_{34} under triaxial compression.

A7.12. Values of stress and strain at o.s.f.p., o.u.f.p. and ultimate for specimens of Mix I_{40} under triaxial compression.

A7.13. Values of stress and strain at o.s.f.p., o.u.f.p. and ultimate for specimens of Mix I_{52} under triaxial compression.

A7.14. Values of stress and strain at o.s.f.p., o.u.f.p. and ultimate for specimens of Mix I_{58} under triaxial compression.

A7.15. Values of stress and strain at o.s.f.p. and ultimate and E and ν at 33% of ultimate for specimens of real concrete mixes under uniaxial tension.

A7.16. Values of stress and strain at o.s.f.p., o.u.f.p. and ultimate for specimens of Mix M1 under triaxial compression.

A7.17. Values of stress and strain at o.s.f.p., o.u.f.p. and ultimate for specimens of Mix C1 under triaxial compression.

A7.18. Values of stress and strain at o.s.f.p., o.u.f.p. and ultimate for specimens of Mix M2 under triaxial compression.

A7.19 Values of stress and strain at o.s.f.p., o.u.f.p. and ultimate for specimens of Mix C2 under triaxial compression.

A7.20 Values of stress and strain at o.s.f.p., o.u.f.p. and ultimate for specimens of Mix C3 under triaxial compression.

A7.21. Values of stress and strain at o.s.f.p., o.u.f.p. and ultimate for specimens of Mix C4 under triaxial compression.

Spec. Type	Spec. Ref.	O.S.F.P.				O.U.F.P.				ULTIMATE			
		Stress	Comp. Strain	Tensile Strain	Vol. Strain	Stress	Comp. Strain	Tensile Strain	Vol. Strain	Stress	Comp. Strain	Tensile Strain	Vol. Strain
		lb/in^2	microstrain			lb/in^2	microstrain			lb/in^2	microstrain		
Cylinder	A	-3851	-1021	+199	-623	-5631	-2038	+544	-952	-6046	-2793	+1186	-426
	B	-4424	-1206	+243	-721	-6112	-2644	+657	-1333	-6112	-2644	+657	-1333
	C	-4567	-1372	+232	-908	-5990	-2460	+544	-1374	-5990	-2460	+544	-1374
	mean	-4281	-1200	+225	-751	-5911	-2381	+582	-1220	-6049	-2632	+796	-1044
Prism	A	-3674	-954	+160	-634	-5670	-2244	+565	-1116	-5789	-2586	+794	-1000
	B	-3987	-1075	+221	-632	-5583	-2066	+538	-991	-5996	-2858	+1161	-542
	C	-4221	-1224	+188	-849	-5950	-2673	+681	-1315	-6065	-3142	+1009	-1130
	mean	-3961	-1084	+190	-705	-5734	-2328	+595	-1141	-5950	-2862	+988	-891
Slab	A	-3098	-816	+183	-449	-4987	-1889	+552	-786	-5840	-3390	+1991	-582
	B	-2820	-723	+168	-405	-4522	-1487	+440	-659	-5758	-3289	+2078	-497
	C	-3008	-757	+170	-432	-5023	-1869	+608	-734	-5791	-3076	+1732	-134
	mean	-2975	-765	+174	-429	-4844	-1748	+533	-726	-5796	-3252	+1934	-404

Table A7.1. Values of stress and strain at o.s.f.p., o.u.f.p. and ultimate for specimens of Mix MBC under uniaxial compression.

Spec. Type	Spec. Ref.	O.S.F.P.				O.U.F.P.				ULTIMATE			
		Stress	Comp. Strain	Tensile Strain	Vol. Strain	Stress	Comp. Strain	Tensile Strain	Vol. Strain	Stress	Comp. Strain	Tensile Strain	Vol. Strain
		lb/in^2	microstrain			lb/in^2	microstrain			lb/in^2	microstrain		
Cylinder	A	-3975	-675	+77	-521	-5369	-1202	+217	-769	-5636	-1679	+630	-422
	B	-3979	-721	+86	-549	-5091	-1116	+194	-728	-5385	-1428	+704	-22
	C	-4901	-932	+111	-710	-5089	-1056	+145	-766	-5888	-1410	+631	-148
	mean	-4285	-776	+91	-593	-5250	-1125	+185	-754	-5636	-1506	+655	-197
Prism	A	-4091	-684	+91	-502	-4713	-839	+124	-591	-5187	-1211	+350	-510
	B	-3315	-523	+67	-390	-5115	-864	+180	-504	-5367	-1030	+601	+171
	C	-4071	-658	+86	-486	-5233	-924	+174	-576	-5435	-1096	+381	-335
	mean	-3826	-622	+81	-459	-5020	-876	+159	-557	-5330	-1112	+444	-225
Slab	A	-2681	-453	+76	-301	-3945	-770	+176	-417	-4989	-1558	+1296	+1032
	B	-2180	-327	+33	-261	-4133	-700	+111	-479	-5274	-1231	+518	-195
	C	-2840	-483	+46	-391	-4343	-813	+151	-511	-5629	-1742	+1575	+1404
	mean	-2567	-421	+52	-318	-4140	-761	+146	-469	-5297	-1510	+1130	+747

Table A7.2. Values of stress and strain at o.s.f.p., o.u.f.p. and ultimate for specimens of Mix 6IC under uniaxial compression.

Spec. Type	Type of Test	Spec. Ref.	O.S.F.P.				O.U.F.P.				ULTIMATE			
			Biaxial Stress	Comp. Strain	Tensile Strain	Vol. Strain	Biaxial Stress	Comp. Strain	Tensile Strain	Vol. Strain	Biaxial Stress	Comp. Strain	Tensile Strain	Vol. Strain
			lb/in^2	microstrain			lb/in^2	microstrain			lb/in^2	microstrain		
Slab	-	A	-2634	-500	+215	-785	-6598	-2466	+2133	-2802	-6718	-2650	+2971	-2337
		B	-3072	-581	+317	-845	-6368	-2020	+1837	-2206	-6775	-2450	+3602	-1311
		C	-3179	-608	+330	-885	-6527	-2199	+1686	-2715	-6709	-1757	+2179	-1340
		Mean	-2962	-563	+287	-838	-6498	-2228	+1885	-2574	-6734	-2286	+2917	-1663
Cylinder	Null	A	At start of test				-6157	-1702	+2320	-1089	-6157	-1702	+2320	-1089
	Null	B	-5758	-1533	+1876	-1193	-6647	-2513	+3484	-1554	-6817	-3000	+4645	-1373
	Null	C	-6307	-1228	+2353	-107	-	-	-	-	-6692	-1841	+3575	-117
	Comp.	D	-4065	-1023	+925	-1122	-5883	-2061	+2503	-1624	-6372	-2769	+4439	-1116
	Comp.	E	-5348	-1380	+1398	-1364	-6642	-2396	+2911	-1890	-6917	-2845	+4057	-1647
	Tens.	F	-5838	-1344	+2633	-60	-	-	-	-			+4502	+673
	Tens.	G	-5453	-911	+1338	-484	-6262	-1351	+2151	-555	-6752	-1865	+4006	+264
		Mean	-4681	-1060	+1503	-619	-6318	-2005	+2674	-1342	-6593	-2276	+3935	-629

Table A7.3. Values of stress and strain at o.s.f.p., o.u.f.p. and ultimate for specimens of Mix MBC under equal biaxial compression.

Spec. Type	Type of Test	Spec. Ref.	O.S.F.P.				O.U.F.P.				ULTIMATE			
			Biaxial Stress	Comp. Strain	Tensile Strain	Vol. Strain	Biaxial Stress	Comp. Strain	Tensile Strain	Vol. Strain	Biaxial Stress	Comp. Strain	Tensile Strain	Vol. Strain
			lb/in^2	microstrain			lb/in^2	microstrain			lb/in^2	microstrain		
Slab	–	A	-3775	-503	-191	-814	-6440	-1027	+621	-1434	-8479	-1096	+1371	-822
	–	B	-3376	-442	-155	-728	-6443	-1054	+681	-1427	-8342	-1432	+7970	-5086
	–	C	-3574	-486	-175	-797	-6079	-951	+609	-1293	-8416	-1059	+3393	-1268
		mean	-3575	-477	-174	-780	-6321	-1011	+637	-1385	-8412	-1196	+4245	-2392
Cylinder	Null	A	at start of test				-1069	-142	+15	-269	-5883	-238	+2453	-1975
	Null	B	at start of test				-2167	-228	+233	-222	-6792	-854	+4122	-2408
	Comp.	C	at start of test				-934	-131	+136	-127	-6048	-361	+2806	-2082
	Comp.	D	at start of test				-5568	-748	+895	-601	-6762	-1294	+2402	-192
	Comp.	E	-	-	-	-	-	-	-	-	-6182	-	-	-
	Tens.	F	at start of test				-1473	-223	+96	-350	-5808	-1001	+3363	-1355
	Tens.	G	at start of test				-1233	-158	+95	-221	-6227	-867	+2503	-766
	Tens.	H	at start of test				-4539	-510	+525	-496	-5893	-1404	+3613	-800
		mean	at start of test				-2426	-306	+285	-327	-6199	-860	+3037	-1313

Table A7.4. Values of stress and strain at o.s.f.p., o.u.f.p. and ultimate for specimens of Mix 6IC under equal biaxial compression

Mix Ref.	Spec. Ref.	O.S.F.P.				ULTIMATE				SECANT E and ν at 33% ULTIMATE	
		Axial Stress	Axial Strain	Lat. Strain	Vol. Strain	Axial Stress	Axial Strain	Lat. Strain	Vol. Strain	E	ν
		lb/in^2	microstrain			lb/in^2	microstrain			lb/in^2	
I_0	A	+319	+73	-9	+56	+456	+115	-10	+95	4.688	-0.131
	B	+413	+101	-14	+73	+413	+101	-14	+73	4.665	-0.136
	C	+307	+77	-6	+65	+333	+87	-5	+77	4.277	-0.071
	mean	+346	+84	-10	+65	+401	+101	-10	+82	4.543	-0.115
I_5	A	+320	+104	-20	+64	+320	+104	-20	+64	3.815	-0.145
	B	+356	+81	-9	+63	+356	+81	-9	+63	4.565	-0.140
	C	+274	+62	-7	+48	+451	+113	-12	+89	4.466	-0.121
	mean	+317	+82	-12	+58	+376	+99	-14	+72	4.282	-0.135
$I_{7.5}$	A	+350	+100	-8	+85	+420	+133	-7	+119	4.148	-0.182
	B	+252	+61	-10	+40	+314	+84	-5	+74	4.236	-0.224
	mean	+301	+81	-9	+63	+367	+109	-6	+97	4.192	-0.203
I_{10}	A	+355	+89	-22	+45	+355	+89	-22	+45	4.497	-0.267
	B	+462	+113	-21	+71	+462	+113	-21	+71	4.217	-0.088
	mean	+409	+101	-22	+58	+409	+101	-22	+58	4.357	-0.178
I_{18}	A	+351	+74	-10	+53	+394	+84	-12	+60	4.923	-0.096
	B	+243	+52	-3	+45	+335	+100	-5	+90	4.962	-0.055
	C	+166	+32	-7	+18	+388	+97	0	+97	5.586	-0.277
	mean	+253	+53	-7	+39	+372	+94	-6	+82	5.156	-0.143
I_{26}	A	+453	+114	-12	+90	+453	+114	-12	+90	4.025	-0.074
	B	+317	+67	-8	+52	+417	+103	-12	+79	4.986	-0.093
	C	+339	+67	-13	+41	+339	+67	-13	+41	5.143	-0.189
	mean	+370	+83	-11	+61	+403	+95	-13	+70	4.718	-0.119

Table A7.5. Values of stress and strain at o.s.f.p. and ultimate and E and ν at 33% of ultimate for specimens of idealised concrete Mixes I_0 to I_{26} under uniaxial tension.

Mix Ref.	Spec. Ref.	O.S.F.P.				ULTIMATE				SECANT E and ν at 33% ULTIMATE	
		Axial Stress	Axial Strain	Lat. Strain	Vol. Strain	Axial Stress	Axial Strain	Lat. Strain	Vol. Strain	E	ν
		lb/in^2	microstrain			lb/in^2	microstrain			lb/in^2	
I_{34}	A	+418	+81	-17	+46	+492	+114	-17	+80	6.083	-0.261
	B	+278	+62	-10	+42	+343	85	-11	+63	4.761	-0.123
	C	+258	+44	-5	+33	+365	+61	-6	+49	5.972	-0.125
	mean	+318	+62	-11	+40	+400	+87	-11	+64	5.605	-0.170
I_{40}	A	+310	+55	-9	+37	+402	+70	-6	+58	5.494	-0.127
	B	+355	+65	-16	+33	+399	+88	-17	+54	6.224	-0.250
	C	+360	+65	-11	+43	+487	+101	-14	+73	6.228	-0.160
	mean	+342	+62	-12	+38	+429	+86	-12	+62	5.981	-0.179
I_{46}	A	+464	+86	-18	+50	+464	+86	-18	+50	6.848	-0.280
	B	+356	+59	-16	+28	+491	+91	-19	+53	6.765	-0.333
	C	+382	+62	-15	+32	+437	+85	-16	+53	7.540	-0.372
	mean	+401	+69	-16	+37	+464	+87	-18	+52	7.057	-0.328
I_{52}	A	+345	+55	-10	+35	+473	+73	-14	+45	7.586	-0.156
	B	+457	+80	-16	+48	+457	+80	-16	+48	6.481	-0.154
	C	+412	+71	-14	+44	+487	+102	-17	+68	6.347	-0.208
	mean	+405	+69	-13	+42	+472	+85	-16	+54	6.804	-0.173
I_{58}	A	+413	+66	-10	+45	+440	+71	-9	+53	7.343	-0.237
	B	+289	+45	-7	+31	+343	+66	0	+66	6.820	-0.125
	mean	+351	+56	-9	+38	+392	+69	-5	+60	7.082	-0.181

Table A7.6. Values of stress and strain at o.s.f.p. and ultimate and E and ν at 33% of ultimate for specimens of idealised concrete Mixes I_{34} to I_{58} under uniaxial tension.

Spec. Ref.	Conf. Press.	O.S.F.P.				O.U.F.P.				ULTIMATE			
		Axial Stress	Axial Strain	Lateral Strain	Vol. Strain	Axial Stress	Axial Strain	Lateral Strain	Vol. Strain	Axial Stress	Axial Strain	Lateral Strain	Vol. Strain
	lb/in^2	lb/in^2	microstrain			lb/in^2	microstrain			lb/in^2	microstrain		
A	0	-7328	-1991	+399	-1195	-10452	-3556	+867	-1828	-10452	-3556	+867	-1828
B	0	-7557	-1936	+377	-1184	-10980	-3754	+899	-1963	-10980	-3754	+899	-1963
C	-512	-8345	-2147	+306	-1536	-12918	-5911	+1463	-3001	-12993	-6521	+1813	-2916
D	-1025	-10496	-3084	+357	-2373	continuous volume decrease				-14798	-9302	+2544	-4254
E	-1985	-11761	-3737	+291	-3157	-16138	-12274	+3000	-6339	-16339	-16643	+5873	-5058
F	-2402	-12962	-4126	+292	-3544	-18060	-15897	+4231	-7551	-18140	-16922	+4766	-7529
G	-2935	-13882	-5072	+315	-4446	-18316	-29944	+8953	-12496	-19288	-24058	+6410	-11507
H	-5448	-17307	-7840	-28	-7894	-25161	-67760	+18158	-33597	-25662	-55333	+12203	-32137
J	-10028	-18554	-8291	-2081	-12414	-37637	-132523	+32903	-74499	-37643	-124975	+29245	-73047
K	-15694	-18710	-6351	-4323	-14923	continuous volume decrease				-53500	-250000	+72000	-106000
L	-17567	-17766	-6566	-6421	-19282	-60738	-221237	+52549	-137241	-61000	-250000	+87500	-75000

Table A7.7. Values of stress and strain at o.s.f.p., o.u.f.p. and ultimate for specimens of Mix I_0 under triaxial compression.

Spec. Ref.	Conf. Press.	O.S.F.P.				O.U.F.P.				ULTIMATE			
		Axial Stress	Axial Strain	Lateral Strain	Vol. Strain	Axial Stress	Axial Strain	Lateral Strain	Vol. Strain	Axial Stress	Axial Strain	Lateral Strain	Vol. Strain
	lb/in^2	lb/in^2	microstrain			lb/in^2	microstrain			lb/in^2	microstrain		
A	0	-6082	-1379	+265	-850	-10650	-3124	+735	-1657	-10650	-3124	+735	-1657
B	-1198	-8300	-1824	+172	-1480	-15290	-6404	+1632	-3159	-15601	-8031	+2668	-2731
C	-2501	-13879	-4095	+263	-3571	-18275	-25777	+6411	-13246	-18983	-17910	+3592	-10842
D	-5057	-19033	-7118	+183	-6756	-25730	-43693	+10062	-24352	-26281	-34327	+6173	-22368
E	-10065	-20732	-7803	-1040	-9865	-	-	-	-	-36605	-	+6194	-
F	-12565	-20543	-7468	-2209	-11848	-	-	-	-	-	-	-	-
G	-15078	-19222	-5641	-3703	-12992	-49283	-77932	+10762	-57979	-50139	-102003	+36187	-35836
H	-17499	-18130	-4759	-3934	-12575	-58940	-124772	+26958	-76947	-59394	-143639	+39391	-74845

Table A7.8. Values of stress and strain at o.s.f.p., o.u.f.p. and ultimate for specimens of Mix I_{10} under triaxial compression.

Spec. Ref.	Conf. Press.	O.S.F.P.				O.U.F.P.				ULTIMATE			
		Axial Stress	Axial Strain	Lateral Strain	Vol. Strain	Axial Stress	Axial Strain	Lateral Strain	Vol. Strain	Axial Stress	Axial Strain	Lateral Strain	Vol. Strain
	lb/in^2	lb/in^2	microstrain			lb/in^2	microstrain			lb/in^2	microstrain		
A	0	-5113	-1005	+212	-583	-9134	-2407	+642	-1126	-9483	-2849	+1329	-197
B	-1198	-7455	-1453	+119	-1217	-13916	-4512	+1118	-2286	-14856	-6448	+2386	-1700
C	-2507	-11716	-2673	+206	-2263	-17531	-7268	+1784	-3724	-18855	-12430	+5233	-2067
D	-5075	-18140	-5410	+113	-5185	-25836	-20495	+4312	-12029	-26070	-23334	+6004	-11571
E	-7570	-19867	-7247	-409	-8060	-31307	-34827	+6981	-21305	-31653	-40920	+10879	-19938
F	-10022	-23937	-8277	-494	-9257	-36354	-27430	+5360	-16977	-37937	-49151	+24176	-2620
G	-10052	-21163	-8026	-1278	-1050	-	-	-	-	-39600	-	-	-
H	-12559	-21346	-6569	-2026	-10590	-44472	-73342	+15457	-44475	-44607	-81182	+20894	-42386
J	-15072	-18616	-5265	-3301	-11820	-51002	-81224	+14539	-54315	-51702	-118246	+44679	-37694
K	-17530	-17961	-4257	-3890	-11989	-56022	-32210	+2081	-28178	-61035	-14502	+29003	+32032

Table A7.9. Values of stress and strain at o.s.f.p., o.u.f.p. and ultimate for specimens of Mix I_{18} under triaxial compression.

Spec. Ref.	Conf. Press.	O.S.F.P.				O.U.F.P.				ULTIMATE			
		Axial Stress	Axial Strain	Lateral Strain	Vol. Strain	Axial Stress	Axial Strain	Lateral Strain	Vol. Strain	Axial Stress	Axial Strain	Lateral Strain	Vol. Strain
	lb/in^2	lb/in^2	microstrain			lb/in^2	microstrain			lb/in^2	microstrain		
A	0	-3209	-698	+131	-437	-8019	-2075	+528	-1021	-8698	-2648	+1009	-633
B	-445	-7317	-1462	+238	-987	-11023	-2676	+626	-1427	-12663	-4613	+2121	-397
C	-1022	-7653	-1477	+143	-1192	-13793	-4186	+999	-2197	-14935	-6764	+3121	-554
D	-2050	-12862	-3594	+192	-3212	-17786	-10903	+2334	-6280	-17942	-12968	+3445	-6156
E	-3014	-16459	-5031	+377	-4281	-20504	-23280	+5323	-12853	-21359	-15082	+2603	-9948
F	-5064	-17233	-5014	+48	-4918	continuous volume decrease				-26988	-28705	+4735	-19485
G	-6705	-18538	-5735	-279	-6290	-30337	-29037	+6763	-15860	-30630	-35517	+10649	-14866
H	-10351	-23169	-8624	-1021	-10646	continuous volume decrease				-40129	-64540	+8141	-49247
J	-15383	-18116	-4533	-3285	-11063	-	-	-	-	-	-	-	-
K	-16040	-22048	-6792	-3470	-13673	continuous volume decrease				-52675	-90000	+15000	-60000
L	-20445	-24823	-7526	-5659	-18727	-	-	-	-	-	-	-	-

Table A7.10 Values of stress and strain at o.s.f.p., o.u.f.p. and ultimate for specimens of Mix I_{26} under triaxial compression.

Spec. Ref.	Conf. Press.	O.S.F.P.				O.U.F.P.				ULTIMATE			
		Axial Stress	Axial Strain	Lateral Strain	Vol. Strain	Axial Stress	Axial Strain	Lateral Strain	Vol. Strain	Axial Stress	Axial Strain	Lateral Strain	Vol. Strain
	lb/in^2	lb/in^2	microstrain			lb/in^2	microstrain			lb/in^2	microstrain		
A	0	-3268	-666	+127	-413	-7235	-1751	+425	-902	-7865	-2238	+887	-468
B	-1002	-5347	-1046	+41	-963	-14371	-5096	+1263	-2582	-14987	-7079	+2624	-1862
C	-2003	-10348	-2113	+133	-1847	-17812	-6647	+1717	-3233	-18729	-10369	+4145	-2148
D	-5063	-16738	-4126	-94	-4313	-26832	-15929	+3629	-8775	-27858	-22244	+7907	-6430
E	-10040	-22372	-5719	-866	-7440	-41943	-32458	+6454	-19929	-42261	-38273	+10525	-17922
F	-15066	-21537	-5265	-2364	-9963	-55160	-74227	+17807	-40963	-55514	-38886	+22530	+4909
G	-20068	-20877	-4874	-4592	-13992	-	-	-	-	-	-	-	-
H	-20055	-20885	-4840	-4555	-13884	-	-	-	-	-	-	-	-
J	-20043	-20862	-3891	-3731	-11311	-69043	-80397	+14852	-52878	-69141	-80463	+14914	-52831

Table A7.11. Values of stress and strain at o.s.f.p., o.u.f.p. and ultimate for specimens of Mix I_{34} under triaxial compression.

Spec. Ref.	Conf. Press.	O.S.F.P.				O.U.F.P.				ULTIMATE			
		Axial Stress	Axial Strain	Lateral Strain	Vol. Strain	Axial Stress	Axial Strain	Lateral Strain	Vol. Strain	Axial Stress	Axial Strain	Lateral Strain	Vol. Strain
	lb/in^2	lb/in^2	microstrain			lb/in^2	microstrain			lb/in^2	microstrain		
A	0	-4005	-643	+115	-413	-6994	-1286	+288	-711	-7807	-1742	+1061	+377
B	-983	-5050	-842	+58	-727	-14754	-5395	+1609	-2192	-15114	-7332	+2593	-2178
C	-2495	-13178	-2580	+197	-2186	-20871	-10521	+3005	-4565	-21028	-12563	+4271	-4110
D	-5002	-17323	-3703	-32	-3768	-28739	-17832	+3716	-10519	-28819	-19474	+4625	-10385
E	-7551	-24338	-7254	-44	-7342	-37525	-28716	+5435	-18130	-37727	-29962	+6110	-18073
F	-7515	-20505	-5217	-308	-5829	-36141	-30466	+7265	-16328	-36175	-36270	+10536	-15855
G	-10040	-24580	-7208	-52	-7208	-41368	-29987	+4739	-20771	-42997	-47239	+26989	+4884
H	-10040	-21466	-5774	-870	-7504	-42176	-42447	+9701	-23780	-42280	-49683	+14505	-21914
J	-15054	-21949	-4418	-1990	-8376	-56976	-43667	+8027	-28253	-57471	-48039	+11091	-26806
K	-15054	-21644	-5120	-2312	-9716	continuous volume decrease				-56024	-80480	+21360	-40779
L	-20061	-22145	-5044	-4572	-14121	-66547	-55808	+5242	-45884	-68514	-37115	+27093	-15766

Table A7.12. Values of stress and strain at o.s.f.p., o.u.f.p. and ultimate for specimens of Mix I_{40} under triaxial compression.

Spec. Ref.	Conf. Press.		O.S.F.P.			O.U.F.P.				ULTIMATE			
		Axial Stress	Axial Strain	Lateral Strain	Vol. Strain	Axial Stress	Axial Strain	Lateral Strain	Vol. Strain	Axial Stress	Axial Strain	Lateral Strain	Vol. Strain
	lb/in^2	lb/in^2	microstrain			lb/in^2	microstrain			lb/in^2	microstrain		
A	0	-4395	-639	+133	-372	-5742	-889	+209	-471	-7331	-1301	+857	+412
B	-989	-6600	-955	+75	-804	-14535	-3213	+1803	-1612	-16348	-5637	+2644	-372
C	-2501	-13289	-2392	+191	-2011	-22434	-7745	+1894	-3982	-23438	-10357	+3570	-3279
D	-5038	-18146	-3527	-63	-3652	-33212	-12335	+2532	-7328	-33833	-14235	+3693	-6940
E	-10003	-	-	-	-	-49227	-22849	+3897	-15218	-49564	-25390	+5506	-14629
F	-10046	-26271	-5569	-447	-6452	continuous volume decrease				-53241	-27005	+3219	-20732
G	-15041	-28240	-5321	-1298	-7901	-62634	-37040	+5308	-26790	-63969	-30461	+3071	-24498
H	-20043	-26968	-5041	-2951	-10905	-71011	-34703	+2498	-29875	-72307	-39522	+5401	-29119

Table A7.13. Values of stress and strain at o.s.f.p., o.u.f.p. and ultimate for specimens of Mix I_{52} under triaxial compression.

Spec. Ref.	Conf. Press.	O.S.F.P.				O.U.F.P.				ULTIMATE			
		Axial Stress	Axial Strain	Lateral Strain	Vol. Strain	Axial Stress	Axial Strain	Lateral Strain	Vol. Strain	Axial Stress	Axial Strain	Lateral Strain	Vol. Strain
	lb/in^2	lb/in^2	microstrain			lb/in^2	microstrain			lb/in^2	microstrain		
A	0	-2488	-461	+83	-295	-5449	-1172	+294	-585	-6732	-1900	+2336	+2770
B	-492	-3405	-522	+31	-461	-10525	-2231	+594	-1046	-11987	-3707	+1744	-229
C	-995	-5681	-907	+47	-813	-14970	-3886	+977	-1938	-16733	-6462	+2985	-522
D	-1702	-	-	-	-	-17560	-4506	+1010	-2494	-21046	-8159	+4238	+266
E	-2501	-13013	-2483	+106	-2270	-23243	-8435	+1817	-4830	-24120	-11244	+3578	-4155
F	-5051	-19804	-3921	+60	-3802	-34942	-15586	+3282	-9113	-35020	-16222	+3633	-9061
G	-7558	-20267	-3759	-201	-4160	-44493	-16741	+3720	-9411	-44493	-16741	+3720	-9411
H	-7564	-26971	-5539	+73	-5394	continuous volume decrease				-44874	-19608	+3052	-13615
J	-10058	-22699	-4373	-731	-5829	-50122	-31145	+7308	-16933	-50632	-25757	+5460	-15088
K	-10065	-28708	-6069	-386	-6837	-49308	-18372	+2434	-13588	-49388	-18776	+2656	-13556
L	-15078	-28487	-6362	-1203	-8752	-64281	-30060	+3533	-23194	-64281	-30060	+3533	-23194
M	-20086	-31080	-6300	-2527	-11317	-73345	-41881	+2112	-37829	-79004	-30590	+136	-30326

A7.14. Values of stress and strain at o.s.f.p., o.u.f.p. and ultimate for specimens of Mix I_{58} under triaxial compression.

Mix Ref.	Spec. Ref.	O.S.F.P.				ULTIMATE				SECANT E and ν at 33% ULTIMATE	
		Axial Stress	Axial Strain	Lat. Strain	Vol. Strain	Axial Stress	Axial Strain	Lat. Strain	Vol. Strain	E	ν
		lb/in^2	microstrain			lb/in^2	microstrain			lb/in^2	
M_1	A	+531	+63	-18	+27	+531	+63	-18	+27	4.91	-0.161
	B	+546	+81	-20	+41	+546	+81	-20	+41	6.77	-0.183
	C	+652	+136	-24	+88	+652	+136	-24	+88	4.15	-0.134
	mean	+576	+93	-21	+29	+576	+93	-21	+29	5.28	-0.159
C_1	A	+307	+52	-8	+36	+499	+109	-12	+85	5.46	-0.160
	B	+360	+48	-9	+30	+602	+93	-17	+59	8.36	-0.197
	C	+426	+67	-11	+45	+567	+95	-14	+67	6.63	-0.177
	mean	+364	+56	-9	+37	+556	+99	-14	+70	6.82	-0.178
M_2	A	+448	+123	-19	+85	+448	+123	-19	+85	3.78	-0.176
	B	+455	+76	-19	+38	+455	+76	-19	+38	5.07	-0.169
	C	+446	+128	-20	+88	+446	+128	-20	+88	3.51	-0.156
	mean	+450	+109	-19	+70	+450	+109	-19	+70	4.12	-0.167
C_2	A	+95	+21	-4	+13	+236	+57	-6	+45	4.29	-0.204
	B	+164	+36	-6	+24	+197	+45	-7	+31	5.11	-0.142
	C	+116	+29	-4	+21	+256	+69	-6	+57	3.97	-0.125
	mean	+125	+29	-5	+19	+230	+57	-6	+44	4.46	-0.157
C_3	A	+493	+85	-22	+41	+493	+85	-22	+41	6.20	-0.164
	B	+598	+93	-22	+53	+598	+93	-20	+53	6.27	-0.156
	mean	+546	+89	-21	+47	+546	+89	-21	+47	6.24	-0.160
C_4	A	+568	+104	-21	+62	+568	+104	-21	+62	5.90	-0.200
	B	+635	+126	-18	+90	+704	+144	-15	+114	5.63	-0.170
	C	+701	+140	-26	+88	+701	+140	-26	+88	5.67	-0.173
		+635	+123	-22	+80	+658	+129	-21	+88	5.73	-0.181

Table A7.15. Values of stress and strain at o.s.f.p. and ultimate and E and ν at 33% of ultimate for specimens of Real Concrete Mixes under uniaxial tension.

Spec. Ref.	Conf. Press.	O.S.F.P.				O.U.F.P.				ULTIMATE			
		Axial Stress	Axial Strain	Lateral Strain	Vol. Strain	Axial Stress	Axial Strain	Lateral Strain	Vol. Strain	Axial Stress	Axial Strain	Lateral Strain	Vol. Strain
	lb./in^2	lb/in^2	microstrain			lb/in^2	microstrain			lb/in^2	microstrain		
A	0	-7036	-1448	+309	-830	-12849	-3189	+845	-1502	-13474	-3725	+1291	-1151
B	0	-6446	-1305	+275	-755	-12904	-3348	+841	-1672	-12904	-3348	+841	-1672
C	0	-7444	-1522	+338	-847	-11353	-2968	+786	-1401	-11867	-2870	+739	-1395
D	-504	-7960	-1653	+256	-1142	-15317	-4661	+1137	-2396	-16178	-6404	+2383	-1664
E	-983	-9752	-2037	+273	-1492	-17402	-5224	+1112	-3011	-18426	-8190	+2813	-2603
F	-1991	-14375	-3373	+408	-2560	-21113	-9415	+2422	-4610	-21568	-13293	+5019	-3364
G	-3275	-16623	-3917	+314	-3292	-25968	-16229	+4764	-6833	-26147	-18862	+6238	-6584
H	-5057	-20681	-6163	+334	-5499	-30105	-40985	+13160	-15577	-30307	-36766	+11021	-15418
J	-10034	-24292	-8055	-768	-9577	-42012	-60222	+15478	-30906	-42015	-65589	+18594	-28401
K	-20037	-24610	-6757	-3725	-14143	Continuous volume decrease				-67385	-118575	+19354	-84126
L	-20043	-24199	-5969	-4304	-14507	-70240	-107693	+20820	-70151	-70299	-112837	+23824	-70063

Table A7.16. Values of stress and strain at o.s.f.p., o.u.f.p. and ultimate for specimens of Mix M1 under triaxial compression.

Spec. Ref.	Conf. Press.	O.S.F.P.				O.U.F.P.				ULTIMATE			
		Axial Stress	Axial Strain	Lateral Strain	Vol. Strain	Axial Stress	Axial Strain	Lateral Strain	Vol. Strain	Axial Stress	Axial Strain	Lateral Strain	Vol. Strain
	lb/in^2	lb/in^2	microstrain			lb/in^2	microstrain			lb/in^2	microstrain		
A	0	-7401	-1187	+215	-757	-8840	-1555	+320	-915	-9105	-1746	+624	-501
B	-504	-6103	-968	+100	-768	-13920	-2984	+623	-1742	-14290	-3506	+945	-1623
C	-989	-13800	-2889	+314	-2262	-16441	-5400	+1092	-3227	-16543	-5985	+1427	-3146
D	-1997	-11872	-2114	+51	-2011	-21202	-9951	+2558	-4880	-21241	-9149	+2186	-4812
E	-3269	-	-	-	-	-26978	-15185	+4121	-7051	-27191	-13211	+3199	-6888
F	-5032	-21190	-4714	+272	-4172	-31762	-18553	+4466	-9766	-31861	-20645	+5636	-9575
G	-9954	-	-	-	-	-45024	-33219	+6348	-20906	-45024	-33219	+6348	-20906
H	-10034	-24693	-4954	-640	-6227	-46564	-25852	+4825	-16429	-46879	-27848	+6010	-16128
J	-20055	-26766	-5018	-3285	-11540	-70463	-52919	+5391	-42680	-70574	-57794	+8244	-42194
K	-20055	-23659	-3919	-3223	-10330	continuous volume decrease				-69610	-48452	+5140	-38645

Table A7.17. Values of stress and strain at o.s.f.p., o.u.f.p. and ultimate for specimens of Mix C1 under triaxial compression.

Spec. Ref.	Conf. Press.	O.S.F.P.				O.U.F.P.				ULTIMATE			
		Axial Stress	Axial Strain	Lateral Strain	Vol. Strain	Axial Stress	Axial Strain	Lateral Strain	Vol. Strain	Axial Stress	Axial Strain	Lateral Strain	Vol. Strain
	lb/in^2	lb/in^2	microstrain			lb/in^2	microstrain			lb/in^2	microstrain		
A	0	-3893	-1124	+224	-676	-5402	-2295	+530	-1236	-5568	-3002	+1387	-235
B	0	-2956	-830	+151	-529	-5718	-2212	+547	-1119	-5985	-2724	+893	-943
C	-479	-4004	-1102	+90	-922	-7727	-3931	+954	-2029	-8171	-6200	+2605	-1016
D	-1008	-5825	-1763	+185	-1394	-9507	-6557	+1769	-3040	-10023	-12343	+5766	-921
E	-1997	-7525	-2829	-60	-2948	-12571	-18587	+4991	-8766	-13076	-31685	+13410	-5541
F	-3287	-9801	-4249	-274	-4795	-17794	-52912	+15258	-23791	-17799	-57035	+16737	-23737
G	-5051	-11268	-6368	-948	-8251	-23052	-72290	+19987	-34836	-23165	-81347	+25263	-34344
H	-10028	-10706	-4733	-4553	-13776	-38127	-116117	+29439	-63310	-38194	-126757	+35834	-63052
J	-20043	at end of hydrostatic region				-66650	-218204	+53713	-131963	-67021	-179915	+29356	-131059

Table A7.18. Values of stress and strain at o.s.f.p., o.u.f.p. and ultimate for specimens of Mix M2 under triaxial compression.

Spec. Ref.	Conf. Pres.	O.S.F.P.				O.U.F.P.				ULTIMATE			
		Axial Stress	Axial Strain	Lateral Strain	Vol. Strain	Axial Stress	Axial Strain	Lateral Strain	Vol. Strain	Axial Stress	Axial Strain	Lateral Strain	Vol. Strain
	lb/in^2	lb/in^2	microstrain			lb/in^2	microstrain			lb/in^2	microstrain		
A	0	-1078	-335	+50	-234	-2102	-917	+234	-450	-2453	-2236	+1597	+955
B	0	-809	-249	+56	-136	-1334	-521	+161	-199	-1975	-1536	+1083	+627
C	-516	-2792	-990	+49	-893	-4958	-5783	+1682	-2435	-5430	-12950	+8526	-3952
D	-989	-2400	-744	-121	-986	-6440	-8139	+2375	-3423	-7421	-22087	+13835	+5159
E	-2009	-4187	-2128	-539	-3204	-10249	-23256	+5715	-12059	-11077	-44416	+19467	-6850
F	-3287	-5751	-3498	-1316	-6120	-15732	-30726	+5987	-19085	-17009	-57230	+27257	-5136
G	-5075	at end of hydrostatic region				-19537	-30461	+3797	-23084	-22035	-29590	+23899	+17349
H	-10028	at end of hydrostatic region				-32057	-38420	+1275	-35966	-37078	-63210	+20228	-24928
J	-20049	at end of hydrostatic region				-61325	-49641	+1869	-46086	-67401	-77747	+19659	-41131
K	-20055	at end of hydrostatic region				-57604	-51869	+1922	-48221	-66831	-112889	+44335	-32485

Table A7.19. Values of stress and strain at o.s.f.p., o.u.f.p. and ultimate for specimens of Mix C2 under triaxial compression.

Spec. Ref.	Conf. Press.	O.S.F.P.				O.U.F.P.				ULTIMATE			
		Axial Stress	Axial Strain	Lateral Strain	Vol. Strain	Axial Stress	Axial Strain	Lateral Strain	Vol. Strain	Axial Stress	Axial Strain	Lateral Strain	Vol. Strain
	lb/in^2	lb/in^2	microstrain			lb/in^2	microstrain			lb/in^2	microstrain		
A	0	-5848	-1088	+258	-573	-7720	-1656	+416	-824	-7720	-1656	+416	-824
B	0	-6447	-1175	+316	-543	-7219	-1459	+439	-582	-7329	-1556	+507	-543
C	0	-5526	-1001	+263	-476	-7251	-1482	+448	-588	-7659	-1690	+631	-429
D	-492	-7777	-1393	+296	-802	-10298	-2413	+630	-1155	-10869	-3183	+1255	-679
E	-989	-9345	-1800	+146	-1509	-12217	-8352	+1977	-4428	-13117	-4916	+798	-3326
F	-1997	-11536	-2482	+311	-1861	-16559	-8466	+2194	-4111	-16844	-11551	+4148	-3334
G	-3257	-12949	-3277	+288	-2702	-20196	-18320	+5350	-7788	-20431	-23258	+8316	-6945
H	-5026	-16201	-4370	+140	-4090	-25484	-18707	+4357	-10136	-26550	-27872	+11402	-5578
J	-10022	-17085	-4165	-1092	-6339	-39494	-43896	+9797	-25070	-40242	-58092	+18505	-22910
K	-10040	-16995	-4379	-1044	-6455	-40729	-61630	+17719	-28080	-40874	-73912	+24935	-27151
L	-20043	at end of hydrostatic region				-65779	-101207	+22007	-61213	-67471	-138812	+48760	-52782
M	-20184	at end of hydrostatic region				-66709	-134634	+43275	-58116	-67445	-149412	+52722	-57359

Table A7.20. Values of stress and strain at o.s.f.p., o.u.f.p. and ultimate for specimens of Mix C3 under triaxial compression.

Spec. Ref.	Conf. Press.	O.S.F.P.				O.U.F.P.				ULTIMATE			
		Axial Stress	Axial Strain	Lateral Strain	Vol. Strain	Axial Stress	Axial Strain	Lateral Strain	Vol. Strain	Axial Stress	Axial Strain	Lateral Strain	Vol. Strain
	lb/in^2	lb/in^2	microstrain			lb/in^2	microstrain			lb/in^2	microstrain		
A	0	-3804	-753	+138	-478	-7768	-2175	+581	-1016	-8219	-2832	+1025	-787
B	-492	-	-	-	-	-9342	-3574	+908	-1763	-9901	-5663	+2383	-919
C	-504	-4968	-1011	+102	-806	-10075	-4167	+1048	-2078	-10308	-5013	+1563	-1901
D	-971	-6629	-1523	+120	-1283	-11844	-6810	+1849	-3134	-12034	-8567	+2832	-2944
E	-2003	-8584	-2075	+ 66	-1943	-15266	-10504	+2697	-5160	-15838	-14831	+5763	-3443
F	-3287	-11476	-3656	- 61	-3777	-18855	-17545	+3941	-9786	-19408	-23182	+7767	-7950
G	-5032	-11644	-3645	-426	-4493	-22852	-21147	+4633	-12056	-24119	-30572	+11476	-8194
H	-10028	-14746	-4350	-1990	-8308	sheath punctured				-	-	-	-
J	-10040	-14406	-4050	-1848	-7727	-38151	-38513	+5438	-28027	-38886	-47273	+6389	-35061
K	-20055	at end of hydrostatic region				-59553	-44222	+1963	-40466	-63573	-75458	+27060	-24744
L	-20061	at end of hydrostatic region				-64190	-63437	+9015	-46475	-65158	-84163	+22870	-41793

Table A7.21. Values of stress and strain at o.s.f.p., o.u.f.p. and ultimate for specimens of Mix C4 under triaxial compression.

APPENDIX 8

The Frictional Resistance of the Axial Load Piston of the Triaxial Cell

As a specimen deforms axially under load the piston assembly applying the load is subjected to frictional restraint at each of the three pressure seals (see Fig. 7.3). This restraint will essentially reduce the load acting on a specimen to a value below that externally applied to the piston by the axial loading system. The main factors affecting the magnitude of this restraint are:-

i) The rate of movement of the piston
The frictional resistance generally increases to a maximum value prior to movement of the piston (stiction) after which it decays to an approximately constant value, this value being dependent on the rate or movement.

ii) The magnitude of the pressure within the cell
Variations of pressure cause the dimensions of the various components of the cell to change. Such changes affect the clearance between the piston and the pressure seals.

iii) The temperature of the hydraulic fluid within the cell
This is considered to be a relatively insignificant factor as the pressurising system for the cell is effectively a 'dead-end' arrangement with virtually no flow of oil. Thus the temperature of the oil remains constant throughout the duration of each test.

The magnitude of the frictional restraint against movement of the axial load piston was assessed by measuring the load necessary to move the piston at a given rate for various values of oil pressure within the cell. The rate of piston movement adopted corresponded to the rate adopted for the tests on concrete cylinders and was controlled by an Amsler hydropacer unit. For each value of cell pressure ranging from zero up to 20,000 lb./in.^{2} the load required to move the piston at the given rate was measured continuously using a sensitive 5 Tonf. capacity load transducer and recorded by a pen-recorder.

For each value of cell pressure the characteristic curve of load vs. piston displacement showed a rapid increase of load up to a maximum followed by a

rapid reduction to a constant value of approximately 80% of the peak value. The mean value of the load over this constant portion was assumed to represent the frictional resistance likely to be experienced in a test on a concrete specimen. Figure A8.1. shows the change in this value with pressure together with the representative bilinear relation which has been adopted for the analysis of the triaxial test results.

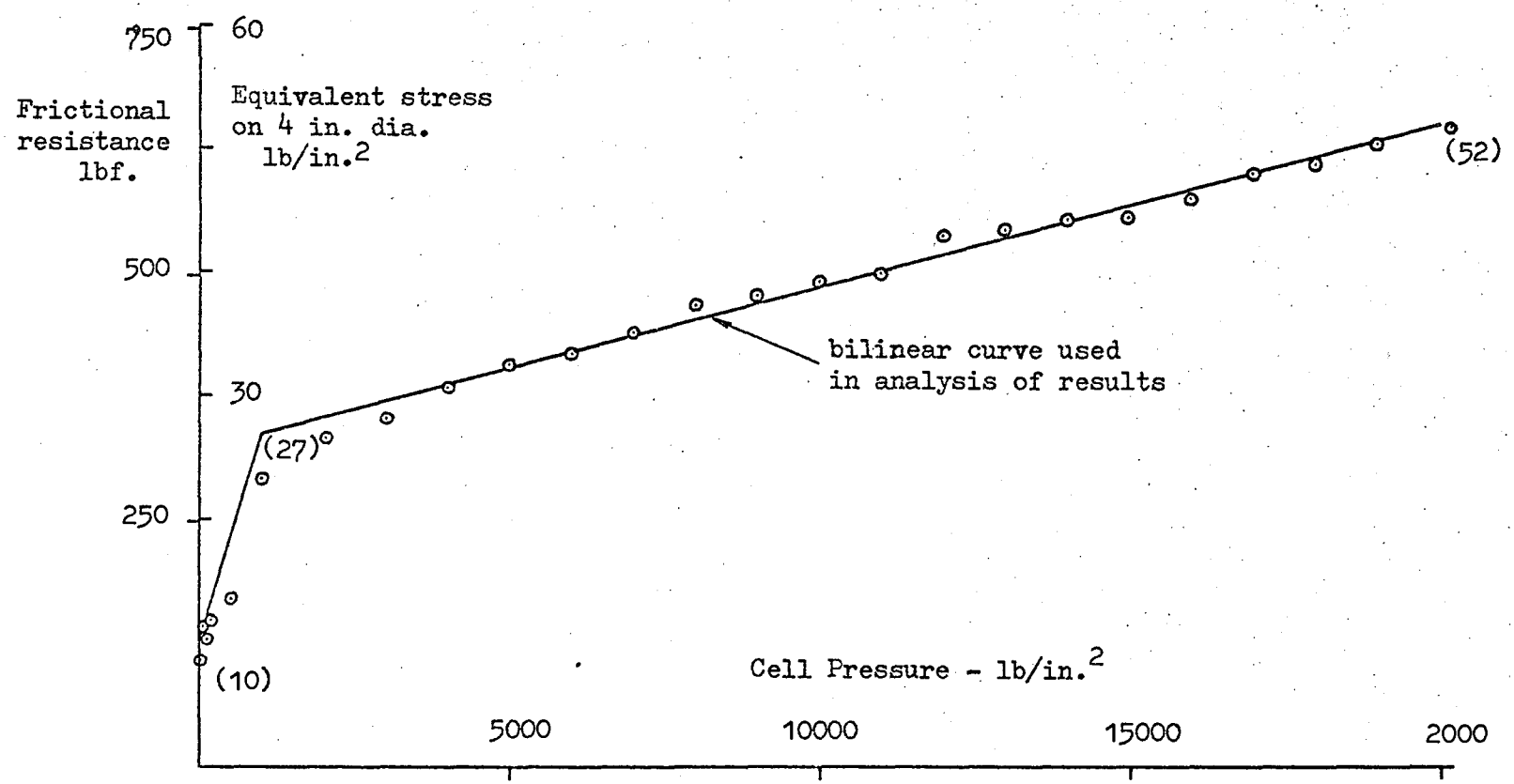


Figure A8.1. Variation of the frictional restraint of the axial load piston with cell pressure.

APPENDIX 9

Effect of Pressure on Strain Gauges

The influence of the cell pressure on the electrical resistance strain gauges used during the triaxial investigation was assessed by calibrating them against hydrostatic pressure when attached to the surface of a material with a known compressibility. The material chosen for this purpose was a stainless steel with a compressibility of 100 lb./in.^{2} which is equivalent to a linear strain of 200 microstrain at a pressure of 20000 lb./in.^{2}.

Two active strain gauges were attached to the surface of a strip of the stainless steel which was placed in hydraulic fluid within the cell. With the dummy gauges attached to a similar strip of steel immersed in hydraulic fluid outside the cell, the development of strain with cell pressure was measured using a digital strain gauge recorder.

The variation of the measured steel strain and cell pressure is given in Figure A9.1. which shows the similarity between the anticipated change of strain of the steel, calculated from its compressibility and the indicated strain at all levels of pressure. This similarly indicates that, for the range of hydrostatic pressures used in the test series, the effect of pressure on the strain gauges is insignificant and can be neglected.

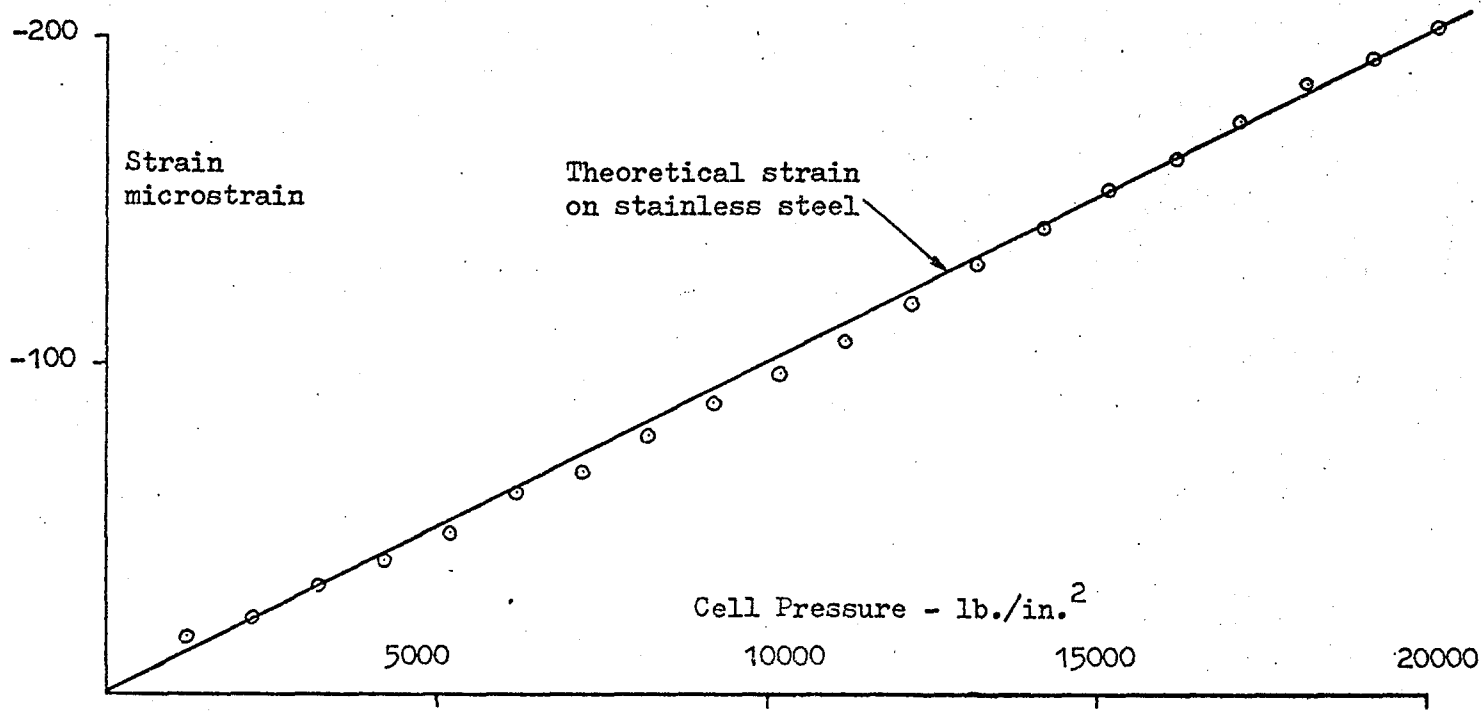


Figure A9.1. Variation of strain on stainless steel specimen as measured by electrical resistance strain gauges type YL-60 with cell pressure.